



HAL
open science

Multivalent systems based on viologen units: redox behaviour and recognition properties by cucurbit[n]urils

Parastoo Dalvand

► **To cite this version:**

Parastoo Dalvand. Multivalent systems based on viologen units: redox behaviour and recognition properties by cucurbit[n]urils. Organic chemistry. Université de Strasbourg, 2015. English. NNT: 2015STRAF051 . tel-01292590

HAL Id: tel-01292590

<https://theses.hal.science/tel-01292590>

Submitted on 23 Mar 2016

HAL is a multi-disciplinary open access archive for the deposit and dissemination of scientific research documents, whether they are published or not. The documents may come from teaching and research institutions in France or abroad, or from public or private research centers.

L'archive ouverte pluridisciplinaire **HAL**, est destinée au dépôt et à la diffusion de documents scientifiques de niveau recherche, publiés ou non, émanant des établissements d'enseignement et de recherche français ou étrangers, des laboratoires publics ou privés.

ÉCOLE DOCTORALE DES SCIENCES CHIMIQUES

UMR 7509

THÈSE présentée par :

Parastoo DALVAND

soutenue le : **29 Septembre 2015**

pour obtenir le grade de : **Docteur de l'université de Strasbourg**

Discipline/ Spécialité : Chimie

**Multivalent Systems Based on Viologen Units:
Redox Behaviour and Recognition Properties by
Cucurbit[n]urils**

THÈSE dirigée par :

M. M. ELHABIRI

Docteur, université de Strasbourg

RAPPORTEURS :

M. O. SIRI

Docteur, Université Aix-Marseille

M. .F. VOCANSON

Professeur, Université Jean Monnet, St Etienne

AUTRES MEMBRES DU JURY :

M. Z. ASFARI

Docteur, Université de Strasbourg

M. J. HAMACEK

Professeur, Université d'Orléans

M. D. TREBOUET

Professeur, Université de Strasbourg

To my parents

KNOWLEDGE IS POWER
FERDOWSI
SHAHNAMEH, 940-1020 AD

Acknowledgements

At first, I owe many thanks to the members of my PhD thesis jury, namely Dr. Olivier Siri, Pr. Francis Vocanson, Pr. Josef Hamacek and Pr. Dominique Trebouet for reading my thesis manuscript and for their valuable feedbacks.

I am most grateful to Dr. Zouhair Afari and Dr. Mourad Elhabiri for giving me the opportunity to work in such an interesting and challenging project as well as for their counseling and guidance during these three years. This thesis wouldn't have been possible without their kindest support, encouragement, consideration and remarkable patience.

I am so grateful to thank Pr. Ali Trabolsi for giving me opportunity to work on such interesting projects.

And also I would like to thank Dr. Elisabeth Davioud-Charvet and Dr. Loic Charbonnière for their support.

I am grateful to Michel Schmitt for his help with NMR analyses, Mathieu Chessé for his help with the ESI-MS identification of the metal complexes and the whole Services Communs d'Analyses de l'Université de Strasbourg.

I owe special thanks to my family especially my two sisters Mastan and Mahnaz for their unconditional love and support, they are always there for me and genuinely love me no matter what, I wish them a happy and healthy life.

I also would like to thank my fiancé, Etienne Gourlay whom joined me in the last year of my thesis, the one who laughs at my jokes and supports me during my heartache and also his parents Fabrice and Monique for treating me like my parents.

I would like to thank Haithem who was a great friend for me, we had a really interesting discussion about calixarene chemistry and more over about life, of course while we were drinking Persian tea.

I am so grateful to thank Max who was a really good friend for me, we passed a memorable time in the lab and I wish him a brilliant future.

I would like to thank Deepak who was not only an excellent friend and neighbor, but also a great chemist and optimistic person who always support me in different aspect of my life.

In the last years, Birgit, Aurelia, Jose and Malika joined our group whom I spent a great time with them and our friendship will continue forever.

I also would like to express my appreciation to all present and former members of the Bioorganic and Medicinal group (Didier, Xavier, Angeline, Liwen, Israel, Selbi and Jaen) and the LIMAA team (Alien, Celine, Sabah, Amandine, Tao, Nabila, Somayeh, Alex, Mohamadu, Rafael and Claudia), those with whom I have had the pleasure to work within the past three years and more over special thanks to Mouhamad Jida for his precious advice.

Abbreviations

ABI	Azo-benzene-imidazole
ANI	Azo-naphthyl-imidazole
API	Azo-phenanthryl-imidazole
BIPY ²⁺	4,4'-Bipyridinium
BMV ²⁺	1-Benzyl-1'-methyl-4,4'-bipyridinium
BV ⁴⁺	Phosphazene <i>bis</i> -viologen
C23 ⁴⁺	1,3-bis-(3-(1'-methyl-[4,4'-bipyridine]-propoxy)- <i>p</i> -tert-butylcalix[4]aren dibromide
C24 ⁴⁺	1,3-bis-(4-(1'-methyl-[4,4'-bipyridine]-butoxy)- <i>p</i> -tert-butylcalix [4]arene)di bromide
Calcd	calculated
CB[7]	cucurbit[7]uril
CB[8]	cucurbit[8]uril
CDCl ₃	Chloroforme d3
CD ₃ OD	Methanol d4
CH ₃ CN	Acetonitrile
CH ₃ I	Methyl iodide
cm	Centimeter
CTP	Cyclotriphosphazene
CV	Cyclic voltammetry
DCM	Dichloromethane
DFT	Density functional theory
DMSO	Dimethyl sulfoxide
DPV ²⁺	1,1'-Diphenyl-4,4'-bipyridinium
EPR	Electron paramagnetic resonance
Equiv	Equivalent
ESI	Electrospray ionization
g	Gram
h	Hour
HR-MS	High resolution mass spectrometry
HV ¹²⁺	Phosphazene Hexaviologen
I1	1-Methyl-[4,4'-bipyridin]-1-ium iodide
I2	1-(3-Bromopropoxy)-4-(<i>tert</i> -butyl)benzene

I3	1-(4-Bromo-butoxy)-4-(<i>tert</i> -butyl)benzene
I4	<i>Tetrakis-p-tert</i> -butyl-calix[4]arene
I5	1,3- <i>Bis</i> (3-bromopropoxy)- <i>p-tert</i> -butyl-calix[4]arene
I6	1,3- <i>Bis</i> (4-bromobutoxy)- <i>p-tert</i> -butyl-calix[4]arene
I	Cell pathlength
M	Molarity
MC3 ²⁺	1-(3-4-(<i>Tert</i> -butyl phenoxy)propyl)-1-methyl-[4,4'-bipyridin]-1,1'-dium bromide iodide
MC4 ²⁺	1-(4-(4-(<i>Tert</i> -butyl)phenoxy)butyl)-1'-methyl-[4,4'-bipyridin]-1,1'-dium bromide iodide
MHz	Megahertz
ml	Milliliter
mm	millimeter
MPV ²⁺	1-Methyl-1'-phenyl-4,4'-bipyridinium
MS	Mass spectrometry
mV	millivolt
MV ²⁺	1,1'-dimethyl-4,4'-bipyridinium
MVTP ²⁺	1-Methyl-1'-tris-phenylene-4,4'-bipyridinium
NIR	Near-infrared
nm	Nanometer
NMR	Nuclear magnetic resonance
pH	Potential hydrogen
s	Second
S1	1-methyl-1 <i>H</i> -imidazole
S2	1 <i>H</i> -imidazole
S3	2-methyl-1 <i>H</i> -imidazole
S4	2-phenyl-1 <i>H</i> -imidazole
SW	Square wave voltammetry
T	Temperature
TBACl	Tetrabutylammonium chloride
TLC	Thin layer chromatography
TV ⁶⁺	<i>tris</i> -viologen
UV	Ultra violet
V	Volume
V	Volt

V _c	Cone voltage
Vis	Visible
ZnL ¹	Zn(II) phenantroline strapped porphyrin
Zn TPP	Zn(II) Tetraphenylporphyrin
λ	Wavelength
δ	Chemical shift scale in NMR
Δ	Heat
μM	micromolar

Table of content

Résumé en Français

Avant propos	i
1 Introduction	iii
1.1. Les cucurbit[n]urils	iii
1.2. Les viologènes	iv
2. Hexamère circulaire et cucurbit[n]uril : vers des interrupteurs moléculaires basés sur des unités viologènes	vi
3. Reconnaissance à plusieurs centres d'un trisviologène circulaire	ix
3.1. Complexes formés avec le CB[7]	ix
3.2. Dimérisation intermoléculaire de dérivés du viologène	xii
3.3. Réduction des [n]pseudorotaxanes formés avec le CB[7]	xiii
4 Etudes physico-chimique de calix[4]arène-viologènes	xvi
4.1. Complexes formés avec les CB[7] et CB[8]	xvii
4.2. Dimérisation intramoléculaire	xviii
4.3. Réduction des [n]pseudorotaxanes formés avec le CB[7]	xix
5 Reconnaissance de substrats azo-imidazoles par une métalloporphyrine à anse phénanthroline	xxii
6 Conclusion	xxvi
7 Partie Bibliographique	xxix

Chapter I: General Introduction

1.1. Introduction	1
1.2. Supramolecular Chemistry	1
1.3. Molecular Recognition	4
1.3.1. Non-covalent Interactions	4
1.3.2. Hydrogen Bonding	5
1.3.3. Electrostatic Interactions	5
1.3.4. Hydrophobic Interactions	6
1.3.5. π - π Bonding	7
1.3.6. Coordination Interaction	7
1.4. Viologen-Cucurbituril Host/Guest Chemistry Toward an Electrochemical Control of Dimerization versus Inclusion for the Development of Novel Nanomechanical Devices	8
1.4.1. Cucurbiturils	8
1.4.1a. <i>Structural and Physico-chemical Features of CB[n]</i>	9
1.4.1b. CB[7] , a Valuable Supramolecular Host	10
1.4.1c. CB[8] , a Homologous Host	11
1.4.2. Viologens	13
1.4.3. CB[n] -Viologen Complexes	14
1.5. Aims of this Work	16

1.5.1.	Host-Guest Recognition Properties of Multimeric Viologen Threads	16
1.5.2.	Azo-Aryl-Imidazole/Zn(II) Metalloporphyrins Host/Guest Chemistry – Toward a Photochemical Control of the Inclusion/Dissociation Processes	19
1.5.3.	Zn(II) Metalloporphyrins	20
1.5.3a.	<i>Absorption Properties of (Metallo)Porphyrins</i>	22
1.5.3b.	<i>Photophysical Properties of (Metallo)Porphyrins</i>	23
1.5.3c.	<i>The Azobenzene System</i>	23
1.5.4.	Aims of this Work	25
Bibliographic Section		25

Chapter II: Cucurbit[n]uril Host and a Hexavalent Phosphazene Guest

2.1.	Introduction	33
2.1.1.	Hexavalent Phosphazene Platform	34
2.2.	Experimental Section and Results	35
2.2.1.	Starting Materials	35
2.2.2.	Analytical Methods	35
2.2.3.	Spectrophotometric Titrations of Viologen Derivatives by CB[7]	36
2.2.3a.	<i>Recognition of MV^{2+} by CB[7]</i>	36
2.2.3b.	<i>Recognition of BMV^{2+} by CB[7]</i>	37
2.2.3c.	<i>Recognition of BV^{4+} by CB[7]</i>	38
2.2.3d.	<i>Recognition of HV^{12+} by CB[7]</i>	38
2.2.4.	Complexation Studies Probed by 1H NMR Spectroscopy	39
2.2.4a.	<i>BMV^{2+} and CB[7] Recognition Probed by 1H NMR Spectroscopy</i>	39
2.2.4b.	<i>BV^{4+} and CB[7] Recognition Probed by 1H NMR Spectroscopy</i>	40
2.2.4c.	<i>HV^{12+} and CB[7] Recognition Probed by 1H NMR Spectroscopy</i>	40
2.2.5.	Stoichiometry of the Complexes for MV^{2+} and BMV^{2+} Probed by ESI-MS	41
2.2.6.	BMV^{*+} Pimerization in Aqueous Solution	42
2.2.7.	Recognition of Radical-Cations by CB[7]	43
2.2.7a.	<i>Recognition of BMV^{*+} by CB[7]</i>	43
2.2.7b.	<i>Recognition of MV^{2+}/MV^{*+} by CB[7]</i>	44
2.2.7c.	<i>Recognition of BMV^{2+}/BMV^{*+} by CB[7]</i>	45
2.2.7d.	<i>Recognition of $BV^{4+}/BV^{2(+*)}$ by CB[7]</i>	46
2.2.7e.	<i>Recognition of $HV^{12+}/HV^{6(*+)}$ by CB[7]</i>	47
2.2.8.	Electrochemistry	48
2.2.9.	Computational Methods	49
2.2.10.	Statistical Processing of the Absorption Spectrophotometric Data	50
2.3.	Discussion	51
2.3.1.	Characterization of the Thread/ CB[7] [n]pseudorotaxanes	51
2.3.1a.	<i>Recognition of MV^{2+} by CB[7]</i>	51
2.3.1b.	<i>Recognition of BMV^{2+} by CB[7]</i>	52
2.3.1c.	<i>Recognition of BV^{4+} and HV^{12+} by CB[7]</i>	54
2.3.2.	Inter- or Intramolecular Dimerization of Viologen Threads	57

2.3.2a.	<i>Intermolecular Dimerization of $BMV^{\bullet+}$</i>	57
2.3.2b.	<i>Intramolecular Pimerization of $BV^{2(\bullet+)}$ and $HV^{6(\bullet+)}$</i>	59
2.3.2c.	<i>Switching Properties of $HV^{12+}/HV_D^{6(\bullet+)}$ on ITO Coated Surface</i>	61
2.3.3.	Reduction of the [n]Pseudorotaxanes	63
2.3.3a.	<i>Monocationic Monoradicals $MV^{\bullet+}$ and $BMV^{\bullet+}$</i>	63
2.3.3b.	<i>Hexacationic Hexaradical $HV^{6(\bullet+)}$</i>	66
2.3.3c.	<i>Dicationic Diradical $BV^{2(\bullet+)}$</i>	70
2.4.	Conclusion	71
	Bibliographic Section	72

Chapter III: Intermolecular Dimerization of a *Tris*-Viologen System and its CB[n] Recognition Properties

3.1.	Introduction	75
3.2.	Experimental Section and Results	77
3.2.1.	Starting Materials	77
3.2.2.	Analytical Methods	77
3.2.3.	Spectrophotometric Titrations of Viologen Derivatives by CB[7]	78
3.2.3a.	<i>Recognition of MPV^{2+} by CB[7]</i>	78
3.2.3b.	<i>Recognition of DPV^{2+} by CB[7]</i>	79
3.2.3c.	<i>Recognition of $MVTP^{2+}$ by CB[7]</i>	80
3.2.3d.	<i>Recognition of TV^{6+} by CB[7]</i>	80
3.2.4.	Stoichiometry of the [n]Pseudorotaxane with MPV^{2+} , DPV^{2+} , $MVTP^{2+}$ and TV^{6+} Probed by ESI-MS	82
3.2.5.	Host-Guest complexation Investigated by 1H NMR Spectroscopy	86
3.2.5a.	<i>Complexation of $MVTP^{2+}/MPV^{2+}$ by CB[7] Probed by 1H NMR Spectroscopy</i>	86
3.2.5b.	<i>TV^{6+} Recognition by CB[7] Probed by 1H NMR Spectroscopy</i>	88
3.2.6.	Pimerization Processes in Aqueous Solution	88
3.2.6a.	<i>$MPV^{\bullet+}$ Pimerization in Aqueous Solution</i>	88
3.2.6b.	<i>Spectrophotometric Titration of $MVTP^{\bullet+}$</i>	90
3.2.6c.	<i>Spectrophotometric Titration of $TV^{3(\bullet+)}$</i>	90
3.2.7.	Recognition of the Radical Cations by CB[7]	91
3.2.7a.	<i>Recognition of $MPV^{\bullet+}$ by CB[7]</i>	91
3.2.7b.	<i>Recognition of $DPV^{\bullet+}$ by CB[7]</i>	93
3.2.7c.	<i>Recognition of $MVTP^{\bullet+}$ by CB[7]</i>	94
3.2.7d.	<i>Recognition of $TV^{3(\bullet+)}$ by CB[7]</i>	95
3.2.8.	Electrochemistry	96
3.2.9.	Recognition by CB[8]	97
3.2.9a.	<i>Recognition of $MPV^{2+}/MPV^{\bullet+}$ by CB[8]</i>	97
3.2.9b.	<i>Recognition of $MVTP^{2+}/MVTP^{\bullet+}$ by CB[8]</i>	98
3.2.9c.	<i>Recognition of $TV^{6+}/TV^{3(\bullet+)}$ by CB[8]</i>	99
3.2.10.	Statistical Processing of the Absorption Spectrophotometric Data	100
3.3.	Discussion	101

3.3.1.	Characterization of the Thread/ CB[7] [n]pseudorotaxanes	101
3.3.1a.	Recognition of MPV²⁺ and DPV²⁺ by CB[7]	101
3.3.1b.	Recognition of MVTP²⁺ and TV⁶⁺ by CB[7]	102
3.3.2.	Recognition of the Viologen Threads by CB[8]	104
3.3.3.	Intermolecular Dimerization of Viologen Threads	104
3.3.3a.	Intermolecular Dimerization of MPV^{•+}	105
3.3.3b.	Intermolecular Dimerization of MVTP^{•+} and TV^{3(•+)}	105
3.3.4.	Reduction of the [n]Pseudorotaxanes with CB[7]	108
3.3.4a.	Monocationic Monoradicals MPV^{•+} and DPV^{•+}	108
3.3.4b.	Monocationic Monoradical MVTP^{•+} and Triscationic Trisradical TV^{3(•+)}	110
3.3.5.	Reduction of the [n]Pseudorotaxanes with CB[8]	111
3.4.	Conclusion	112
	Bibliographic Section	114

Chapter IV: Recognition of Calix[4]arene-Based Viologens by CB[n]

4.1.	Introduction	116
4.1.1.	Calix[n]arene	117
4.1.2.	Historical Background	117
4.1.3.	Conformational and Structural Properties of Calix[4]arenes	118
4.1.4.	Aim of this Work	120
4.2.	Experimental Section and Results	121
4.2.1.	Synthesis of the Calix[4]arene-Bis-Viologens and the Corresponding Models	121
4.2.1a.	1-methyl-[4,4'-bipyridin]-1-ium iodide (I1)	121
4.2.1b.	1-(3-bromopropoxy)-4-(tert-butyl)benzene (I2)	121
4.2.1c.	1-(3-4-(tert-butyl)phenoxy)propyl)-1-methyl-[4,4'-bipyridin]-1,1'-dium bromide iodide (MC3²⁺)	122
4.2.1d.	1-(4-bromo-butoxy)-4-(tert-butyl)benzene (I3)	123
4.2.1e.	1-(4-4-(tert-butyl) phenoxy)butyl)-1'-methyl-[4,4'-bipyridin]-1,1'-dium bromide iodide (MC4²⁺)	123
4.2.1f.	Tetrakis-p-tert-butyl-calix[4]arene (I4)	124
4.2.1g.	1,3-bis(3-bromopropoxy)-p-tert-butyl-calix[4]arene (I5)	125
4.2.1h.	1,3-bis(3-(1'-methyl-[4,4'-bipyridin]-1,1'-dium)propoxy)-p-tert-butyl-calix[4]arene dibromide diiodide (C23⁴⁺)	125
4.2.1i.	1,3-bis(4-bromobutoxy)-p-tert-butyl-calix[4]arene (I6)	126
4.2.1j.	1,3-bis(3-(1'-methyl-[4,4'-bipyridin]-1,1'-dium)butoxy)-p-tert-butyl-calix[4]arene dibromide diiodide (C24⁴⁺)	127
4.2.2.	Physico-Chemistry	128
4.2.2a.	Solvents and Starting Materials	128
4.2.2b.	Analytical Methods	129
4.2.3.	Spectrophotometric Titrations of Viologen Derivatives by CB[7]	129

4.2.3a.	<i>Recognition of $MC3^{2+}$ by $CB[7]$</i>	129
4.2.3b.	<i>Recognition of $MC4^{2+}$ by $CB[7]$</i>	130
4.2.3c.	<i>Recognition of $C23^{4+}$ by $CB[7]$</i>	131
4.2.3d.	<i>Recognition of $C24^{4+}$ by $CB[7]$</i>	132
4.2.4.	Stoichiometry of the [n]Pseudorotaxane with $MC3^{2+}$, $MC4^{2+}$, $C23^{4+}$ and $C24^{4+}$ Probed by ESI-MS	132
4.2.5.	$MC3^{2+}/MC4^{2+}$ Recognition by $CB[7]$ Probed by 1H NMR Spectroscopy	136
4.2.5a.	<i>1H NMR Titration of $MC3^{2+}$ by $CB[7]$</i>	137
4.2.5b.	<i>1H NMR Titration of $MC4^{2+}$ by $CB[7]$</i>	138
4.2.6.	$C23^{4+}/C24^{4+}$ Recognition by $CB[7]$ Probed by 1H NMR Spectroscopy	138
4.2.6a.	<i>1H NMR Titration of $C23^{4+}$ by $CB[7]$</i>	138
4.2.6b.	<i>1H NMR Titration of $C24^{4+}$ by $CB[7]$</i>	139
4.2.7.	$MC3^{*+}$ and $MC4^{*+}$ Pimerization in Aqueous Solution	140
4.2.8.	Recognition of the Radical Cations by $CB[7]$	141
4.2.8a.	<i>Recognition of $MC3^{*+}$ by $CB[7]$</i>	141
4.2.8b.	<i>Recognition of $MC4^{*+}$ by $CB[7]$</i>	143
4.2.8c.	<i>Recognition of $C23^{2(*+)}$ by $CB[7]$</i>	144
4.2.8d.	<i>Recognition of $C24^{2(*+)}$ by $CB[7]$</i>	145
4.2.9.	Electrochemical Properties of the Threads and the [n]Pseudorotaxanes	145
4.2.10	EPR Spectroscopy	147
4.2.10a.	<i>EPR Characterization of the Chemically Generated Radical Cation $MC3^{*+}$ and its Inclusion Complex $MC3^{*+} \subset (CB7)_2$</i>	147
4.2.10b.	<i>EPR Characterization of the Chemically Generated Radical Cation $MC4^{*+}$ and its Inclusion Complex $MC4^{*+} \subset (CB7)_2$</i>	148
4.2.10c.	<i>EPR Characterization of the Chemically Generated Radical Cations $C23^{2(*+)}$ and $C24^{2(*+)}$ in the Presence and in the Absence of $CB[7]$</i>	148
4.2.11.	Recognition of $MC3^{2+}/MC3^{*+}$ and $MC4^{2+}/MC4^{*+}$ by $CB[8]$	149
4.2.12.	Behaviour of $C23^{2(*+)}$ and $C24^{2(*+)}$ Radical Species in the Presence of $CB[8]$	151
4.2.13.	Statistical Processing of the Absorption Spectrophometric Data	153
4.3.	Discussion	154
4.3.1.	Characterization of the Thread/ $CB[7]$ [n]pseudorotaxanes	154
4.3.1a.	<i>Recognition of $MC3^{2+}$ and $MC4^{2+}$ by $CB[7]$</i>	154
4.3.1b.	<i>Recognition of $C23^{4+}$ and $C24^{4+}$ by $CB[7]$</i>	155
4.3.2.	Intermolecular <i>versus</i> Intramolecular Dimerization of the Radical Cations	156
4.3.3.	Reduction of the [n]Pseudorotaxanes with $CB[7]$	158
4.3.3a.	<i>Monocationic Monoradicals $MC3^{*+}$ and $MC4^{*+}$</i>	158
4.3.3b.	<i>Bisradicals $C23^{2(*+)}$ and $C24^{2(*+)}$</i>	160
4.3.4.	Recognition of the Viologen Threads by $CB[8]$	162
4.3.5.	Reduction of the [n]Pseudorotaxanes with $CB[8]$	163
4.4.	Conclusion	163
	Bibliographic Section	165

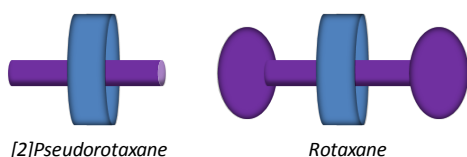
Chapter V: Recognition of Azo-Aryl-Imidazoles by Phen-Strapped Porphyrins

5.1. Introduction	167
5.2. Experimental Section and Results	168
5.2.1. Starting Materials and Solvents	168
5.2.2. UV-Vis. Absorption Spectrophotometric Titrations	168
5.2.3. Luminescence Titrations	171
5.2.4. Statistical Processing of the Absorption Spectrophotometric Data	173
5.2.5. Formation Kinetics and Statistical Analyses	174
5.3. Discussion	176
5.3.1. Recognition Properties	176
5.3.2. Formation Mechanism	178
5.3.3. Activation and Energetic Parameters	179
5.4. Conclusion	181
Bibliographic Section	183
General Conclusion	185

Avant-propos

Le travail de recherche effectué au cours de thèse a été en particulier centré sur la synthèse et l'étude des propriétés de reconnaissance de dérivés du 4,4'-bipyridinium ou d'imidazoles par des récepteurs, respectivement, de type curcubit[n]uril ou porphyrinique. Ces travaux ont été menés en étroite collaboration avec l'équipe du Professeur Ali Trabolsi (Center for Science and Engineering, New York University Abu Dhabi – NYUAD, préparation des systèmes multivalents basés sur des unités 4,4'-bipyridinium et des substrats azo-aryl-imidazoles), l'équipe du Docteur Jean Weiss (CLAC, UMR 7177, Strasbourg, préparation des récepteurs porphyriniques) et le Professeur Carlos Platas-Iglesias (Universidade da Coruña, Spain, calculs DFT and modélisation). En tirant profit d'interactions inter- ou intramoléculaires fortes au sein de nouveaux systèmes multivalents pré-organisés, nous avons démontré que la dimérisation de monoradicaux-cationiques (générés à partir d'unités viologènes) pouvait entrer en compétition thermodynamique avec le processus d'inclusion de ces mêmes substrats avec le curcubituril (**CB[7]** ou **CB[8]**) et conduire, grâce à une réaction (électro)chimique, à la dissociation rapide et efficace des complexes "host-guest". Alternativement, la ré-oxydation sous forme de bipyridiniums prévient le processus de dimérisation et régénère de manière réversible les systèmes "host-guest" initiaux.

Mon travail de thèse a donc été consacré à l'ingénierie et à l'étude de nouveaux systèmes basés sur les propriétés de reconnaissance de bipyridiniums rédox-actifs par des macrocycles de type curcubit[n]uril ($n = 7$ ou 8) (Figure 1). Les systèmes nano-mécaniques qui ont été développées concernent, entre autres, un [3]pseudorotaxane, un [4]pseudorotaxane et un [7]pseudorotaxane, chacun composé d'un multimère basé sur des unités viologènes (Figure 2, Figure 3 et Figure 4) et de macrocycles, le curcubit[7]uril (noté **CB[7]**) ou le curcubit[8]uril (noté **CB[8]**).



[2]Pseudorotaxane

Rotaxane

En solution aqueuse, ces systèmes peuvent être interconvertis électrochimiquement entre un état complexé, définis par les pseudorotaxanes eux-mêmes, et un état non complexé comprenant leurs composants séparés. La force motrice du processus de dissociation est une forte dimérisation intra- ou intermoléculaire des radicaux viologènes cationiques. Une analogie peut être établie entre ces systèmes artificiels et des canaux membranaires voltage-dépendants, leurs composants protéiques subissant de larges changements conformationnels sous l'action d'un potentiel.¹

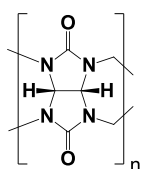


Figure 1. Structure chimique des composés de la famille des cucurbit[n]urils **CB[n]**.

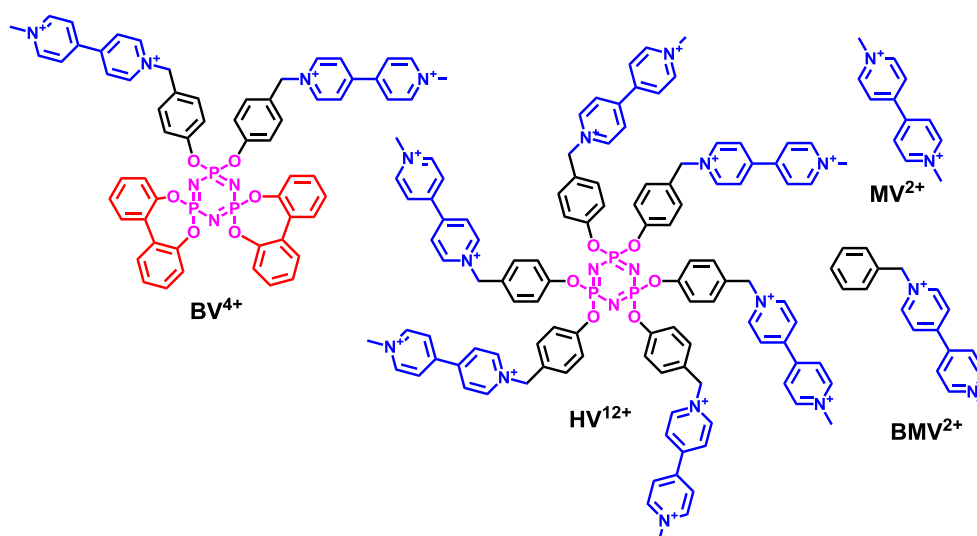


Figure 2. Structures chimiques d'un hexamère circulaire basé sur des unités viologènes HV^{12+} et de ses modèles BMV^{2+} , BV^{4+} et MV^{2+} .

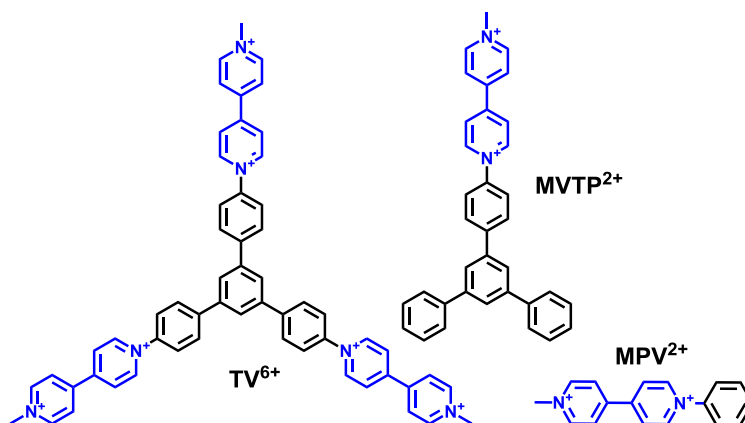


Figure 3. Structures chimiques d'un trimère circulaire basé sur des unités viologènes TV^{6+} et de ses modèles $MVTP^{2+}$ et MPV^{2+} .

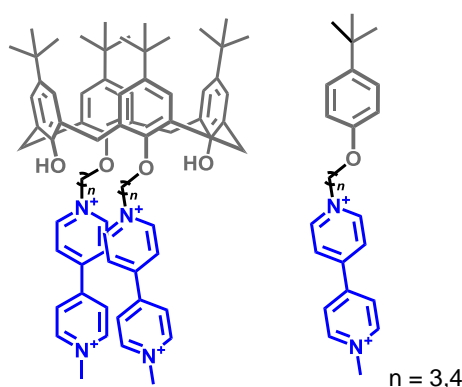


Figure 4. Structures chimiques de calix[4]arènes basés sur des unités viologènes $C23^{4+}$ and $C24^{4+}$ et de ses composés de référence $MC3^{2+}$ and $MC4^{4+}$. Le chiffre 2 correspond au nombre d'unités viologènes tandis que les chiffres 3-4 indiquent le nombre de carbones qui sépare la plateforme calix[4]arène des unités viologènes terminales.

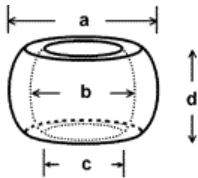
1. Introduction

En raison des nombreuses applications potentielles, la capacité d'induire des mouvements rapides et réversibles de grande amplitude au sein d'entités nanométriques est devenue un objectif scientifique majeur. À cette fin, de nombreux modèles supramoléculaires et de dispositifs mécaniques ont été synthétisés au cours de ces deux dernières décennies. Ceux-ci comprennent, entre autres, des systèmes fonctionnels à l'échelle nanométrique tels que des pincettes,²¹ des engrenages,³ des rotors,⁴⁻⁸ des navettes,⁹ des actionneurs,¹⁰⁻¹² ou encore des ascenseurs,¹³ dont les mouvements répondent à une grande variété de stimuli externes, tels que des changements de pH,¹⁴⁻¹⁶ de potentiel rédox,^{2,17} de température,¹⁸ ou d'intensité lumineuse.^{19,20} Dans cette partie, je rappellerai tout d'abord brièvement les principales propriétés des curcubit[n]uril, puis des viologènes. Par la suite, je décrirai les résultats qui ont été obtenus sur les systèmes étudiés au cours de ce travail de Doctorat.

1.1. Les curcubit[n]urils

Les curcubit[n]urils (**CB[n]**, $n = 5-10$) sont une classe de macrocycles²¹ synthétisés par condensation sous catalyse acide du formaldéhyde avec 5, 6, 7, 8 ou 10 molécules de glycoluril. Ils possèdent une forme de citrouille et deux portails carbonylés identiques, ainsi qu'une cavité hydrophobe qui peut accueillir une large variété de molécules hôtes.

Tableau 1. Propriétés structurales and physico-chimiques des macrocycles **CB[n]**.^a



	CB[5]	CB[6]	CB[7]	CB[8]	CB[10]
Diamètre externe a (Å)	13,1	14,4	16,0	17,5	20-21,1
Diamètre de la cavité b (Å)	4,4	5,8	7,3	8,8	11,3-12,4
Diamètre du portail c (Å)	2,4	3,9	5,4	6,9	9,0-11,0
Profondeur de la cavité ^b	7,4	7,5	7,6	7,7	7,8
Hauteur d (Å)	9,1	9,1	9,1	9,1	9,1
Volume (Å ³)	82	164	279	479	870
S _{H₂O} (mM)	20-30	0,018	20-30	< 0.01	-

^a Calculé à partir des données obtenues à l'état solide (Structures RX). ^b La profondeur de la cavité est déterminée à partir des minima du potentiel électrostatique. S_{H₂O} = solubilité dans l'eau à 25°C.

La chimie "host-guest" avec des **CB[n]** a suscité un énorme intérêt,^{21,22} et possède de nombreuses applications potentielles dans le domaine des nanotechnologies ou des sciences des matériaux.²¹⁻²⁴ Les récepteurs macrocycliques **CB[n]** ont été largement utilisés pour la préparation d'une large gamme de systèmes auto-assemblés, y compris les précurseurs de molécules mécaniquement imbriquées (MIMs) et les interrupteurs moléculaires.^{21,22} Le **CB[7]** a attiré le plus d'attention en raison de sa plus grande solubilité dans l'eau.²¹ Ce

macrocycle présente une cavité interne hydrophobe qui mesure 7,3 Å de diamètre et 9,1 Å de hauteur²⁵ (Tableau 1) et peut accueillir un large éventail de substrats^{21, 26,28} tels que des imidazoles,^{21,29,30} des stilbènes,³¹ des viologènes,³²⁻³⁷ des acridiniums,³⁸ des pyridine/pyridiniums,^{39,40} des adamantanes,²⁸ naphthalènes,⁴¹ ou ferrocènes,^{42,43} juste pour en citer quelques-uns. Du fait de sa taille de cavité réduite, le **CB[7]** ne peut toutefois reconnaître qu'un seul substrat. Le **CB[8]**, qui possède une taille de cavité plus grande, peut accueillir deux substrats identiques (complexes 1:2) ou deux substrats différents (complexes ternaires 1:1:1). Cependant, le **CB[8]** est caractérisé par une solubilité moindre dans l'eau.

1.2. Les viologènes

Les viologènes (notés V^{2+}), diversement substitués, constituent une classe de composés qui contiennent le noyau dicationique 1,1'-dialkyl-4,4'-bipyridinium (noté $BIPY^{2+}$), formé à partir de la diquaternization de la 4,4'-bipyridine.⁴⁴ Le prototype viologène, 1,1'-diméthyl-4,4'-bipyridinium (MV^{2+}), est connu sous le nom de diméthyl-viologène (ou paraquat), tandis que les autres analogues symétriques ou asymétriques sont désignés comme des sels de viologène substitués.

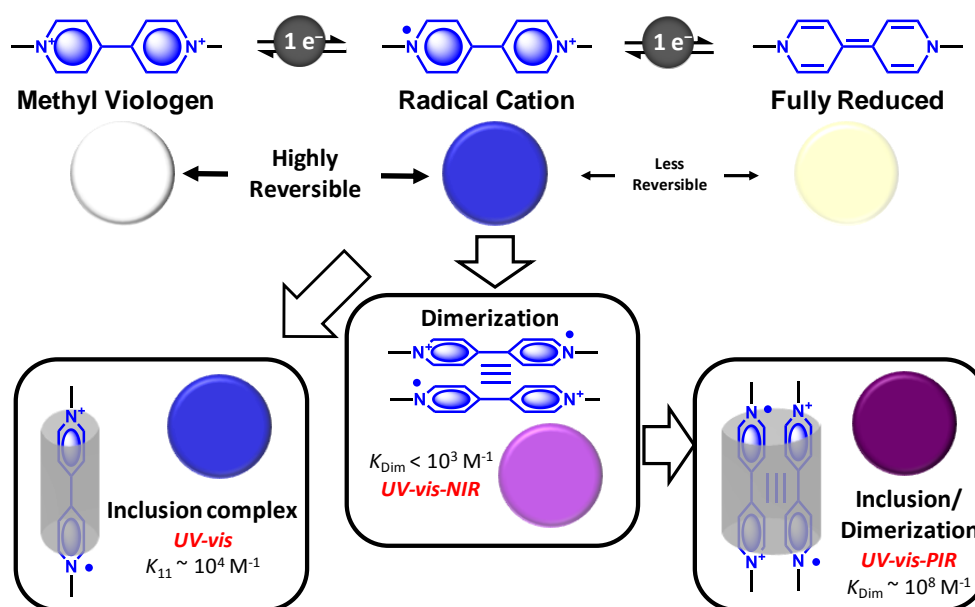


Figure 5. Représentation schématique des propriétés physico-chimiques, électrochimiques et de reconnaissance du diméthyl-viologène par des curcubit[n]urils **CB[n]** (n =7 ou 8).

Les sels de viologène ont acquis leur dénomination du fait de l'apparition dans l'eau d'une couleur mauve lors de la réduction monoélectronique du $BIPY^{2+}$ en un monoradical cationique stable $BIPY^{\bullet+}$.⁴⁵⁻⁵⁰ Sous l'effet de la dilution, la couleur mauve disparaît au profit d'une couleur bleue qui résulte de la présence majoritaire du monomère radical $BIPY^{\bullet+}$.^{51,52} Contrairement aux dications $BIPY^{2+}$ incolores, les monoradicaux-cations $BIPY^{\bullet+}$ sont d'un bleu intense. Leurs coefficients d'absorption molaires élevés résultent d'un transfert de charge intramolécule entre les deux atomes d'azote qui portent, respectivement, les charges formelles +1 et 0.^{52,53} En outre, les monoradicaux-cations $BIPY^{\bullet+}$ s'auto-associent spontanément dans l'eau^{48,51} pour donner naissance au dimère $(BIPY^{\bullet+})_2$ du fait

d'interactions radical-radical qui favorisent la formation d'un état singlet. La dimérisation du monoradical-cation est peu favorisée dans l'eau ($K_{\text{Dim}} = 10^{2,86} \text{ M}^{-1}$ pour $\text{MV}^{\bullet+54}$ et $10^{3,46} \text{ M}^{-1}$ pour $\text{BMV}^{\bullet+}$, Figure 6) ce limite leurs potentiels pour des applications en électrochromisme (UV-vis-PIR). Ce phénomène, également connu sous le terme de π -dimérisation ou de pimérisation, a été très utilisé pour générer des mouvements de translation ou de rotation au sein de molécules mécaniquement imbriquées (MIMs).⁵⁵

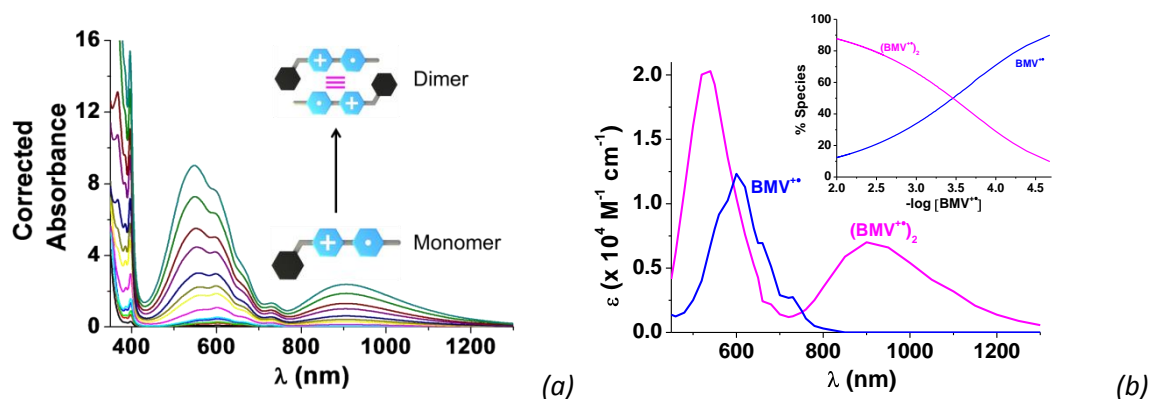


Figure 6. Titration spectrophotométrique (absorption UV-Vis.-PIR) (a) et spectres électroniques (b) du benzyl-méthyl-viologène BMV^{2+} sous sa forme monoradical. Solvant : tampon à pH 7,0 (0,1 M $\text{Na}_2\text{HPO}_4/\text{NaH}_2\text{PO}_4$). Pour $10^{-5} \text{ M} \leq [\text{BMV}^{\bullet+}]_0 < 10^{-4} \text{ M}$; $l = 1 \text{ cm}$; pour $2 \times 10^{-4} \text{ M} \leq [\text{BMV}^{\bullet+}]_0 < 10^{-3} \text{ M}$; $l = 0,2 \text{ cm}$; $T = 25,0(1) \text{ }^\circ\text{C}$. La figure encadrée décrit les courbes de distribution des espèces (monomère *versus* dimère) pour le monoradical-cation $\text{BMV}^{\bullet+}$ (travail de thèse).

Ces composés, substitués ou non, possèdent donc une chimie rédox riche et disposent de multiples propriétés physico-chimiques qui les rendent intéressants pour une utilisation dans des applications d'électrochromisme,⁵⁶ de catalyse,⁵⁷ ou de bioanalyse.⁵⁸

L'utilisation de macrocycles de type **CB[7]** est, en outre, connue pour empêcher la dimérisation de $\text{MV}^{\bullet+}$ (issue de la réduction à un électron du diméthyl-viologène MV^{2+}) par inclusion du monomère $\text{MV}^{\bullet+}$ au sein du récepteur. Le **CB[7]** est en effet capable de conduire en solution aqueuse à des complexes d'inclusion de stœchiométrie 1: 1 avec les deux états d'oxydation du diméthyl-viologène ($\text{MV}^{2+} \subset \text{CB[7]}$ et $\text{MV}^{\bullet+} \subset \text{CB[7]}$).^{22,26} Les constantes d'association $K_{\text{MV}^{\bullet+} \subset \text{CB[7]}}$ sont de l'ordre de 10^4 à 10^6 M^{-1} pour le complexe $\text{MV}^{\bullet+} \subset \text{CB[7]}$ et sont plus fortes que celles associées à la dimérisation spontanée de $\text{MV}^{\bullet+}$ ($K \sim 10^2$ à 10^5 M^{-1} selon les conditions expérimentales). Ceci indique que le processus d'inclusion de monoradicaux-cations par le **CB[7]** est thermodynamiquement favorisé pour prévenir la formation de dimères en solution.⁵⁹ En revanche, l'utilisation de **CB[8]** favorise la pimérisation de $\text{MV}^{\bullet+}$ par la formation d'un complexe binaire $(\text{MV}^{\bullet+})_2 \subset \text{CB[8]}$. Sans la présence de **CB[8]**, la pimérisation intermoléculaire serait très largement défavorisée. Le **CB[7]**, ne peut quant à lui reconnaître qu'un seul substrat du fait de sa taille de cavité réduite. Malgré tout, il demeure un récepteur d'intérêt du fait de sa meilleure solubilité dans l'eau et de forte capacité à accommoder divers substrats viologènes (interactions ions-dipôles et hydrophobes).

2. Hexamère circulaire et cucurbit[n]uril : vers des interrupteurs moléculaires basés sur des unités viologènes

Je me suis intéressé dans la première partie de mon travail de thèse à de nouveaux dispositifs moléculaires basés sur des unités bipyridiniums pour l'élaboration de systèmes électrochromes et/ou de machines moléculaires. Mon équipe d'accueil avait décrit en 2013 les propriétés d'une plateforme phosphazène fonctionnalisée par 6 viologènes (**HV**¹²⁺, Figure 2) dont la réduction à 6 électrons conduit à sa "pimérisation" intramoléculaire et lui confère des propriétés exploitables dans le domaine des électrochromes (Figure 7). Ce système de nature dendritique contient six unités **BIPY**²⁺ terminales réparties harmonieusement autour d'un cœur cyclotriphosphazène (CTP). Le CTP peut être facilement polyfonctionnalisé par substitution nucléophile de l'hexachlorure correspondant (NPCI_2)₃ conduisant à un système plus ou moins plan où les atomes de phosphore approchent une géométrie tétraédrique (sp^3) et les atomes d'azote tendent vers une géométrie sp^2 .⁶⁰ Les dérivés du CTP possèdent d'excellentes stabilités thermiques et chimiques et sont photochimiquement et électrochimiquement inertes. De ce fait, ils ne perturbent pas les propriétés des unités viologènes qui ont été combinées. L'ensemble de ces propriétés (facilité de fonctionnalisation, stabilité, géométrie...) plaide donc pour son utilisation comme brique moléculaire dans le développement de nouveaux systèmes multifonctionnels.

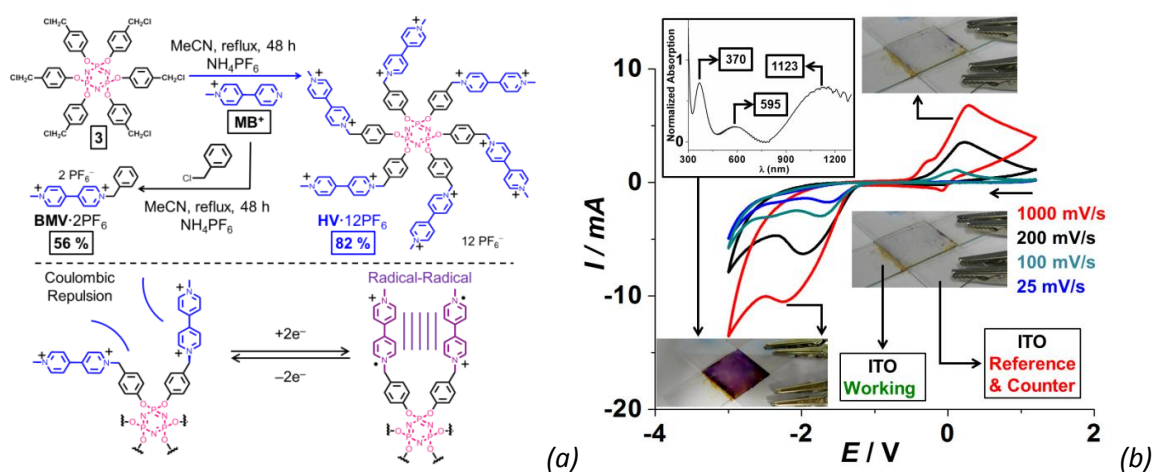


Figure 7. (a) Synthèse de **HV**¹²⁺ et **BMV**²⁺ et représentation schématique de la π -dimérisation de **HV**¹²⁺ rédox-activée (pour des raisons de simplicité, seuls deux bras viologènes sont représentés). Sous réduction, 1 électron est transféré à chaque **BIPY**²⁺ au sein de **HV**¹²⁺ (6 **BIPY**²⁺) pour générer l'intermédiaire **HV**⁶⁽⁺⁾. Une dimérisation intramoléculaire concomitante de 2 **BIPY**²⁺ adjacents portés par le même phosphore conduit à l'espèce **HV**_D⁶⁽⁺⁾. La ré-oxydation de **HV**_D⁶⁽⁺⁾ en **HV**¹²⁺ régénère les **BIPY**²⁺ qui se repoussent pour des raisons électrostatiques. (b) Voltampérogrammes cycliques à balayage variable d'une solution de **HV**¹²⁺ (NaCl 1 M) prise en sandwich entre deux lames de verre recouvertes d'ITO (4-8 Ohms, 1500–2000 Å d'épaisseur nominale de revêtement). Une des lames ITO est utilisée comme électrode de travail, tandis que l'autre est utilisée comme électrode de mesure et de référence. Un changement de couleur (incolore au violet) est observée lors de la réduction. Figure encadrée : spectre d'absorption du dispositif sous une tension appliquée de -2V.

Les complexes d'inclusion formés avec le **CB**[7] ont été tout d'abord donc été examinés. Contrairement au **CB**[8], le **CB**[7] conduit à l'inhibition de la pimérisation dans l'eau du

monoradical viologène $\text{BMV}^{\bullet+}$, du fait de sa taille de cavité plus petite et pour des raisons thermodynamiques ($\log K_{\text{BMV}^{\bullet+}+\text{CB}[7]} = 4,9(1)$ versus $\log K_{(\text{BMV}^{\bullet+})_2} = 3,46(5)$, Figure 8).

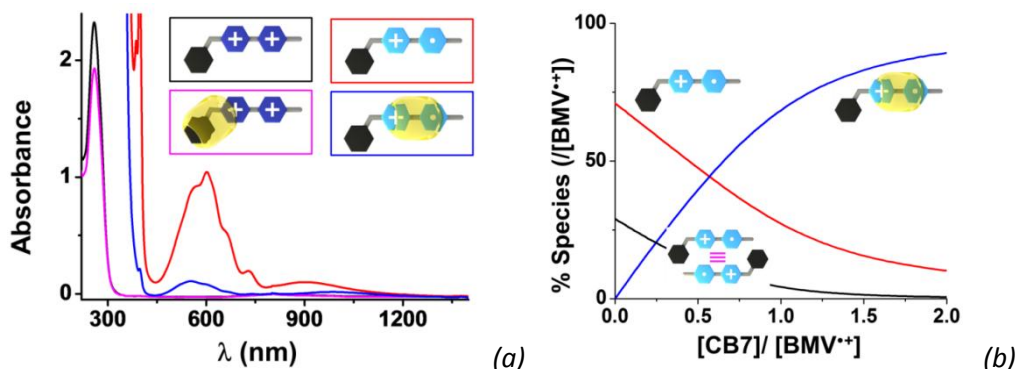


Figure 8. (a) spectres d'absorption de BMV^{2+} (noir), de son complexe d'inclusion avec $\text{BMV}^{2+} \subset \text{CB}[7]$ (magenta) ainsi que de son radical $\text{BMV}^{\bullet+}$ (rouge, mélange monomère + dimère). L'addition de $\text{CB}[7]$ (bleu) empêche la dimérisation du $\text{BMV}^{\bullet+}$. La formation de $\text{BMV}^{\bullet+} \subset \text{CB}[7]$ est caractérisée par un fort déplacement hypochrome de l'absorption centrée à ~ 550 nm. (b) Diagrammes de distribution du complexe d'inclusion de $\text{BMV}^{\bullet+}$ avec $\text{CB}[7]$ et du dimère $(\text{BMV}^{\bullet+})_2$ qui montrent que la formation de $\text{BMV}^{\bullet+} \subset \text{CB}[7]$, en compétition avec le processus de pimérisation, est thermodynamiquement favorisée. Solvant : tampon à pH 7,0 (0,1 M $\text{Na}_2\text{HPO}_4/\text{NaH}_2\text{PO}_4$).

Nous avons montré, grâce à nos outils physico-chimiques et électrochimiques, que les radicaux $\text{MV}^{\bullet+}$ et $\text{BMV}^{\bullet+}$ possédaient une affinité comparable ($\log K_{\text{BMV}^{\bullet+}+\text{CB}[7]} = 4,9(1)$ et $\log K_{\text{MV}^{\bullet+}+\text{CB}[7]} = 4,79$) pour le $\text{CB}[7]$, ce qui suppose un mode d'interaction unique (l'unité radical-cation interagit avec la cavité hydrophobe du $\text{CB}[7]$ dans l'eau). Par contre, sous sa forme oxydée, le benzyl-méthyl-viologène BMV^{2+} possèdent une meilleure affinité pour le $\text{CB}[7]$ du fait d'interactions hydrophobes stabilisantes entre le $\text{CB}[7]$ et le substituant benzylique ($\log K_{\text{BMV}^{2+}+\text{CB}[7]} = 6,9(8)$ versus $\log K_{\text{MV}^{2+}+\text{CB}[7]} = 5,30(2)$). Il apparait donc que lorsque le [2]pseudorotaxane $\text{BMV}^{2+} \subset \text{CB}[7]$ est réduit pour conduire à l'espèce $\text{BMV}^{\bullet+} \subset \text{CB}[7]$, le macrocycle effectue un mouvement de translocation de l'unité benzylique vers le radical-cation viologène (Figure 9).

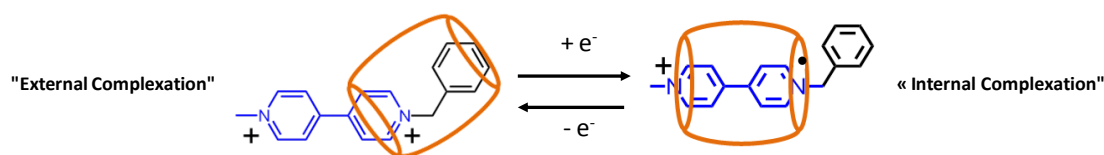


Figure 9. Translocation de $\text{CB}[7]$ contrôlée électrochimiquement pour les complexes avec BMV^{2+} .

L'hexaviologène HV^{12+} (Figure 2 et Figure 7a) a ensuite été examiné en présence de $\text{CB}[7]$. Sous sa forme oxydée, nous avons mis en évidence (absorption, ^1H RMN et ESI-MS) la formation d'un [7]pseudorotaxane ($\log K^*_{\text{HV}^{12+}+(\text{CB}[7])_6} = 4,23(7)$ avec K^* = constante apparente versus $\log K_{\text{MV}^{2+}+\text{CB}[7]} = 5,30(2)$). Malgré la similitude structurale apparente entre le modèle BMV^{2+} et les unités terminales des multimères BV^{4+} et HV^{12+} (Figure 2), les unités viologènes de ces derniers se lient au $\text{CB}[7]$ de la même façon que MV^{2+} , c.à.d. que le macrocycle $\text{CB}[7]$ interagit avec la partie BIPY^{2+} . Ceci résulte d'effets stériques dû au noyau

focal cyclotriphosphazène qui empêchent les macrocycles **CB[7]** d'interagir avec les espaces de type benzyl.

Contrairement à $MV^{2+} \subset CB[7]$ et $BMV^{2+} \subset CB[7]$ (*i.e.* la réduction monoélectronique conduit à des complexes d'inclusion $MV^{\bullet+} \subset CB[7]$ et $BMV^{\bullet+} \subset CB[7]$), la réduction à 1 électron de chaque unité viologène du [7]pseudorotaxane $HV^{12+} \subset [CB[7]]_6$ se traduit par une dissociation des macrocycles du fait d'une pimérisation intramoléculaire très largement favorisée par rapport à la reconnaissance des radicaux-cations par les **CB[7]**. Les macrocycles **CB[7]** se dissocient donc spontanément pour conduire aux espèces pimérisées $BV_D^{2(\bullet+)}$ et $HV_D^{6(\bullet+)}$, respectivement. Ces résultats confortent l'idée que la dimérisation intramoléculaire de radicaux-cations (*i.e.* interaction relativement faible) peut être favorisée grâce à une pré-organisation judicieuse d'unités viologènes autour d'une plateforme moléculaire et ainsi être exploitée pour la conception de nouveaux interrupteurs moléculaires. Notre approche est originale au regard des données de la littérature. Un article récent a montré qu'une réorganisation moléculaire (de douze à six directions) autour d'un noyau C_{60} peut être accomplie par une réduction monoélectronique de chacune des douze sous-unités viologènes terminales.⁶¹

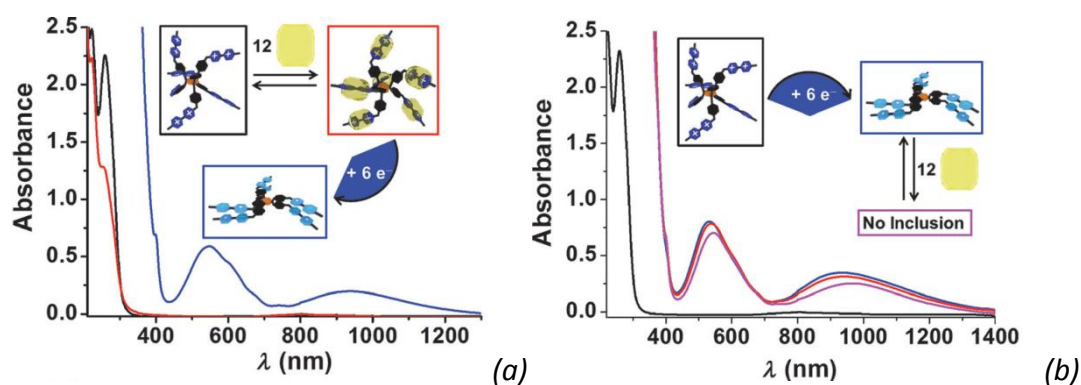


Figure 10. (a) Spectres d'absorption de HV^{12+} et de $HV^{12+} \subset [CB[7]]_6$. L'addition de $Na_2S_2O_4$ à $HV^{12+} \subset [CB[7]]_6$ induit la dissociation des macrocycles **CB[7]** comme en témoigne la signature spectroscopique caractéristique (absorption dans le PIR) de l'espèce entièrement dimérisée $HV_D^{6(\bullet+)}$. (b) Spectres d'absorption de HV^{12+} et de son produit de réduction $HV_D^{6(\bullet+)}$. L'addition d'excès de **CB[7]** n'a aucun effet apparent sur le spectre d'absorption de $HV_D^{6(\bullet+)}$.

Ces résultats ont été publiés dans *Chem. Eur. J.* (2014, 20, 7334).

Pseudorotaxanes

- Radical-Cation Dimerization Overwhelms Inclusion in [n]Pseudorotaxanes (pages 7334–7344)

Dr. Katia Nchimi-Nono, Parastoo Dalvand, Dr. Kuldeep Wadhwa, Selbi Nuryyeva, Shaikha Alneyadi, Dr. Thirumurugan Prakasam, Dr. Albert C. Fahrenbach, Prof. John-Carl Olsen, Dr. Zouhair Asfari, Carlos Platas-Iglesias, Dr. Mourad Elhabiri and Prof. Ali Trabolsi

Article first published online: 7 MAY 2014 | DOI: 10.1002/chem.201400069



Multimeric threads in which two and six viologen subunits are covalently bonded to a phosphazene core form the corresponding [3]- and [7]pseudorotaxanes on complexation with cucurbit[7]uril. In aqueous solution, these systems can be electrochemically switched between the complexed and uncomplexed states (*i.e.*, the separate components). The driving force for dethreading is intramolecular dimerization of the viologen radical cation (see figure).

3. Reconnaissance à plusieurs centres d'un trisviologène circulaire

3.1. Complexes formés avec le CB[7]

Dans cette deuxième partie, j'ai étudié les processus de reconnaissance et de pimérisation intermoléculaire d'un système trimérique circulaire TV^{6+} basé sur un benzène focal qui a été étendu sur ses positions 1, 3 et 5 par des unités méthyl-phényl-viologènes. Les modèles correspondants, le méthyl-phényl-viologène MPV^{2+} , le diphenyl-viologène DPV^{2+} et le méthyl-triphényl-benzène-viologène $MVTP^{2+}$, ont été également étudiés (Figure 3). Je vais décrire ci-dessous les principaux résultats issus d'une étude physico(électro)chimique (1H RMN, spectrophotométrie d'absorption UV-Vis.-PIR, électrochimie, ESI-MS) de cette série homogène de quatre dérivés viologènes en combinaison avec le **CB[7]** et le **CB[8]**.

Un titrage par spectrophotométrie d'absorption de MPV^{2+} avec le **CB[7]** en solution aqueuse a tout d'abord confirmé la formation d'un complexe d'inclusion de stœchiométrie 1:1 ($MPV^{2+} \subset CB[7]$) en accord avec des mesures ESI-MS. La constante d'association de ce [2]pseudorotaxane ($\log K_{MPV^{2+} \subset CB[7]} = 6,1(3)$ dans un tampon phosphate à 0,1 M, pH 7,0) est 6 fois plus stable que celle mesurée pour $MV^{2+} \subset CB[7]$ ($\log K_{MV^{2+} \subset CB[7]} = 5,30(2)$ à pH 7,0). Cette stabilisation de $MPV^{2+} \subset CB[7]$ peut être attribuée au groupement phényl supplémentaire et donc à des interactions hydrophobes plus fortes. Lors de ce titrage spectrophotométrique, de faibles variations spectrales ont été enregistrées. La complexation en mode interne ($BIPY^{2+} \subset CB[7]$) est généralement caractérisée par des variations hypochromes et bathochromes significatives des transitions $\pi-\pi^*$ centrées sur le noyau $BIPY^{2+}$. La complexation du mode externe (Figure 11) par le **CB[7]**, dont la force motrice est le caractère hydrophobe du groupe phényl additionnel, a été confirmée par la 1H RMN qui a révélé de larges variations vers des champs forts des protons de l'unité phényl tandis que des variations beaucoup plus faibles sont observées pour les protons associés à l'unité $BIPY^{2+}$.

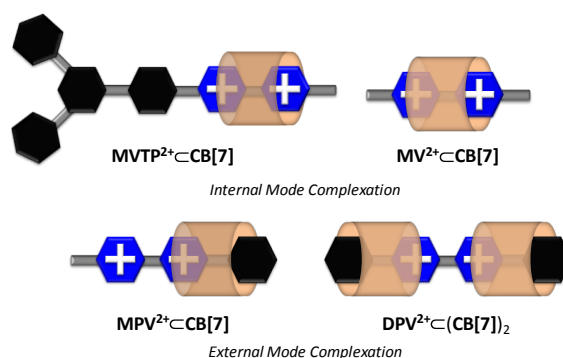


Figure 11. Représentation schématique d'une reconnaissance en mode interne (MV^{2+} et $MVTP^{2+}$, la cavité hydrophobe du **CB[7]** occupe l'unité bipyridinium) and externe (MPV^{2+} et DPV^{2+} , la cavité hydrophobe du **CB[7]** est localisée sur le groupement phényl terminal).

Ces observations suggèrent donc la formation d'un [2]pseudorotaxane $MPV^{2+} \subset CB[7]$ dont la cavité hydrophobe du **CB[7]** entoure préférentiellement le substituent phényl au lieu de

l'électrophore **BIPY²⁺** (comme pour **MV²⁺**) qui contribue à la stabilisation de ce dernier. Un tel mode d'inclusion avait déjà été décrit par ¹H RMN pour l'analogue symétrique, le diphenyl-viologène **DPV²⁺**.⁶² Une stœchiométrie 1:2 (**DPV²⁺:CB[7]**) avait été suggérée dans cette étude. La formation d'un [3]pseudorotaxane **DPV²⁺⊂(CB[7])₂** a été confirmée dans le cadre de mon travail de thèse. Lors de la reconnaissance du **DPV²⁺** par le **CB[7]**, les transitions π - π^* centrées sur le **DPV²⁺** subissent de faibles variations hypsochromes et hypochromes qui confirme un mode d'inclusion externe. La spectrométrie de masse en mode électrospray a, en outre, mis en évidence la formation de deux complexes : un [2]pseudorotaxane **DPV²⁺⊂CB[7]** et un [3]pseudorotaxane **DPV²⁺⊂(CB[7])₂**. Seule la stabilité globale du [3]pseudorotaxane a été déterminée dans nos conditions expérimentales ($\log \beta_{\text{DPV}^{2+}\subset(\text{CB}[7])_2} = 8,29(9)$). En faisant l'hypothèse que la constante de stabilité calculée pour **MPV²⁺⊂CB[7]** ($\log K_{\text{MPV}^{2+}\subset\text{CB}[7]} = 6,1(3)$) est comparable à celle du [2]pseudorotaxane **DPV²⁺⊂CB[7]**, une reconnaissance statistique ($K_{\text{DPV}^{2+}\subset(\text{CB}[7])_2}/K_{\text{DPV}^{2+}\subset\text{CB}[7]} = 0,25$)⁶³ conduirait à une constante de stabilité globale $\log \beta_{\text{DPV}^{2+}\subset(\text{CB}[7])_2} = 11,6$, très supérieure à celle déterminée expérimentalement. Ceci rend donc compte de fortes interactions stériques entre les deux macrocycles **CB[7]** au sein du [3]pseudorotaxane **DPV²⁺⊂(CB[7])₂** qui altèrent les propriétés de reconnaissance (*i.e.* coopérativité négative) par rapport à **MPV²⁺⊂CB[7]**.

La formation de complexes d'inclusion de **MVTP²⁺** et **TV⁶⁺** avec le **CB[7]** a également été mis en évidence par des mesures d'absorption UV-visible. Contrairement aux systèmes précédents, des déplacements hypochromes et bathochromes importants des transitions π - π^* centrées sur le noyau **BIPY²⁺** suggèrent une reconnaissance du chromophore **BIPY²⁺** par la cavité hydrophobe du macrocycle **CB[7]** (complexation en mode interne, Figure 11) malgré la présence d'un groupement triphényl-benzène également de nature hydrophobe. Des titrages ¹H RMN ont également confirmé l'association du **CB[7]** au dication **BIPY²⁺** comme observé précédemment pour **MV²⁺**.

Tableau 2. Paramètres thermodynamiques and spectroscopiques des [n]pseudorotaxanes entre plusieurs viologènes substitués et les **CB[7]** et **CB[8]**.

Viologène V	$\log K_{V\subset\text{CB}[7]}$	$\log K_{V\subset\text{CB}[8]}$	λ (V) (nm) ϵ^m ($10^4 \text{ M}^{-1} \text{ cm}^{-1}$)	λ (V⊂CB[7]) (nm) ϵ^d ($10^4 \text{ M}^{-1} \text{ cm}^{-1}$)
MV²⁺	5,30(2)	5,04 ⁶⁶	227(2,96) / 257(2,06)	226(3,13) / 281(sh)
MPV²⁺	6,1(3)	-	227(2,20) / 286(1,19)	227(2,22) / 286 (1,14)
DPV²⁺	$\log \beta_{\text{DPV}^{2+}\subset\text{CB}[7]} =$ 8,29(9)		250(1,14) / 293(sh) / 312(2,03)	250 (1,47) / 298(2,31) / 310(2,18)
MVTP²⁺	4,8(4)	4,6(4)	349(0,85)	372(0,75)
TV⁶⁺	$\log K^*_{\text{TV}^{6+}\subset(\text{CB}[7])_3}$ = 4,7(1)	5,5(1)	226(4,66) / 262(4,16) / 346(1,62)	226(5,07) / 262(3,47) / 378(1,41)

Solvant : tampon aqueux à pH 7,0 avec 0,1 M Na₂H₂PO₄/NaH₂PO₄ ; l = 1 cm ; T = 25,0(1)° C. Les valeurs en italique sont caractéristiques de complexes pour lesquels un mode de liaison externe a été mis en évidence, tandis que les valeurs en gras suggèrent un mode d'association interne.

Nous avons ensuite examiné les complexes d'inclusion formés avec le **CB[7]** et **TV⁶⁺** sous sa forme oxydée et mis en évidence un [4]pseudorotaxane **TV⁶⁺⊂(CB[7])₃** (Figure 12). Cette espèce a été caractérisée et quantifiée par spectrophotométrie d'absorption (Figure 12A), ESI-

MS (Figure 12B) et ^1H RMN. Pour TV^{6+} , seule une association constant^{64,65} apparente ($\log K^*_{\text{TV}^{6+}\text{-(CB[7])}_3} = 4,7(1)$, tampon phosphate 0,1 M à pH 7,0) a été calculée à partir du traitement statistiques des données spectrophotométriques. Cela reflète le fait que les trois sous-unités BIPY^{2+} du trisviologène TV^{6+} se comportent comme des sites de liaison indépendants, et que chaque CB[7] lié aux unités BIPY^{2+} de TV^{6+} induit des variations spectrales comparables. La constante de stabilité moyenne ($\log K^*_{\text{calc.}} = 4,5$) qui peut être déduit à partir d'un modèle d'association statistique est comparable à la valeur apparente déterminée à partir de titrage d'absorption à pH 7,0 ($\log K^*_{\text{TV}^{6+}\text{-(CB[7])}_3} = 4,7(1)$).

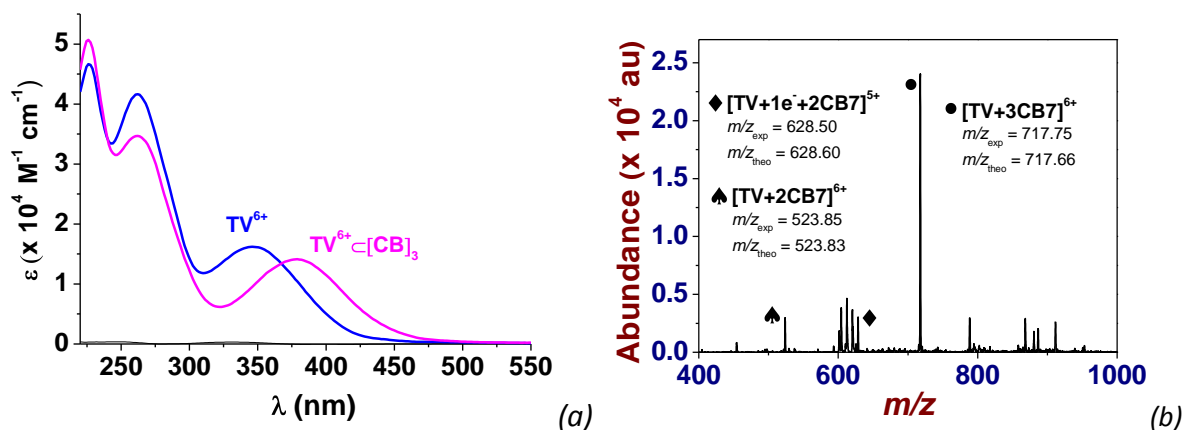


Figure 12. (a) Spectres d'absorption électronique des complexes d'inclusion de TV^{6+} avec le CB[7] . Solvant : tampon à pH 7,0 (0,1 M $\text{Na}_2\text{HPO}_4/\text{NaH}_2\text{PO}_4$) ; $T = 25,0(1)^\circ\text{C}$ (b) Spectre de masse ESI-MS des complexes d'inclusion TV^{6+} avec le CB[7] . $[\text{TV}^{6+}]_0 = 5 \times 10^{-5} \text{ M}$; $[\text{CB[7]}] = 2 \times 10^{-4} \text{ M}$. Solvant : eau ; mode positif. $V_c = 180 \text{ V}$. $\bullet = [\text{TV}+3\text{CB[7]}]^{6+}$, $m/z_{\text{exp}} = 717,75$, $m/z_{\text{theo}} = 717,66$. $\blacklozenge = [\text{TV}+1\text{e}^-+2\text{CB[7]}]^{5+}$, $m/z_{\text{exp}} = 628,50$, $m/z_{\text{theo}} = 628,60$. $\blackspade = [\text{TV}+2\text{CB[7]}]^{6+}$, $m/z_{\text{exp}} = 523,85$, $m/z_{\text{theo}} = 523,83$. Le spectre de masse ESI-MS a été limité à sa zone d'intérêt. Aucun autre signal n'a été observé dans la zone omise.

La caractérisation et la quantification des complexes "host-guest" formés avec les viologènes MPV^{2+} , DPV^{2+} , MVTP^{2+} et TV^{6+} et le cucurbit[8]uril CB[8] ont été ensuite menées par spectrophotométrie d'absorption et ESI-MS. Tout comme pour les [n]pseudorotaxanes avec le CB[7] , nous avons pu caractériser également les complexes $\text{MPV}^{2+}\text{-(CB[8])}$, $\text{DPV}^{2+}\text{-(CB[8])}_2$, $\text{MVTP}^{2+}\text{-(CB[8])}$ ($\log K_{\text{MVTP}^{2+}\text{-(CB[8])}} = 4,6(4)$) et $\text{TV}^{6+}\text{-(CB[8])}_3$ ($\log K_{\text{TV}^{6+}\text{-(CB[8])}_3} = 5,5(1)$). Aucun complexe de stœchiométrie 2:1 ($(\text{V}^{2+})_2\text{-(CB[8])}$) n'a été mis en évidence en accord avec les données issues de la littérature.^{50,66} En raison de la solubilité limitée du CB[8] , nous n'avons pu effectuer de titrages ^1H RMN, ce qui limite l'information sur le mode de complexation de ces espèces. De plus, de faibles variations spectrales centrées sur l'unité BIPY^{2+} ont été observées lors de la complexation de MPV^{2+} et DPV^{2+} par le CB[8] . Les effets de dilution du à la faible solubilité du CB[8] ne nous pas permis de déterminer avec précision les constantes de formation des [n]pseudorotaxanes correspondants. De même, la constante de stabilité apparente mesurée pour TV^{6+} semble être surestimée par rapport à celle déterminée pour MVTP^{2+} . Toutefois, les spectres électroniques calculés pour MVTP^{2+} et TV^{6+} en présence de CB[8] semblent suggérer un mode de complexation interne (*i.e.* reconnaissance du chromophore BIPY^{2+}).

3.2. Dimérisation intermoléculaire de dérivés du viologène

Nous avons montré que les radicaux-cations $\text{MPV}^{\bullet+}$ s'auto-associaient en solution avec une valeur de $\log K_{\text{Dim}}$ de 3,5(1), qui est comparable avec celle mesurée pour le benzyl-méthyl-viologène $\text{BMV}^{\bullet+}$ ($\log K_{\text{Dim}} = 3,46(5)$) et supérieure à celle du diméthyl-viologène $\text{MV}^{\bullet+}$ ($\log K_{\text{Dim}} \sim 2,5-2,9$).^{67,68} Ceci montre que l'augmentation du caractère hydrophobe autour de l'unité BIPY^{2+} avec des substituants aromatiques favorise la pimérisation des radicaux-cations. Le spectre électronique de MVTP^{2+} diffère de celui de MPV^{2+} (déplacement bathochrome des transitions $\pi-\pi^*$ centrées sur l'unité BIPY^{2+}) qui peut être expliqué par une conjugaison étendue du système aromatique. Le noyau central triphényl-benzène conduit à une forte conjugaison et une planéité accrue augmentant ainsi la probabilité d'empilements π -aromatiques. Le radical-cation $\text{MVTP}^{\bullet+}$ se caractérise par une absorption centrée à 563 nm. Contrairement à son analogue $\text{MPV}^{\bullet+}$, une absorption intense centrée à 1034 nm est observée. Cette caractéristique est attribuée à un transfert de charge qui se produit au sein d'une espèce dimérisée ($K_{\text{Dim}} \gg 10^7 \text{ M}^{-1}$) favorisée par π -stacking du fait de la présence de l'unité triphényl-benzène (Figure 13). Le spectre électronique de $\text{TV}^{3(\bullet+)}$ présente les mêmes caractéristiques spectrales que $\text{MVTP}^{\bullet+}$ (absorption à 560 nm et CT à ~ 1170 nm). La réduction monoélectronique de chacune des unités viologènes de TV^{6+} conduit à une espèce trisradicalaire $\text{TV}^{3(\bullet+)}$ qui s'auto-associe spontanément en solution pour conduire au dimère $(\text{TV}^{3(\bullet+)})_2$. Contrairement à de simples viologènes sous forme monoradicalaire, la constante de pimérisation ($K_{\text{Dim}} \gg 10^7 \text{ M}^{-1}$) est très largement augmentée du fait de la multiplication des centres de pimérisation. Le dimère $(\text{TV}^{3(\bullet+)})_2$ constitue donc l'espèce prédominante à des concentrations sub- μM . Cette stratégie novatrice démontre que des interactions intermoléculaires peuvent aussi être utilisées pour augmenter la stabilité de pimères en solution grâce à une approche multivalente et à une ingénierie adaptée.

Un processus d'agrégation a été mis en évidence du fait de l'empilement aromatique de dimères $(\text{TV}^{3(\bullet+)})_2$. Ce processus est réversible par ajout de **CB[8]** et non altéré par l'ajout de **CB[7]** (Figure 14).

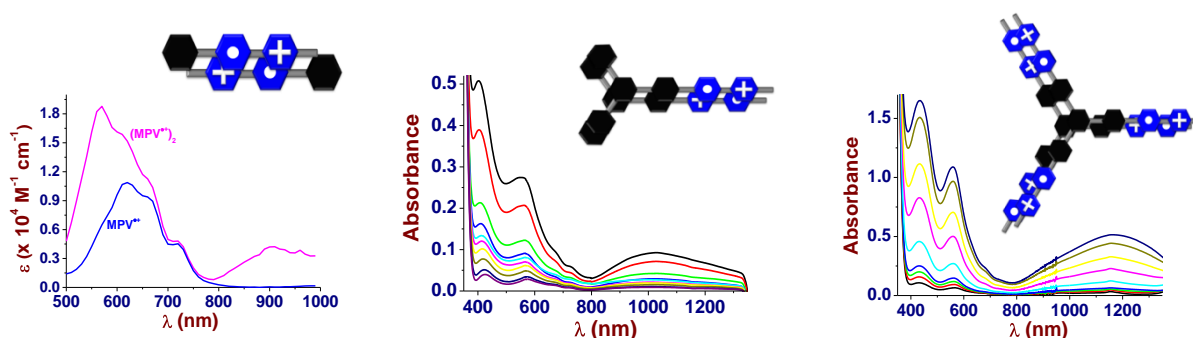


Figure 13. (a) Titrages par spectrophotométrie d'absorption UV-Vis.-PIR de $\text{MPV}^{\bullet+}$, $\text{MVTP}^{\bullet+}$ et $\text{TV}^{3(\bullet+)}$ en solution aqueuse. $10^{-5} \text{ M} \leq [\text{MPV}^{\bullet+}]_0 \leq 10^{-4} \text{ M}$; $l = 1 \text{ cm}$ et $2,5 \times 10^{-4} \text{ M} \leq [\text{MPV}^{\bullet+}]_0 \leq 2 \times 10^{-3} \text{ M}$; $l = 2 \text{ mm}$. $10^{-6} \text{ M} \leq [\text{MVTP}^{\bullet+}]_0 \leq 4 \times 10^{-5} \text{ M}$; $l = 1 \text{ cm}$. $10^{-6} \text{ M} \leq [\text{TV}^{3(\bullet+)})_0 \leq 4 \times 10^{-5} \text{ M}$; $l = 1 \text{ cm}$. Solvant : tampon aqueux à pH 7,0 avec 0,1 M $\text{Na}_2\text{H}_2\text{PO}_4/\text{NaH}_2\text{PO}_4$; $T = 25,0(1)^\circ \text{C}$. Dans chacune des solutions, le radical-cation a été généré à partir de $\text{Na}_2\text{S}_2\text{O}_4$ (*ca.* 10^{-2} M) fraîchement préparée en conditions d'atmosphère inerte. Les spectres d'absorption ne sont pas corrigés des effets de dilution.



Figure 14. Mélanges de $\text{TV}^{3(++)}$ et **CB[8]** (pas de précipitation, couleur verte, à gauche) et de $\text{TV}^{3(++)}$ et **CB[7]** (précipitation, couleur rougeâtre, à droite).

3.3. Réduction des [n]pseudorotaxanes formés avec le **CB[7]**

Des expériences voltamétriques (cyclique – CV et à ondes carrées – SWV) en solution aqueuse à pH 7,0 ont été réalisées sur le premier composé de référence (MPV^{2+}) en absence et en présence de **CB[7]**. L'ajout de **CB[7]** modifie profondément les propriétés électrochimiques de ce dérivé viologène. En présence de 2 équivalents de **CB[7]**, la première vague rédox est déplacée à un potentiel plus négatif ($\Delta E_{1/2}^1 = 100$ mV) et conserve sa forme réversible, tandis que la seconde vague de réduction subit un déplacement cathodique plus important ($\Delta E_{1/2}^2 = 190$ mV). Ces changements témoignent des affinités relatives du récepteur **CB[7]** pour les différents états d'oxydation de MPV^{2+} . En tenant compte de la constante d'association ($\log K_{\text{MPV}^{2+} \cdot \text{CB}[7]} = 6,1(3)$) déterminée précédemment pour $\text{MPV}^{2+} \cdot \text{CB}[7]$, les affinités de $\text{MPV}^{\bullet+}$ et MPV^0 pour **CB[7]** peuvent être estimées ($\log K_{\text{MPV}^{\bullet+} \cdot \text{CB}[7]} \sim 4,41$ and $\log K_{\text{MPV}^0 \cdot \text{CB}[7]} \sim 1,2$). Si le **CB[7]** a une plus grande affinité pour MPV^{2+} ($\log K_{\text{MPV}^{2+} \cdot \text{CB}[7]} = 6,1(3)$) que pour l'analogue MV^{2+} ($\log K_{\text{MV}^{2+} \cdot \text{CB}[7]} = 5,30(2)$), il possède une affinité similaire pour les deux radicaux-cations $\text{MPV}^{\bullet+}$ ($\log K_{\text{MPV}^{\bullet+} \cdot \text{CB}[7]} \sim 4,41$) et $\text{MV}^{\bullet+}$ ($\log K_{\text{MV}^{\bullet+} \cdot \text{CB}[7]} \sim 4,79$). La forme réduite neutre à 2 électrons MPV^0 est faiblement liée au **CB[7]**. Tout comme BMV^{2+} (voir le chapitre précédent), le **CB[7]** possède deux modes de liaison selon l'état rédox du viologène MPV^{2+} (MPV^{2+} versus $\text{MPV}^{\bullet+}$). Suite à la réduction à 1 électron de MPV^{2+} en $\text{MPV}^{\bullet+}$, le macrocycle **CB[7]** subit un court mouvement de translocation de l'unité phényle vers le radical-cation de l'unité bipyridinium (Figure 15). Ce processus est réversible après ré-oxydation du radical-cation et vice-versa.

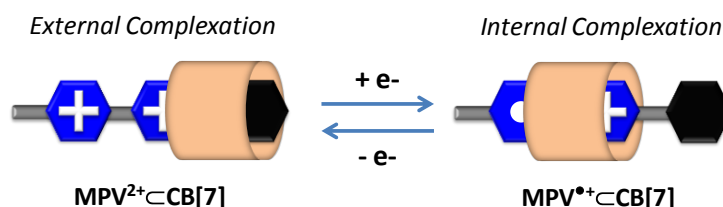


Figure 15. Translocation électrochimiquement contrôlée du macrocycle **CB[7]** au sein du complexe "host-guest" formé avec MPV^{2+} .

Une approche spectrophotométrique (absorption UV-Vis.-PIR) a permis de confirmer ces résultats. Le titrage de $\text{MPV}^{\bullet+}$ par le **CB[7]** dans l'eau à pH 7,0 montre un déplacement hypochrome important des transitions associées au radical-cation $\text{MPV}^{\bullet+}$ lors de la

formation du [2]pseudorotaxane $\text{MPV}^{\bullet+} \subset \text{CB}[7]$, confirmant ainsi l'inclusion du radical-cation $\text{BIPY}^{\bullet+}$ au sein de $\text{CB}[7]$. La constante d'association calculée par voie spectrophotométrique ($\log K_{\text{MPV}^{\bullet+} \subset \text{CB}[7]} = 4,60(7)$) est en excellent accord avec celle estimée à partir des données électrochimiques ($\log K_{\text{MPV}^{\bullet+} \subset \text{CB}[7]} \sim 4,41$).

En absence de $\text{CB}[7]$, le radical-cation $\text{DPV}^{\bullet+}$, généré chimiquement dans l'eau avec $\text{Na}_2\text{S}_2\text{O}_4$, a également une forte tendance à dimériser/oligomériser et former des particules insolubles. L'exposition de cette solution à l'air ré-oxyde $\text{DPV}^{\bullet+}$ en DPV^{2+} qui se re-solubilise du fait de son incapacité à s'auto-associer. Afin de surmonter ces limitations, la spectrophotométrie d'absorption en temps résolue (ms) a été utilisée et a permis d'enregistrer le spectre d'absorption du radical-cation $\text{DPV}^{\bullet+}$ en absence ou en présence de $\text{CB}[7]$ avant qu'il ne soit sujet à des réactions d'oligomérisation/précipitation. Le traitement statistique des données spectrales ainsi reconstituées a permis de proposer la formation d'un complexe de stœchiométrie 1:1 $\text{DPV}^{\bullet+} \subset \text{CB}[7]$ ($\log K_{\text{DPV}^{\bullet+} \subset \text{CB}[7]} = 4,9(1)$). La stabilité de $\text{DPV}^{\bullet+} \subset \text{CB}[7]$ est comparable à celles mesurées pour $\text{MPV}^{\bullet+} \subset \text{CB}[7]$ ($\log K_{\text{MPV}^{\bullet+} \subset \text{CB}[7]} = 4,60(7)$), $\text{BMV}^{\bullet+} \subset \text{CB}[7]$ ($\log K_{\text{BMV}^{\bullet+} \subset \text{CB}[7]} = 4,9(1)$) ou $\text{MV}^{\bullet+} \subset \text{CB}[7]$ ($\log K_{\text{MV}^{\bullet+} \subset \text{CB}[7]} \sim 4,79$), ce qui atteste d'un mode de reconnaissance comparable pour chacune de ces systèmes "host-guest". Comme observé désormais pour plusieurs systèmes viologène/ $\text{CB}[7]$, le [2]pseudorotaxane $\text{DPV}^{\bullet+} \subset \text{CB}[7]$ se caractérise par un déplacement hypochrome très important des bandes d'absorption associées au radical-cation, ce qui confirme une inclusion préférentielle du radical-cation $\text{BIPY}^{\bullet+}$ par le $\text{CB}[7]$. Lors de la réduction monoélectronique du 4,4'-bipyridinium du [2]pseudorotaxane $\text{DPV}^{2+} \subset (\text{CB}[7])_2$, l'un des deux macrocycles $\text{CB}[7]$ se dissocie tandis qu'une translocation concomitante de l'autre $\text{CB}[7]$ s'effectue (Figure 16).

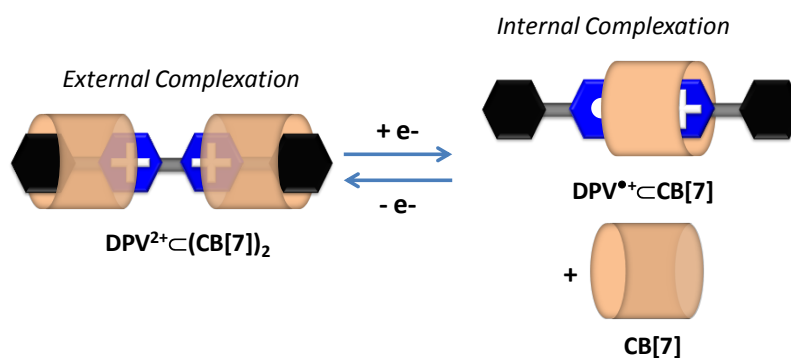


Figure 16. Dissociation et translocation électrochimiquement contrôlée des macrocycles $\text{CB}[7]$ dans le [3]pseudorotaxane formé avec DPV^{2+} pour conduire à un [2]pseudorotaxane avec $\text{DPV}^{\bullet+}$.

Pour le trimère TV^{6+} , la réduction monoélectronique de chacune des unités viologènes conduit au triradical-trication $\text{TV}^{3(\bullet+)}$ qui s'auto-associe spontanément en solution aqueuse pour conduire au dimère $(\text{TV}^{3(\bullet+)})_2$. Contrairement aux simples dérivés viologènes sous leur état radicalaire, la constante de pimérisation de $\text{TV}^{3(\bullet+)}$ est significativement augmentée ($K_{\text{Dim}} \gg 10^7 \text{ M}^{-1}$) du fait de la multiplication des centres de pimérisation (effet de multivalence). Le dimère $(\text{TV}^{3(\bullet+)})_2$ reste l'espèce prédominante, même en solution très diluée ($< 10^{-6} \text{ M}$). Ceci reste vrai même en présence du macrocycle $\text{CB}[7]$ qui permettrait, en présence de la forme oxydée TV^{6+} , de conduire à la formation du [4]pseudorotaxane $\text{TV}^{6+} \subset (\text{CB}[7])_3$. Tout comme

pour le système hexavalent HV^{12+} , ceci suppose la dissociation des macrocycles **CB[7]** (Figure 17) lors de la réduction monoélectronique de chacune des unités viologènes de l'espèce $\text{TV}^{6+} \subset (\text{CB}[7])_3$. Ce processus de dissociation \rightarrow pimérisation \rightarrow oligomérisation *versus* inclusion est réversible par ré-oxydation des monoradicaux de $(\text{TV}^{3(\bullet+)})_2$. Contrairement à HV^{12+} , ce sont des processus de pimérisation intermoléculaire qui constituent des processus compétitifs par rapport aux processus d'inclusion avec le **CB[7]**.

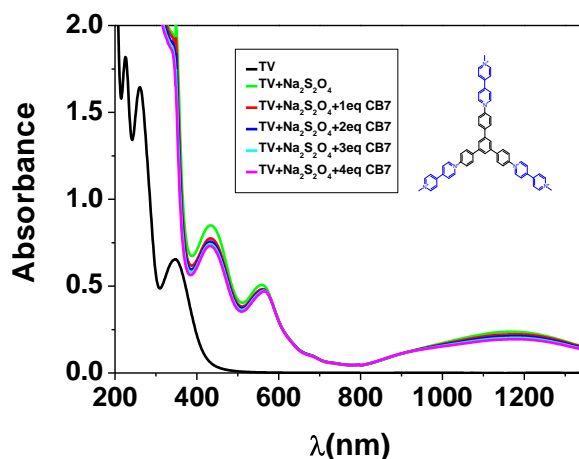


Figure 17. Spectres d'absorption UV-Vis-PIR de TV^{6+} ($[\text{TV}^{6+}]_0 = 5 \times 10^{-5}$ M, noir) et de son dérivé réduit $\text{TV}^{3(\bullet+)}$ (addition de $\text{Na}_2\text{S}_2\text{O}_4$ avant (vert) et après (cyan) addition de **CB[7]** ($[\text{CB}[7]]_0 = 3,3 \times 10^{-3}$ M). Solvant : tampon à pH 7,0 (0,1 M $\text{Na}_2\text{HPO}_4/\text{NaH}_2\text{PO}_4$) ; $l = 1$ cm ; $T = 25.0(1)$ °C. Dans chacune des solutions examinées, l'espèce $\text{TV}^{3(\bullet+)}$ a été générée à partir de TV^{6+} en utilisant $\text{Na}_2\text{S}_2\text{O}_4$ à $ca. 10^{-2}$ M sous conditions d'atmosphère contrôlée. Les spectres d'absorption ne sont pas corrigés des effets de dilution.

Un processus d'agrégation du dimère $(\text{TV}^{3(\bullet+)})_2$ a été mis en évidence qui peut s'expliquer par l'empilement aromatique et l'oligomérisation consécutive de plusieurs dimères. Si le **CB[7]** n'a aucun effet sur ce processus d'oligomérisation du fait de sa taille réduite, ce dernier peut être empêché par l'addition d'un macrocycle plus volumineux, le **CB[8]** (Tableau 1 et Figure 14). Le **CB[8]** est donc capable de stabiliser au sein de sa plus grande cavité deux monoradical-cation du viologène qui pimérisent pour conduire à un [5]pseudorotaxane $(\text{TV}^{3(\bullet+)})_2 \subset (\text{CB}[8])_3$, limitant ainsi le processus d'oligomérisation/précipitation.

Ce travail a permis de montrer que la multiplication de centres viologènes judicieusement organisés autour d'une plateforme robuste et inerte (ici le triphényl-benzène) peut constituer une stratégie alternative à la préparation de nouveaux matériaux électrochromes ou de molécules de fonction.

4. Etudes physico-chimique de calix[4]arène-viologènes

Le troisième volet de mes activités de recherches a concerné la synthèse et l'étude de nouveaux systèmes constitués de viologènes ancrés sur une plateforme calix[4]arène. Au début de ce projet, nous souhaitions utiliser les propriétés de ces derniers pour développer de nouveaux dérivés pour des applications en électrochromisme. Le travail de synthèse a été effectué sous la supervision du Docteur Zouhair Asfari (IPHC, UMR 7518, Strasbourg). Ce projet a été également mené en collaboration avec le Professeur Ali Trabolsi. Deux calixarènes di-substitués par des résidus 4,4-bipyridiniums et qui diffèrent par la longueur des espaceurs (3 ou 4 carbones) séparant les unités viologènes de la plateforme calix[4]arène ont été synthétisés (Figure 4). Leurs propriétés physico-chimiques et de reconnaissance avec le **CB[7]** ont été évaluées au moyen des mêmes méthodes analytiques décrites précédemment. Le **CB[7]** complexe fortement les unités viologènes et des processus de pimérisation intramoléculaire entre les deux viologènes réduits positionnés en face-à-face ont été mis en évidence. Ces processus sont aussi thermodynamiquement favorisés par rapport aux processus d'inclusion avec des **CB[7]** ou des **CB[8]**.

La dimérisation intermoléculaire de radicaux organiques a déjà été étudiée avec une large gamme de composés électroactifs. Toutefois, le principal obstacle de cette approche réside dans le fait, qu'en solution aqueuse, ces radicaux organiques s'auto-associent faiblement en π -dimères et nécessite donc de fortes concentrations. L'utilisation d'hôtes de nature macrocyclique possédant une cavité volumineuse tels que les cucurbiturils (*e.g.* **CB[8]**) ou les cyclodextrines (*e.g.* β -CD) favorisent les π -dimères intermoléculaires par encapsulation. Nous⁶⁹ ainsi que d'autres groupes avons démontré que la pré-organisation de deux ou plusieurs radicaux organiques grâce à des plates-formes moléculaires et des longueurs de chaîne appropriées (alkyle,^{53,70,71} porphyrine,² ferrocène,⁶⁰ phényl,^{53,72} C₆₀⁶¹ ou calixarène⁷³, Figure 18) pouvaient constituer une stratégie appropriée pour conduire à des pimères intramoléculaires stables utilisable en électrochromisme ou dans d'autres applications.

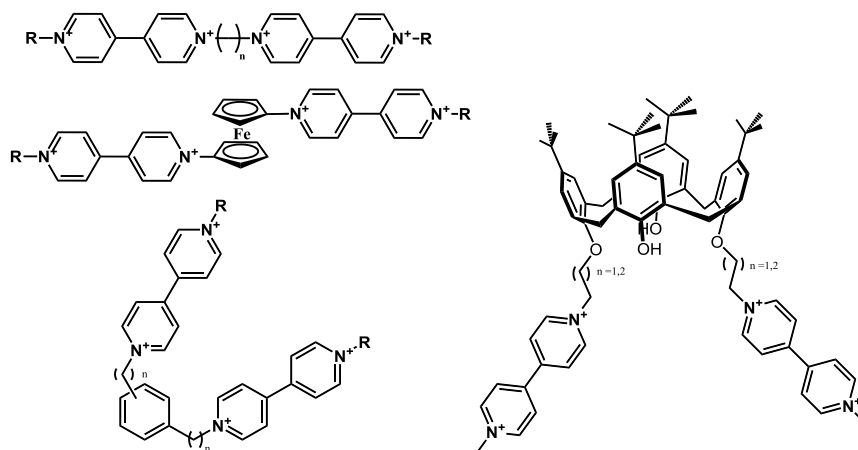


Figure 18. Structures chimiques de dérivés *bis*-viologènes qui permettent de favoriser la dimérisation intramoléculaire des radicaux-cations correspondants.

Ces plateformes d'ancrage d'unités viologènes doivent cependant remplir un cahier des charges exigeant (*e.g.* facilité de fonctionnalisation, inertie électrochimique, forte stabilité thermique et chimique, pimérisation efficace et rapide, reconnaissance rédox-dépendant, et potentiel pour nouveau matériau électrochrome). Les calix[4]arènes remplissent ce cahier des charges et ont donc été choisis. En outre, jusqu'à quatre positions peuvent être substituées (bord inférieur ou bord supérieur). Leurs propriétés conformationnelles (cône, 1,2- ou 1,3-alternée) du calix[4]arène peuvent également être contrôlées.

4.1. Complexes formés avec les CB[7] et CB[8]

Les calix[4]arène-viologènes **C23⁴⁺** et **C24⁴⁺** ont été étudiés à pH 7,0 en utilisant les mêmes méthodes analytiques décrites précédemment. Deux monomères (**MC3²⁺** et **MC4²⁺**), utilisés comme modèles des composés **C23⁴⁺** et **C24⁴⁺** ont d'abord été étudiés. Les titrages spectrophotométriques par le **CB[7]** et le **CB[8]** ont mis en évidence des complexes d'inclusion de stœchiométrie 1:1 (**MC3²⁺⊂CB[7]** et **MC4²⁺⊂CB[7]**, Tableau 3).

Tableau 3. Paramètres thermodynamiques et spectroscopiques de [n]pseudorotaxanes avec le **CB[7]**.

Viologène V	$\log K_{V\subset CB[7]}$	$\lambda (V) (nm)$ $\epsilon^m (10^4 M^{-1} cm^{-1})$	$\lambda (V\subset CB[7]) (nm)$ $\epsilon^d (10^4 M^{-1} cm^{-1})$
MV²⁺	5,30(2)	227(2,96) / 257(2,06)	226(3,13) / 281(sh)
MC3²⁺	4,51(6)	224(2,29) / 259(2,17)	223(2,49) / 255(1,51)
MC4²⁺	4,68(5)	224(2,17) / 260(2,29)	224(2,48) / 252(1,40)
C23⁴⁺	4,5(1)	224(7,42) / 262(3,20)	225(7,50) / 275(2,10)
C23⁴⁺	4,44(8)	220(7,16) / 263(2,99)	220(7,29) / 280(1,83)
Solvant: pH 7,0 avec 0,1 M Na ₂ H ₂ PO ₄ /NaH ₂ PO ₄ ; l = 1 cm; T = 25,0(1)° C.			

Aucune décomplexation ou dimérisation des radicaux-cations n'a été observée dans des expériences qui combinent le **CB[7]** ou le **CB[8]** et les formes réduites à 1 électron (**MC3^{•+}** and **MC4^{•+}**). Aucune translocation du macrocyclique hôte n'a, en outre, été observée entre les deux sites de liaison possibles (*i.e.* unités **BIPY²⁺** et alcoxy-phényl). Des résultats inattendus ont, par contre, été obtenus à fortes concentrations par ¹H RMN (Figure 19). Des [3]pseudorotaxanes tels que **MC3²⁺⊂(CB[7])₂** et **MC4²⁺⊂(CB[7])₂** ont été caractérisées. Avec le **CB[8]**, les mêmes propriétés ont été identifiées pour les modèles **MC3²⁺** et **MC4²⁺**.

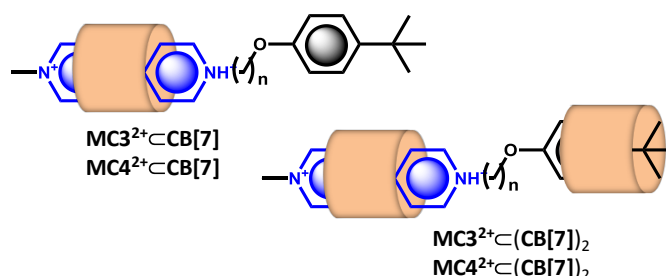


Figure 19. Représentation schématique des [2]pseudorotaxanes **MC3²⁺⊂CB[7]** et **MC4²⁺⊂CB[7]** (le **CB[7]** interagit principalement le groupement bipyridinium) et des [3]pseudorotaxanes **MC3²⁺⊂(CB[7])₂** et **MC4²⁺⊂(CB[7])₂** (la cavité hydrophobe du second **CB[7]** interagit avec le groupement phényl terminal).

Avec **C23⁴⁺** et **C24⁴⁺**, nous avons caractérisé des [3]pseudorotaxanes avec le **CB[7]** ou le **CB[8]**. Les récepteurs curcubit[n]urils (n = 7 ou 8) résident essentiellement au cœur des dications **BIPY²⁺** probablement du fait d'interactions stériques avec la plateforme calix[4]arène. Ce mode de complexation a été confirmé par des mesures ¹H RMN. Les valeurs des stabilités apparentes ($\log K^*_{\text{CB234}^+ \subset (\text{CB}[7])_2} = 4,5(1)$ and $\log K^*_{\text{CB244}^+ \subset (\text{CB}[7])_2} = 4,44(8)$) sont proches de celles déterminées pour les modèles **MC3²⁺** and **MC4²⁺** (Tableau 3). Une déstabilisation systématique de près d'un ordre de grandeur est observée par rapport au modèle **MV²⁺** ($\log K_{\text{MV}^{2+} \subset \text{CB}[7]} = 5,30(2)$) du fait à la présence de l'ancre calix[4]arène.

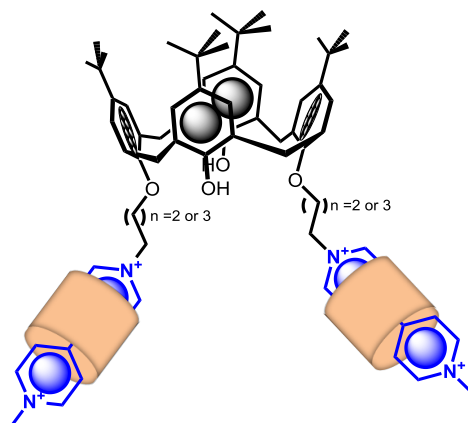


Figure 20. Représentation schématique des [3]pseudorotaxanes **C23⁴⁺⊂(CB[7])₂** et **C24⁴⁺⊂(CB[7])₂** (la cavité hydrophobe du **CB[7]** interagit avec les groupements bipyrindiniums).

4.2. Dimérisation intramoléculaire

Des spectres d'absorption UV-Vis.-PIR (220-1300 nm, Figure 21) de concentrations croissantes de solutions de **MC3^{•+}** ou **MC4^{•+}** (préparées par addition de $\text{Na}_2\text{S}_2\text{O}_4$ sous atmosphère contrôlée) à pH 7,0 ont été enregistrés. Lorsque la concentration augmente, la formation graduelle d'une large bande d'absorption intense dans le domaine PIR est la signature spectrophotométrique d'un processus de dimérisation s'effectuant entre deux radicaux-cations générés chimiquement. Le traitement des données a permis d'évaluer les constantes de dimérisation de **MC3^{•+}** ou de **MC4^{•+}** (**MC4^{•+}** et **MC3^{•+}** : $\log K_{\text{Dim}} = 3,4(2)$). Ces valeurs sont comparables à celles mesurées pour les radicaux-cations du méthyl-benzylviologène **BMV^{•+}** ($\log K_{\text{Dim}} = 3,46(5)$) ou d'autres viologènes diversement décorés par des chaînes alkyles hydrophobes⁵¹. Elles sont par contre plus élevées que celle décrite pour le diméthylviologène **MV^{•+}** ($\log K_{\text{Dim}} = 2,5-2,9$). Ceci démontre que l'accroissement du caractère hydrophobe à proximité de l'unité **BIPY^{•+}** par des substituants aryl et/ou alkyl favorise la pimérisation intermoléculaire en solution aqueuse. D'autre part, nous avons montré que le plus grand espaceur de **MC4^{•+}** (n = 4) ne modifie pas ses propriétés de pimérisation par rapport à l'analogue **MC3^{•+}** (n = 3) puisque des valeurs similaires de K_{Dim} ont été mesurées.

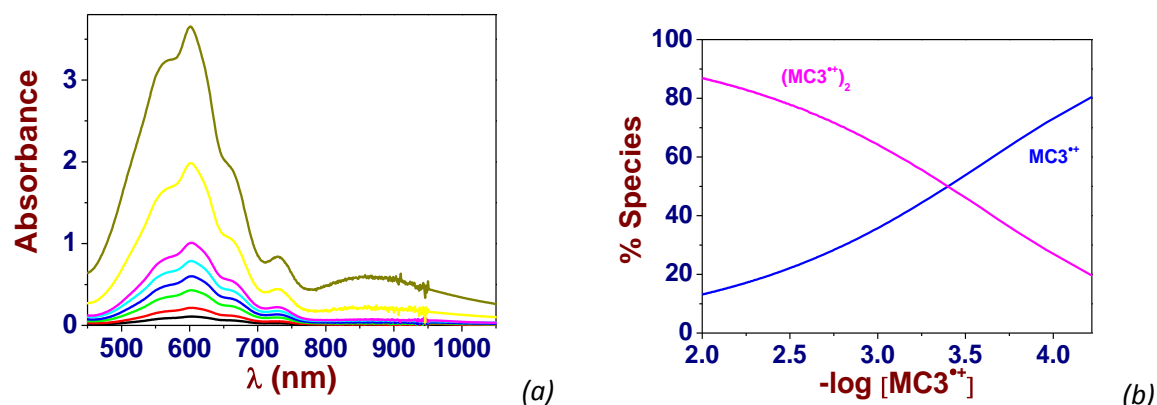


Figure 21. (a) Titrage spectrophotométrique d'absorption UV-Vis.-PIR de MC3^{2+} en solution aqueuse. (b) diagrammes de distribution du monomère *versus* dimère en fonction de la concentration de MC3^{2+} . Solvant : pH 7,0 (0,1 M $\text{Na}_2\text{HPO}_4/\text{NaH}_2\text{PO}_4$). $10^{-5} \text{ M} \leq [\text{MC3}^{2+}]_0 \leq 10^{-4} \text{ M}$; $l = 1 \text{ cm}$; $2 \times 10^{-4} \text{ M} \leq [\text{MC3}^{2+}]_0 \leq 4 \times 10^{-4} \text{ M}$; $l = 2 \text{ mm}$; $T = 25,0(1) \text{ }^\circ\text{C}$. Dans chacune des solutions examinées, l'espèce MC3^{2+} a été générée à partir de MC3^{2+} en utilisant $\text{Na}_2\text{S}_2\text{O}_4$ à $ca. 10^{-2} \text{ M}$ sous conditions d'atmosphère inerte. Les spectres d'absorption ne sont pas corrigés de la dilution.

Lors de la caractérisation des radicaux-cations $\text{C23}^{2(\bullet+)}$ et $\text{C24}^{2(\bullet+)}$, des bandes d'absorption intenses ont été également observées à $\sim 530 \text{ nm}$ (Figure 22) et témoignent de la réduction monoélectronique de chacune des unités viologènes. Une bande d'absorption intense et centrée à plus faible énergie (1072 nm pour $\text{C23}^{2(\bullet+)}$ et 925 nm pour $\text{C24}^{2(\bullet+)}$) sont attribuables à des transferts de charge intramolécule entre les deux viologènes réduits et témoignent d'une pimérisation intramolécule des deux bras viologènes positionnés en face-à-face. En d'autres termes, la réduction à deux électrons conduit aux espèces $\text{C23}^{2(\bullet+)}$ et $\text{C24}^{2(\bullet+)}$ qui dimérisent spontanément de manière intramolécule.

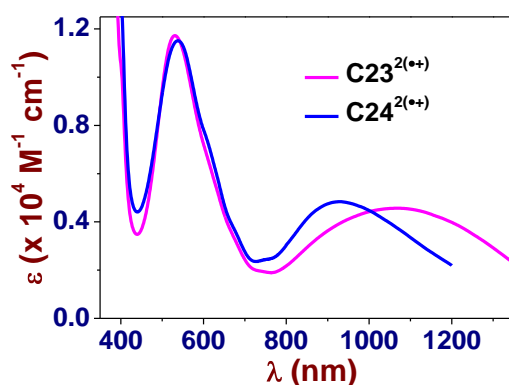


Figure 22. Spectres d'absorption électronique UV-Vis.-PIR de $\text{C23}^{2(\bullet+)}$ et $\text{C24}^{2(\bullet+)}$ dans l'eau. Solvant : pH 7,0 avec 0,1 M $\text{Na}_2\text{HPO}_4/\text{NaH}_2\text{PO}_4$. $T = 25,0(1) \text{ }^\circ\text{C}$.

4.3. Réduction des [n]pseudorotaxanes formés avec le CB[7]

Des expériences électrochimiques (CV et SWV, Figure 23) ont été menées sur les systèmes modèles MC3^{2+} et MC4^{2+} en absence et en présence de **CB[7]** dans l'eau à pH 7,0. L'ajout de **CB[7]** modifie sensiblement les propriétés électrochimiques de deux dérivés viologènes. En

présence de trois équivalents de **CB[7]** (les [3]pseudorotaxanes $\text{MC3}^{2+} \subset (\text{CB}[7])_2$ et $\text{MC4}^{2+} \subset (\text{CB}[7])_2$ coexistent avec les [2]pseudorotaxanes $\text{MC3}^{2+} \subset \text{CB}[7]$ et $\text{MC4}^{2+} \subset \text{CB}[7]$), les deux vagues rédox subissent des déplacements cathodiques et conservent leurs caractères réversibles. En considérant $\log K_{\text{MC4}^{2+} \subset \text{CB}[7]} = 4,5$, des valeurs $\log K_{\text{MC4}^{0+} \subset \text{CB}[7]} \sim 4,2$ and $\log K_{\text{MC4}^{0} \subset \text{CB}[7]} \sim 3,8$ sont calculées pour les complexes d'inclusion du **CB[7]** avec les différents états d'oxydation de MC4^{2+} . Ceci rend donc compte des affinités relatives de **CB[7]** pour les différents états rédox des systèmes modèles. En considérant $\log K_{\text{MC3}^{2+} \subset \text{CB}[7]} = 4,68$ pour $\text{MC3}^{2+} \subset \text{CB}[7]$ déterminée par absorption, les stabilités $\log K_{\text{MC3}^{0+} \subset \text{CB}[7]} \sim 4,0-4,2$ and $\log K_{\text{MC3}^{0} \subset \text{CB}[7]} \sim 3,5-3,9$ peuvent être estimées pour les différents états d'oxydation de MC4^{2+} en présence de **CB[7]**.^{26,74} Les valeurs calculées pour $\text{MC3}^{0+} \subset \text{CB}[7]$ ($\log K_{\text{MC3}^{0+} \subset \text{CB}[7]} \sim 4,0-4,2$) and $\text{MC4}^{0+} \subset \text{CB}[7]$ ($\log K_{\text{MC4}^{0+} \subset \text{CB}[7]} \sim 4,2$) par une approche électrochimique sont en bon accord avec les valeurs déterminées grâce à des titrages spectrophotométrique d'absorption de MC3^{0+} ou MC4^{0+} par le **CB[7]** ($\log K_{\text{MC3}^{0+} \subset \text{CB}[7]} = 3,8(4)$ and $\log K_{\text{MC4}^{0+} \subset \text{CB}[7]} = 4,5(5)$). Ces titrages spectrophotométriques ont, en outre, mis en évidence un déplacement hypochrome important des absorptions relatives aux monoradicaux-monocations, signe d'une forte interaction entre les unités BIPY^{0+} et le **CB[7]**. Contrairement à BMV^{2+} , MPV^{2+} or DPV^{2+} (une translocation du **CB[7]** avait été mise en évidence lors de la réduction électrochimique de l'unité électroactive), le macrocycle **CB[7]** reste localisé sur l'unité BIPY^{2+} quel que soit son état d'oxydation. Ceci peut s'expliquer soit par un encombrement stérique plus important de la chaîne aryle terminale (espèces $\text{MC3}^{2+} \subset \text{CB}[7]$ et $\text{MC4}^{2+} \subset \text{CB}[7]$) ou alors par la présence d'un second macrocycle **CB[7]** (espèce $\text{MC3}^{2+} \subset (\text{CB}[7])_2$ et $\text{MC4}^{2+} \subset (\text{CB}[7])_2$).

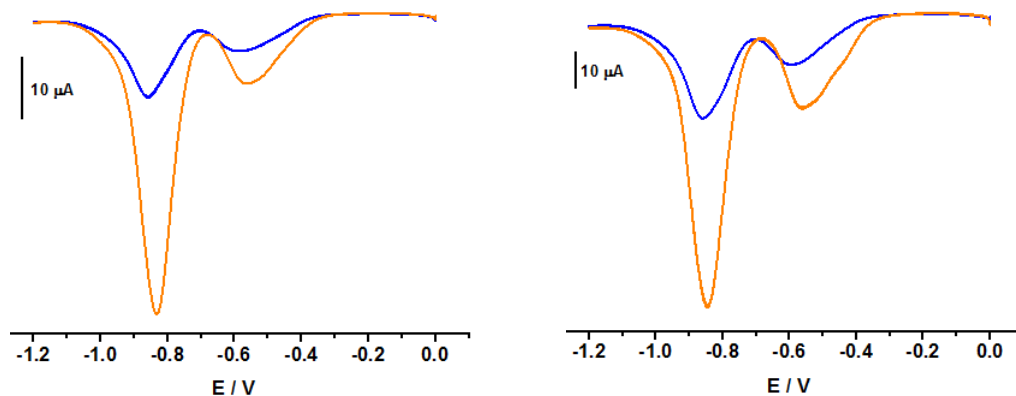


Figure 23. Voltampérogrammes à ondes carrées de MC3^{2+} , $[\text{MC3}^{2+}] = 0,05$ mM (gauche) et de MC4^{2+} , $[\text{MC4}^{2+}] = 0,06$ mM (droite) en absence (orange) et en présence de **CB[7]** (bleu, 3 équivalents de **CB[7]**). Tous les voltampérogrammes ont été mesurés sur des solutions aqueuses dégazées et tamponnées à pH 7,0 (0,1 M $\text{Na}_2\text{HPO}_4/\text{NaH}_2\text{PO}_4$) à 25°C (*E* versus Ag/AgCl).

Des études électrochimiques (Figure 24) ont été menées avec les calix[4]arène-viologènes C23^{4+} and C24^{4+} pour évaluer l'effet du macrocycle **CB[7]** sur les processus de pimérisation intramoléculaire des deux radicaux-cations BIPY^{0+} positionnés en face-à-face. Pour les [3]pseudorotaxanes $\text{C23}^{4+} \subset (\text{CB}[7])_2$ et $\text{C24}^{4+} \subset (\text{CB}[7])_2$, aucune variation notable n'a été observée pour la seconde vague de réduction par rapport aux mêmes données enregistrées pour C23^{4+} et C24^{4+} , ce qui aurait dû en fait correspondre aux réactions suivantes : $\text{C23}^{2(\bullet+)} \subset (\text{CB}[7])_2 \rightarrow \text{C23}^0 \subset (\text{CB}[7])_2$ et $\text{C24}^{2(\bullet+)} \subset (\text{CB}[7])_2 \rightarrow \text{C24}^0 \subset (\text{CB}[7])_2$. Cela indique qu'après

le premier processus de réduction, les calix[4]arène-viologènes sont non complexés au **CB[7]** ($\text{C23}^{2(\bullet+)}$ et $\text{C24}^{2(\bullet+)}$). En d'autres termes, la réduction monoélectronique de chacune des unités viologènes de $\text{C23}^{4+} \subset (\text{CB}[7])_2$ et $\text{C24}^{4+} \subset (\text{CB}[7])_2$ induit une dissociation spontanée des macrocycles **CB[7]** dont la force motrice est la forte dimérisation intramoléculaire des unités **BIPY^{•+}**. Tout comme pour l'hexaviologène **HV¹²⁺** basé sur une ancre phosphazène, les [3]pseudorotaxanes $\text{CB23}^{4+} \subset (\text{CB}[7])_2$ et $\text{CB24}^{4+} \subset (\text{CB}[7])_2$ se dissocient donc spontanément à la suite de la réduction monoélectronique de chacun des bras bipyridiniums qui résulte d'une forte pimérisation intramoléculaire des radicaux-cations positionnés en face-à-face.

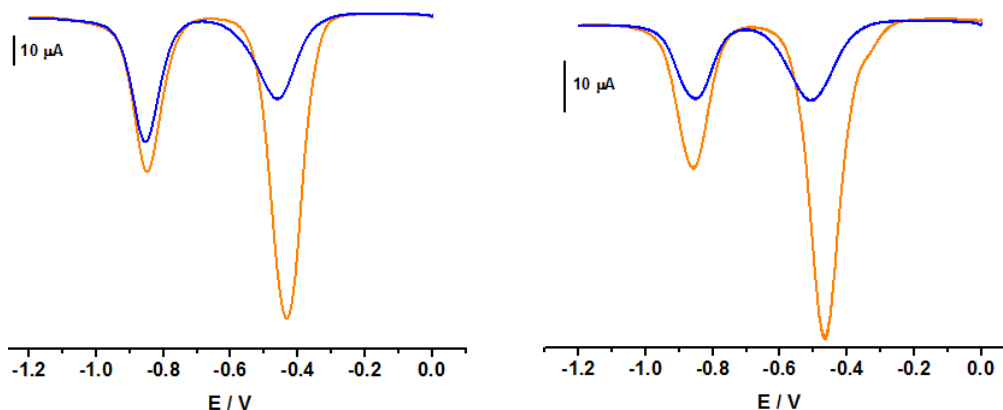


Figure 24. Voltampérogrammes à ondes carrées de C23^{4+} , $[\text{C23}^{4+}] = 0,05 \text{ mM}$ (gauche) et de C24^{4+} , $[\text{C24}^{4+}] = 0,05 \text{ mM}$ (droite) en absence (orange) et en présence de **CB[7]** (bleu, 3 et 4 équivalents de **CB[7]** ont été respectivement ajoutés). Tous les voltampérogrammes ont été mesurés sur des solutions aqueuses dégazées et tamponnées à pH 7,0 (0,1 M $\text{Na}_2\text{HPO}_4/\text{NaH}_2\text{PO}_4$) à 25°C (E versus Ag/AgCl).

De même que pour les calix[4]arène-viologènes C23^{4+} et C24^{4+} en présence de **CB[7]**, la réduction chimique des unités électroactifs **BIPY²⁺** conduit également à une dissociation des macrocycliques **CB[8]** et ce, malgré une taille de la cavité plus grande. Ceci suggère donc de fortes contraintes stériques avec la plate-forme calix[4]arène et/ou une flexibilité inappropriée des espaceurs, même s'ils sont paraissent suffisamment longs et flexibles. Les modèles MC3^{2+} et MC4^{2+} conduisent, par contre, aux [3]pseudorotaxanes attendus ($\text{MC3}^{\bullet+}$)₂ \subset **CB[8]** and ($\text{MC4}^{\bullet+}$)₂ \subset **CB[8]** soulignant le rôle critique de la plate-forme d'ancrage plutôt que la longueur des espaceurs. La formation de [3]pseudorotaxanes (($\text{MC3}^{\bullet+}$)₂ \subset **CB[8]**) and ($\text{MC4}^{\bullet+}$)₂ \subset **CB[8]**) est en accord avec des données de la littérature^{35,66} pour le diméthylviologène MV^{2+} qui ont montré que la stabilité du dimère ($\text{MV}^{\bullet+}$)₂ dans l'eau était significativement accrue en présence de **CB[8]** suite à la formation d'un [3]pseudorotaxane (($\text{MV}^{\bullet+}$)₂ \subset **CB[8]**).

5. Reconnaissance de substrats azo-imidazoles par une métalloporphyrine à anse phénanthroline

Ce dernier projet a été mené en collaboration avec les équipes du Docteur Jean Weiss (UMR 7177, Strasbourg) et du Professeur Ali Trabolsi et a concerné la synthèse et l'étude en solution de nouveaux substrats imidazoles et l'élucidation de leurs propriétés de reconnaissance (aspects thermodynamiques et cinétiques) par des récepteurs porphyriniques à anse phénanthroline. Mon travail a été essentiellement centré sur l'étude physico-chimique en solution (aspects spectroscopiques, thermodynamiques et cinétiques) de complexes pentacoordinés formés à partir d'un récepteur porphyrinique avec des substrats azo-aryl-imidazoles. Une série homogène d'azo-aryl-imidazoles, dont l'encombrement en position 2 de l'imidazole a été varié, a été considéré (Figure 25). L'objectif de ce projet sera d'étudier la photo-éjection de ces substrats imidazoles complexés à une porphyrine de Zn(II) grâce à l'isomérisation photo-induite (*trans-cis*) des unités azobenzènes (Figure 26). La relaxation thermique du système doit permettre de rétablir en solution les complexes pentacoordinés thermodynamiquement les plus stables. Ces systèmes pourraient permettre le développement de nouveaux matériaux intelligents.

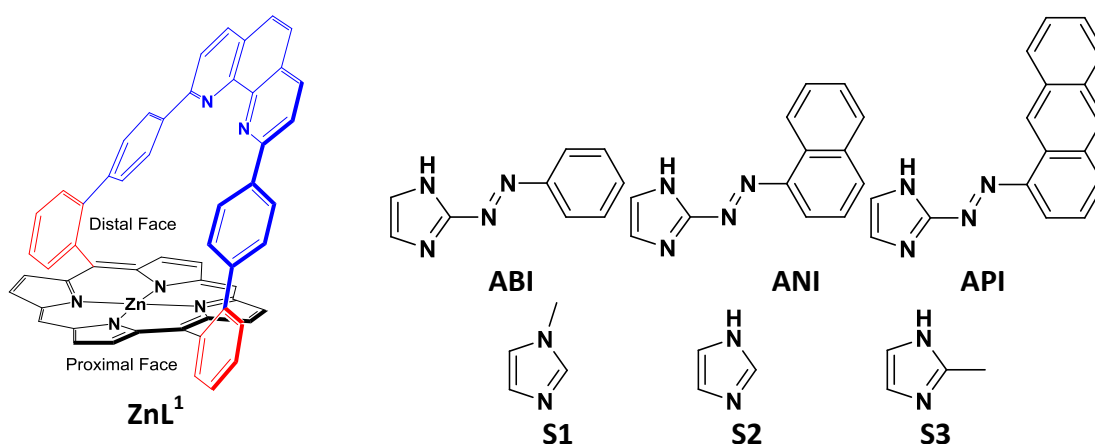


Figure 25. Structures chimiques d'un récepteur à anse phénanthroline (ZnL^1) et des substrats imidazole (S1-S3) et azo-aryl-imidazole (ABI, ANI et API) examinés au cours de ce travail.

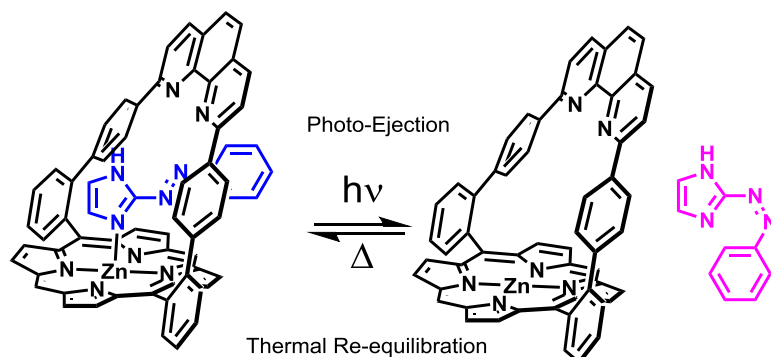


Figure 26. Représentation schématique du principe de photo-éjection d'un azo-aryl-imidazole de son complexe pentacoordiné avec ZnL^1 .

La porphyrine à anse phénanthroline ZnL^1 présente une topographie adaptée pour lier fortement et sélectivement divers substrats imidazoles non substitués en position N_1 . La discrimination distale de la coordination axiale Zn-N est favorisée par la mise en place de liaisons hydrogène bifurquées du groupement N_1H de l'imidazole avec les azotes phénanthroline du récepteur ZnL^1 . Cette propriété a pour conséquence de stabiliser les complexes pentacoordinés correspondants et de conduire à des systèmes "host-guest" multi-centres (Figure 29). La flexibilité importante du récepteur ZnL^1 (c.-à-d. la distorsion du système tétrapyrrolique conjugué et la forte inclinaison de l'unité diphenylphénanthroline) constitue des caractéristiques structurales qui minimisent les interactions stériques et ajuste le substrat au sein de la cavité du récepteur au cours du processus de reconnaissance. Deux structures RX ont été obtenus avec le récepteur porphyrinique ZnL^1 et les substrats **ABI** et **ANI** (Figure 27) et témoignent de ces ajustements structuraux.

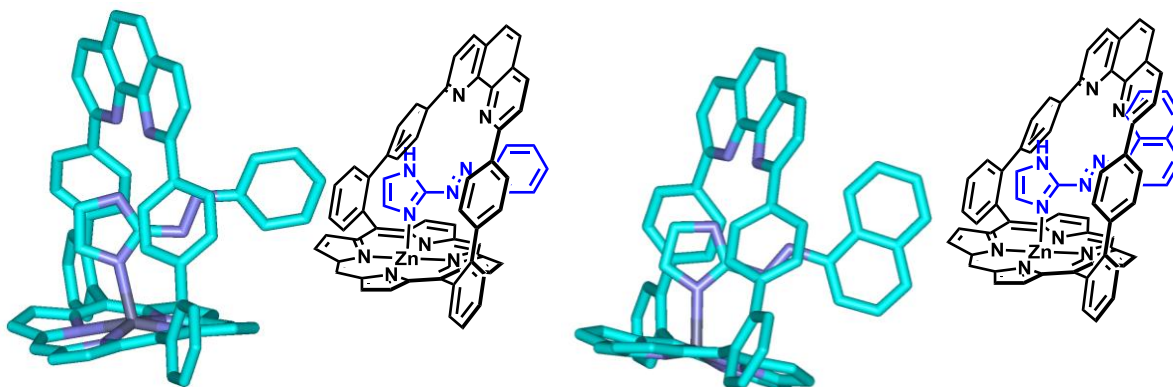


Figure 27. Représentation schématique des structures RX des complexes ZnL^1 .ABI et ZnL^1 .ANI.

J'ai démontré au cours de cette étude que, malgré la substitution en position 2 par des chromophores encombrants (isomérisation conformationnelle *trans-cis* photo-induite), les substrats azo-aryl-imidazoles **ABI** et **ANI** pouvaient former des espèces pentacoordinées stables avec ZnL^1 (reconnaissance distale). Cependant, une déstabilisation est observée lorsque les données sont comparées à celles obtenues avec des substrats et une porphyrine de référence ($ZnTPP$, 1-méthyl-1*H*-imidazole **S1**, 1*H*-imidazole **S2** ou le 2-méthyl-1*H*-imidazole **S3**, Figure 28). Ceci résulte probablement d'interactions stériques de l'azo-chromophore avec l'anse phénanthroline conduisant à des déformations du cycle porphyrinique (Figure 27). La substitution du substrat azo-imidazole par un groupe phénanthryle (**API**) va jusqu'à empêcher la formation du complexe pentacoordiné avec ZnL^1 (Figure 28).

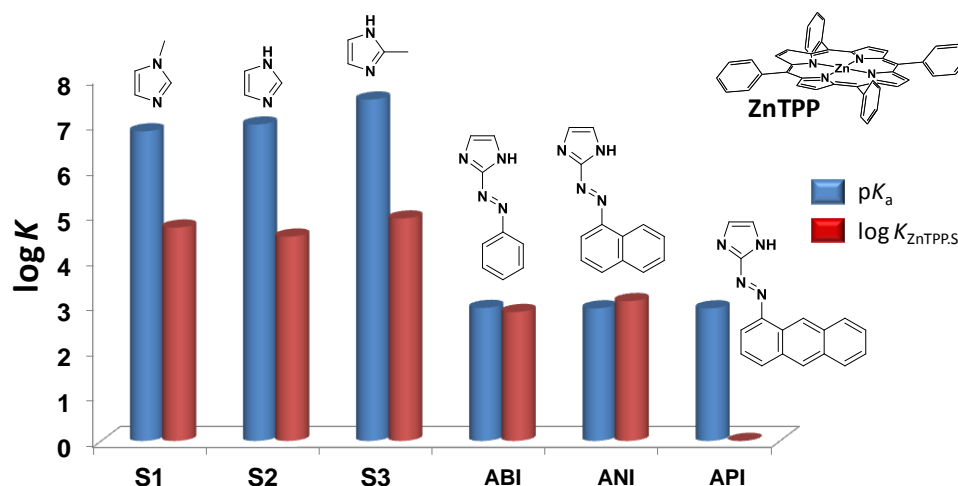


Figure 28. Représentation schématique des valeurs de $\log K_{\text{ZnTPP.S}}$ en fonction des valeurs de $\text{p}K_{\text{a}}$ (estimée à l'aide de ChemAxon $\text{p}K_{\text{a}}$ calculator) qui illustre les effets stériques induits par l'encombrement des azo-chromophores.

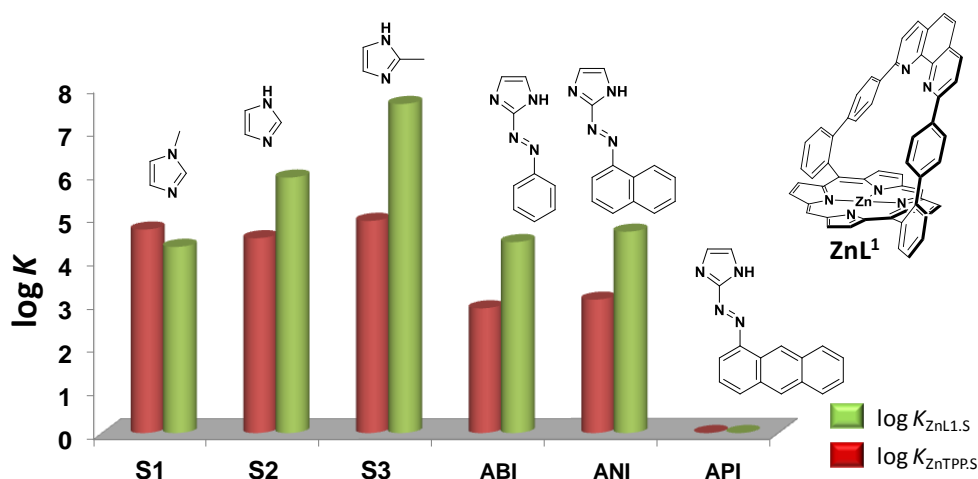


Figure 29. Représentation schématique des valeurs de $\log K_{\text{ZnTPP.S}}$ et $\log K_{\text{ZnL1.S}}$ qui montre l'importance des liaisons hydrogène avec l'anse phénanthroline sur la stabilisation des complexes pentacoordinés indépendamment du volume d'encombrement de l'azo-chromophore.

Le mécanisme de formation a été élucidé grâce à l'utilisation d'un spectrophotomètre à flux stoppé. La formation du complexe se déroule en une étape limitante concertée (Tableau 4). Des effets importants sont observés sur la constante de vitesse de formation bimoléculaire k_f lorsque l'encombrement de la position 2 de l'imidazole augmente (**ABI** et 2-phényl-1*H*-imidazole). Des interactions stériques entre l'azo-chromophore et l'anse phénanthroline de ZnL^1 expliquent également l'augmentation de la labilité des espèces ZnL^1 .**ABI** par rapport à des systèmes modèles (*e.g.* ZnL^1 .**S3**). La mesure des paramètres d'activation et énergétiques ΔG^\ddagger , en outre, permis une meilleure compréhension du mécanisme de la formation. La formation du complexe pentacoordiné ZnL^1 .**ABI** suit un mécanisme associatif enthalpiquement contrôlée. Un gain enthalpique de $\sim 20 \text{ kJ mol}^{-1}$ peut être observée lorsque l'on compare $\text{ZnTPP}.$ **ABI** à ZnL^1 .**ABI** du fait des interactions

stabilisantes (*i.e.* liaisons hydrogène) entre le substrat imidazole et l'anse phénanthroline.

Tableau 4. Constantes de vitesse déterminées au moyen d'approches cinétiques pour le mécanisme de formation de complexes pentacoordinés avec ZnL¹.^a

	S2	S3	2-Phenyl- 1H-Imidazole ^{75,76}	1H-Benz- imidazole ^{75,76}	ABI
k_f (M ⁻¹ s ⁻¹) ^d	Trop rapide	$2,2(9) \times 10^7$	$2,0(7) \times 10^4$	$6,4(8) \times 10^7$	$2,35(4) \times 10^5$
k_d (s ⁻¹) ^d	na	16(8)	1,4(2)	162(51)	27(3)
$\log(k_f/k_d)$	na	6,2	4,2	5,6	9,9
$\log K_{ZnL1.S}$	5,9(1)	7,6(4)	3,92(7)	5,8(4)	4,4(1)
^a Solvant : 1,2-dichloroethane; T = 25.0(2) °C. $k_{obs} = k_f[S^n]_{tot} + k_d$. na = non applicable					

6. Conclusion

Ce travail de thèse a été centré sur la synthèse et l'étude physico-chimique de systèmes "host guest" en utilisant des "multimères" basés sur des unités viologènes et des récepteurs macrocycliques de type cucurbit[n]uril ($n = 7$ et 8). Une attention toute particulière a été portée sur la compréhension de leurs propriétés rédox qui leur confèrent un comportement particulier et un potentiel pour la conception de nouveaux outils moléculaires rédox-dépendant à l'échelle nanométrique.

Les nano-machines développés dans ce travail comprennent entre autres : un [3]pseudorotaxane, un [4]pseudorotaxane et un [7]pseudorotaxane, chacun d'entre eux étant constitué d'un multimère basé sur des unités viologènes et les cucurbit[7]uril (**CB[7]**) ou cucurbit[8]uril (**CB[8]**). En solution aqueuse, ces systèmes peuvent être interconvertis électrochimiquement entre un état complexé, définis par les pseudorotaxanes eux-mêmes, et un état non complexé comprenant leurs composants de départ. La force motrice du processus de dissociation est une forte dimérisation intra- ou intermoléculaire des radical-cations issus des unités viologènes qui les composent. Les propriétés de reconnaissance et de dissociation ont été analysées au moyen d'un ensemble d'outils analytiques complémentaires tels que la spectrophotométrie d'absorption UV-visible-PIR, la ^1H RMN, l'électrochimie (CV et SWV), l'ESI-MS et la RPE. Ces données ont été complétées par des calculs DFT.

Dans la première partie, nous avons étudié les propriétés rédox et de reconnaissance d'un hexaviologène de nature dendritique (**HV¹²⁺**) qui utilise les propriétés d'un cœur de type phosphazène. Les ligands (**BV⁴⁺**, **MV²⁺** and **BMV²⁺**) ont été étudiés afin d'évaluer le rôle du cyclotriphosphazène sur les propriétés de reconnaissance et de dimérisation. J'ai d'abord démontré que **MV²⁺** et **MV^{•+}** se liaient au **CB[7]** selon un même mode de reconnaissance, c.-à-d. avec l'unité viologène interagissant avec la cavité hydrophobe du récepteur macrocyclique. Ainsi, lorsque le pseudorotaxane **MV²⁺⊂CB[7]** est réduit en **MV^{•+}⊂CB[7]**, aucun changement conformationnel ne se produit. En revanche, **BMV²⁺** se lie au **CB[7]** avec son substituant benzylique au sein de la cavité du macrocycle **CB[7]**. Lorsque le pseudorotaxane **BMV²⁺⊂CB[7]** est réduit en **BMV^{•+}⊂CB[7]**, le macrocycle **CB[7]** navigue (translocation intramoléculaire) de l'unité benzylique vers le radical-cation du viologène. En dépit de la similitude structurale entre **BMV²⁺** et les bras des multimères **BV⁴⁺** et **HV¹²⁺**, ceux-ci se lient au **CB[7]** de la même manière que **MV²⁺** (site de reconnaissance **BIPY²⁺**). Les effets stériques avec le noyau cyclotriphosphazène empêchent les **CB[7]** de se lier aux espaceurs benzyliques pourtant plus hydrophobes. Lorsque chacune des unités bipyridiniums de **BV⁴⁺⊂CB[7]** et **HV¹²⁺⊂CB[7]** subit une réduction monoélectronique, les macrocycles **CB[7]** se dissocient spontanément pour des raisons thermodynamiques pour donner naissance, respectivement, aux espèces pimérisées **BV_D^{2(•+)}** and **HV_D^{6(•+)}**. Ces données confortent l'idée que la dimérisation du radical-cation du viologène (une interaction dite faible) peut être sensiblement améliorée dans l'eau grâce à une approche intramoléculaire et exploitée pour la conception de nouveaux interrupteurs moléculaires. Cette approche a été peu exploitée jusqu'à ici.

Grâce à une stratégie alternative qui utilise des interactions intermoléculaires avec des systèmes multivalents, nous avons démontré que la forte dimérisation de radicaux-cations pouvait aussi concurrencer, pour des raisons thermodynamiques, l'inclusion de macrocycles **CB[7]** et induire une dissociation rapide et efficace des systèmes "host-guest". La ré-oxydation des radicaux-cations en bipyridiniums prévient le processus de dimérisation et régénère de manière réversible les complexes "host-guest" de départ. Un système trimérique de nature circulaire (**TV**⁶⁺) composé d'un noyau benzénique, qui a été étendu sur ses positions 1, 3 et 5 par des sous-unités méthyl-phényl-viologènes (**MPV**²⁺), a été considéré. Les modèles (**MVTP**²⁺, **MPV**²⁺ et **DPV**²⁺) ont été étudiés en combinaison avec les macrocycles **CB[7]** et **CB[8]** en utilisant les mêmes méthodes analytiques.

L'étude de la reconnaissance de **TV**⁶⁺ par le **CB[7]** (ou **CB[8]**) a mis en évidence la formation d'un [4]pseudorotaxane **TV**⁶⁺⊂**CB[n]**₃ (n = 7, 8). La réduction monoélectronique de chacune des unités viologènes conduit à un triradical-trication **TV**^{3(•+)} qui s'auto-associe spontanément en solution pour conduire au dimère (**TV**^{3(•+)})₂. Contrairement aux simples dérivés viologènes sous leur état réduits à 1 électron, la pimérisation de **TV**^{3(•+)} est fortement augmenté ($K_{\text{Dim}} \gg 10^7 \text{ M}^{-1}$) grâce à la multiplication des centres de pimérisation (multivalence). Un processus d'agrégation a été, en outre, observé et résulte d'un processus d'empilement aromatique de dimères (**TV**^{3(•+)})₂ qui peut être déjoué par l'ajout de **CB[8]** mais pas de **CB[7]**. Le **CB[8]** dispose d'une cavité de reconnaissance plus grande qui permet d'accueillir et de renforcer la pimérisation de deux monoradicaux terminaux issus de deux **TV**^{3(•+)} pour conduire au [5]pseudorotaxane ((**TV**^{3(•+)})₂⊂**CB[8]**)₃. Cette espèce empêche l'oligomérisation du dimère (**TV**^{3(•+)})₂. Cette stratégie novatrice démontre que des interactions intermoléculaires peuvent aussi être utilisées pour augmenter sensiblement en solution la stabilité de dimères de radicaux-cations de viologène grâce à un design particulier (plusieurs centres de reconnaissance répartis à la périphérie d'un benzène central) et à une approche multi-centre. C'est probablement une stratégie à considérer pour la préparation de nouveaux matériaux électrochromes.

Motivés par la recherche d'autres plateformes d'ancrage pour pré-organiser et distribuer efficacement plusieurs unités viologènes, nous avons considéré les calix[4]arènes. Le calix[4]arène possède de nombreuses propriétés que nous souhaitons mettre à profit. Deux calix[4]arène-*bis*viologènes, **C23**⁴⁺ and **C24**⁴⁺, ont été synthétisés. Leurs études avec le **CB[7]** et le **CB[8]** ont démontré leurs aptitudes à accueillir deux macrocycles liés aux dications **BIPY**²⁺ terminaux. Suite à une réduction monoélectronique des bipyridiniums terminaux, les [3]pseudorotaxanes avec **C23**⁴⁺ and **C24**⁴⁺ se dissocient spontanément du fait d'une forte dimérisation intramoléculaire des deux radicaux-cations positionnés en face-à-face. Aucune décomplexation du macrocycle ou de dimérisation forte n'a été observée avec les monomères **MC3**²⁺ and **MC4**²⁺, que ce soit en présence de **CB[7]** ou de **CB[8]**. Cette étude a fourni des informations importantes pour le développement de nouveaux systèmes fonctionnels sensibles à des stimuli rédox.

Le dernier chapitre de ce travail de thèse a porté sur des systèmes tout à fait différents. Nous avons considéré une métalloporphyrine de Zn(II) fonctionnalisée par une anse

diphényl-phénanthroline qui présente une topographie adaptée à la complexation forte et sélective de substrats de type imidazole. Nous avons démontré que des substrats imidazoles judicieusement décorés en position 2 avec des azo-chromophores fonctionnels (isomérisation *trans-cis* photoinduite) pouvaient conduire à des espèces pentacoordinées stables avec le récepteur ZnL¹ (reconnaissance distale). Cependant, une déstabilisation est constatée lorsque les données thermodynamiques recueillies sont comparées à celles obtenues avec des composés de référence (ZnTPP, 1*H*-imidazole, 1-méthyl-1*H*-imidazole ou le 2-méthyl-1*H*-imidazole) probablement du fait d'interactions stériques de l'azo-chromophore avec l'anse phénanthroline qui induit des contraintes sur le macrocycle tétrapyrrolique. La substitution du substrat imidazole par un groupement azo-phénanthryle (**API**) peut aller jusqu'à limiter la formation d'un complexe avec le récepteur ZnL¹.

La cinétique de formation des complexes pentacoordinés suit un processus à une étape limitante de nature concertée. Les constantes de vitesse de formation bimoléculaires k_f et de dissociation monomoléculaires k_d rendent compte de l'encombrement de l'imidazole en position 2. La combinaison de ZnL¹ avec des substrats imidazoles fonctionnalisés avec des azo-chromophores présente un fort potentiel pour la préparation de systèmes fonctionnels innovants. Sous photo-excitation de l'azo-chromophore, un changement conformationnel *cis-trans* induirait une dissociation de l'imidazole du fait de fortes interactions stériques. La relaxation thermique permettrait de rétablir les complexes pentacoordinés thermodynamiquement favorisés.

7. Partie bibliographique

- 1 Bargiello, T. A.; Tang, Q.; Oh, S.; Kwon, T. *Biochim. Biophys. Acta-Biomembranes* **2012**, *1818*, 1807.
- 2 Iordache, A.; Retegan, M.; Thomas, F.; Royal, G.; Saint-Aman, E.; Bucher, C. *Chem. Eur. J.* **2012**, *18*, 7648-7653.
- 3 Bryan, J.; Sachleben, R.; Gakh, A.; Bunick, G. *J. Chem. Crystallogr.* **1999**, *29*, 513-521.
- 4 Vogelsberg, C. S.; Bracco, S.; Beretta, M.; Comotti, A.; Sozzani, P.; Garcia-Garibay, M. A. *J. Phys. Chem. B* **2012**, *116*, 1623-1632.
- 5 Kay, E. R.; Leigh, D. A.; Zerbetto, F. *Angew. Chem. Int. Ed.* **2007**, *46*, 72-191.
- 6 Skopek, K.; Hershberger, M. C.; Gladysz, J. A. *Coord. Chem. Rev.* **2007**, *251*, 1723-1733.
- 7 Browne, W. R.; Feringa, B. L. *Nat. Nanotechnol.* **2006**, *1*, 25-35.
- 8 Kottas, G. S.; Clarke, L. I.; Horinek, D.; Michl, J. *Chem. Rev.* **2005**, *105*, 1281-1376.
- 9 Yoon, I.; Benítez, D.; Zhao, Y.-L.; Miljanić, O. Š.; Kim, S.-Y.; Tkatchouk, E.; Leung, K. C. F.; Khan, S. I.; Goddard, W. A.; Stoddart, J. F. *Chem.-Eur. J.* **2009**, *15*, 1115-1122.
- 10 Li, D.; Paxton, W. F.; Baughman, R. H.; Huang, T. J.; Stoddart, J. F.; Weiss, P. S. *MRS Bulletin* **2009**, *34*, 671-681.
- 11 Juluri, B. K.; Kumar, A. S.; Liu, Y.; Ye, T.; Yang, Y.-W.; Flood, A. H.; Fang, L.; Stoddart, J. F.; Weiss, P. S.; Huang, T. J. *ACS Nano* **2009**, *3*, 291-300.
- 12 Saha, S.; Stoddart, J. F.; Wiley-VCH: Weinheim, Germany, **2007**.
- 13 Badjic, J. D.; Ronconi, C. M.; Stoddart, J. F.; Balzani, V.; Silvi, S.; Credi, A. *J. Am. Chem. Soc.* **2006**, *128*, 1489-1499.
- 14 Angelos, S.; Khashab, N. M.; Yang, Y.-W.; Trabolsi, A.; Khatib, H. A.; Stoddart, J. F.; Zink, J. I. *J. Am. Chem. Soc.* **2009**, *131*, 12912-12914.
- 15 Hmadeh, M.; Fang, L.; Trabolsi, A.; Elhabiri, M.; Albrecht-Gary, A.-M.; Stoddart, J. F. *J. Mater. Chem.* **2010**, *20*, 3422-3430.
- 16 Badjić, J. D.; Balzani, V.; Credi, A.; Silvi, S.; Stoddart, J. F. *Science* **2004**, *303*, 1845-1849.
- 17 Khashab, N. M.; Trabolsi, A.; Lau, Y. A.; Ambrogio, M. W.; Friedman, D. C.; Khatib, H. A.; Zink, J. I.; Stoddart, J. F. *Eur. J. Org. Chem.* **2009**, 1669-1673.
- 18 Fernández-Mato, A.; García, M. D.; Peinador, C.; Quintela, J. M.; Sánchez-Andújar, M.; Pato-Doldán, B.; Señaris-Rodríguez, M. A.; Tordera, D.; Bolink, H. J. *Cryst. Growth Des.* **2013**, *13*, 460-464.
- 19 Muraoka, T.; Kinbara, K.; Kobayashi, Y.; Aida, T. *J. Am. Chem. Soc.* **2003**, *125*, 5612-5613.
- 20 Muraoka, T.; Kinbara, K.; Aida, T. *Nature* **2006**, *440*, 512-515.
- 21 Lagona, J.; Mukhopadhyay, P.; Chakrabarti, S.; Isaacs, L. *Angew. Chem. Int. Ed.* **2005**, *44*, 4844-4870.
- 22 Choi, S.; Lee, J. W.; Ko, Y. H.; Kim, K. *Macromolecules* **2002**, *35*, 3526-3531.
- 23 McNally, B. A.; Leevy, W. M.; Smith, B. D. *Supramol. Chem.* **2007**, *19*, 29-37.
- 24 Mohanty, J.; Nau, W. M. *Angew. Chem. Int. Ed.* **2005**, *44*, 3750-3754.
- 25 Bardelang, D.; Udachin, K. A.; Leek, D. M.; Margeson, J. C.; Chan, G.; Ratcliffe, C. I.; Ripmeester, J. A. *Cryst. Growth Des.* **2011**, *11*, 5598-5614.
- 26 Lee, J. W.; Samal, S.; Selvapalam, N.; Kim, H.-J.; Kim, K. *Acc. Chem. Res.* **2003**, *36*, 621-630.
- 27 Dsouza, R. N.; Pischel, U.; Nau, W. M. *Chem. Rev.* **2011**, *111*, 7941-7980.
- 28 Liu, S.; Ruspic, C.; Mukhopadhyay, P.; Chakrabarti, S.; Zavalij, P. Y.; Isaacs, L. *J. Am. Chem. Soc.* **2005**, *127*, 15959-15967.

- 29 Wang, R.; Yuan, L.; Macartney, D. H. *Chem. Commun.* **2006**, 2908-2910.
- 30 Hettiarachchi, D. S. N.; Macartney, D. H. *Can. J. Chem.* **2006**, *84*, 905-914.
- 31 Choi, S.; Park, S. H.; Ziganshina, A. Y.; Ko, Y. H.; Lee, J. W.; Kim, K. *Chem. Commun.* **2003**, 2176-2177.
- 32 Jansen, K.; Buschmann, H. J.; Wego, A.; Döpp, D.; Mayer, C.; Drexler, H. J.; Holdt, H. J.; Schollmeyer, E. *J. Inclusion Phenom.* **2001**, *39*, 357-363.
- 33 Buschmann, H. J.; Cleve, E.; Jansen, K.; Schollmeyer, E. *Anal. Chim. Acta* **2001**, *437*, 157-163.
- 34 Buschmann, H. J.; Cleve, E.; Jansen, K.; Wego, A.; Schollmeyer, E. *J. Inclusion Phenom.* **2001**, *40*, 117-120.
- 35 Ong, W.; Gómez-Kaifer, M.; Kaifer, A. E. *Org. Lett.* **2002**, *4*, 1791-1794.
- 36 Ong, W.; Kaifer, A. E. *J. Org. Chem.* **2004**, *69*, 1383-1385.
- 37 Abouderbala, L. O.; Belcher, W. J.; Boutelle, M. G.; Cragg, P. J.; Steed, J. W.; Turner, D. R.; Wallace, K. J. *Proc. Natl. Acad. Sci. U.S.A.* **2002**, *99*, 5001-5006.
- 38 Wang, R.; Yuan, L.; Ihmels, H.; Macartney, D. H. *Chem. Eur. J.* **2007**, *13*, 6468-6473.
- 39 Thangavel, A.; Rawashdeh, A. M. M.; Sotiriou-Leventis, C.; Leventis, N. *Org. Lett.* **2009**, *11*, 1595-1598.
- 40 Ong, W.; Kaifer, A. E. *Angew. Chem. Int. Ed.* **2003**, *42*, 2164-2167.
- 41 Wagner, B. D.; Stojanovic, N.; Day, A. I.; Blanch, R. J. *J. Phys. Chem. B* **2003**, *107*, 10741-10746.
- 42 Cui, L.; Gadde, S.; Li, W.; Kaifer, A. E. *Langmuir* **2009**, *25*, 13763-13769.
- 43 Ong, W.; Kaifer, A. E. *Organometallics* **2003**, *22*, 4181-4183.
- 44 Monk, P. M. S. *The Viologens: Physicochemical Properties, Synthesis and Applications of the Salts of 4, 4'-Bipyridine* Chichester, **1998**.
- 45 Bruinink, J.; Kregting, C. G. A.; Ponjeé, J. J. *J. Electrochem. Soc.* **1977**, *124*, 1854-1858.
- 46 Evans, A. G.; Evans, J. C.; Baker, M. W. *J. Am. Chem. Soc.* **1977**, *99*, 5882-5884.
- 47 Meisel, D.; Mulac, W. A.; Matheson, M. S. *J. Phys. Chem.* **1981**, *85*, 179-187.
- 48 Adar, E.; Degani, Y.; Goren, Z.; Willner, I. *J. Am. Chem. Soc.* **1986**, *108*, 4696-4700.
- 49 Yasuda, A.; Mori, H.; Seto, J. *J. Appl. Electrochem.* **1987**, *17*, 567-573.
- 50 Trabolsi, A.; Hmadeh, M.; Khashab, N. M.; Friedman, D. C.; Humbert, N.; Elhabiri, M.; Khatib, H. A.; Belowich, M. E.; Coskun, A.; Albrecht-Gary, A. M.; Stoddart, J. F. *J. Am. Chem. Soc.* **2009**, *131*, 254-263.
- 51 Kosower, E.M.; Cotter, J.L. *J. Am. Chem. Soc.* **1964**, *86*, 5524-5527.
- 52 (a) Kosower, E. M.; Hajdu, J. *J. Am. Chem. Soc.* **1971**, *93*, 2534-2535.
- 53 Geuder, W.; Hünig, S.; Suchy, A. *Tetrahedron* **1986**, *42*, 1665-1677.
- 54 Monk, P. M.S.; Hodgkinson, N. M.; Ramzan, S.A. *Dyes & Pigments* **1999**, *43*, 207-217.
- 55 Fahrenbach, A. C.; Barnes, J. C.; Lanfranchi, D. A.; Li, H.; Coskun, A.; Gassensmith, J. J.; Liu, Z.; Benítez, D.; Trabolsi, A.; Goddard, W. A.; Elhabiri, M.; Stoddart, J. F. *J. Am. Chem. Soc.* **2011**, *133*, 3061-3072.
- 56 (a) Mortimer, R.J. *Electrochim. Acta* **1999**, *44*, 2971-2981. (b) Cao, L.-C.; Mou, M.; Wang, Y. *J. Mater. Chem.* **2009**, *19*, 3412-3418. (c) Asaftei, S.; Ciobanu, M.; Lepadatu, A.M.; Song, E.; Beginn, U. *J. Mater. Chem.* **2012**, *22*, 14426-14437.
- 57 Kuroboshi, M.; Shiba, T.; Tanaka, H. *Tetrahedron Lett.* **2013**, *54*, 3666-3668.
- 58 Ciepluch, K.; Katir, N.; El Kadib, A.; Felczak, A.; Zawadzka, K.; Weber, M.; Klajnert, B.; Lisowska, K.; Caminade, A.-M.; Bousmina, M.; Bryszewska, M.; Majoral, J. P. *Mol. Pharmaceutics* **2012**, *9*, 448-457.
- 59 Park, J. W.; Ko, S. H.; Park, J. Y. *Bull. Korean Chem. Soc.* **1992**, *13*, 259.

- 60 Iordache, A.; Oltean, M.; Milet, A.; Thomas, F.; Saint-Aman, E.; Bucher, C. *J. Am. Chem. Soc.* **2012**, *134*, 2653-2671.
- 61 Iehl, J.; Frasconi, M.; Jacquot de Rouville, H.-P.; Renaud, N.; Dyar, S. M.; Strutt, N. L.; Carmieli, R.; Wasielewski, M. R.; Ratner, M. A.; Nierengarten, J.-F.; Stoddart, J. F. *Chem. Sci.* **2013**, *4*, 1462-1469.
- 62 Benyettou, F.; Nchimi Nono, K.; Jouiad, M.; Lalatonne, Y.; Milosevic, I.; Motte, L.; Olsen, J.-C.; Saleh, N.; Trabolsi, A. *Chem. Eur. J.* **2015**, *21*, 4607-4613.
- 63 Perlmutter-Hayman, B. *Acc. Chem. Res.* **1986**, *19*, 90-96.
- 64 Hou, J. L.; Yi, H. P.; Shao, X. B.; Li, C.; Wu, Z. Q.; Jiang, X. K.; Wu, L. Z.; Tung, C. H.; Li, Z. T. *Angew. Chem. Int. Ed.* **2006**, *45*, 796-800.
- 65 Trabolsi, A.; Urbani, M.; Delgado, J. L.; Ajamaa, F.; Elhabiri, M.; Solladi, N.; Nierengarten, J.-F.; Albrecht-Gary, A.-M. *New J. Chem.* **2008**, *32*, 159-165.
- 66 Jeon, W. S.; Kim, H.-J.; Lee, C.; Kim, K. *Chem. Commun.* **2002**, 1828-1829.
- 67 Lee, C.; Moon, M. S.; Park, J. W. *J. Electroanal. Chem.* **1996**, *407*, 161-167.
- 68 Stargardt, J. F.; Hawkridge, F. M. *Anal. Chim. Acta* **1983**, *146*, 1-8.
- 69 (a) Nchimi Nono, K.; Dalvand, P.; Wadhwa, K.; Nuryyeva, S.; Alneyadi, S.; Fahrenbach, A.; Olsen, J.-C.; Asfari, Z.; Platas-Iglesias, C.; Elhabiri, M.; Trabolsi, A. *Chem. Eur. J.* **2014**, *20*, 7334-7344. (b) K. Wadhwa, S. Nuryyeva, A. C. Fahrenbach, M. Elhabiri, C. Platas-Iglesias, A. Trabolsi, *J. Mater. Chem. C* **2013**, *1*, 2302-2307.
- 70 Kannappan, R.; Bucher, C.; Saint-Aman, E.; Moutet, J. C.; Milet, A.; Oltean, M.; Métay, Pellet-Rostaing, E. S.; Lemaire, M.; Chaix, C. *New J. Chem.* **2010**, *34*, 1373-1386.
- 71 Atherton, S. J.; Tsukahara, K.; Wilkins, R. G. *J. Am. Chem. Soc.* **1986**, *108*, 3380-3385.
- 72 Mohammad, M. *Electrochim. Acta* **1988**, *33*, 417-419.
- 73 (a) Iordache, A.; Kanappan, R.; Métay, E.; Duclos, M. C.; Pellet-Rostaing, S.; Lemaire, M.; Milet, A.; Saint-Aman, E.; Bucher, C. *Org. Biomol. Chem.* **2013**, *11*, 4383-4389. (b) Kahlfuss, C.; Métay, E.; Duclos, M. C.; Lemaire, M.; Oltean, M.; Milet, A.; Saint-Aman, E.; Bucher, C. *C. R. Chimie* **2014**, *17*, 505-511.
- 74 Kim, H.-J.; Jeon, W. S.; Ko, Y. H.; Kim, K. *Proc. Natl. Acad. Sci. USA* **2002**, *99*, 5007-5011.
- 75 Brandel, J.; Trabolsi, A.; Melin, F.; Elhabiri, M.; Weiss, J.; Albrecht-Gary, A. M. *Inorg. Chem.* **2007**, *46*, 9534-9536.
- 76 Brandel, J.; Trabolsi, A.; Trabolsi, H.; Melin, F.; Koepf, M.; Wytko, J. A.; Elhabiri, M.; Weiss, J.; Albrecht-Gary, A. M. *Inorg. Chem.* **2009**, *48*, 3743-3754.

Chapter I: General Introduction

1.1. Introduction

The PhD research work described in this manuscript was carried out in the Laboratoire de Chimie Bioorganique et Médicinale (UMR 7509, CNRS-UdS, Strasbourg) and the Laboratoire d'Ingénierie Moléculaire Appliquée à l'Analyse (IPHC, UMR 7178 CNRS-UdS) under the joint supervision of Dr Mourad Elhabiri, Chargé de Recherche CNRS and Dr Zouhair Asfari, Ingénieur de Recherche CNRS. It has been developed in the frame of a broader research topic investigated in the team which is focussed on ionic and molecular recognition processes in supramolecular chemistry. The ongoing achievements in synthetic methodologies allowed (and are still) creating increasingly sophisticated supramolecular devices for the development of valuable functional nanomaterials. If their preparations and characterizations are now better controlled and well described, the understanding of their mechanisms of recognition and/or self-assembly has been, however, rarely addressed. These physico-chemical parameters would have been essential to gain a deeper understanding and a better control of their self-assembly processes in order to afford more efficient non-covalent nano-objets. Elucidation of these mechanisms in solution typically requires spectroscopic, thermodynamic and kinetic studies. The research work described has been focussed to understand the self-assembly/recognition processes and the mode of action of several supramolecular systems. This was achieved in the frame of scientific collaborations with French and international research teams who possess the skills and the know-how of supramolecular ligands. With Dr Jean Weiss (Controlled Ligand Architectures in Coordination Chemistry, UMR 7177 CNRS-UdS, Strasbourg) and Pr Ali Trabolsi (Supramolecular Multifunctional Systems, New York Abu Dhabi University NYUAD, Abu Dhabi, UAE), we have examined the physico-chemical properties (absorption spectrophotometric and structural properties in solution, electrochemistry, thermodynamics...) of hosts based on Zn(II) metalloporphyrins with azo-chromophore guests, as well as the recognition processes of viologen based multimeric substrates by curcubit[n]uril ($n = 7, 8$) macrocyclic receptors.

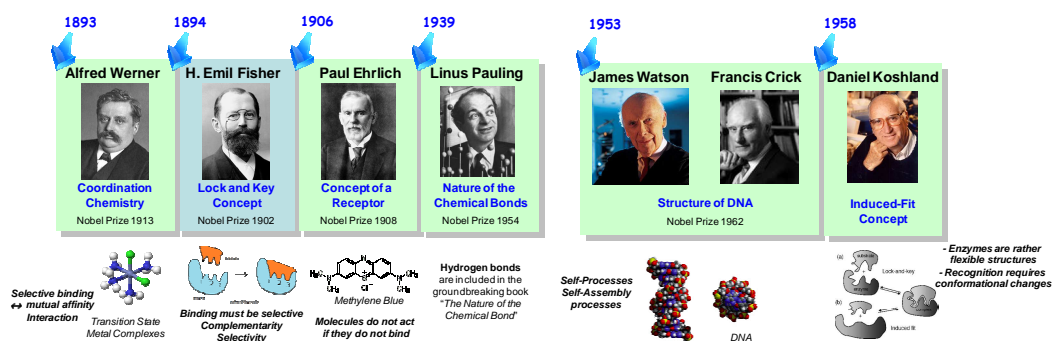
1.2. Supramolecular Chemistry

Even though the roots of supramolecular chemistry (*i.e.* Lat: supra = beyond, above....) have been discovered in the beginning of the XX century (Figure 1), it has been initially defined long after in 1978 by J. M. Lehn as being "*the chemistry of molecular assemblies and of the intermolecular bond*"¹⁻³ It encompasses the entities that are formed by the association of at least two discrete chemical subunits or components. Other outstanding authors such as F. Vögtle have defined the supramolecular chemistry as being the domain of chemistry "*beyond that of molecules*".⁴

While traditional chemistry primarily focuses on the covalent bond, supramolecular chemistry involves non-covalent interactions between two or more species (*e.g.* molecules, ion, molecular building blocks, macromolecules, proteins...) with the purpose of forming, for instance, a supramolecule complex (Figure 2). Archetypal examples are provided by Nature such as enzymes which play the role of a host. Its guest (substrate) selectively, efficiently and reversibly binds thanks to non-covalent interactions to afford a targeted enzyme-substrate

complex that is devoted to achieve a given function. Many other examples of natural (*e.g.* cyclodextrins...) and synthetic hosts (*e.g.* cucurbiturils, calixarenes...) (Figure 3) can be also mentioned.⁵⁻⁷ Representative concepts that arose from supramolecular chemistry included self-assembly, folding, molecular and/or ionic recognition, host-guest chemistry, mechanically-interlocked molecular systems – MIMs, molecular machines, topological devices to cite a few (Figure 1).⁸

Concepts and Roots of Supramolecular Chemistry



Supramolecular Chemistry, a Young Scientific Discipline

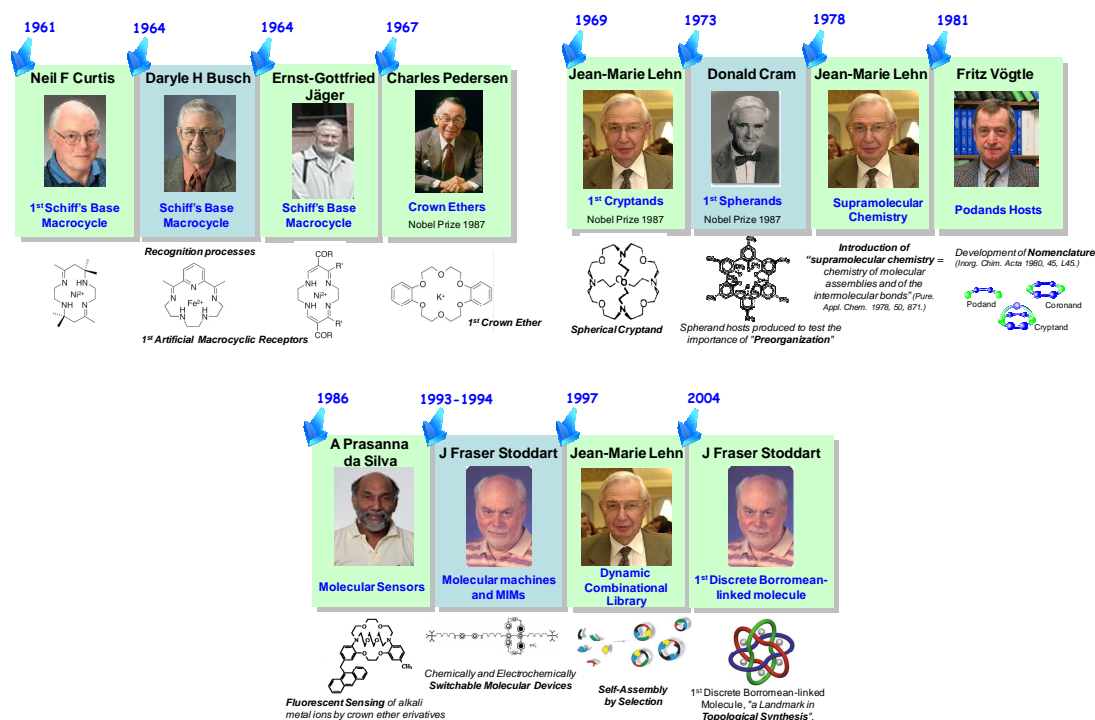
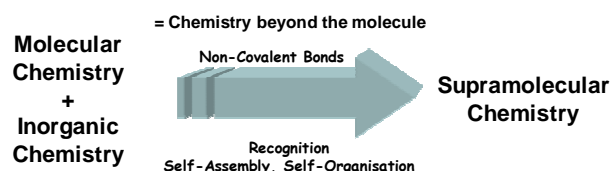


Figure 1. Timeline of supramolecular chemistry



Preprogrammed Synthesis or Construction
Self-Assembly of Discrete Chemical Structures
Self-Organization of Higher-order Structures
Weak Chemical Forces
Molecular rather than Atomic Building Blocks
Nanoscale rather than Angstrom Scale

Figure 2. Key aspects of supramolecular chemistry

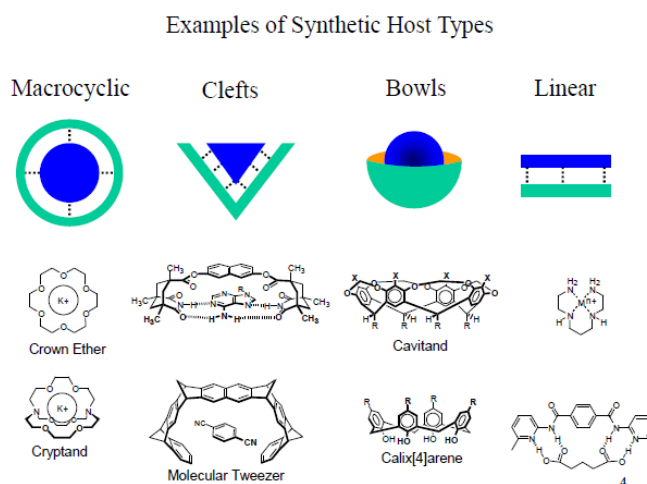


Figure 3. Examples of common synthetic molecular hosts with different topologies

A broad "range" of strong or weak interactions (Figure 4) can be used as a toolbox to design supramolecular architectures. Among them, one can cite the metal-ligand, ion-ion, ion-dipole or dipole-dipole, hydrogen bonding, Van der Waals', π - π stacking, cation- π , anion- π ,⁹ electrostatic or hydrophobic interactions.

Strong	Metal-Ligand	200 – 400 kJ mol ⁻¹
	Ion-Ion	50 – 300 kJ mol ⁻¹
	Ion-Dipole	50 – 200 kJ mol ⁻¹
	Dipole-Dipole	5 – 50 kJ mol ⁻¹
	Hydrogen Bond	4 – 120 kJ mol ⁻¹
	Cation-π	5 – 80 kJ mol ⁻¹
	Anion-π	20 – 70 kJ mol ⁻¹
	π-π	0 – 50 kJ mol ⁻¹
Weak	CH-π	0 – 50 kJ mol ⁻¹
	Van der Waals	< 5 kJ mol ⁻¹
	Hydrophobic	0 – 0.2 kJ mol ⁻¹ Å ⁻²

Figure 4. Strong to weak non-covalent interactions.

1.3. Molecular Recognition

As outlined above, molecular recognition represents a broad research domain of supramolecular chemistry and is as a rule defined as the specific, selective and reversible binding of a guest molecule to a complementary host molecular receptor through non-covalent interactions (Figure 5). The bioorganic edifices such as antigen-antibody, DNA-protein, sugar-lectin, RNA-ribosome or enzyme-ligand constitute representative examples of host-guest complexes that can be found in Nature and which rely on molecular recognition processes. Two or more molecules have the capacity to identify to each other and to fit together in an optimal manner. There are several parameters that influence the nature of these systems: their steric and interactional complementarity (shape and size) of the components, large contact areas, multiplication of interaction sites and nature and strength of the interactions (Figure 5).^{10,11} The well tailored design and construction of hosts that are capable to selectively and firmly accommodate guest molecules then requires precise control over geometrical and interactional features.¹² Historically, the matching in size and shape between the binding sites of the host and the guest that can be illustrated by the lock and key principle was introduced by H. E. Fisher more than one century ago (Figure 1). However, the host and the guest components can be also regarded as flexible systems that can alter their shape during the recognition process. This recent view on the molecular recognition, designated as the induced fit concept, was introduced later by D. Koshland in 1958.

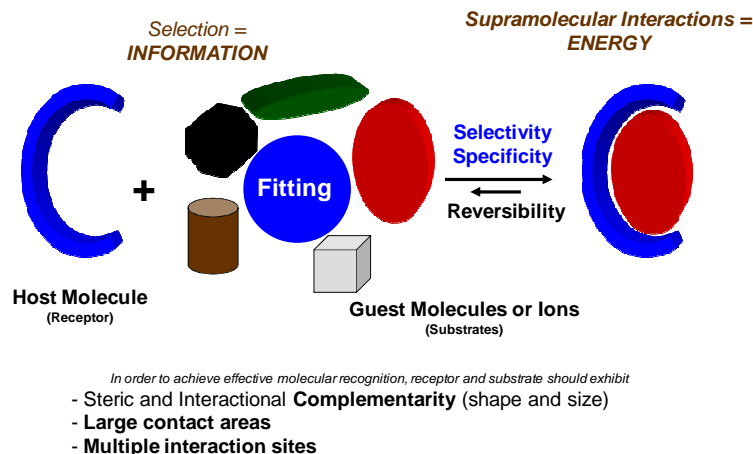


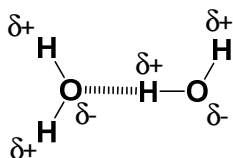
Figure 5. Principles of molecular recognition.

1.3.1. Non-Covalent Interactions

As described above, non-covalent interactions are considered as the spine of supramolecular chemistry: they are the main forces that support the supramolecular systems together.^{13,14} Non-covalent bonding energies are generally weaker than those of the covalent bonds, but the combination of many of them is sufficient to strongly stabilize the host-guest complexes (Figure 4). The next section will review the principle of the different types of non-covalent interactions that are relevant in the context of this research work.

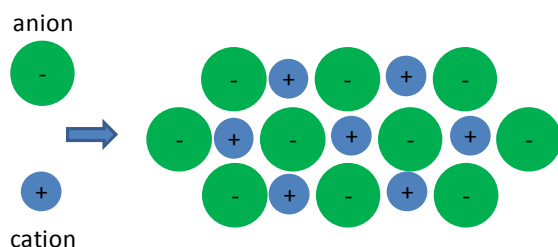
1.3.2. Hydrogen Bonding¹⁵

The hydrogen bond is considered to be among the most important non-covalent forces in supramolecular chemistry. It was described by Pimentel and McClellan¹⁶ as the interaction between a functional group (X-H) (hydrogen bond donor) and an atom or a group of atoms (AC) (hydrogen bond acceptor) within the same (intramolecular) molecule or between two different molecules (intermolecular). A more recent definition proposed in 2011 by IUPAC states that “*The hydrogen bond is an attractive interaction between a hydrogen atom from a molecule or a molecular fragment X–H in which X is more electronegative than H, and an atom or a group of atoms in the same or a different molecule, in which there is evidence of bond formation*”.¹⁷ The hydrogen bond can be classified into three categories according to its strength.¹³ A strong hydrogen bond forms with energies ranging from 60 to 120 kJ mol⁻¹, while moderate hydrogen bond energy ranges from 15 to 50 kJ mol⁻¹. A weak hydrogen bond is then used to describe an interaction characterized by energies below 15 kJ mol⁻¹. The strength of the hydrogen bond mainly depends on stereochemical properties such as the distance between the hydrogen bond donor Dn-H and the hydrogen bond acceptor AC. Shorter will be the distance, stronger will be the hydrogen bond interaction. Another important feature is the angle between the three centres (**Dn-H...AC**) that can also affect the hydrogen bond strength. It has been shown that linear angles usually lead to strong hydrogen bonds.



1.3.3. Electrostatic Interactions

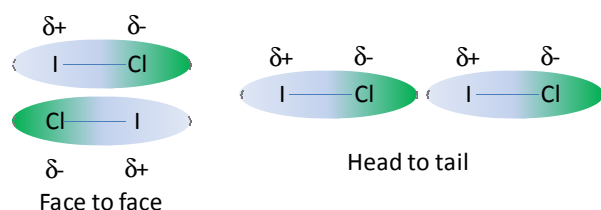
Electrostatic interactions are interactions between and among cations and anions or partially charged molecules that, depending on the sign of the charges, can be either attractive or repulsive. These interactions can be divided into three sub-categories: ion pairing, ion-dipole or dipole-dipole interactions.¹³ Electrostatic interactions between two charged centres are non-directional and usually strong interactions that fall off gradually with the distance ($1/r$).



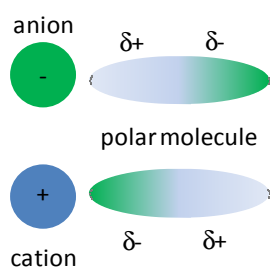
Ion pairing (ion-ion) interaction describes the association of an anion and a cation that are firmly held together due to Coulombic attraction without formation of a covalent bond. These interactions are characterized by bond energies ranging from 100 to 350 kJ mol⁻¹ and are among the strongest non-covalent

forces. They are comparable to some typical covalent bond energies (~ 350 kJ mol⁻¹) such as C-C, C-O or C-Cl. Importantly, ion pairing takes place between cation and anion that are very close in space, so the energy formed from their electrostatic attraction is greater than the energy required to separate them. Although these interactions do not depend on the orientation of the ions, they are dependent on the distance (r) between them ($1/r$).¹⁴

Dipole-dipole interactions exist between two or more dipoles. Two dipoles can feel each other through space. The positive end of the first dipole is attracted to the negative end of the second dipole. The strength of a dipole-dipole interaction ($5\text{-}50 \text{ kJ mol}^{-1}$) depends on several parameters such as the size of the dipoles, their proximity and mutual orientations. This type of interaction can be either attractive or repulsive and its energy falls off with $1/r^3$.¹⁴

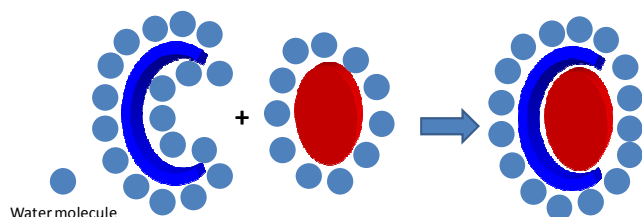


When an ion is close to a molecule that displays a dipole moment, ion-dipole interactions can take place. Ion-dipole is, in a sense, comparable to dipole-dipole interactions but involves ions rather than only polar molecules. Ion-dipole forces are stronger than dipole-dipole interactions because the charge of an ion is greater than the charge of a dipole moment. In contrast with ion-ion interaction, ion-dipole interactions are dependent on the orientation of the partners, as the ion should oppositely face the partial charge of the dipole. Their strengths ($50\text{-}200 \text{ kJ mol}^{-1}$) depend on the distance between the ion and the dipole ($1/r^2$).¹⁴



1.3.4. Hydrophobic Interactions

*“Proverbially, Oil and water do not mix. The repelling of oil for water, with its unusual temperature dependence, is called the hydrophobic effect”*¹⁸ The hydrophobic effect was explained using the fact that in water or other protic media, the non-polar regions of molecules or non-polar molecules (low water-soluble molecules also called hydrophobes) tend to clump up together to reach the most energetically stable status. The driving force of such a process is designated as the hydrophobic interaction. Surprisingly, water is usually the most favourable solvent for the association of non-polar species (hydrophobes). For instance, in the case of recognition processes which involve hydrogen bonding interactions, the host-guest inclusion process might be altered in water or protic media. During the recognition process, the non-polar partners exclude water (or the protic solvent) from their respective solvation shell in order to come closer so the host-guest complexation induces partial or full desolvation of the host and guest. This solvation effects therefore play a critical role in mediating the final stability of supramolecular edifice.^{1,19} Even though the origin of



the hydrophobic interactions is not fully understood, it seems to arise from two different factors. The first is an enthalpic contribution, which results from the tendency of water molecules to form a solvating layer around the non-polar molecules (e.g. non-polar guests) that could be very costly in terms of energy. Water molecules also interact with the walls of a host cavity (which is often hydrophobic) such as

the macrocyclic cyclodextrin, cucurbit[n]urils or calix[n]arenes receptors. By releasing these water molecules from the cavity to interact with the bulk solvent, which is more favourable, there will be an enthalpic cost. Another important factor that affects the hydrophobic interaction is the entropic gain that results from combining the host and the guest as it induces two different holes in the water solvation structure. Hydrophobes indeed tends to clump up together rather than distributing itself in a water medium, because this will allow the hydrophobes to display a minimal contact with the unfavourable protic solvent. By forming such a host-guest species, they will cause less disruption to the whole system.^{1,14,20}

1.3.5. π - π Bonding

The weak π - π stacking interactions (0-50 kJ/mol), which usually occur between aromatic rings in which one ring is relatively electron rich and the other is electron poor, are caused by intermolecular overlapping of p-orbitals in π -conjugated systems that results in an energetic gain. Therefore, the strength of the interaction increases with the number of π electrons. The stacking between aromatic rings can be edge-to-face or T-shape, or a face-to-face (parallel or shifted) arrangement (Figure 6).²¹

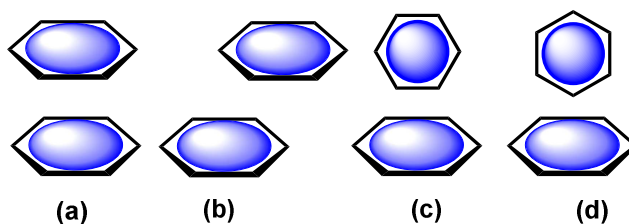


Figure 6. π - π stacking interactions. Face-to-face: (a) parallel (b) shifted, (c) edge to face and (d) T-shaped.²¹

1.3.6. Coordination Interaction

Metal complexes can be regarded as the products of a Lewis acid-base reaction in which a central metal ion (*i.e.* a Lewis acids that can accept electrons from a Lewis base) is surrounded by several neutral molecules or anions (*i.e.* called ligand, a Lewis base that contains at least one pair of electrons to donate to a metal centre). In the absence of other non-covalent interactions, the coordination bond (or interaction) which is directional and brought close together the ligands and the metal ion is among the more stable non-covalent interactions and its energy lies within the 200 to 400 kJ mol⁻¹ range. Coordination compounds and complexes are distinct chemical species, their properties and behaviour being different from those of the metal ion and the ligands from which they result. Coordination number usually ranges from 2 up to 12, with 4 and 6 being common for the upper transition metals.

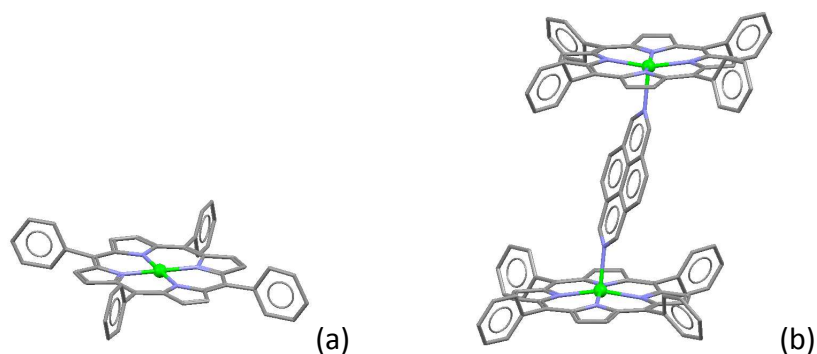


Figure 7. Crystallographic X-ray structures of a) **ZnTPP** (tetracoordinated Zn^{2+} cation) and b) of the complex (2,7-diazapyrène- N,N')-bis(5,10,15,20-tétraphénylporphyrinato- N,N',N'',N''')-di-zinc(II) (pentacoordinated Zn^{2+} cation).²²

1.4. Viologen-Cucurbituril Host/Guest Chemistry – Toward an Electrochemical Control of Dimerization *versus* Inclusion for the Development of Novel Nanomechanical devices

A first part of my PhD work has been devoted to study, in aqueous solution, novel systems based on recognition properties of redox active bipyridiniums by macrocycles such as cucurbit[n]uril. The nanomechanical systems that have been developed include among other: [3]pseudorotaxane, [4]pseudorotaxane and [7]pseudorotaxane, each composed of a “multimeric” viologen-based thread molecule and the macrocycles, cucurbit[7]uril (noted **CB[7]**) or cucurbit[8]uril (noted **CB[8]**). These systems can be electrochemically switched between a complexed state, defined by the pseudorotaxanes themselves, and an uncomplexed state comprising their separate components. The driving force for the disassembly process (*i.e.* "dethreading") is a strong intramolecular or intermolecular dimerization of the viologen radical cations. I will recall in the following section the structural and physico-chemical properties of cucurbit[n]uril and viologen.

1.4.1. Cucurbiturils

Cucurbit[n]urils (**CB[n]**) can then be considered as a class of macrocycles²³ that are synthesized by the acid-catalyzed condensation of formaldehyde with 5, 6, 7, 8, or 10 glycoluril molecules. They have a pumpkin-like shape and two identical carbonyl-rimmed portals, as well as a hydrophobic cavity that can accommodate a large variety of guest molecules. Historically, Behrend, Mayer, and Rusche described in 1905 the acidic condensation of an excess of formaldehyde and *bis*(ureido)glycoluril that produced a crystalline precipitate which was exceedingly stable towards a number of potent reagents.²⁴ Due to the inappropriate characterization tools available at that time, they were not able to elucidate the chemical structure of the corresponding substance. It was not until the early 1980s that Freeman, Mock, and Shih repeated the synthesis and then characterized the product as a hexameric macropolycyclic structure of composition $C_{36}H_{36}N_{24}O_{12}$. A crystal structure further showed that the macrocyclic molecule is based on six glycoluril units bridged together thanks to twelve methylene units. Two calcium cations were found to interact with the carbonyl portals. Mock first designated the compound as “cucurbituril”

with respect to their likeness to the pumpkin fruit (*Cucurbitaceae*). At that time, cucurbit[6]uril **CB[6]** was the only isolated product (Figure 8).²⁵

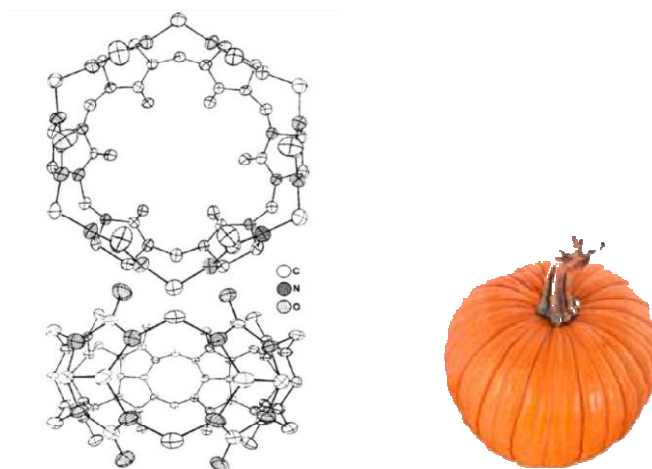


Figure 8. First illustration of **CB[6]** by Freeman et al. (crystallographic structure from top and edge-on view, taken from ref.25 (Freeman et al., 1981).

In 2000, Kim and his co-workers isolated and characterized three more homologues; **CB[5]**, **CB[7]**, and **CB[8]** using milder reaction conditions (Figure 9).^{26,27} Since then, the family of cucurbit[n]urils **CB[n]** has grown and attracted the interest of many research groups who synthesize other derivatives (*e.g.* **CB[10]**).²⁸⁻³³ They are now commercially available.

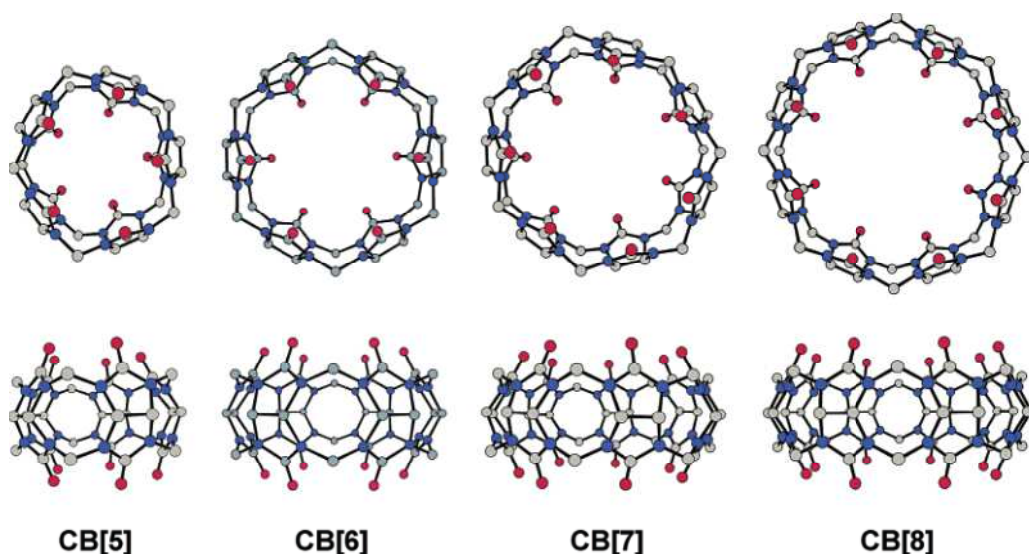


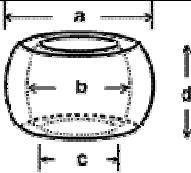
Figure 9. X-ray crystal structures of **CB[n]** ($n = 5-8$). Colour codes: carbon, gray; nitrogen, blue; oxygen, red. Cucurbituril homologues and derivatives; Figure taken from ref. 27 (Lee *et al.*, 2003).

1.4.1a. Structural and Physico-chemical Features of **CB[n]**

The available crystallographic structures of **CB[n]** showed that they display structural parameters (external and internal diameter, volume) that differ from one macrocycle to each other, except for their height, which remains identical within the series (Table 1).^{23,34} **CB[n]**s have two polar carbonyl portals and a hydrophobic cavity. Although they display

similar depth and height, they possess different external and internal diameters depending on the number of glycoluril units.^{34,35} The diameter of the **CB[n]** portals is generally 2 Å narrower than the diameter of the cavity. The geometrical parameters of the **CB[n]** are given in Table 1.

Table 1. Structural^a and physico-chemical parameters of the **CB[n]** macrocycles.

	CB[5]	CB[6]	CB[7]	CB[8]	CB[10]
External diameter a (Å)	13.1	14.4	16.0	17.5	20-21.1
Cavity diameter b (Å)	4.4	5.8	7.3	8.8	11.3-12.4
Portal diameter c (Å)	2.4	3.9	5.4	6.9	9.0-11.0
Cavity depth ^b	7.4	7.5	7.6	7.7	7.8
Height d (Å)	9.1	9.1	9.1	9.1	9.1
Volume (Å ³)	82	164	279	479	870
S _{H2O} (mM)	20-30	0.018	20-30	< 0.01	-
^a Calculated from the X-ray crystal structures. ^b Cavity depth determined from electrostatic potential minima. S _{H2O} = solubility in water at 25°C.					

This particular structure allows these **CB[n]** macrocycles establishing ion-dipole, hydrogen bond or hydrophobic interactions with a wide range of substrates and is at the origin of their high affinities/selectivities as compared to cyclodextrins, crown ethers or other relevant macrocycles.³⁶⁻³⁹ In addition, the cavity size and the macrocycle diameter play a major role in the recognition/inclusion process (induced fit process).²⁷ Last but not the least, water solubility of **CB[n]** is another important aspect. **CB[6]** and **CB[8]** are sparingly soluble while **CB[5]** and **CB[7]** are fairly soluble in water.²³ Consequently, some of these macrocyclic compounds are interesting molecular tools for supramolecular chemists due to their ability to host a wide range of cationic and neutral guests in water, through cation-dipole and/or hydrophobic interactions. During the last years, significant progress has been made in the control of the size and shape and in the functionalization during the synthesis of cucurbit[n]uril. As said previously, **CB[7]** (279 Å³) and **CB[8]** (479 Å³) display comparable cavities, respectively, to those of β- and γ-cyclodextrins and are therefore among the most interesting and most studied compounds of this series.^{40,41} My research work has therefore been focussed in the study of **CB[7]** and **CB[8]** with viologen-based monomeric or multimeric systems. The following section will describe the recognition properties of these two macrocyclic systems.

1.4.1b. **CB[7]**, a Valuable Supramolecular Host

As stated previously, the host-guest chemistry of **CB[n]** has attracted tremendous interest^{23,42} and has many potential applications in nanotechnology and materials science to cite a few.^{23,43} **CB[n]** hosts have been used for the synthesis of a range of self-assembled

compounds including precursors to mechanically interlocked molecules and molecular switches.^{23,42} **CB[7]** has some advantages over the other homologues belonging to the cucurbituril family (e.g. higher solubility in water²³), and has drawn much more attention. **CB[7]** has a hydrophobic internal cavity that measures 7.3 Å in diameter and 9.1 Å in height⁴⁴ (Table 1) that allow to accommodate in a 1:1 fashion a broad variety of guest substrates^{23,27,45-47} such as the positively charged substrates as dicationic or tetracationic viologen^{48,49} stilbenes,⁵⁰ naphthalenes,^{51,52} protonated amino-adamantanes,⁴⁶ imidazolium cations,⁵³ chiral N-benzyl-1-(1-naphthyl)ethylamines⁵⁴ and pyridinium derivatives,⁵⁵ or neutral guests including adamantanes and bicyclooctanes^{27,56-58}, o-carborane,⁵⁹ fullerene,⁶⁰ ferrocene and cobaltocene derivatives,^{40,61,62} among others.^{63,64} Moreover, **CB[7]** can form inclusion complexes with a series of small neutral polar organic guests such as acetone, butan-2-one, acetophenone, methyl acetate, and others.⁶⁵ The binding constants generally varied with to the nature, size, and hydrophobicity of the guest, which supports that the hydrophobic and dipole-dipole interactions are the main forces responsible for complex formation.

1.4.1c. **CB[8]**, a Homologous Host

With respect to **CB[7]**, **CB[8]** possesses a larger cavity, which opens more possibilities in molecular recognition processes. Similarly to **CB[7]**, **CB[8]** can bind to positively charged guests such as adamantane or methyl viologen (**MV**²⁺) derivatives,^{66,67,68} by inducing mainly ion-dipole interactions with the guests. However, the striking recognition property of **CB[8]** with respect to **CB[7]** (279 Å³) is that it is capable of encapsulating two aromatic guests simultaneously into its larger cavity (479 Å³) to form a 1:2 host-guest complex. As an example, the 2,6-*bis*(4,5-dihydro-1H-imidazol-2-yl)naphthalene, even from a 1:1 mixture with **CB[8]**, leads to a 1:2 stoichiometry host-guest species. As depicted in the X-ray crystal structure in Figure 10, the naphthalene moieties are encapsulated inside the **CB[8]** cavity (hydrophobic interactions), while the terminal protonated dihydro-imidazolium rings are forming hydrogen bonds with the two carbonyl portals of **CB[8]** (Figure 6).²⁶

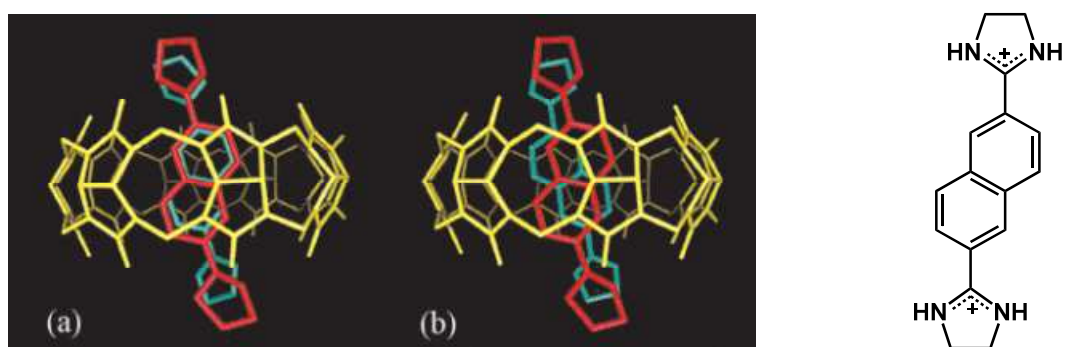


Figure 10. X-ray crystal structure of two 2,6-*bis*(4,5-dihydro-1H-imidazol-2-yl)naphthalene guests with **CB[8]** complex. (a) *syn* conformation and (b) *anti* conformation. Figure taken from ref. 26 (Kim *et al.* 2000).

CB[8] can also bind two different guests, such as methyl viologen (**MV**²⁺)⁶⁹ and 2,6-dihydroxynaphthalene (**DNP**), to form a 1:1:1 hetero host/guest complex. In addition to the

classical non-covalent interactions described for the host-guest chemistry of **CB[n]**, strong charge-transfer (CT) interactions take place between the electron-deficient **MV²⁺** guests and the electron-rich unit (**HN**) within the **CB[8]** cavity and constitute an additional driving force of the recognition process.⁷⁰ For instance, the **MV²⁺•DNP⊂CB[8]** displays a CT absorption band centred at 580 nm that is red-shifted ($\Delta\lambda = 120$ nm) and increased by comparison with the CT complex **MV²⁺•DNP** in the absence of **CB[8]**. Strong fluorescence quenching of **DNP** was also observed upon formation of the CT complex in the **CB[8]** cavity (Figure 7).^{27,70}

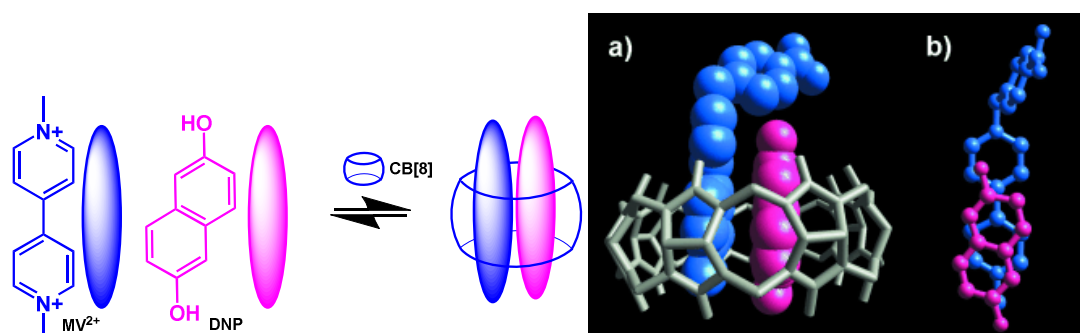


Figure 11. Schematic representation of the host-guest complex involving CT interactions and X-ray crystal structure (a) **MV²⁺•DNP⊂CB[8]** and (b) **MV²⁺•DNP**. Figure (right) taken from ref. 70 (Kim *et al.* 2001).

These properties were advantageously used to prepare self-assembled charge-transfer (CT) complexes between donor-acceptor thread-like compounds incorporating viologen (**V²⁺**) units and 1,5-dihydroxynaphthalene (**DNP**) stations and cucurbit[8]uril (**CB[8]**).⁷¹ Binding and characterization studies show the formation of 1:1 and 2:1 complexes between **CB[8]** and a thread-like compound containing two viologen units, while only a 1:1 inclusion complex was observed between **CB[8]** and a thread-like compound containing only a single viologen unit. The switching behaviour of the threads within their pseudorotaxane frameworks was investigated as well (Figure 12).

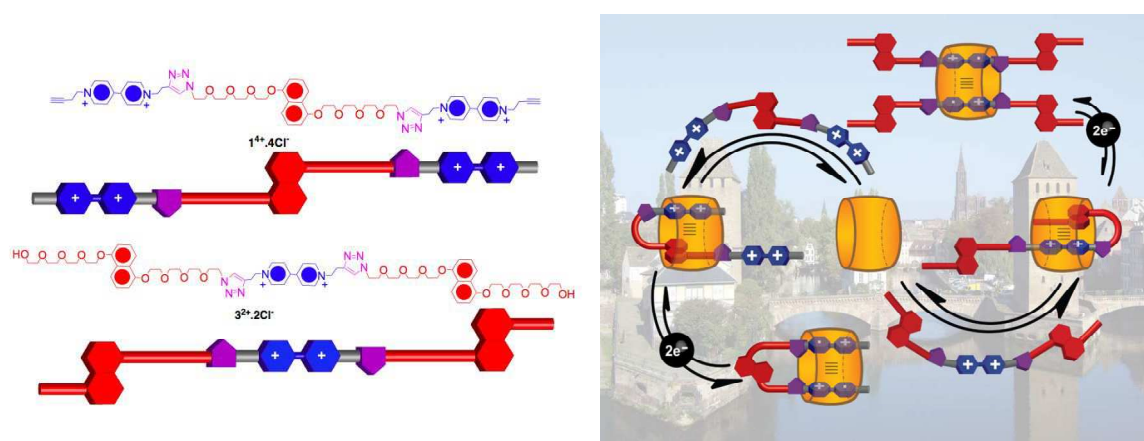


Figure 12. Schematic representation of two thread-like compounds incorporating viologen (**V²⁺**) units and 1,5-dihydroxynaphthalene (**DNP**) stations and their host-guest complexes with **CB[8]**. Figures taken from ref. 71 (Trabolsi *et al.* 2009).

1.4.2. Viologens

Substituted viologens V^{2+} are a class of compounds that contain the dicationic 1,1'-dialkyl-4,4'-bipyridinium (**BIPY** $^{2+}$) core (Figure 13), formed by diquaternization of 4,4'-bipyridine.⁷² It is indeed known since a long time that diquaternization of 4,4'-bipyridine can lead to dialkylated bipyridinium with valuable redox properties. In 1881, A. F. Hofmann prepared the first dibenzyl-bipyridinium diiodide by condensing two pyridinium with sodium amalgam and successive oxidation.⁷³ 40 years later, O. Dimroth and collaborators improved the synthesis of 4,4'-bipyridine and performed a direct diquaternization on it.⁷⁴ Later on, in 1933, L. Michaelis noticed that the one electron reduction of 1,1'-dimethyl-4,4'-bipyridinium (**MV** $^{2+}$) led a marked violet colour in solution.^{72,75}

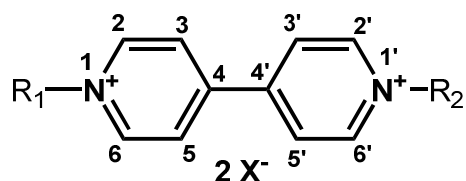


Figure 13. Chemical structure of a viologen dication, R_1 , R_2 = alkyl or aryl groups, X^- = counter anion.

Since then, 1,1'-dimethyl-4,4'-bipyridinium (**MV** $^{2+}$), the prototype viologen, is known as methyl viologen or paraquat, while the other simple (un)symmetrical bipyridinium analogues are referred as substituted viologens.⁶² In contrast to the colourless **BIPY** $^{2+}$ dications, the stable viologen radical monocations **BIPY** $^{\bullet+}$ are intensely blue.⁷¹ Their high molar absorption coefficients result from charge transfer between the two nitrogen atoms, which carry formal charges of +1 and 0, respectively (Figure 14).⁷⁷ Furthermore, **BIPY** $^{\bullet+}$ radical cations spontaneously dimerize⁷⁸ to give the (**BIPY** $^{\bullet+}$)₂ dimer in aqueous solution in a process driven by radical-radical interactions that favour the formation of the singlet state (strong absorption of the UV-visible-NIR domain of the solar spectrum, Figure 15).⁷⁷⁻⁷⁹

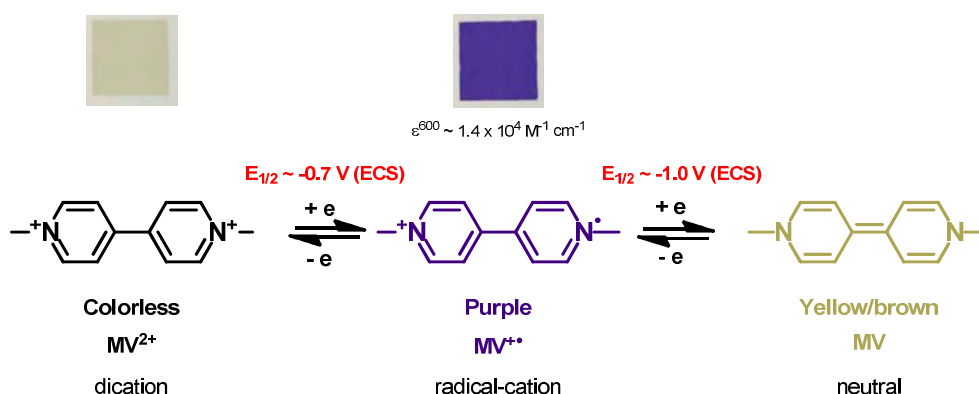


Figure 14. The three common redox states of viologens and their physico-chemical properties. The bipyridinium dication is the most stable. The first reduction process is reversible and can be cycled many times without fatigue of the device. The second one is usually a non-reversible electrochemical process that produces an insoluble yellow neutral species (**MV**⁰).

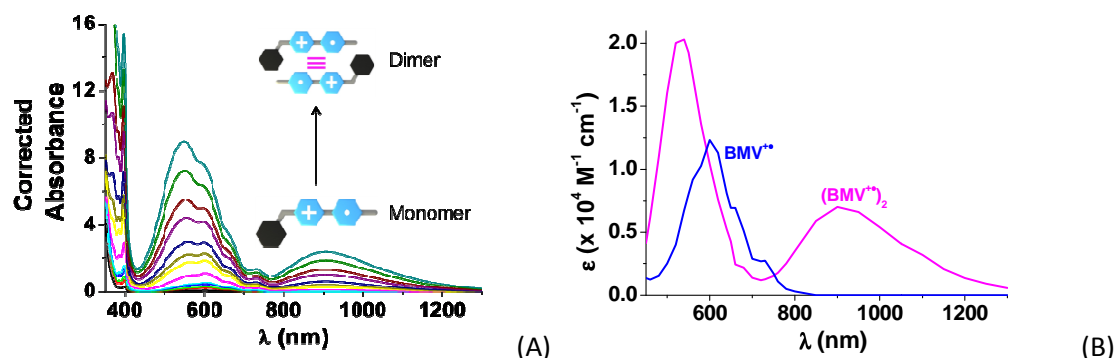


Figure 15. Spectrophotometric (absorption) (A) and electronic spectra (B) of benzyl-methyl-viologen BMV^{2+} under its monoradical monocationic state. Solvent: phosphate buffer at pH 7 (0.1 M $\text{Na}_2\text{HPO}_4/\text{NaH}_2\text{PO}_4$). For $10^{-5} \text{ M} \leq [\text{BMV}^{2+}]_0 < 10^{-4} \text{ M}$; $l = 1 \text{ cm}$; For $2 \times 10^{-4} \text{ M} \leq [\text{BMV}^{2+}]_0 < 10^{-3} \text{ M}$; $l = 0,2 \text{ cm}$; $T = 25,0(1) \text{ }^\circ\text{C}$. (Results obtained in the frame of this PhD work).

This phenomenon, which is also known as π -dimerization or pimerization, has been used to generate translation and rotation in mechanically interlocked molecules.⁸⁰ In addition, 4,4'-bipyridinium group has one single nitrogen atoms per ring and reveals a rotational degree of freedom along their connecting C-C axis. Therefore, the two pyridine rings are not always coplanar. These compounds therefore display a rich redox chemistry and exhibit many physico-chemical properties that make them attractive for use in electrochromic,^{81,82} catalytic,⁸³ or bioanalytical systems.⁸⁴ More precisely, electrochromic compounds are capable of reversibly change their optical properties upon a redox process.⁸⁵⁻⁸⁷ Generally, in the visible region, where the redox active compound absorbs light, an electrochromic compound can be switched between a transparent state and a colored state.^{88,89} This phenomenon give possibility to used for building flexible electrochromic displays (ECD).⁹⁰⁻⁹⁴ Commercial and research interests particularly focus on inorganic^{95,96} and/or organic⁹⁷⁻⁹⁹ molecules exhibiting electrochromism throughout the visible-NIR spectrum.

1.4.3. CB[n]-Viologen Complexes

In 2002, A. E. Kaifer, K. Kim and their co-workers described for the first time the interaction of MV^{2+} with cucurbit[n]uril hosts such as **CB[7]** and **CB[8]**.^{48,49,67} With **CB[8]**, it was found that the substrate strongly binds inside the macrocycle cavity, the major driving force being ion-dipole interactions between the positively charged viologen and the oxygen rich host portals atoms. Although the size of the **CB[8]** cavity was large enough to welcome two viologen units, the 1:2 ($(\text{MV}^{2+})_2 \subset \text{CB[8]}$) was not observed. Electrostatic repulsions between the two positively charged viologen prevent the formation of such an inclusion complex.⁶⁷ **CB[8]** exclusively forms a 1:1 species ($\text{MV}^{2+} \subset \text{CB[8]}$) in water with a rather large stability constant of $1.1 \times 10^5 \text{ M}^{-1}$. By contrast, the one electron reduction of methyl viologen MV^{2+} allowed the formation of a bisradical species ($(\text{MV}^{\bullet+})_2 \subset \text{CB[8]}$). The dimerization constant of the $\text{MV}^{\bullet+}$ in the presence of the **CB[8]** was estimated to be $\sim 2 \times 10^7 \text{ M}^{-1}$ which is about 10^5 times larger than $\text{MV}^{\bullet+}$ alone (Table 2).^{27,67}

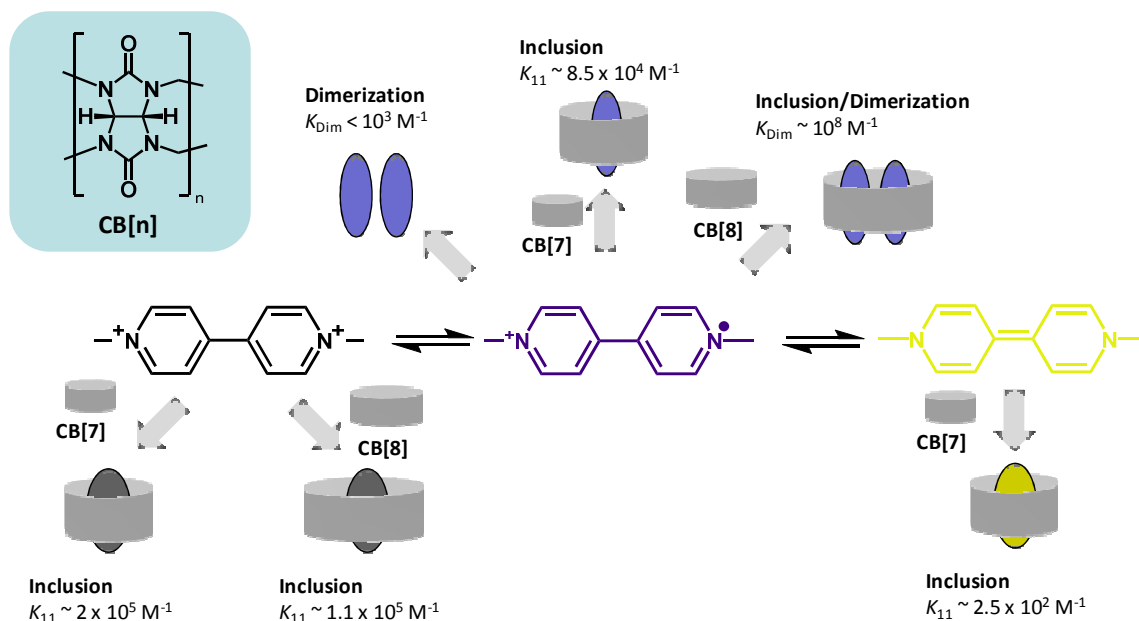


Figure 16. Schematic representation of host-guest recognition of 1,1'-dimethyl-4,4'-bipyridinium (MV^{2+}) with **CB[8]** and **CB[8]** under its different oxidation states.

Table 2. Thermodynamic and spectroscopic parameters of viologens radical cations under monomeric and dimeric states.

	Anion	$\log K_{Dim}$	λ^m (nm) ϵ^m ($10^4 \text{ M}^{-1} \text{ cm}^{-1}$)	λ^d (nm) ϵ^d ($\text{M}^{-1} \text{ cm}^{-1}$)	Ref.
$R = R' = \text{CH}_3$ $C_1C_1V^{•+}$ $(MV^{•+})$	Cl-	2.70 ^c	396 (4.2)/602 (1.37)	362 (5.0)/518 (2.1)	100,104
	nd	2.58 ^e	675 (0.38)/604 (1.69)/ 396 (3.49)	537 (3.24)/369 (8.97)	78
	nd	2.86 ^f			101
	CH_3SO_4^-	5.10 ^a	598 (1.37)/606 (1.37)	480/565/670	102 103
$C_1C_6V^{•+}$ $R = \text{CH}_3; R' = \text{C}_6\text{H}_{13}$	Cl-	2.75 ^c	nd	nd	100,104
$C_1C_7V^{•+}$ $R = \text{CH}_3; R' = \text{C}_7\text{H}_{15}$	Cl-	2.89	nd	nd	100
	Cl-	2.81			104
$C_1C_8V^{•+}$ $R = \text{CH}_3; R' = \text{C}_8\text{H}_{17}$	Cl-	2.93	396 (4.2)/602 (1.37)	362 (5.0)/518 (2.10)	100
	Cl-	2.89 ^c			104
$C_1C_9V^{•+}$ $R = \text{CH}_3; R' = \text{C}_9\text{H}_{19}$	Cl-	4.04 ^c	nd	nd	104
$C_1C_{10}V^{•+}$ $R = \text{CH}_3; R' = \text{C}_{10}\text{H}_{21}$	Cl-	4.86 ^c	nd	nd	104
$C_2C_2V^{•+}$ $R = R' = \text{C}_2\text{H}_5$	Br-	5.03 ^a	597 (1.22)	564 (0.890)	102
$C_3C_3V^{•+}$ $R = R' = \text{C}_3\text{H}_7$	Br-	4.68 ^a	597 (1.06)	550 (0.887)	102
$C_4C_4V^{•+}$ $R = R' = \text{C}_4\text{H}_9$	Cl-	2.74 ^c	nd	nd	104
$C_5C_5V^{•+}$ $R = R' = \text{C}_5\text{H}_{11}$	Br-	4.33 ^a	602 (1.04)	563 (0.869)	102
$C_6C_6V^{•+}$	Br-	3.85 ^a	600 (1.025)	558 (0.870)	102

$R = R' = C_6H_{13}$					
$C_7C_7V^{•+}$ $R = R' = C_7H_{15}$	Br-	3.85 ^a	571 (1.016)	515 (0.856)	102
	Br-	4.00 ^d	600 (1.38)	600 (0.4)	105
$C_8C_8V^{•+}$ $R = R' = C_8H_{17}$	Br-	3.29 ^a	548 (0.892)	504 (0.855)	102
	Br-	5.33 ^d	600 (1.38)	600 (0.4)	105
$BzBzV^{•+}$ (BBV ^{•+}) $R = R' = CH_2C_6H_6$	-	4.0	560 (1.72)/604 (1.22)	560 (1.7)/604 (2.44)	106
^a water, $I = 0$. ^b water, pH 7.0 (sodium phosphate buffer 0.1 M). ^c 0.1 KCl. ^d pH 8.1 (0.1 M tris/H ₂ SO ₄ buffer); ^e 1 M salt concentration; ^f pH 10.0 (glycine buffer 0.1 M); nd: not defined.					

Although MV^{2+} better fits into **CB[7]** cavity and consequently forms a very stable 1:1 host-guest complex (inclusion stability constant $\sim 2 \times 10^5 M^{-1}$), its cavity is not large enough to accommodate a dimer radical⁴⁹ as observed with **CB[8]**. The use of **CB[7]** macrocycle is indeed known to suppress $MV^{•+}$ dimerization by sequestering $MV^{•+}$ monomers. **CB[7]** exclusively forms 1:1 inclusion complexes in aqueous solution with the three different oxidation states of methyl viologen: $MV^{2+} \subset CB[7]$ and $MV^{•+} \subset CB[7]$ and $MV^0 \subset CB[7]$ (Figure 16).^{42,27} Typical binding constants K reported in a wide range of experimental conditions for the $MV^{•+} \subset CB[7]$ complex are in the range of $K_{11} = 10^4 - 10^6 M^{-1}$ and are usually larger than those associated with the dimerization of $MV^{•+}$ ($K_{Dim} \sim 10^2 - 10^5 M^{-1}$). This comparison indicates that the inclusion process of the radical cations is thermodynamically favourable enough to prevent dimerization.¹⁰⁷ In terms of structural behaviour, the $MV^{2+} \subset CB[7]$ and $MV^{•+} \subset CB[7]$ can be considered as [2]pseudorotaxane in which the bipyridinium or the monoradical monocation moieties reside inside the **CB[7]** cavity and the two methyl groups are located outside (*i.e.* the strong binding can be explained by a combination of ion-dipole and hydrophobic interactions).⁴⁸

1.5. Aims of this Work

1.5.1. Host-Guest Recognition Properties of Multimeric Viologen Threads

This work has been mainly focused on the synthesis and physico-chemical characterizations of host guest complexes using several viologen based systems (monomeric or multimeric viologen-based derivatives) and cucurbituril macrocycles (*i.e.* **CB[7]** and **CB[8]**). The use of synthetic receptors that have both a high affinity and a high selectivity for the binding of guests in water is a very interesting prospect.¹⁰⁸⁻¹¹¹ The recognition properties were analyzed using a set of complementary analytical methods such as UV-visible absorption spectrophotometry, ¹H-NMR, electrochemistry, EPR and ESMS. The host-guest stability constants as well as the stoichiometric ratios with **CB[7]** and **CB[8]** of the oxidized and the one-electron reduced forms of a large series of viologen-based systems were evaluated and discussed. In the absence of cucurbit[n]uril, the pimerization properties of these latter systems were also examined. In the presence of cucurbit[n]uril, particular attention was paid on the competition between dimerisation and inclusion, the objective being to develop multivalent systems which favour inter or intramolecular dimerisation of the monoradical cations over inclusion with cucurbituril. The redox properties of these systems confer them interesting behaviour and high potential for designing new nanometric

mechanical or electrochemical tools. Thanks to these new properties, molecular switches and/or electrochromic materials were developed. This work, which is described in the following sections, has been mainly done in close collaboration with the group of Pr Ali Trabolsi (NYUAD, Abu Dhabi, UAE).

A first system that has been considered consists of a hexaviologen dendritic like system (noted HV^{12+} , Figure 17) which takes advantage of the properties of a phosphazene anchor. Six terminal BIPY^{2+} units were homogeneously distributed along the periphery of a cyclotriphosphazene (noted CTP). Interestingly, CTP moieties exhibit excellent thermal and chemical stabilities and are photochemically and electrochemically inert. As a consequence, they do not interfere with the photophysical and electrochemical properties centred on the grafted redox active viologens. The easiness of CTP rings functionalization coupled to the structural rigidity of the products make CTP an attractive core for the development of multifunctional and robust systems. In combination with $\text{CB}[7]$, we were able to characterize and quantify a stable [7]pseudorotaxane. Upon one electron reduction of each of the viologen subunits, decomplexation of the $\text{CB}[7]$ macrocycles occurs as a result of strong pimerization of a pair of viologen monoradical cations. This process is fully reversible and processes without fatigue as demonstrated by cyclic voltammetry. Model ligands (BV^{4+} and BMV^{2+}) were also employed to assess the critical role of the core on the recognition and dimerization processes.

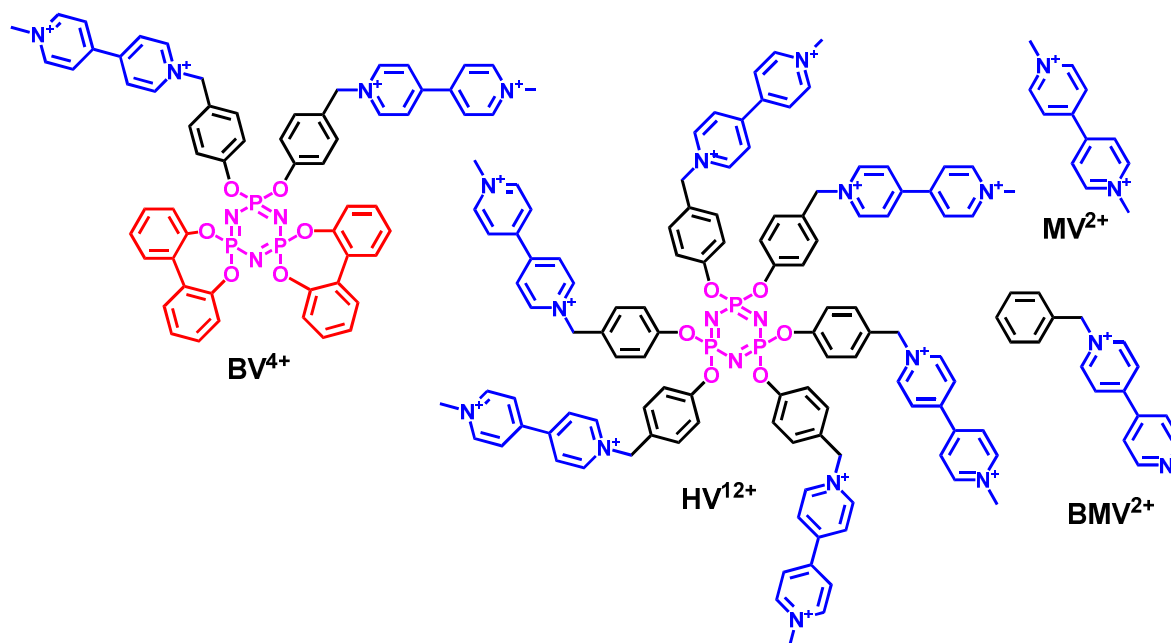


Figure 17. Chemical structures of a hexameric viologen-based system HV^{12+} and its models BMV^{2+} , BV^{4+} and MV^{2+} .

Alternatively, we have also considered a circular trimeric system composed of a benzenic core which is extended on its 1, 3 and 5 positions by terminal viologen subunits (Figure 18). The recognition properties of $\text{CB}[7]$ and $\text{CB}[8]$ have been also thoroughly investigated. Interestingly, the presence of three redox active centres within the molecule strongly favours the dimerization process with respect to recognition and increases by several orders

of magnitude the so-called “dimerization” constant. This innovative strategy demonstrates that intermolecular interactions can also be used to enhance the stability of radical dimers in solution thank to a peculiar design and to a multicenter approach.

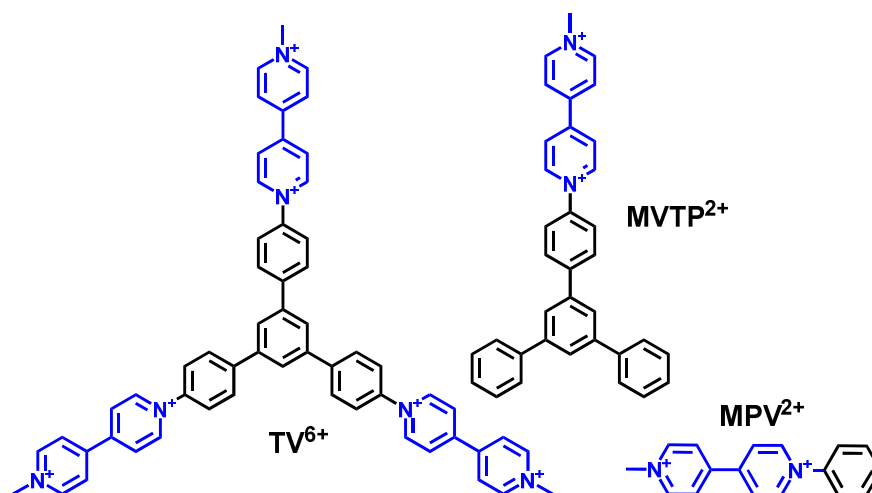


Figure 18. Chemical structures of a trimeric viologen-based system **TV⁶⁺** and its reference compounds **MVTP²⁺** and **MPV²⁺**.

For these last systems, we used the peculiar calix[4]arene properties (structural and geometrical) to introduce face to face at a suitable distance two terminal viologen units. The length of the spacers separating the platform calix[4]arene from the viologen moieties was varied. Two calix[4]arene systems, namely **C23⁴⁺** and **C24⁴⁺**, (2 stands for the number of viologens and 3-4 correspond to the number of carbons of the chain connecting the viologens to the macrocyclic core, Figure 19) have been synthesized and led to [3]pseudorotaxanes in combination with either **CB[7]** or **CB[8]**. These [3]pseudorotaxanes spontaneously dissociate on reduction of the bipyridiniums as the result of a strong intramolecular dimerization of the two face-to-face viologen radical cations. Decomplexation and dimerization do not occur in experiments involving **CB[7]** (or **CB[8]**) and either of the two monomeric viologen models **MC3²⁺** and **MC4²⁺**, which were taken as the corresponding models.

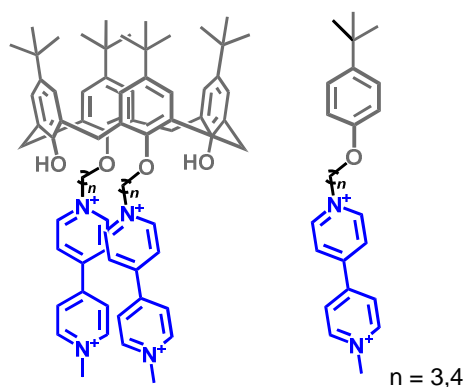


Figure 19. Chemical structures of the calixarene viologen-based systems **C23⁴⁺** and **C24⁴⁺** and the reference compounds **MC3²⁺** and **MC4⁴⁺**. The number 2 stands for the number of viologens and 3-4 correspond to the number of carbons of the chain connecting the viologens to the macrocyclic core

1.5.2. Azo-Aryl-Imidazole/Zn(II) metalloporphyrins Host/Guest Chemistry – Toward a Photochemical Control of the Inclusion/Dissociation Processes

This second and last project was done in close collaboration with the groups of Dr Jean Weiss (UMR 7177, CNRS-UdS, Strasbourg) and Pr Ali Trabolsi (NYUAD, Abu Dhabi, UAE) and was focused on the synthesis of new azo-imidazole substrates and the physico-chemical characterization of their pentacoordinated complexes with phenanthroline strapped porphyrins (Figure 20). A series of azo-imidazoles whose bulkiness of the aromatic moiety was varied have been considered. The aim of this study was to use the valuable properties of the azobenzene (*trans-to-cis* isomerization induced by light – so called “photoejection” process) to induce dissociation of the pentacoordinated systems (Figure 21). Thermal re-equilibration is expected to reinstate the pentacoordinated complexes. As a preliminary step toward this goal, spectroscopic, thermodynamic and kinetic aspects of the recognition processes leading to the pentacoordinated porphyrinic complexes with these azo-imidazoles substrates have been thoroughly studied (absorption/emission spectrophotometries, stopped-flow measurements, electrochemistry...) in this work. I will first recall in the following section the physico-chemical and spectroscopic properties of Zn(II) metalloporphyrins.

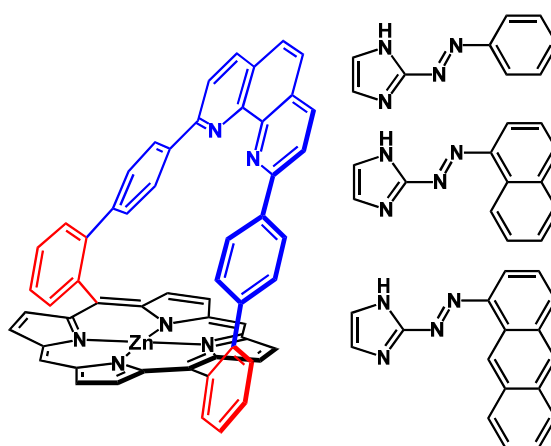


Figure 20. Chemical structures of the strapped Zn(II) porphyrin receptor and the azo-aryl-imidazole substrates examined in this work.

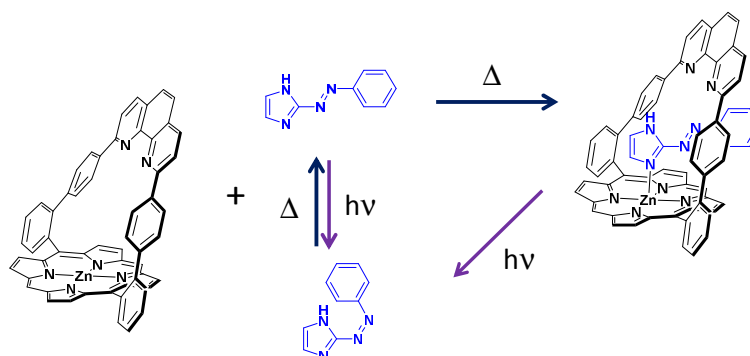


Figure 21. Principle of the “photoejection” of the azo-imidazole upon light excitation due to *trans-to-cis* isomerization of the substrate.

1.5.3. Zn(II) Metalloporphyrins

Porphyrins, which are aromatic tetrapyrrolic macrocycles (Figure 22a), are one of the most common and versatile chromophores in living systems and artificial mimics. These molecular building blocks induce peculiar photochemical and redox properties to the assembled architectures in which they partake. In a free form, these porphyrinic macrocycles (also called "free bases") behave either as acids or dibases^{112,113} and can be metallated (called metalloporphyrins) with almost all the metal ions (Figure 22b). Porphyrins can also be partially reduced and thus successively lead to chlorins (reduction of one double bond, Figure 22c) or (iso)bacteriochlorines (two double bonds are hydrogenated, Figure 22d,e). These compounds (from the Greek: porphyrá = purple) were named Porphyrin as a result of their intense purple colour. Porphyrins can also display a red colour such as in blood (heme) or green colour such as in leaves (chlorophyll).

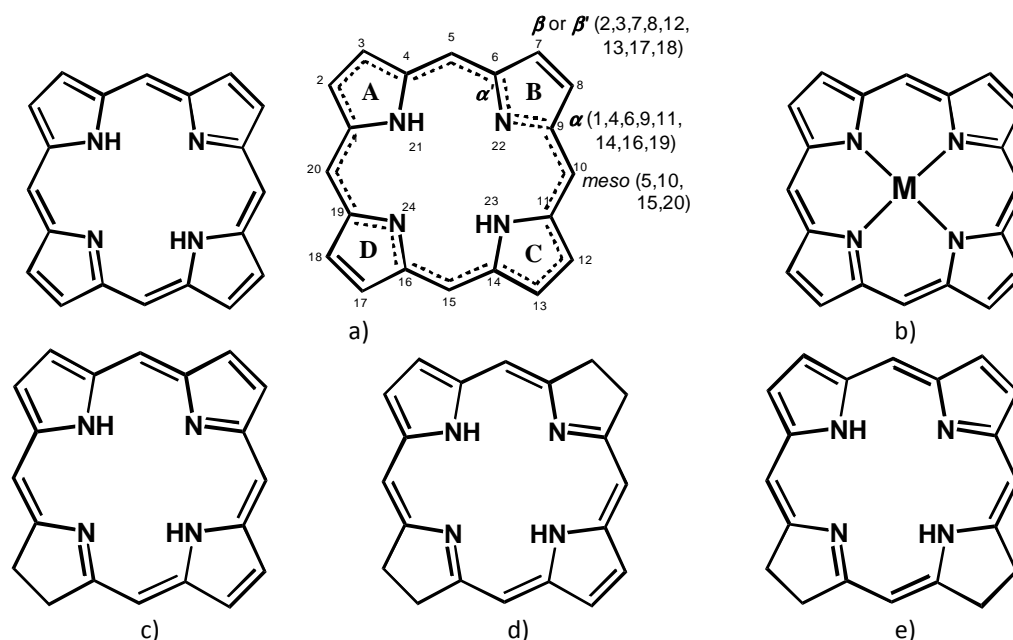


Figure 22. Chemical Structures of a) free-base porphyrin (numbering according to the IUPAC system representation of the 18 aromatic π electrons system), b) metalloporphyrin, c) chlorine d), bacteriochlorine and e) isobacteriochlorine.

Porphyrin is then the simplest representative of the broad porphyrin family (Figure 22) and consists of four pyrrolic units connected together by methine bridges. Two of the four nitrogen atoms are of pyrrole type with a lone pair of electrons pointing toward the macrocyclic cavity. The chromophore is then a highly conjugated system with twenty two π electrons whose eighteen (*i.e.* $4n + 2$, $n = 4$, Hückel Rule) contribute to the aromaticity of the macrocyclic system (Figure 22). The *meso*- and β -positions correspond to the most frequent and easiest functionalization sites (Figure 1). In addition, porphyrins offer a wide range of valuable features such as a rigid and planar geometry, a high stability, an intense absorption in the UV-visible region, fluorescence emission properties, and a small HOMO-LUMO energy gap. Metalloporphyrins display other physico-chemical properties that are at the origin of various fundamental biological processes.¹¹⁴ They are commonly associated with proteins

and act as cofactors. They are involved in substrates recognition (*e.g.* hemoglobin, myoglobin), electron transfer (*e.g.* cytochromes) or energy transfer (photosynthesis, Figure 23).¹¹⁴

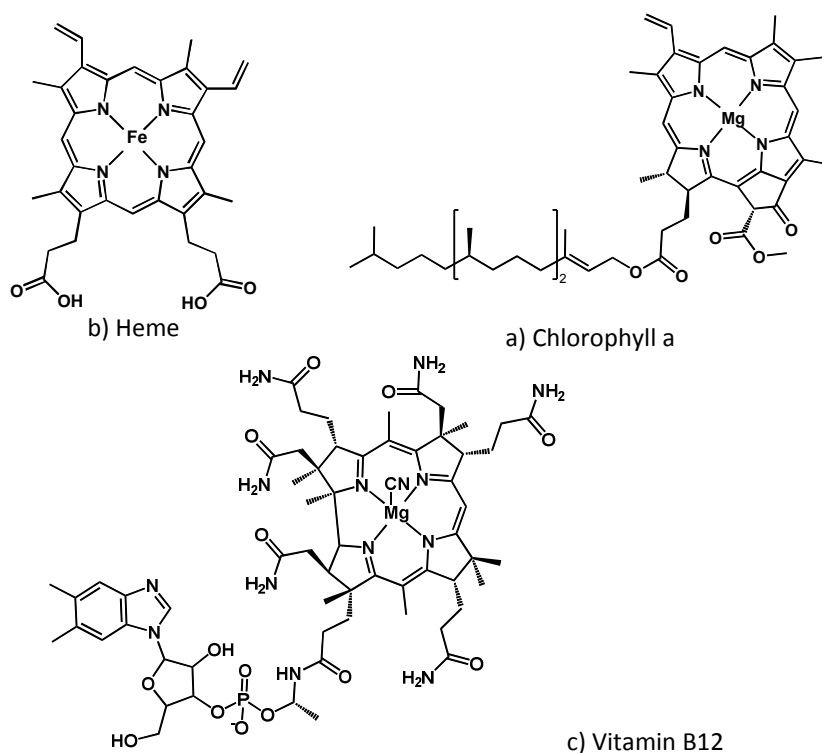


Figure 23. Examples of natural tetrapyrrolic macrocycles. a) heme b, cofactor of protein such as hemoglobin, b) chlorophyll a, pigment involved in the photosynthesis process, c) vitamin B12, cofactor of enzymes involved in the nucleic acids metabolism.

Due to their intrinsic properties and their easiness of functionalization, porphyrins and metalloporphyrins have been (and are still) widely applied in different areas of chemistry.¹¹⁵ They have led to the design of biomimetic systems²¹¹⁶⁻¹²¹ (*e.g.* artificial antenna systems¹²² or photosynthetic centre mimics¹²³) and new molecules for therapeutic purposes such as in oncology (photodynamic therapy¹²⁴⁻¹²⁷). Furthermore, the photochemical properties of these (metallo)porphyrin macrocycles have been advantageously employed for the development of photoactive materials (*e.g.* dyads,¹²⁸ triads,¹²⁹ polymers for electronic and/or photonic conduction¹³⁰⁻¹³² gates and redox switches¹³³ and the fabrication of smart devices and molecular machines.¹³⁴ The Zn(II) metalloporphyrins have often been considered in combination with nitrogen-based substrates (pyridine, imidazole) because the Zn-N coordination bond allows stabilizing the targeted complexes and induces a significant exchange rate of the exogenous molecule essential for the development of dynamic systems.¹³⁵ In addition, the long lived (ns) excited state¹³⁶⁻¹³⁸ of zinc(II) porphyrins provides to the final building interesting photophysical properties. This Zn-N coordination ($200 - 400 \text{ kJ mol}^{-1}$) usually gives rise to complexes whose stability constants (K) varies from 10^2 to 10^5 M^{-1} depending on the nature of the substrate and experimental conditions.

1.5.3a. Absorption Properties of (Metallo)Porphyrins

Absorption spectra of porphyrinic systems usually display two characteristic absorption bands¹³⁹⁻¹⁴². As an example, the absorption spectra of the free base tetraphenylporphyrin (noted **H₂TPP**) and the Zn(II) tetraphenylporphyrin (noted **ZnTPP**) (Figure 24) show an intense absorption ($\epsilon \geq 10^5 \text{ M}^{-1} \text{ cm}^{-1}$) between 380 nm and 420 nm (Soret band or B band or γ band in natural systems) that vanishes upon alteration of the aromaticity of the molecule. Additionally, a set of absorption bands (Q bands responsible for the colour of the porphyrins) of lower intensities ($\epsilon \sim 10^4 \text{ M}^{-1} \text{ cm}^{-1}$) can be observed in the visible region (between 500 nm and 700 nm). The free base porphyrins (D_{2h} symmetry) are usually characterized by a set of four to five Q absorptions (Q_x and Q_y), while the metalloporphyrins of higher symmetry (D_{4h} symmetry) display only one to two Q absorptions (Q_x).

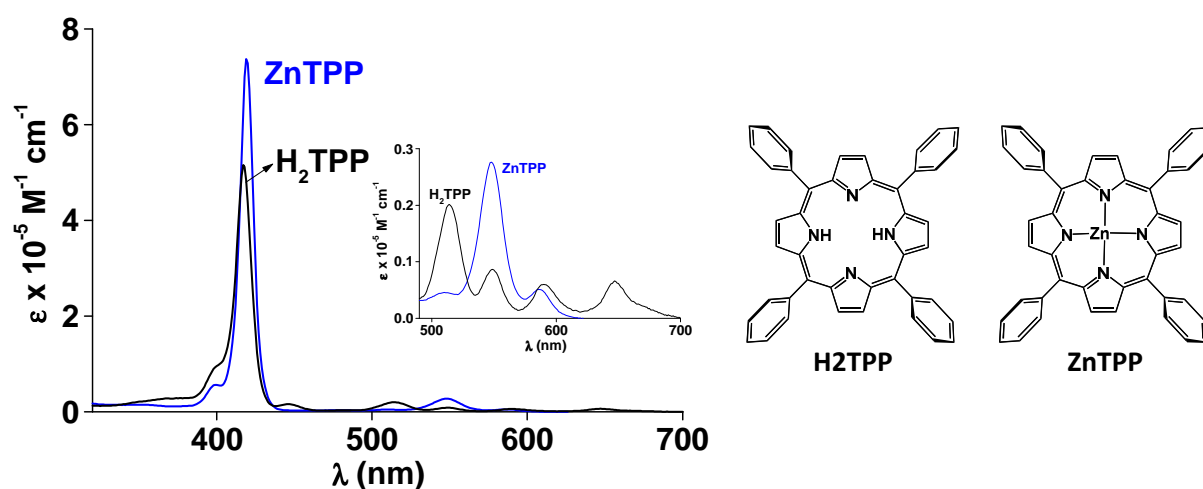


Figure 24. Electronic spectra **H₂TPP** and **ZnTPP**. Solvent: 1,2-dichloroethane; $T = 25.0 \text{ }^\circ \text{C}$.

Table 3 depicts the two labelling systems (Fischer-Stern and Platt-Gouterman systems) used to describe the absorption bands of UV-visible absorption spectra of free base and metallated porphyrins.^{143,144}

Table 3. Nomenclature of the UV-visible absorption of porphyrins.

	Free Base Porphyrin		Metalloporphyrin	
Symmetry	D _{2h}		D _{4h}	
Classification	Fischer-Stern	Platt-Gouterman	Fischer-Stern	Platt-Gouterman
Absorption band	Soret	B	Soret (γ)	B
	IV	Q _{y(0-1)}	α	Q ₍₀₋₁₎
	III	Q _{y(0-0)}		
	II	Q _{x(0-1)}	β	Q ₍₀₋₀₎
	I	Q _{x(0-0)}		

1.5.3b. Photophysical Properties of (Metallo)Porphyrins

The free base and Zn(II) porphyrins are usually characterized by two broad luminescence emissions. The $S_2 \rightarrow S_0$ transitions are usually centred between 400 nm and 500 nm, while those of $S_1 \rightarrow S_0$ transitions are lying between 550 and 800 nm. Figure 25 depicts the absorption and emission spectra of **H2TPP** and **ZnTPP** in benzene. A. Zewail and his colleagues^{145,146} have thoroughly described the photophysical properties of these two porphyrins using ultrafast laser spectroscopy (fs) and evaluated the dynamics of the main radiative and non-radiative desexcitation routes (Figure 26) resulting from photo-excitation of these two chromophores at 397 nm (B band).

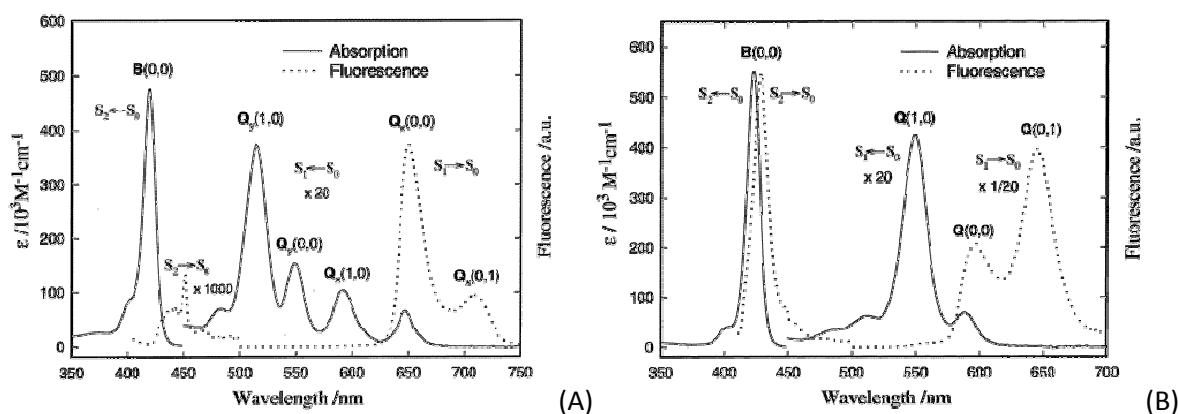


Figure 25. Absorption (—) and emission (···) spectra of (A) **H2TPP** and (B) **ZnTPP**. Solvent: benzene, $\lambda_{\text{exc}} = 397$ nm (B band).

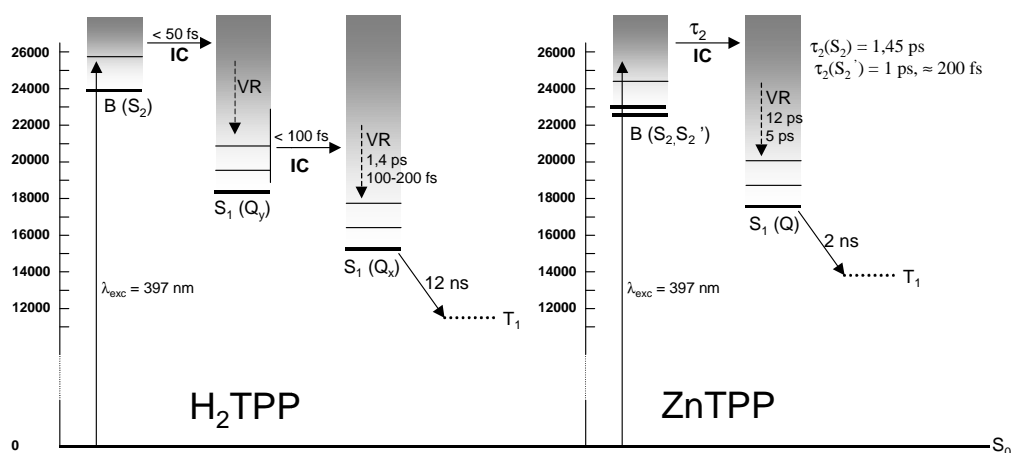


Figure 26. Schematic diagrams of the dynamics of energetic relaxation of **H2TPP** et **ZnTPP**. IC : internal conversion ; VR : vibrational relaxation.

1.5.3c. The Azobenzene System

The azo compounds are known since the mid of XIX century (A. Noble, 1856)¹⁴⁷ and have been mainly used as synthetic colouring agents in the dye industry for a very long period.¹⁴⁸ A broad range of azo derivatives have been developed with the aim of varying the colour of applicable robust and cheap dyes. The structural variations of azo-benzene dye such as the number of azo moieties, the nature of the aromatic ring (*e.g.* benzene, naphthalene) or the

nature, position and number of various substituents have been therefore extensively investigated.¹⁴⁹

More than 80 years after, G. S. Hartley first reported, isolated and characterized in 1937 the *cis*-conformer of azo-benzene after evidencing a lack of reproducibility in absorbance measurements of an azo-benzene solution that was exposed to sunlight.¹⁵⁰ Since then, significant achievements have made such as photo-switches.¹⁵¹⁻¹⁵⁶

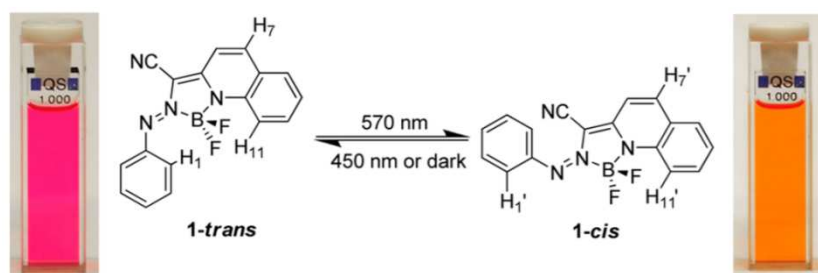


Figure 27. A visible light-induced *trans* to *cis* isomerization of a bodipy chromophore containing a photoactive azo-benzene unit. Figures taken from ref. 157 (Yang *et al.*, 2012).

Trans-azobenzene displays a weak $n-\pi^*$ band centred at ~ 440 nm and strong $\pi-\pi^*$ transitions at ~ 320 nm. *Cis*-azo-benzene is characterized by a more intense $n-\pi^*$ absorption at same energies but a less intense $\pi-\pi^*$ transitions that are hypsochromically shifted to 250 nm - 280 nm. The *trans* conformation is nearly planar (dipole moment ~ 0 ,^{155,158} while the *cis*-conformer adopts a bent conformation with its phenyl rings twisted of about 55° out of the plane from the azo group (dipole moment ~ 3 Debye). The *trans*-isomer is ~ 10 -12 kcal/mol more stable than the *cis*- so that the *trans*-derivative predominates ($> 99.99\%$) in the absence of light input.^{151,159} A substantial amount of the *cis* isomer can be produced by irradiation with 340 nm light. This light-induced isomerization is efficient ($\Phi_{tc} \sim 0.1$) and proceeds with minimal photo-bleaching.¹⁵² The *trans*-isomer is regenerated either by thermal re-equilibration or by photo-irradiation at 450 nm ($\Phi_{ct} \sim 0.45$). The end-to-end distance of each isomer is also different and amounts to ~ 3.5 Å for the two carbons at the para-positions.¹⁵⁵

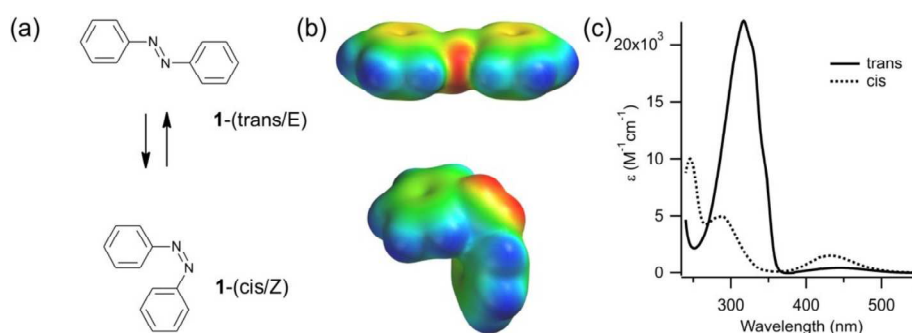


Figure 28. a) Chemical structures of the *trans*- and *cis*-isomers of azo-benzene. B) Space-filling models are coloured by electrostatic potential (red-negative to blue-positive). c) Electronic absorption spectra of the *trans*- and *cis*-isomers of azo-benzene in ethanol. Taken from ref. 160 (Beharry, 2012)

1.5.4. Aims of this Work

Inspired by the strong binding of nitrogen-based substrate by zinc porphyrins as a powerful assembling tool, my hosting group has evidenced, in collaboration with the group of Dr Jean Weiss (UMR 7177, CNRS-UdS, Strasbourg), a selective recognition of imidazoles (Figure 20)^{128,161-163} by phenanthroline super-structured porphyrins. A careful ligand design based on the induced-fit principle led to the selective and strong recognition of various imidazoles, whose bulkiness has been varied, by receptors that differ by the nature of substitution in the *meso*-positions (Figure 29). The selective distal imidazole recognition results from a strong *N*-imidazolyl-Zn(II) axial coordination¹⁶⁴⁻¹⁶⁷ and bifurcated hydrogen bonds between the substrate and the nitrogen atoms of the 1,10-phenanthroline strap of the receptor. Moreover, introduction of secondary interactions (π - π stacking, CH- π , hydrophobic interactions) also contributed to strengthen the final assemblies. This self-assembly approach was successfully implemented in photodyads^{163,168} and linear porphyrin arrays.¹²⁹

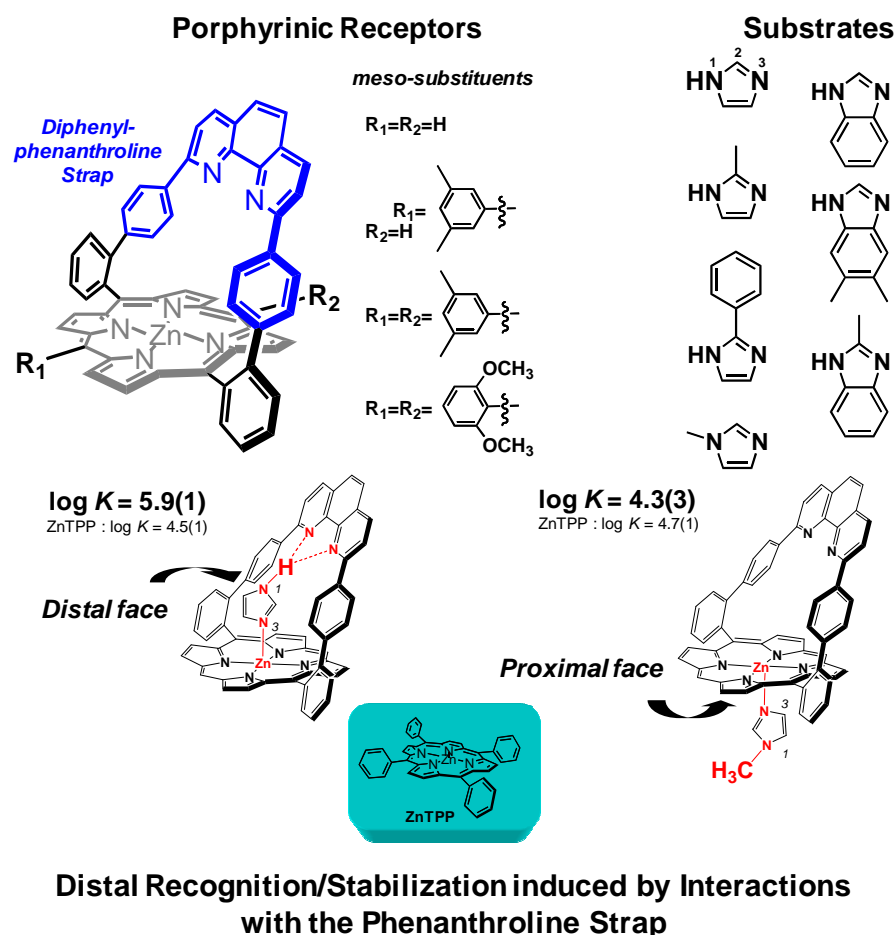


Figure 29. Chemical structures of the phenanthroline strap metalloporphyrins and of the substrate previously investigated in my hosting group. Distal *versus* proximal recognition of substrates controlled by the *N*-substitution of the imidazole.

My PhD work has been mainly focused on the physico-chemical understanding of the recognition properties of novel azo-aryl-imidazole substrates (synthesized by the group of Pr

Ali Trabolsi, NYUAD, Abu Dhabi, UAE) by the phenanthroline strapped zinc(II) porphyrins previously described. The presence of the phenanthroline strap differentiates the two faces of the porphyrin macrocycle and the axial coordination of the substrates is herein also expected to occur on the "distal" (most hindered face)^{128,162} for most of the substrates thanks to secondary non-covalent interactions. The recognition properties of a homogeneous series of new imidazoles substrates displaying an azo-aryl substituent have been studied using absorption and emission spectrophotometries. The formation mechanism has been elucidated using fast kinetic techniques. The effect of the bulkiness of these substrates (*i.e.* aryl = benzene → naphthalene → anthracene) has been evaluated. The influence of the phenanthroline strap and of the *meso*-substituents of the Zn(II) receptors have been also considered. The objective of this preliminary work was to develop supramolecular devices that can undergo ejection of the coordinated imidazole (*i.e.* steric hindrance between the receptor and the photo-generated *cis*-conformers) upon light stimulus (*i.e.* photoejection) thank to isomerization of the azobenzene unit. The Chemical structures of novel azo-aryl-imidazoles substrates as well as valuable models and of the investigated Zn(II) porphyrinic receptors are given in the Figure 30.

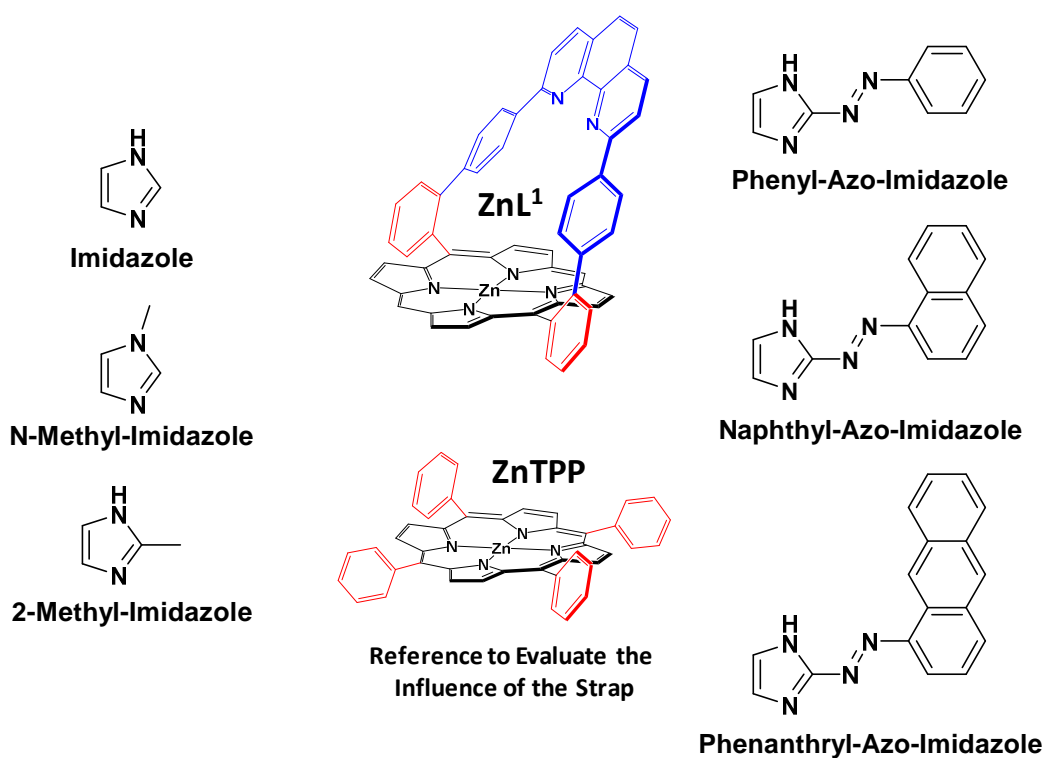


Figure 30. Chemical structures of the Zn(II) metalloporphyrins and imidazole substrates examined on this work.

Bibliographic Section

- 1 Lehn, J. M. *Pure. Appl. Chem.* **1978**, *50*, 871-892.
- 2 Steed, J. W.; Atwood, J. L. *Supramolecular chemistry*; John Wiley: Chichester; New York, **2000**.
- 3 Tian, J. *Annu. Rep. Prog.Chem Sect. B.* **2012**, *108*, 171-185.
- 4 a) Vögtle, F. *Supramolecular Chemistry*, John Wiley & Sons, New York, **1991**. b) *Comprehensive Supramolecular Chemistry*, Atwood, J. L.; Davies, J. E. D.; MacNicol, D. D.; Vögtle, F., Lehn, J. M., Eds., Pergamon, Oxford, **1996**.
- 5 http://chem.rutgers.edu/sites/default/files/coursefiles/Courses_f09/310/Host-Guest-Chemistry_I_Part_1.pdf
- 6 Koshland, D. E. *Angew. Chem., Int. Ed. Engl.* **1994**, *33*, 2375-2378.
- 7 Zhang, X. X.; Bradshaw, J. S.; Izatt, R. M. *Chem. Rev.* **1997**, *97*, 3313-3362.
- 8 Oshovsky, G. V.; Reinhoudt, D. N., Verboom, W. *Angew. Chem. Int. Ed.* **2007**, *46*, 2366–2393.
- 9 Robertazzi, A.; Krull, F.; Knapp, E.-W.; Gamez, P. *CrystEngComm*, **2011**, *13*, 3293-3300.
- 10 Gellman, S. H. *Chem. Rev.* **1997**, *97*, 1231-1232.
- 11 Lehn, J. M. *Angew. Chem. Int. Ed.* **1988**, *27*, 89-112.
- 12 Steed, J. W.; Turner, D. R.; Wallace, K. J. *Core concepts in supramolecular chemistry and nanochemistry*, John Wiley, Chichester, **2007**.
- 13 Anslyn, E. V.; Dougherty, D. A. *Modern physical organic chemistry*, University Science, Sausalito, CA, **2006**.
- 14 Schneider, H.-J. *Angew. Chem. Int. Ed.* **1991**, *30*, 1417-1436.
- 15 Weinhold, F.; Klein, R. A. *Chem. Educ. Res. Pract.* **2014**, *15*, 276-285.
- 16 Pimentel, G. C.; McClellan, A. L. *The Hydrogen Bond*, Freeman, San Francisco, **1960**.
- 17 (a) Arunan, E.; Desiraju, G. R.; Klein, R. A.; Sadlej, J.; Scheiner, S.; Alkorta, I.; Clary, D. C.; Crabtree, R. H.; Dannenberg, J. J.; Hobza, P.; Kjaergaard, H. G.; Legon, A. C.; Mennucci, B.; Nesbitt D. J. *Pure Appl. Chem.* **2011**, *83*, 1637-1641. (b) Arunan, E.; Desiraju, G. R.; Klein, R. A.; Sadlej, J.; Scheiner, S.; Alkorta, I.; Clary, D. C.; Crabtree, R. H.; Dannenberg, J. J.; Hobza, P.; Kjaergaard, H. G.; Legon, A. C.; Mennucci, B.; Nesbitt D. J. *Pure Appl. Chem.* **2011**, *83*, 1619-1636.
- 18 Southall, N. T.; Dill, K. A.; Haymet, A. D. J. *J. Phys. Chem. B* **2002**, *106*, 521-533.
- 19 Lindoy, L. F.; Atkinson, I. M. *Self-assembly in Supramolecular Systems*, Royal Society of Chemistry, Cambridge, **2000**.
- 20 Atwood, J. L.; Steed, J. W. *Encyclopedia of supramolecular chemistry*, Marcel Dekker, New York, **2004**.
- 21 Riley, K. E.; Hobza, P. *Acc. Chem. Res.* **2013**, *46*, 927–936.
- 22 Diskin-Posner, Y.; Patra, G. K.; Goldberg, I. *J. Chem. Soc., Dalton Trans.* **2001**, *19*, 2775-2782.
- 23 Lagona, J.; Mukhopadhyay, P.; Chakrabarti, S.; Isaacs, L. *Angew. Chem. Int. Ed.* **2005**, *44*, 4844-4870.
- 24 Behrend, R.; Meyer, E.; Rusche, F. *Liebigs Ann. Chem.* **1905**, *339*, 1-40.
- 25 Freeman, W. A.; Mock, W. L.; Shih, N. Y. *J. Am. Chem. Soc.* **1981**, *103*, 7367-7368.
- 26 Kim, J.; Jung, I.-S.; Kim, S.-Y.; Lee, E.; Kang, J.-K.; Sakamoto, S.; Yamaguchi, K.; Kim, K. *J. Am. Chem. Soc.* **2000**, *122*, 540-541.
- 27 Lee, J. W.; Samal, S.; Selvapalam, N.; Kim, H. J.; Kim, K. *Acc. Chem. Res.* **2003**, *36*, 621-630.
- 28 Day, A. I.; Arnold, A. P.; Blanch, R. J. *Molecules* **2003**, *8*, 74-84.

- 29 Day, A. I.; Blanch, R. J.; Arnold, A. P.; Lorenzo, S.; Lewis, G. R.; Dance, I. *Angew. Chem., Int. Ed.* **2002**, *41*, 275-277.
- 30 Gürbüz, S.; Idris, M.; Tuncel, D. *Org. & Biomol. Chem.* **2015**, *13*, 330-347.
- 31 (a) Lü, J.; Lin, J.-X.; Cao, M.-N.; Cao, R. *Coord. Chem. Rev.* **2013**, *257*, 1334-1356. (b) Masson, E.; Ling, X.; Roymon, J.; Kyeremeh-Mensah, L.; Lu, X. *RSC Advances* **2012**, *2*, 1213-1247. (c) Day, A. I.; Xiao, X.; Zhang, Y.-Q.; Xue, S.-F.; Tao, Z. *J. Incl. Phenom. Macrocycl. Chem.* **2011**, *71*, 281-286.
- 32 Fukuhara, G. *J. Synth. Org. Chem. Jpn.* **2009**, *67*, 1282-1283.
- 33 Yang, H.; Tan, Y.; Huang, X.; Wang, Y. *Prog. Chem.* **2009**, *21*, 164-173.
- 34 Isaacs, L. *Chem. Commun.* **2009**, 619-627.
- 35 Gobre, V. V.; Pinjari, R. V.; Gejji, S. P. *J. Phys. Chem. A* **2010**, *114*, 4464-4470.
- 36 Mock, W. L.; Shih, N. Y. *J. Org. Chem.* **1986**, *51*, 4440-4446.
- 37 Izatt, R. M.; Terry, R. E.; Haymore, B. L.; Hansen, L. D.; Dalley, N. K.; Avondet, A. G.; Christensen, J. J. *J. Am. Chem. Soc.* **1976**, *98*, 7620-7626.
- 38 Sun, Sh.; Shi, J.; Dong, Y.; Hu, X.; Wang, L.; *J. Prog. Chemistry.* **2014**, *26*, 1409-1426.
- 39 Liu, Y.; Yang, H.; Wang, Zh.; Xi, Zh. *Chem Asian J.* **2013**, *8*, 1626-1632
- 40 Jeon, W. S.; Moon, K.; Park, S. H.; Chun, H.; Ko, Y. H.; Lee, J. Y.; Lee, E. S.; Samal, S.; Selvapalam, N.; Rekharsky, M. V.; Sindelar, V.; Sobransingh, D.; Inoue, Y.; Kaifer A. E.; Kim, K. J. *Am. Chem. Soc.*, **2005**, *127*, 12984-12989.
- 41 Cong, H.; Tao, Z.; Xue, S-F.; Zhu, Q-J. *Curr. Org. Chem.* **2011**, *15*, 86-95.
- 42 Choi, S.; Lee, J. W.; Ko, Y. H.; Kim, K. J. *Macromolecules.* **2002**, *35*, 3526-3531.
- 43 McNally, B. A.; Leevy, W. M.; Smith, B. D. *J. Supramol. Chem.* **2007**, *19*, 29-37.
- 44 Bardelang, D.; Udachin, K. A.; Leek, D. M.; Margeson, J. C.; Chan, G.; Ratcliffe, C. I.; Ripmeester, J. A. *Cryst. Growth Des.* **2011**, *11*, 5598-5614.
- 45 D' Souza, R. N.; Pischel, U.; Nau, W. M. *Chem. Rev.* **2011**, *111*, 7941-80.
- 46 Liu, S.; Ruspic, C.; Mukhopadhyay, P.; Chakrabarti, S.; Zavalij, P. Y.; Isaacs, L. *J. Am. Chem. Soc.* **2005**, *127*, 15959-15967.
- 47 Kim, K. *Chem. Soc. Rev.* **2002**, *31*, 96-107.
- 48 Kim, H. J.; Jeon, W. S.; Ko, Y. H.; Kim, K. *Proc. Natl. Acad. Sci. USA* **2002**, *99*, 5007-5011.
- 49 Ong, W.; Gomez-Kaifer, M.; Kaifer, A. E. *Org. Lett.* **2002**, *4*, 1791-1794.
- 50 Choi, S.; Park, S. H.; Ziganshina, A. Y.; Ko, Y. H.; Lee, J. W.; Kim, K. *Chem. Commun.* **2003**, *17*, 2176-2177.
- 51 Wagner, B. D.; Stojanovic, N.; Day, A. I.; Blanch, R. J. *J. Phys. Chem. B* **2003**, *107*, 10741-10746.
- 52 Zhang, K. C.; Mu, T. W.; Liu, L.; Guo, Q. X. *Chin. J. Chem.* **2001**, *19*, 558-561.
- 53 Wang, R. B.; Yuan, L. N.; Macartney, D. H. *Chem. Commun.* **2006**, 2908-2910.
- 54 Yuan, L.; Wang, R.; Macartney, D. H. *Tetrahedron: Asymmetry* **2007**, *18*, 483-487.
- 55 Wang, R.; Yuan, L.; Macartney, D. H. *J. Org. Chem.* **2006**, *71*, 1237-1239.
- 56 Shen, Y.; Xue, S.; Zhao, Y.; Zhu, Q.; Tao, Z. *Chin. Sci. Bull.* **2003**, *48*, 2694.
- 57 Mukhopadhyay, P.; Wu, A.; Isaacs, L. *J. Org. Chem.* **2004**, *69*, 6157-6164.
- 58 Ma, P.; Dong, J.; Xiang, S.; Xue, S.; Zhu, Q.; Tao, Z.; Zhang, J.; Zhou, X. *Sci. China Ser. B* **2004**, *47*, 301-310.
- 59 Blanch, R. J.; Sleeman, A. J.; White, T. J.; Arnold, A. P.; Day, A. I. *Nano Lett.* **2002**, *2*, 147-149.
- 60 Constabel, F.; Geckeler, K. E. *Fuller. Nanotub. Carbon Nanostruct.* **2004**, *12*, 811-818.
- 61 Wang, R.; Yuan, L.; Macartney, D. H. *Organometallics* **2006**, *25*, 1820-1823.
- 62 Ong, W.; Kaifer, A. E. *Organometallics* **2003**, *22*, 4181-4183.

- 63 Jeon, Y. J.; Kim, S. Y.; Ko, Y. H.; Sakamoto, S.; Yamaguchi, K.; Kim, K. *Org. Biomol. Chem.* **2005**, *3*, 2122-2125.
- 64 Wheate, N. J.; Day, A. I.; Blanch, R. J.; Arnold, A. P.; Cullinane, C.; Collins, J. G. *Chem. Commun.* **2004**, 1424-1425.
- 65 Wyman, I. W.; Macartney, D. H. *Org. Biomol. Chem.* **2008**, *6*, 1796-1801.
- 66 Yang, S. L.; Xue, S. F.; Zhu, Q. J.; Tao, Z.; Zhang, J. X.; Zhou, X. *Chin. J. Org. Chem.* **2005**, *25*, 427-432.
- 67 Jeon, W. S.; Kim, H. J.; Lee, C.; Kim, K. *Chem. Commun.* **2002**, 1828-1829.
- 68 Sun, S. G.; Zhang, R.; Andersson, S.; Pan, J. X.; Akermark, B.; Sun, L. C. *Chem. Commun.* **2006**, 4195-4197.
- 69 Gadde, Suresh; Kaifer, Angel E. J. *Curr. Org. Chem.* **2011**, *15*, 27-38.
- 70 Kim, H.-J.; Heo, J.; Jeo, W. S.; Lee, E.; Kim, J.; Sakamoto, S.; Yamaguchi, K.; Kim, K. *Angew. Chem. Int. Ed.* **2001**, *40*, 1526-1529.
- 71 Trabolsi, A.; Hmadeh, H.; M.Khashab, N.; Douglas, C. F.; E.Belowich, M.; Humbert, N.; Elhabiri, M.; A.Khatib, H.; Albrecht-Gary, A M.; Stoddart, J.F. *New. J. Chem.* **2009**, *33*, 254-263.
- 72 Monk, P. M. S. *The Viologens: Physicochemical Properties, Synthesis and Applications of the Salts of 4, 4'-Bipyridine*, Chichester, **1998**.
- 73 Hofmann, A. W.; Bee. *Ber. Dtsch. Chem. Ges.* **1881**, *14*, 1497-1506.
- 74 (a) Dimroth, O.; Heene, R. *Ber. Dtsch. Chem. Ges.* **1921**, *54*, 2934-2942. (b) Dimroth, O., Frister, F. *Ber. Dtsch. Chem. Ges.* **1922**, *55*, 1223-1232.
- 75 (a) Michaelis, L.; Hill, E. S. *J. Gen. Physiol.* **1933**, *16*, 859-873. (b) Michaelis, L. *Chem. Rev.* **1935**, *16*, 243-286; (c) Bird, C. L. Kuhn, A. T. *Chem. Soc. Rev.* **1981**, *10*, 49-82.
- 76 (a) Bruinink, J.; Kregting, C.G.A.; Ponjeé, J. J. *J. Electrochem. Soc.* **1977**, *124*, 1854-1858. (b) Evans, A. G.; Evans, J. C.; Baker, M. W. *J. Am. Chem. Soc.* **1977**, *99*, 5882-5884. (c) Meisel, D.; Mulac, W. A.; Matheson, M. S. *J. Phys. Chem.* **1981**, *85*, 179-187. (d) Adar, E.; Degani, Y.; Goren, Z.; Willner, I. *J. Am. Chem. Soc.* **1986**, *108*, 4696-4700. (e) Yasuda, A.; Mori, H.; Seto, J. *J. Appl. Electrochem.* **1987**, *17*, 567-573.
- 77 Geuder, W.; Hünig, S.; Suchy, A. *Tetrahedron* **1986**, *42*, 1665-1677.
- 78 Kosower, E. M.; Cotter, J. L. *J. Am. Chem. Soc.* **1964**, *86*, 5524-5527.
- 79 Kosower, E. M.; Hajdu, J. *J. Am. Chem. Soc.* **1971**, *93*, 2534-2535.
- 80 Fahrenbach, A. C.; Barnes, J. C.; Lanfranchi, D. A.; Li, H.; Coskun, A.; Gassensmith, J. J.; Liu, Z.; Benítez, D.; Trabolsi, A.; Goddard, W. A.; Elhabiri, M.; Stoddart, J. F. *J. Am. Chem. Soc.* **2012**, *134*, 3061-3072.
- 81 Wadhwa, K.; Nuryyeva, S.; Fahrenbach, A. C.; Elhabiri, M.; Platas-Iglesias, C.; Trabolsi, A. *J. Mater. Chem. C* **2013**, *1*, 2302-2307.
- 82 (a) Mortimer, R. J. *Electrochim. Acta* **1999**, *44*, 2971-2981. (b) Cao, L.-C.; Mou, M.; Wang, Y. *J. Mater. Chem.* **2009**, *19*, 3412-3418. (c) Asaftei, S.; Ciobanu, M.; Lepadatu, A. M.; Song, E.; Beginn, U. *J. Mater. Chem.* **2012**, *22*, 14426-14437.
- 83 Kuroboshi, M.; Shiba, T.; Tanaka, H. *Tetrahedron Lett.* **2013**, *54*, 3666-3668.
- 84 Ciepluch, K.; Katir, N.; El Kadib, A.; Felczak, A.; Zawadzka, K.; Weber, M.; Klajnert, B.; Lisowska, K.; Caminade, A.-M.; Bousmina, M.; Bryszewska, M.; Majoral, J. P. *Mol. Pharmaceutics.* **2012**, *9*, 448-457.
- 85 Granqvist, G. C. *Handbook of Inorganic Electrochromic Materials*, Elsevier, Amsterdam, **1995**.
- 86 Monk, P. M. S.; Mortimer, R. J.; Rosseinsky, D. R., *Electrochromism and Electrochromic Devices*, Cambridge University Press, Cambridge, UK, **2007**.

- 87 Platt, J. R. J. *J. Chem. Phys.* **1961**, *34*, 862-863.
- 88 Corr, D.; Bach, U.; Fay, D.; Kinsella, M.; McAtamney, C.; O'Reilly, F.; Rao, S. N.; Stobie, N. *Solid State Ionics* **2003**, *165*, 315-321.
- 89 Cinnsealach, R.; Boschloo, G.; Nagaraja Rao, S.; Fitzmaurice, D. *Sol. Energy Mater. Sol. Cells* **1999**, *57*, 107-125.
- 90 Berger, S.; Ghicov, A.; Nah, Y. C.; Schmuki, P. *Langmuir* **2009**, *25*, 4841-4844.
- 91 Cummins, D.; Boschloo, G.; Ryan, M.; Corr, D.; Rao, S. N.; Fitzmaurice, D. *J. Phys. Chem. B.* **2000**, *104*, 11449-11459.
- 92 De Filpo, G.; Nicoletta, F. P.; Chidichimo, G. *Chem. Mater.* **2006**, *18*, 4662-4666.
- 93 Cinnsealach, R.; Boschloo, G.; Nagaraja Rao, S.; Fitzmaurice, D. *Sol. Energy Mater. Sol. Cells.* **1998**, *55*, 215-223.
- 94 Bonhôte, P.; Gogniat, E.; Grätzel, M.; Ashrit, P. V. *Thin Solid Films* **1999**, *350*, 269-275.
- 95 Avendaño, E.; Berggren, L.; Niklasson, G. A.; Granqvist, C. G.; Azens, A. *Thin Solid Films* **2006**, *496*, 30-36.
- 96 Jain, V.; Sahoo, R.; Jinschek, J. R.; Montazami, R.; Yochum, H. M.; Beyer, F. L.; Kumar, A.; Heflin, J. R. *Chem. Commun.* **2008**, 3663-3665.
- 97 Mortimer, R. J. *Electrochim. Acta.* **1999**, *44*, 2971-2981.
- 98 Ma, C.; Taya, M.; Xu, C. *Polym. Eng. Sci.* **2008**, *48*, 2224-2228.
- 99 Invernale, M. A.; Ding, Y.; Sotzing, G. A. *ACS. Appl. Mater. Inter.* **2010**, *2*, 296-300.
- 100 Park, J. W.; Choi, N. H.; Kim, J. H. *J. Phys. Chem.* **1996**, *100*, 769-774.
- 101 Stargardt, J. F.; Hawkridge, F. M. *Anal. Chim. Acta.* **1983**, *146*, 1-8.
- 102 Monk, P. M. S.; Hodgkinson, N. M.; Ramzan, S. A. *Dyes Pigm.* **1999**, *43*, 207-217.
- 103 Watanabe, T.; Honda, K. *J. Phys. Chem.* **1982**, *86*, 2617-2619.
- 104 Lee, C.; Moon, M. S.; Park, J. W. *J. Electroanal. Chem.* **1996**, *407*, 161-167.
- 105 Claude-Montigny, B.; Merlin, A.; Tondre, C. *J. Phys. Chem.* **1992**, *96*, 4432-4437.
- 106 Mayhew, S. G.; Müller, F. *Biochem. Soc. Trans.* **1982**, *10*, 176-177.
- 107 Park, J. W.; Ko, S. H.; Park, J. Y. *Bull. Korean Chem. Soc.* **1992**, *13*, 259-265.
- 108 *Functional Synthetic Receptors*, Schrader, T.; Hamilton, A. D., Eds., Wiley-VCH, Weinheim, **2005**.
- 109 Ariga, K.; Kunitake, T. *Supramolecular Chemistry—Fundamentals and Applications*, Springer, Berlin, **2005**.
- 110 *Highlights in Bioorganic Chemistry: Methods and Applications*, Schmuck, C.; Wennemers, H. Eds., Wiley-VCH, Weinheim, **2004**.
- 111 Kubik, S.; Reyheller, C.; Stuwe, S. J. *Incl. Phenom. Macro. Chem.* **2005**, *52*, 137-187.
- 112 Braun, J.; Hasenfratz, C.; Schwesinger, R.; Limbach, H.-S. *Angew. Chem. Int. Ed. Engl.* **1994**, *33*, 2215-2217.
- 113 Vogel, G. C.; Searby, L. A. *Inorg. Chem.* **1973**, *12*, 936-939.
- 114 *The Porphyrin Handbook*, Kadish, K. M.; Smith, K. M.; Guillard, R. Eds., Academic, New York, **2000**, *4*.
- 115 *The Porphyrin Handbook*, Kadish, K. M.; Smith, K. M.; Guillard, R. Eds., Academic, New York. **2000**, *6*.
- 116 Balaban, T. S.; Eichhöfer, A.; Lehn, J. M. *Eur. J. Org. Chem.* **2000**, 4047-4057.
- 117 Sun, L.; von Gersdorff, J.; Niethammer, D.; Tian, P.; Kurreck, H. *Angew. Chem., Int. Ed. Engl.* **1994**, *33*, 2318-2320.
- 118 Molt, O.; Rübeling, D.; Schrader, T. *J. Am. Chem. Soc.* **2003**, *125*, 12086-12087.

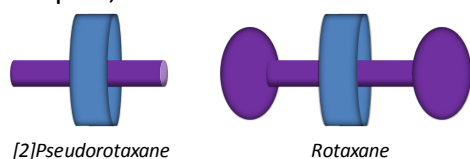
- 119 Feiters, M. C.; Rowan, A. E.; Nolte, R. J. M. *Chem. Soc. Rev.* **2000**, *29*, 375-384.
- 120 Collman, J. P. *Inorg. Chem.* **1997**, *36*, 5145-5155.
- 121 Choi, M.; Yamazaki, T.; Yamazaki, I.; Aida, T. *Angew. Chem. Int. Ed.* **2004**, *43*, 150-158.
- 122 Balaban, T. S. *Acc. Chem. Res.* **2005**, *38*, 612-623.
- 123 Maruyama, K.; Osuka, A. *Pure Appl. Chem.* **1990**, *62*, 1511-1520.
- 124 Pandey, R. K.; Zheng, G. In *The Porphyrin Handbook*, Kadish, K. M.; Smith, K. M.; Guillard, R. Eds., Academic Press, New York **2000**, *6*, 157-230.
- 125 Marcus, S. L. *Proc. IEEE.* **1992**, *80*, 869-886.
- 126 Dougherty, T. J.; Gomer, C. J.; Henderson, B.W. *J. Natl. Cancer Inst.* **1998**, *90*, 88-905.
- 127 Dougherty, T. J.; Marcus, S. L. *Eur. J. Cancer.* **1992**, *28A*, 1734-1742.
- 128 Paul, D.; Wytko, J. A.; Koepf, M.; Weiss, J. *Inorg. Chem.* **2002**, *41*, 3699-3704.
- 129 Koepf, M.; Trabolsi, A.; Elhabiri, M.; Wytko, J. A.; Paul, D.; Albrecht-Gary, A. M.; Weiss, J. *Org. Lett.* **2005**, *7*, 1279-1282.
- 130 *The Porphyrin Handbook*, Kadish, K. M.; Smith, K. M.; Guillard, R. Eds., Academic Press, New York **2000**, *8*.
- 131 Harvey, P. D. In *The Porphyrin Handbook* Kadish, K. M.; Smith, K. M.; Guillard, R. Eds., Elsevier Science, **2003**, *18*, 63-250.
- 132 Aratani, N.; Cho, H. S.; Ahn, T. K.; Cho, S.; Kim, D.; Sumi, H.; Osuka, A. *J. Am. Chem. Soc.* **2003**, *125*, 9668-9681.
- 133 Otsuki, J.; Yasuda, A.; Takido, T. *Chem. Commun.* **2003**, 608-609.
- 134 Hush, N. S.; Reimers, J. R.; Hall, L. E.; Johnston, L. A.; Crossley, M. J. *Ann. New York Acad. Sci.* **1998**, *852*, 1-21.
- 135 Satake, A.; Kobuke, Y. *Tetrahedron.* **2005**, *61*, 13-41.
- 136 Tobita, S.; Kaizu, H.; Kobayashi, H.; Tanaka, I. *J. Chem. Phys.* **1984**, *81*, 2962-2969.
- 137 Reed, R. A.; Purello, R.; Prendergast, K.; Spiro, T. G. *J. Phys. Chem.* **1991**, *95*, 9720-9727.
- 138 Harriman, A.; Porter, G.; Searle, N. *J. Chem. Soc. Faraday Trans.* **1979**, *75*, 1515-1521.
- 139 Dorrough, G. D.; Miller, J. R.; Huennekens, F. M. *J. Am. Chem. Soc.* **1951**, *73*, 4315-4320.
- 140 Thomas, D. W.; Martell, A. E. *J. Am. Chem. Soc.* **1956**, *78*, 1338-1343.
- 141 Edwards, L.; Dolphin, D. H.; Gouterman, M.; Adler, A. D. *J. Mol. Spectrosc.* **1971**, *38*, 16-32.
- 142 Seybold, P. G.; Gouterman, M. *J. Mol. Spectrosc.* **1969**, *31*, 1-13.
- 143 Gouterman, M. *The Porphyrins*, Dolphin, D., Ed., Academic Press, New York, **1978**, *3*, 1-165.
- 144 Gouterman, M. *J. Chem. Phys.* **1959**, *30*, 1139-1161.
- 145 Baskin, J. S.; Yu, H. Z.; Zewail, A. *J. Phys. Chem. A.* **2002**, *106*, 9837-9844.
- 146 Yu, H. Z.; Baskin, J. S.; Zewail, A. *J. Phys. Chem. A.* **2002**, *106*, 9845-9854.
- 147 Noble, A. *Justus Liebigs Ann. Chem.* **1856**, *98*, 253-256.
- 148 Griffiths, J. *Chem. Soc. Rev.* **1972**, *1*, 481-493.
- 149 Venkataraman, K. *The chemistry of synthetic dyes*, Academic Press, New York, **1956**.
- 150 Hartley, G. S. *Nature* **1937**, *140*, 281-281.
- 151 Rau, H. *Angew. Chem. Int. Ed. Engl.* **1973**, *12*, 224-235.
- 152 Rau, H. In *Azo Compounds in Photochromism. Molecules and Systems*, Durr, H., Bouas-Laurent, H., Eds., Elsevier, Amsterdam, **1990**, 165-192.
- 153 Tiberio, G.; Muccioli, L.; Berardi, R.; Zannoni, C. *Chem. Phys. Chem.* **2010**, *11*, 1018-1028.
- 154 Dokic, J.; Gothe, M.; Wirth, J.; Peters, M. V.; Schwarz, J.; Hecht, S.; Saalfrank, P. *J. Phys. Chem. A.* **2009**, *113*, 6763-6773.

- 155 Fliegl, H.; Kohn, A.; Hattig, C.; Ahlrichs, R. *J. Am. Chem. Soc.* **2003**, *125*, 9821-9827.
- 156 Knoll, H. In *Photoisomerism of azobenzenes* in *CRC Handbook of organic photochemistry and photobiology*, Horspool, W., Lenci, F., Eds., 2nd ed., CRC Press, Boca Raton, **2004**, 1-16.
- 157 Yang, Y.; Hughes, R. P.; Aprahamian, I. *J. Am. Chem. Soc.* **2012**, *134*, 15221-15224.
- 158 Tsuji, T.; Takeuchi, H.; Egawa, T.; Konaka, S. *J. Am. Chem. Soc.* **2001**, *123*, 6381-6387.
- 159 Dias, A. R., Minas da Piedade, M. E., Martinho Simoes, J. A., Simoni, J. A., Teixeira, C., Diogo, H. P., Meng-Yan, Y., Pilcher, G. *J. Chem. Thermodynamics* **1992**, *24*, 439-447.
- 160 A. A. Beharry, PhD thesis from the Department of Chemistry, University of Toronto, **2012**.
- 161 Froidevaux, J.; Ochsenbein, P.; Bonin, M.; Schenk, K.; Maltese, P.; Gisselbrecht, J. P.; Weiss, J. *J. Am. Chem. Soc.* **1997**, *119*, 12362-12363.
- 162 Dharam, P.; Melin, F.; Hirtz, C.; Wytko, J. A.; Ochsenbein, P.; Bonin, M.; Schenk, K.; Maltese, P.; Weiss, J. *Inorg. Chem.*, **2003**, *42*, 3779-3787.
- 163 Brandel, J.; Trabolsi, A.; Traboulsi, H.; Melin, F.; Koepf, M.; A. Wytko, J.; Elhabiri, M.; Weiss, J.; Albrecht-Gary, A-M. *Inorg. Chem.* **2009**, *48*, 3743-3754.
- 164 Sanders, J. K. M. In *The Porphyrin Handbook*; Kadish, K. M.; Smith, K. M.; Guillard, R., Eds.; Academic Press, New York **2000**, *3*, 347-368.
- 165 Imamura, T.; Fukushima, K. *Coord. Chem. Rev.* **2000**, *198*, 133-156.
- 166 Wojaczynski, J.; Latos-Grazynski, L. *Coord. Chem. Rev.* **2000**, *204*, 113-171.
- 167 a) Iengo, E.; Zangrando, E.; Alessio, E. *Eur. J. Inorg. Chem.* **2003**, 2371-2384. c) Heitz, V.; Chambron, J. C.; Sauvage, J. P. In *The Porphyrin Handbook*, Kadish, K. M.; Smith, K. M.; Guillard, R. Eds.; Academic Press, New York, **2000**, *6*, 1-42. d) Haycock, R. A.; Hunter, C. A.; James, D. A.; Michelsen, U.; Sutton, L. R. *Org. Lett.* **2000**, *2*, 2435-2438.
- 168 Leray, I.; Valeur, B.; Paul, D.; Regnier, E.; Koepf, M.; Wytko, J. A.; Boudon, C.; Weiss, J. *Photochem. Photobiol. Sci.* **2005**, *4*, 280-286.

**Chapter II:
Cucurbit[n]uril Host and
a Hexavalent
phosphazene Guest**

2.1. Introduction

The ability to induce fast and reversible movements of large amplitude within molecular bodies has become a major scientific goal. To that end, many nanometric mimics of mechanical tools and devices have been synthesized. These include nanoscale tweezers,¹ gears,² rotors,³⁻⁷ shuttles,⁸ actuators,⁹⁻¹¹ and elevators,¹² the movements of which respond to a variety of external stimuli including changes in pH,¹³⁻¹⁵ redox potential,^{1,16} temperature,¹⁷ and light intensity.^{18,19} Toward this goal, my PhD work has been partly devoted to engineer and study novel systems based on recognition properties of redox active bipyridiniums by macrocycles such as cucurbit[n]uril. The novel nanomechanical systems that have developed include among other: a [3]pseudorotaxane (*i.e.* rotaxane-like complex, but in which the linear unit does not possess bulky terminal groups); a rotaxane



consists of a mechanically-interlocked molecular ensemble displaying of a "dumbbell shaped molecule" that is threaded through a "macrocyclic molecule"), a [4]pseudorotaxane and a [7]pseudorotaxane, each composed of a "multimeric" viologen-based thread molecule and the macrocycles, cucurbit[7]uril (noted **CB[7]**) and cucurbit[8]uril (noted **CB[8]**). In aqueous solution, these systems can be electrochemically switched between a complexed state, defined by the pseudorotaxanes themselves, and an uncomplexed state comprising their separate components. The driving force for the disassembly process (*i.e.*, "dethreading") is strong

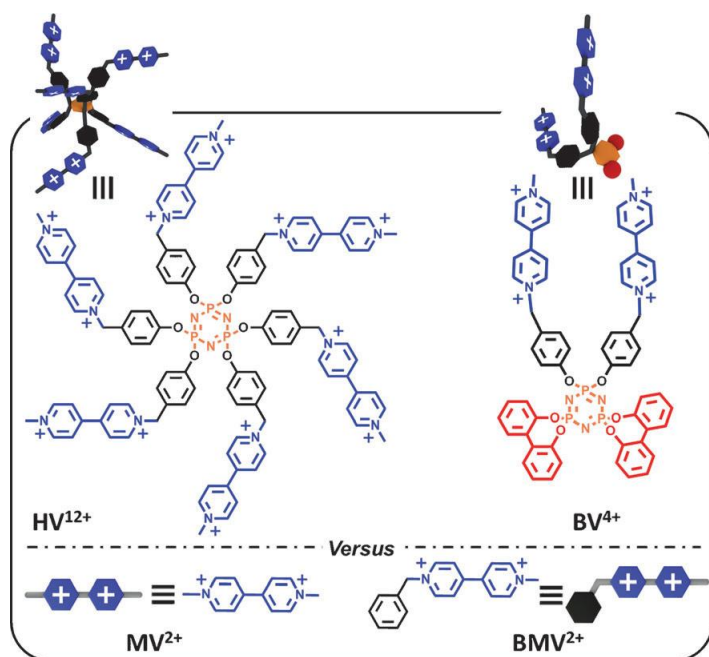


Figure 1. Structural formulas and 3D representations of phosphazene derivatives bearing six 4,4'-bipyridinium subunits (**HV¹²⁺**) and two 4,4'-bipyridinium subunits and two [1,1'-biphenyl]-2,2'-diol protective groups (**BV⁴⁺**).

Methyl viologen (**MV²⁺**) and 1-benzyl-1'-methyl-4,4'-bipyridinium (**BMV²⁺**) were used as reference compounds.

intramolecular and / or intermolecular dimerization of the viologen radical cations. An analogy can be made between these artificial systems and voltage-gated membrane channels, the protein components of which undergo large conformational changes under the influence of an action potential.²⁰

In this chapter,²¹ we have principally demonstrated that the intramolecular dimerization of viologen monoradical cations can thermodynamically overwhelm the inclusion to **CB[7]** and induce fast and efficient host-guest "dethreading". Reinstating the oxidized bipyridiniums prevent the dimerization process and reversibly led to the initial host-guest species.

A cyclotriphosphazene (noted phosphazene or **CTP**) platform functionalized with 6 terminal viologens (noted **HV¹²⁺**) was prepared (by the group of Pr Ali Trabolsi, NYUAD, Abu Dhabi, UAE) and thoroughly studied (Figure 1) in combination with **CB[7]** using analytical methods such as absorption spectrophotometry, electro-chemistry, electrospray mass spectrometry, ¹H NMR, ¹H DOSY NMR and electron paramagnetic resonance (EPR) spectroscopies. Model ligands (**BV⁴⁺** and **BMV²⁺**) were also employed to assess the critical role of the anchoring core on the recognition and dimerization processes. **BV⁴⁺** only contains two viologen subunits that are distributed face to face along the periphery of the phosphazene core while the benzyl methyl viologen **BMV²⁺** represents the basic electroactive unit (Figure 1).

2.1.1. Hexavalent Phosphazene Platform

Phosphazenes can be described as a class of compounds that display alternating phosphorus and nitrogen atoms in their backbone. They are considered as a class of chemical compounds possessing at least one double bond between a pentavalent phosphorus atom and a nitrogen atom. In 1895, H. N. Stokes was the first to suggest that (NPCl₂)₃ can exhibit a cyclic arrangement (Figure 2).²² The phosphazene can be actually defined as a class of compounds that are in the form of cyclic, linear short-chain or high molecular weight polymers and displaying -N=PR₂-repeating units.

In particular, cyclotriphosphazene (noted CTP) can be easily hexa-functionalized through nucleophilic substitution reactions on the corresponding hexachloride (NPCl₂)₃ analogue leading to a nearly planar system where the phosphorous atoms are almost tetrahedral (sp³) and the nitrogen atoms approach a sp² geometry.²³ CTP moieties exhibit excellent thermal and chemical stabilities and are photochemically and electrochemically inert. As a consequence, they do not interfere with the photophysical and electrochemical properties centred on the grafted redox active viologens. The easiness of CTP rings functionalization coupled to the structural rigidity of the products make CTP an attractive core for the development of multifunctional and robust systems.

Phosphazene Scaffolds

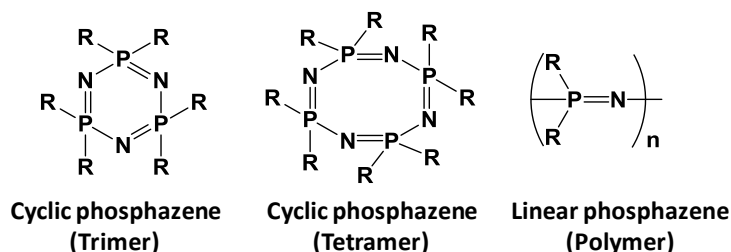


Figure 2. Chemical structures of the possible phosphazene scaffolds. a) cyclic trimer, b) cyclic tetramer, c) linear polymer. The halogen groups (R) can be easily substituted by alkoxy, aryloxy or amino groups via nucleophilic substitutions.

2.2. Experimental Section and Results

2.2.1. Starting Materials

The reagents and the starting materials were purchased from commercial source and used without further purification. The dicationic dimethyl viologen **MV**•2I was prepared according to literature procedures.²⁴ **HV**•6Cl.6I, **BMV**•Cl.I and **BV**•2Cl.2I were prepared by our collaborators (Pr Ali Trabolsi, NYUAD, Abu Dhabi, UAE).²⁵ Cucurbit[7]uril (**CB[7]**) ($C_{42}H_{42}N_{28}O_{14}$, M. W. = 1162.96 g mol⁻¹, Strem chemicals) is a commercial product that was used without further purification.

All solutions were prepared in distilled H₂O which was further purified by passing it through a mixed bed of ion-exchanger (Bioblock Scientific R3-83002, M3-83006) and activated carbon (Bioblock Scientific ORC-83005). It was then boiled and de-oxygenated using CO₂ and O₂ free argon prior to use (Sigma Oxiclear cartridge). All stock solutions were prepared using an AG 245 Mettler Toledo balance (precision 0.01 mg), and complete dissolution in phosphate buffer was achieved using an ultrasonic bath. The experiments were carried out at 25.0(2) °C maintained with the help of a Haake FJ thermostat.

In all the solutions, the pH was maintained at 7.00 ± 0.05 by the use of a 0.1 M phosphate buffer, which was prepared by mixing 30.5 mL of Na₂HPO₄•2H₂O (0.2 M) (Prolabo) with 19.5 ml of NaH₂PO₄ (0.2 M) (Prolabo) and diluting to a total volume of 100 mL. The final pH of the solution was then set at the required value by using phosphoric acid (85%, Labosi). The pH was measured with an Ag/AgCl combined glass electrode (Metrohm 6.0234.500, long life) filled with 0.1 M NaCl (Fluka, p.a.) in H₂O. Standardization of the millivoltmeter and the verification of the linearity of the electrode response were performed using a set of NIST certified commercial Merck buffered solutions (pH 1.68, 4.00, 6.86, 7.41 and 9.18).

Reduction of **HV**¹²⁺ and **BMV**²⁺ into their corresponding radical cationic forms was achieved under argon (CO₂- and O₂-free argon) with the addition of Na₂S₂O₄ solution in argon purged H₂O. The formation of the radicals was monitored by absorption spectrophotometry using a Cary 5000 UV-Vis.-NIR spectrophotometer.

2.2.2. Analytical Methods

Routine Nuclear Magnetic Resonance (NMR) spectra were recorded at 298 K on a Bruker Advance 600 spectrometer with working frequencies of 600 and 150 MHz for ¹H and ¹³C, respectively. Chemical shifts are reported in ppm relative to the signals corresponding to the residual non-deuterated solvents (D₂O δ = 4.97, d₆-DMSO δ = 2.50).

Electrospray mass (ESI-MS) spectra were measured on an ion-trap instrument (Bruker Esquire 3000plus, Bruker Daltonic, Bremen, Germany) equipped with an Agilent Technologies 6120 quadrupole equipped with an electrospray (ESI) interface.

Cyclic (CV) and Square wave (SW) voltammetries were carried out at room temperature in Ar-purged H₂O and DMSO solutions with a Gamry Multipurpose instrument. The experiments were performed using a glassy carbon working electrode (0.071 cm², BASi). The electrode surface was polished routinely with 0.05 μm alumina-water slurry on a felt surface immediately before use. The counter electrode was a Pt coil and the reference electrode was an Ag/AgCl electrode. The concentration of the electrolyte, tetrabutylammonium chloride (TBACl), was 0.1 M. The experimental errors on the potentials are estimated to ± 10 mV.

UV-Vis.-NIR spectra were recorded on a Cary 5000 (Agilent) spectrophotometer maintained at 25.0(2) °C by the flow of a Dual Cell Pelletier Accessory (Cary Varian)

2.2.3. Spectrophotometric Titrations of Viologen Derivatives by CB[7]

The spectrophotometric titrations of **MV²⁺** (1.51×10^{-4} M), **BMV²⁺** (1.15×10^{-4} M), **BV⁴⁺** (2.32×10^{-5} M) and **HV¹²⁺** (2.42×10^{-5} M) with cucurbit[7]uril (**CB[7]**) were carried out in Hellma quartz optical cells of 2, 5 or 10 mm pathlengths in water at pH 7 (0.1 M phosphate buffer). Microvolumes of a concentrated solution of **CB[7]** ($1\text{--}2 \times 10^{-3}$ M) were added to the viologen derivatives **MV²⁺** ($l = 2$ mm, $v = 500$ μL), **BMV²⁺** ($l = 5$ mm, $v = 1$ mL), **BV⁴⁺** ($l = 10$ mm, $v = 2.5$ mL) or **HV¹²⁺** ($l = 2$ mm, $v = 500$ μL) with the help of a microburette (Eppendorf). The $[\text{CB[7]}]_0/[\text{BIPY}^{2+}]_0$ ratios were varied from 0 to 2.68 for **MV²⁺**, from 0 to 1.56 for **BMV²⁺**, from 0 to 5.5 for **BV⁴⁺** and from 0 to 20.21 for **HV¹²⁺**, respectively. Special care was taken to ensure that complete equilibration was attained. After each addition, a UV-Vis. spectrum was recorded from 220 to 800 nm on a Cary 5000 spectrophotometer maintained at 25.0(2) °C by the flow of a Dual Cell Pelletier Accessory (Cary Varian).

2.2.3a. Recognition of MV²⁺ by CB[7]

Figure 3A portrays the spectrophotometric titration of **MV²⁺** by **CB[7]**. Figure 3B presents the electronic spectra of **MV²⁺** and its inclusion complex **MV²⁺⊂CB[7]**. The Job plot in Figure 4 confirms the expected 1:1 complex formation between **MV²⁺** and **CB[7]**.

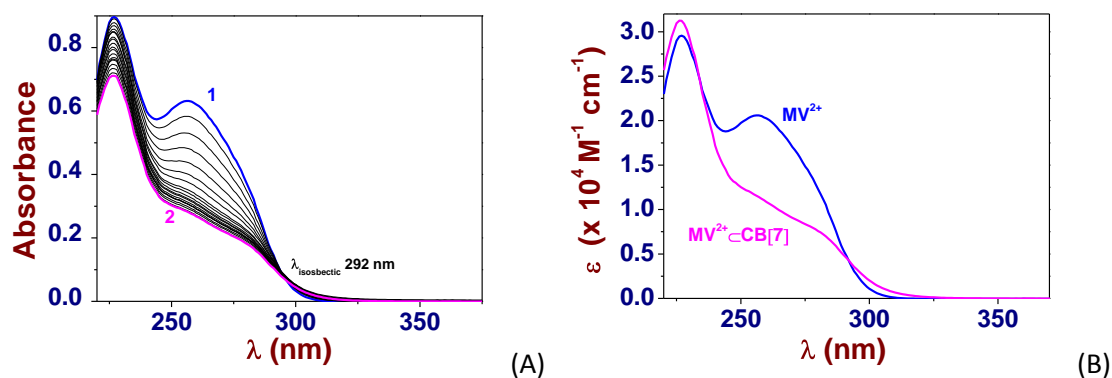


Figure 3. (a) UV-Vis. Absorption titration of **MV²⁺** by **CB[7]**. (b) Electronic spectra of **MV²⁺** and of its inclusion complex with **CB[7]** (**MV²⁺⊂CB[7]**). Solvent: water pH 7.0 (0.1 M Na₂HPO₄/NaH₂PO₄). $[\text{MV}^{2+}]_0 = 1.51 \times 10^{-4}$ M; (1) $[\text{CB[7]}]_0/[\text{MV}^{2+}]_0 = 0$; (2) $[\text{CB[7]}]_0/[\text{MV}^{2+}]_0 = 2.68$; $l = 2$ mm; $T = 25.0(1)$ °C. The absorption spectra are not corrected from dilution effects.

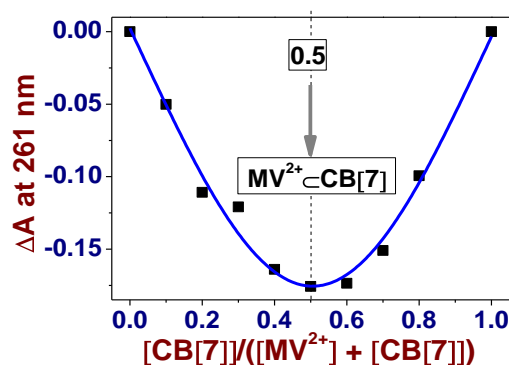


Figure 4. Job plot (ΔA at 261 nm) upon mixing MV^{2+} and $CB[7]$. ($[MV^{2+}]_0 + [CB[7]]_0 = 2.0 \times 10^{-4}$ M; Solvent: water pH 7.0 (0.1 M Na_2HPO_4/NaH_2PO_4); $l = 2$ mm; $T = 25.0(1)$ °C)

2.2.3b. Recognition of BMV^{2+} by $CB[7]$

Figure 5A illustrates the spectrophotometric titration of BMV^{2+} by $CB[7]$. Figure 5B presents the electronic spectra of BMV^{2+} and its inclusion complex $BMV^{2+} \subset CB[7]$. The Job plot presented in Figure 6 confirms that a 1:1 complex is formed between BMV^{2+} and $CB[7]$.

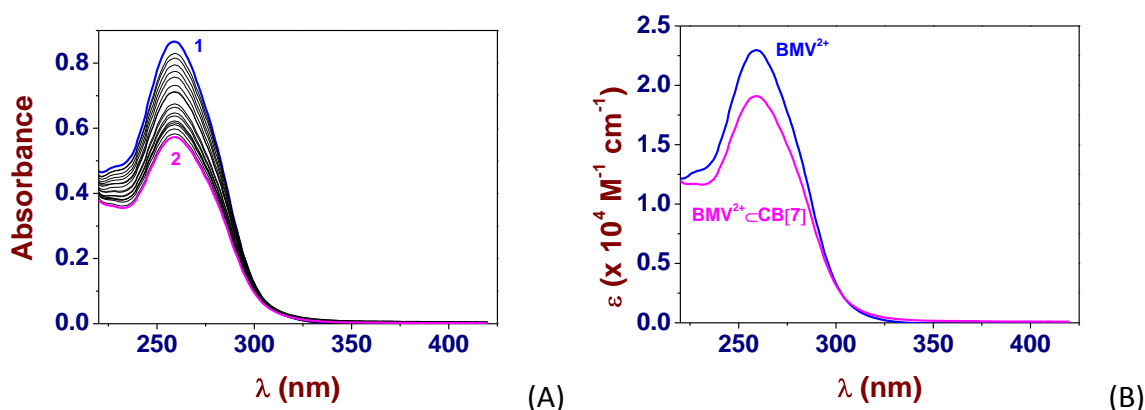


Figure 5. (A) UV-Vis. Absorption titration of BMV^{2+} by $CB[7]$. (B) Electronic spectra of BMV^{2+} and of its inclusion complex with $CB[7]$ ($BMV^{2+} \subset CB[7]$). Solvent: water pH 7.0 (0.1 M Na_2HPO_4/NaH_2PO_4). $[BMV^{2+}]_0 = 1.15 \times 10^{-4}$ M; (1) $[CB[7]]_0/[BMV^{2+}]_0 = 0$; (2) $[CB[7]]_0/[BMV^{2+}]_0 = 1.56$; $l = 5$ mm; $T = 25.0(1)$ °C. The absorption spectra are not corrected from dilution effects.

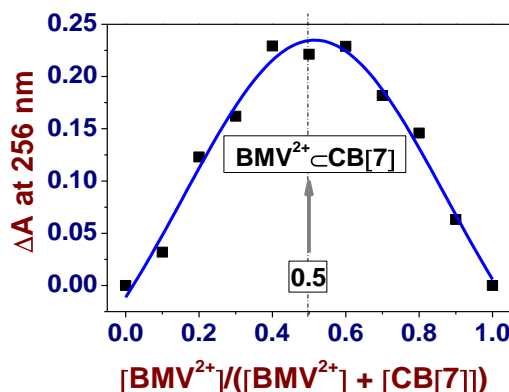


Figure 6. Job plot (ΔA at 256 nm) upon mixing BMV^{2+} and $CB[7]$. ($[BMV^{2+}]_0 + [CB[7]]_0 = 10^{-4}$ M; Solvent: water pH 7.0 (0.1 M Na_2HPO_4/NaH_2PO_4); $l = 5$ mm; $T = 25.0(1)$ °C.

2.2.3c. Recognition of BV^{4+} by CB[7]

Figure 7A illustrates the spectrophotometric titration of BV^{4+} by CB[7]. Figure 7B shows the electronic spectra of BV^{4+} and its inclusion complexes $BV^{4+} \subset CB[7]$ and $BV^{4+} \subset (CB[7])_2$. The Job plot presented in Figure 14 clearly confirms that a ternary 1:2 complex is formed between BV^{4+} and CB[7].

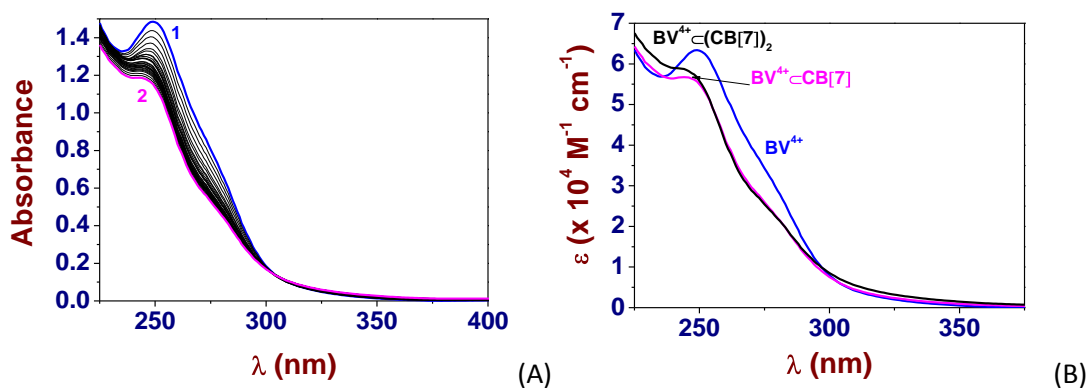


Figure 7. (A) UV-Vis. Absorption titration of BV^{4+} by CB[7]. (B) Electronic spectra of BV^{4+} and of its inclusion complexes with CB[7] ($BV^{4+} \subset CB[7]$ and $BV^{4+} \subset (CB[7])_2$). Solvent: water pH 7.0 (0.1 M Na_2HPO_4/NaH_2PO_4). $[BV^{4+}]_0 = 2.32 \times 10^{-5}$ M; (1) $[CB[7]]_0/[BV^{4+}]_0 = 0$; (2) $[CB[7]]_0/[BV^{4+}]_0 = 4.66$; $l = 1$ cm; $T = 25.0(1)$ °C.

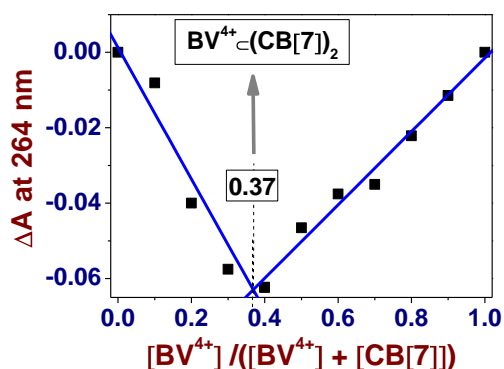


Figure 8. Job plot (ΔA at 264 nm) upon mixing BV^{4+} and CB[7]. ($[BV^{4+}]_0 + [CB[7]]_0 = 5.80 \times 10^{-5}$ M; Solvent: water pH 7.0 (0.1 M Na_2HPO_4/NaH_2PO_4); $l = 1$ cm; $T = 25.0(1)$ °C.

2.2.3d. Recognition of HV^{12+} by CB[7]

Figure 9A illustrates the spectrophotometric titration of HV^{12+} by CB[7]. Figure 9B shows the electronic spectra of HV^{12+} and its corresponding [7]pseudorotaxane $HV^{4+} \subset (CB[7])_6$. The Job plot presented in Figure 10 clearly confirms that a 1:6 complex is formed between HV^{12+} and CB[7].

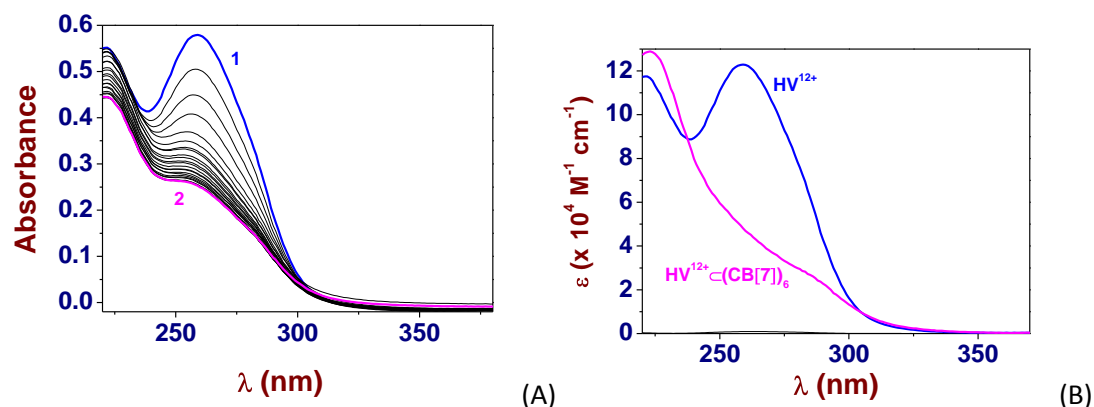


Figure 9. (A) UV-Vis. Absorption titration of HV^{12+} by $\text{CB}[7]$. (B) Electronic spectra of HV^{12+} and of its inclusion complex with $\text{CB}[7]$ ($\text{HV}^{12+} \subset (\text{CB}[7])_6$). Solvent: water pH 7.0 (0.1 M $\text{Na}_2\text{HPO}_4/\text{NaH}_2\text{PO}_4$). $[\text{HV}^{12+}]_0 = 2.42 \times 10^{-5}$ M; (1) $[\text{CB}[7]]_0/[\text{HV}^{12+}]_0 = 0$; (2) $[\text{CB}[7]]_0/[\text{HV}^{12+}]_0 = 20.21$; $l = 2$ mm; $T = 25.0(1)^\circ\text{C}$.

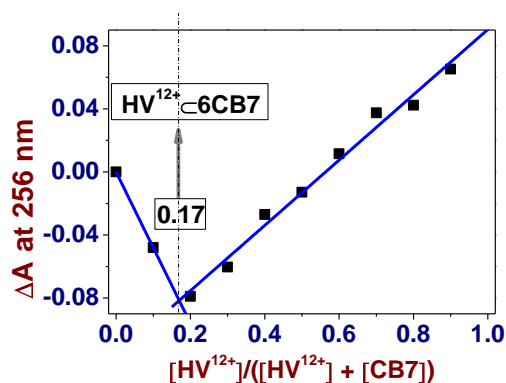


Figure 10. Job plot (ΔA at 256 nm) upon mixing HV^{12+} and $\text{CB}[7]$. ($[\text{HV}^{12+}]_0 + [\text{CB}[7]]_0 = 4 \times 10^{-5}$ M; Solvent: water pH 7.0 (0.1 M $\text{Na}_2\text{HPO}_4/\text{NaH}_2\text{PO}_4$); $l = 5$ mm; $T = 25.0(1)^\circ\text{C}$)

2.2.4. Complexation Studies Probed by ^1H NMR Spectroscopy

2.2.4a. BMV^{2+} and $\text{CB}[7]$ Recognition Probed by ^1H NMR Spectroscopy

To study the interaction between guests MV^{2+} and BMV^{2+} and host $\text{CB}[7]$, titration experiments were carried-out and monitored using ^1H NMR spectroscopy (Figure 11). The NMR spectra clearly reveal an upfield shift of the *c* protons of the benzylic unit which confirm the location of $\text{CB}[7]$ around the benzyl group. The recorded NMR spectra clearly reveal two different binding modes of $\text{CB}[7]$ with MV^{2+} and BMV^{2+} where the $\text{CB}[7]$ resides on the bipyridinium part in the case of MV^{2+} and on the benzyl group in BMV^{2+} .

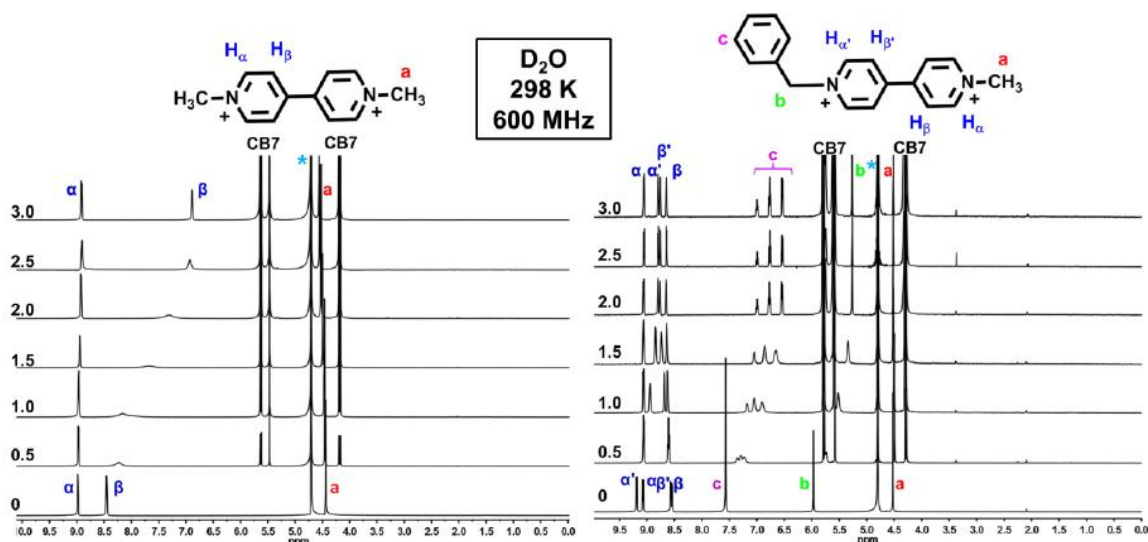


Figure 11. Full ^1H NMR spectra (600 MHz, D_2O , 298 K) of MV^{2+} (left) and BMV^{2+} (right) in the presence of increasing amounts of $\text{CB}[7]$. *Solvent peak.

2.2.4b. BV^{4+} and $\text{CB}[7]$ Recognition Probed by ^1H NMR Spectroscopy

To study the interaction between the guest BV^{4+} and host $\text{CB}[7]$ a titration in DMSO was performed and monitored by ^1H NMR spectroscopy (Figure 12). The NMR data clearly indicate the host-guest complex formation as indicated by the upfield shift and the masking of the β and β' signals. These confirm the arrangement of $\text{CB}[7]$ around the 4,4'-bipyridyl group.

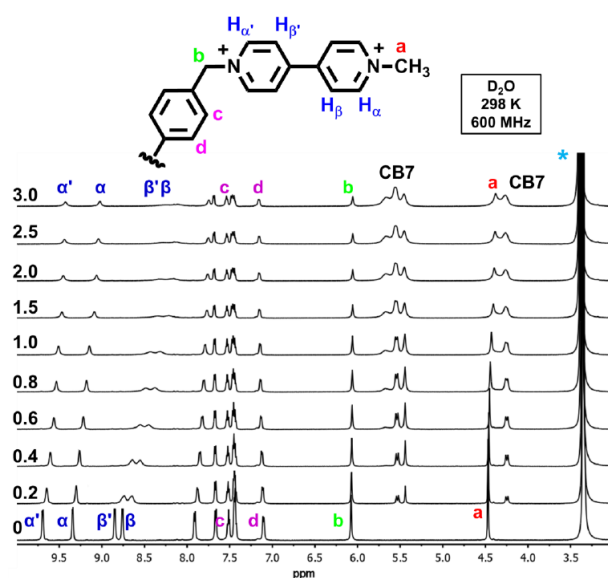


Figure 12. ^1H NMR partial spectra (600 MHz, 1.0 M $\text{NaCl}/\text{D}_2\text{O}$) of BV^{4+} in the presence of increasing amount of $\text{CB}[7]$.

2.2.4c. HV^{12+} and $\text{CB}[7]$ Recognition Probed by ^1H NMR spectroscopy

To study the interaction between the guest HV^{12+} and the $\text{CB}[7]$ host, a titration experiment was also performed using ^1H NMR spectroscopy (Figure 13). These studies

clearly indicate an upfield shift and shielding of β/β' proton along the formation of the inclusion complex and confirm the location of **CB[7]** around the 4,4'-bipyridyl group.

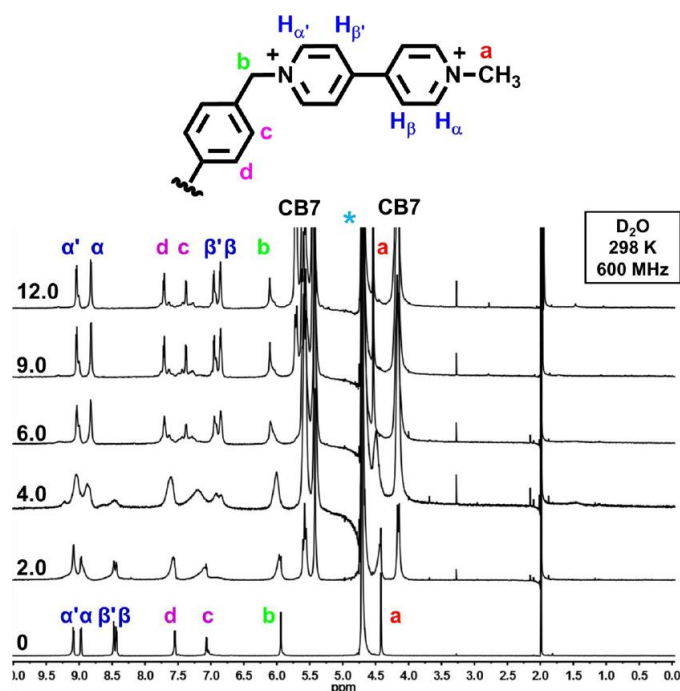


Figure 13. ^1H NMR partial spectra (600 MHz, 1.0 M NaCl/ D_2O) of HV^{12+} in the presence of 0 equiv, 1 equiv, 3 equiv, 7 equiv, 9 equiv, and 12 equiv of **CB[7]**.

2.2.5. Stoichiometry of the Complexes for MV^{2+} and BMV^{2+} Probed by ESI-MS

Electrospray ionization mass spectra (ESI-MS) of the host-guest complexes formed with either MV^{2+} or BMV^{2+} with **CB[7]** (or **CB[8]**) were carried out with an ion-trap instrument (Bruker Esquire 3000plus, Bruker Daltonic, Bremen, Germany) equipped with an Agilent Technologies 6120 quadrupole equipped with an electrospray (ESI) interface. The sample solutions were continuously introduced into the spectrometer source with a syringe pump (Kd Scientific) with a flow rate of $800 \mu\text{L}\cdot\text{h}^{-1}$. For electrospray ionization, the drying gas was heated at 250°C and its flow was set at $6 \text{ L}\cdot\text{min}^{-1}$. The capillary exit voltage was fixed at 5 kV and the skimmer voltage was varied from 50 to 200 V in order to optimize the signal responses. Scanning was performed from $m/z = 100$ to 1500. Different attempts to characterize the complexes formed with HV^{12+} and **CB[7]** were unsuccessful, either in the positive or negative mode, due to the easy fragmentation even at very low skimmer voltage of the viologen-based derivative HV^{12+} . The stoichiometries of the MV^{2+} and BMV^{2+} complexes formed with **CB[7]** and **CB[8]** were investigated by electrospray mass spectrometry (ESI-MS) in the positive mode in aqueous solutions. Regardless of the nature of the viologen (MV^{2+} or BMV^{2+}) and of the macrocyclic receptors used, Figure 14 and Figure 15 clearly evidence the formation of 1:1 complexes. The ionization of the viologen derivatives (mainly observed as positively monocharged species) takes place by reduction and addition of sodium cations. Fragmentations such as demethylation or loss of a benzyl group were observed.

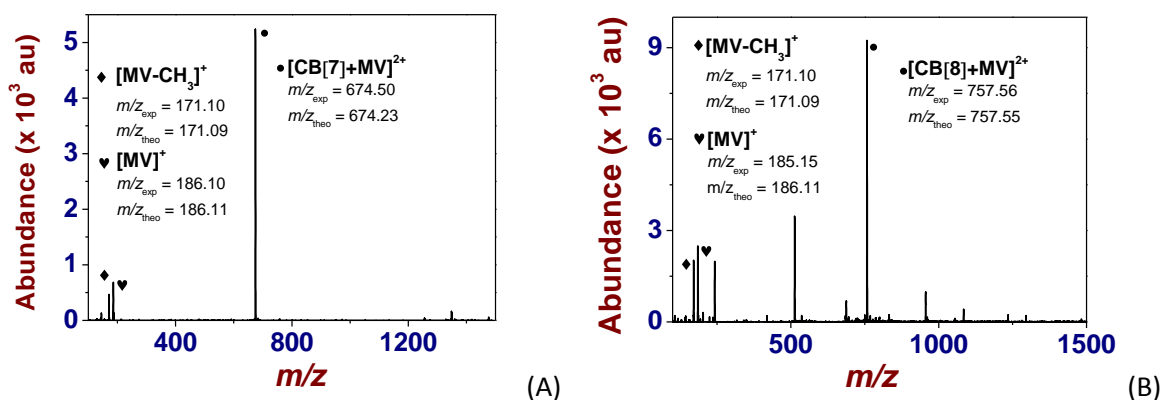


Figure 14. ESI mass spectra of the MV^{2+} complex formed with (A) $\text{CB}[7]$ and (B) $\text{CB}[8]$. (A) $[\text{MV}^{2+}]_0 = 55 \mu\text{M}$ with 1 equivalent of $\text{CB}[7]$; $V_c = 300$ V. (B) $[\text{MV}^{2+}]_0 = 100 \mu\text{M}$ with 1 equivalent of $\text{CB}[8]$. $V_c = 150$ V. Solvent: water; positive mode.

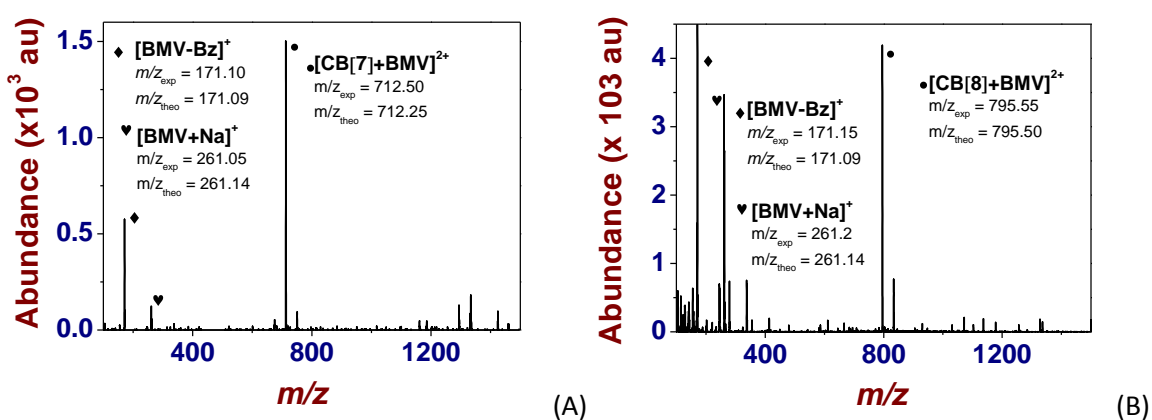


Figure 15. ESI mass spectra of the BMV^{2+} complex formed with (A) $\text{CB}[7]$ and (B) $\text{CB}[8]$. (A) $[\text{BMV}^{2+}]_0 = 50 \mu\text{M}$ with 1 equivalent of $\text{CB}[7]$; $V_c = 280$ V. (B) $[\text{BMV}^{2+}]_0 = 100 \mu\text{M}$ with 1 equivalent of $\text{CB}[8]$. $V_c = 280$ V. Solvent: water; positive mode.

2.2.6. $\text{BMV}^{\bullet+}$ Pimerization in Aqueous Solution

UV-Vis.-NIR absorption spectra (220 nm - 1500 nm) of increasing concentration of $\text{BMV}^{\bullet+}$ (prepared by addition of sodium dithionite under a controlled atmosphere of argon) in 2 mL ($10^{-4} \text{ M} \geq [\text{BMV}^{\bullet+}] \geq 10^{-5} \text{ M}$) or 1 mL ($10^{-3} \text{ M} \geq [\text{BMV}^{\bullet+}] \geq 2 \times 10^{-5} \text{ M}$) 0.1 M phosphate solutions (pH 7.0) were recorded in 10 mm or 5 mm optical cells, respectively, at 25 °C (Dual Cell Pelletier Accessory) with a Cary 5000 spectrophotometer. The absorbances at any wavelength have been correlated to the absorptivities of both the monomer and the dimer, which are related by:

$$A_t = \frac{1}{2} \left[\varepsilon_d C_t + \frac{(2\varepsilon_m - \varepsilon_d) \sqrt{(1 + 8K_{\text{Dim}} C_t) - 1}}{4K_{\text{Dim}}} \right]_{26,27}$$

$$\text{With } K_{\text{Dim}} = [(\text{BMV}^{\bullet+})_2] / [\text{BMV}^{\bullet+}]^2$$

Figure 16 clearly shows the formation of a broad and intense absorption in the NIR region ($\lambda > 800$ nm) upon increasing the concentration of the $\text{BMV}^{\bullet+}$ monoradical cation in solution,

which constitutes a valuable spectrophotometric probe of the dimerization process). The data have been processed with the Origin program and allowed us to evaluate the dimerization constant ($\log K_{\text{Dim}}$ value of 3.46(5)) and to calculate the electronic spectra of $\text{BMV}^{\bullet+}$ under its monomeric and dimeric states (Figure 17).

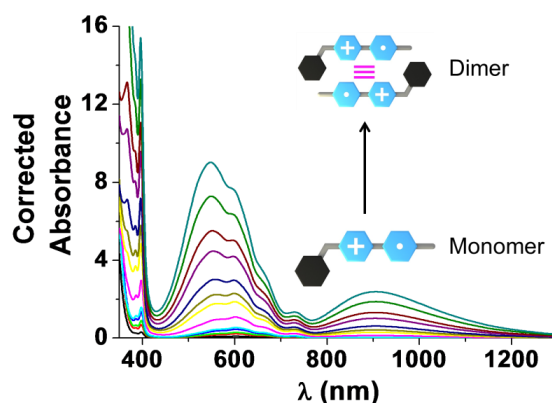


Figure 16. UV-Vis.-NIR absorption titration of $\text{BMV}^{\bullet+}$ in aqueous solution. Solvent: Water pH 7.0 (0.1 M $\text{Na}_2\text{HPO}_4/\text{NaH}_2\text{PO}_4$). For $10^{-5} \text{ M} \leq [\text{BMV}^{\bullet+}]_0 < 10^{-4} \text{ M}$, $l = 1 \text{ cm}$; for $2 \times 10^{-4} \text{ M} \leq [\text{BMV}^{\bullet+}]_0 < 10^{-3} \text{ M}$, $l = 2 \text{ mm}$; $T = 25.0(1) \text{ }^\circ\text{C}$. In each of the solutions considered, the $\text{BMV}^{\bullet+}$ species was generated from BMV^{2+} using freshly prepared sodium dithionite solution at $ca. 10^{-2} \text{ M}$ under O_2 free conditions.

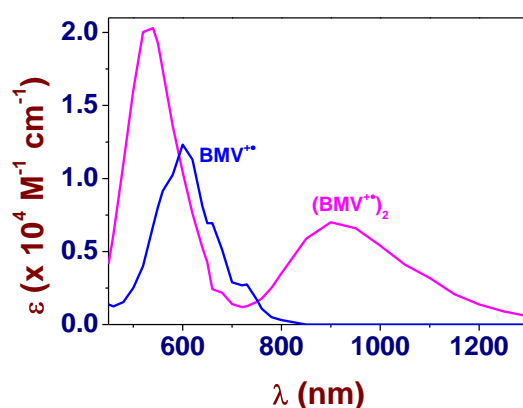


Figure 17. UV-Vis.-NIR electronic spectra of $\text{BMV}^{\bullet+}$ under its monomeric or dimeric form. Solvent: Water pH 7.0 (0.1 M $\text{Na}_2\text{HPO}_4/\text{NaH}_2\text{PO}_4$); $T = 25.0(1) \text{ }^\circ\text{C}$.

2.2.7. Recognition of the Radical Cations by CB[7]

2.2.7a. Recognition of $\text{BMV}^{\bullet+}$ by CB[7]

To determine the association constant of the $\text{BMV}^{\bullet+} \subset \text{CB}[7]$ inclusion complex, 2 mL of BMV^{2+} ($9 \times 10^{-5} \text{ M}$) were reacted with an excess of sodium dithionite (sodium hydrosulfite, $\text{Na}_2\text{S}_2\text{O}_4$, 85%, Sigma Aldrich) in a 10 mm Hellma quartz optical cell in water at pH 7 (0.1 M phosphate buffer). The solution was constantly flushed with O_2 -free argon to avoid re-oxidation of the $\text{BMV}^{\bullet+}$ radicals. The $[\text{CB}[7]]_0/[\text{BMV}^{\bullet+}]_0$ ratio was varied from 0 to 1.0. Special care was taken to ensure that complete equilibration was attained. After each addition, a UV-

Vis.-NIR spectrum was recorded from 220 to 1500 nm on a Cary 5000 (Agilent) spectrophotometer maintained at 25.0(2) °C by the flow of a Dual Cell Pelletier Accessory (Cary Varian). Figure 18A illustrates the spectrophotometric titration of BMV^{2+} by $\text{CB}[7]$. Figure 18B shows the electronic spectra of BMV^{2+} , its dimer $(\text{BMV}^{2+})_2$ and its corresponding inclusion complex $\text{BMV}^{2+} \subset \text{CB}[7]$.

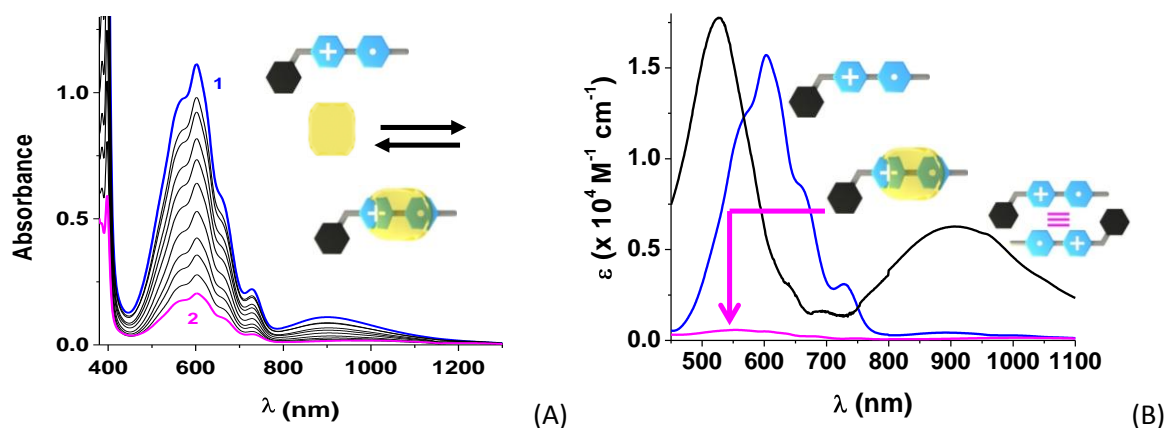


Figure 18. (A) UV-Vis. Absorption batch titration of BMV^{2+} by $\text{CB}[7]$ in water. (B) Electronic spectra of BMV^{2+} and of its inclusion complex with $\text{CB}[7]$ ($\text{BMV}^{2+} \subset \text{CB}[7]$). Solvent: water pH 7.0 (0.1 M $\text{Na}_2\text{HPO}_4/\text{NaH}_2\text{PO}_4$). $[\text{BMV}^{2+}]_0 = 9 \times 10^{-5}$ M; (1) $[\text{CB}[7]]_0/[\text{BMV}^{2+}]_0 = 0$; (2) $[\text{CB}[7]]_0/[\text{BMV}^{2+}]_0 = 1.0$; $l = 1$ cm; $T = 25.0(1)$ °C. In each of the solutions considered, the BMV^{2+} species was generated from BMV^{2+} using freshly prepared sodium dithionite solution at *ca.* 10^{-2} M under O_2 free conditions.

2.2.7b. Recognition of $\text{MV}^{2+}/\text{MV}^{\bullet+}$ by $\text{CB}[7]$

Figure 19A shows the UV-Vis-NIR spectra of MV^{2+} ($[\text{MV}^{2+}]_0 = 10^{-4}$ M) and of its inclusion complex $\text{MV}^{2+} \subset \text{CB}[7]$ ($[\text{CB}[7]]_0 = 2 \times 10^{-4}$ M).

Addition of freshly prepared and O_2 -free sodium dithionite reduces the MV^{2+} into its monoradical cationic species which is still located within the $\text{CB}[7]$ cavity (the absorbance measured for the $\text{MV}^{\bullet+} \subset \text{CB}[7]$ is lower than that obtained for free $\text{MV}^{\bullet+}$, blue line). Figure 19B displays the UV-Vis-NIR spectra of MV^{2+} ($[\text{MV}^{2+}]_0 = 10^{-4}$ M, black line) and of its monoradical cationic species $\text{MV}^{\bullet+}$ (red line, addition of freshly prepared and O_2 -free sodium dithionite). No dimer is evidenced under these experimental conditions. Addition of $\text{CB}[7]$ ($[\text{CB}[7]]_0 = 5 \times 10^{-5}$ M, blue line and $[\text{CB}[7]]_0 = 2 \times 10^{-4}$ M, green line) induces a hypochromic shift of the absorption characteristics of the monoradical cationic $\text{MV}^{\bullet+}$. This spectral variation is indicative of the inclusion process of $\text{MV}^{\bullet+}$ within the $\text{CB}[7]$ cavity. Figure 19C illustrates the distribution diagrams of the $\text{MV}^{\bullet+}/\text{CB}[7]$ system which agree with our experimental observations.

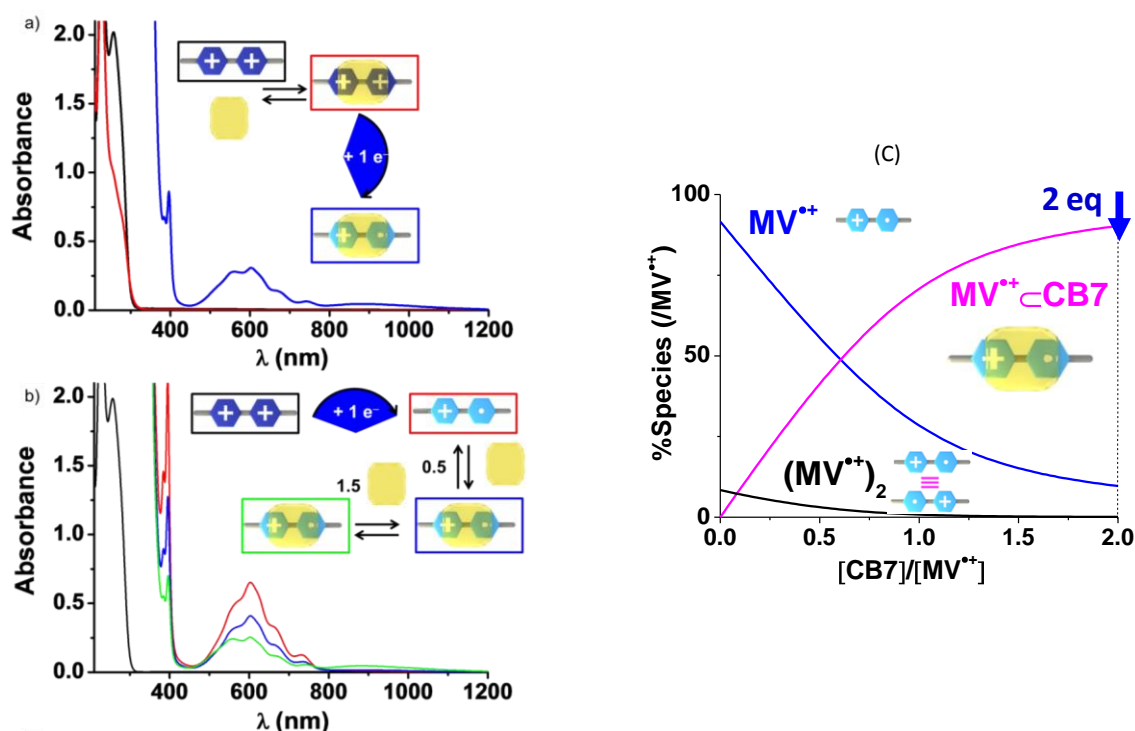


Figure 19. (A) UV-Vis-NIR spectra of MV^{2+} ($[MV^{2+}]_0 = 10^{-4}$ M, black line) and of its $MV^{2+} \subset CB[7]$ complex ($[MV^{2+}]_0 = 10^{-4}$ M and $[CB[7]]_0 = 2 \times 10^{-4}$ M, red line). (B) UV-Vis-NIR spectra of MV^{2+} ($[MV^{2+}]_0 = 10^{-4}$ M, black line) and of its monoradical cationic species $MV^{\bullet+}$ (red line, addition of freshly prepared and O_2 -free sodium dithionite). (C) Distribution diagrams of the $MV^{\bullet+}$ species as a function of its concentration. Solvent: water pH 7.0 (0.1 M Na_2HPO_4/NaH_2PO_4); $l = 1$ cm; $T = 25.0(1)$ °C. In each of the solutions considered, $MV^{\bullet+}$ was generated from MV^{2+} using freshly prepared sodium dithionite solution at *ca.* 10^{-2} M under O_2 free conditions.

2.2.7c. Recognition of $BMV^{2+}/BMV^{\bullet+}$ by $CB[7]$

Figure 20A displays the UV-Vis-NIR spectra of BMV^{2+} ($[BMV^{2+}]_0 = 10^{-4}$ M) and of its inclusion complex $BMV^{2+} \subset CB[7]$ ($[CB[7]]_0 = 2 \times 10^{-4}$ M).

Addition of freshly prepared and O_2 -free sodium dithionite reduces the BMV^{2+} into its monoradical cationic species which is still located within the $CB[7]$ cavity (the absorbance measured for the $BMV^{\bullet+} \subset CB[7]$ is much lower than that obtained for free $BMV^{\bullet+}$, blue spectrum). Figure 20B shows the UV-Vis-NIR spectra of BMV^{2+} ($[BMV^{2+}]_0 = 10^{-4}$ M, black spectrum) and of its monoradical cationic species $BMV^{\bullet+}$ (red line, addition of freshly prepared and O_2 -free sodium dithionite). The presence of weak amount of the $(BMV^{\bullet+})_2$ dimer can be evidenced under these experimental conditions (absorption at about 900 nm). Upon addition of $CB[7]$ ($[CB[7]]_0 = 5 \times 10^{-5}$ M, blue line and $[CB[7]]_0 = 2 \times 10^{-4}$ M, green line), the absorption characteristics of the monoradical cationic $BMV^{\bullet+}$ vanishes. This spectral variation is indicative of the inclusion process of $BMV^{\bullet+}$ within the $CB[7]$ cavity. Figure 20C displays the distribution diagrams of the $BMV^{\bullet+}/CB[7]$ system which agree with our experimental observations.

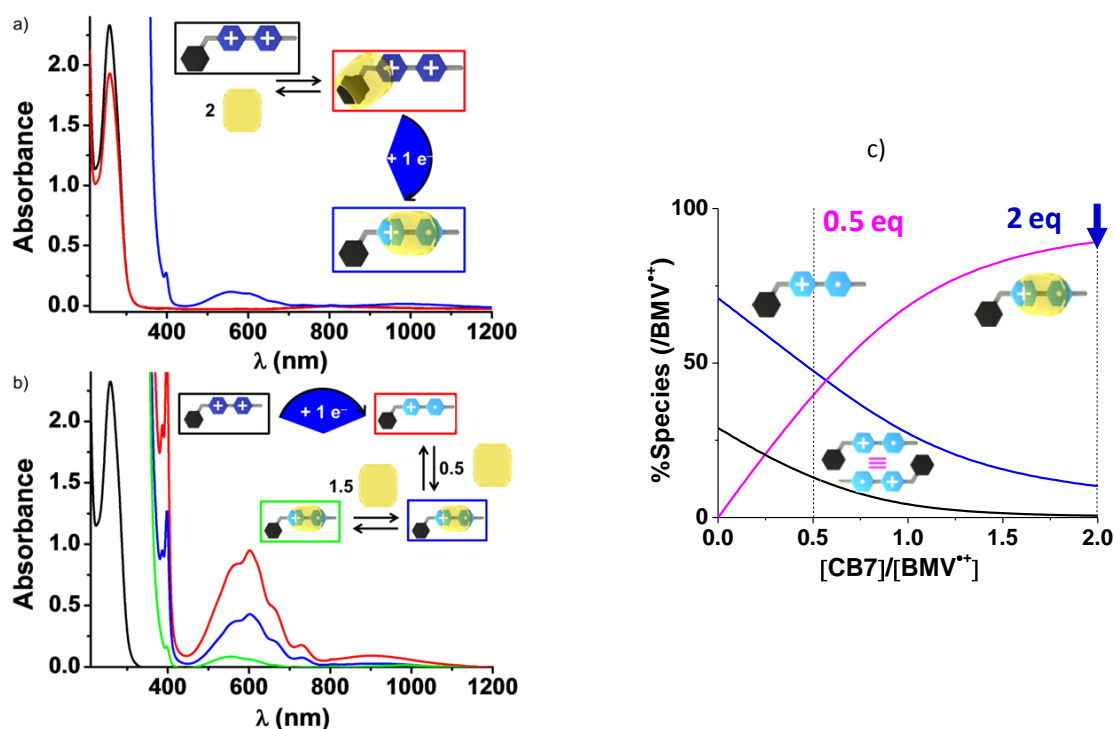


Figure 20. (A) UV-Vis-NIR spectra of **BMV²⁺** ($[\text{BMV}^{2+}]_0 = 10^{-4}$ M, black line) and of its **BMV²⁺ ⊂ CB[7]** complex ($[\text{BMV}^{2+}]_0 = 10^{-4}$ M and $[\text{CB}[7]]_0 = 2 \times 10^{-4}$ M, red line). (B) UV-Vis-NIR spectra of **BMV²⁺** ($[\text{BMV}^{2+}]_0 = 10^{-4}$ M, black line), of its monoradical cationic species **BMV^{•+}** (red line, addition of freshly prepared and O₂-free sodium dithionite) and upon addition of **CB[7]** ($[\text{CB}[7]]_0 = 5 \times 10^{-5}$ M, blue line and $[\text{CB}[7]]_0 = 2 \times 10^{-4}$ M, green line). (C) Distribution diagrams of the **BMV^{•+}/CB[7]** system. Solvent: water buffered at pH 7.0 with 0.1 M Na₂HPO₄/ NaH₂PO₄; $l = 1$ cm; $T = 25.0(1)$ °C. In each of the solutions considered, the **BMV^{•+}** species was generated from **BMV²⁺** using freshly prepared sodium dithionite solution at *ca.* 10⁻² M under O₂ free conditions.

2.2.7d. Recognition of **BV⁴⁺/BV^{2(•+)}** by **CB[7]**

Figure 21A displays the UV-Vis-NIR spectra of **BV⁴⁺** ($[\text{BV}^{4+}]_0 = 5.3 \times 10^{-5}$ M) and of its **BV⁴⁺ ⊂ (CB[7])₂** complex ($[\text{CB}[7]]_0 = 2.12 \times 10^{-4}$ M).

Addition of freshly prepared and O₂-free sodium dithionite reduces the **BV⁴⁺** into its radical state. Strong intramolecular interactions between the two monoradical monocations within **BV^{2(•+)}** induce release of the **CB[7]** macrocycles as evidence by the NIR CT absorption (blue line). Figure 21B shows the UV-Vis-NIR spectra of **BV⁴⁺** ($[\text{BV}^{4+}]_0 = 5.3 \times 10^{-5}$ M, black line) and of its radical analogue **BV^{2(•+)}** (blue line, addition of freshly prepared and O₂-free sodium dithionite). The intramolecular stacking interactions between the two viologen monoradicals are evidenced by the two absorptions lying in the visible and NIR regions. Upon addition of **CB[7]** ($[\text{CB}[7]]_0 = 5.3 \times 10^{-5}$ M, red line and $[\text{CB}[7]]_0 = 2.12 \times 10^{-4}$ M, pink line), the absorptions originating from the intramolecular dimer remain unchanged supporting the fact that speciation of the monoradical cations with **CB[7]** does not compete with dimerization.

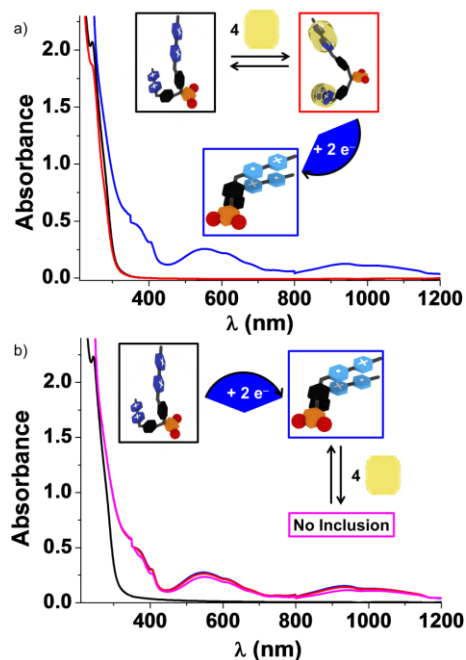


Figure 21. (a) UV-Vis-NIR spectra of BV^{4+} ($[\text{BV}^{4+}]_0 = 5.3 \times 10^{-5}$ M, black line) and of its $\text{BV}^{4+} \subset (\text{CB}[7])_2$ complex ($[\text{BV}^{4+}]_0 = 5.3 \times 10^{-5}$ M and $[\text{CB}[7]]_0 = 2.12 \times 10^{-4}$ M, red line). (b) UV-Vis-NIR spectra of BV^{4+} ($[\text{BV}^{4+}]_0 = 5.3 \times 10^{-5}$ M, black line) and of its radical analogue $\text{BV}^{2(\bullet+)}$ (blue line, addition of freshly prepared and O_2 -free sodium dithionite), and upon addition of $\text{CB}[7]$ ($[\text{CB}[7]]_0 = 5.3 \times 10^{-5}$ M, red line and $[\text{CB}[7]]_0 = 2.12 \times 10^{-4}$ M, pink line). Solvent: water buffered at pH 7.0 with 0.1 M $\text{Na}_2\text{HPO}_4/\text{NaH}_2\text{PO}_4$; $l = 1$ cm; $T = 25.0(1)$ °C. In each of the solutions considered, the $\text{BV}^{2(\bullet+)}$ species was generated from BV^{4+} using freshly prepared sodium dithionite solution at ca. 10^{-2} M under O_2 free conditions.

2.2.7e. Recognition of $\text{HV}^{12+}/\text{HV}^{6(\bullet+)}$ by $\text{CB}[7]$

Figure 22A displays the UV-Vis-NIR spectra of HV^{12+} ($[\text{HV}^{12+}]_0 = 2.6 \times 10^{-5}$ M) and of its $\text{HV}^{12+} \subset (\text{CB}[7])_6$ complex ($[\text{CB}[7]]_0 = 3.12 \times 10^{-4}$ M).

Addition of freshly prepared and O_2 -free sodium dithionite reduces the HV^{12+} into its radical state. Strong intramolecular interactions between the six monoradical monocations within $\text{HV}^{6(\bullet+)}$ induce release of the $\text{CB}[7]$ macrocycles as evidence by the NIR CT absorption (blue line). Figure 22B illustrated the UV-Vis-NIR spectra of HV^{12+} ($[\text{HV}^{12+}]_0 = 2.6 \times 10^{-5}$ M, black line) and of its hexaradical analogue $\text{HV}^{6(\bullet+)}$ (blue line, addition of freshly prepared and O_2 -free sodium dithionite). The intramolecular stacking interactions between the viologen radicals are evidenced by the two absorptions lying in the visible and NIR regions. Upon addition of $\text{CB}[7]$ ($[\text{CB}[7]]_0 = 1.56 \times 10^{-4}$ M, red line and $[\text{CB}[7]]_0 = 3.12 \times 10^{-4}$ M, pink line), the absorptions originating from the intramolecular dimer remain almost unchanged supporting the fact that speciation of the monoradical cations with $\text{CB}[7]$ does not compete with dimerization.

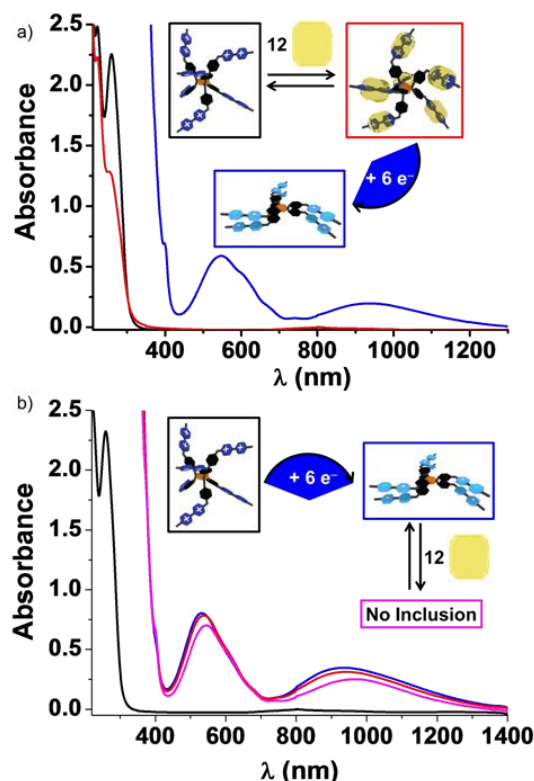


Figure 22. (A) UV-Vis.-NIR spectra of HV^{12+} ($[\text{HV}^{12+}]_0 = 2.6 \times 10^{-5}$ M, black line) and of its $\text{HV}^{12+} \cdot (\text{CB}[7])_6$ complex ($[\text{HV}^{12+}]_0 = 2.6 \times 10^{-5}$ M and $[\text{CB}[7]]_0 = 3.12 \times 10^{-4}$ M, red line). (B) UV-Vis.-NIR spectra of HV^{12+} ($[\text{HV}^{12+}]_0 = 2.6 \times 10^{-5}$ M, black line) and of its hexaradical analogue $\text{HV}^{6(\bullet+)}$ (blue line, addition of freshly prepared and O_2 -free sodium dithionite), and upon addition of $\text{CB}[7]$ ($[\text{CB}[7]]_0 = 1.56 \times 10^{-4}$ M, red line and $[\text{CB}[7]]_0 = 3.12 \times 10^{-4}$ M, pink line). Solvent: water buffered at pH 7.0 with 0.1 M $\text{Na}_2\text{HPO}_4 / \text{NaH}_2\text{PO}_4$; $l = 1$ cm; $T = 25.0(1)^\circ\text{C}$. In each of the solutions considered, the $\text{HV}^{6(\bullet+)}$ species was generated from HV^{12+} using freshly prepared sodium dithionite solution at *ca.* 10^{-2} M under O_2 free conditions.

2.2.8. Electrochemistry

Cyclic Voltammetry (CV) and Square Wave voltammetry (SW) experiments were carried out at room temperature in argon-purged H_2O and DMSO solutions with a Gamry Multipurpose instrument (Reference 600) interfaced to a PC. The electrochemical experiments were performed using a glassy carbon working electrode (0.071 cm^2 , BASi). The electrode surface was polished routinely with $0.05 \mu\text{m}$ alumina-water slurry on a felt surface immediately before use. The counter electrode was a Pt coil and the reference electrode was an Ag/AgCl electrode, unless otherwise noted. The concentration of the supporting electrolyte, tetrabutylammonium chloride (TBACl) was 0.1 M. The experimental errors on the potential values are estimated to ± 10 mV. All measurements were recorded in phosphate buffer solutions (pH 7). In order to overcome the precipitation effect that normally occurs upon reduction of viologen, the scan rate was set to 1000 mV s^{-1} . Figure 23 represents the cyclic voltammograms of all four viologens studied in the absence and the presence of $\text{CB}[7]$. Values of $E_{1/2}$ calculated for each redox processes are in excellent agreement with the ones determined by SW experiments.

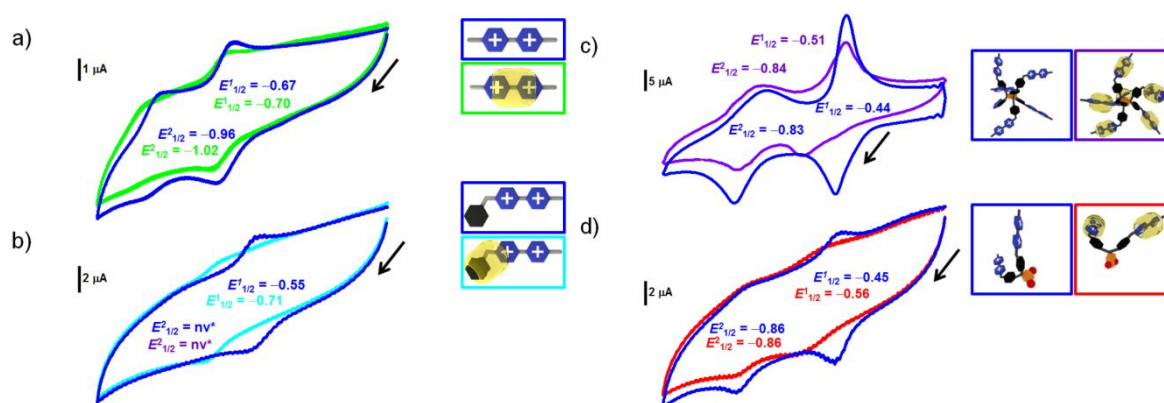


Figure 23. Cyclic voltammograms (CVs) MV^{2+} , $[MV^{2+}] = 0.06$ mM (A), BMV^{2+} , $[BMV^{2+}] = 0.08$ mM (B), HV^{12+} , $[HV^{12+}] = 0.024$ mM (C), and BV^{4+} , $[BV^{4+}] = 0.065$ mM (D) in the absence and the presence of **CB[7]** (respectively 3, 3, 18 and 4 equivalents of **CB[7]**). All voltammograms were recorded in Argon-purged phosphate buffer solutions (pH 7) at 298 K with 0.1 M TBACl. The scan rate was set at 1000 mVs^{-1} . * Under our conditions, the second redox wave was not visible by CV in the case of BMV^{2+} but was detectable by SW. E versus Ag/AgCl.

2.2.9. Computational Methods

All calculations presented in this work were performed by the group of Pr Carlos Platas-Iglesias (Departamento de Química Fundamental, Universidade da Coruña, Coruña, Spain) and were employing the Gaussian 09 package (Revision B.01).²⁸ Full geometry optimizations of the **CB[7]**, MV^{2+} , BMV^{2+} , $MV^{2+} \subset CB[7]$ and $BMV^{2+} \subset CB[7]$ systems were carried out without any symmetry constraints using hybrid DFT with the B3LYP exchange-correlation functional^{29,30} and the standard 6-31G(d) basis set. The X-ray structure of **CB[7]** was used as input geometry for structure optimization purposes.³¹ The stationary points found on the potential energy surfaces as a result of the geometry optimizations have been tested to represent energy minima rather than saddle points via frequency analysis (0 imaginary frequencies). The relative free energies of the different isomers of $BMV^{2+} \subset CB[7]$ were calculated including non-potential-energy contributions (zero point energies and thermal terms) obtained through frequency analysis. In aqueous solution relative free energies of the different conformations of the complexes were calculated from solvated single point energy calculations on the geometries optimized *in vacuo*. In these calculations, solvent effects (water) were evaluated by using the polarizable continuum model (PCM), in which the solute cavity is built as an envelope of spheres centred on atoms or atomic groups with appropriate radii. In particular, the integral equation formalism (IEFPCM)³² variant as implemented in Gaussian 09 was employed with the radii and non-electrostatic terms obtained by D. G. Truhlar et al. (SMD solvation model).³³

Due to the large size of the $HV^{12+} \subset (CB[7])_6$ system, semi-empirical calculations are the only practical alternative to high-level calculations using DFT or more sophisticated *ab initio* methods. Among the different semi-empirical methods, we have selected the PM6 semi-empirical MO method,³⁴ which has been shown to provide more accurate results than the classical PM3 and AM1 semi-empirical methods for different systems.^{35,36}

2.2.10. Statistical Processing of the Absorption Spectrophotometric Data

The spectrophotometric data were processed using the Specfit program³⁷⁻⁴⁰ which adjusts the stability constants and the corresponding extinction coefficients of the species formed at equilibrium. Specfit uses factor analyses to reduce the absorbance matrix and to extract the eigenvalues prior to the multi-wavelength fit of the reduced data set according to the Marquardt algorithm.^{41,42}

2.3. Discussion

2.3.1. Characterization of the Thread/CB[7] [n]pseudorotaxanes

2.3.1a. Recognition of MV^{2+} by CB[7]

An absorption spectrophotometric binding titration of $MV^{2+} 2I^-$ with **CB[7]** was performed in water at pH 7.0 to confirm the 1:1 stoichiometry ($MV^{2+} \subset CB[7]$). Preliminary measurements such as a Job plot determined from absorption spectrophotometric data (Figure 4) or ESI-MS (Figure 14) evidenced the presence of [2]pseudorotaxane $MV^{2+} \subset CB[7]$ in solution. The host-guest binding constant ($\log K_{MV^{2+} \subset CB[7]} = 5.30(2)$ at 0.1 M phosphate buffer, pH 7.0) that was calculated from our spectral data set perfectly agrees with those previously determined and constituted a benchmark for our further studies. The complexation of MV^{2+} with **CB[7]** has been extensively studied, in particular by the groups of K. Kim⁴³ or A. E. Kaifer,⁴⁴ who reported that MV^{2+} forms a thermodynamically stable ($\log K_{MV^{2+} \subset CB[7]} = 5.01$ at 0.2 M NaCl⁴⁴ and $\log K_{MV^{2+} \subset CB[7]} = 5.3$ at 0.1 M phosphate buffer pH 7.0⁴³) and a reasonably inert kinetic 1:1 inclusion species with **CB[7]** ($k_{diss} = 1.9 \times 10^2 \text{ s}^{-1}$)⁴³ in aqueous solutions.

The formation of $MV^{2+} \subset CB[7]$ is characterized by a significant hypochromic shift of the signal that corresponds to the $\pi-\pi^*$ transition centred on the **BIPY**²⁺ core (Figure 10 and Figure 25). This shift allows detection of the complex in solution. Taken together, the spectroscopic data point to an inclusion complex strongly stabilized by hydrophobic and charge--dipole interactions and suggest that the **CB[7]** host has a cavity that is well tailored for binding the **BIPY**²⁺ moiety. The ¹H NMR studies (Figure 11) on aqueous $MV^{2+} \subset CB[7]$ also support a binding model in which the bipyridinium moiety sits within the cavity of **CB[7]** and the two methyl groups are projected outward.⁴⁵ The upfield shift of the β protons perfectly matches with such binding mode. DFT calculations performed by the group of Pr Carlos Platas-Iglesias (Departamento de Química Fundamental, Universidad da Coruña, Coruña, Spain) were also found to agree with such arrangement. The geometry of the $MV^{2+} \subset CB[7]$ system optimized at the B3LYP/6-31G(d) level (Figure 24) indicates that the MV^{2+} unit is positioned within the **CB[7]** cavity with the methyl groups pointing outward. Four CH \cdots O hydrogen-bonding interactions with C \cdots O distances of 3.16–3.17 Å, CH \cdots O distances of 2.20–2.33 Å, and CH \cdots O angles of 133–146° appear to be also responsible of the stabilization of the $MV^{2+} \subset CB[7]$ complex.

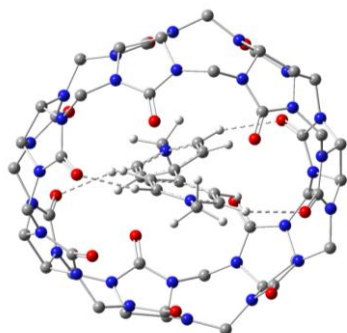


Figure 24. Molecular geometry of $\text{MV}^{2+}@\text{CB}[7]$ optimized at the B3LYP/6-31G(d) level.

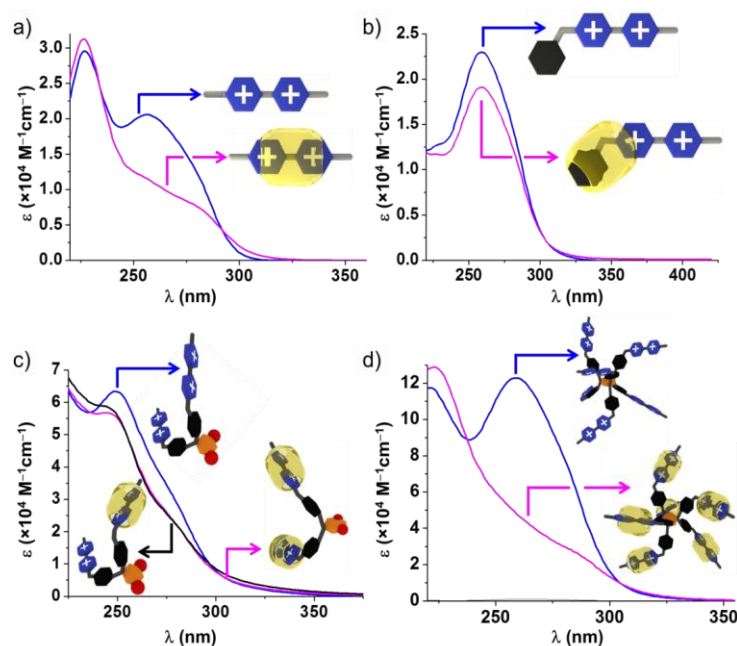


Figure 25. Electronic spectra of MV^{2+} (a), BMV^{2+} (b), BV^{4+} (c) and HV^{12+} (d) and their corresponding complexes with $\text{CB}[7]$. Solvent: water pH 7.0 (0.1 M $\text{Na}_2\text{HPO}_4/\text{NaH}_2\text{PO}_4$); $T = 25.0(1)^\circ\text{C}$.

2.3.1b. Recognition of BMV^{2+} by $\text{CB}[7]$

To elucidate the interactions between $\text{CB}[7]$ and the BIPY^{2+} units of the hexaviologen dendrimer HV^{12+} , we first analyzed the asymmetrical benzyl methyl viologen BMV^{2+} as a model system. BMV^{2+} readily forms a stable 1:1 inclusion complexes with $\text{CB}[7]$ in water, as evidenced by ^1H NMR spectroscopy (Figure 11). In D_2O the singlet that corresponds to the methyl group of BMV^{2+} remains unchanged on addition of $\text{CB}[7]$, whereas the singlet that corresponds to the aromatic protons (H_c) of the benzyl ring is split into one doublet and two triplets. This differentiation is due to $\text{CB}[7]$'s restricting the rotation of the benzyl ring. The multiplets are shifted upfield because of the increased shielding the protons experienced inside the macrocycle. The singlet associated with the methylene bridge (H_b) is shifted upfield by more than 0.7 ppm, and the signals of the α' aromatic protons of the viologen are shifted upfield by about 0.6 ppm. Those of the α aromatic protons are nearly unchanged. By contrast with MV^{2+} , the signals of both β and β' aromatic protons experience a small

downfield shift. Together, these results are consistent with complexation of the benzyl ring by **CB[7]** through hydrophobic and dipole–charge attractions, and its interaction with only part of the viologen moiety.^{46,47}

The 1:1 stoichiometric complexation between **BMV**²⁺ by **CB[7]** was further confirmed by Job plot experiments (Figure 6) and ESI-MS (Figure 15) and the strength of binding of the **BMV**²⁺⊂**CB[7]** species was evaluated by absorption spectrophotometry (Figure 5). Unlike recognition of **MV**²⁺ by **CB[7]**, the recognition of **BMV**²⁺ by **CB[7]** has little influence on the **BIPY**²⁺ π–π transitions, which indicates, as do the ¹H NMR data, that the **CB[7]** host does not fully encircle this chromophore but is instead positioned on the benzyl moiety. The binding constant of the **BMV**²⁺⊂**CB[7]** complex in water was calculated to be $\log K_{\text{BMV}^{2+}\text{CB[7]}} \sim 6.9(8)$. Although this value is only a rough estimate (spectral changes observed during the titration were weak), it suggests that **BMV**²⁺ forms a significantly more stable [2]pseudorotaxane with **CB[7]** than **MV**²⁺ does. This value is similar in magnitude to those determined for other cations (ammonium,^{48,49} pyridinium, or 4,4'-bipyridinium)⁴⁷ that display a hydrophobic benzyl substituent attached to a cationic core (*e.g.*, $\log K = 8.398(4)$ for $(\text{PhCH}_2)\text{N}(\text{CH}_3)_3^+$ versus 5.079(2) for $\text{N}(\text{CH}_3)_4^+$ and $\log K = 8.613(2)$ for $(\text{PhCH}_2)(\text{CH}_3)_2\text{N}^+(\text{CH}_2)_2\text{OH}$ versus 5.813(2) for $(\text{CH}_3)_3\text{N}^+(\text{CH}_2)_2\text{OH}$).

For the **BMV**²⁺⊂**CB[7]** system, two different minimum energy conformations were deduced from DFT calculations (Figure 26): one in which the viologen unit resides inside the **CB[7]** host, and a second isomer in which the benzyl unit of **BMV**²⁺ resides inside. The free energy difference between these two forms, calculated in the gas-phase indicates that the conformation with the viologen unit inside the cavity is more stable by 18.0 kcal mol⁻¹. However, this is not surprising considering the electrostatic potential on the molecular surface of **BMV**²⁺. This property, as defined by the 0.001 electrons·bohr⁻³ contour of the electron density following the suggestion of Bader⁵⁰ was calculated at the B3LYP/6-311G** level (Figure 26). Due to the net positive charge on the molecule, the surface is completely positive. The most positive region located on the hydrogens of the bipyridinium unit (as is observed for related viologens)⁵¹ which suggests that the primary interaction between **BMV**²⁺ and **CB[7]** in the gas-phase involves the bipyridinium unit rather than the benzyl moiety. When solvent effects were accounted for with the aid of the PCM model, the free energy difference between the two binding modes decreased from 18.0 kcal mol⁻¹ to 7.3 kcal mol⁻¹. Because the NMR spectral data provide strong evidence of binding to the benzyl unit, it is clear that, at least in aqueous solution, our DFT calculations overestimate the stability of the inclusion complex in which the viologen unit sits inside the cavity of **CB[7]**.

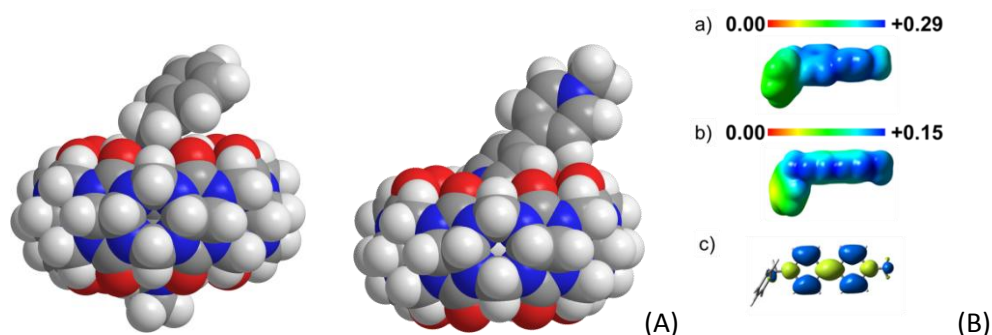


Figure 26. (A) Space-filling representation of the two minimum energy geometries of $\text{BMV}^{2+} \subset \text{CB}[7]$ optimized at the B3LYP/6-31G(d) level. (B) Computed B3LYP/6-311G** electrostatic potential (Hartree) of BMV^{2+} (a) and $\text{BMV}^{\bullet+}$ (b) on the molecular surface defined by the 0.001 electrons-bohr⁻³ contour of the electronic density and view of the SOMO of $\text{BMV}^{\bullet+}$ (c) calculated in aqueous solution at the same computational level.

This discrepancy is likely due to the frequent inadequacy of continuum dielectric solvent models for investigating ionic solutes that have concentrated charge densities with strong local solute-solvent interactions.⁵²⁻⁵⁴ The calculated 10.7 kcal mol⁻¹ stabilization of the complex that has the benzyl group inside $\text{CB}[7]$ can be explained in terms of more efficient solvation, as this binding mode leaves the bipyridinium unit (with its positive electrostatic potential) exposed to the solvent.

2.3.1c. Recognition of BV^{4+} and HV^{12+} by $\text{CB}[7]$

The solubility of BV^{4+} in water was found to be low most likely due to the dioxybiphenyl groups which were introduced on the phosphazene anchor. Thus, monitoring of the interaction of BV^{4+} with $\text{CB}[7]$ by ¹H NMR was carried out in a 3 mM solution of BV^{4+} in [d₆]DMSO. The spectra (Figure 12) were recorded for additions of up to three equivalents of $\text{CB}[7]$. As observed with HV^{12+} (Figure 13), the signals for the β and β' aromatic protons are the most affected by $\text{CB}[7]$, with both types shifted significantly upfield. The α and α' proton signals are shifted upfield as well but at a lesser extent than the β and β' aromatic protons. All other signals, including those corresponding to the methylene groups, remain nearly unchanged. These results confirm the formation of a $\text{BV}^{4+} \subset (\text{CB}[7])_2$ inclusion complex in which the bipyridinium chromophores are positioned inside the hydrophobic cavities of the two $\text{CB}[7]$ macrocycles, and the methyl groups and hindered benzyl moieties are outside. In this complex, the dioxybiphenyl groups increase steric hindrance near the phosphazene core and prevent inclusion of the benzyl group. The ¹H NMR titration results indeed suggest that conformational rearrangements of the dioxybiphenyl protecting groups and the phosphazene core occur on recognition by $\text{CB}[7]$. For example, the signals between 7.3 and 8 ppm associated with the dioxybiphenyl protecting groups are shifted upfield, which is consistent with steric effects upon $\text{CB}[7]$ binding.

Absorption titration of BV^{4+} in 0.1 M phosphate buffer at pH 7.0 (Figure 7) allowed us to detect the formation of a [2]pseudorotaxane ($\text{BV}^{4+} \subset \text{CB}[7]$, $\log K_{\text{BV}^{4+} \subset \text{CB}[7]} \sim 5.9(2)$) and a

[3]pseudorotaxane ($\text{BV}^{4+} \subset (\text{CB}[7])_2$, $\log K_{\text{BV}^{4+} \subset (\text{CB}[7])_2} \approx 4.7(4)$). In addition, the large decrease of the BIPY^{2+} π - π transitions of BV^{4+} upon binding with $\text{CB}[7]$ confirmed a binding mode in which the bipyridinium chromophores are located inside the hydrophobic cavities of the $\text{CB}[7]$ hosts (*i.e.* comparable to MV^{2+}). In addition, the job plot experiments supported the formation of the $\text{BV}^{4+} \subset (\text{CB}[7])_2$ species (Figure 8). Interestingly, the stability constant of the [2]pseudorotaxane $\text{BV}^{4+} \subset \text{CB}[7]$ is comparable to that measured for $\text{MV}^{2+} \subset \text{CB}[7]$ ($\log K_{\text{MV}^{2+} \subset \text{CB}[7]} = 5.30(2)$), which supports the fact that $\text{CB}[7]$ prefers the bipyridinium moiety in BV^{4+} most likely due to steric hindrance as mentioned above. Furthermore, a comparison of the stabilities of the [2]pseudorotaxane $\text{BV}^{4+} \subset \text{CB}[7]$ and the [3]pseudorotaxane $\text{BV}^{4+} \subset (\text{CB}[7])_2$ ($K_{\text{BV}^{4+} \subset (\text{CB}[7])_2} / K_{\text{BV}^{4+} \subset \text{CB}[7]} = 0.03 \ll 0.25$) indicates that binding of the first $\text{CB}[7]$ sterically inhibits binding of the second;^{55,56} in other words, the system exhibits a negative cooperativity that originates from the bulky protecting groups, which decrease the flexibility of the phosphazene core and limit its ability to rearrange to accommodate the second $\text{CB}[7]$ macrocycle.

With respect to the hexaviologen system HV^{12+} , evidence for the formation of the [7]pseudorotaxane $\text{HV}^{12+} \subset (\text{CB}[7])_6$ was observed thanks to ^1H NMR titration experiments in which 1 to 12 equivalents of $\text{CB}[7]$ were successively added to a 1 mM solution of HV^{12+} . As illustrated in Figure 13, the most significant change in the spectra of HV^{12+} are related to the β and β' aromatic protons, which exhibit a large upfield shift of more than 1.5 ppm. This large shift is consistent with those already observed for the β/β' protons of MV^{2+} . The smaller shifts of the other corresponding signals in HV^{12+} and MV^{2+} , such as those of the methyl groups, are also similar. These data indicate that the mode of interaction between $\text{CB}[7]$ and BIPY^{2+} in HV^{12+} is very similar to that observed in $\text{MV}^{2+} \subset \text{CB}[7]$, namely, that in which the bipyridinium chromophore resides within the cavity of $\text{CB}[7]$ (I). Although benzyl spacers in HV^{12+} have been used to anchor the BIPY^{2+} groups on the phosphazene core, strong steric interactions near the core likely prevent the type of benzyl-group inclusion seen in $\text{BMV}^{2+} \subset \text{CB}[7]$.

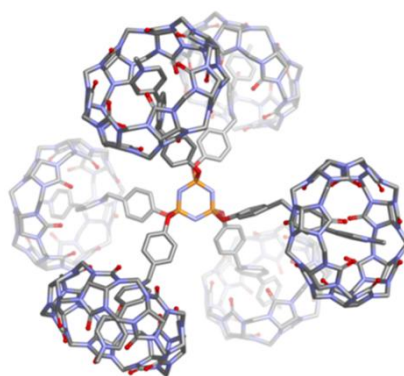


Figure 27. Capped-Stick representation of the minimum energy geometry of $\text{HV}^{12+} \subset (\text{CB}[7])_6$ obtained with PM6 calculations.

The existence in solution of the [7]pseudorotaxane $\text{HV}^{12+} \subset (\text{CB}[7])_6$ was further confirmed by a Job plot experiment (Figure 10), which supports the $\text{HV}^{12+} : \text{CB}[7]$ binding stoichiometry

of 1:6. The electronic spectrum of \mathbf{HV}^{12+} ($\epsilon^{259} = 12.29 \times 10^4 \text{ M}^{-1} \text{ cm}^{-1}$) was found to be similar to the sum of six spectra of \mathbf{MV}^{2+} ($\epsilon^{256} = 2.06 \times 10^4 \text{ M}^{-1} \text{ cm}^{-1} \sim (1/6) \times \epsilon^{\mathbf{HV}^{12+}}$) or six spectra of \mathbf{BMV}^{2+} ($\epsilon^{259} = 2.29 \times 10^4 \text{ M}^{-1} \text{ cm}^{-1} \approx (1/6) \times \epsilon^{\mathbf{HV}^{12+}}$). For both \mathbf{HV}^{12+} and \mathbf{MV}^{2+} , recognition by $\mathbf{CB}[7]$ resulted in a significant hypochromic shift of the electronic transition at $\lambda = 259 \text{ nm}$. On the other hand, \mathbf{BV}^{4+} contains two 2,2'-dioxybiphenyl protecting groups, which do not act as binding sites for $\mathbf{CB}[7]$ but do absorb UV light strongly. Owing to their presence, the electronic spectrum of \mathbf{BV}^{4+} ($\epsilon^{249} = 6.34 \times 10^4 \text{ M}^{-1} \text{ cm}^{-1}$) was significantly different than those of \mathbf{HV}^{12+} , \mathbf{MV}^{2+} , and \mathbf{BMV}^{2+} , and complexation by $\mathbf{CB}[7]$ led to relatively modest spectral changes.

Interestingly, only an apparent association constant^{57,58} ($\log K_{\mathbf{HV}^{12+} \subset (\mathbf{CB}[7])_6}^* = 4.23(7)$) at 0.1 M phosphate buffer pH 7.0) was deduced from the processing of the spectrophotometric titrations (Figure 9). This reflects the fact that the \mathbf{BIPY}^{2+} subunits in \mathbf{HV}^{12+} behave as independent binding sites and that each $\mathbf{CB}[7]$ binding to the \mathbf{BIPY}^{2+} units of \mathbf{HV}^{12+} induces comparable spectral variations. In the case of a statistical binding for a multivalent system (*i.e.* for \mathbf{HV}^{12+} , $n = 6$), the ratio between the successive stability constants related to each successive binding event (*i.e.* binding of $\mathbf{CB}[7]$ to each of the terminal viologen units) can be estimated using the following equation: $K_{i+1}/K_i = (n-i)/(i+1)(n-i+1)$ with $n = 6$ (number of identical and independent sites) and $1 \leq i \leq 6$ number of sites occupied.⁵⁵ Therefore for $n = 6$, $K_1/K_2 = 5/12$; $K_2/K_3 = 8/15$; $K_4/K_3 = 9/16$; $K_5/K_4 = 8/15$; $K_6/K_5 = 5/12$.

If we first assume that $\log K_{\mathbf{HV}^{12+} \subset \mathbf{CB}[7]} = \log K_{\mathbf{MV}^{2+} \subset \mathbf{CB}[7]} = 5.3$, the corresponding successive stability constants can be accordingly evaluated: $\log K_{\mathbf{HV}^{12+} \subset (\mathbf{CB}[7])_2} = 4.92$; $\log K_{\mathbf{HV}^{12+} \subset (\mathbf{CB}[7])_3} = 4.65$; $\log K_{\mathbf{HV}^{12+} \subset (\mathbf{CB}[7])_4} = 4.40$; $\log K_{\mathbf{HV}^{12+} \subset (\mathbf{CB}[7])_5} = 4.12$ and $\log K_{\mathbf{HV}^{12+} \subset (\mathbf{CB}[7])_6} = 3.74$. The average stability constant ($\log K_{\text{calcd}}^* = 4.8$) that can be deduced assuming statistical interactions is significantly higher than the apparent value determined from absorption titration at pH 7.0 ($\log K_{\mathbf{HV}^{12+} \subset (\mathbf{CB}[7])_6}^* = 4.23(7)$). Similarly, assuming $\log K_{\mathbf{HV}^{12+} \subset \mathbf{CB}[7]} = \log K_{\mathbf{BV}^{4+} \subset \mathbf{CB}[7]} = 5.9$, an average stability constant of $\log K_{\text{calcd}}^* = 5.4$ was deduced for a statistical binding and is also significantly higher than the experimental apparent value determined from absorption titration at pH 7.0 ($\log K_{\mathbf{HV}^{12+} \subset (\mathbf{CB}[7])_6}^* = 4.23(7)$). This suggests negative steric interactions^{55,56} due to the bulkiness of the $\mathbf{CB}[7]$ macrocycles and \mathbf{HV}^{12+} and thereby a negatively cooperative binding of $\mathbf{CB}[7]$ to \mathbf{HV}^{12+} . Thus, the apparent stability constant of $\mathbf{HV}^{12+} \subset (\mathbf{CB}[7])_6$ $K_{\mathbf{HV}^{12+} \subset (\mathbf{CB}[7])_6}^*$ is more than an order of magnitude lower than those calculated for $\mathbf{MV}^{2+} \subset \mathbf{CB}[7]$ ($\log K_{\mathbf{MV}^{2+} \subset \mathbf{CB}[7]} = 5.30(2)$) and $\mathbf{BV}^{4+} \subset \mathbf{CB}[7]$ ($\log K_{\mathbf{MV}^{2+} \subset \mathbf{CB}[7]} = 5.9(2)$). Last but not the least, significant hypochromic shifts of the $\pi-\pi^*$ transitions of the \mathbf{BIPY}^{2+} chromophores of \mathbf{HV}^{12+} were observed (Figure 15) on complexation with $\mathbf{CB}[7]$ macrocycles, which substantiates the ^1H NMR data and the proposed $\mathbf{BIPY}^{2+}/\mathbf{CB}[7]$ binding mode. To illustrate this binding feature, Figure 28 shows the distribution curves of the successive inclusion complexes which might be formed when \mathbf{HV}^{12+} is mixed with $\mathbf{CB}[7]$.

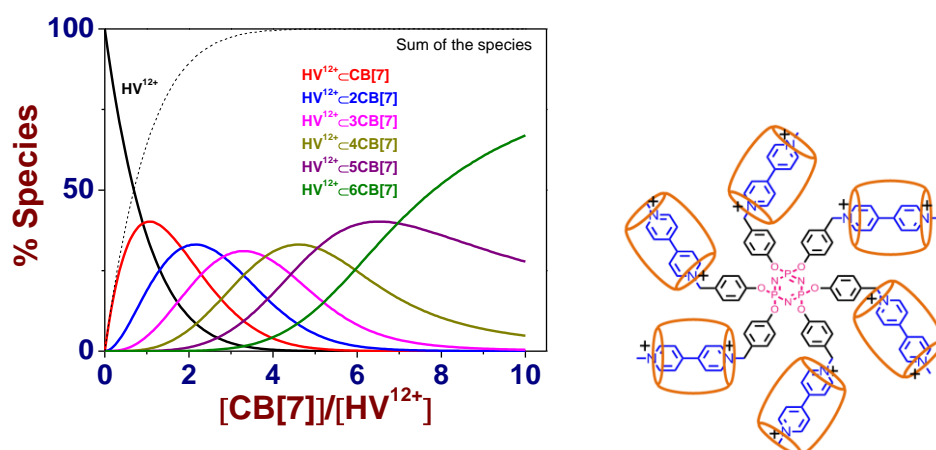


Figure 28. Distribution curves of the inclusion complexes which might be formed when HV^{12+} is mixed with $\text{CB}[7]$. The dash line corresponds to the sum of all the species. Distribution diagram calculated using $\log K_{\text{HV}^{12+}+\text{CB}[7]} = \log K_{\text{MV}^{2+}+\text{CB}[7]} = 5.3$ and a statistical binding process. Solvent: water pH 7.0 (0.1 M $\text{Na}_2\text{HPO}_4/\text{NaH}_2\text{PO}_4$); $[\text{HV}^{12+}] = 10^{-4}$ M; $T = 25.0(1)$ °C.

2.3.2. Inter- or Intramolecular Dimerization of Viologen Threads

In aqueous solution, monomers $\text{V}^{\bullet+}$ and dimers $(\text{V}^{\bullet+})_2$ of viologen radical cations coexist in equilibrium. Table 1 gathers the thermodynamic and spectroscopic data measured for the dimerization of a large variety of viologens. The differences between the corresponding values for the same viologen compound reflect the different experimental conditions that were employed (*e.g.* $\text{MV}^{\bullet+}$ or $\text{C}_8\text{C}_8\text{V}^{\bullet+}$). Concentrations, ionic strength, pH, and polarity of the solvent, as well as temperature and nature of the counter-anion all influence the position of the equilibrium. Factors such as high solvent polarity that diminish electrostatic repulsion between the cationic monomers tend to favour dimerization,^{24,59} as do attractive hydrophobic interactions between alkyl substituents borne by the electroactive chromophores.

2.3.2a. Intermolecular Dimerization of $\text{BMV}^{\bullet+}$

According to the UV-Vis.-NIR absorption data that were collected for $\text{BMV}^{\bullet+}$, we were able to correlate the total absorbance at each wavelength to the absorptivities of both the monomer and the dimer, the concentrations of which being related by the equilibrium constant for dimerization K_{Dim} .^{27,26} From the absorbance data and concentrations, we determined that $\text{BMV}^{\bullet+}$ self-associates in solution with a $\log K_{\text{Dim}}$ value of 3.46(5), which is in the same range as $\log K_{\text{Dim}}$ values determined for the methyl viologen radical cation $\text{MV}^{\bullet+}$ ($\log K_{\text{Dim}} \sim 2.5\text{-}2.9$,^{60,61} Table 1) and the bis-benzyl viologen radical cation $\text{BBV}^{\bullet+}$ ($\log K_{\text{Dim}} = 4.0$ ⁶², Table 1). The fact that these values increase in the order $\text{MV}^{\bullet+} < \text{BMV}^{\bullet+} < \text{BBV}^{\bullet+}$ indicates that the benzyl substituents reinforce the strength of binding between the two $\text{BIPY}^{\bullet+}$ units, likely by means of hydrophobic interactions.

Table 1. Thermodynamic and spectroscopic parameters of viologens radical cations under monomeric and dimeric states.

	Anion	log K_{Dim}	λ^m (nm) ϵ^m ($10^4 M^{-1} cm^{-1}$)	λ^d (nm) ϵ^d ($10^4 M^{-1} cm^{-1}$)	Ref.
R = R' = CH ₃ C ₁ C ₁ V ^{•+} (MV ^{•+})	Cl-	2.70 ^c	396 (4.2)/602 (1.37)	362 (5.0)/518 (2.1)	60,63,64
	nd	2.58 ^e	675 (0.38)/604 (1.69)/ 396 (3.49) 600	537 (3.24)/369 (8.97)	61
	nd	2.86 ^f			59
CH ₃ SO ₄ ⁻	5.10 ^a	598 (1.37)/606 (1.37)	480/565/670	65	
C ₁ C ₆ V ^{•+} R = CH ₃ ; R' = C ₆ H ₁₃	Cl-	2.75 ^c	nd	nd	60,63
C ₁ C ₇ V ^{•+} R = CH ₃ ; R' = C ₇ H ₁₅	Cl-	2.89	nd	nd	63
	Cl-	2.81			60
C ₁ C ₈ V ^{•+} R = CH ₃ ; R' = C ₈ H ₁₇	Cl-	2.93	396 (4.2)/602 (1.37)	362 (5.0)/518 (2.10)	63
	Cl-	2.89 ^c			60
C ₁ C ₉ V ^{•+} R = CH ₃ ; R' = C ₉ H ₁₉	Cl-	4.04 ^c	nd	nd	60
C ₁ C ₁₀ V ^{•+} R = CH ₃ ; R' = C ₁₀ H ₂₁	Cl-	4.86 ^c	nd	nd	60
C ₂ C ₂ V ^{•+} R = R' = C ₂ H ₅	Br-	5.03 ^a	597 (1.22)	564 (0.890)	59
C ₃ C ₃ V ^{•+} R = R' = C ₃ H ₇	Br-	4.68 ^a	597 (1.06)	550 (0.887)	59
C ₄ C ₄ V ^{•+} R = R' = C ₄ H ₉	Cl-	2.74 ^c	nd	nd	60
C ₅ C ₅ V ^{•+} R = R' = C ₅ H ₁₁	Br-	4.33 ^a	602 (1.04)	563 (0.869)	59
C ₆ C ₆ V ^{•+} R = R' = C ₆ H ₁₃	Br-	3.85 ^a	600 (1.025)	558 (0.870)	59
	Br-	3.85 ^a	571 (1.016)	515 (0.856)	59
C ₇ C ₇ V ^{•+} R = R' = C ₇ H ₁₅	Br-	4.00 ^d	600 (1.38)	600 (0.4)	62
	Br-	3.29 ^a	548 (0.892)	504 (0.855)	59
C ₈ C ₈ V ^{•+} R = R' = C ₈ H ₁₇	Br-	5.33 ^d	600 (1.38)	600 (0.4)	62
	-	4.0	560 (1.72)/604 (1.22)	560 (1.7)/604 (2.44)	66
BzBzV ^{•+} (BBV ^{•+}) R = R' = CH ₂ C ₆ H ₆	-	4.0	560 (1.72)/604 (1.22)	560 (1.7)/604 (2.44)	66
C ₁ BzV ^{•+} (BMV ^{•+}) R = CH ₃ ; R' = CH ₂ C ₆ H ₆	Cl ⁻ /I ⁻	3.46 ^b	600 (1.23)	540 (2.03)/900 (0.7)	this work

^a water, $I = 0$. ^b water, pH 7.0 (sodium phosphate buffer 0.1 M). ^c 0.1 KCl. ^d pH 8.1 (0.1 M tris/H₂SO₄ buffer); ^e 1 M salt concentration; ^f pH 10.0 (glycine buffer 0.1 M); nd: not defined.

Figure 16 shows the electronic spectra and distribution diagram of the **BMV^{•+}** monomer and dimer. The spectrum of **BMV^{•+}** is characterized by an intense and structured absorption in the visible region ($\lambda_{max} \sim 600$ nm, $\epsilon^{600} = 1.23 \times 10^4 M^{-1} cm^{-1}$), in agreement with the spectroscopic parameters determined for **MV^{•+}** and **BBV^{•+}** (Table 1). Formation of the dimer (**BMV^{•+}**)₂ induces a significant hypsochromic shift of the absorption around 600 nm ($\Delta\lambda \sim 60$ nm) and gives rise to an intense absorption in the near-IR region ($\lambda_{max} \sim 900$ nm, $\epsilon^{900} = 7.0 \times$

$10^3 \text{ M}^{-1} \text{ cm}^{-1}$). This new signal likely results from an allowed radical–radical transition that occurs in the dimer,⁶⁴ and consequently serves as a valuable and discrete reporter of the dimer occurrence in solution.

2.3.2b. Intramolecular Pimerization of $\text{BV}^{2(\bullet+)}$ and $\text{HV}^{6(\bullet+)}$

My hosting group recently reported the intramolecular pimerization process that occurs on electrochemical reduction of HV^{12+} .²⁵ A six-electron reduction led to $\text{HV}^{6(\bullet+)}$, a hexaradical hexavalent cation, which immediately pimerizes intramolecularly to form three pairs of viologen radical cation dimers (referred as the fully pimerized species $\text{HV}_D^{6(\bullet+)}$).

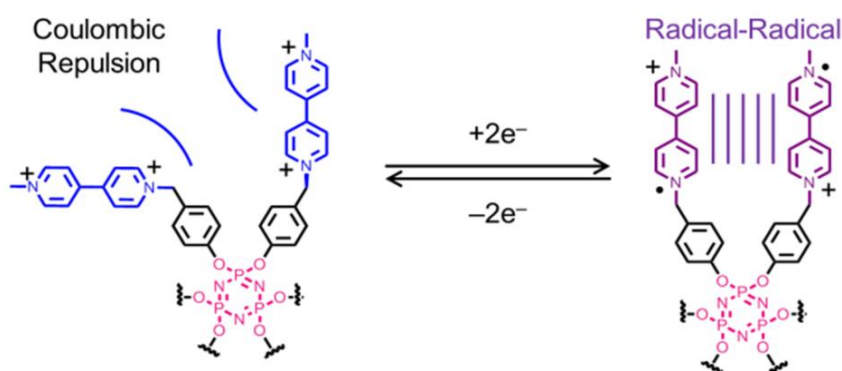


Figure 29. Schematic representation of the redox-activated π -dimerization of HV^{12+} (only two arms are represented for the sake of clarity). Upon reduction, one electron to each BIPY^{2+} present in HV^{12+} (total of six electron for the six BIPY^{2+}) are transferred to generate the $\text{HV}^{6(\bullet+)}$ intermediate species leading to the intramolecular dimerization of each two adjacent $\text{BIPY}^{\bullet+}$ located on the same P atom leading to $\text{HV}_D^{6(\bullet+)}$ species. Exposure to O_2 re-oxidizes $\text{HV}_D^{6(\bullet+)}$ back to HV^{12+} where the BIPY^{2+} units repel each other through Coulombic forces.

The pre-organization of the designed dendrimer allows efficient intramolecular dimerization of the two viologens borne by the same phosphorous atom in a wide range of solvents upon reduction leading to a reversible colour change (colourless – purple). The equilibrium constants β_{Dim} for the formation of $\text{HV}_D^{6(\bullet+)}$ from $\text{HV}^{6(\bullet+)}$ was measured in several solvents (Table 2).²⁵ The high β_{Dim} values indicate nearly complete dimerization of all six viologen subunits. In water, the global dimerization constant β_{Dim} is equal to 1.69×10^{14} .

Table 2. Thermodynamic parameters associated with the intramolecular dimerization of $\text{BIPY}^{\bullet+}$ radical cations in the dendrimer HV^{12+} after reduction in different solvents (Data taken from reference 25, Wadhwa et al., 2013)

Solvent	E_0 (V)	E_{eq} (V)	ΔE (V)	β_{Dim}
Me_2CO^a	-0.299	-0.267	0.0316	1.16×10^3
DMF^a	-0.318	-0.277	0.0404	1.26×10^4
MeCN^a	-0.351	-0.274	0.0775	7.32×10^7
H_2O^b	-0.593	-0.450	0.1402	1.69×10^{14}
$T = 298 \text{ K}$. Determined from Square wave differential pulse. ^a Reference ferrocene. ^b Reference Ag/AgCl				

Herein, we generated $\text{HV}_D^{6(\bullet+)}$ in water with $\text{Na}_2\text{S}_2\text{O}_4(\text{aq})$ and measured the UV-Vis.-NIR absorption spectrum of the pimerized complex. As shown in Figure 30, two intense absorption bands, one centred at 530 nm ($\epsilon^{530} = 3.69 \times 10^4 \text{ M}^{-1} \text{ cm}^{-1}$) and another, charge-transfer (CT) absorption band, lying at 944 nm ($\epsilon^{944} = 1.62 \times 10^4 \text{ M}^{-1} \text{ cm}^{-1}$), characterize the absorption spectrum of $\text{HV}_D^{6(\bullet+)}$. For comparison purposes, the absorption properties of $\text{BV}^{2(\bullet+)}$ (generated similarly in aqueous solution from BV^{4+} using $\text{Na}_2\text{S}_2\text{O}_4(\text{aq})$), which contains only one pair of firmly pimerized $\text{BIPY}^{\bullet+}$ subunits was measured. The absorption spectrum of $\text{BV}^{2(\bullet+)}$ (Figure 31) displays an intense CT absorption band at 933 nm ($\epsilon^{933} = 2.87 \times 10^3 \text{ M}^{-1} \text{ cm}^{-1}$) that clearly confirms pimerization and corroborates the observations made for $\text{HV}_D^{6(\bullet+)}$. Importantly, it indicates that the dimerization occur between viologen units that are borne by the same phosphorus atom of the phosphazene core. However, discrepancies are observed between the electronic spectrum of $\text{HV}_D^{6(\bullet+)}$ ($\epsilon^{944} = 1.62 \times 10^4 \text{ M}^{-1} \text{ cm}^{-1}$) and that deduced from the $\text{BMV}^{\bullet+}$ dimer ($3 \times \epsilon^{(\text{BMV}^{\bullet+})_2}$, Figure 31), and suggest that ground-state interactions⁶⁷ occur between $(\text{BIPY}^{\bullet+})_2$ dimers within the dendrimeric structure, but not between dimerized monomers of $\text{BMV}^{\bullet+}$.

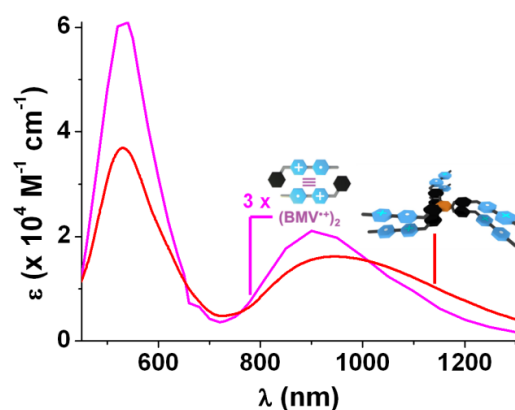


Figure 30. Electronic UV-Vis-NIR absorption spectra of $\text{HV}_D^{6(\bullet+)}$ compared to that of $(\text{BMV}^{\bullet+})_2$ in water. Solvent: water buffered at pH 7.0 with 0.1 M $\text{Na}_2\text{HPO}_4/\text{NaH}_2\text{PO}_4$. $T = 25.0(1) \text{ }^\circ\text{C}$.

A comparison of the electronic spectrum of $\text{HV}_D^{6(\bullet+)}$ and that deduced from $\text{BV}^{2(\bullet+)}$ ($= 3 \times \epsilon^{\text{BV}^{2(\bullet+)}}$, Figure 31) reveals similar discrepancies.

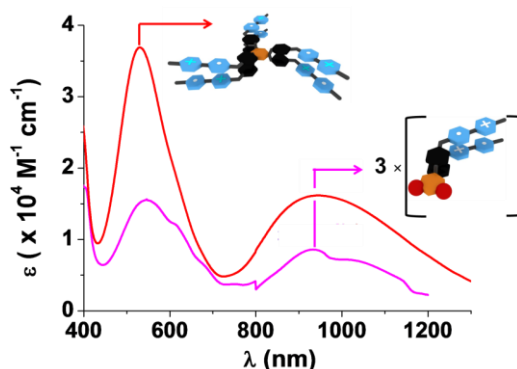


Figure 31. Electronic UV-Vis-NIR absorption spectra of $\text{HV}_D^{6(\bullet+)}$ compared to that of $(\text{BV}^{\bullet+})_2$ in water. Solvent: water buffered at pH 7.0 with 0.1 M $\text{Na}_2\text{HPO}_4/\text{NaH}_2\text{PO}_4$. $T = 25.0(1) \text{ }^\circ\text{C}$.

In order to get insight into the nature of the pimerization process, a computational approach (collaboration with Pr Carlos Platas-Iglesias (Departamento de Química Fundamental, Universidad de Coruña, Coruña, Spain) using density functional theory calculations at the M06/6-31G(d,p) level⁶⁸ that have shown to provide good results for inclusion complexes of **BIPY^{•+}** radical cations was performed.⁶⁹ Due to the large size of the system of interest, the calculations (Figure 32) were performed on a simplified model noted **BV⁴⁺** where four of the six **BMV²⁺** units of **HV¹²⁺** were replaced by methyl groups.

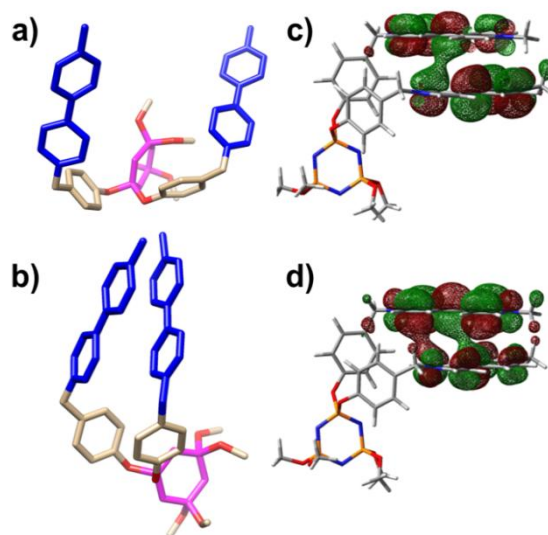


Figure 32. Optimized geometries of the **BV⁴⁺** a) and **BV^{2(•+)}** b) models, and representations of SOMO c) and SOMO-1 d) in **BV^{2(•+)}** computed in aqueous solution at the M06/6-31G(d,p) level.

This model system was fully optimized in its oxidized **BV⁴⁺** and reduced **BV^{2(•+)}** forms. Structure optimizations performed in aqueous solution (IEFPCM model)³² resulted in a molecular geometry where the two **BIPY^{•+}** units are stacked in a nearly parallel fashion, with the angle between the two least-square planes defined by the **BIPY^{•+}** units amounting to 3.1°, and up to six C...C distances in the range 3.30-3.56 Å. A twist angle of ~ 37° is obtained for its fully oxidized form, while two **BIPY^{•+}** fragments show virtually no twisting about their 4,4'-C-C bonds. The decrease in the torsion angle is accompanied by a significant shortening of the 4,4'-C-C distance, which amounts to 1.474 and 1.426 Å in the **BV⁴⁺** and **BV^{2(•+)}** systems, respectively. This is in line with recent crystallographic studies, in which small torsion angles in **BIPY^{•+}** were considered as a signature of its radical cation nature.⁶⁹ Indeed, both SOMO and SOMO-1 in **BV^{2(•+)}** show significant overlap (bonding character) between the 4,4' ring carbon atoms of both **BIPY^{•+}** units. Interestingly, an important delocalization of the SOMO and SOMO-1 (Figure 32) among the two **BIPY^{•+}** units is also observed.

2.3.2c. Switching Properties of **HV¹²⁺**/**HV_D^{6(•+)}** on ITO Coated Surface

Taking advantage of its electrochemical properties (*i.e.* showing a change in the absorption spectrum of **HV¹²⁺** by providing external stimuli in the form of electrons) **HV¹²⁺** has been tested as a potential electrochromic material. A device (Figure 33) consisting of

two transparent indium tin oxide (ITO) electrodes has been elaborated (work done in collaboration with the group of Pr Ali Trabolsi, NYUAD, Abu Dhabi, UAE).

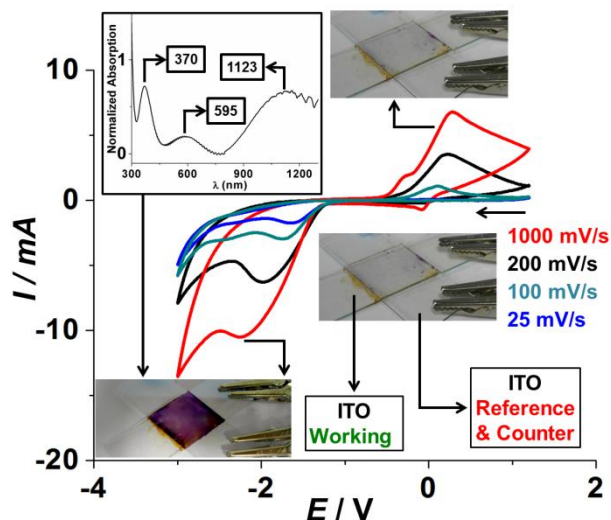


Figure 33. Variable scan cyclic voltammograms of a solution of $\text{HV}^{12+} \cdot 12\text{Cl}$, in 1 M NaCl H_2O , sandwiched between two ITO coated glass slides (4–8 Ohms, 1500–2000 Å nominal coating thickness). One of the ITO slides is used as a working electrode while the other is used as counter and reference electrode. A colour change (colourless to purple) is observed upon reduction. Inset: UV-Vis-NIR spectrum of the device switched at -2 V.

A concentrated solution of 5.0 mM HV^{12+} in 1 M NaCl in H_2O was sandwiched between two ITO slides under nitrogen. The electrochemistry of the resulting device was investigated in open air employing one of the ITO as a working electrode, while the second ITO slide was used as the counter electrode as well as the reference electrode. Figure 33 depicts the electrochemical properties of HV^{12+} on an ITO electrode. The obtained cyclic voltammograms exhibit wave shapes typical for surface confined redox processes indicating adsorption of the compound onto the electrode surface.⁷⁰ The large peak-to-peak separation in the case of the ITO electrode is attributed to the high resistance of the electrode material. Moreover, the prepared window exhibited a reversible and relatively fast (*i.e.* based on the rate of the electrochemical redox processes, the electrochromic device can be switched as fast as 2.5 sec for 1000 mV/s to 10 sec for 200 mV/s. colour change (up to ten cycles without any significant changes, Figure 34) from colourless to purple upon reduction as shown in Figure 33. The electrochromic property of the device was also examined by UV-Vis-NIR spectroscopy (Figure 33). Maintaining the voltage at -2 V resulted in absorption spectra similar to that obtained in solution. Large NIR band centred at 1123 nm as well as two absorption bands at 595 and 370 nm characteristic of the dimer formation were observed (Figure 33). The larger intensity of the NIR band can be explained by the formation of aggregates on the surface of the ITO slides upon reduction (Figure 33).

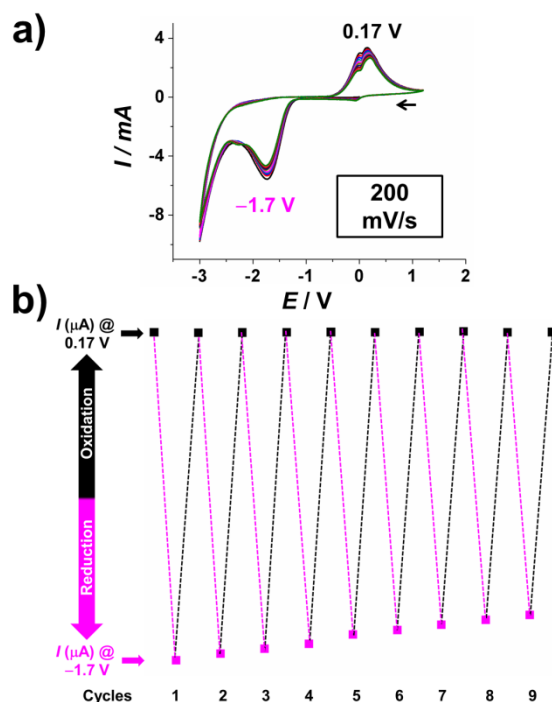


Figure 34. a) Reversible Redox cycles of the ITO device and b) change in the current intensity as a function of reduction/oxidation processes.

2.3.3. Reduction of the [n]Pseudorotaxanes

2.3.3a. Monocationic Monoradicals $MV^{•+}$ and $BMV^{•+}$

Cyclic voltammetric (CV, Figure 23) and square-wave voltammetric (SWV, Figure 36) experiments in phosphate-buffered solutions at pH 7 were performed on the reference compounds MV^{2+} and BMV^{2+} in the absence and presence of **CB[7]**. MV^{2+} (Figure 36a) is characterized by two successive one-electron reversible redox waves: $E_{1/2}^1 (MV^{2+}/MV^{•+}) = -0.66$ V and $E_{1/2}^2 (MV^{•+}/MV^0) = -0.96$ V. Addition of **CB[7]** markedly alters its electrochemical properties. In the presence of three equivalents of **CB[7]**, the first redox wave shifts slightly to a more negative potential ($\Delta E_{1/2}^1 = 30$ mV) and retains its reversible shape, while the second reduction wave shifts to a much more negative potential ($\Delta E_{1/2}^2 = 60$ mV). These shifts reflect the relative affinities of **CB[7]** for the different redox states of methyl viologen. Assuming a thermodynamic and kinetic high stable inclusion complexes between **CB[7]** and viologen derivatives V^{2+} , the binding constant ($K_{V^{•+}+CB[7]}$) between the one-electron reduced species $V^{•+}$ and **CB[7]** can be evaluated (*vide infra*) from the previously determined $K_{V^{2+}+CB[7]}$ values (binding constants between **CB[7]** and the oxidized viologens V^{2+}), where $\Delta E_{1/2}^1$ corresponds to the difference between the half-wave potentials of the complexed and free viologen (*i.e.* $E_{1/2}^1(V^{•+}+CB[7]) - E_{1/2}^1(V^{•+})$). Similarly, the same approach can be applied for the evaluation of the stability constant of the two electrons reduced viologen species V^0 and **CB[7]** by calculating $E_{1/2}^2(V^0+CB[7]) - E_{1/2}^2(V^0)$.

$$K_{V^{•+}+CB[7]}/K_{V^{2+}+CB[7]} \exp(-F\Delta E_{1/2}^1/RT)$$

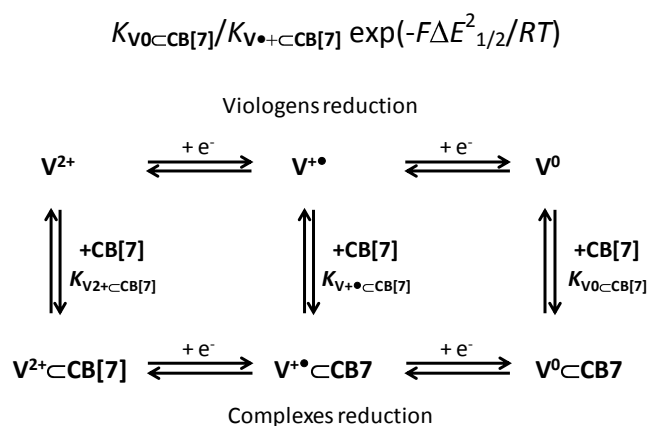


Figure 35. Plausible electrochemical and chemical routes involved in the reduction of viologen guests in the presence of **CB[7]**. The electron transfers involving the redox-active inclusion complexes with **CB[7]** can proceed either: (i) directly from inclusion complexes, and (ii) indirectly after dissociation of the complexes.

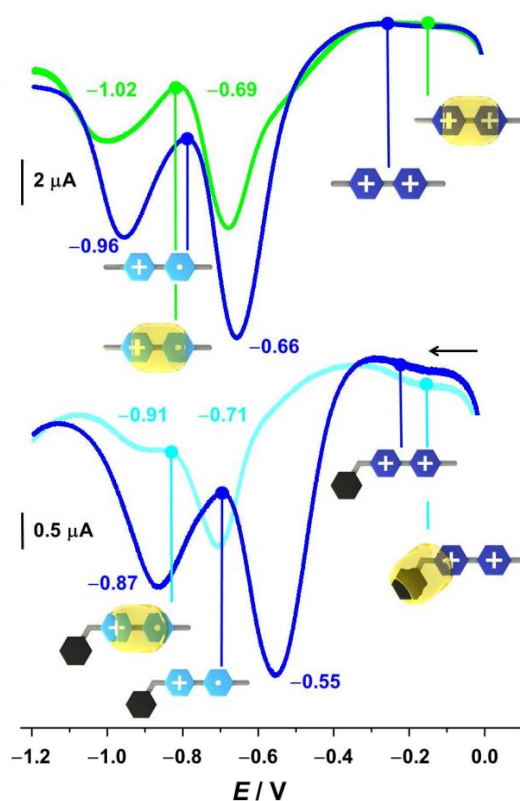


Figure 36. Square Wave voltammograms of MV^{2+} , $[MV^{2+}] = 0.06$ mM (top) and BMV^{2+} , $[BMV^{2+}] = 0.08$ mM (bottom) in the absence and the presence of **CB[7]** (respectively 3 and 3 equivalents of **CB[7]**). All voltammograms were recorded in Argon-purged phosphate buffer solutions (pH 7) at 298 K with 0.1 M TBACl. E versus Ag/AgCl.

For MV^{2+} , assuming a $\log K_{MV^{2+} \subset CB[7]} = 5.3$ for $MV^{2+} \subset CB[7]$ previously determined using absorption spectrophotometric titrations, $\log K_{MV^{+\bullet} \subset CB[7]} \sim 4.79$ and $\log K_{MV^0 \subset CB[7]} \sim 3.77$ values can be accordingly calculated.⁴³ This indicates that $MV^{+\bullet}$ remains firmly complexed within the **CB[7]** host, whereas the neutral MV^0 is more loosely bound. The relatively high

affinity of **CB[7]** for $\text{MV}^{\bullet+}$ is consistent with prevention of $\text{MV}^{\bullet+}$ dimerization by the macrocycle in aqueous solutions (Table 1 and Figure 19c).

As anticipated, BMV^{2+} is also characterized by two reversible one-electron redox processes (Figure 36b): $E_{1/2}^1(\text{BMV}^{2+}/\text{BMV}^{\bullet+}) = -0.55$ V and $E_{1/2}^2(\text{BMV}^{\bullet+}/\text{BMV}^0) = -0.87$ V, and the addition of three equivalents of **CB[7]** to BMV^{2+} also induced major changes in the SW voltammograms of the viologen, including a marked shift of the first peak to a more negative potential: $\Delta E_{1/2}^1 = 140$ mV for BMV^{2+} as compared to only 30 mV for MV^{2+} . The second reduction wave for BMV^{2+} is also shifted to a more negative potential, but, in this case, by a similar amount as was observed for MV^{2+} : $\Delta E_{1/2}^1 = 40$ mV for BMV^{2+} versus 60 mV for MV^{2+} . These results substantiate that **CB[7]** has a greater binding affinity for BMV^{2+} ($\log K_{\text{BMV}^{2+}\text{CB[7]}} = 6.9(8)$) than for MV^{2+} ($\log K_{\text{MV}^{2+}\text{CB[7]}} = 5.30(2)$) but a similar affinity for both radical cationic forms $\text{BMV}^{\bullet+}$ ($\log K_{\text{BMV}^{\bullet+}\text{CB[7]}} \sim 4.53$) and $\text{MV}^{\bullet+}$ ($\log K_{\text{MV}^{\bullet+}\text{CB[7]}} \sim 4.79$). This is consistent with **CB[7]** having two redox-state-dependent binding modes for the BMV^{2+} species (depending on its redox state), and one for the MV^{2+} species. Thus, we infer that on reduction of BMV^{2+} to $\text{BMV}^{\bullet+}$, translocation of **CB[7]** from the benzyl unit to the bipyridinium moiety occurs (Figure 37). In its oxidized form, the benzyl methyl viologen BMV^{2+} has a much better affinity for **CB[7]** than MV^{2+} due to hydrophobic stabilizing interactions between the **CB[7]** and the hydrophobic benzyl substituent. The NMR data that have been measured (Figure 11) confirm this peculiar property. It thus appears that when the [2]pseudorotaxane $\text{BMV}^{2+}\text{CB[7]}$ (*i.e.* **CB[7]** encircles the benzylic unit) is reduced to its $\text{BMV}^{\bullet+}\text{CB[7]}$ analogue (*i.e.* **CB[7]** encircles the monoradical viologen centre), the macrocycle reversibly performs a translocation movement from the benzyl to the viologen radical cation (Figure 37). This process is reversible on oxidation of the radical cation and *vice-versa*.

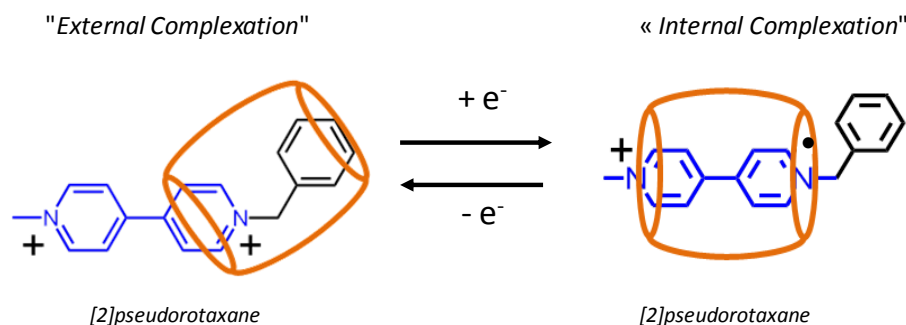


Figure 37. Electrochemically controlled translocation of the macrocycle **CB[7]** in the host/guest complex with BMV^{2+} .

Similarly, we have also estimated the stability constants of $\text{BMV}^0\text{CB[7]}$ ($\log K_{\text{BMV}^0\text{CB[7]}} \sim 3.86$) using the measured potential shifts and the estimated binding constant for BMV^{2+} [$\log K_{\text{BMV}^{2+}\text{CB[7]}} = 6.9(8)$] and $\text{BMV}^{\bullet+}$ ($\log K_{\text{BMV}^{\bullet+}\text{CB[7]}} \sim 4.53$).^{43,44} Similarly to methyl-viologen MV^{2+} , the stability sequence of the three redox-related **CB[7]**/**BMV** complexes is $\text{BMV}^{2+}\text{CB[7]} > \text{BMV}^{\bullet+}\text{CB[7]} > \text{BMV}^0\text{CB[7]}$, which confirms that **CB[7]** preferentially binds cationic species over neutral ones.⁴³

In order to go further, we undertook a UV-Vis.-NIR absorption titration of $\text{BMV}^{\bullet+}$ by $\text{CB}[7]$ in water at pH 7.0 (Figure 18a). $\text{BMV}^{\bullet+}$ was generated with an excess of freshly prepared $\text{Na}_2\text{S}_2\text{O}_4(\text{aq})$ under O_2 -free argon. As usually observed for viologen/ $\text{CB}[7]$ complexes, $\text{BMV}^{\bullet+}\text{-CB}[7]$ is characterized by significant hypochromic shifts of the absorption signals associated with the radical cation, and such shifts provide additional evidence for inclusion of the radical cation within $\text{CB}[7]$ (Figure 20). Also the disappearance of the CT absorption band at 900 nm and the vanishing of the π - π^* transitions of $\text{BMV}^{\bullet+}$ are clear signatures of $\text{BMV}^{\bullet+}\text{-CB}[7]$ formation (Figure 20). Statistical processing of the corresponding spectral data allowed us to evaluate the $K_{\text{BMV}^{\bullet+}\text{-CB}[7]}$ value ($\log K_{\text{BMV}^{\bullet+}\text{-CB}[7]} = 4.9(1)$) which is in excellent agreement with that determined from the electrochemical data ($\log K_{\text{BMV}^{\bullet+}\text{-CB}[7]} \sim 4.53$). In the absence of $\text{CB}[7]$ and on one-electron reduction of BMV^{2+} with $\text{Na}_2\text{S}_2\text{O}_4$, $\text{BMV}^{\bullet+}$ was found to self-associate with a dimerization constant of $\log K_{\text{Dim}} = 3.46$. As expected, the presence of $\text{CB}[7]$ suppressed dimerization (Figure 38) by forming 1:1 inclusion complex $\text{BMV}^{\bullet+}\text{-CB}[7]$, which has a higher stability constant ($\log K_{\text{BMV}^{\bullet+}\text{-CB}[7]} = 4.9(1)$) than the dimer ($\log K_{(\text{BMV}^{\bullet+})_2} = 3.4(6)$).

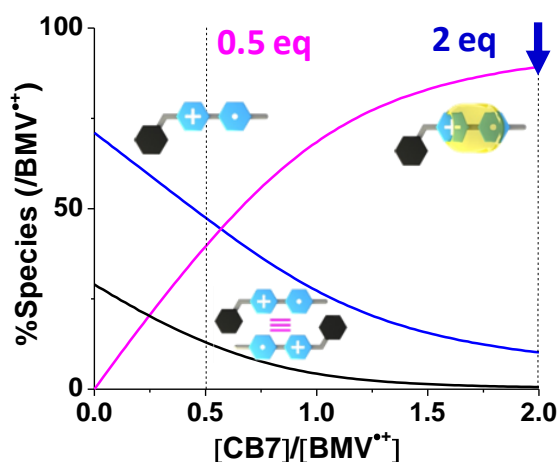


Figure 38. Distribution diagrams of the $\text{BMV}^{\bullet+}/\text{CB}[7]$ system. Solvent: water buffered at pH 7.0 with 0.1 M $\text{Na}_2\text{HPO}_4/\text{NaH}_2\text{PO}_4$; $T = 25.0(1)^\circ\text{C}$.

The same inferences apply to the $\text{MV}^{\bullet+}/\text{CB}[7]$ system (Figure 19). In the case of $\text{MV}^{\bullet+}$, the smaller dimerization constant ($\log K_{\text{Dim}} = 2.70^{61,71}$) necessitates much higher concentrations of $\text{MV}^{\bullet+}$ for self-association to be easily measured (Figure 19).

2.3.3b. Hexacationic Hexaradical $\text{HV}^{6(\bullet+)}$

The cyclic voltammograms recorded for the hexaviologen dendrimer (Figure 39) clearly shows two distinct and reversible redox waves. The relative amplitudes and shapes of the peaks for each wave at the anode (oxidation) are similar to those observed at the cathode (reduction). Such a pattern is a strong indication of the redox reversibility of the system. Quantitatively, the difference ($\Delta E = E_{\text{pc}} - E_{\text{pa}}$) between the potential at the peak of the first reduction wave and the potential of the corresponding oxidation were calculated and were found to be 40 and 60 mV respectively for the first and second reduction processes, which represent an excellent proof for reversibility of the two redox processes.

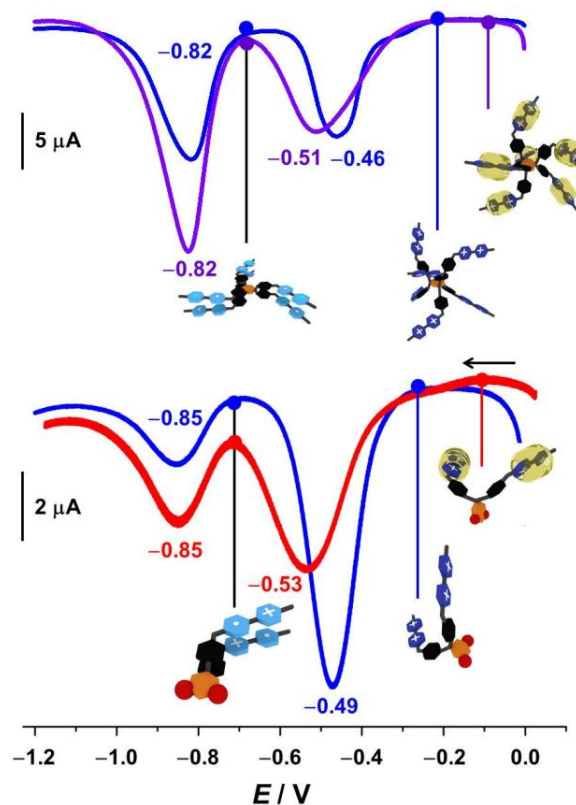


Figure 39. Square Wave voltammograms of HV^{12+} , $[\text{HV}^{12+}] = 0.024$ mM (top) and BV^{4+} , $[\text{BV}^{4+}] = 0.065$ mM (bottom) in the absence and the presence of **CB[7]** (respectively 18 and 4 equivalents of **CB[7]**). All voltammograms were recorded in Argon-purged phosphate buffer solutions (pH 7) at 298 K with 0.1 M TBACl. E versus Ag/AgCl.

The SWVs of HV^{12+} (Figure 39) show two reversible six-electron processes ($E_{1/2}^1$ ($\text{HV}^{12+}/\text{HV}^{6(\bullet+)} = -0.46$ V and $E_{1/2}^2$ ($\text{HV}^{6(\bullet+)}/\text{HV}^0 = -0.82$ V). Chronocoulometric experiments²⁵ confirmed that the first reversible redox process $\text{HV}^{12+}/\text{HV}^{6(\bullet+)}$ involves six electrons, while those associated with the monomeric viologens ($\text{MV}^{2+}/\text{MV}^{\bullet+}$ and $\text{BMV}^{2+}/\text{BMV}^{\bullet+}$) involve only one. The voltammogram of HV^{12+} has a shape that is similar to that of BV^{4+} , which displays only two electroactive centres, as well as to that of BMV^{2+} , which possesses one. This observation is consistent with the inference that each pair of geminal viologen subunits is independent of the others and that, overall, the six viologen subunits in HV^{12+} are identical, non-interacting electroactive centres.⁷² This result is consistent with the spectrophotometric and thermodynamic analyses of the $\text{HV}^{12+}/\text{CB[7]}$ pseudorotaxanes (*vide supra*). On the other hand, the difference in the magnitude of the peak-to-peak separations in the voltammograms of BMV^{2+} and HV^{12+} ($\Delta E_{1/2} = 320$ mV and 360 mV for BMV^{2+} and HV^{12+} , respectively) is a strong indication that intramolecular dimerization occurs in $\text{HV}^{6(\bullet+)}$. It has been shown previously that the thermodynamic stability of $\text{BIPY}^{\bullet+}$ π dimers induces positive shifts in the first redox potential, whereas the second reduction process leading to BIPY^0 is negatively shifted.⁵⁸ Interestingly, for $\text{HV}^{12+} \subset (\text{CB[7]})_6$, no shift ($\Delta E_{1/2}^2 = 0$ mV) was detected for the second reduction wave, which would be expected to correspond to the following reaction: $\text{HV}^{6(\bullet+) \subset (\text{CB[7]})_6} \rightarrow \text{HV}^0 \subset (\text{CB[7]})_6$. This result indicates that, after the first six-electron reduction, the thread behaves like free $\text{HV}^{6(\bullet+)}$. In other words, the first reduction of

$\text{HV}^{12+} \subset (\text{CB}[7])_6$ induces complete dissociation of **CB[7]** and is followed by concomitant intramolecular dimerization of the three pairs of geminal **BIPY**^{•+} groups to form the tertiary dimer $\text{HV}_\text{D}^{6\bullet+}$. An electrochemical study on HV^{12+} in different media (H_2O , CH_3CN , DMF, Me_2CO , Table 2) demonstrated that this intramolecular dimerization is associated with large β_{Dim} values (where β_{Dim} represents the overall equilibrium constant for dimerization of all three pairs of viologen radical cations in $\text{HV}_\text{D}^{6\bullet+}$). Absorption spectra of $\text{HV}_\text{D}^{6\bullet+}$ in the presence and absence of **CB[7]** provided additional evidence for radical-induced dissociation of **CB[7]** (Figure 22). The addition of $\text{Na}_2\text{S}_2\text{O}_4$ to a solution of the [7]pseudorotaxane $\text{HV}^{12+} \subset (\text{CB}[7])_6$ resulted in an absorption spectrum identical to that obtained for $\text{HV}_\text{D}^{6\bullet+}$ in the absence of **CB[7]**. This result also suggests that six-electron reduction of the HV^{12+} thread within the [7]pseudorotaxane forms **BIPY**^{•+} radicals and, in turn, leads to dimerization of geminal **BIPY**^{•+} units and, ultimately, to the formation of a tertiary dimer $\text{HV}_\text{D}^{6\bullet+}$, in which three pairs of geminal **BIPY**^{•+} are firmly stacked. A direct consequence of intramolecular dimerization is the impossibility to determine the binding constant for $\text{HV}^{6\bullet+}$ and **CB[7]**.

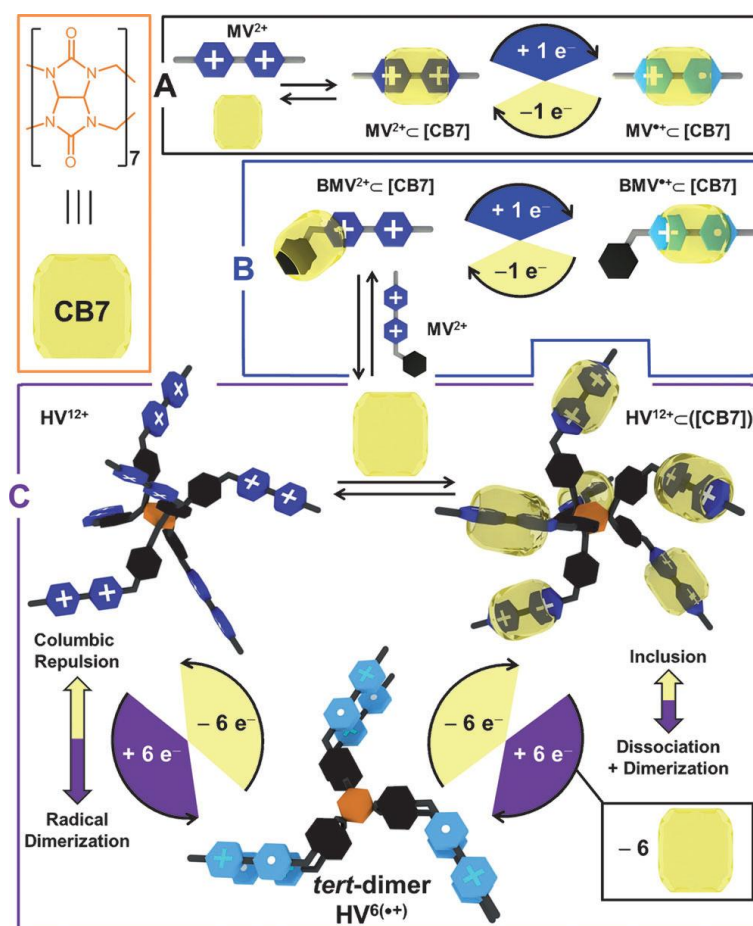


Figure 40. Schematic representation of reversible redox processes involving MV^{2+} (A), BMV^{2+} (B), and HV^{12+} (C) in the presence of the **CB[7]** host. The process involving $\text{BV}^{4+}/\text{CB}[7]$ is analogous to that of HV^{12+} .

Diffusion-ordered spectroscopy (DOSY) and chronocoulometry were used to examine the constitution of the different pseudorotaxanes that arise from the interaction of **CB[7]** with the viologen-containing threads. Firstly, the ^1H DOSY experiments showed that the

magnitude of the diffusion coefficients ($\text{cm}^2 \text{s}^{-1}$) in the absence of **CB[7]** decreases with increasing hydrodynamic size of the viologen substrate in the order $D_{\text{MV}^{2+}} (5.84 \times 10^{-6}) > D_{\text{BMV}^{2+}} (1.71 \times 10^{-6}) > D_{\text{BV}^{4+}} (9.7 \times 10^{-7}) > D_{\text{HV}^{12+}} (7.27 \times 10^{-7})$. For solubility reasons, the diffusion coefficients for **BV⁴⁺** and **HV¹²⁺** were measured in *d*₆-DMSO while those of **MV²⁺** and **BMV²⁺** were determined in D₂O. As anticipated, diffusion coefficients decreased for all four viologen substrates upon addition of **CB[7]**. These results are consistent with the ¹H NMR and UV-Vis spectrophotometric titrations which indicate strong interactions between the threads and **CB[7]**. After **CB[7]** addition, the diffusion coefficients were found to be 2.52×10^{-6} , 7.55×10^{-7} , 8.6×10^{-7} , and $5.02 \times 10^{-7} \text{ cm}^2 \text{ s}^{-1}$ for **MV²⁺CB[7]**, **BMV²⁺CB[7]**, **BV⁴⁺CB[7]**, and **HV¹²⁺CB[7]**, respectively.

Table 3. Diffusion constants ($\text{cm}^2 \text{s}^{-1}$) calculated from chronocoulometric^a and ¹H NMR DOSY^b experiments in H₂O (0.1 M TBACl).

– CB[7]		+ CB[7]	
HV ¹²⁺	HV ^{6(•+)}	HV ¹²⁺	HV ^{6(•+)}
$2.32(4) \times 10^{-7a}$ 7.27×10^{-7b}	$5.87(3) \times 10^{-7a}$	$2.06(6) \times 10^{-7a}$ 5.02×10^{-7b}	$7.00(9) \times 10^{-7a}$
BV ⁴⁺	BV ^{2(•+)}	BV ⁴⁺	BV ^{2(•+)}
$9.80(1) \times 10^{-7a}$ 9.7×10^{-7b}	$1.78(1) \times 10^{-6a}$	$8.63(1) \times 10^{-7a}$ 8.6×10^{-7b}	$2.90(1) \times 10^{-6a}$
BMV ²⁺	BMV ^{•+}	BMV ²⁺	BMV ^{•+}
$5.66(3) \times 10^{-6a}$ 1.71×10^{-6b}	$7.86(4) \times 10^{-6a}$	$4.75(5) \times 10^{-6a}$ 7.55×10^{-7b}	$4.21(5) \times 10^{-6a}$
MV ²⁺	MV ^{•+}	MV ²⁺	MV ^{•+}
5.84×10^{-6b}	nd	2.52×10^{-6b}	nd
^a [HV ¹²⁺] = 0.04 mM, [BV ⁴⁺] = 0.065 mM, and [BMV ²⁺] = 0.13 mM with 12, 3 and 5 equivalents of CB[7] , respectively. Reference electrode = Ag/AgCl. ^b In <i>d</i> ₆ -DMSO: [HV ¹²⁺] = 3mM and [BV ⁴⁺] = 5mM, in D ₂ O [MV ²⁺] = 10 mM and [BMV ²⁺] = 5mM with 12, 6, 3 and 3 equivalents of CB[7] , respectively			

Chronocoulometry was also used to determine the diffusion coefficients of the fully oxidized and radical cationic states of the different species in aqueous solution (H₂O, 0.1 M tetrabutylammonium chloride (TBACl) as electrolyte). During the reduction process (0V → -0.7V) the fully oxidized species are predominant and diffuse to the electrode surface where they are reduced. By measuring the reduction rates, we calculated the diffusion constants for **HV¹²⁺**, **BV⁴⁺** and **BMV²⁺** in the absence and in the presence of **CB[7]**. The values (D₂O) are in a reasonable good agreement with those determined by DOSY (D₂O or DMSO) and, in general, follow the same decreasing sequence $D_{\text{BMV}^{2+}} > D_{\text{BV}^{4+}} > D_{\text{HV}^{12+}}$. Furthermore, by setting the voltage to -0.7V and performing the oxidation process, we measured the rates of oxidation of the corresponding radical cationic species and calculated their diffusion coefficients. In the absence of **CB[7]**, larger diffusion coefficients were observed for **HV^{6(•+)}** and **BV^{2(•+)}** than for their corresponding fully oxidized forms (Table 2). This is consistent with the decrease in hydrodynamic size that occurs upon reduction and subsequent pimerization. The slight D value increase observed for reduction of **BMV²⁺** may arise from increased

hydrophobic character and consequent decreases in solvation and effective hydrodynamic size.⁷² In the presence of **CB[7]**, the diffusion coefficients determined during the reduction process were much smaller as a consequence of inclusion complex formation. Moreover, large differences in the D coefficient were observed for the oxidized *versus* reduced forms of **BV** and **HV**, with the D value for the radical cationic form being significantly larger, in each case, and comparable to the value determined in the absence of **CB[7]**. These results provide clear evidence for reduction-induced decomplexation of **CB[7]** and subsequent dimerization of geminal viologen radical cations in both **BV^{2(•+)}** and **HV^{6(•+)}**. Changes in D value were not pronounced in the case of **BMV** because reduction of **BMV²⁺** to **BMV^{•+}** does not induce **CB[7]** dissociation and consequently does not lead to dimerization.

The volumes (inside a contour of 0.001 electrons·Bohr³) of **MV²⁺**, **BMV²⁺**, **BV⁴⁺**, **MV²⁺⊂CB[7]** and **BMV²⁺⊂CB[7]** were computed using DFT and found to be 239.9, 342.54, 1153.6, 1325.3 and 1364.4 Å³, respectively. The corresponding radii of these species, evaluated by considering spheres having the same volumes, were then used to estimate diffusion coefficients with the aid of the Stokes-Einstein equation.^{73,74} The calculated diffusion coefficients for **MV²⁺**, **BMV²⁺**, **BV⁴⁺**, **MV²⁺⊂CB[7]** and **BMV²⁺⊂CB[7]** were found to be 5.70×10^{-6} , 5.06×10^{-6} , 3.38×10^{-6} , 3.22×10^{-6} , and 3.19×10^{-6} cm²s⁻¹, respectively, and are in reasonably good agreement with the data obtained from DOSY and chronocoulometry. The volume calculated for **BMV^{•+}** (316.79 Å³) was found to be somewhat smaller than that obtained for **BMV²⁺** (342.54 Å³), which is also consistent with the higher diffusion coefficient determined for the radical cation using chronocoulometry (Table 3).

2.3.3c. Dicationic Diradical **BV^{2(•+)}**

To further provide evidence of the reduction-induced pimerization mechanism of **HV¹²⁺⊂(CB[7])₆**, SWVs of **BV⁴⁺** in the absence and in the presence of **CB[7]** were recorded in phosphate buffer (Figure 39). As observed for the other derivatives, their shapes can be ascribed to two reversible reduction processes. Assuming that, in the absence of **CB[7]**, the electrochemical properties of **BV⁴⁺** are related to those of **HV¹²⁺**, we infer that each reduction process of the former involves two electrons. This deduction is confirmed by the values of the reduction potentials of **BV⁴⁺** ($(E_{1/2}^1(\text{BV}^{4+}/\text{BV}^{2(•+)}) = -0.49$ V, and $E_{1/2}^2(\text{BV}^{2(•+)}/\text{BV}^0) = -0.85$ V) and by the peak-to-peak separation $\Delta E_{1/2} = 360$ mV, which are almost identical to the corresponding values determined for **HV¹²⁺**. On addition of **CB[7]** to **BV⁴⁺**, a shift of ~ 40 mV to a more negative potential was observed for the first reduction peak, whereas no shift was detected for the second reduction process, in agreement with the results previously obtained with **HV¹²⁺**. Thus, formation of radical cations on two-electron reduction of **BV⁴⁺** induces dissociation of **CB[7]** and subsequent pimerization. The negative shifts of $\Delta E_{1/2}^1$ observed for **BV⁴⁺** (40 mV) and **HV¹²⁺** (50 mV) in the presence of **CB[7]** are similar in magnitude to the shift observed for **MV²⁺** (30 mV) after addition of **CB[7]**, which is an indication that the same binding mode (**CB[7]**/bipyridinium) is shared by **BV⁴⁺⊂(CB[7])₂**, **HV¹²⁺⊂(CB[7])₆** and **MV²⁺⊂CB[7]**. By contrast, the marked negative shift of $\Delta E_{1/2}^1$ observed for **BMV²⁺** (140 mV) strongly suggests a different binding mode (*i.e.* **CB[7]** is suggested to

encircle the benzylic unit for \mathbf{BMV}^{2+} , while it encircles the corresponding viologen monoradical upon one electron reduction).

2.4. Conclusion

UV-Vis.-NIR, ^1H NMR and electrochemical analyses have clearly demonstrated that \mathbf{MV}^{2+} and $\mathbf{MV}^{\bullet+}$ bind to $\mathbf{CB[7]}$ in a similar way, with a viologen unit encircled inside the hydrophobic cavity of the macrocycle. Therefore, when the pseudorotaxane $\mathbf{MV}^{2+}\subset\mathbf{CB[7]}$ is reduced to $\mathbf{MV}^{\bullet+}\subset\mathbf{CB[7]}$, no major conformational changes occur, although $\mathbf{MV}^{\bullet+}\subset\mathbf{CB[7]}$ is a less stable complex (Figure 40). In contrast, \mathbf{BMV}^{2+} binds to $\mathbf{CB[7]}$ with its benzyl substituent inside the cavity of the macrocycle. However, $\mathbf{BMV}^{\bullet+}$ and $\mathbf{MV}^{\bullet+}$ have nearly the same binding affinity for $\mathbf{CB[7]}$, which suggests that $\mathbf{BMV}^{\bullet+}$ also binds with its radical cationic moiety inside $\mathbf{CB[7]}$. It follows that, when the pseudorotaxane $\mathbf{BMV}^{2+}\subset\mathbf{CB[7]}$ is reduced to $\mathbf{BMV}^{\bullet+}\subset\mathbf{CB[7]}$, the macrocycle shuttles (intramolecular translocation) from the benzyl unit to the viologen radical cation (Figure 40).

Despite the structural similarity between \mathbf{BMV}^{2+} and the arms of the multimeric threads \mathbf{BV}^{4+} and \mathbf{HV}^{12+} (Figure 40), the latter bind to $\mathbf{CB[7]}$ in the same fashion that \mathbf{MV}^{2+} does. This is due to steric effects near the cyclophosphazene core, which prevent $\mathbf{CB[7]}$ from properly encircling the benzyl substituents. However, unlike $\mathbf{MV}^{2+}\subset\mathbf{CB[7]}$, when each of the bipyridinium units of $\mathbf{BV}^{4+}\subset\mathbf{CB[7]}$ and $\mathbf{HV}^{12+}\subset\mathbf{CB[7]}$ (Figure 40) are reduced to their corresponding monoradical monocations, $\mathbf{CB[7]}$ spontaneously dissociates for thermodynamic reasons to give the pimerized species $\mathbf{BV}^{2(\bullet+)}$ and $\mathbf{HV}_D^{6(\bullet+)}$, respectively. In fact, no evidence for interactions between $\mathbf{CB[7]}$ and the multimeric viologen radical cations could be detected by any of the analytical methods employed. More generally, the data lend credence to the idea that radical cation dimerization (a relatively weak interaction, see introduction) can be enhanced intramolecularly and exploited for the design of novel molecular switches. This approach is scarce in the literature, even though a recent report has demonstrated that molecular reorganization (from twelve to six directions) around a C_{60} core can be achieved by one electron reduction of each of the twelve viologen subunits homogeneously substituted.⁷⁵

Bibliographic Section

- 1 Iordache, A.; Retegan M.; Thomas F.; Royal, G.; Saint-Aman, E.; Bucher C. *Chem. Eur. J.* **2012**, *18*, 7648-7653.
- 2 Bryan, J. C.; Sachleben, R. A.; Gakh, A. A., Bunick, G. J. *J. Chem. Crystallogr.* **1999**, *29*, 513-521.
- 3 Vogelsberg, C. S.; Bracco, S.; Beretta, M.; Comotti, A.; Sozzani, P.; A.Garcia-Garibay, M. *J. Phys. Chem. B.* **2012**, *116*, 1623-1632.
- 4 Kay, E. R.; Leigh, D. A.; Zerbetto, F. *Angew. Chem. Int. Ed.* **2007**, *46*, 72-191.
- 5 Skopek, K.; Hershberger, M. C.; Gladysz, J. A. *Coord. Chem. Rev.* **2007**, *251*, 1723-1733.
- 6 Browne, W. R.; Feringa, B. L. *Nat. Nanotechnol.* **2006**, *1*, 25-35.
- 7 Kottas, G. S.; Clarke, L. I.; Horinek, D.; Michl, J. *Chem. Rev.* **2005**, *105*, 1281-1376.
- 8 Yoon, I.; Benitez, D.; Zhao, Y.-L.; Miljanic, O.S.; Kim, S.-Y.; Tkatchouk, E.; Leung, K. C. F.; Khan, S. I.; Goddard, W. A.; Stoddart, J. F. *Chem. Eur. J.* **2009**, *15*, 1115-1122.
- 9 Li, D.; Paxton, W. F.; Baughman, R. H.; Huang, T. J.; Stoddart, J. F.; Weiss, P. S. *MRS Bull.* **2009**, *34*, 671-681.
- 10 Juluri, B. K.; Kumar, A. S.; Liu, Y.; Ye, T.; Yang, Y.-W., Flood, A. H.; Fang, L.; Stoddart, J. F.; Weiss, P. S.; Huang, T. J. *ACS Nano* **2009**, *3*, 291-300.
- 11 Saha, S.; Stoddart, J. F. *Molecular Motors and Muscles*, in *Functional Organic Materials* Müller, T. J. J.; Bunz, U. H. F., Eds., Wiley-VCH, Weinheim, Germany, **2007**, 295-327.
- 12 Badjic, D.; Ronconi, C. M.; Stoddart, J. F.; Balzani, V.; Silvi, S.; Credi, A. *J. Am. Chem. Soc.* **2006**, *128*, 1489-1499.
- 13 Angelos, S.; Khashab, N. M.; Yang, Y.-W.; Trabolsi, A.; Khatib, H. A.; Stoddart, J. F.; Zink, J. I. *J. Am. Chem. Soc.* **2009**, *131*, 12912-12914.
- 14 Hmadeh, M.; Fang, L.; Trabolsi, A.; Elhabiri, M.; Albrecht-Gary, A.-M.; Stoddart, J. F. *J. Mater. Chem.* **2010**, *20*, 3422-3430.
- 15 Badjic, J. D.; Balzani, V.; Credi, A.; Silvi, S.; Stoddart, J. F. *Science* **2004**, *303*, 1845-1849.
- 16 Khashab, N. M.; Trabolsi, A.; Lau, Y. A.; Ambrogio, M. W.; Friedman, D. C.; Khatib, H. A.; Zink, J. I.; Stoddart, J. F. *Eur. J. Org. Chem.* **2009**, 1669-1673.
- 17 Fernandez-Mato, A.; Garcia, M. D.; Peinador, C.; Quintela, J. M.; Sanchez-Andujar, M.; Pato-Doldan, B.; Senaris-Rodriguez, M. A.; Tordera, D.; Bolink, H. J. *Cryst. Growth Des.* **2013**, *13*, 460-464.
- 18 Muraoka, T.; Kinbara, K.; Kobayashi, Y.; Aida, T. *J. Am. Chem. Soc.* **2003**, *125*, 5612-5613.
- 19 Muraoka, T.; Kinbara, K.; Aida, T. *Nature* **2006**, *440*, 512-515.
- 20 Bargiello, T. A.; Tang, Q.; Oh, S.; Kwon, T. *Biochim. Biophys. Acta-Biomembranes* **2012**, *18*, 1807-1822.
- 21 Nchimi Nono, K.; Dalvand, P.; Wadhwa, K.; Nuryyeva, S.; Alneyadi, S.; Fahrenbach, A.; Olsen, J.-C.; Asfari, Z.; Platas-Iglesias, C.; Elhabiri, M.; Trabolsi, A. *Chem. Eur. J.* **2014**, *20*, 7334-7344.
- 22 Stokes, H. N. *Amer. Chem. J.* **1895**, *17*, 275-290.
- 23 Iordache, A.; Oltean, M.; Milet, A.; Thomas, F.; Baptiste, B.; Saint-Aman, E.; Bucher, C. *J. Am. Chem. Soc.*, **2012**, *134*, 2653-2671.
- 24 Monk, P. M. S. *The Viologens: Physicochemical Properties, Synthesis and Applications of the Salts of 4, 4'-Bipyridine* Chichester, **1998**

- 25 Wadhwa, K.; Nuryyeva, S.; Fahrenbach, A. C.; Elhabiri, M.; Platas-Iglesias, C.; Trabolsi, A. *J. Mater. Chem. C* **2013**, *1*, 2302-2307.
- 26 Georges, J. *Spectrochim. Acta A: Mol. Biomol. Spectro.* **1995**, *51*, 985-994.
- 27 Blank, O.; Davioud-Charvet, E.; Elhabiri, M. *Antioxid. Redox Signal.* **2012**, *17*, 544-554.
- 28 Gaussian 09, Revision A.01, Frisch, M. J.; Trucks, G. W.; Schlegel, H. B.; Scuseria, G. E.; Robb, M. A.; Cheeseman, J. R.; Scalmani, G.; Barone, V.; Mennucci, B.; Petersson, G. A.; Nakatsuji, H.; Caricato, M.; Li, X.; Hratchian, H. P.; Izmaylov, A. F.; Bloino, J.; Zheng, G.; Sonnenberg, J. L.; Hada, M.; Ehara, M.; Toyota, K.; Fukuda, R.; Hasegawa, J.; Ishida, M.; Nakajima, T.; Honda, Y.; Kitao, O.; Nakai, H.; Vreven, T.; Montgomery, Jr., J. A.; Peralta, J. E.; Ogliaro, F.; Bearpark, M.; Heyd, J. J.; Brothers, E.; Kudin, K. N.; Staroverov, V. N.; Kobayashi, R.; Normand, J.; Raghavachari, K.; Rendell, A.; Burant, J. C.; Iyengar, S. S.; Tomasi, J.; Cossi, M.; Rega, N.; Millam, N. J.; Klene, M.; Knox, J. E.; Cross, J. B.; Bakken, V.; Adamo, C.; Jaramillo, J.; Gomperts, R.; Stratmann, R. E.; Yazyev, O.; Austin, A. J.; Cammi, R.; Pomelli, C.; Ochterski, J. W.; Martin, R. L.; Morokuma, K.; Zakrzewski, V. G.; Voth, G. A.; Salvador, P.; Dannenberg, J. J.; Dapprich, S.; Daniels, A. D.; Farkas, Ö.; Foresman, J. B.; Ortiz, J. V.; Cioslowski, J.; Fox, D. J. Gaussian, Inc., Wallingford CT, **2009**.
- 29 Becke, A. D. *J. Chem. Phys.* **1993**, *98*, 5648-5652.
- 30 Lee, C.; Yang, W.; Parr, R. G. *Phys. Rev. B.* **1988**, *37*, 785-789.
- 31 Kim, J.; Jung, I.-S.; Kim, S.-Y.; Lee, E.; Kang, J.-K.; Sakamoto, S.; Yamaguchi, K.; Kim, K. *J. Am. Chem. Soc.* **2000**, *112*, 540-541.
- 32 Tomasi, J.; Mennucci, B.; Cammi, R. *Chem. Rev.* **2005**, *105*, 2999-3093.
- 33 Marenich, A. V.; Cramer, C. J.; Truhlar, D. G. *J. Phys. Chem. B.* **2009**, *113*, 6378-6396.
- 34 Stewart, J. J. P. *J. Mol. Model.* **2007**, *13*, 1173-1213.
- 35 Puzyn, T.; Suzuki, N.; Haranczyk, M.; Rak, J. *J. Chem. Inf. Model.* **2008**, *48*, 1174-1180.
- 36 Zhang, J.; Li, H.; Fan, Y.-R.; Zhou, X. *J. Phys. Org. Chem.* **2012**, *25*, 1306-1314.
- 37 Gampp, H.; Maeder, M.; Meyer, C. J.; Zuberbühler, A. D. *Talanta.* **1985**, *32*, 95-101.
- 38 Rossotti, F. J. C.; Rossotti, H. S.; Whewell, R. J. *J. Inorg. Nucl. Chem.* **1971**, *33*, 2051-2065.
- 39 Gampp, H.; Maeder, M.; Meyer, C. J.; Zuberbühler, A. D. *Talanta.* **1985**, *32*, 257-264.
- 40 Gampp, H.; Maeder, M.; Meyer, C. J.; Zuberbühler, A. D. *Talanta.* **1986**, *33*, 943-951.
- 41 Marquardt, D. W. *J. Soc. Ind. Appl. Math.* **1963**, *11*, 431-441.
- 42 Maeder, M.; Zuberbuehler, A. D. *Anal. Chem.* **1990**, *62*, 2220-2224.
- 43 (a) Kim, H.-J.; Jeon, W.S.; Ko, Y.H.; Kim, K. *Proc. Natl. Acad. Sci. U.S.A.*, **2002**, *99*, 5007-5011. (b) Lee, J.W.; Samal, S.; Selvapalam, N.; Kim, H.-J.; Kim, K. *Acc. Chem. Res.* **2003**, *36*, 621-630.
- 44 (a) Jansen, K.; Buschmann, H.-J.; Wego, A.; Döpp, D.; Mayer, C.; Drexler, H. J.; Holdt, H. J.; Schollmeyer, E. *J. Incl. Phenom. Macrocycl. Chem.* **2001**, *39*, 357-363. (b) Buschmann, H.-J.; Cleve, E.; Jansen, K.; Schollmeyer, E. *Anal. Chim. Acta* **2001**, *437*, 157-163. (c) Buschmann, H.-J.; Cleve, E.; Jansen, K.; Wego, A.; Schollmeyer, E. *J. Incl. Phenom. Macrocycl. Chem.* **2001**, *40*, 117-120. (d) Ong, W.; Gomez-Kaifer, M.; Kaifer, A.E. *Org. Lett.*, **2002**, *4*, 1791-1794. (e) Ong, W.; Kaifer, A.E. *J. Org. Chem.* **2004**, *69*, 1383-1385.
- 45 Freitag, M. PhD dissertation, The State University of New Jersey, **2011**.
- 46 Yang, H.; Hao, J.; Tan, Y. *J. Polym. Sci. Part A.* **2011**, *49*, 2138-2146.
- 47 Sindelar, V.; Moon, K.; Kaifer, A. E. *Org. Lett.* **2004**, *6*, 2665-2668.
- 48 St-Jacques, A. D.; Wyman, I. W.; Macartney, D. H. *Chem. Commun.* **2008**, 4936-4938.

- 49 Wyman, I. W.; Macartney, D. H. *Org. Biomol. Chem.* **2010**, *8*, 253-260.
- 50 Bader, R. F. W.; Carroll, M. T.; Cheeseman, J. R.; Chang, C. J. *Am. Chem. Soc.* **1987**, *109*, 7968-7979.
- 51 López-Vidal, E. M.; Regueiro-Figueroa, M.; García, M. D.; Platas-Iglesias, C.; Peinador, C.; Quintela, J. M. *Inorg. Chem.* **2012**, *51*, 4429-4431.
- 52 Pliego, J. R.; Riveros, J. M. *J. Phys. Chem. A* **2001**, *105*, 7241-7247.
- 53 Bryantsev, V. S.; Diallo, M. S.; Goddard III, W. A. *J. Phys. Chem. B* **2008**, *112*, 9709-9719.
- 54 Bryantsev, V. S.; Diallo, M. S.; Goddard III, W. A. *J. Phys. Chem. A* **2009**, *113*, 9559-9567.
- 55 Perlmutter-Hayman, B. *Acc. Chem. Res.* **1986**, *19*, 90-96.
- 56 Ercolani, G. *J. Am. Chem. Soc.* **2003**, *125*, 16097-16103.
- 57 Hou, J. L.; Yi, H. P.; Shao, X. B.; Li, C.; Wu, Z. Q.; Jiang, X. K.; Wu, L. Z.; Tung, C. H.; Li, Z. T. *Angew. Chem. Int. Ed.* **2006**, *45*, 796-800.
- 58 Trabolsi, A.; Urbani, M.; Delgado, J. L.; Ajamaa, F.; Elhabiri, M.; Solladie, N.; Nierengarten, J.-F.; Albrecht-Gary, A.-M. *New J. Chem.* **2008**, *32*, 159-165.
- 59 Monk, P.; Hodgkinson, N. M.; Ramzan, S. A. *Dyes. Pigm.* **1999**, *43*, 207-217.
- 60 Lee, C.; Moon, M. S.; Park, J. W.; *J. Electroanal. Chem.* **1996**, *407*, 161-167.
- 61 Stargardt, J. F.; Hawkridge, F. M.; *Anal. Chim. Acta.* **1983**, *146*, 1-8.
- 62 Claude-Montigny, B.; Merlin, A.; Tondre, C. *J. Phys. Chem.* **1992**, *96*, 4432-4437.
- 63 Park, J. W.; Choi, N. H.; Kim, J. H. *J. Phys. Chem.* **1996**, *100*, 769-774.
- 64 Kosower, E. M.; Cotter, J. L. *J. Am. Chem. Soc.* **1964**, *86*, 5524-5527.
- 65 Watanabe, T.; Honda, K. *J. Phys. Chem.* **1983**, *86*, 2617-2619.
- 66 Mayhew, S. G.; Müller, F. *Biochem. Soc. Trans.* **1982**, *10*, 176-177.
- 67 In contrast to aqueous solutions, the monomer–dimer equilibrium is indeed usually not observed in polar organic solvents such as MeOH, MeCN, and DMF, presumably because the radical cation exists as an ion pair rather than as a fully dissociated species, and thus dimerization is prevented.
- 68 (a) Zhao, Y.; Truhlar, D. G. *Theor. Chem. Acc.* **2008**, *120*, 215-241 (b) Frisch, M. J.; *Gaussian 09, Revision B.1, Gaussian, Inc.*, Wallingford CT, **2009**.
- 69 Fahrenbach, A. C.; Barnes, J. C.; Lanfranchi, D. A.; Li, H.; Coskun, A.; Gassensmith, J. J.; Liu, Z.; Benítez, D.; Trabosi, A.; Goddard III, W. A.; Elhabiri, M.; Stoddart, J. F. *J. Am. Chem. Soc.* **2012**, *134*, 3061-3072.
- 70 Bernhard, S.; Goldsmith, J. I.; Takada, K.; Abruña, H. D. *Inorg. Chem.* **2003**, *42*, 4389-4393.
- 71 Flanagan, J. B.; Margel, S.; Bard, A. J.; Anson, F. C. *J. Am. Chem. Soc.* **1978**, *100*, 4242-4248.
- 72 Cohen, Y.; Ayalon, A. *Angew. Chem. Int. Ed. Engl.* **1995**, *34*, 816-818.
- 73 Rast, S.; Fries, P. H.; Belorizky, E. *J. Chem. Phys.* **2000**, *113*, 8724-8735.
- 74 Roca-Sabio, A. N.; Bonnet, C. L. S.; Mato-Iglesias, M.; Esteban-Gomez, D.; Toth, E. V.; Blas, A. S. D.; Rodriguez-Blas, T.; Platas-Iglesias, C. *Inorg. Chem.* **2012**, *51*, 10893-10903.
- 75 Iehl, J.; Frasconi, M.; Jacquot de Rouville, H.-P.; Renaud, N.; Dyar, S. M.; Strutt, N. L.; Carmieli, R.; Wasielewski, M. R.; Ratner, M. A.; Nierengarten, J.-F.; Stoddart, J. F. *Chem. Sci.* **2013**, *4*, 1462-1469.

**Chapter III:
Intermolecular
Dimerization of a *Tris-*
Viologen System and its
CB[n] Recognition
Properties**

3.1. Introduction

Radical cationic species of viologen derivatives possess a high propensity to form non-covalent dimers in aqueous solution. This dimerization results from the lessening of the Coulombic repulsions that usually take place between two identical viologen dications. Upon one-electron reduction, the electrostatic interaction between the positively charged nitrogen atom of a molecule and the reduced nitrogen radical of an adjoining molecule becomes favourable to the formation of a cation-radical molecular pair. Besides, the resulting planarity of the conjugated systems allows the formation of the supramolecular species. Planarity and hydrophobicity of the conjugated monoradical viologens and π - π stacking interactions therefore play a key-role in the formation of the corresponding dimer.^{1,2}

In the preceding chapter, we have demonstrated that intramolecular dimerization, both in organic and inorganic solvents, of viologen monoradical cations judiciously distributed around a preorganized multivalent system can, thermodynamically overwhelm the inclusion to **CB[7]** and induce fast and efficient host-guest dethreading. Reinstating the oxidized bipyridiniums in turn prevent the intramolecular dimerization processes and reversibly led to the initial host-guest species with **CB[7]**. Consequently, molecular switches triggered by (electro)chemical stimuli can be envisaged. A phosphazene platform functionalized with 6 terminal viologens was prepared and thoroughly studied in combination with **CB[7]** using a fruitful combination of analytical methods such as absorption spectrophotometry, electrochemistry (CV and SWV), ESI-MS and ¹H NMR.^{3,4}

Herein, we now developed a new strategy to enhance the dimerization strength of bipyridinium moieties by the synergistic combination of the preorganization of multiple viologens on the same platform and the hydrophobicity of the directly attached aromatic substituents. A tritopic system in which three viologen moieties were assembled around a triphenylbenzene platform has been synthesised. This circular trimeric system can be regarded as benzenic core that has been extended on its 1, 3 and 5 positions by phenyl-methyl viologen subunits (Figure 1). The recognition properties of **CB[7]** and **CB[8]** have been thoroughly investigated. Interestingly, the presence of three redox-active centres within the same molecule favours the dimerization process with respect to the recognition by **CB[7]** and increases by several orders of magnitude the so-called “dimerization” constant. This innovative strategy demonstrates that intermolecular interactions can be beneficially employed to enhance the stability of radical dimers in solution thank to a peculiar design and to a multicenter strategy. For the sake of comparison, three model compounds were synthesized and concomitantly studied. The first one is an original platform embedding the tris-phenylene conjugated platform on which only one arm has been substituted by a methyl-viologen residue (**MVTP²⁺**); the second and third models are the monomeric and homologous methyl-phenyl viologen (**MPV²⁺**) and diphenyl-viologen derivative (**DPV²⁺**) that are still rigid compounds.

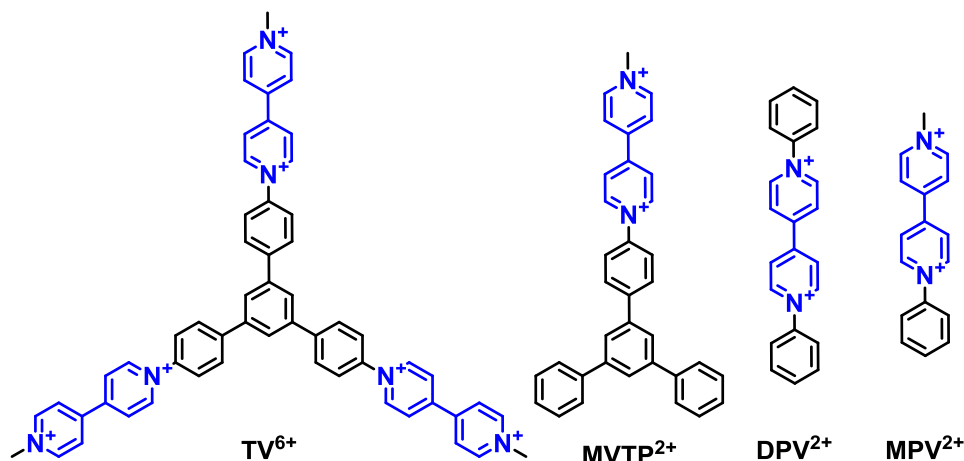


Figure 1. Chemical structures of the trimeric viologen system **TV⁶⁺** and its reference compounds **MVTP²⁺**, **MPV²⁺** and **DPV²⁺**.

In the following sections, we will thoroughly describe a physico-(electro)chemical investigation of this homogeneous series of four viologen derivatives in combination with the **CB[7]** and **CB[8]** macrocyclic guests. In particular, we have investigated the formation of the multimeric pseudorotaxanes **TV⁶⁺⊂(CB[7])₃** by ¹H NMR and UV-Vis. spectroscopy and measured their switching properties using electrochemistry and UV-Vis.-NIR absorption spectroscopy. For comparison, we also characterized the pseudorotaxanes **MPV²⁺⊂CB[7]**, **MVTP²⁺⊂CB[7]** and **DPV²⁺⊂(CB[7])₂** that were formed from the monomeric threads **MPV²⁺**, **MVTP²⁺** and **DPV²⁺**, respectively. These pseudorotaxanes species have been fully characterized by ESI-MS, absorption spectrophotometry and ¹H NMR. Their switching properties upon redox reactions were also characterized. With respect to the trisviologen compound **TV⁶⁺**, the one electron reduction of each of the viologen units leads to a trisradicalar tricationic species **TV^{3(•+)}** that spontaneously self-associate in solution to afford a very stable face-to-face dimer (**TV^{3(•+)}**)₂. Similarly to the above-mentioned hexavalent system **HV¹²⁺** system, formation of this (**TV^{3(•+)}**)₂ dimer concomitantly induces dethreading of the **CB[7]** macrocycles. A comparative study is also provided for **MPV^{•+}**, **MVTP^{•+}** and **DPV^{2(•+)}**.

3.2. Experimental Section and Results

3.2.1. Starting Materials

The reagents and the starting materials were purchased from commercial source and used without further purification. $\text{TV}^{6+} \cdot 3\text{I}/3\text{Cl}$, $\text{MPV}^{2+} \cdot \text{Br}/\text{Cl}$, $\text{MVTP}^{2+} \cdot \text{Cl}/\text{I}$ and $\text{DPV}^{2+} \cdot 2\text{Cl}$ were prepared by our collaborators (group of Pr Ali Trabolsi, NYUAD, Abu Dhabi, UAE).³

Cucurbit[7]uril (**CB[7]**) ($\text{C}_{42}\text{H}_{42}\text{N}_{28}\text{O}_{14}$, M. W. = 1162.96 g mol⁻¹, Strem chemicals) and cucurbit[8]uril (**CB[8]**) ($\text{C}_{48}\text{H}_{48}\text{N}_{32}\text{O}_{16}$, M.W. = 1329.11 g.mol⁻¹, Aldrich) are commercial products that were used without further purification.

All solutions were prepared in distilled H₂O which was further purified by passing it through a mixed bed of ion-exchanger (Bioblock Scientific R3-83002, M3-83006) and activated carbon (Bioblock Scientific ORC-83005). It was then boiled and de-oxygenated using CO₂ and O₂ free argon prior to use (Sigma Oxiclear cartridge). All stock solutions were prepared using an AG 245 Mettler Toledo analytical balance (precision 0.01 mg), and complete dissolution in phosphate buffer was achieved using an ultrasonic bath. The experiments were carried out at 25.0(2) °C maintained with the help of Haake FJ thermostats.

In all the solutions, the pH was maintained at 7.00 ± 0.05 by the use of a 0.1 M phosphate buffer, which was prepared by mixing 30.5 mL of Na₂HPO₄•2H₂O (0.2 M) (Prolabo) with 19.5 ml of NaH₂PO₄ (0.2 M) (Prolabo) and diluting to a total volume of 100 mL. The final pH of the solution was then set at the required value by using phosphoric acid (85%, Labosi). The pH was measured with an Ag/AgCl combined glass electrode (Metrohm 6.0234.500, long life) filled with 0.1 M NaCl (Fluka, p.a.) in H₂O. Standardization of the millivoltmeter and the verification of the linearity of the electrode response were performed using a set of NIST certified commercial Merck buffered solutions (pH 1.68, 4.00, 6.86, 7.41 and 9.18).

Reduction of TV^{6+} and its model derivatives into their corresponding radical cationic forms ($\text{TV}^{3(\bullet+)}$, $\text{MPV}^{\bullet+}$, $\text{MVTP}^{\bullet+}$ and $\text{DPV}^{\bullet+}$) was achieved under argon (CO₂- and O₂-free argon) with the addition of Na₂S₂O₄ solution in argon purged H₂O. The formation of the radicals was monitored by absorption spectrophotometry using a Cary 5000 UV-Vis.-NIR spectrophotometer.

3.2.2. Analytical Methods.

Routine Nuclear Magnetic Resonance (NMR) spectra were recorded at 298 K on a Bruker Advance 600 spectrometer with working frequencies of 600 and 150 MHz for ¹H and ¹³C, respectively. Chemical shifts are reported in ppm relative to the signals corresponding to the residual non-deuterated solvents (D₂O δ = 4.97).

Electrospray mass (ESI-MS) spectra were measured on an ion-trap instrument (Bruker Esquire 3000plus, Bruker Daltonic, Bremen, Germany) equipped with an Agilent Technologies 6120 quadrupole equipped with an electrospray (ESI) interface.

Square wave voltammetry (SW) was carried out at room temperature in argon-purged H₂O and DMSO solutions with a Gamry Multipurpose instrument (Reference 600) interfaced to a PC. SW experiments were performed using a glassy carbon working electrode (0.071 cm², BASi). The electrode surface was polished routinely with 0.05 μm alumina-water slurry on a felt surface immediately before use. The counter electrode was a Pt coil and the reference electrode was an Ag/AgCl electrode, unless otherwise noted. The concentration of the supporting electrolyte, tetrabutylammonium chloride (TBACl) was 0.1 M. The experimental errors on the potential values are estimated to +/– 10 mV.

UV-Vis.-NIR spectra were recorded on a Cary 5000 (Agilent) spectrophotometer maintained at 25.0(2) °C by the flow of a Dual Cell Pelletier Accessory (Cary Varian)

3.2.3. Spectrophotometric Titrations of Viologen Derivatives by CB[7]

The spectrophotometric titrations of **TV⁶⁺** (3×10^{-4} M), **MPV²⁺** (9.5×10^{-5} M), **MVTP²⁺** (10^{-4} M) and **DPV¹²⁺** (5×10^{-5} M) with cucurbit[7]uril (**CB[7]**) were carried out in Hellma quartz optical cells of 10 mm pathlength in water at pH 7 (0.1 M phosphate buffer). Microvolumes of a concentrated solution of **CB[7]** ($2\text{--}5 \times 10^{-3}$ M) were added to the viologen derivatives **MPV²⁺** ($l = 10$ mm, $v = 2.5$ mL), **DPV²⁺** ($l = 10$ mm, $v = 1$ mL), **MVTP²⁺** ($l = 10$ mm, $v = 1$ mL) or **TV⁶⁺** ($l = 10$ mm, $v = 2.5$ mL) with the help of a microburette (Eppendorf). The $[\text{CB[7]}]_0/[\text{BIPY}^{2+}]_0$ ratios were varied from 0 to 3.75 for **MPV²⁺**, from 0 to 5.5 for **DPV²⁺**, from 0 to 2.62 for **MVTP²⁺** and from 0 to 9.3 for **TV⁶⁺**, respectively. The spectrophotometric titration of **TV⁶⁺** (8.02×10^{-6} M), **MVTP²⁺** (1.54×10^{-5} M) with cucurbit[8]uril (**CB[8]**) was also carried out in a 10 mm Hellma quartz optical cell at pH 7 (0.1 M phosphate buffer). Microvolumes of a concentrated solution of **CB[8]** were added to the bipyridinium solutions with the help of a microburette (Eppendorf). The $[\text{CB[8]}]_0/[\text{BIPY}^{2+}]_0$ ratios were varied from 0 to 1.26 for **MVTP²⁺** and from 0 to 5.44 for **TV⁶⁺**, respectively. Special care was taken to ensure that complete equilibration was attained. After each addition, a UV-Vis. spectrum was recorded from 220 to 800 nm on a Cary 5000 (Agilent) spectrophotometer maintained at 25.0(2) °C by the flow of a Dual Cell Pelletier Accessory (Cary Varian).

3.2.3a. Recognition of MPV²⁺ by CB[7]

Figure 2a depicts the UV-Vis. absorption spectrophotometric titration of the **MPV²⁺** by **CB[7]**. Figure 2b shows the electronic spectra of **MPV²⁺** and its inclusion complex **MPV²⁺⊂CB[7]**. The isosbestic point at 274 nm is a strong indication of a single equilibrium in solution. The Job plot presented in Figure 8 confirms the expected 1:1 complex formation between **MPV²⁺** and **CB[7]**. The **MPV²⁺⊂CB[7]** [2]pseudorotaxane is characterized by a stability constant of $\log K_{\text{MPV}^{2+}\text{⊂CB[7]}} = 6.1(3)$.

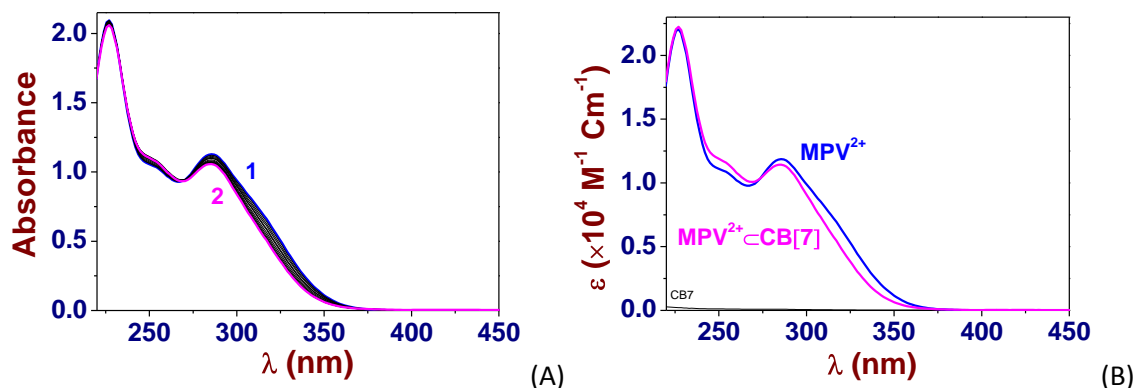


Figure 2. A) UV-Vis. absorption titration of MPV^{2+} by $CB[7]$. B) Electronic spectra of MPV^{2+} and its inclusion complex with $CB[7]$ ($MPV^{2+} \subset CB[7]$). Solvent: water pH 7.0 (0.1 M $Na_2H_2PO_4/NaH_2PO_4$). $[MPV^{2+}]_0 = 9.5 \times 10^{-5}$ M; (1) $[CB[7]]_0/[MPV^{2+}]_0 = 0$; (2) $[CB[7]]_0/[MPV^{2+}]_0 = 3.75$; $l = 1$ cm; $T = 25.0(1)^\circ C$. The absorption spectra are not corrected from dilution effects.

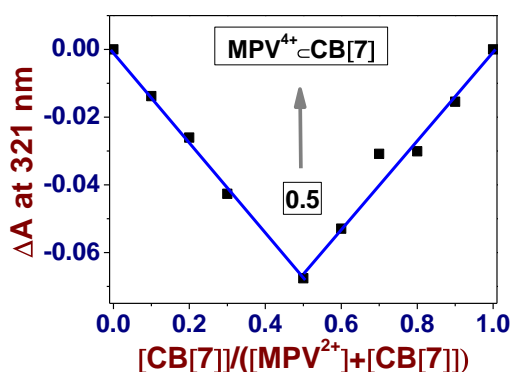


Figure 3. Job plot (ΔA at 321 nm) upon mixing MPV^{2+} with $CB[7]$ at pH 7. ($[MPV^{2+}]_0 + [CB[7]]_0 = 9.5 \times 10^{-5}$ M; Solvent: water pH 7.0 (0.1 M $Na_2H_2PO_4/NaH_2PO_4$); $l = 1$ cm; $T = 25.0(1)^\circ C$).

3.2.3.b. Recognition of DPV^{2+} by $CB[7]$

Figure 4A illustrates the spectrophotometric titration of DPV^{2+} by $CB[7]$ (isosbestic point at 316 nm).

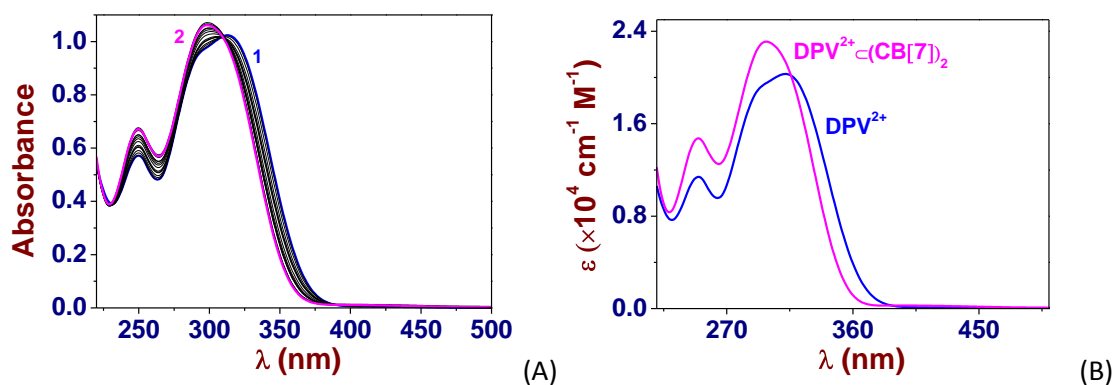


Figure 4. A) UV-Vis. absorption titration of DPV^{2+} by $CB[7]$. B) Electronic spectra of DPV^{2+} and its inclusion complex with $CB[7]$ ($DPV^{2+} \subset (CB[7])_2$). Solvent: water pH 7.0 (0.1 M $Na_2H_2PO_4/NaH_2PO_4$). $[DPV^{2+}]_0 = 5.0 \times 10^{-5}$ M; (1) $[CB[7]]_0/[DPV^{2+}]_0 = 0$; (2) $[CB[7]]_0/[DPV^{2+}]_0 = 5.5$; $l = 1$ cm; $T = 25.0(1)^\circ C$. The absorption spectra are not corrected from dilution effects.

Figure 4B shows the electronic spectra of DPV^{2+} and its inclusion complexes $\text{DPV}^{2+}\text{C}(\text{CB}[7])_2$. The Job plot presented in Figure 5 further confirms that a ternary 1:2 complex might be formed between DPV^{2+} and $\text{CB}[7]$. Only the global stability constant of the [3]pseudorotaxane $\text{DPV}^{2+}\text{C}(\text{CB}[7])_2$ was calculated ($\log \beta_{\text{DPV}^{2+}\text{C}(\text{CB}[7])_2} = 8.29(9)$).

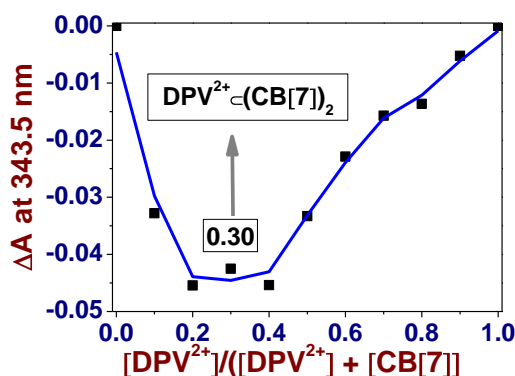


Figure 5. Job plot (ΔA at 343.5 nm) upon mixing DPV^{2+} with $\text{CB}[7]$ at pH 7. ($[\text{DPV}^{2+}]_0 + [\text{CB}[7]]_0 = 7.0 \times 10^{-5} \text{ M}$; Solvent :water pH 7.0 (0.1 M $\text{Na}_2\text{H}_2\text{PO}_4/\text{NaH}_2\text{PO}_4$); $l = 1 \text{ cm}$; $T = 25.0(1)^\circ\text{C}$).

3.2.3c. Recognition of MVTP^{2+} by $\text{CB}[7]$

The host-guest complexes formed between MVTP^{2+} and $\text{CB}[7]$ were characterized using UV-Vis. absorption spectrophotometric titrations (Figure 6A). Figure 6B displays the electronic spectra of MVTP^{2+} and its inclusion complexes $\text{MVTP}^{2+}\text{C}(\text{CB}[7])$ that were calculated (two isosbestic points at 370 and 451 nm). The $\text{MVTP}^{2+}\text{C}(\text{CB}[7])$ [2]pseudorotaxane that was clearly characterized is associated to a stability constant of $\log K_{\text{MVTP}^{2+}\text{C}(\text{CB}[7])} = 4.8(4)$.

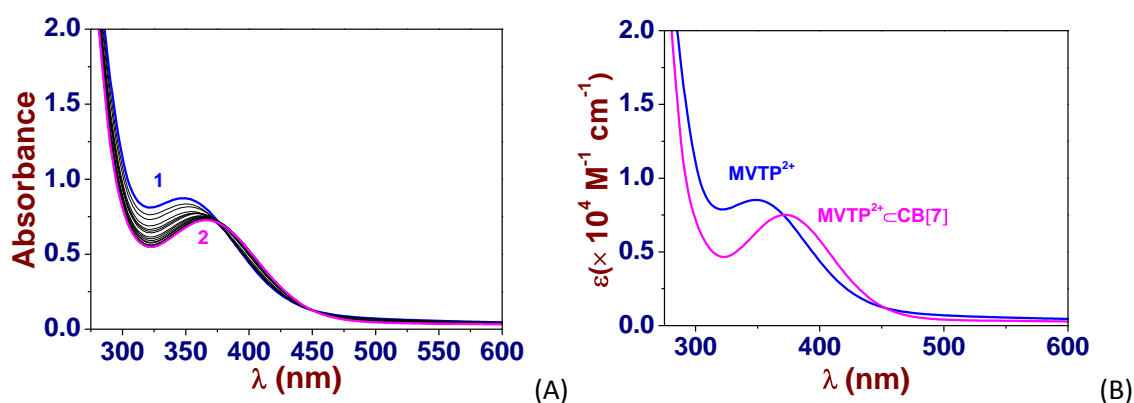


Figure 6. A) UV-Vis. absorption titration of MVTP^{2+} by $\text{CB}[7]$. B) Electronic spectra of MVTP^{2+} and its inclusion complex with $\text{CB}[7]$ ($\text{MVTP}^{2+}\text{C}(\text{CB}[7])$). Solvent: water pH 7.0 (0.1 M $\text{Na}_2\text{H}_2\text{PO}_4/\text{NaH}_2\text{PO}_4$). $[\text{MVTP}^{2+}]_0 = 10^{-4} \text{ M}$; (1) $[\text{CB}[7]]_0/[\text{MVTP}^{2+}]_0 = 0$; (2) $[\text{CB}[7]]_0/[\text{MVTP}^{2+}]_0 = 2.62$; $l = 1 \text{ cm}$; $T = 25.0(1)^\circ\text{C}$. The absorption spectra are not corrected from dilution effects.

3.2.3d. Recognition of TV^{6+} by $\text{CB}[7]$

Figure 7A illustrates the spectrophotometric titration of TV^{6+} by $\text{CB}[7]$. Figure 7B shows the electronic spectra of TV^{6+} and its corresponding [4]pseudorotaxane $\text{TV}^{4+}\text{C}(\text{CB}[7])_3$ (two

isosbestic point at 238 and 367 nm). Similarly to HV^{12+} (see previous chapter), only an apparent association constant^{5,6} ($\log K^*_{\text{TV}^{6+}\text{C}(\text{CB}[7])_3} = 4.7(1)$) was deduced from the processing of the absorption spectrophotometric titrations.

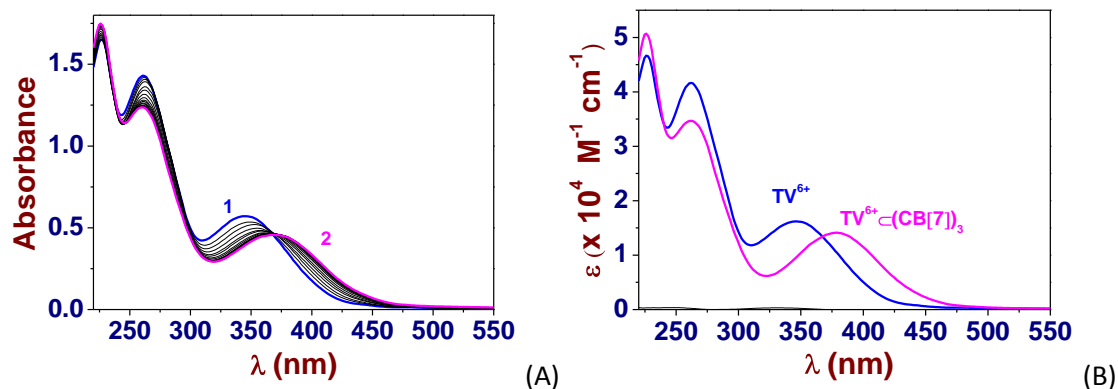


Figure 7. A) UV-Vis. absorption titration of TV^{6+} by $\text{CB}[7]$. B) Electronic spectra of TV^{6+} and its inclusion complex with $\text{CB}[7]$ ($\text{TV}^{6+}\text{C}(\text{CB}[7])_3$). Solvent: water pH 7.0 (0.1 M $\text{Na}_2\text{H}_2\text{PO}_4/\text{NaH}_2\text{PO}_4$). $[\text{TV}^{6+}]_0 = 10^{-4}$ M; (1) $[\text{CB}[7]]_0/[\text{TV}^{6+}]_0 = 0$; (2) $[\text{CB}[7]]_0/[\text{TV}^{6+}]_0 = 9.3$; $l = 1$ cm; $T = 25.0(1)^\circ\text{C}$. The absorption spectra are not corrected from dilution effects.

The characterization of the host-guest complexes formed with MVTP^{2+} or TV^{6+} and $\text{CB}[8]$ was investigated by absorption spectrophotometry (Figure 8A and Figure 9A). Figure 8B and Figure 9B depict the calculated electronic spectra of the inclusion complexes $\text{BIPY}^{2+}\text{C}(\text{CB}[8])$.

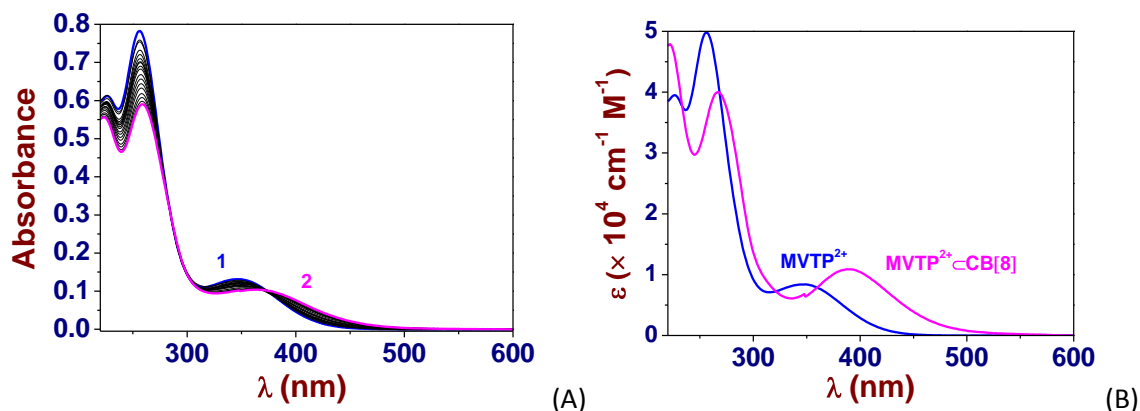


Figure 8. A) UV-Vis. absorption titration of MVTP^{2+} by $\text{CB}[8]$. B) Electronic spectra of MVTP^{2+} and its inclusion complex with $\text{CB}[8]$ ($\text{MVTP}^{2+}\text{C}(\text{CB}[8])$). Solvent: water pH 7.0 (0.1 M $\text{Na}_2\text{H}_2\text{PO}_4/\text{NaH}_2\text{PO}_4$). $[\text{MVTP}^{2+}]_0 = 1.54 \times 10^{-5}$ M; (1) $[\text{CB}[8]]_0/[\text{MVTP}^{2+}]_0 = 0$; (2) $[\text{CB}[8]]_0/[\text{MVTP}^{2+}]_0 = 1.26$; $l = 1$ cm; $T = 25.0(1)^\circ\text{C}$. The absorption spectra are not corrected from dilution effects.

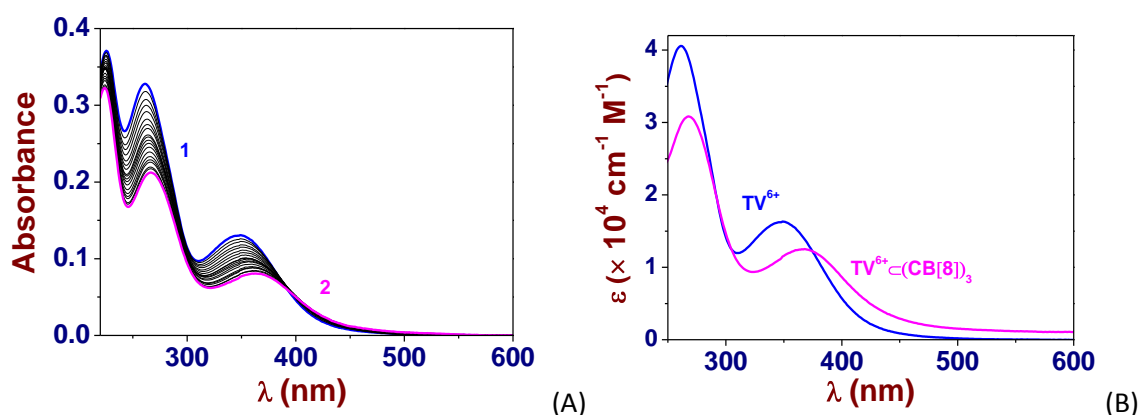


Figure 9. A) UV-Vis. absorption titration of TV^{6+} by $\text{CB}[8]$. B) Electronic spectra of TV^{6+} and its inclusion complex with $\text{CB}[8]$ ($\text{TV}^{6+} \subset (\text{CB}[8])_3$). Solvent: water pH 7.0 (0.1 M $\text{Na}_2\text{H}_2\text{PO}_4/\text{NaH}_2\text{PO}_4$). $[\text{TV}^{6+}]_0 = 10^{-5}$ M; (1) $[\text{CB}[8]]_0/[\text{TV}^{6+}]_0 = 0$; (2) $[\text{CB}[8]]_0/[\text{TV}^{6+}]_0 = 5.44$; $l = 1$ cm; $T = 25.0(1)^\circ\text{C}$. The absorption spectra are not corrected from dilution effects.

3.2.4. Stoichiometry of the [n]Pseudorotaxane with MPV^{2+} , DPV^{2+} , MVTP^{2+} and TV^{6+} Probed by ESI-MS

Electrospray ionization mass spectra (ESI-MS) of the host-guest complexes formed with either MV^{2+} or BMV^{2+} with $\text{CB}[7]$ (or $\text{CB}[8]$) were carried out with an ion-trap instrument (Bruker Esquire 3000plus, Bruker Daltonic, Bremen, Germany) equipped with an Agilent Technologies 6120 quadrupole equipped with an electrospray (ESI) interface. The sample solutions were continuously introduced into the spectrometer source with a syringe pump (Kd Scientific) with a flow rate of $800 \mu\text{L}\cdot\text{h}^{-1}$. For electrospray ionization, the drying gas was heated at 250°C and its flow was set at $6 \text{ L}\cdot\text{min}^{-1}$. The capillary exit voltage was fixed at 5 kV and the skimmer voltage was varied from 50 to 200 V in order to optimize the signal responses. Scanning was performed from $m/z = 100$ to 1500. The stoichiometries of the pseudorotaxanes formed with $\text{CB}[7]$ and $\text{CB}[8]$ were investigated by electrospray mass spectrometry (ESI-MS) in the positive mode in aqueous solutions. The ionization of the viologen derivatives and complexes (mainly observed as mono- or doubly positively charged species) takes place by reduction, deprotonation and/or by addition of sodium cations. Fragmentations such as demethylation were also observed.

Figure 10 depicts the ESI-MS spectrum obtained for a $55 \mu\text{M}$ solution of MPV^{2+} combined to 5 equivalents of $\text{CB}[7]$ while Figure 11 presents the ESI-MS spectrum obtained for a $100 \mu\text{M}$ solution of MPV^{2+} combined to 1 equivalent of $\text{CB}[8]$. A [2]pseudorotaxane species $\text{MPV}^{2+} \subset \text{CB}[n]$ ($n = 7,8$) has been clearly identified and its presence matches with the observations made by absorption spectrophotometry (*vide supra*).

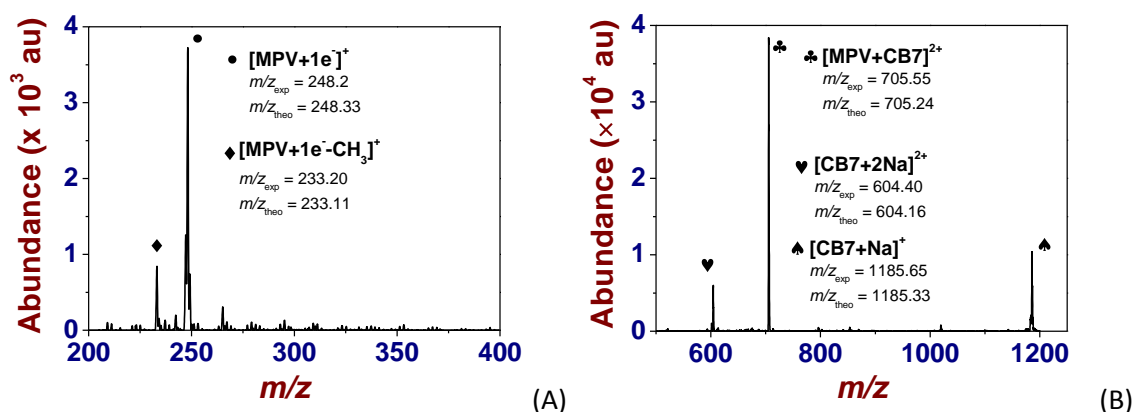


Figure 10. (A) ESI mass spectrum of free MPV^{2+} . $[\text{MPV}^{2+}]_0 = 5.5 \times 10^{-5}$ M. Solvent: H_2O ; positive mode. $V_c = 100$ V. • = $[\text{MPV}+1\text{e}^-]^+$, $m/z_{\text{exp}} = 248.20$, $m/z_{\text{theo}} = 248.33$. ♦ = $[\text{MPV}+1\text{e}^- \cdot \text{CH}_3]^+$, $m/z_{\text{exp}} = 233.20$, $m/z_{\text{theo}} = 233.11$.

(B) ESI mass spectrum of inclusion complexes of MPV^{2+} with $\text{CB}[7]$. $[\text{MPV}^{2+}]_0 = 5.5 \times 10^{-5}$ M; $[\text{CB}[7]]_0 = 2.75 \times 10^{-4}$ M. Solvent: H_2O ; positive mode. $V_c = 300$ V. ♥ = $[\text{CB}[7]+2\text{Na}]^{2+}$, $m/z_{\text{exp}} = 604.40$, $m/z_{\text{theo}} = 604.16$. ♣ = $[\text{MPV}+\text{CB}[7]]^{2+}$, $m/z_{\text{exp}} = 705.55$, $m/z_{\text{theo}} = 705.24$. ♠ = $[\text{CB}[7]+\text{Na}]^+$, $m/z_{\text{exp}} = 1185.65$, $m/z_{\text{theo}} = 1185.33$. The ESI-MS spectra were limited to the areas of interest. No peaks were detected in the excluded m/z regions.

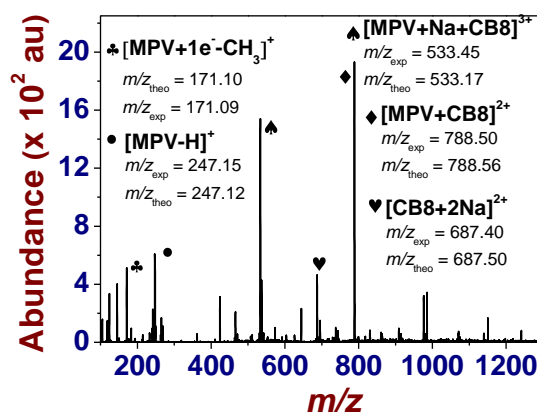


Figure 11. ESI mass spectrum of inclusion complexes of MPV^{2+} with $\text{CB}[8]$. $[\text{MPV}^{2+}]_0 = 1 \times 10^{-4}$ M; $[\text{CB}[8]]_0 = 1 \times 10^{-4}$ M. Solvent: H_2O ; positive mode. $V_c = 120$ V. ♥ = $[\text{CB}[8]+2\text{Na}]^{2+}$, $m/z_{\text{exp}} = 687.40$, $m/z_{\text{theo}} = 687.50$. • = $[\text{MPV}-\text{H}]^+$, $m/z_{\text{exp}} = 247.15$, $m/z_{\text{theo}} = 247.12$. ♦ = $[\text{MPV}+\text{CB}[8]]^{2+}$, $m/z_{\text{exp}} = 788.50$, $m/z_{\text{theo}} = 788.56$. ♣ = $[\text{MPV}-1\text{e}^- \cdot \text{CH}_3]^+$, $m/z_{\text{exp}} = 171.10$, $m/z_{\text{theo}} = 171.09$. ♠ = $[\text{MPV}+\text{Na}+\text{CB}[8]]^{3+}$, $m/z_{\text{exp}} = 533.45$, $m/z_{\text{theo}} = 533.17$. The ESI-MS spectra were limited to the areas of interest. No peaks were detected in the excluded m/z regions.

Figure 12 and Figure 13 gather the ESI-MS data obtained for the $\text{MVTP}^{2+}/\text{CB}[7]$ and $\text{MVTP}^{2+}/\text{CB}[8]$ system, respectively. As anticipated, they demonstrate that the [2]pseudorotaxanes $\text{MVTP}^{2+} \subset \text{CB}[n]$ ($n = 7, 8$) are also the predominant species formed in solution.

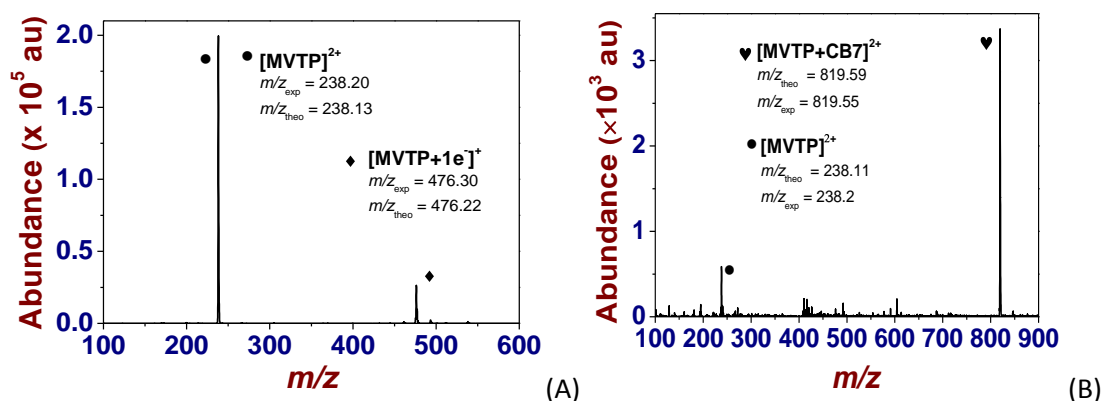


Figure 12. (A) ESI mass spectrum of free MVTP²⁺. [MVTP²⁺]₀ = 4 × 10⁻⁶ M. Solvent: H₂O; positive mode. V_c = 100 V. ● = [MVTP]²⁺, m/z_{exp} = 238.20, m/z_{theo} = 238.11. ◆ = [MVTP+1e]⁺, m/z_{exp} = 476.30, m/z_{theo} = 476.22.

(B) ESI mass spectrum of inclusion complexes of MVTP²⁺ with CB[7]. [MVTP²⁺] = 4 × 10⁻⁶ M; [CB[7]] = 2.75 × 10⁻⁴ M. Solvent: H₂O; positive mode. V_c = 100 V. ● = [MVTP]²⁺, m/z_{exp} = 238.2, m/z_{theo} = 238.11. ♥ = [MVTP+CB[7]]²⁺, m/z_{exp} = 819.55, m/z_{theo} = 819.59. The ESI-MS spectra were limited to the areas of interest. No peaks were detected in the excluded m/z regions.

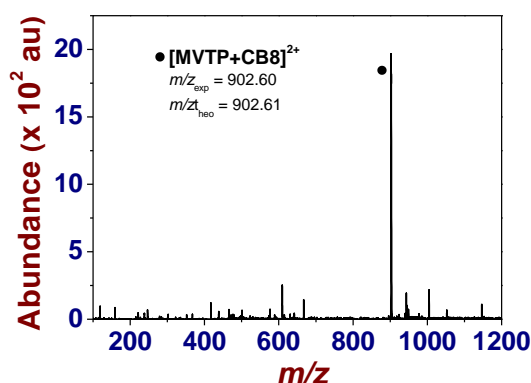


Figure 13. ESI mass spectrum of inclusion complexes of MVTP²⁺ with CB[8]. [MVTP²⁺] = 1 × 10⁻⁴ M; [CB[7]] = 1 × 10⁻⁴ M. Solvent: H₂O; positive mode. V_c = 120 V. ● = [MVTP+CB[8]]²⁺, m/z_{exp} = 902.60, m/z_{theo} = 902.61. The ESI-MS spectra were limited to the areas of interest. No peaks were detected in the excluded m/z regions.

ESI-MS mass spectra were also recorded for aqueous solutions containing 50 μM of DPV²⁺ with 4 equivalents of CB[7] (Figure 14) or 1 equivalent of CB[8] (Figure 15) and suggested, in agreement with the absorption spectrophotometric studies, the formation of a [2]pseudorotaxane DPV²⁺⊂CB[n] as well as a [3]pseudorotaxane DPV²⁺⊂(CB[n])₂ (n = 7,8).

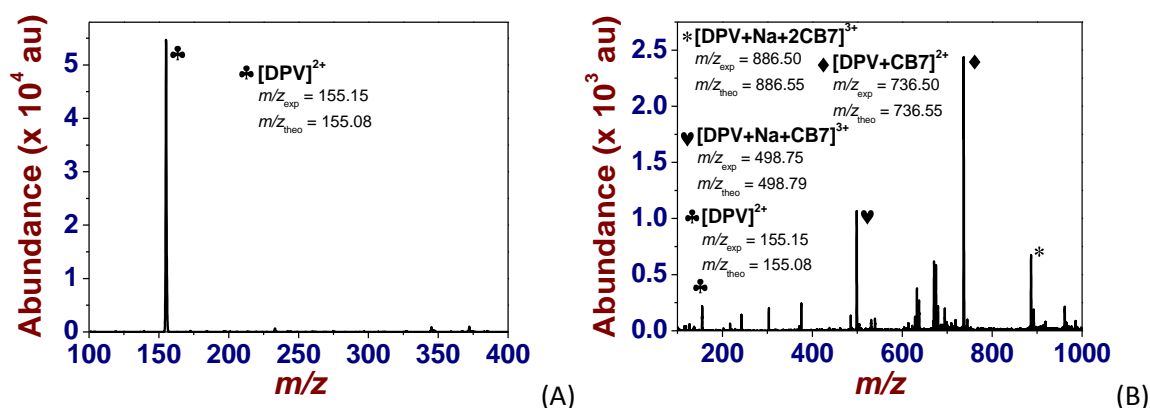


Figure 14. (A) ESI mass spectrum of free DPV^{2+} . $[\text{DPV}^{2+}]_0 = 5 \times 10^{-5}$ M. Solvent: H_2O ; positive mode. $V_c = 20$ V. $\clubsuit = [\text{DPV}]^{2+}$, $m/z_{\text{exp}} = 155.15$, $m/z_{\text{theo}} = 155.08$.

(B) ESI mass spectrum of inclusion complexes of DPV^{2+} with $\text{CB}[7]$. $[\text{DPV}^{2+}]_0 = 5 \times 10^{-5}$ M; $[\text{CB}[7]]_0 = 2 \times 10^{-4}$ M. Solvent: H_2O ; positive mode. $V_c = 20$ V. $\clubsuit = [\text{DPV}]^{2+}$, $m/z_{\text{exp}} = 155.15$, $m/z_{\text{theo}} = 155.08$. $\blacklozenge = [\text{DPV}+\text{CB}[7]]^{2+}$, $m/z_{\text{exp}} = 736.50$, $m/z_{\text{theo}} = 736.55$. $\spadesuit = [\text{DPV}+\text{Na}+2\text{CB}[7]]^{3+}$, $m/z_{\text{exp}} = 886.50$, $m/z_{\text{theo}} = 886.55$. The ESI-MS spectra were limited to the areas of interest. No peaks were detected in the excluded m/z regions.

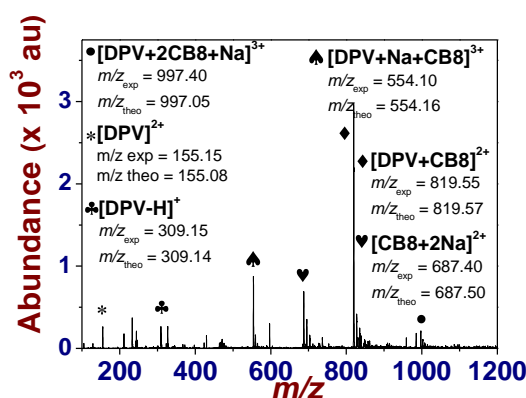


Figure 15. ESI mass spectrum of inclusion complexes of DPV^{2+} with $\text{CB}[8]$. $[\text{DPV}^{2+}]_0 = 5 \times 10^{-5}$ M; $[\text{CB}[8]]_0 = 2 \times 10^{-4}$ M. Solvent: H_2O ; positive mode. $V_c = 150$ V. $\clubsuit = [\text{DPV}]^{2+}$, $m/z_{\text{exp}} = 155.15$, $m/z_{\text{theo}} = 155.08$. $\clubsuit = [\text{DPV}-\text{H}]^+$, $m/z_{\text{exp}} = 309.15$, $m/z_{\text{theo}} = 309.14$. $\heartsuit = [\text{CB}[8]+2\text{Na}]^{2+}$, $m/z_{\text{exp}} = 687.40$, $m/z_{\text{theo}} = 687.50$. $\blacklozenge = [\text{DPV}+\text{CB}[8]]^{2+}$, $m/z_{\text{exp}} = 819.55$, $m/z_{\text{theo}} = 819.57$. $\spadesuit = [\text{DPV}+\text{Na}+\text{CB}[8]]^{3+}$, $m/z_{\text{exp}} = 554.10$, $m/z_{\text{theo}} = 554.16$. $\bullet = [\text{DPV}+\text{Na}+2\text{CB}[8]]^{3+}$, $m/z_{\text{exp}} = 997.40$, $m/z_{\text{theo}} = 997.05$. The ESI-MS spectra were limited to the areas of interest. No peaks were detected in the excluded m/z regions.

The stoichiometry of the TV^{6+} complexes formed with $\text{CB}[7]$ and $\text{CB}[8]$ was investigated as well by electrospray mass spectrometry in the positive mode. ESI-MS mass spectra were recorded for aqueous solutions containing 50 μM of the TV^{6+} mixed with 4.5 equivalent of $\text{CB}[7]$ (Figure 16) and for 100 μM of the TV^{6+} mixed with 3 equivalent of $\text{CB}[8]$ (Figure 17).

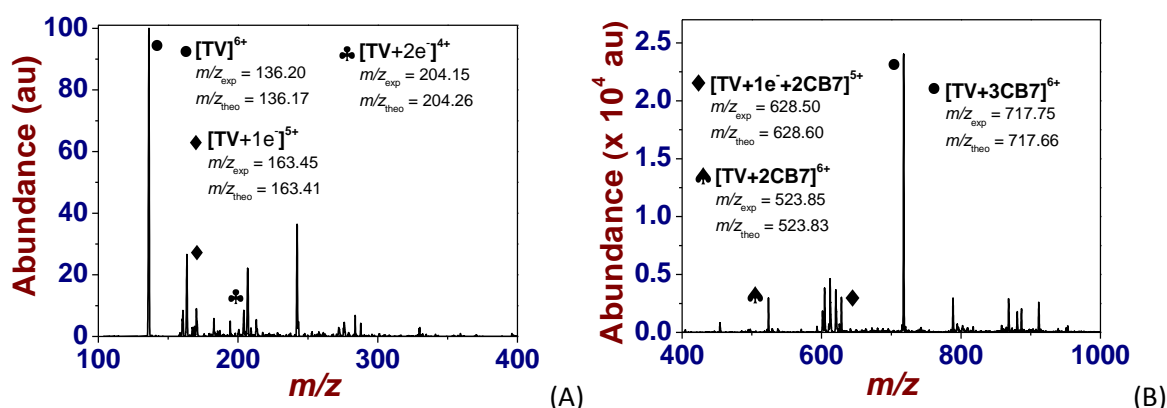


Figure 16. (A) ESI mass spectrum of free TV^{6+} . $[\text{TV}^{6+}]_0 = 5 \times 10^{-5}$ M. Solvent: H_2O ; positive mode. $V_c = 20$ V. $\bullet = [\text{TV}]^{6+}$, $m/z_{\text{exp}} = 136.20$, $m/z_{\text{theo}} = 136.17$, $\blacklozenge = [\text{TV}+1\text{e}^{-}]^{5+}$, $m/z_{\text{exp}} = 163.45$, $m/z_{\text{theo}} = 163.41$; $\clubsuit = [\text{TV}+2\text{e}^{-}]^{4+}$, $m/z_{\text{exp}} = 204.15$, $m/z_{\text{theo}} = 204.26$.

(B) ESI mass spectrum of the inclusion complexes of TV^{6+} with $\text{CB}[7]$. $[\text{TV}^{6+}]_0 = 5 \times 10^{-5}$ M; $[\text{CB}[7]] = 2 \times 10^{-4}$ M. Solvent: H_2O ; positive mode. $V_c = 180$ V. $\bullet = [\text{TV}+3\text{CB}[7]]^{6+}$, $m/z_{\text{exp}} = 717.75$, $m/z_{\text{theo}} = 717.66$. $\blacklozenge = [\text{TV}+1\text{e}^{-}+2\text{CB}[7]]^{5+}$, $m/z_{\text{exp}} = 628.50$, $m/z_{\text{theo}} = 628.60$. $\spadesuit = [\text{TV}+2\text{CB}[7]]^{6+}$, $m/z_{\text{exp}} = 523.85$, $m/z_{\text{theo}} = 523.83$. The ESI-MS spectra were limited to the areas of interest. No peaks were detected in the excluded m/z regions.

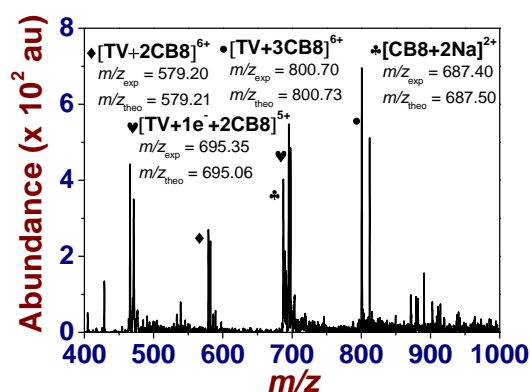


Figure 17. ESI mass spectrum of the inclusion complexes of TV^{6+} with $\text{CB}[8]$. $[\text{TV}^{6+}]_0 = 1 \times 10^{-4}$ M; $[\text{CB}[8]] = 3 \times 10^{-4}$ M. Solvent: H_2O ; positive mode. $V_c = 100$ V. $\bullet = [\text{TV}+3\text{CB}[8]]^{6+}$, $m/z_{\text{exp}} = 800.70$, $m/z_{\text{theo}} = 800.73$. $\heartsuit = [\text{TV}+1\text{e}^{-}+2\text{CB}[8]]^{5+}$, $m/z_{\text{exp}} = 695.35$, $m/z_{\text{theo}} = 695.06$. $\blacklozenge = [\text{TV}+2\text{CB}[8]]^{6+}$, $m/z_{\text{exp}} = 579.20$, $m/z_{\text{theo}} = 579.21$. \spadesuit $[\text{CB}[8]+2\text{Na}]^{2+}$, $m/z_{\text{exp}} = 687.40$, $m/z_{\text{theo}} = 687.50$. The ESI-MS spectra were limited to the areas of interest. No peaks were detected in the excluded m/z regions.

3.2.5. Host-Guest Complexation Investigated by ^1H NMR Spectroscopy.

3.2.5a. Complexation of $\text{MVTP}^{2+}/\text{MPV}^{2+}$ by $\text{CB}[7]$ Probed by ^1H NMR Spectroscopy.

To evaluate the interactions between the MVTP^{2+} and MPV^{2+} guests by the $\text{CB}[7]$ host, titration experiments were carried out and monitored using ^1H NMR spectroscopy (Figure 18). For MPV^{2+} , the ^1H NMR spectra clearly revealed a large upfield shift (fast exchange on the NMR timescale) of the *b* and *c* (and at a lesser extent that of *i*) protons of the phenyl unit together with an upfield shift of some of the protons associated to the viologen unit

($\alpha/\beta/\beta'$). The protons signal arising from the methyl group were found to be unaltered by **CB[7]** complexation. These NMR data evidenced the formation of a [2]pseudorotaxane **MPV**²⁺⊂**CB[7]** whose the hydrophobic cavity of **CB[7]** mainly resides on the phenyl group instead of the bipyridinium group (as seen for **MV**²⁺, see previous chapter) and also interacts with a part of the viologen core. These data are in agreement with those previously obtained for the homologous system **DPV**²⁺.⁷ By contrast with **MPV**²⁺, the shifts of the signals of **DPV**²⁺ were at a maximum after the addition of two equivalents of **CB[7]**, which lends support for the proposed 1:2 stoichiometric complexation in solution at room temperature already observed by absorption spectrophotometry (*i.e.* **DPV**²⁺⊂(**CB[7]**)₂).

MVTP²⁺ stands in an interesting contrast with **MPV**²⁺. The protons of the central conjugated platform (*d* and *e*) are slightly shifted in the downfield region, while those of the unsubstituted phenyl rings remain unaffected on complexation by **CB[7]**. The α and α' are shielded upon **CB[7]** but at a much lesser extent than the upfield shifts experienced by the β and β' protons. Importantly, the presence of two resonances indicates a slow exchange on the NMR timescale. Such a behaviour suggests the formation of an inclusion complex where the **CB[7]** macrocycle stands at the peripheral of the ligand and encapsulates the bipyridinium group.

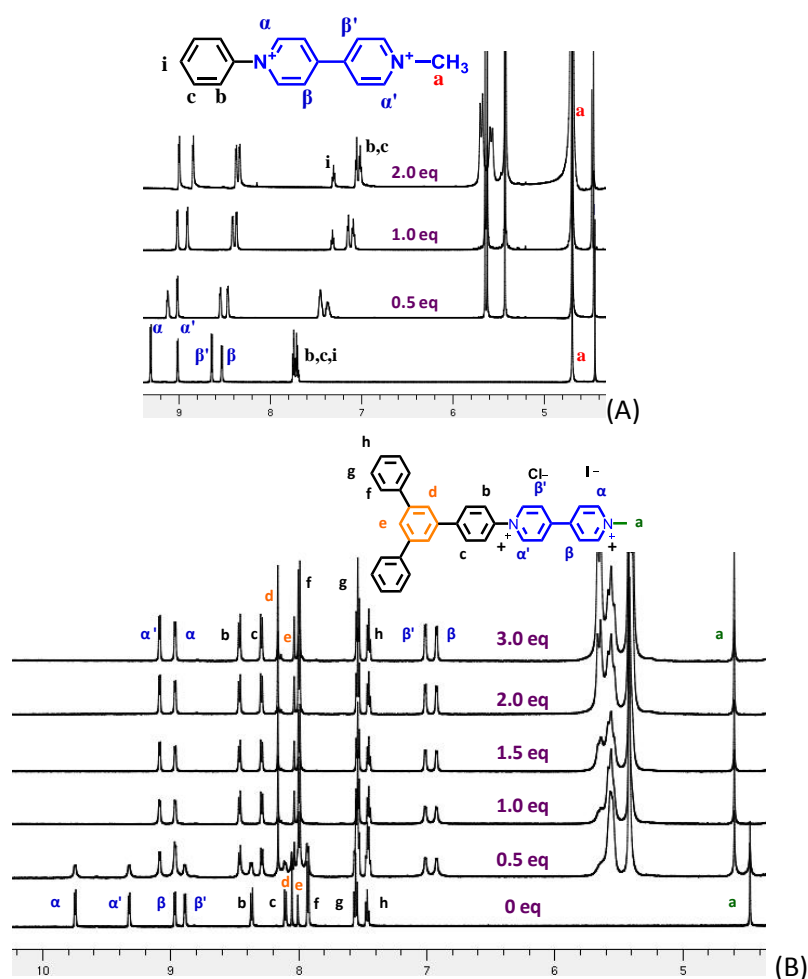


Figure 18. Full ¹H NMR spectra (600 MHz, D₂O, 298 K) of **MVTP**²⁺ (A) and **MPV**²⁺ (B) in the presence of increasing amounts of **CB[7]**.

3.2.5b. TV^{6+} Recognition by CB[7] Probed by ^1H NMR Spectroscopy.

To study the interaction between, The ^1H NMR titration experiment of TV^{6+} by **CB[7]** is given in Figure 19. In the absence of **CB[7]**, the ^1H NMR spectrum of TV^{6+} matches with that of a symmetrical species. Upon addition of **CB[7]**, the shape of the spectrum was gradually altered until 3 equivalents of **CB[7]** were added. Addition of excess of **CB[7]** did not induce further variations. Importantly, the overall set of protons corresponded to a new symmetrical species, whose number and multiplicity of the protons are the same than the parent TV^{6+} . These results provided strong evidences of the formation of a 3:1 guest/host complex of TV^{6+} with **CB[7]** as already suggested by absorption spectrophotometry. Upon **CB[7]** complexation, the protons of the central conjugated platform *b*, *c* and *d* and the α and α' protons of the bipyridinium core were slightly shielded. However, the shifts were found to be significantly greater for the β and β' protons ($\Delta\delta > 1$ ppm). Similarly to the **MVTP** $^{2+}$ model, these observations supports the formation of an inclusion complex ($\text{TV}^{6+} \subset (\text{CB}[7])_3$) where the macrocycles stand at the peripheral of the tritopic ligand, encircling the bipyridinium groups.

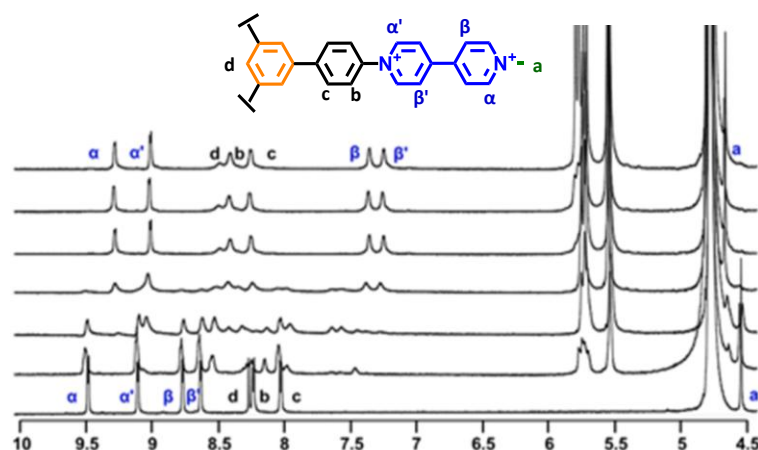


Figure 19. Full ^1H NMR spectra (600 MHz, D_2O , 298 K) of TV^{6+} in the presence of increasing amounts of **CB[7]**.

3.2.6. Pimerization Processes in Aqueous Solution

3.2.6a. MPV^{++} Pimerization in Aqueous Solution

UV-Vis.-NIR absorption spectra (220 nm - 1400 nm) of increasing concentration of MPV^{++} (prepared by addition of sodium dithionite under a controlled atmosphere of argon) in 1 mL ($10^{-4} \text{ M} \geq [\text{MPV}^{++}] \geq 10^{-5} \text{ M}$) or 0.5 mL ($2 \times 10^{-3} \text{ M} \geq [\text{MPV}^{++}] \geq 2.5 \times 10^{-4} \text{ M}$) 0.1 M phosphate solutions (pH 7.0) were recorded in 10 mm or 2 mm optical cells, respectively, at 25 °C (Dual Cell Pelletier Accessory) with a Cary 5000 spectrophotometer. The absorbances at any wavelength have been correlated to the absorptivities of both the monomer and the dimer, which are related by:

$$A_t = \frac{1}{2} \left[\varepsilon_d C_t + \frac{(2\varepsilon_m - \varepsilon_d) \sqrt{(1 + 8K_{\text{Dim}} C_t) - 1}}{4K_{\text{Dim}}} \right]_{8,9}$$

$$\text{With } K_{\text{Dim}} = [(\text{MPV}^{\bullet+})_2] / [\text{MPV}^{\bullet+}]^2$$

Figure 20 evidences the formation of a broad and intense absorption in the NIR region ($\lambda > 800 \text{ nm}$) upon increasing the concentration of the $\text{MPV}^{\bullet+}$ monoradical cation in solution, which constitutes a valuable spectrophotometric probe of the dimerization process). The data have been processed with the Origin program and allowed us to evaluate the dimerization constant ($\log K_{\text{Dim}}$ value of 3.5(1)) and to calculate the electronic spectra of $\text{MPV}^{\bullet+}$ under its monomeric and dimeric states (Figure 20B).

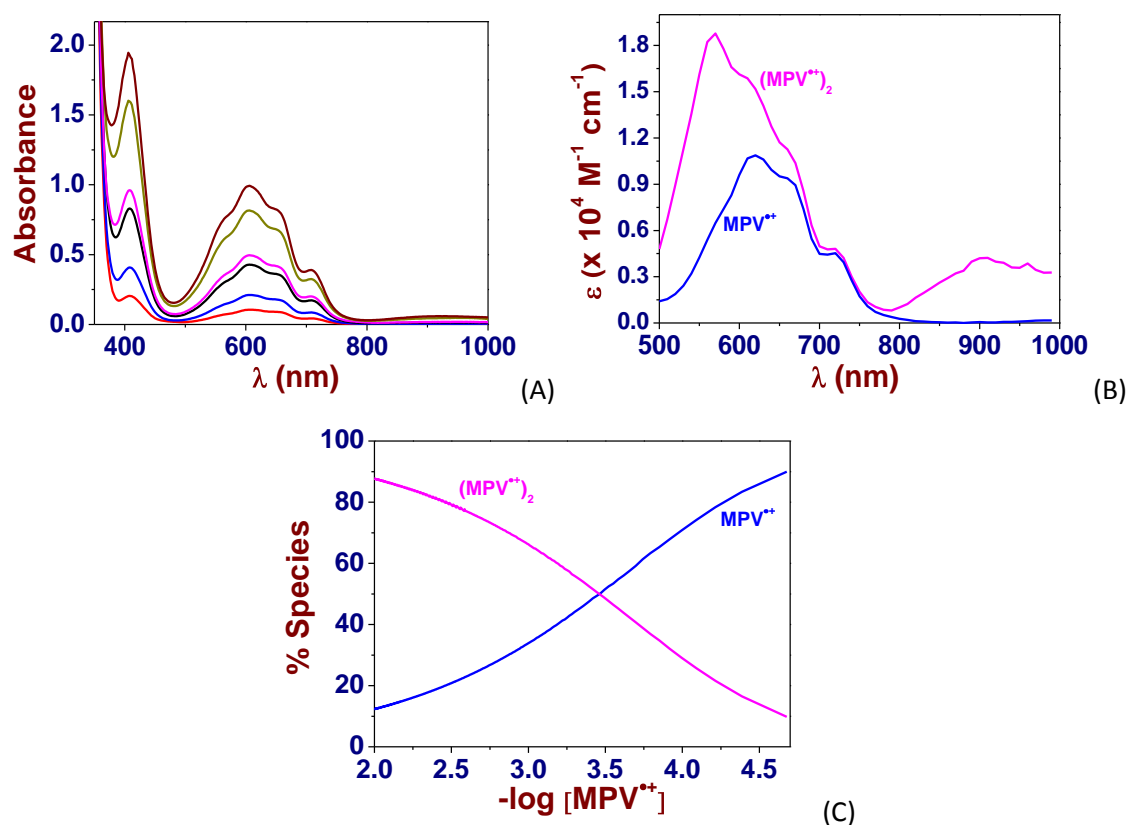


Figure 20. (A) UV-Vis.-NIR absorption titration of $\text{MPV}^{\bullet+}$ in aqueous solution, (B) UV-Vis.-NIR electronic spectra of $\text{MPV}^{\bullet+}$ under its monomeric or dimeric form and (C) distribution diagram of the monomer *versus* dimer as a function of $\text{MPV}^{\bullet+}$ concentration. Solvent: Water pH 7.0 (0.1 M $\text{Na}_2\text{HPO}_4/\text{NaH}_2\text{PO}_4$). For $10^{-5} \text{ M} \leq [\text{MPV}^{\bullet+}]_0 < 10^{-4} \text{ M}$; $l = 1 \text{ cm}$; for $2.5 \times 10^{-4} \text{ M} \leq [\text{MPV}^{\bullet+}]_0 < 2 \times 10^{-3} \text{ M}$; $l = 2 \text{ mm}$; $T = 25.0(1) \text{ }^\circ\text{C}$. In each of the solutions considered, the $\text{MPV}^{\bullet+}$ species was generated from MPV^{2+} using freshly prepared sodium dithionite solution at *ca.* 10^{-2} M under O_2 free conditions. The absorption spectra are not corrected from dilution effects.

3.2.6b. Spectrophotometric Titration of $\text{MVTP}^{\bullet+}$

Similarly to $\text{MPV}^{\bullet+}$, UV-Vis.-NIR absorption spectra (220 nm - 1400 nm) of increasing concentration of $\text{MVTP}^{\bullet+}$ ($10^{-6} \text{ M} \leq [\text{MVTP}^{\bullet+}]_0 < 4 \times 10^{-5} \text{ M}$) were recorded in aqueous solutions at pH 7.0. Figure 21 clearly shows the presence of a broad and intense absorption in the NIR region ($\lambda_{\text{max}} \sim 1025 \text{ nm}$) which is indicative of the dimeric species. Interestingly, the absorbances at 1025 nm linearly vary with the concentrations of $\text{MVTP}^{\bullet+}$ and obey the Beer-Lambert law which strongly suggests that the $(\text{MVTP}^{\bullet+})_2$ is the predominant species in solution even under diluted conditions. As a consequence, the dimerization constant K_{Dim} can be estimated to be greater than 10^7 M^{-1} . This unexpected result demonstrates that the substitution of the phenyl group by a triaryl-phenyl moiety favours by far the pimerization process of the monoradical monocationic viologen unit.

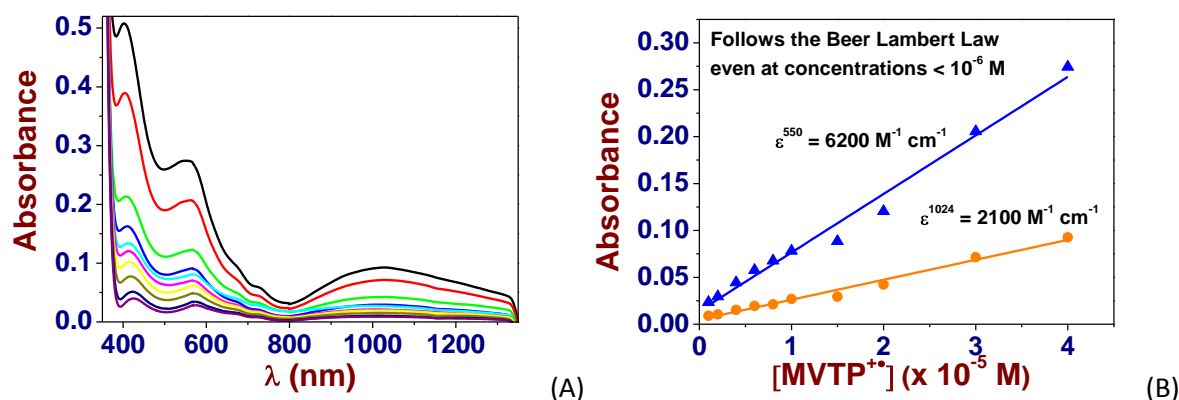


Figure 21. (A) UV-Vis.-NIR absorption titration of $\text{MVTP}^{\bullet+}$ in aqueous solution and (B) absorbances at typical wavelengths as a function of $\text{MVTP}^{\bullet+}$ concentrations. Solvent: Water pH 7.0 (0.1 M $\text{Na}_2\text{HPO}_4/\text{NaH}_2\text{PO}_4$); $10^{-6} \text{ M} \leq [\text{MVTP}^{\bullet+}]_0 < 4 \times 10^{-5} \text{ M}$; $l = 1 \text{ cm}$; $T = 25.0(1) \text{ }^\circ\text{C}$. In each of the solutions considered, the $\text{MVTP}^{\bullet+}$ species was generated from MVTP^{2+} using freshly prepared sodium dithionite solution at *ca.* 10^{-2} M under O_2 free conditions. The absorption spectra are not corrected from dilution effects.

3.2.6c. Spectrophotometric Titration of $\text{TV}^{3(\bullet+)}$

The same procedure described above for $\text{MPV}^{\bullet+}$ and $\text{MVTP}^{\bullet+}$ was applied to $\text{TV}^{3(\bullet+)}$ (Figure 22). Similarly to $\text{MVTP}^{\bullet+}$, $\text{TV}^{3(\bullet+)}$ self-assembles to form in solution a very stable dimeric species $(\text{TV}^{3(\bullet+)})_2$ that is characterized by a broad and intense absorption in the NIR region ($\lambda_{\text{max}} \sim 1215 \text{ nm}$, Figure 22) and a high $\log K_{\text{Dim}}$ value (> 7).

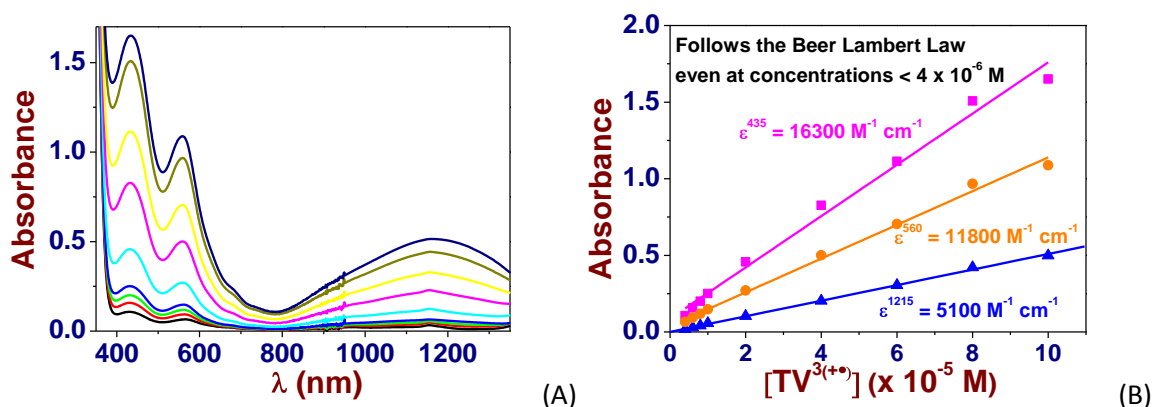


Figure 22. (A) UV-Vis.-NIR absorption titration of $\text{TV}^{3(\bullet+)}$ in aqueous solution and (B) absorbances at typical wavelengths as a function of $\text{TV}^{3(\bullet+)}$ concentrations. Solvent: Water pH 7.0 (0.1 M $\text{Na}_2\text{HPO}_4/\text{NaH}_2\text{PO}_4$); $10^{-6} \text{ M} \leq [\text{TV}^{3(\bullet+)}]_0 < 4 \times 10^{-5} \text{ M}$; $l = 1 \text{ cm}$; $T = 25.0(1) \text{ }^\circ\text{C}$. In each of the solutions considered, the $\text{TV}^{3(\bullet+)}$ species was generated from TV^{6+} using freshly prepared sodium dithionite solution at $ca. 10^{-2} \text{ M}$ under O_2 free conditions. The absorption spectra are not corrected from dilution effects.

3.2.7. Recognition of the Radical Cations by CB[7]

3.2.7a. Recognition of $\text{MPV}^{\bullet+}$ by CB[7]

Figure 23A shows the UV-Vis.-NIR spectra of MPV^{2+} (black line) and of its inclusion complex $\text{MPV}^{2+} \subset \text{CB}[7]$ (red line).

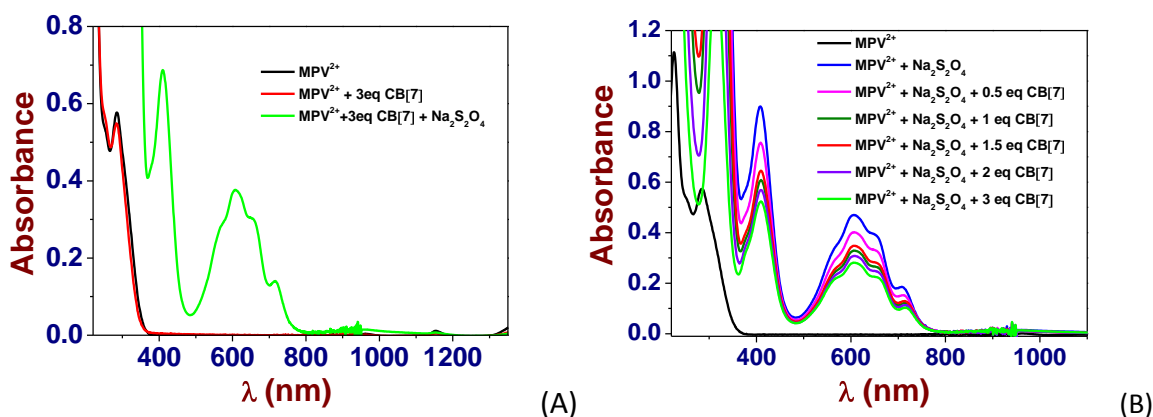


Figure 23. (A) UV-Vis.-NIR spectra of MPV^{2+} ($[\text{MPV}^{2+}]_0 = 5 \times 10^{-5} \text{ M}$, black line) and of its $\text{MPV}^{2+} \subset \text{CB}[7]$ complex ($[\text{CB}[7]]_0/[\text{MPV}^{2+}]_0 = 3$, red line). Addition of a freshly prepared O_2 -free sodium dithionite (green line) induces formation of absorptions in the visible region that are characteristics of the radical species $\text{MPV}^{\bullet+}$. (B) UV-Vis.-NIR spectra of MPV^{2+} ($[\text{MPV}^{2+}]_0 = 5 \times 10^{-5} \text{ M}$, black line) and of its radical species $\text{MPV}^{\bullet+}$ (blue line, addition of freshly prepared and O_2 -free sodium dithionite). Upon addition of $\text{CB}[7]$ ($[\text{CB}[7]]_0/[\text{MPV}^{\bullet+}]_0 = 0$, blue line and $[\text{CB}[7]]_0/[\text{MPV}^{\bullet+}]_0 = 3.09$, green line), the absorptions experienced a hypochromic shift that is indicative of host/guest complexation. Solvent: water buffered at pH 7.0 with 0.1 M $\text{Na}_2\text{H}_2\text{PO}_4/\text{NaH}_2\text{PO}_4$; $l = 1 \text{ cm}$; $T = 25.0(1) \text{ }^\circ\text{C}$. In each of the solutions considered, the $\text{MPV}^{\bullet+}$ species was generated from MPV^{2+} using freshly prepared sodium dithionite solution at $ca. 10^{-2}$ under O_2 free conditions. The absorption spectra are not corrected from dilution effects.

Addition of a freshly prepared O₂-free sodium dithionite solution reduces the **MPV**²⁺ into its monoradical cationic species **MPV**^{•+} which is still located within the **CB[7]** cavity (*i.e.* the absorbance measured for the **MPV**^{•+}⊂**CB[7]** is much lower than the one recorded for free **MPV**^{•+} under the same experimental conditions, Figure 23B, blue line). Alternatively, Figure 23B shows the UV-Vis.-NIR spectra of **MPV**²⁺ (black line) and of its monoradical cationic species **MPV**^{•+} (blue line). No dimer was evidenced under these experimental conditions. Addition of increasing amount of **CB[7]** clearly induces a hypochromic shift of the absorption bands of **MPV**^{•+} hence suggesting that the monoradical monocation viologen unit is encircled by the **CB[7]** host.

To determine the association constant of the **MPV**^{•+}⊂**CB[7]** inclusion complex, 1 mL of **MPV**²⁺ (5×10^{-5} M) were reacted with an excess of sodium dithionite (sodium hydrosulfite or sodium dithionite, Na₂S₂O₄, 85%, Sigma Aldrich) in a 10 mm Hellma quartz optical cell in water at pH 7 (0.1 M phosphate buffer). The solution was constantly flushed with O₂- free argon to avoid re-oxidation of the **MPV**^{•+} radicals. The [CB[7]]₀/[MPV^{•+}]₀ ratio was varied from 0 to 3.09. Special care was taken to ensure that complete equilibration was attained. After each addition, a UV-Vis.-NIR spectrum was recorded from 220 to 1500 nm on a Cary 5000 (Agilent) spectrophotometer maintained at 25.0(2) °C by the flow of a Dual Cell Pelletier Accessory (Cary Varian). Figure 24A depicts the absorption spectrophotometric titration whereas Figure 24B shows the electronic spectra of **MPV**^{•+} and its corresponding inclusion complex **MPV**^{•+}⊂**CB[7]**. The [2]pseudorotaxane **MPV**^{•+}⊂**CB[7]** is characterized by a stability constant of $\log K_{\text{MPV}^{\bullet+} \subset \text{CB}[7]} = 4.60(7)$ in agreement with that measured for **BMV**^{•+}⊂**CB[7]** ($\log K_{\text{BMV}^{\bullet+} \subset \text{CB}[7]} = 4.9(1)$) or **MV**^{•+}⊂**CB[7]** ($\log K_{\text{MV}^{\bullet+} \subset \text{CB}[7]} \sim 4.79$, see previous chapter) thus substantiating the proposed binding mode (*i.e.* the monoradical monocation of the bipyridinium moiety is encapsulated by the **CB[7]**).

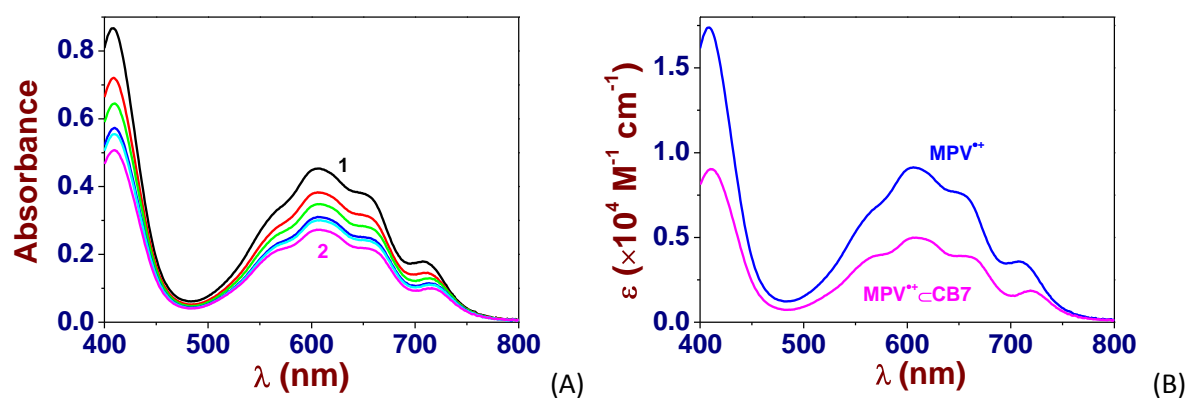


Figure 24. (A) UV-Vis. Absorption batch titration of **MPV**^{•+} by **CB[7]** in water. (B) Electronic spectra of **MPV**^{•+} and of its inclusion complex with **CB[7]** (**MPV**^{•+}⊂**CB[7]**). Solvent: water pH 7.0 (0.1 M Na₂HPO₄/NaH₂PO₄). [MPV^{•+}]₀ = 5×10^{-5} M; (1) [CB[7]]₀/[MPV^{•+}]₀ = 0; (2) [CB[7]]₀/[MPV^{•+}]₀ = 3.09; *l* = 1 cm; *T* = 25.0(1) °C. In each of the solutions considered, the **MPV**^{•+} species was generated from **MPV**²⁺ using freshly prepared sodium dithionite solution at *ca.* 10⁻² M under O₂ free conditions. The absorption spectra are not corrected from dilution effects.

3.2.7b. Recognition of $\text{DPV}^{\bullet+}$ by $\text{CB}[7]$

In the absence of $\text{CB}[7]$ in water, the monoradical cationic $\text{DPV}^{\bullet+}$, that was generated with an excess of freshly prepared O_2 -free $\text{Na}_2\text{S}_2\text{O}_4(\text{aq})$, has a strong tendency to rapidly dimerize/oligomerize leading to fast formation of insoluble particles (Figure 25). Exposure of the latter solution to air reinstates the DPV^{2+} (*i.e.* DPV^{2+} is unable to dimerize/oligomerize) and leads to colourless and limp solution. The same feature was also observed for TV^{6+} but precipitation occurs only after a few minutes allowing us to study its behaviour in solution.

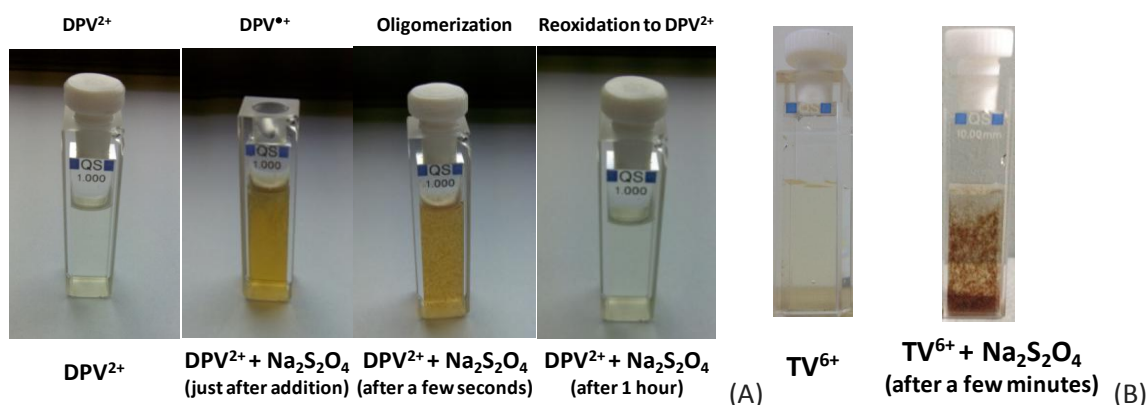


Figure 25. Solutions of (A) DPV^{2+} and (B) TV^{6+} before and after addition of $\text{Na}_2\text{S}_2\text{O}_4$ showing the formation of an insoluble aggregate that re-dissolves upon re-oxidation under open air conditions.

To overcome these limitations, time resolved absorption spectrophotometry was employed (stopped flow apparatus equipped with a diode array spectrophotometer) and allowed measuring the absorption spectrum of $\text{DPV}^{\bullet+}$ in the milliseconds time range (Figure 26) prior its dimerization and further fast oligomerization.

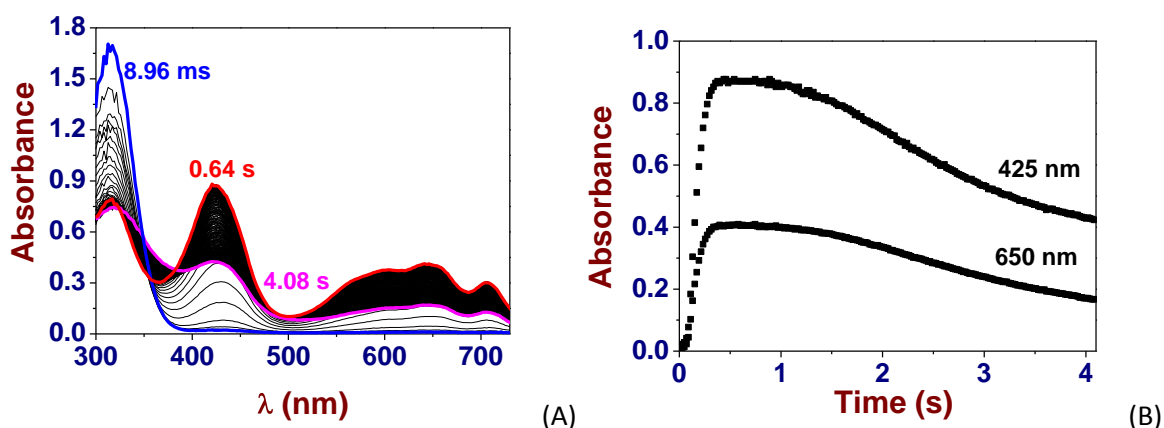


Figure 26. (A) Time-resolved absorption spectra of DPV^{2+} in the presence of sodium dithionite ($\text{Na}_2\text{S}_2\text{O}_4$) showing the very fast formation (< 1 second) of the 1 electron reduced form $\text{DPV}^{\bullet+}$ and the fast oligomerization and (B) absorption variation at 425 nm and 650 nm (absorptions that are characteristic of the $\text{DPV}^{\bullet+}$ species). Solvent: water buffered at pH 7.0 with 0.1 M $\text{Na}_2\text{HPO}_4/\text{NaH}_2\text{PO}_4$; $l = 1$ cm; $T = 25.0(1)^\circ\text{C}$. $[\text{DPV}^{2+}] = 5.23 \times 10^{-5}$ M; $[\text{Na}_2\text{S}_2\text{O}_4] = 9.88 \times 10^{-4}$ M.

Using such an approach, an absorption spectrophotometric titration of the chemically generated $\text{DPV}^{\bullet+}$ by $\text{CB}[7]$ was performed (Figure 27, *i.e.* only the first absorption spectrum of repeated spectral kinetic experiments was recorded for each of the $[\text{CB}[7]]/[\text{DPV}^{\bullet+}]$ ratio considered). By contrast with DPV^{2+} and $\text{CB}[7]$, the statistical processing of the absorption spectral data set allowed us to evidence the formation of only the [2]pseudorotaxane $\text{DPV}^{\bullet+}\subset\text{CB}[7]$ that is characterized by a stability constant of $\log K_{\text{DPV}^{\bullet+}\subset\text{CB}[7]} = 4.9(1)$ in agreement with that measured for $\text{MV}^{\bullet+}\subset\text{CB}[7]$ (MV^{2+} = methyl viologen, $\log K_{\text{MV}^{\bullet+}\subset\text{CB}[7]} \sim 4.79$, see previous chapter) or $\text{BMV}^{\bullet+}\subset\text{CB}[7]$ (BMV^{2+} = benzyl methyl viologen, $\log K_{\text{BMV}^{\bullet+}\subset\text{CB}[7]} = 4.9(1)$, see previous chapter) thus substantiating the proposed binding mode (*i.e.* only the radical cation of the BIPY^{2+} moiety is encapsulated by $\text{CB}[7]$). It is noteworthy that the stability of the $\text{DPV}^{\bullet+}\subset\text{CB}[7]$ species is also comparable to that measured for the homologous [2]pseudorotaxane $\text{MPV}^{\bullet+}\subset\text{CB}[7]$ ($\log K_{\text{MPV}^{\bullet+}\subset\text{CB}[7]} = 4.60(7)$) once again confirming similar binding mode for each of the considered radical host-guest complexes.

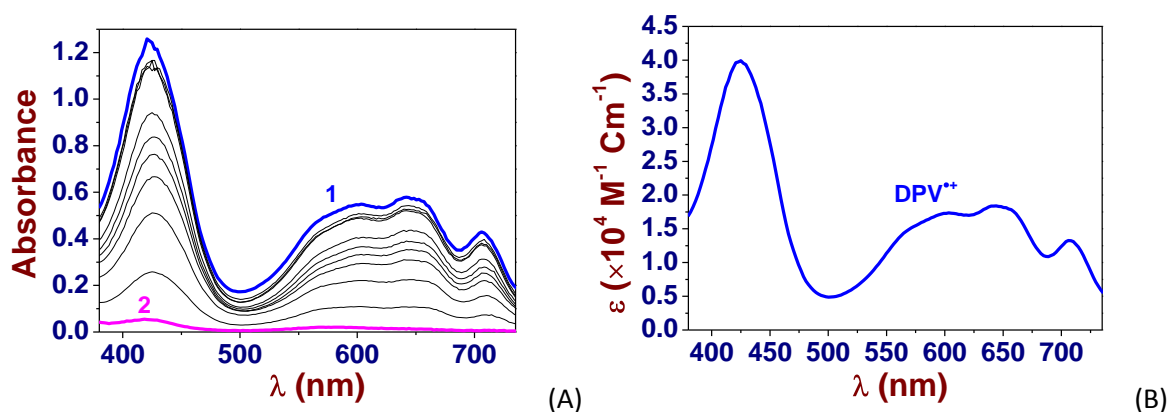


Figure 27. (A) UV-Vis Absorption titration of $\text{DPV}^{\bullet+}$ by $\text{CB}[7]$ in water. (B) Electronic spectra of $\text{DPV}^{\bullet+}$.

The inclusion of $\text{DPV}^{\bullet+}$ within the $\text{CB}[7]$ cavity led to an almost complete fading of the $\text{DPV}^{\bullet+}$ absorption in the Vis.-NIR region. The electronic absorption spectrum of $\text{DPV}^{\bullet+}\subset\text{CB}[7]$ could not be calculated with a good accuracy and was considered as a non colored species during the statistical process. Solvent: water buffered at pH 7.0 with 0.1 M $\text{Na}_2\text{HPO}_4/\text{NaH}_2\text{PO}_4$. $[\text{DPV}^{\bullet+}]_0 = 5.23 \times 10^{-5}$ M; (1) $[\text{CB}[7]]_0/[\text{DPV}^{\bullet+}]_0 = 0$; (2) $[\text{CB}[7]]_0/[\text{DPV}^{\bullet+}]_0 = 2.95$; $l = 1$ cm; $T = 25.0(1)$ °C. The absorption spectra are corrected from dilution effects.

3.2.7c. Recognition of $\text{MVTP}^{\bullet+}$ by $\text{CB}[7]$

Figure 28A shows the UV-Vis.-NIR spectra of MVTP^{2+} (black line) and of its [2]pseudorotaxane $\text{MVTP}^{2+}\subset\text{CB}[7]$ (red line). Reduction of MVTP^{2+} into its corresponding one electron reduced species $\text{MVTP}^{\bullet+}$ (green line) demonstrate by contrast with $\text{MPV}^{\bullet+}$ that the viologen radical $\text{MVTP}^{\bullet+}$ has been dissociated from the host/guest complex as evidenced by the broad and intense absorption in the NIR region. As shown above, this absorption is a clear signature of the dimer $(\text{MVTP}^{\bullet+})_2$ occurrence in solution. The high stability of the dimer species prevents for thermodynamic reasons the inclusion process. This feature was further emphasized with the experiments described in Figure 28B which first shows the UV-Vis.-NIR spectra of MPV^{2+} (black line) and of its monoradical cationic species $\text{MPV}^{\bullet+}$ (green line). Addition of $\text{CB}[7]$ up to 4 equivalents has no effect neither on the shape nor on the intensity

of the $\text{MPV}^{\bullet+}$ radical absorption thus demonstrating that when the viologen compound is reduced, it spontaneously self-assembles in solution and prevents recognition by $\text{CB}[7]$.

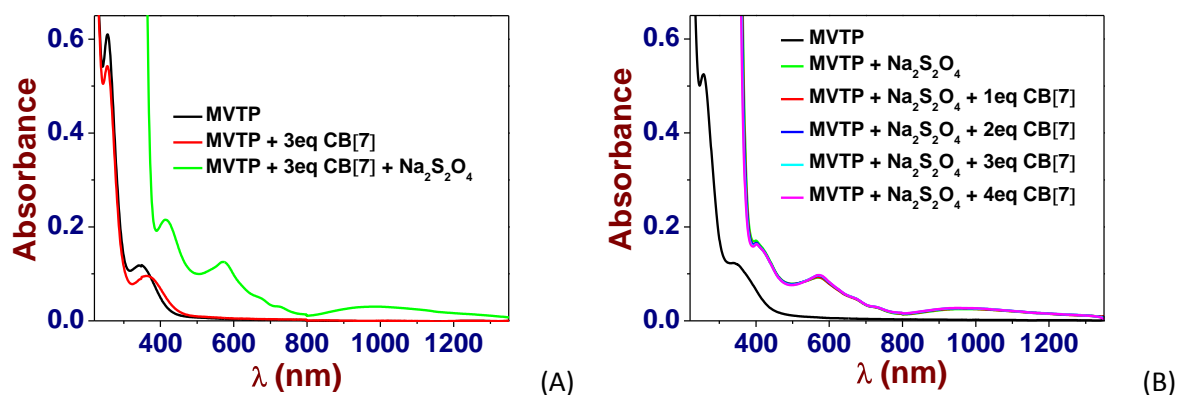


Figure 28. (A) UV-Vis.-NIR spectra of MVTP^{2+} ($[\text{MVTP}^{2+}]_0 = 2.0 \times 10^{-5}$ M, black line) and of its $\text{MPV}^{2+} \subset \text{CB}[7]$ complex ($[\text{MVTP}^{2+}]_0/[\text{CB}[7]]_0 = 3$, red line). Addition of a freshly prepared O₂-free sodium dithionite (green line) induces formation of absorptions in the visible and NIR regions that are characteristics of the radical dimeric species $(\text{MVTP}^{\bullet+})_2$. (B) UV-Vis.-NIR spectra of MVTP^{2+} ($[\text{MVTP}^{2+}]_0 = 2.0 \times 10^{-5}$ M, black line) and of its radical species $\text{MVTP}^{\bullet+}$ under its dimeric state (green, addition of freshly prepared and O₂-free sodium dithionite). Upon addition of $\text{CB}[7]$ ($[\text{CB}[7]]_0/[\text{MVTP}^{\bullet+}]_0 = 0$, green line and $[\text{CB}[7]]_0/[\text{MVTP}^{\bullet+}]_0 = 4$, magenta), no alteration of the absorption spectrum of $(\text{MVTP}^{\bullet+})_2$ can be observed thus confirming the incapacity of $\text{CB}[7]$ to revert the dimerisation reaction. Solvent: water buffered at pH 7.0 with 0.1 M Na₂H₂PO₄/NaH₂PO₄; $l = 1$ cm; $T = 25.0(1)^\circ\text{C}$. In each of the solutions considered, the $\text{MVTP}^{\bullet+}$ species was generated from MVTP^{2+} using freshly prepared sodium dithionite solution at *ca.* 10^{-2} under O₂ free conditions. The absorption spectra are not corrected from dilution effects.

3.2.7d. Recognition of $\text{TV}^{3(\bullet+)}$ by $\text{CB}[7]$

In agreement with the high dimerization constant of the $\text{TV}^{3(\bullet+)}$ and as shown above for $\text{MVTP}^{\bullet+}$, no influence of $\text{CB}[7]$ has been observed. Figure 29A shows the UV-Vis.-NIR spectra of TV^{6+} (black line) and of its [4]pseudorotaxane $\text{TV}^{6+} \subset (\text{CB}[7])_3$ (red line). Reduction of TV^{6+} into its corresponding three electron reduced species (one electron per viologen unit) $\text{TV}^{3(\bullet+)}$ (green line) evidenced the presence of the broad NIR absorption that is a signature of the $(\text{TV}^{3(\bullet+)})_2$ dimer. Figure 29B depicts the UV-Vis.-NIR spectra of TV^{6+} (black line) and of its triradical tricationic species $\text{TV}^{3(\bullet+)}$ under its dimeric state (green line). Addition of $\text{CB}[7]$ (up to 4 equivalents) has no effect on the absorption of the $\text{TV}^{3(\bullet+)}$ radical demonstrating that the $(\text{TV}^{3(\bullet+)})_2$ dimer is thermodynamically favoured with respect to the inclusion complexes with $\text{CB}[7]$.

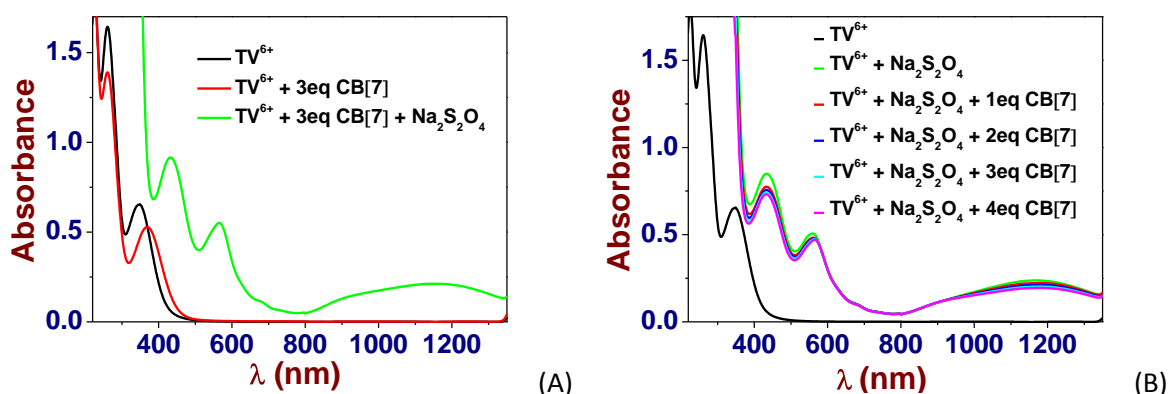


Figure 29. (A) UV-Vis.-NIR spectra of TV^{6+} ($[\text{TV}^{6+}]_0 = 5.0 \times 10^{-5}$ M, black line) and of its $\text{TV}^{6+} \subset (\text{CB}[7])_3$ complex ($[\text{CB}[7]]_0/[\text{TV}^{6+}]_0 = 3$, red line). Addition of a freshly prepared O_2 -free sodium dithionite (green line) induces formation of absorptions in the visible and NIR regions that are characteristics of the radical dimeric species $(\text{TV}^{3(\bullet+)})_2$. (B) UV-Vis.-NIR spectra of TV^{6+} ($[\text{TV}^{6+}]_0 = 5.0 \times 10^{-5}$ M, black line) and of its radical species $\text{TV}^{3(\bullet+)}$ under its dimeric state (green line, addition of freshly prepared and O_2 -free sodium dithionite). Upon addition of $\text{CB}[7]$ ($[\text{CB}[7]]_0/[\text{TV}^{3(\bullet+)}]_0 = 0$, green line and $[\text{CB}[7]]_0/[\text{TV}^{3(\bullet+)}]_0 = 4$, magenta line), no alteration of the absorption spectrum of $(\text{TV}^{3(\bullet+)})_2$ is observed thus confirming the incapacity of $\text{CB}[7]$ to revert the dimerisation reaction. Solvent: water buffered at pH 7.0 with 0.1 M $\text{Na}_2\text{H}_2\text{PO}_4/\text{NaH}_2\text{PO}_4$; $l = 1$ cm; $T = 25.0(1)^\circ$ C. In each of the solutions considered, the $\text{TV}^{3(\bullet+)}$ species was generated from TV^{6+} using freshly prepared sodium dithionite solution at *ca.* 10^{-2} under O_2 free conditions. The absorption spectra are not corrected from dilution effects.

3.2.8. Electrochemistry

Cyclic Voltammetry (CV) and Square Wave (SW) voltammetry experiments were carried out at room temperature in argon-purged aqueous solutions and DMSO solutions with a Gamry Multipurpose instrument (Reference 600) interfaced to a PC. The electrochemical experiments were performed using a glassy carbon working electrode (0.071 cm^2 , BASi). The electrode surface was polished routinely with $0.05 \mu\text{m}$ alumina-water slurry on a felt surface immediately before use. The counter electrode was a Pt coil and the reference electrode was an Ag/AgCl electrode, unless otherwise noted. The concentration of the supporting electrolyte, tetrabutylammonium chloride (TBACl) was 0.1 M. The experimental errors on the potential values are estimated to ± 10 mV. All measurements were recorded in phosphate buffer solutions (pH 7). In order to overcome the precipitation effect that can occur on reduction of viologens, the scan rate was set to 1000 mV s^{-1} . Figure 30, represents the SWVs of the three viologens MPV^{2+} , MVTP^{2+} and TV^{6+} studied in the absence and the presence of $\text{CB}[7]$. It is noteworthy that the values of $E_{1/2}$ calculated by SWV for each redox processes are in excellent agreement with the ones determined by CV experiments.

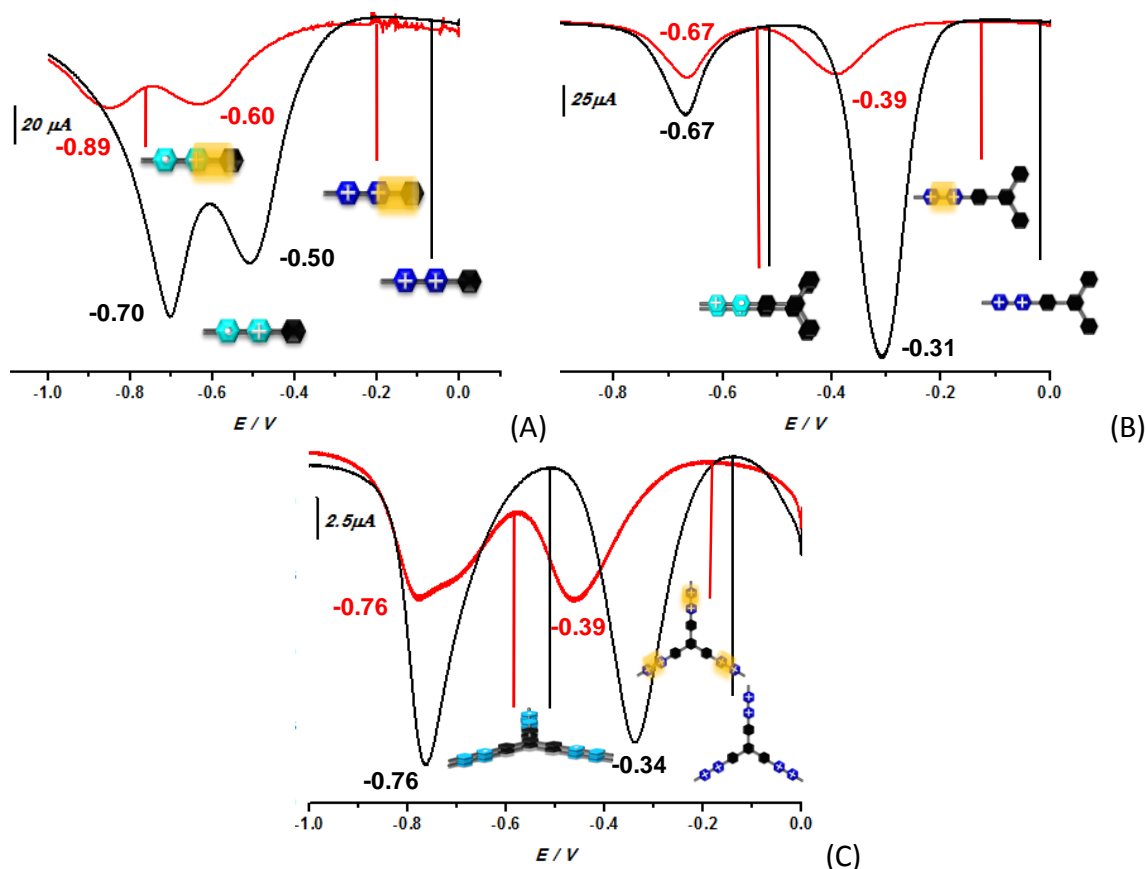


Figure 30. Square wave voltammograms (SWVs) of (A) MPV^{2+} , (B) $MVTP^{2+}$, and (C) TV^{6+} in the absence and the presence of **CB[7]** (respectively 2, 4, and 8 equivalents of **CB[7]**). All voltammograms were recorded in Argon-purged phosphate buffer solutions (pH 7) at 298 K. The scan rate was set at 1000 mVs^{-1} . E versus Ag/AgCl.

In the next section, we then evaluated the ability of the viologen derivatives considered in this work to lead to host-guest complexes with **CB[8]**, a **CB[7]** homologous macrocyclic receptor whose the cavity size is appropriate for the recognition of two different or similar guests.

3.2.9. Recognition by **CB[8]**

3.2.9a. Recognition of $MPV^{2+}/MPV^{\bullet+}$ by **CB[8]**

Figure 31A first shows the UV-Vis.-NIR spectra of MPV^{2+} (black line) and of its inclusion complex $MPV^{2+} \subset CB[8]$ (red line). It is noteworthy that only a 1:1 complex was previously evidenced by absorption spectrophotometric titrations and ESI-MS experiments. Addition of freshly prepared O_2 -free sodium dithionite reduces the MPV^{2+} into its monoradical monocationic species $MPV^{\bullet+}$ (green line) whose the absorption is markedly different from that observed in the presence of **CB[7]** (Figure 23). This UV-Vis.-NIR absorption spectrum is characterized by a broad absorption in the NIR ($\lambda_{\text{max}} = 926 \text{ nm}$) and an intense and sharper absorption in the visible region ($\lambda_{\text{max}} = 558 \text{ nm}$) that are associated to the dimeric form of $MPV^{\bullet+}$ hosted by **CB[8]** ($(MPV^{\bullet+})_2 \subset CB[8]$). This indicates that the larger size of **CB[8]** with

respect to that of **CB[7]** allows accommodating two monoradical monocations **MPV^{•+}** that are firmly stacked together within the macrocyclic host cavity. Figure 31B further confirmed this observation. The monoradical monocationic species **MPV^{•+}** (red line), chemically generated from **MPV²⁺** by addition of O₂-free sodium dithionite, is characterized by a set of structured absorptions centred at 601 nm suggestive of the monomer occurrence in solution. Incremental additions of **CB[8]** induces a hypsochromic shift of the absorptions lying in the visible region concomitant to the formation of NIR transitions. This spectral feature is clearly related to the formation of the (**MPV^{•+}**)₂⊂**CB[8]** species.

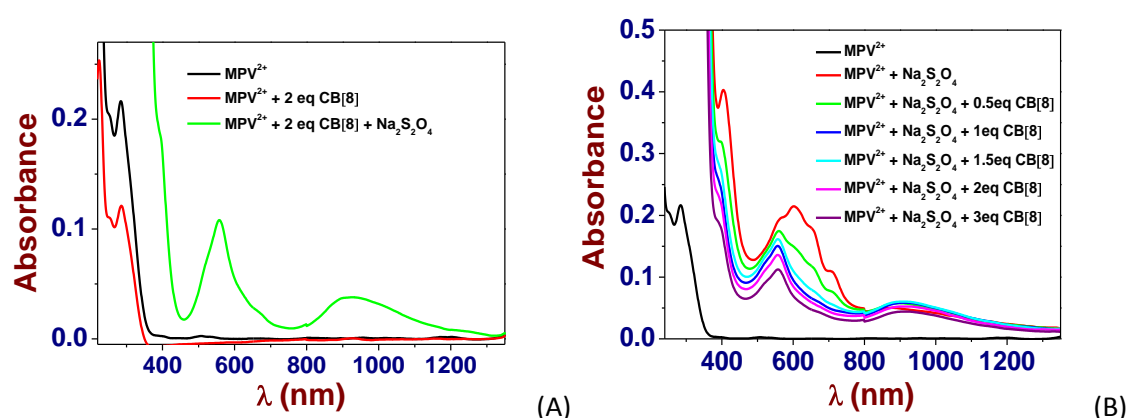


Figure 31. (A) UV-Vis.-NIR spectra of **MPV²⁺** ($[\text{MPV}^{2+}]_0 = 2.0 \times 10^{-5}$ M, black line) and of its **MPV²⁺⊂CB[8]** complex ($[\text{CB[8]}]_0/[\text{MPV}^{2+}]_0 = 2$, red line). Addition of a freshly prepared O₂-free sodium dithionite (green line) induces formation of absorptions in the visible and NIR regions that are characteristics of the radical dimeric species (**MPV^{•+}**)₂ that is favoured thanks to encapsulation by **CB[8]** (*i.e.* (**MPV^{•+}**)₂⊂**CB[8]**, see Figure 23 for comparison propose with **CB[7]**). (B) UV-Vis.-NIR spectra of **MPV²⁺** ($[\text{MPV}^{2+}]_0 = 2.0 \times 10^{-5}$ M, black line) and of its radical species **MPV^{•+}** under its predominant monomeric state (red line, addition of freshly prepared O₂-free sodium dithionite). Upon addition of **CB[8]** ($[\text{CB[8]}]_0/[\text{MPV}^{•+}]_0 = 0$, green line and $[\text{CB[8]}]_0/[\text{MPV}^{•+}]_0 = 3$, purple line), significant alteration of the absorption spectrum of **MPV^{•+}** is observed thus confirming the dimerization of **MPV^{•+}** aided by **CB[8]** inclusion. Solvent: water buffered at pH 7.0 with 0.1 M Na₂H₂PO₄/NaH₂PO₄; $l = 1$ cm; $T = 25.0(1)^\circ\text{C}$. In each of the solutions considered, the **MPV^{•+}** species was generated from **MPV²⁺** using freshly prepared sodium dithionite solution at *ca.* 10⁻² under O₂ free conditions. The absorption spectra are not corrected from dilution effects.

3.2.9b. Recognition of MVTP²⁺/MVTP^{•+} by CB[8]

Figure 32A depicts the UV-Vis.-NIR spectra of **MVTP²⁺** (black line) and its inclusion complex **MVTP²⁺⊂CB[8]** (red line). Addition of sodium dithionite reduces the **MVTP²⁺** into its predominant monoradical cationic species under its dimeric form (**MVTP^{•+}**)₂ as already observed with **CB[7]** (Figure 28). Figure 32B demonstrates that addition of **CB[8]** to a solution of (**MVTP^{•+}**)₂ (red line) has negligible effects on the Vis.-NIR absorptions of the dimer species. This can indicate either that **CB[8]** is not able to accommodate two **MVTP^{•+}** radicals or that recognition of (**MVTP^{•+}**)₂ by **CB[8]** has weak influence on its absorption properties.

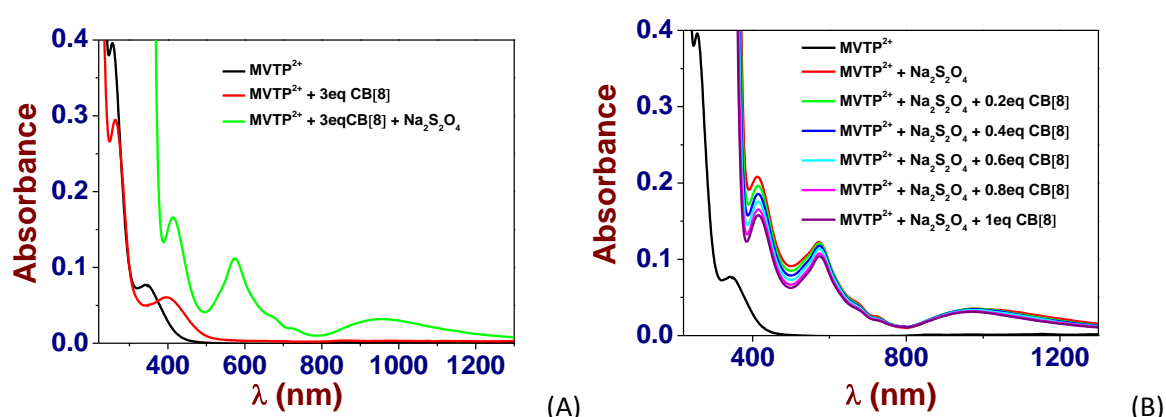


Figure 32. (A) UV-Vis.-NIR spectra of MVTP^{2+} ($[\text{MVTP}^{2+}]_0 = 2.0 \times 10^{-5}$ M, black line) and of its $\text{MVTP}^{2+} \subset \text{CB}[8]$ complex ($[\text{CB}[8]]_0 / \text{MVTP}^{2+} = 3$, red line). Addition of a freshly prepared O_2 -free sodium dithionite (green line) induces formation of absorptions in the visible and NIR regions that are characteristics of the stable radical dimeric species $(\text{MVTP}^{\bullet+})_2$, see Figure 28 for comparison propose with $\text{CB}[7]$). (B) UV-Vis.-NIR spectra of MVTP^{2+} ($[\text{MVTP}^{2+}]_0 = 2.0 \times 10^{-5}$ M, black line) and of its radical species $\text{MVTP}^{\bullet+}$ under its predominant dimeric state (red line, addition of freshly prepared O_2 -free sodium dithionite). Upon addition of $\text{CB}[8]$ ($[\text{CB}[8]]_0 / [\text{MVTP}^{\bullet+}]_0 = 0$, red line and $[\text{CB}[7]]_0 / [\text{MVTP}^{\bullet+}]_0 = 1$, purple line), weak variations of the absorption spectrum of $(\text{MVTP}^{\bullet+})_2$ are observed. Solvent: water buffered at pH 7.0 with 0.1 M $\text{Na}_2\text{H}_2\text{PO}_4 / \text{NaH}_2\text{PO}_4$; $l = 1$ cm; $T = 25.0(1)^\circ \text{C}$. In each of the solutions considered, the $\text{MVTP}^{\bullet+}$ species was generated from MVTP^{2+} using freshly prepared sodium dithionite solution at *ca.* 10^{-2} under O_2 free conditions. The absorption spectra are not corrected from dilution effects.

3.2.9c. Recognition of $\text{TV}^{6+} / \text{TV}^{3(\bullet+)}$ by $\text{CB}[8]$

Figure 33A first depicts the UV-Vis.-NIR spectra of TV^{6+} (black line) and of its inclusion complex $\text{TV}^{6+} \subset (\text{CB}[8])_3$ (red line). Addition of O_2 -free sodium dithionite reduces TV^{6+} into its triradical tricationic species $\text{TV}^{3(\bullet+)}$ (green line) that spontaneously pimerizes ($(\text{TV}^{3(\bullet+)})_2$) thanks to strong intermolecular interactions between the monoradical viologen sub-units (green line). It is noteworthy that the absorption spectrum ($\text{NIR-}\lambda_{\text{max}} \sim 936$ nm) is strikingly different from that measured in the presence of $\text{CB}[7]$ ($\text{NIR-}\lambda_{\text{max}} \sim 1168$ nm, Figure 29) suggesting that one $\text{CB}[8]$ accommodates two monoradical viologen subunits that are firmly stacked together within the macrocyclic host cavity ultimately leading to $(\text{TV}^{3(\bullet+)})_2 \subset (\text{CB}[8])_3$ species. It is noteworthy that no precipitation of oligomeric species $(\text{TV}^{3(\bullet+)})_n$ occurs in the presence of $\text{CB}[8]$ (Figure 34), while $\text{CB}[7]$ has no effect (Figure 29) on the polymerisation and aggregation processes. These observations are confirmed in the reversed experiments (Figure 33B). The NIR absorption of the $(\text{TV}^{3(\bullet+)})_2$ dimer ($\text{NIR-}\lambda_{\text{max}} \sim 1170$ nm) that is chemically produced with $\text{Na}_2\text{S}_2\text{O}_4$ experiences a hypsochromic shift to 915 nm in the presence of $\text{CB}[8]$ confirming the formation of host-guest species. Similarly, the Vis. transitions are also blue shifted in the presence of $\text{CB}[8]$.

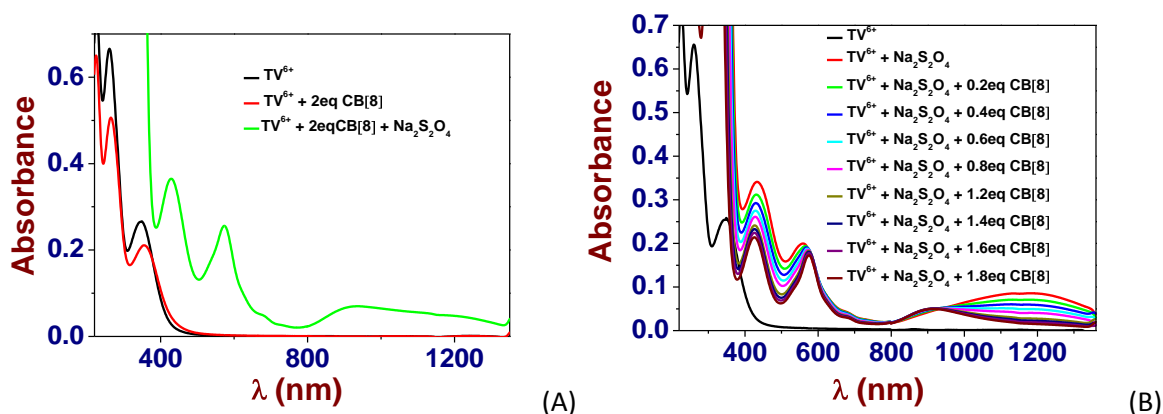


Figure 33. (A) UV-Vis.-NIR spectra of TV^{6+} ($[\text{TV}^{6+}]_0 = 2.0 \times 10^{-5}$ M, black line) and of its $\text{TV}^{6+} \subset (\text{CB}[8])_3$ complex ($[\text{CB}[8]]_0/[\text{TV}^{6+}]_0 = 2$, red line). Addition of a fresh O_2 -free sodium dithionite (green line) induces formation of absorptions in the visible and NIR regions that are characteristics of the stable radical dimeric species $(\text{TV}^{3(\bullet+)})_2$, see Figure 29 for comparison propose with **CB[7]**). The NIR absorption however displays a broader shape with respect to that measured in the absence of **CB[7]** or **CB[8]**. (B) UV-Vis.-NIR spectra of TV^{6+} ($[\text{TV}^{6+}]_0 = 2.0 \times 10^{-5}$ M, black line) and of its triradical species $\text{TV}^{3(\bullet+)}$ under its predominant dimeric state (red line, addition of freshly prepared O_2 -free sodium dithionite). Upon addition of **CB[8]** ($[\text{CB}[8]]_0/[\text{TV}^{3(\bullet+)}]_0 = 0$, red line and $[\text{CB}[8]]_0/[\text{TV}^{3(\bullet+)}]_0 = 1.8$, wine line), large spectral variations of the absorption spectrum of $(\text{TV}^{3(\bullet+)})_2$ are observed indicating host-guest complexation with **CB[8]**. In addition to this feature, no precipitation of oligomeric species $(\text{TV}^{3(\bullet+)})_n$ occurs. Solvent: water buffered at pH 7.0 with 0.1 M $\text{Na}_2\text{H}_2\text{PO}_4/\text{NaH}_2\text{PO}_4$; $l = 1$ cm; $T = 25.0(1)^\circ\text{C}$. In each of the solutions considered, the $\text{MVTP}^{\bullet+}$ species was generated from MVTP^{2+} using freshly prepared sodium dithionite solution at $ca. 10^{-2}$ under O_2 free conditions. The absorption spectra are not corrected from dilution effects.



Figure 34. Solutions of $\text{TV}^{3(\bullet+)}$ and **CB[8]** (no precipitation, green colour, left) and $\text{TV}^{3(\bullet+)}$ and **CB[7]** (precipitation, reddish colour, right).

3.2.10. Statistical Processing of the Absorption Spectrophotometric Data

The spectrophotometric data were processed using the Specfit program¹⁰⁻¹³ which adjusts the stability constants and the corresponding extinction coefficients of the species formed at equilibrium. Specfit uses factor analyses to reduce the absorbance matrix and to extract the eigenvalues prior to the multi-wavelength fit of the reduced data set according to the Marquardt algorithm.^{14,15}

3.3. Discussion

3.3.1. Characterization of the Thread/CB[7] [n]pseudorotaxanes

3.3.1a. Recognition of MPV²⁺ and DPV²⁺ by CB[7]

An absorption spectrophotometric binding titration (Figure 2) of **MPV²⁺** with **CB[7]** was carried out in aqueous solution at pH 7.0 to substantiate the 1:1 stoichiometry (**MPV²⁺⊂CB[7]**) that was evidenced by preliminary Job plot (Figure 3) and ESI-MS measurements (Figure 10). The host-guest binding constant ($\log K_{\text{MPV}^{2+}\text{⊂CB[7]}} = 6.1(3)$) at 0.1 M phosphate buffer, pH 7.0) is 6 times more stable than that measured for the **MV²⁺⊂CB[7]** ($\log K_{\text{MV}^{2+}\text{⊂CB[7]}} = 5.30(2)$) at 0.1 M phosphate buffer, pH 7.0).^{1,2} This extra-stabilization of the [2]pseudorotaxane **MPV²⁺⊂CB[7]** can be ascribed by the additional phenyl ring and therefore to enhanced hydrophobic interactions. During the titration of **MPV²⁺** by **CB[7]**, weak spectral variations (Table 1) were indeed observed. The internal mode complexation is usually characterized by significant hypochromic and bathochromic shifts of the signal that corresponds to the π - π^* transitions centred on the **BIPY²⁺** core (Table 1). It is noteworthy that the introduction of phenyl or triaryl substitution increases the delocalization of the **BIPY²⁺** core and hence leads to a bathochromic shifts of the π - π^* transitions (*e.g.* **MV²⁺** $\lambda^{\text{max}} = 257$ nm, **MPV²⁺** $\lambda^{\text{max}} = 286$ nm and **DPV²⁺** $\lambda^{\text{max}} = 312$ nm; **MVTP²⁺** $\lambda^{\text{max}} = 349$ nm).

Table 1. Thermodynamic and spectroscopic parameters of [n]pseudorotaxanes formed with viologens and **CB[n]** (n = 7, 8).

Viologen V	$\log K_{V\text{⊂CB[7]}}$	$\log K_{V\text{⊂CB[8]}}$	λ (V) (nm) ϵ^m ($10^4 \text{ M}^{-1} \text{ cm}^{-1}$)	λ (V⊂CB[7]) (nm) ϵ^d ($10^4 \text{ M}^{-1} \text{ cm}^{-1}$)
MV²⁺	5.30(2)	5.04 ¹⁹	227(2.96) / 257(2.06)	226(3.13) / 281(sh)
MPV²⁺	6.1(3)	-	227(2.20) / 286(1.19)	227(2.22) / 286 (1.14)
DPV²⁺	$\log \beta_{\text{DPV}^{2+}\text{⊂CB[7]}} =$ 8.29(9)		250(1.14) / 293(sh) / 312(2.03)	250 (1.47) / 298(2.31) / 310(2.18)
MVTP²⁺	4.8(4)	4.6(4)	349(0.85)	372(0.75)
TV⁶⁺	$\log K^*_{\text{TV}^{6+}\text{⊂(CB[7])}_3}$ = 4.7(1)	5.5(1)	226(4.66) / 262(4.16) / 346(1.62)	226(5.07) / 262(3.47) / 378(1.41)

Solvent: water buffered at pH 7.0 with 0.1 M Na₂H₂PO₄/NaH₂PO₄; l = 1 cm; T = 25.0(1)° C. The values in italics are characteristics of the external mode inclusion while those in bold illustrate the internal mode complexation.

The external mode complexation of **CB[7]** guided by the hydrophobic character of the additional phenyl group was further confirmed by a ¹H NMR titrations (Figure 18) that revealed large upfield shifts of the *b* and *c* (and at a lesser extent that of *i*) protons of the phenyl unit together with a modest upfield shift of some protons associated to the **BIPY²⁺** unit. Altogether, these observations suggest the formation of a [2]pseudorotaxane **MPV²⁺⊂CB[7]** whose the hydrophobic cavity of **CB[7]** mainly resides on the phenyl group instead of the **BIPY²⁺** group (as seen for **MV²⁺**) contributing to the stabilization of the latter species (Figure 35).

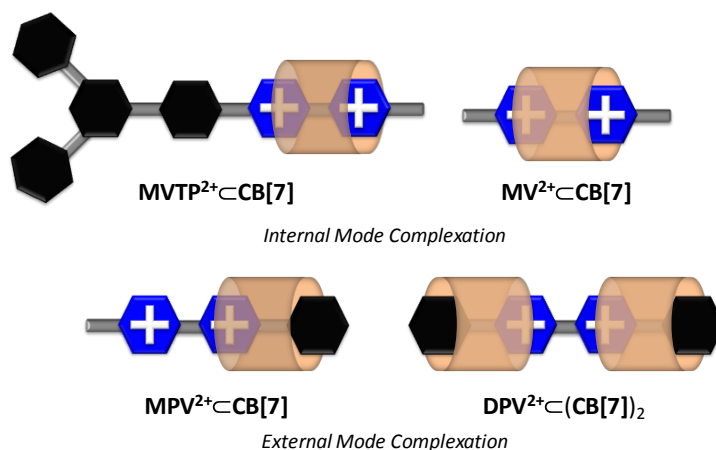


Figure 35. Schematic representation of the internal (MV^{2+} and $MVTP^{2+}$, the hydrophobic cavity of $CB[7]$ mainly resides on the bipyridinium group) and external (MPV^{2+} and DPV^{2+} , the hydrophobic cavity of $CB[7]$ mainly resides on the terminal phenyl group).

Such an inclusion pattern has been previously described by 1H -NMR spectroscopy with the symmetrical diphenyl viologen DPV^{2+} analogue.⁷ However, the shifts of the proton signals of DPV^{2+} were at a maximum after the addition of two equivalents of $CB[7]$ thus suggesting the formation of a [3]pseudorotaxane $DPV^{2+} \subset (CB[7])_2$. UV-visible absorption spectrophotometric titrations of DPV^{2+} with $CB[7]$ clearly supported the formation of this species in solution (Figure 4). The 1:2 ($DPV^{2+} : CB[7]$) stoichiometry was also assessed using a Job plot approach (Figure 5) and ESI-MS experiments (Figure 14). On recognition by the $CB[7]$, the π - π^* transitions centred on the DPV^{2+} also undergo weak hypsochromic and hypochromic shifts which supports an external binding of the DPV^{2+} by the two $CB[7]$ macrocycles (Figure 35 and Table 1). These spectrophotometric data stand in contrast with those of methyl viologen MV^{2+} for which large hypochromic shift of the UV absorption band has been measured on internal binding of the dicationic $BIPY^{2+}$ chromophore by $CB[7]$.⁴ Only a global binding constant ($\log \beta_{DPV^{2+} \subset (CB[7])_2} = 8.29(9)$) could be determined under our experimental conditions. Assuming the stability constant calculated for $MPV^{2+} \subset CB[7]$ ($\log K_{MPV^{2+} \subset CB[7]} = 6.1(3)$) as being closely related to the first binding event occurring for DPV^{2+} and $CB[7]$ ($K_{DPV^{2+} \subset CB[7]}$), the statistical recognition ($K_{DPV^{2+} \subset (CB[7])_2} / K_{DPV^{2+} \subset CB[7]} = 0.25$)¹⁶ of a second $CB[7]$ macrocycle ($K_{DPV^{2+} \subset (CB[7])_2} / K_{DPV^{2+} \subset CB[7]}$) would lead to a global stability constant of $\log \beta_{DPV^{2+} \subset (CB[7])_2} = 11.6$ far above the one experimentally determined. This suggests that strong steric interactions between the two $CB[7]$ macrocycles are taking place within the [3]-pseudorotaxane $DPV^{2+} \subset (CB[7])_2$ that lead to altered recognition properties (*i.e.* negative cooperativity) with respect to $MPV^{2+} \subset CB[7]$.

3.3.1b. Recognition of $MVTP^{2+}$ and TV^{6+} by $CB[7]$

The formation of the inclusion complexes of $MVTP^{2+}$ and TV^{6+} with $CB[7]$ was also evidenced by UV-Vis. measurements. Interestingly, hypochromic and bathochromic shifts of the π - π^* transitions centred on the $BIPY^{2+}$ core were observed in both case (Table 1) as a consequence of the encapsulation of the $BIPY^{2+}$ chromophore by the macrocycle cavity.

Despite the presence of the hydrophobic triaryl substituent, the ^1H NMR titrations also confirmed that the **CB[7]** is encircling the **BIPY** $^{2+}$ cation as seen previously for **MV** $^{2+}$. The α/α' and β/β' protons of the **BIPY** $^{2+}$ experienced an upfield shift upon **CB[7]** inclusion confirming the formation of a [2]pseudorotaxane where the **CB[7]** macrocycle stands at the peripheral of the **MVTP** $^{2+}$ ligand. This different behaviour with respect to **MPV** $^{2+}$ can be explained by steric hindrance of the triaryl unit which prevent the recognition of the more hydrophobic moiety. Consequently, the stability constant ($\log K_{\text{MVTP}^{2+}\text{CB}[7]} = 4.8(4)$) is decreased with respect to that of **MPV** $^{2+}$ ($\log K_{\text{MPV}^{2+}\text{CB}[7]} = 6.1(3)$) or **MV** $^{2+}$ ($\log K_{\text{MV}^{2+}\text{CB}[7]} = 5.30(2)$).

For **TV** $^{6+}$, only an apparent association constant^{5,6} ($\log K_{\text{TV}^{6+}\text{CB}[7]}^* = 4.7(1)$) at 0.1 M phosphate buffer pH 7.0) was calculated from the processing of the spectrophotometric data (Figure 7). This reflects the fact that the three **BIPY** $^{2+}$ subunits in **TV** $^{6+}$ behave as independent binding sites and that each **CB[7]** binding to the **BIPY** $^{2+}$ units of **TV** $^{6+}$ induces comparable spectral variations (Figure 7 and Table 1). In the case of a statistical binding for a multivalent system (*i.e.* for **TV** $^{6+}$, $n = 3$), the successive stability constants related to each binding event (*i.e.* binding of **CB[7]** to each of the terminal viologen units) can be estimated using the following equation: $K_{i+1}/K_i = (n-i)/(i+1)(n-i+1)$ with $n = 3$ (number of identical and independent sites) and $1 \leq i \leq 3$ number of sites occupied.¹⁶ Therefore for $n = 3$, $K_1/K_2 = 2/6$; $K_2/K_3 = 1/6$. If we first assume that $\log K_{\text{TV}^{6+}\text{CB}[7]} = \log K_{\text{MVTP}^{2+}\text{CB}[7]} = 4.8$, the corresponding successive stability constants can be accordingly evaluated: $\log K_{\text{TV}^{6+}\text{CB}[7]}_2 = 4.32$ and $\log K_{\text{TV}^{6+}\text{CB}[7]}_3 = 3.54$. The average stability constant ($\log K_{\text{calcd}}^* = 4.5$) that can be deduced is comparable within experimental errors to the apparent value determined from absorption titration at pH 7.0 ($\log K_{\text{TV}^{6+}\text{CB}[7]}^* = 4.7(1)$). In addition, significant hypochromic and bathochromic shifts of the $\pi-\pi^*$ transitions of the three **BIPY** $^{2+}$ chromophores of **TV** $^{6+}$ were observed (Figure 7) on complexation with **CB[7]** macrocycles, which substantiates the ^1H NMR (Figure 19), the ESI-MS (Figure 16) data and the proposed **BIPY** $^{2+}$ /**CB[7]** binding mode. To illustrate this binding feature, Figure 36 shows the distribution curves of the successive inclusion complexes that coexist when **TV** $^{6+}$ is mixed with **CB[7]**.

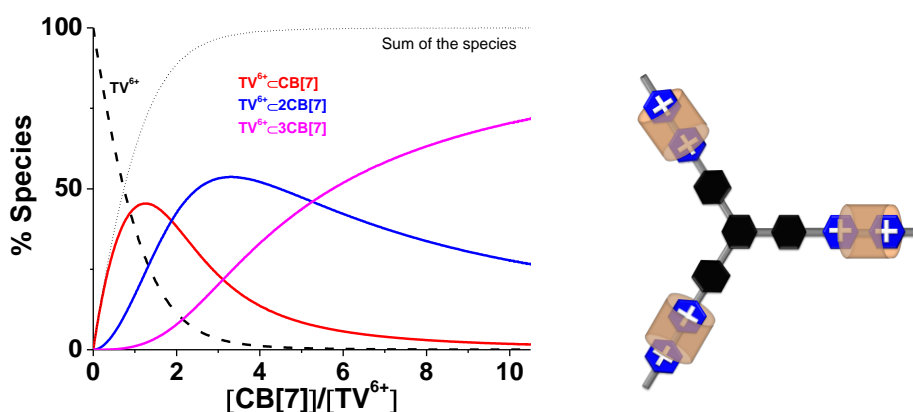


Figure 36. Distribution curves of the inclusion complexes which might be formed when **TV** $^{6+}$ is mixed with **CB[7]**. The dash line corresponds to the sum of all the species. Distribution diagram calculated using $\log K_{\text{TV}^{6+}\text{CB}[7]} = \log K_{\text{MVTP}^{2+}\text{CB}[7]} = 4.8$ and a statistical binding process. Solvent: water pH 7.0 (0.1 M $\text{Na}_2\text{HPO}_4/\text{NaH}_2\text{PO}_4$); $[\text{TV}^{6+}] = 10^{-4}$ M; $T = 25.0(1)$ °C.

3.3.2. Recognition of the Viologen Threads by CB[8]

Cucurbit[8]uril **CB[8]** which displays a cavity size comparable to that of γ -cyclodextrin can include two identical guest molecules to form¹⁷ a binary 1:2 complex, or two different guest molecules to form a ternary 1:1:1 complex¹⁸. Kim et al.¹⁹ also showed that methyl viologen exclusively forms with **CB[8]** a 1:1 complex for which the formation constant was calculated to be $K_{MV2+CB[8]} = (1.1 \pm 0.3) \times 10^5 \text{ M}^{-1}$ ($\log K_{MV2+CB[8]} = 5.04$). Although **CB[8]** has a cavity large enough²⁰ to encapsulate two viologen molecules, only a single dicationic viologen unit is hosted by the macrocyclic ligand.²¹ The formation of the 2:1 complex is precluded by the strong electrostatic repulsions between the two dications. However, these recognition properties can be tuned by simple redox chemistry and **CB[8]** was then shown to be able to accommodate two radical cations of methyl viologen (*vide infra*).¹⁹ Kim et al.²² have exploited this redox-coupled, guest-exchange process²³ in designing a molecular machine reminiscent of a loop lock.

In our work, the characterization of the host-guest complexes formed with **MPV**²⁺, **DPV**²⁺, **MVTP**²⁺ or **TV**⁶⁺ and **CB[8]** was investigated by absorption spectrophotometry (Figure 8 and Figure 9) and ESI-MS measurements (Figure 11, Figure 13, Figure 15 and Figure 17). Similarly to the [n]pseudorotaxanes formed with **CB[7]**, we were able to also characterize a **MPV**²⁺⊂**CB[8]**, a **DPV**²⁺⊂(**CB[8]**)₂, a **MVTP**²⁺⊂**CB[8]** ($\log K_{MVTP2+CB[8]} = 4.6(4)$) and a **TV**²⁺⊂(**CB[8]**)₃ ($\log K_{TV6+CB[8]3} = 5.5(1)$). No 2:1 (**V**²⁺:**CB[8]**) complexes were evidenced in agreement with the reported studies for other viologens.^{19,21} Due to the limited solubility of **CB[8]**, we were not able to perform ¹H NMR titrations of the viologens and therefore information about the mode of complexation is unluckily lacking. In addition, for **MPV**²⁺ and **DPV**²⁺, the weak spectral variations centred on the **BIPY**²⁺ chromophore upon **CB[8]** binding and the high dilution effects induced by the low solubility of the **CB[8]** host preclude any accurate determination of the host-guest binding constants. Similarly, the apparent stability constant measured for **TV**⁶⁺ seems to be overestimated with respect to that of **MVTP**²⁺ (Table 1). However, the electronic spectra depicted in Figure 8B and Figure 9B for **MVTP**²⁺ and **TV**⁶⁺ strongly support an internal complexation mode with **CB[8]** as previously evidenced with **CB[7]**. An ¹H NMR spectrum of **TV**⁶⁺ (data not shown) in the presence of an excess of **CB[8]** at very low concentration shows the formation of a symmetrical species whose spectral footprint is almost identical to that measured for **TV**⁶⁺⊂(**CB[7]**)₃. It confirmed, in addition to the absorption and ESI-MS data (*vide supra*), the formation of the 3:1 supramolecular complex **TV**⁶⁺⊂(**CB[8]**)₃ with a similar binding mode, although **CB[8]** has a larger hydrophobic cavity than **CB[7]**.

3.3.3. Intermolecular Dimerization of Viologen Threads

As mentioned in the previous chapter, monomers **V**⁺ and dimers (**V**⁺)₂ of viologen radical cations coexist in equilibrium in aqueous solution. We will discuss in the following section the influence of the substituents on the dimer formation and strength in water at pH 7.0 (0.1 M Na₂HPO₄/NaH₂PO₄).

3.3.3a. Intermolecular Dimerization of $\text{MPV}^{\bullet+}$

According to the UV-Vis.-NIR absorption data (Figure 20) that were collected for $\text{MPV}^{\bullet+}$, the absorbance at each wavelength can be correlated to the absorptivities of both the monomer and the dimer, the concentrations of which being related by the equilibrium constant for dimerization K_{Dim} .^{8,9} We showed that $\text{MPV}^{\bullet+}$ self-associates in solution with a log K_{Dim} value of 3.5(1), which is in the same range as the value previously determined for the benzyl methyl viologen radical cation $\text{BMV}^{\bullet+}$ (log $K_{\text{Dim}} = 3.46(5)$) and higher than that reported for the methyl viologen radical cation $\text{MV}^{\bullet+}$ (log $K_{\text{Dim}} \sim 2.5-2.9$ ^{24,25}). This feature clearly shows that increasing the hydrophobicity of the BIPY^{2+} unit with aryl substituent favours the dimerization of the radical cations. Figure 20 shows the electronic spectra and the distribution diagram of the $\text{MPV}^{\bullet+}$ species in solution (monomer *versus* dimer). $\text{MPV}^{\bullet+}$ is characterized by an intense and structured absorption in the visible region ($\lambda_{\text{max}} \sim 620$ nm, $\epsilon^{620} = 1.09 \times 10^4 \text{ M}^{-1} \text{ cm}^{-1}$), in agreement with the spectroscopic parameters determined for $\text{MV}^{\bullet+}$ (600-606 nm)^{NOTEREF_Ref420356478 \hbar 25-28} and $\text{BMV}^{\bullet+}$ (600 nm, see the previous chapter). Formation of the dimer ($\text{MPV}^{\bullet+}$)₂ induces a significant hypsochromic shift of the absorption at ~ 620 nm ($\Delta\lambda \sim 50$ nm) and gives rise to intense radical-radical transitions in the near-IR region ($\lambda_{\text{max}} \sim 910$ nm, $\epsilon^{910} = 4.2 \times 10^3 \text{ M}^{-1} \text{ cm}^{-1}$).²⁷

3.3.3b. Intermolecular Dimerization of $\text{MVTP}^{\bullet+}$ and $\text{TV}^{3(\bullet+)}$

UV-Vis absorption studies performed with the $\text{MPV}^{\bullet+}$ model demonstrated that no significant π -stacking interaction occurs (dimerization) except if the concentration of the radical cation is high enough ($> 10^{-3}$ M, Figure 20C). The electronic absorption spectrum of the π -conjugated MVTP^{2+} model markedly differs from the one of MPV^{2+} by a very high absorptivity in the UV region and a significant bathochromic shift of the BIPY^{2+} π - π^* transitions close to the visible region. This spectral shift can be explained by an extended conjugation of the aromatic system to the two additional phenyl rings. Such an important aromaticity is a strong indication of the fact that the triaryl phenyl central core exhibiting a high aromaticity is entirely flat, enhancing the probability of π -stacking. Upon generation of the radical cation $\text{MVTP}^{\bullet+}$, an absorption band in the visible region emerges as anticipated and is centred at 563 nm. Moreover and in contrast to what was observed during the titration of $\text{MPV}^{\bullet+}$, an additional and intense absorption centred at 1034 nm can be observed. This feature can be assigned to the intramolecular charge resonance that is occurring in the dimerized viologen species and clearly demonstrates the formation of a radical cation dimer ($K_{\text{Dim}} \gg 10^7 \text{ M}^{-1}$) strongly stabilized by the π -stacking interaction of the triarylphenyl central unit (Figure 37).

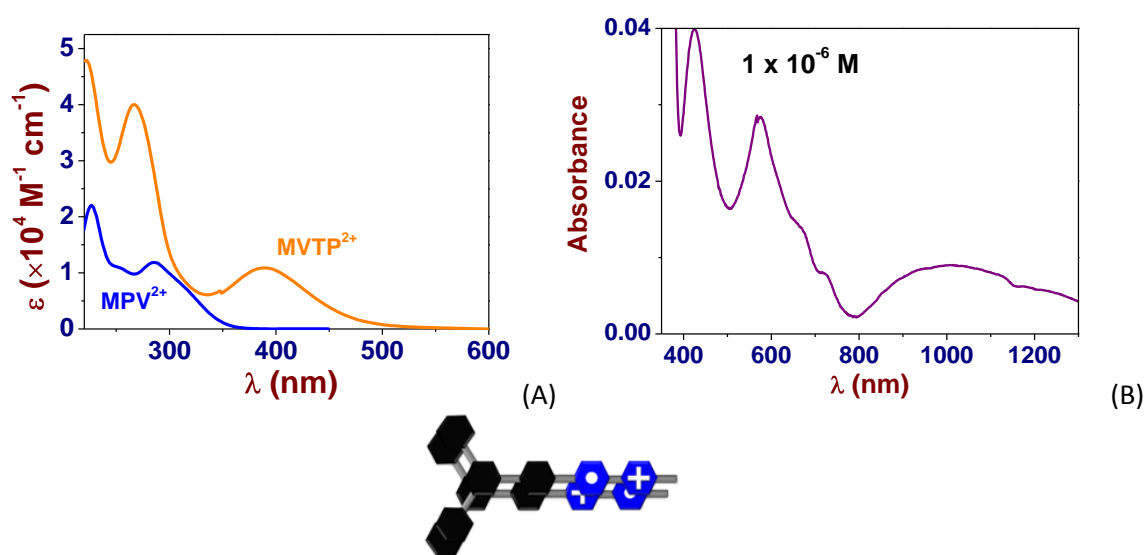


Figure 37. (A) UV-Vis. electronic absorption spectra of MPV^{2+} and $MVTP^{2+}$ and (B) UV-Vis.-NIR electronic absorption spectrum of a diluted $MVTP^{\bullet+}$ solution ($10^{-6} M$) Solvent: Water pH 7.0 (0.1 M Na_2HPO_4/NaH_2PO_4); $MVTP^{\bullet+}$ was generated from $MVTP^{2+}$ using freshly prepared sodium dithionite solution at *ca.* $10^{-2} M$ under O_2 free conditions.

The absorption titration of the trisviologen platform TV^{6+} by sodium dithionite displays the same spectral features than $MVTP^{2+}$. The electronic absorption spectrum of the fully oxidized ligand exhibits two strong absorption bands centred at 346 nm and 262 nm, characteristic of the π - π^* transitions of the $BIPY^{2+}$ and the triarylphenyl units, respectively. Strikingly, the $BIPY^{2+}$ π - π^* transitions are hypsochromically shifted with respect to $MVTP^{2+}$ as a consequence of the presence of three bipyridinium units. Formation of the radical cation species is evidenced by the formation of a new band at 560 nm which account for the charge transfer (CT) transitions as observed for the $MVTP^{\bullet+}$ control ligand. This new band is accompanied with absorption at ~ 1170 nm in the NIR region, which is assigned to the charge resonance (CR) transfer allowed upon the formation of radical cation dimers. It is suggested that the three radical cation subunits of a $TV^{3\bullet+}$ molecule interact with the same radical cation moieties of an adjoining $TV^{3\bullet+}$ (i.e. multicenter dimerization, Figure 38) thus leading to $(TV^{3\bullet+})_2$ that is further stabilized by π -stacking of the central triarylphenyl central groups. The multivalent $TV^{3\bullet+}$ system then affords in aqueous solution a very stable dimeric species ($K_{Dim} \gg 10^7 M^{-1}$).

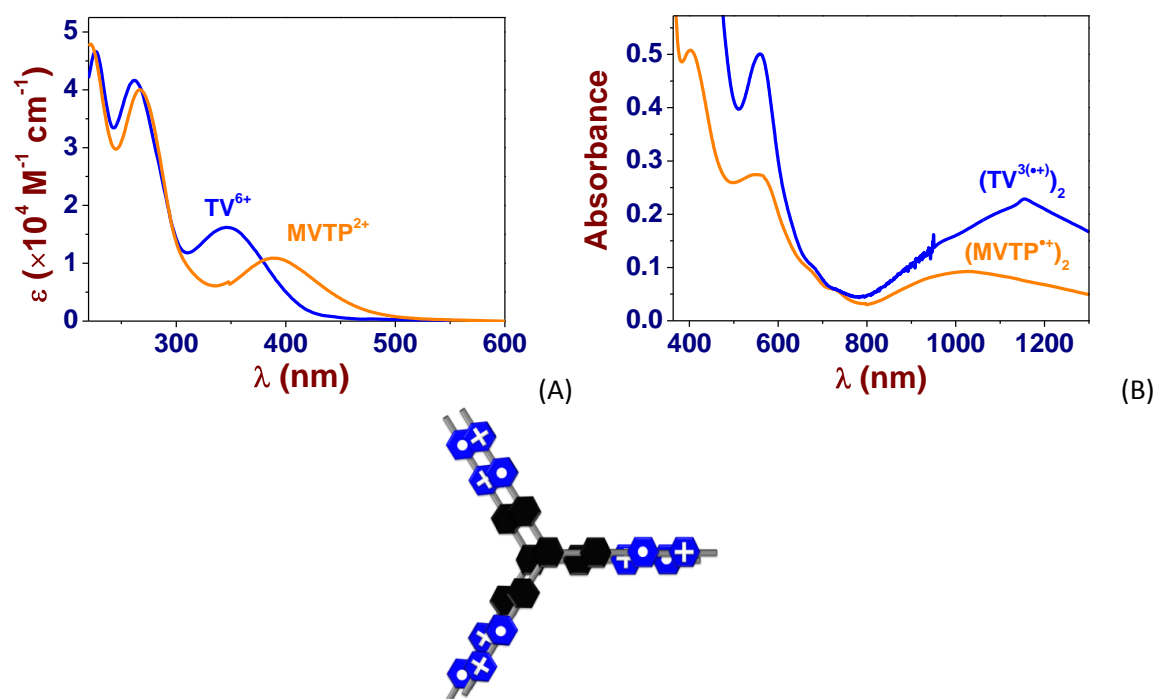


Figure 38. (A) UV-Vis. electronic absorption spectra of TV^{6+} and MVTP^{2+} and (B) UV-Vis.-NIR electronic absorption spectrum of a diluted $\text{TV}^{3(\bullet+)}$ solution. Solvent: Water pH 7.0 (0.1 M $\text{Na}_2\text{HPO}_4/\text{NaH}_2\text{PO}_4$); $\text{TV}^{3(\bullet+)}$ was generated from TV^{6+} using freshly prepared sodium dithionite solution at *ca.* 10^{-2} M under O_2 free conditions.

It is worth noticing the physico-chemical alterations occurring in solution during the reduction of the control ligands MPV^{2+} and MVTP^{2+} and the tritopic platform TV^{6+} . Under their fully oxidized states, dissolution of both viologens derivatives gives pale yellow solutions (strong absorption below 400 nm). Meanwhile, after addition of reducing agent, the solution of $\text{MPV}^{\bullet+}$ exhibits a deep blue colour (strong absorption centred at $\sim 600\text{-}620$ nm) that is typical of the non-pimerized radical cationic viologen. By contrast, the chemically reduced solutions of MVTP^{2+} and TV^{6+} turned reddish (strong absorption centred at ~ 560 nm) instead of purple as it is commonly observed for the pimerized viologen radical cations (e.g. $\text{MV}^{\bullet+}$, $\text{BMV}^{\bullet+}$ or $\text{MPV}^{\bullet+}$). This feature strongly supports that the equilibrium is entirely displaced towards the dimerized species, highlighting the strong effect of the central π -conjugated system (MVTP^{2+} and TV^{6+}) as well as the multivalency (TV^{6+}) on the stabilization of the dimer. Importantly, when solutions of $(\text{TPV}^{\bullet+})_2$ and $(\text{TV}^{3(\bullet+)})_2$ are allowed to stand for a few minutes, a phenomenon of precipitation is clearly observed (Figure 25 and Figure 34). This can be rationalized by additional π -stacking between the dimers (Figure 39).

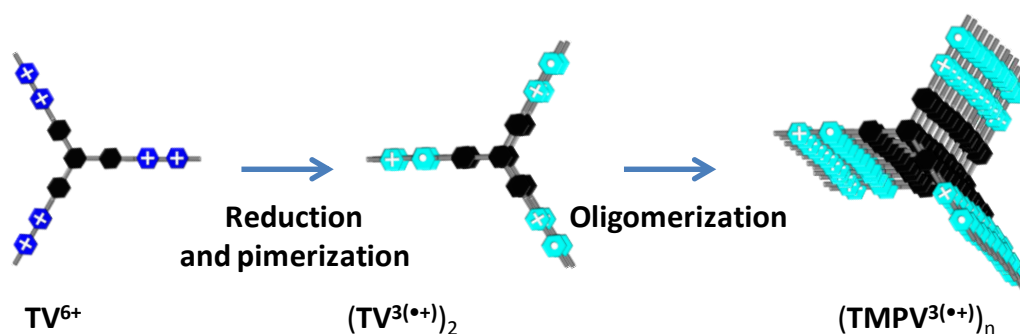


Figure 39. Schematic representation of the pimerization and oligomerization of TV^{6+} upon reduction with sodium dithionite.

3.3.4. Reduction of the [n]Pseudorotaxanes with CB[7]

3.3.4a. Monocationic Monoradicals $MPV^{\bullet+}$ and $DPV^{\bullet+}$

Cyclic voltammetric and square-wave voltammetric (Figure 30) experiments in phosphate-buffered solutions at pH 7 were performed on the reference compounds MPV^{2+} in the absence and presence of **CB[7]**. MPV^{2+} (Figure 30A) is characterized by two successive one-electron reversible redox waves: $E_{1/2}^1 (MPV^{2+}/MPV^{\bullet+}) = -0.50$ V and $E_{1/2}^2 (MV^{\bullet+}/MV^0) = -0.89$ V). Addition of **CB[7]** alters its electrochemical properties. In the presence of two equivalents of **CB[7]**, the first redox wave shifts slightly to a more negative potential ($\Delta E_{1/2}^1 = 100$ mV) and retains its reversible shape, while the second reduction wave shifts to a much more negative potential ($\Delta E_{1/2}^2 = 190$ mV). These shifts reflect the relative affinities of **CB[7]** for the different redox states of MPV^{2+} . Assuming a $\log K_{MPV^{2+}+CB[7]} = 6.1(3)$ for $MPV^{2+}+CB[7]$ previously determined using absorption spectrophotometric titrations, $\log K_{MPV^{\bullet+}+CB[7]} \sim 4.41$ and $\log K_{MV^0+CB[7]} \sim 1.2$ values can be accordingly calculated. These results show that **CB[7]** has a greater binding affinity for MPV^{2+} ($\log K_{MPV^{2+}+CB[7]} = 6.1(3)$) than for MV^{2+} ($\log K_{MV^{2+}+CB[7]} = 5.30(2)$). However, a similar affinity of both radical cationic forms $MPV^{\bullet+}$ ($\log K_{MPV^{\bullet+}+CB[7]} \sim 4.41$) and $MV^{\bullet+}$ ($\log K_{MV^{\bullet+}+CB[7]} \sim 4.79$) for **CB[7]** can be observed. The neutral MPV^0 is loosely bound to **CB[7]**. Similarly to what was observed for BMV^{2+} (see previous chapter, $\log K_{BMV^{2+}+CB[7]} = 6.9(8)$) and $\log K_{BMV^{\bullet+}+CB[7]} \sim 4.53$), **CB[7]** displays two redox-state-dependent binding modes for the MPV species (MPV^{2+} versus $MPV^{\bullet+}$). On reduction of MPV^{2+} to $MPV^{\bullet+}$, translocation of **CB[7]** from the terminal phenyl moiety to the radical cation of the bipyridinium unit occurs (Figure 40). Similarly to benzyl methyl viologen BMV^{2+} , MPV^{2+} exhibits a much better affinity for **CB[7]** than MV^{2+} due to hydrophobic stabilizing interactions between the **CB[7]** and the more hydrophobic phenyl substituent. The NMR data that have been measured (Figure 18) confirmed this peculiar property. It thus appears that when the [2]pseudorotaxane $MPV^{2+}+CB[7]$ (*i.e.* **CB[7]** encircles the benzylic unit) is reduced to its $MPV^{\bullet+}+CB[7]$ form (*i.e.* **CB[7]** encircles the monoradical viologen centre), the macrocycle host performs a translocation movement from the benzyl to the viologen radical

cation (Figure 23 and Figure 40). This process is reversible on oxidation of the radical cation and *vice-versa*.

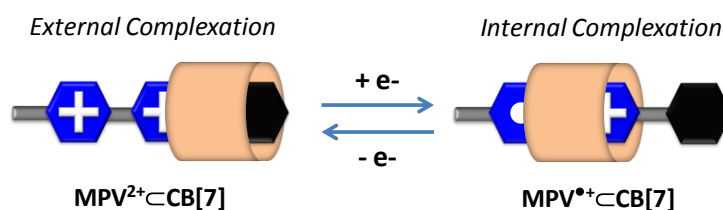


Figure 40. Electrochemically controlled translocation of the macrocycle **CB[7]** in the host-guest complex with **MPV²⁺**.

In order to go further, we undertook a UV-Vis.-NIR absorption titration of **MPV^{•+}** by **CB[7]** in water at pH 7.0 (Figure 23). **MPV^{•+} ⊂ CB[7]** was characterized by a significant hypochromic shift of the absorption signals associated with the radical cation, providing solid proof for inclusion of the radical cation within **CB[7]**. Statistical processing of the corresponding spectral data allowed us to evaluate the $K_{\text{MPV}^{\bullet+} \subset \text{CB}[7]}$ value ($\log K_{\text{BMV}^{\bullet+} \subset \text{CB}[7]} = 4.60(7)$) that is in excellent agreement with that determined from the electrochemical data ($\log K_{\text{MPV}^{\bullet+} \subset \text{CB}[7]} \sim 4.41$). The [2]pseudorotaxane **MPV^{•+} ⊂ CB[7]** is also characterized by a stability constant in agreement with that spectrophotometrically measured for **BMV^{•+} ⊂ CB[7]** ($\log K_{\text{BMV}^{\bullet+} \subset \text{CB}[7]} = 4.9(1)$, see previous chapter) or electrochemically determined for **MV^{•+} ⊂ CB[7]** ($\log K_{\text{MV}^{\bullet+} \subset \text{CB}[7]} \sim 4.79$, see previous chapter) thus substantiating the proposed binding mode (*i.e.* the radical cation of the bipyridinium moiety is encapsulated by the **CB[7]**).

After one-electron reduction under O₂-free environment, **DPV²⁺** forms a monoradical cationic intermediate **DPV^{•+}** (Figure 26). However, in the absence of **CB[7]** in water, the monoradical cationic **DPV^{•+}**, that was generated with an excess of freshly prepared Na₂S₂O_{4(aq)}, has a strong tendency to dimerize/oligomerize leading to formation of insoluble particles (Figure 25). Exposure of the latter solution to air reinstates the **DPV²⁺** (*i.e.* **DPV²⁺** is unable to dimerize/oligomerize) and leads to colourless and limpid solution. To overcome these limitations, time resolved absorption spectrophotometry was employed (stopped flow apparatus equipped with a diode array spectrophotometer) and allowed measuring the absorption spectrum of **DPV^{•+}** in the ms time range (Figure 26) prior its dimerization and further fast oligomerization (*i.e.* for **MPV^{•+}**, $\log K_{\text{Dim}} = 3.5(1)$). Using such an approach, an absorption spectrophotometric titration of the chemically generated **DPV^{•+}** by **CB[7]** was performed (*i.e.* the first absorption spectrum of repeated spectral kinetic experiments was recorded for each of the $[\text{CB}[7]]/[\text{DPV}^{\bullet+}]$ ratio considered). The statistical processing of the corresponding spectral data (Figure 27) allowed us to evaluate that unlike **DPV²⁺** that forms the ternary complex **DPV²⁺ ⊂ (CB[7])₂**, a 1:1 inclusion complex **DPV^{•+} ⊂ CB[7]** is observed with a binding constant value of $\log K_{\text{DPV}^{\bullet+} \subset \text{CB}[7]} = 4.9(1)$. The stability of the **DPV^{•+} ⊂ CB[7]** species is comparable to that measured for **MPV^{•+} ⊂ CB[7]** ($\log K_{\text{MPV}^{\bullet+} \subset \text{CB}[7]} = 4.60(7)$) or **BMV^{•+} ⊂ CB[7]** ($\log K_{\text{BMV}^{\bullet+} \subset \text{CB}[7]} = 4.9(1)$, see previous chapter) further confirming similar binding mode for each of the considered radical host-guest complexes. As it is usually observed for viologen/**CB[7]** complexes, **DPV^{•+} ⊂ CB[7]** is characterized by a significant

hypochromic shift of the absorption signals associated to the radical cation, and such shift provide additional evidence for the preferred radical cation's inclusion within **CB[7]**. In other words, the reduction of **DPV²⁺** induces the dissociation of one of the **CB[7]** macrocycles whether the second one undergoes a translocation from the phenyl ring to the viologen unit (Figure 41).

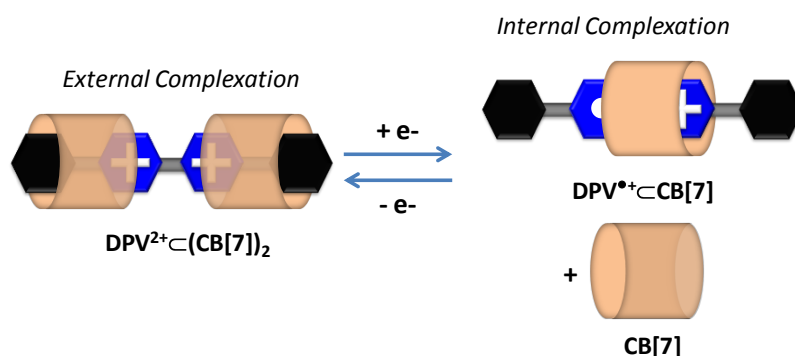


Figure 41. Electrochemically controlled dissociation and translocation of the macrocycles **CB[7]** in the host-guest complex with **DPV²⁺**.

3.3.4b. Monocationic Monoradical **MVTP^{•+}** and Triscationic Trisradical **TV^{3(•+)}**

The cyclic and square wave voltammograms recorded for the trisviologen **TV⁶⁺** and its **MVTP²⁺** model (Figure 30) clearly shows two distinct and reversible redox waves. The SWVs of **TV⁶⁺** (Figure 30) display two reversible three-electron processes ($E_{1/2}^1(\text{TV}^{6+}/\text{TV}^{3(•+)}) = -0.39$ V and $E_{1/2}^2(\text{TV}^{3(•+)}/\text{HV}^0) = -0.67$ V). For the **MVTP²⁺** model compound, the $E_{1/2}^1(\text{MVTP}^{2+}/\text{MVTP}^{•+})$ and $E_{1/2}^2(\text{MVTP}^{•+}/\text{MVTP}^0)$ values were measured to be -0.34 V and -0.76 V, respectively. Chronocoulometric experiments confirmed that the first reversible redox process **TV⁶⁺/TV^{3(•+)}** involves three electrons, while those associated with the monomeric viologen (**MVTP²⁺/MVTP^{•+}**) involve only one. Upon addition of 4 and 8 equivalents of **CB[7]** to **MPTV²⁺** and **TV⁶⁺**, respectively, the inclusion complexes are formed and the SW profile of each of them shows a marked shift of the first redox peak to a more negative value ($\Delta E_{1/2}^1 = 80$ mV for **MVTP²⁺** and $\Delta E_{1/2}^1 = 50$ mV for **TV⁶⁺**). Meanwhile, the second reduction peak is unaffected by the presence of **CB[7]**. For **TV⁶⁺ ⊂ (CB[7])₃** and **MVTP²⁺ ⊂ CB[7]**, no shift ($\Delta E_{1/2}^2 = 0$ mV) was then detected for the second reduction wave, which is expected to correspond to the following reaction: **TV^{3(•+) ⊂ (CB[7])₃}** → **TV^{0 ⊂ (CB[7])₃}** and **MVTP^{•+ ⊂ CB[7]}** → **MVTP^{0 ⊂ CB[7]}**. This unanticipated result is a strong indication that after the first (one-electron) three-electron reduction, the threads actually behave like free **MVTP^{•+}** or **TV^{3(•+)}**. The first reduction of **TV⁶⁺ ⊂ (CB[7])₃** or **MVTP²⁺ ⊂ CB[7]** induces complete dissociation of **CB[7]** and is followed by spontaneous intermolecular dimerization of the **BIPY^{•+}** groups to form the dimers (**TV^{3(•+)})₂** (or **MVTP^{•+})₂**). These features were further clearly confirmed by absorption spectrophotometric experiments depicted in Figure 28 and Figure 29. The one electron reduction of **MVTP²⁺ ⊂ CB[7]** (Figure 28A) induces dethreading of the radical cation **MVTP^{•+}** from the [2]pseudorotaxane and intermolecular dimerization as evidenced by the broad NIR absorption that constitutes a solid proof of the dimer (**MVTP^{•+})₂** occurrence in

solution. The high stability of the dimer species ($K_{\text{Dim}} \gg 10^7 \text{ M}^{-1}$) indeed prevents the inclusion process for thermodynamic reasons. Alternatively (Figure 28B), addition of **CB[7]** up to 4 equivalents to the $(\text{MVTP}^{\bullet+})_2$ dimer has no effect on its absorption properties thus demonstrating that when the viologen is reduced, it spontaneously self-assembles in solution and prevents **CB[7]** complexation. The same observations can be also proposed for TV^{6+} (Figure 29A and B).

A quantitative study of this phenomenon was carried out through the determination of the diffusion coefficients values by chronocoulometry of the redox active species including in the absence and in the presence of **CB[7]** and **CB[8]** which have been demonstrated to lead to inclusion complexes with TV^{6+} but not with $\text{TV}^{3(\bullet+)}$. The calculated D_i values from chronocoulometric experiments are reported in water (Table 2).

Table 2. Diffusion constants ($\text{cm}^2 \text{ s}^{-1}$) calculated from chronocoulometric experiments in H_2O (0.1 M TBACl).

– CB[7]		+ CB[7]		+ CB[8]	
TV^{6+}	$\text{TV}^{3(\bullet+)}$	TV^{6+}	$\text{TV}^{3(\bullet+)}$	TV^{6+}	$\text{TV}^{3(\bullet+)}$
6.71×10^{-5}	1.26×10^{-5}	17.7×10^{-5}	1.68×10^{-5}	7.19×10^{-5}	4.47×10^{-6}
Reference electrode = Ag/AgCl.					

The diffusion coefficient of $\text{TV}^{3(\bullet+)}$ was not sensitive to the absence ($1.26 \times 10^{-5} \text{ cm}^2 \text{ s}^{-1}$) or the presence of **CB[7]** ($1.68 \times 10^{-5} \text{ cm}^2 \text{ s}^{-1}$) in excellent agreement with the inability of **CB[7]** to interact with $\text{TV}^{3(\bullet+)}$ due to the formation of a very stable pimer ($\text{TV}^{3(\bullet+)})_2$. On the other hand, the diffusion coefficient of $\text{TV}^{3(\bullet+)}$ experienced a significant decrease in the presence of **CB[8]** ($4.47 \times 10^{-6} \text{ cm}^2 \text{ s}^{-1}$) that can be explained by the formation of the 3:2 inclusion complex $(\text{TV}^{3(\bullet+)})_2 \subset (\text{CB}[8])_3$. The larger cavity size of **CB[8]** indeed allow accommodating two radical cations and was shown to prevent oligomerization and precipitation of $\text{TV}^{3(\bullet+)}$ (Figure 33) and $\text{MVTP}^{\bullet+}$ (Figure 32).

3.3.5. Reduction of the [n]Pseudorotaxanes with CB[8]

We have highlighted that the π -stacking properties of the triaryl phenyl central core and the multivalency effect of TV^{6+} (3 homogeneously distributed bipyridinium centres) increase by far the capacity of the trisradical cation $\text{TV}^{3(\bullet+)}$ to firmly pimerize in solution ($K_{\text{Dim}} \gg 10^7 \text{ M}^{-1}$ in water at pH 7). Consequently, upon reduction in water and even in the presence of **CB[7]**, formation of aggregates (*i.e.* oligomers) and precipitation of stacked dimers was observed (Figure 34). In the presence of **CB[8]**, the absorption spectrum ($\text{NIR-}\lambda_{\text{max}} \sim 936 \text{ nm}$) of $\text{TV}^{3(\bullet+)}$ was markedly different from that measured in the absence or presence of **CB[7]** ($\text{NIR-}\lambda_{\text{max}} \sim 1168 \text{ nm}$, Figure 29) suggesting that one **CB[8]** (*i.e.* the **CB[8]** cavity is large enough to accommodate two radical cations of viologen) accommodates two monoradical viologen subunits that are firmly stacked together within the macrocyclic host cavity

ultimately leading to $(\text{TV}^{3(\bullet+)})_2 \subset (\text{CB}[8])_3$ species. This significant hypsochromic shift of the NIR absorption can be explained the hydrophobic environment of the $(\text{TV}^{3(\bullet+)})_2$ dimer upon recognition by **CB[8]**. This observation is also in line with the reported studies^{1,2,19} that showed that the stability of methyl viologen dimer $(\text{MV}^{\bullet+})_2$ was significantly increased (enhancement of dimerization process by a factor of 10^5) in the presence of **CB[8]** following the formation of a 2:1 $(\text{MV}^{\bullet+})_2 \subset \text{CB}[8]$ supramolecular complex in water. By contrast, **CB[7]** displays a recognition site that is not large enough to welcome two radical cations of methyl viologen and was found to hinder the formation of this radical dimer. It is noteworthy that no precipitation of oligomeric species $(\text{TV}^{3(\bullet+)})_n$ occurs in the presence of **CB[8]** (Figure 34), while **CB[7]** has no effect (Figure 29) on this aggregation process. These observations were confirmed in the reversed experiments (Figure 33B). The NIR absorption of the $(\text{TV}^{3(\bullet+)})_2$ dimer (NIR- $\lambda_{\text{max}} \sim 1170$ nm) that was chemically generated with $\text{Na}_2\text{S}_2\text{O}_4$ in O_2 -free aqueous solution experienced a hypsochromic shift to 915 nm in the presence of **CB[8]** confirming the formation of host-guest species. The low solubility of **CB[8]** prevent the use of electrochemistry to gauge the redox properties of the $(\text{TV}^{3(\bullet+)})_2 \subset (\text{CB}[8])_3$ species.

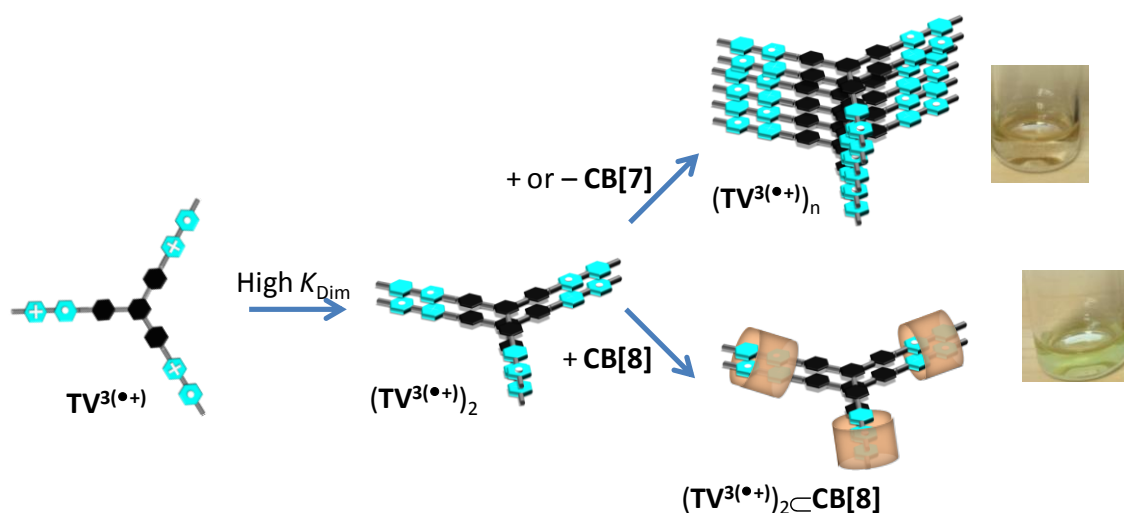


Figure 42. Schematic representation of the host-guest complexes and speciation of the trisradical cation $\text{TV}^{3(\bullet+)}$.

3.4. Conclusion

Using an alternative strategy with intermolecular interactions on multivalent systems, we have demonstrated that the very strong dimerization of radical cations can thermodynamically overwhelm the inclusion to **CB[7]** and induce fast and efficient host-guest dethreading. Reinstating the oxidized bipyridiniums prevent the dimerization process and reversibly led to the initial host-guest species. A circular trimeric system (TV^{6+}) composed of a benzenic core which has been extended on its 1, 3 and 5 positions by methyl-phenyl-viologen (MPV^{2+}) subunits has been considered. For the comparison purposes, model systems (MVTP^{2+} , MPV^{2+} and DPV^{2+}) were systematically studied using the same set of analytical methods (absorption spectrophotometry, electrochemistry, electrospray mass

spectrometry, ^1H NMR). The recognition properties of **CB[7]** and **CB[8]** have been thoroughly investigated.

The inclusion complexes of TV^{6+} formed with **CB[7]** (and **CB[8]**) clearly evidenced the main formation of a [4]pseudorotaxane $\text{TV}^{6+}\subset[\text{CB}[n]]_3$ ($n = 7, 8$). These species have been fully characterized both by absorption spectrophotometry, ESI-MS and ^1H NMR.

The redox properties of the trimeric circular TV^{6+} system and its corresponding models were then examined. The one electron reduction of each of the viologen units leads to a trisradical viologen $\text{TV}^{3(\bullet+)}$ that spontaneously self-associate in solution to afford the dimer $(\text{TV}^{3(\bullet+)})_2$. Unlike simpler viologen derivatives under their monoradical state, the pimerization constant of $\text{TV}^{3(\bullet+)}$ was found to be significantly increased ($K_{\text{Dim}} \gg 10^7 \text{ M}^{-1}$) due to the multiplication of pimerization centres (multivalency effect). The $(\text{TV}^{3(\bullet+)})_2$ dimer remains the predominant species even in the sub-micromolar concentrations. Furthermore, a slow aggregation process has been highlighted due to a stacking process between the aromatic dimers that can be reversible prevented by addition of **CB[8]** but not with **CB[7]**.

In the presence of **CB[7]**, the one electron reduction of each of the viologen unit (similarly to the above-mentioned hexavalent HV^{12+} system) led to the dethreading of the macrocycles from the (electro)chemically generated $\text{TV}^{3(\bullet+)}\subset[\text{CB}[7]]_3$ species. This process is fully reversed upon re-oxidation of the viologen monoradical subunits. Importantly, this intermolecular pimerization here competes thermodynamically with the inclusion process. The more voluminous **CB[8]** was shown to accommodate two monoradical viologen subunits that are firmly stacked together within the macrocyclic host cavity ultimately leading to $(\text{TV}^{3(\bullet+)})_2\subset[\text{CB}[8]]_3$ species and then preventing oligomerization of the $(\text{TV}^{3(\bullet+)})_2$ dimers.

This innovative strategy demonstrates that intermolecular interactions can be used as well to enhance the stability of radical dimers in solution thank to a peculiar design (recognition centres judiciously distributed along the periphery of a benzenic central core) and to a multicenter approach. This can constitute a smart strategy for the preparation of new electrochromic materials.

Bibliographic Section

- 1 (a) Kim, H.-J.; Jeon, W.S.; Ko, Y.H.; Kim, K. *Proc. Natl. Acad. Sci. U.S.A.* **2002**, *99*, 5007-5011. (b) Lee, J. W.; Samal, S.; Selvapalam, N.; Kim, H.-J.; Kim, K. *Acc. Chem. Res.* **2003**, *36*, 621-630.
- 2 (a) Jansen, K.; Buschmann, H.-J.; Wego, A.; Döpp, D.; Mayer, C.; Drexler, H. J.; Holdt, H. J.; Schollmeyer, E. *J. Incl. Phenom. Macrocycl. Chem.*, **2001**, *39*, 357-363. (b) Buschmann, H.-J.; Cleve, E.; Jansen, K.; Schollmeyer, E. *Anal. Chim. Acta* **2001**, *437*, 157-163. (c) Buschmann, H.-J.; Cleve, E.; Jansen, K.; Wego, A.; Schollmeyer, E. *J. Incl. Phenom. Macrocycl. Chem.* **2001**, *40*, 117-120. (d) Ong, W.; Gomez-Kaifer, M.; Kaifer, A. E. *Org. Lett.* **2002**, *4*, 1791-1794. (e) Ong, W.; Kaifer, A. E. *J. Org. Chem.* **2004**, *69*, 1383-1385.
- 3 Wadhwa, K.; Nuryyeva, S.; Fahrenbach, A. C.; Elhabiri, M.; Platas-Iglesias, C.; Trabolsi, A. *J. Mater. Chem. C* **2013**, *1*, 2302-2307.
- 4 Nchimi Nono, K.; Dalvand, P.; Wadhwa, K.; Nuryyeva, S.; Alneyadi, S.; Fahrenbach, A.; Olsen, J.-C.; Asfari, Z.; Platas-Iglesias, C.; Elhabiri, M.; Trabolsi, A. *Chem. Eur. J.* **2014**, *20*, 7334-7344.
- 5 Hou, J. L.; Yi, H. P.; Shao, X. B.; Li, C.; Wu, Z. Q.; Jiang, X. K.; Wu, L. Z.; Tung, C. H.; Li, Z. T. *Chem Angew. Chem. Int. Ed.* **2006**, *45*, 796-800.
- 6 Trabolsi, A.; Urbani, M.; Delgado, J. L.; Ajamaa, F.; Elhabiri, M.; Solladi, N.; Nierengarten, J.-F.; Albrecht-Gary, A.-M. *New J. Chem.* **2008**, *32*, 159-165.
- 7 Benyettou, F.; Nchimi-Nono, K.; Jouiad, M.; Lalatonne, Y.; Milosevic, I.; Motte, L.; Olsen, J.-C.; Saleh, N.; Trabolsi, A. *Chem. Eur. J.* **2015**, *21*, 4607-4613.
- 8 Georges, J. *Spectrochim. Acta A: Mol. Biomol. Spectro.* **1995**, *51*, 985-994.
- 9 Blank, O.; Davioud-Charvet, E.; Elhabiri, M. *Antioxid. Redox Signal.* **2012**, *17*, 544-554.
- 10 Gampp, H.; Maeder, M.; Meyer, C. J.; Zuberbühler, A. D. *Talanta*, **1985**, *32*, 95-101.
- 11 Rossotti, F. J. C.; Rossotti, H. S.; Whewell, R. J. *J. Inorg. Nucl. Chem.* **1971**, *33*, 2051-2065.
- 12 Gampp, H.; Maeder, M.; Meyer, C. J.; Zuberbühler, A. D. *Talanta* **1985**, *32*, 257-264.
- 13 Gampp, H.; Maeder, M.; Meyer, C. J.; Zuberbühler, A. D. *Talanta* **1986**, *33*, 943-951.
- 14 Marquardt, D. W. *J. Soc. Ind. Appl. Math.* **1963**, *11*, 431-441.
- 15 Maeder, M.; Zuberbuehler, A. D. *Anal. Chem.* **1990**, *62*, 2220-2224.
- 16 Perlmutter-Hayman, B. *Acc. Chem. Res.* **1986**, *19*, 90-96.
- 17 (a) Freeman, W. A.; Mock, W. L.; Shih, N.-Y. *J. Am. Chem. Soc.* **1981**, *103*, 7367-7368; (b) Kim, J.; Jung, I. S.; Kim, S. Y.; Lee, E.; Kang, J.-K.; Sakamoto, S.; Yamaguchi, K.; Kim, K. *J. Am. Chem. Soc.* **2000**, *122*, 540-541; (c) Day, A.; Arnold, A. P.; Blanch, R. J.; Snushall, B. *J. Org. Chem.* **2001**, *66*, 8094-8100; (d) Liu, S.; Zavalij, P. Y.; Isaacs, L. *J. Am. Chem. Soc.* **2005**, *127*, 16798-16799.
- 18 Kim, H.-J.; Heo, J.; Jeon, W. S.; Lee, E.; Kim, J.; Sakamoto, S.; Yamaguchi, K.; Kim, K. *Angew. Chem. Int. Ed.* **2001**, *40*, 1526-1529.
- 19 Jeon, W. S.; Kim, H.-J.; Lee, C.; Kim, K. *Chem. Commun.* **2002**, 1828-1829.
- 20 Kim, J.; Jung, I. S.; Kim, S. Y.; Lee, E.; Kang, J. K.; Sakamoto, S.; Yamaguchi, K.; Kim, K. *J. Am. Chem. Soc.* **2000**, *122*, 540-541.
- 21 Trabolsi, A.; Hmadeh, M.; Khashab, N. M.; Friedman, D. C.; Humbert, N.; Elhabiri, M.; Khatib, H. A.; Belowich, M. E.; Coskun, A.; Albrecht-Gary, A. M.; Stoddart, J. F. *New J. Chem.* **2009**, *33*, 254-263.
- 22 (a) Ko, Y. H.; Kim, K.; Kang, J.-K.; Chun, H.; Lee, J. W.; Sakamoto, S.; Yamaguchi, K.; Fettingner, J. C.; Kim, K. *J. Am. Chem. Soc.* **2004**, *126*, 1932-1933. (b) Jeon, Y. J.; Bharadwaj, P. K.; Choi, S. W.; Lee, J. W.; Kim, K. *Angew. Chem. Int. Ed.* **2002**, *41*, 4474-4476. (c) Wang, W.; Kaifer, A. E. *Angew. Chem. Int. Ed.* **2006**, *45*, 7042-7046. (d) Kim, S.-Y.; Ko, Y. H.; Lee, J. W.; Sakamoto, S.;

- Yamaguchi, K.; Kim, K. *Chem. Asian J.* **2007**, *2*, 747-754. (e) Lee, J. W.; Han, S. C.; Kim, J. H.; Ko, Y. H.; Kim, K. *Bull. Korean Chem. Soc.* **2007**, *28*, 1837-1840; f) Lee, J. W.; Kim, K.; Choi, S.; Ko, Y. H.; Sakamoto, S.; Yamaguchi, K.; Kim, K. *Chem. Commun.* **2002**, 2692-2693. (g) Kim, K.; Kim, D.; Lee, J. W.; Ko, Y. H.; Kim, K. *Chem. Commun.* **2004**, 848-849. (h) Bush, M. E.; Bouley, N. D.; Urbach, A. R. *J. Am. Chem. Soc.* **2005**, *127*, 14511-14517. (i) Sindelar, V.; Cejas, M. A.; Raymo, F. M.; Chen, W.; Parker, S. E.; Kaifer, A. E. *Chem. Eur. J.* **2005**, *11*, 7054-7059. (j) Ko, Y. H.; Kim, K.; Kim, E.; Kim, K. *Supramol. Chem.* **2007**, *19*, 287-293. (k) Kang, J.-K.; Hwang, I.; Ko, Y. H.; Jeon, W. S.; Kim, H.-J.; Kim, K. *Supramol. Chem.* **2008**, *20*, 149-155.
- 23 Jeon, W. S.; Kim, E.; Ko, Y. H.; Hwang, I.; Lee, J. W.; Kim, S.-Y.; Kim, H.-J.; Kim, K. *Angew. Chem. Int. Ed.* **2005**, *44*, 87-91.
- 24 Lee, C.; Moon, M. S.; Park, J. W. *J. Electroanal. Chem.* **1996**, *407*, 161-167.
- 25 Stargardt, J. F.; Hawkrige, F. M. *Anal. Chim. Acta* **1983**, *146*, 1-8.
- 26 Park, J. W.; Choi, N. H.; Kim, J. H. *J. Phys. Chem.* **1996**, *100*, 769-774.
- 27 Kosower, E. M.; Cotter, J. L. *J. Am. Chem. Soc.* **1964**, *86*, 5524-5527.
- 28 Monk, P. M. S.; Hodgkinson, N. M.; Ramzan, S. A. *Dyes Pigm.* **1999**, *43*, 207-217.

Chapter IV: Recognition of Calix[4]arene-Based Viologens by CB[n]

4.1. Introduction

As mentioned previously, my PhD work has been mainly devoted to engineer and study novel systems based on recognition properties of redox active bipyridiniums by macrocycles such as cucurbit[n]uril. The novel nanomechanical systems that have described in the previous chapter include among other: a [4]pseudorotaxane and a [7]pseudorotaxane, each composed of a “multimeric” viologen-based thread molecule (*i.e.* **TV**⁶⁺ and **HV**¹²⁺) and the macrocycles, cucurbit[7]uril (noted **CB[7]**) and cucurbit[8]uril (noted **CB[8]**). In aqueous solution, these systems were shown to be electrochemically switched between a complexed state, defined by the pseudorotaxanes themselves, and an uncomplexed state comprising their separate components. The driving force for the disassembly process (*i.e.* dethreading process) was a strong intramolecular or intermolecular dimerization (*i.e.* pimerization) of the viologen radical cations.

As being already mentioned, intermolecular dimerization of organic radicals has been extensively studied with a broad range of aromatic derivatives. However, the main issue of such an approach is that formation of the loosely associated π -dimers in solution usually requires high concentrations due to the low dimerization constants (see the previous chapter for an exhaustive list of thermodynamic values and compounds). Low temperatures or use of macrocyclic hosts with large cavity size such as cucurbiturils (e.g. **CB[8]**) or cyclodextrins (e.g. β -CD) favour the intermolecular π -dimer complexes. We¹ and other authors have shown that preorganizing two or more organic radicals with adequate anchoring platforms and appropriate chain lengths favour by far the intramolecular π -dimers in solution. Alkyl,²⁻⁴ porphyrinic,⁵ ferrocenyl,⁶ phenyl^{3,7}, C₆₀⁸ or calixarene⁹ linkers (Figure 1) have already been demonstrated to promote the intramolecular dimerization of the corresponding bipyridinium radicals.

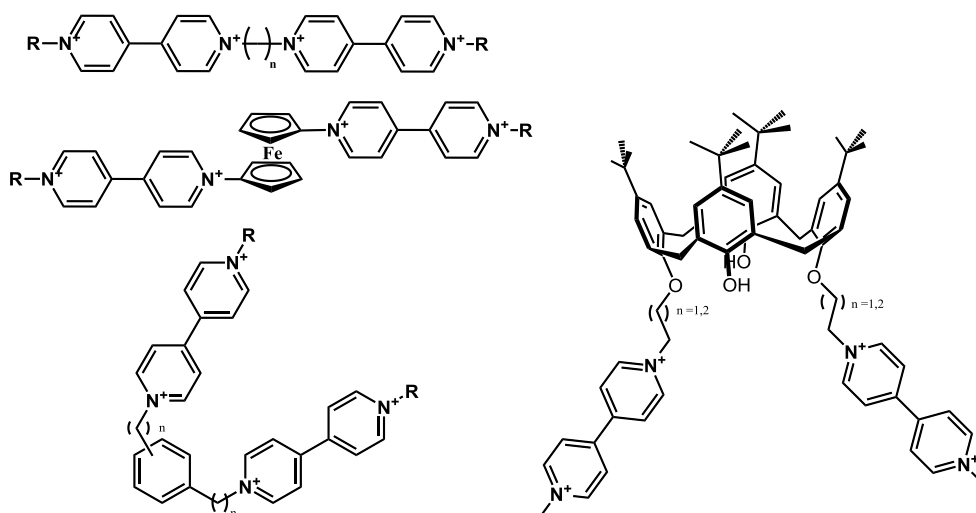


Figure 1. Chemical structures of *bis*-viologen compounds that favour intramolecular dimerization of their corresponding radical cations.

Hereafter, we employed the calix[4]arene as an anchoring platform (*i.e.* similarly to phosphazene with **HV**¹²⁺) that was functionalized with 2 terminal viologens using spacers of

different length (*i.e.* 3 and 4 carbons). It is noteworthy that analogous derivatives with 2 and 3 carbons spacers have been already described but only studied in acetonitrile in the absence of **CB[7]** and **CB[8]**.⁹ These new calix[4]arene-viologen derivatives that were synthesized were thoroughly studied in water in combination with **CB[7]** and **CB[8]** using the analytical methods already described such absorption spectrophotometry, electrochemistry, electrospray mass spectrometry, ¹H NMR and electron paramagnetic resonance (EPR) spectroscopies. Before describing the results of this extensive study, I will first briefly recall below the main properties of calixarene.

4.1.1. Calix[n]arene

Calixarenes are phenol derived macrocyclic hosts (synthesized through the condensation of a phenol with formaldehyde (base induction)^{10,11} that represent an important and extensively investigated family in host-guest supramolecular chemistry.¹² The term “calixarene” was originally introduced by C. D. Gutsche and R. Muthukrishnan¹³ for the resemblance of its shape to a type of ancient Greek vase (calyx Krater¹⁴) whereas arene denotes the presence of aryl moieties (Figure 2). Although the most popular calixarenes are built of 4 to 8 aromatic cycles, it is possible to prepare calix[n]arenes that contain from 4 to 20 aromatic rings in their structure.



Figure 2. Chemical structure of a calix[4]arene and its likeness to the Calyx Krater, a large vase which was used to mix wine and water in Ancient Greece.

4.1.2. Historical Background

The first condensation reaction of a phenol with formaldehyde was described by A. von Baeyer in 1872.¹⁵ By performing several experiments, he obtained a tarry like resinous product that he could neither characterize nor isolate the pure substance. Thirty years later, L. Baekeland discovered that, by controlling the amount of the base, it was possible to transform this tarry material into a brittle substance that he then designated as “Bakelite”. The main attempt to control the formaldehyde condensation reaction with various *para*-alkylated phenols in the presence of aqueous sodium hydroxide was conducted much later in 1942 by A. Zinke and E. Ziegler (designated as “Zinke synthesis”).¹⁶ The aim of their work was to produce linear polymers, easier to study than the phenol condensates. They

successfully obtained highly insoluble compounds for which they proposed a cyclic tetrameric structure.^{17,18}

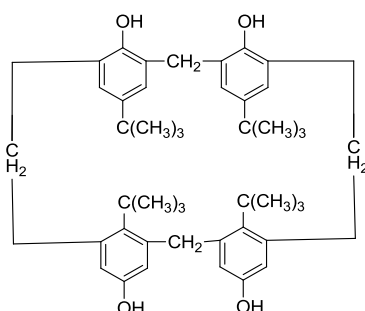


Figure 3. First cyclic condensate from *p*-alkylphenol/ CH_2O based on the Zinke and Ziegler synthesis.¹⁷

In 1955, experiments were carried out by J. W. Cornforth (an Australian-British chemist that was awarded by the Nobel prize in chemistry in 1975) and his colleagues^{19,20} that demonstrated that the product which was described by A. Zinke and E. Ziegler was a mixture of three related compounds. Twenty years later, a fundamental work was done by C. D. Gutsche who rationalized their structural properties and their preparation in larger scale.^{11,23} For the first time, he introduced the term "calixarene" for the cyclic tetramer previously described by A. Zinke and E. Ziegler to establish definitively the nomenclature of these new macrocycles. Last but not the least, he also showed that the condensation of *p*-tert-butylphenol with formaldehyde, in the presence of catalytic amounts of base, lead to cyclic oligomers such as the tetramer, the hexamer or the octamer. It is in fact the subtle combination of several parameters including among other the nature and the amount of base, the nature of the phenol and the cation associated to the base that determined the final number of aromatic components of the cyclic oligomer.

Since then, in addition to the cyclic oligomers consisting of 4, 6 or 8 recurring units, other teams have been interested in the preparation of calixarene having an odd number of phenolic units²¹ such as the *p*-tert-butyl-calix[7]arene. The *p*-tert-butyl-calix[9]arene, *p*-tert-butyl-calix[10]arene, *p*-tert-butyl-calix[11]arene and *p*-tert-butyl-calix[12]arene were obtained in one step after optimization of the synthetic procedures.²² In 1999, C. D. Gutsche and his colleagues isolated a wider series of calix[n]arenes with *n* ranging from between 9 to 20.²³ Calix[n]arenes are now easy to prepare in high yields from inexpensive starting materials and are easy to modify with a wide range of functional groups either at the aromatic rings or at the O-centres of the phenolic moieties. Another reason of interest is the bowl shaped cavity that is capable of including a broad range of guests. The cavity displays two opening edges, the one at the lower rim (which has the phenol hydroxyl groups) being considerably smaller than the one at the upper rim (Figure 5)

4.1.3. Conformational and Structural Properties of Calix[4]arenes

Calix[n]arenes can adopt various conformations and form cavities. J. W. Cornforth^{19,20} first evidenced that the calix[4]arene can exist in four conformations in solution with various aryl groups oriented upward or downward relative to an average plane defined by the methylene groups (Figure 4). Calix[4]arenes then display four potential conformations,²⁴ namely the

cone, partial cone, 1,2-alternate and 1,3-alternate conformations (Figure 4). At room temperature, the cone conformation is usually favoured because of the formation of circular hydrogen bonds (O–H···O hydrogen bonds at the lower rim, Figure 5). Substitution of the phenolic units markedly alters the conformational properties of the calix[4]arene. For instance, *p*-*tert*-butyl-tetramethoxy-calix[4]arene is still a flexible macrocycle (e.g. the interconversion rate at room temperature is $\sim 100 \text{ s}^{-1}$)²⁴ but the partial cone conformation is the most stable one. The tetraethyl ether analogue can also be regarded as a flexible compound but only at temperatures above 100°C and it then exists at room temperature as an equal mixture of partial cone and 1,2-alternate cone conformers.²⁵

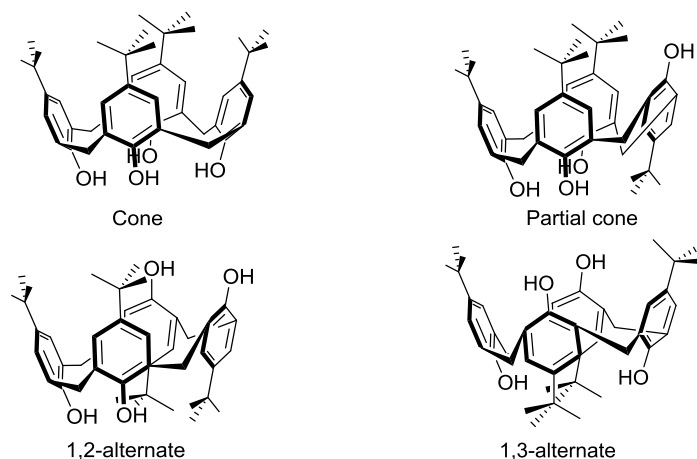


Figure 4. Conformational aspects of calix[4]arene.

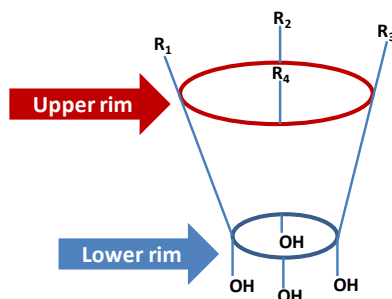


Figure 5. Positions of calix[4]arene that can be chemically modified.

The alkylation selectivity (*i.e.* the number of substituted phenols) can be controlled by the reaction conditions therefore giving rise to a broad range of conformers and cavity sizes (Table 1).²⁶

Table 1. Experimental conditions for selective alkylation of calix[4]arene.

Substitution targeted	Base	Solvent
<i>Mono</i> -	K_2CO_3	Acetone
<i>1,2-Bis</i> -	NaH	DMF/THF
<i>1,3-Bis</i> -	K_2CO_3 or Na_2CO_3	Acetone/ CH_3CN
<i>Tris</i> -	BaO/BaOH_2	DMF
<i>Tetrakis</i> -	NaH or K_2CO_3	DMF or Acetone

4.1.4. Aim of this Work

My research work was focused on the synthesis of viologen-based systems using calix[4]arene as an inert anchoring platform. The structural and conformational properties and the broad range of substitution of calix[4]arene make them interesting tools in electrochromic applications and host/guest chemistry. Di-substituted calix[4]arenes with 4,4'-bipyridiniums have been synthesized. The chain length connecting the viologens to the calix[4]arene unit has been varied from 3 to 4. Recognition properties with respect to **CB[7]** and **CB[8]** as well as the pimerization processes have been thoroughly investigated in aqueous solutions using the fruitful combination of analytical methods previously described in the PhD report.

Particularly, two calix[4]arene systems, namely **C23⁴⁺** and **C24⁴⁺**, (2 stands for the number of viologens and 3-4 correspond to the number of carbons of the chain connecting the viologens to the macrocyclic core, Figure 6) have been synthesized and led to [3]pseudorotaxanes in combination with either **CB[7]** or **CB[8]**. These [3]pseudorotaxanes spontaneously dissociate on reduction of the bipyridiniums as the result of a strong intramolecular dimerization of the two face-to-face viologen radical cations. Decomplexation and dimerization do not occur in experiments involving **CB[7]** (or **CB[8]**) and either of the two monomeric viologen guests **MC3²⁺** and **MC4²⁺**, which correspond to the reliable models.

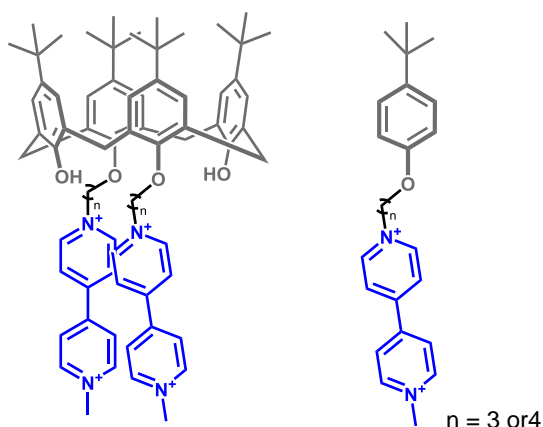


Figure 6. Chemical structures of the calixarene viologen-based systems **C23⁴⁺** and **C24⁴⁺** and the reference compounds **MC3²⁺** and **MC4⁴⁺**. The number 2 stands for the number of viologens while 3-4 correspond to the number of carbons of the chain connecting the terminal viologens to the calix[4]arene backbone.

4.2. Experimental Section and Results

4.2.1. Synthesis of the Calix[4]arene-Bis-viologens and the Corresponding Models

All commercially reagents were purchased from Sigma-Aldrich and used without further purification. Thin layer chromatography (TLC) was used to follow the reactions and was performed on aluminium sheets bearing silica gel 60 F254 (E. Merck). Column chromatography was performed using silica gel provided by Merck (40-63 μm). Routine Nuclear Magnetic Resonance (NMR) spectra were recorded on a Bruker AC 400 with working frequencies of 400 and 100 MHz for ^1H and ^{13}C , respectively. Chemical shifts are reported in ppm relative to the signals corresponding to the residual non-deuterated solvents (CDCl_3 ($\delta = 7.26$), CD_3OD ($\delta = 3.34$), and d_6 -DMSO ($\delta = 2.50$). High-resolution electrospray mass (HR-ESI) spectra were measured on a micro Q-TOF (Bruker) spectrometer.

4.2.1a. 1-methyl-[4,4'-bipyridin]-1-ium iodide (**I1**)

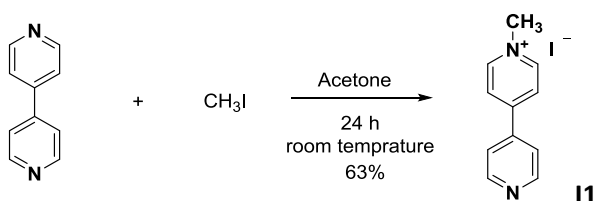


Figure 7. Synthesis of 1-methyl-[4,4'-bipyridin]-1-ium iodide (**I1**).

This compound was prepared according to literature procedures²⁷ (Figure 7). To a solution of 4,4'-bipyridine (90.3 mmol, 14.1 g) in 250 ml acetone, 12.8 g (90.3 mmol) of CH_3I were added. The mixture was stirred at RT for 24 hours. The yellow precipitate were filtered and washed with acetone. The solid part was dissolved in acetonitrile and filtered. Then, solid phase was dried under vacuum to afford **I1** as a yellow solid (yield: 63%)

I1: Light yellow solid; Chemical formula: $\text{C}_{11}\text{H}_{11}\text{N}_2\text{I}$; Molecular weight: 298 g mol^{-1} .

^1H NMR (400 MHz, d_6 -DMSO): δ [ppm]: 9.13 [d, 2H, $J=6.8$ Hz, Ar-H], 8.86 [d, 2H, $J=6$ Hz, Ar-H], 8.62 [d, 2H, $J=6.8$ Hz, Ar-H], 8.04 [d, 2H, $J=6.4$ Hz, Ar-H], 4.39 [s, 3H, CH_3]

4.2.1b. 1-(3-bromopropoxy)-4-(*tert*-butyl)benzene (**I2**)

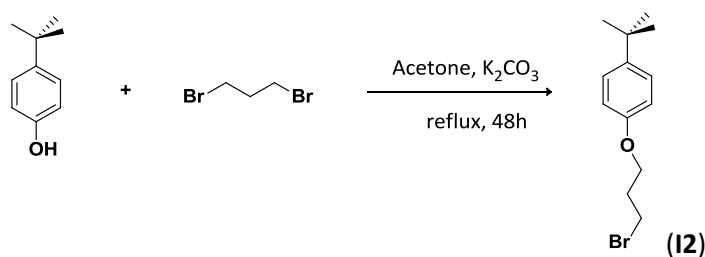


Figure 8. Synthesis of 1-(3-bromopropoxy)-4-(*tert*-butyl)benzene (**I2**)

1.5 g of *tert*-butyl-phenol (~ 10 mmol) was mixed with 1.4 g of K_2CO_3 (~ 10 mmol) and stirred for two hours in 100 ml of acetone at RT. Then 1.21 ml (~ 12 mmol) of 1,3-dibromopropane in 200 ml of acetone were added and the mixture was kept under reflux for three days. The solvent was fully evaporated and then the reaction mixture was dissolved in 200 ml of dichloromethane and washed with 400 ml of water. The organic phase was then dried under Na_2SO_4 and the solvent was evaporated. 0.8 g of crude product was obtained (Figure 8) which was involved directly in the next step without further purification.

I2: Colourless oil; Chemical formula: $C_{13}H_{19}BrO$; Molecular weight: $270.06 \text{ g mol}^{-1}$

1H NMR (400 MHz, CD_3OD): δ [ppm]: 7.21 [d, 2H, $J=8.8$ Hz, Ar-*H*], 6.76 [d, 2H, $J=8.8$ Hz, Ar-*H*], 3.91 [t, 2H, $J=6.4$ Hz, $-CH_2-Br$], 3.70 [t, 2H, $J=6.8$ Hz, O- CH_2-], 2.09-2.01 [m, 2H, Br- CH_2-CH_2-], 1.35 [s, 9H, $C(CH_3)_3$].

4.2.1c. 1-(3-4-(*tert*-butyl)phenoxy)propyl)-1-methyl-[4,4'-bipyridin]-1,1'-dium bromide iodide ($MC3^{2+}$)

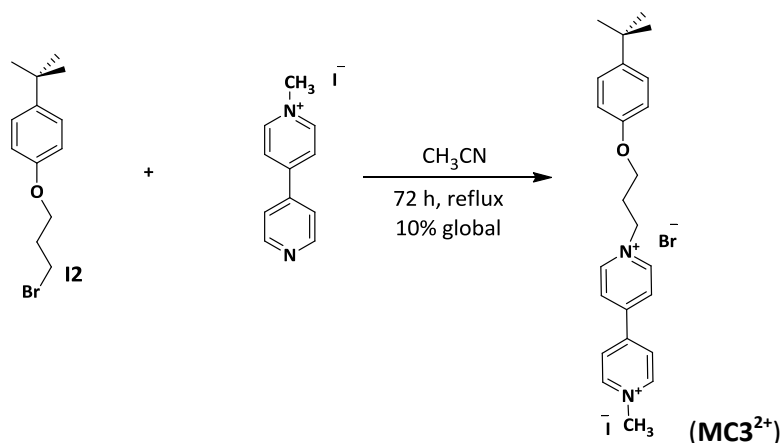


Figure 9. Synthesis of 1-(3-4-(*tert*-butyl) phenoxy)propyl)-1-methyl-[4,4'-bipyridin]-1,1'-dium bromide iodide ($MC3^{2+}$)

0.8 g (~ 2.95 mmol) of **I2** was mixed with 0.88 g (~2.95 mmol) of **I1** (1-methyl-[4,4'-bipyridin]-1-ium iodide) in 30 ml of acetonitrile and the mixture was refluxed for two days. The reaction mixture was filtered and washed with acetonitrile to afford 0.53 g of $MC3^{2+}$ (0.933 mmol) as a red-orange solid (global yield from **4.2.1b**: 9.33%).

$MC3^{2+}$: red-orange solid; Chemical formula: $C_{24}H_{30}ON_2IBr$; Molecular weight: $568.06 \text{ g mol}^{-1}$; Melting point: $258-9$ °C.

HR-MS for $C_{24}H_{30}ON_2$: [$MC3^{2+}$] calcd. $m/z = 181.1174$ and exp. $m/z = 181.1172$.

1H NMR (400 MHz, CD_3OD): δ [ppm]: 9.36 [d, 2H, $J=6.8$ Hz, Ar-*H*], 9.23 [d, 2H, $J=6.8$ Hz, Ar-*H*], 8.70 [t, 4H, $J=7.2$ Hz, Ar-*H*], 7.30 [d, 2H, $J=8.8$ Hz, Ar-*H*], 6.77 [d, 2H, $J=9.2$ Hz, Ar-*H*], 5.04 [t, 2H, $J=6.8$ Hz, N- CH_2-CH_2], 4.57 [s, 3H, N- CH_3], 4.19 [t, 2H, $J=5.6$ Hz, O- CH_2-CH_2], 2.66-2.60 [m, 2H, N- $CH_2-CH_2-CH_2-O$], 1.29 [s, 9H, $C(CH_3)_3$].

^{13}C NMR (100 MHz, CD_3OD): δ [ppm]: 158.08, 152.66, 152.21, 151.75, 148.88, 148.34, 145.96, 129.04, 128.84, 128.20, 124.39, 115.78, 66.58, 62.13, 35.75, 32.78.

4.2.1d. 1-(4-bromo-butoxy)-4-(*tert*-butyl)benzene (I3)

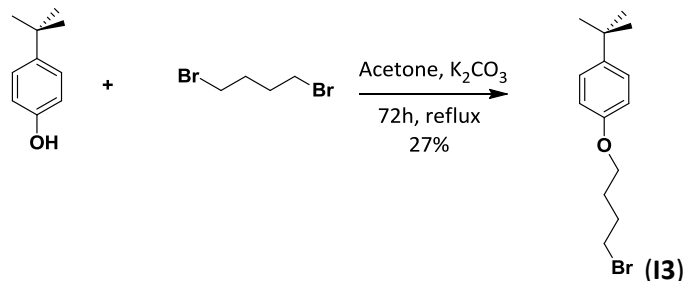


Figure 10. Synthesis of 1-(4-bromo-butoxy)-4-(*tert*-butyl)benzene (I3)

3 g of *p-tert*-butyl-phenol (~ 20 mmol) was mixed with 3 g of K_2CO_3 (~ 20 mmol) and stirred for two hours in 250 ml of acetone at RT. 2.8 ml (~ 24 mmol) of 1,4-dibromobutane in 200 ml acetone was then added and the mixture was kept under reflux for 3 days. Then, 5 ml of methanol were added, the solvent was evaporated under vacuum. The reaction mixture was dissolved in 200 ml of dichloromethane and washed with 400 ml of water. The organic phase was then dried under Na_2SO_4 and the solvent was removed under vacuum. The reaction mixture was purified by column chromatography (dichloromethane / cyclohexane, 3:7), to give afford 1-(4-bromo-butoxy)-4-(*tert*-butyl)benzene (yield: 27%)

I3: Colourless oil; Chemical formula: $\text{C}_{14}\text{H}_{21}\text{BrO}$; Molecular weight: $284.08 \text{ g mol}^{-1}$.

^1H NMR (400 MHz, CD_3OD): δ [ppm]: 7.30 [d, 2H, $J=8.8$ Ar-*H*], 6.83 [d, 2H, $J=8.8$, Ar-*H*], 3.98 [t, 2H, $J=6$ Hz, $-\text{CH}_2-\text{Br}$], 3.49 [t, 2H, $J=6.8$, O- CH_2-], 2.11-2.03 [m, 2H, Br- CH_2-CH_2-], 1.97-1.90 [m, 2H, $\text{CH}_2-\text{CH}_2-\text{O}-$], 1.30 [s, 9H, $\text{C}(\text{CH}_3)_3$].

4.2.1e. 1-(4-(4-(*tert*-butyl)phenoxy)butyl)-1'-methyl-[4,4'-bipyridin]-1,1'-dium bromide iodide (MC4^{2+})

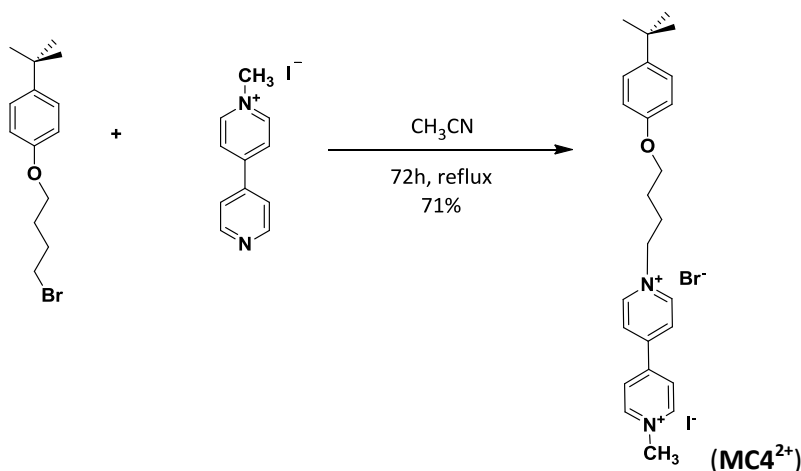


Figure 11. Synthesis of 1-(4-(4-(*tert*-butyl)phenoxy)butyl)-1'-methyl-[4,4'-bipyridin]-1,1'-dium bromide iodide (MC4^{2+})

1.58 g (~ 5.53 mmol) of **I3** was mixed with 1.5 g (~ 5.02 mmol) of **I1** (N-methyl-4,4'-bipyridinium iodide) in 30 ml of acetonitrile and the mixture was refluxed for three days. The reaction mixture was filtered and washed with acetonitrile to afford **MC4²⁺** (Figure 11) as a yellow-orange solid (yield: 71%).

MC4²⁺: yellow-orange solid; Chemical formula: C₂₅H₃₂ON₂I⁺Br⁻; Molecular weight: 582.07 g mol⁻¹; Melting point: 254-5 °C.

HR-MS for C₂₅H₃₂ON₂: [MC4²⁺] calcd. *m/z* = 188.1252 and exp. *m/z* = 188.1245.

¹H NMR (400 MHz, CD₃OD): δ [ppm]: 9.36 [d, 2H, *J*=7.2 Hz, Ar-*H*], 9.23 [d, 2H, *J*=6.8 Hz, Ar-*H*], 8.73 [d, 2H, *J*=6.8 Hz, Ar-*H*], 8.70 [d, 2H, *J*=6.8 Hz, Ar-*H*], 7.32 [d, 2H, *J*=8.8 Hz, Ar-*H*], 6.88 [d, 2H, *J*=8.8 Hz, Ar-*H*], 4.90 [t, 2H, *J*=7.6 Hz, N-CH₂-CH₂], 4.57 [s, 3H, N-CH₃], 4.10 [t, 2H, *J*=6 Hz, CH₂-O-Ar], 2.39-2.32 [m, 2H, N-CH₂-CH₂-CH₂], 2.00-1.93 [m, 2H, O-CH₂-CH₂-CH₂], 1.31 [s, 9H, C(CH₃)₃].

¹³C NMR (100 MHz, CD₃OD): δ [ppm]: 158.73, 152.13, 148.64, 148.01, 145.52, 129.21, 128.84, 128.09, 115.94, 69.03, 63.95, 35.70, 32.80, 30.55, 27.92.

4.2.1f. Tetrakis-*p*-*tert*-butyl-calix[4]arene (**I4**)

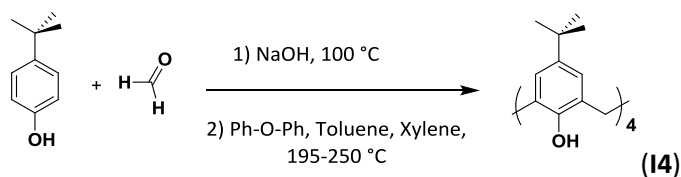


Figure 12. Synthesis of tetrakis-*p*-*tert*-butyl-calix[4]arene (**I4**)

The synthesis of the tetrakis-*p*-*tert*-butyl-calix[4]arene (Figure 12) was done in two steps. In the first step, 2.4 g (~ 60 mmol) of NaOH was added to the flask containing 200 gr (~ 1330 mmol) of *p*-*tert*-butylphenol in 125 ml formaldehyde (37%). The mixture was stirred at 100 °C for 2 hours to remove the water. The mixture started to become clear and then formed foam. After that step, the products that were obtained were the oligomers of *p*-*tert*-butylphenol. In a second step, the oligomers were mixed with 2 L of diphenylether, 80 ml of oxylene and 80 ml of toluene and the temperature was increased slowly until 185-195 °C and stirred for 2 h to remove the rest of the water as an azeotrope with toluene (bp = 110.6 °C) and with xylene (bp = 137 °C). The temperature of the reaction mixture was further increased to 250 °C for two additional hours. The mixture was then cooled down to 100 °C and 2 L of ethylacetate were added. The crude product was precipitated and washed with acetic acid and methanol. 137 g (211 mmol, yield: 63%) of a white powder was obtained as a pure product (**I4**). The ¹H and ¹³C NMR characterization of **I4** matches with that described in reference.^{28,29}

In the following, the calixarene-*bis*-viologens **C23⁴⁺** and **C24⁴⁺** (displaying a cone conformation) were prepared according to a two steps synthetic procedure. The first step

led to the intermediates **I5** (1,3-bis(3-bromopropoxy)-*p*-*tert*-butyl-calix[4]arene, Figure 13) and **I6** (1,3-bis(4-bromobutoxy)-*p*-*tert*-butyl-calix[4]arene) and were prepared according to the procedure described in the R. Pomecko's PhD work.²⁸ These intermediates were then reacted with **I1** (Figure 7) to obtain the targeted products **C23⁴⁺** and **C24⁴⁺** that were prepared following the method which was described by our collaborators (group of Pr Ali Trabolsi, NYUAD, Abu Dhabi, UAE) for synthesizing **HV¹²⁺**.¹

4.2.1g. 1,3-bis(3-bromopropoxy)-*p*-*tert*-butyl-calix[4]arene (**I5**)

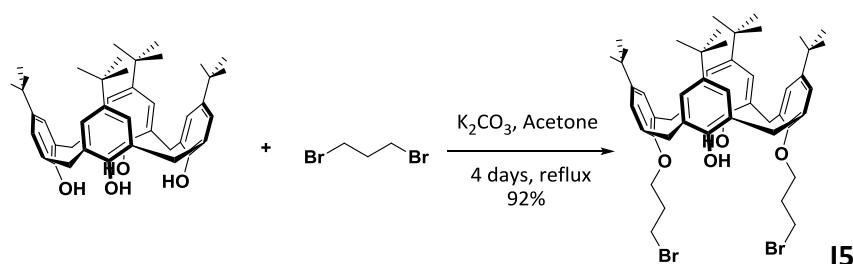


Figure 13. Synthesis of 1,3-bis(3-bromopropoxy)-*p*-*tert*-butyl-calix[4]arene (**I5**)

2.766 g (20 mmol) of K_2CO_3 was added to 6.49 g (10 mmol) of *tetrakis-p*-*tert*-butyl-calix[4]arene (**I4**) in 100 ml of acetone. The reaction mixture was stirred at RT for 2 hours, then 3 ml (30 mmol) of 1,3-dibromopropane in 100 ml of acetone was added into the flask. The reaction mixture was kept under reflux for 4 days. 5 ml of methanol was then added to the reaction mixture and the solvent was evaporated in vacuum. The reaction mixture was dissolved in 200 ml dichloromethane and washed with 400 ml of water. The organic phase was dried with Na_2SO_4 and the solvent was removed under vacuum. The crude product was purified by crystallization from 1/10 dichloromethane/methanol solvent to obtain 1,3-bis(3-bromopropoxy)-*p*-*tert*-butyl-calix[4]arene **I5** (Figure 13, yield: 92%). The 1H and ^{13}C NMR characterization of **I5** compares well with that described in reference²⁸ and will not be herein described.

I5: White solid; Chemical formula: $C_{50}H_{66}O_4Br_2$; Molecular weight: $888.33g\ mol^{-1}$.

1H NMR (400 MHz, $CDCl_3$): δ [ppm]: 7.69 [s, 2H, OH], 7.05 [s, 4H, Ar-H], 6.88 [s, 4H, Ar-H], 4.25 [d, 4H, $J=12.8$ Hz, Ar- CH_2 -Ar], 4.12 [t, 4H, $J=5.6$ Hz CH_2-CH_2-O], 4.01 [t, 4H, CH_2-CH_2-Br , $J=6.4$ Hz], 3.34 [d, 4H, $J=12$ Hz, Ar- CH_2 -Ar], 2.53-2.48 [m, 4H, CH_2-CH_2-O], 1.27 [s, 18H, $C(CH_3)_3$], 1.02 [s, 18H, $C(CH_3)_3$].

4.2.1h. 1,3-bis(3-(1'-methyl-[4,4'-bipyridin]-1,1'-diium)propoxy)-*p*-*tert*-butyl-calix[4]-arene dibromide diiodide (C23⁴⁺**)**

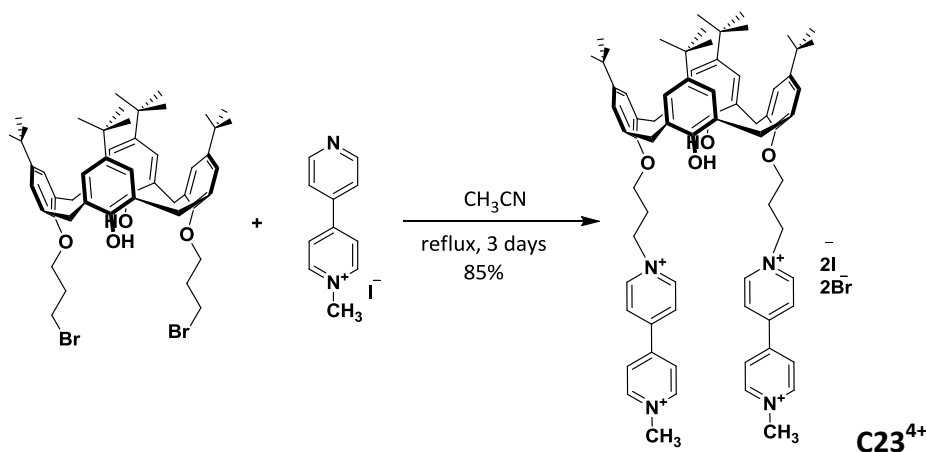


Figure 14. Synthesis of 1,3-bis(3-(1'-methyl-[4,4'-bipyridin]-1,1'-diium)propoxy)-*p*-*tert*-butyl-calix[4]arene dibromide diiodide (**C23⁴⁺**).

1.192 g (~ 4 mmol) of **I1** (1-methyl-[4,4'-bipyridin]-1-ium iodide, Figure 7) was added to the flask containing 0.365 g (~ 0.4 mmol) of **I5** and 30 ml of CH₃CN. The mixture was left under reflux for 3 days. The solvent was fully removed under vacuum. The product (**C23⁴⁺**, yield: 85%) was washed with water, filtrated and dried under vacuum.

C23⁴⁺: Red-orange solid; Chemical formula: C₇₂H₈₈O₄N₄I₂Br₂; Molecular weight: 1486 g mol⁻¹; Melting point: 295-6 °C.

HR-MS for C₇₂H₈₈O₄N₄: [**C23⁴⁺**+2e⁻]²⁺ calcd. *m/z* = 536.3397 and exp. *m/z* = 536.3382.

¹H NMR (400 MHz, CD₃OD): δ [ppm]: 9.60 [d, 4H, *J*=6.8 Hz, Ar-*H*], 9.22 [d, 4H, *J*=6.8 Hz, Ar-*H*], 8.82 [d, 4H, *J*=5.6 Hz, Ar-*H*], 8.74 [d, 4H, *J*=6.8 Hz, Ar-*H*], 7.22 [s, 4H, Ar(calix)-*H*], 7.07 [s, 4H, Ar(calix)-*H*], 5.30 [t, 4H, *J*=7.2 Hz, N-CH₂-CH₂], 4.56 [s, 6H, N-CH₃], 4.32-4.23 [d, 8H, Ar-CH₂-Ar and CH₂-O-Ar], 3.50 [d, 4H, *J*=13.6, Ar-CH₂-Ar], 3.02-2.95 [m, 4H, CH₂-CH₂-CH₂], 1.30 [s, 18H, C(CH₃)₃], 1.02 [s, 18H, C(CH₃)₃].

¹³C NMR (100 MHz, d₆-DMSO): δ [ppm]: 150.65, 150.36, 149.54, 148.80, 148.26, 147.52, 146.77, 142.61, 133.91, 128.37, 127.70, 127.00, 126.662, 126.31, 73.26, 58.88, 49.04, 34.92, 37.55, 32.39, 32.29, 31.76, 31.61.

4.2.1i. 1,3-bis(4-bromobutoxy)-*p*-*tert*-butyl-calix[4]arene (**16**)

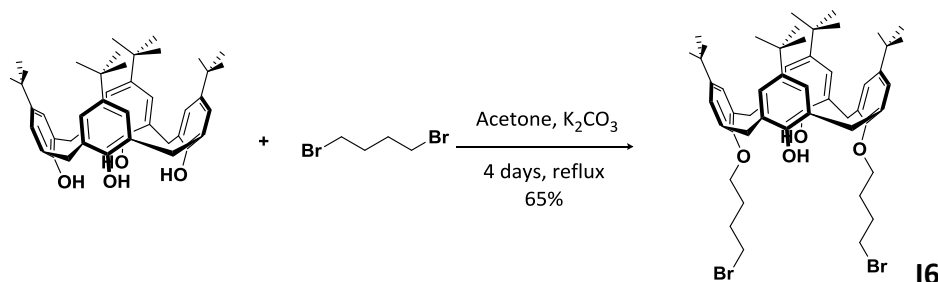


Figure 15. Synthesis of 1,3-bis(4-bromobutoxy)-*p*-*tert*-butyl-calix[4]arene (**16**).

3.244 g (~ 5 mmol) of *tetrakis-p-tert-butyl-calix[4]arene* and 1.383 g (~10 mmol) of K_2CO_3 were added to 50 ml of acetone and the mixture was stirred at RT for 2h. Then 3.236 g (~15 mmol) of 1,4-dibromobutane in 50 ml of acetone was added and the mixture was kept under reflux for four days. 5 ml of methanol were then added and the solvent was evaporated under vacuum. The reaction crude product was dissolved in 200 ml of dichloromethane and washed with 400 ml of water. The organic phase was dried under Na_2SO_4 and solvent was then removed under vacuum. The reaction mixture was purified by column chromatography (dichloromethane/cyclohexane 3:7) to give **I6** (Figure 15) as a white solid (yield: 65%). The 1H and ^{13}C NMR characterization of **I6** compares well with that described in reference²⁸ and will not be herein described.

I6: White solid; Chemical formula: $C_{52}H_{70}O_4Br_2$; Molecular weight: $918.92 \text{ g mol}^{-1}$.

1H NMR (400 MHz, $CDCl_3$): δ [ppm]: 7.40 [s, 2H, OH], 7.08 [s, 4H, Ar-H], 6.88 [s, 4H, Ar-H], 4.20 [d, 4H, $J=13 \text{ Hz}$, Ar- CH_2 -Ar], 4.05 [t, 4H, $J=5.4 \text{ Hz}$ CH_2 - CH_2 -O], 3.92 [t, 4H, CH_2 - CH_2 -Br], $J=6.6 \text{ Hz}$], 3.30 [d, 4H, $J=12 \text{ Hz}$, Ar- CH_2 -Ar], 2.58-2.52 [m, 4H, CH_2 - CH_2 -Br], 2.33-2.25 [m, 4H, CH_2 - CH_2 -O], 1.24 [s, 18H, $C(CH_3)_3$], 1.02 [s, 18H, $C(CH_3)_3$].

4.2.1j. 1,3-bis(3-(1'-methyl-[4,4'-bipyridin]-1,1'-diium)butoxy)-*p-tert-butyl-calix[4]arene* dibromide diiodide (**C24⁴⁺**)

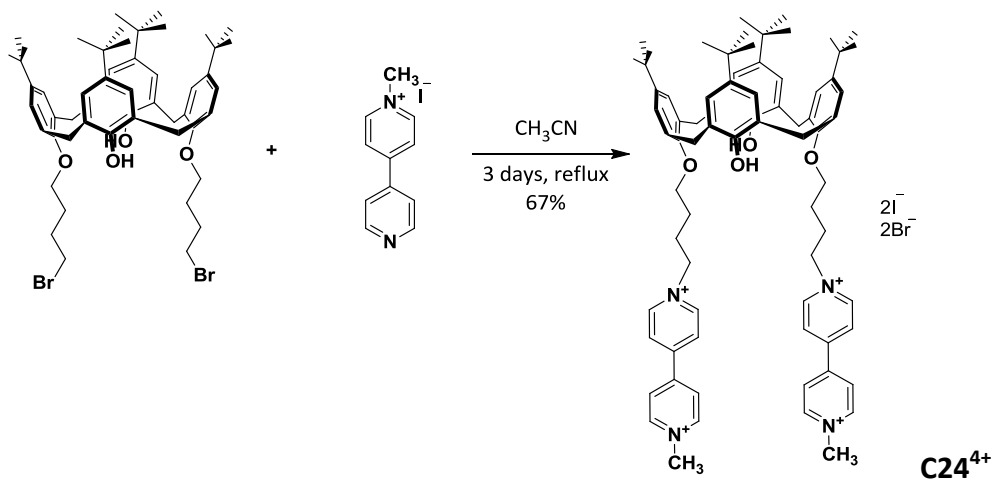


Figure 16. Synthesis of 1,3-bis(3-(1'-methyl-[4,4'-bipyridin]-1,1'-diium)butoxy)-*p-tert-butyl-calix[4]arene* dibromide diiodide (**C24⁴⁺**)

0.368 g (~ 0.4 mmol) of **I6** (1,3-bis(4-bromobutoxy)-*p-tert-butyl-calix[4]arene*, Figure 15) was dissolved in 30 ml of CH_3CN . 1.192 g (~ 4 mmol) of **I1** (1-methyl-[4,4'-bipyridin]-1-ium iodide, Figure 7) was added. The mixture was left under reflux for 3 days. The solvent was fully removed under vacuum. The product (**C24⁴⁺**, yield: 67%) was washed with water (due to its poor solubility in water), filtrated and dried under vacuum.

C24⁴⁺: Orange solid; Chemical formula: $C_{74}H_{92}O_4N_4I_2Br_2$; Molecular weight: $1514.93 \text{ g mol}^{-1}$; Melting point: $224-5 \text{ }^\circ\text{C}$.

HR-MS for C₇₄H₉₂O₄N₄: [C24⁴⁺+2e⁻]²⁺ calcd. *m/z* = 550.3554 and exp. *m/z* = 550.3561.

¹H NMR (400 MHz, CD₃OD): δ [ppm]: 9.54 [d, 4H, *J*=6.4 Hz, Ar-*H*], 9.21 [d, 4H, *J*=6.4 Hz, Ar-*H*], 8.78 [d, 4H, *J*=6.4 Hz, Ar-*H*], 8.71 [d, 4H, *J*=6.8 Hz, Ar-*H*], 7.19 [s, 4H, Ar(calix)-*H*], 7.05 [s, 4H, Ar(calix)-*H*], 5.15 [t, 4H, *J*=7.6 Hz, N-CH₂-CH₂], 4.56 [s, 6H, N-CH₃], 4.32 [d, 4H, *J*=12.8, Ar-CH₂-Ar], 4.16 [t, 4H, *J*=6.8 Hz, CH₂-O-Ar], 3.48 [d, 4H, *J*=12.8, Ar-CH₂-Ar], 2.66-2.58 [m, 4H, N-CH₂-CH₂-], 2.25-2.17 [m, 4H, -CH₂-CH₂-O], 1.29 [s, 18H, C(CH₃)₃], 1.02 [s, 18H, C(CH₃)₃].

¹³C NMR (100 MHz, DMSO): δ [ppm]: 150.79, 150.46, 149.51, 148.89, 148.10, 147.48, 146.74, 142.42, 134.02, 128.41, 127.57, 127.01, 126.56, 126.21, 76.01, 61.22, 49.02, 34.92, 34.52, 32.29, 31.79.

4.2.2. Physico-Chemistry

4.2.2a. Solvents and Starting Materials.

The reagents and the starting materials were purchased from commercial source and used without further purification. C24•2Br/2I, C23•2Br/2I and MC4•Br/I and MC3•Br/I were prepared as previously described. Cucurbit[7]uril (CB[7]) (C₄₂H₄₂N₂₈O₁₄, M. W. = 1162.96 g mol⁻¹, Strem chemicals) and cucurbit[8]uril (CB[8]) (C₄₈H₄₈N₃₂O₁₆, M.W. = 1329.11 g mol⁻¹, Aldrich) are commercial products that were used without further purification.

All solutions were prepared in distilled H₂O which was further purified by passing it through a mixed bed of ion-exchanger (Bioblock Scientific R3-83002, M3-83006) and activated carbon (Bioblock Scientific ORC-83005). It was then boiled and de-oxygenated using CO₂ and O₂ free argon prior to use (Sigma Oxiclear cartridge). All stock solutions were prepared using a Sartorius analytical balance (precision 0.1 mg), and complete dissolution in phosphate buffer was achieved using an ultrasonic bath (Branson 2510). The experiments were carried out at 25.0(2) °C maintained with the help of Haake FJ thermostats.

In all the solutions, the pH was maintained at 7.00 ± 0.05 by the use of a 0.1 M phosphate buffer, which was prepared by mixing 30.5 ml of Na₂HPO₄•2H₂O (0.2 M) (Prolabo) with 19.5 ml of NaH₂PO₄ (0.2 M) (Prolabo) and diluting to a total volume of 100 ml. The final pH of the solution was then set at the required value by using phosphoric acid (85%, Labosi). The pH was measured with an Ag/AgCl combined glass electrode (Metrohm 6.0234.500, long life) filled with 0.1 M NaCl (Fluka, p.a.) in H₂O. Standardization of the millivoltmeter and the verification of the linearity of the electrode response were performed using a set of NIST certified commercial Merck buffered solutions (pH 1.68, 4.00, 6.86, 7.41 and 9.18).

Chemical reduction of C24⁴⁺ and C23⁴⁺ and their corresponding models MC4²⁺ and MC3²⁺ into their corresponding radical cationic forms (C24^{2(•+)}, C23^{2(•+)}, MC4^{•+} and MC3^{•+}) was achieved under argon (CO₂- and O₂-free argon) with the addition of Na₂S₂O₄ solution in argon purged H₂O. The formation of the radicals was monitored by absorption spectrophotometry using a Cary 5000 UV-Vis.-NIR spectrophotometer.

4.2.2b. Analytical Methods

Routine Nuclear Magnetic Resonance (NMR) spectra were recorded at 298 K on Bruker Advance 400 spectrometers with working frequencies of 400 and 100 MHz for ^1H and ^{13}C , respectively. Chemical shifts are reported in ppm relative to the signals corresponding to the residual non-deuterated solvents (D_2O $\delta = 4.97$).

Electrospray mass (ESI-MS) spectra were measured on an ion-trap instrument (Bruker Esquire 3000plus, Bruker Daltonic, Bremen, Germany) equipped with an Agilent Technologies 6120 quadrupole equipped with an electrospray (ESI) interface.

Square wave voltammetry (SW) was carried out at room temperature in argon-purged H_2O and DMSO solutions with a Gamry Multipurpose instrument (Reference 600) interfaced to a PC. SW experiments were performed using a glassy carbon working electrode (0.071 cm^2 , BASi). The electrode surface was polished routinely with $0.05\text{ }\mu\text{m}$ alumina-water slurry on a felt surface immediately before use. The counter electrode was a Pt coil and the reference electrode was an Ag/AgCl electrode, unless otherwise noted. The concentration of the supporting electrolyte, tetrabutylammonium chloride (TBACl) was 0.1 M . The experimental errors on the potential values are estimated to $\pm 10\text{ mV}$.

UV-Vis.-NIR spectra were recorded on a Cary 5000 (Agilent) spectrophotometer maintained at $25.0(2)\text{ }^\circ\text{C}$ by the flow of a Dual Cell Pelletier Accessory (Cary Varian)

4.2.3. Spectrophotometric Titrations of Viologen Derivatives by CB[7].

The spectrophotometric titration of MC3^{2+} ($3.8 \times 10^{-5}\text{ M}$), MC4^{2+} ($3.3 \times 10^{-5}\text{ M}$), C23^{4+} ($3.3 \times 10^{-5}\text{ M}$) and C24^{4+} ($5.6 \times 10^{-5}\text{ M}$) with cucurbit(7)uril (CB[7]) were carried out in Hellma quartz optical cells of 10 mm pathlength in water at pH 7 (0.1 M phosphate buffer). Microvolumes of a concentrated solution of CB[7] ($1.2\text{--}5.16 \times 10^{-3}\text{ M}$) were added to the viologen derivatives MC3^{2+} ($l = 1\text{ cm}$, $v = 2\text{ ml}$), MC4^{2+} ($l = 1\text{ cm}$, $v = 2\text{ ml}$), C23^{4+} ($l = 1\text{ cm}$, $v = 2\text{ ml}$) and C24^{4+} ($l = 1\text{ cm}$, $v = 2\text{ ml}$) with the help of a microburette (Eppendorf). The $[\text{CB}[7]]_{\text{tot}}/[\text{BIPY}^{2+}]_{\text{tot}}$ ratios were varied from 0 to 2.9 for MC3^{2+} , from 0 to 1.9 for MC4^{2+} , from 0 to 42 for C23^{4+} and from 0 to 30.6 for C24^{4+} , respectively. Special care was taken to ensure that complete equilibration was attained. After each addition, a UV-Vis. spectrum was recorded from $220\text{ to }800\text{ nm}$ on a Cary 5000 (Agilent) spectrophotometer maintained at $25.0(2)\text{ }^\circ\text{C}$ by the flow of a Dual Cell Pelletier Accessory (Cary Varian).

4.2.3a. Recognition of MC3^{2+} by CB[7]

Figure 17A portrays the spectrophotometric titration of MC3^{2+} by CB[7], and Figure 17B presents the electronic spectra of MC3^{2+} and its inclusion complex $\text{MC3}^{2+}\text{--CB}[7]$ (isosbestic point at 292 nm). The expected 1:1 complex formation between MC3^{2+} and CB[7] has been confirmed by a Job plot measurement (Figure 18). The $\text{MC3}^{2+}\text{--CB}[7]$ [2]pseudorotaxane is characterized by a stability constant of $\log K_{\text{MC3}^{2+}\text{--CB}[7]} = 4.51(6)$.

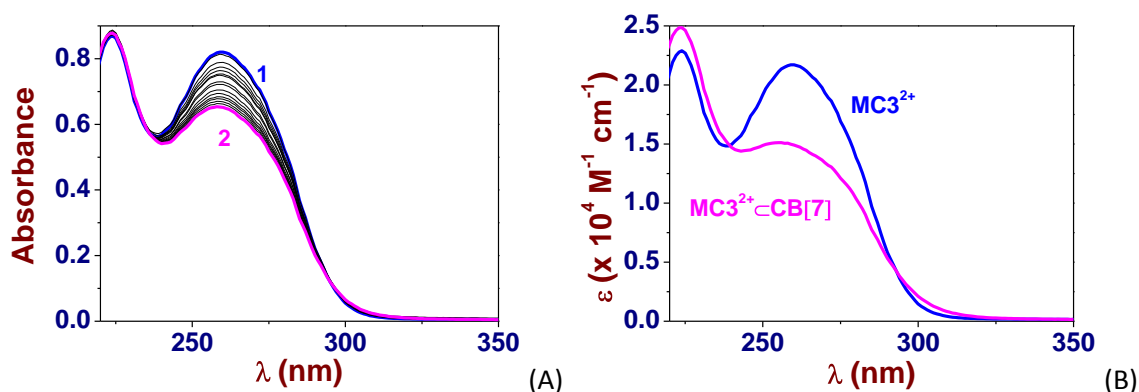


Figure 17. A) UV-Vis. absorption titration of MC3^{2+} by CB[7] . B) Electronic spectra of MC3^{2+} and its inclusion complex with CB[7] ($\text{MC3}^{2+} \subset \text{CB[7]}$). Solvent: water pH 7.0 (0.1 M $\text{Na}_2\text{H}_2\text{PO}_4/\text{NaH}_2\text{PO}_4$). $[\text{MC3}^{2+}]_0 = 3.8 \times 10^{-5} \text{ M}$; (1) $[\text{CB[7]}]_0/[\text{MC3}^{2+}]_0 = 0$; (2) $[\text{CB[7]}]_0/[\text{MC3}^{2+}]_0 = 2.9$; $l = 1 \text{ cm}$; $T = 25.0(1)^\circ\text{C}$. The absorption spectra are not corrected from dilution effects.

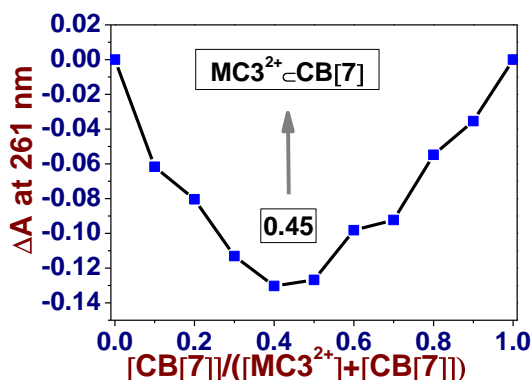


Figure 18. Job plot (ΔA at 261 nm) upon mixing MC3^{2+} with CB[7] at pH 7. ($[\text{MC3}^{2+}]_0 + [\text{CB[7]}]_0 = 7.0 \times 10^{-5} \text{ M}$; Solvent: water pH 7.0 (0.1 M $\text{Na}_2\text{H}_2\text{PO}_4/\text{NaH}_2\text{PO}_4$); $l = 1 \text{ cm}$; $T = 25.0(1)^\circ\text{C}$).

4.2.3b. Recognition of MC4^{2+} by CB[7]

Similarly to MC3^{2+} with CB[7] , Figure 19A gathers the spectral absorption data that have been recorded during the spectrophotometric titration of MC4^{2+} by CB[7] .

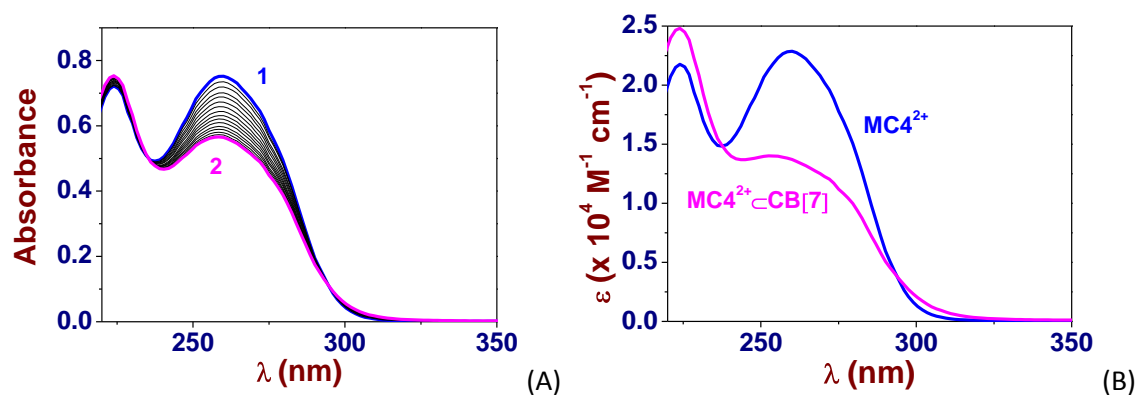


Figure 19. A) UV-Vis. absorption titration of MC4^{2+} by CB[7] . B) Electronic spectra of MC4^{2+} and its inclusion complex with CB[7] ($\text{MC4}^{2+} \subset \text{CB[7]}$). Solvent: water pH 7.0 (0.1 M $\text{Na}_2\text{H}_2\text{PO}_4/\text{NaH}_2\text{PO}_4$). $[\text{MC4}^{2+}]_0 = 3.3 \times 10^{-5} \text{ M}$; (1) $[\text{CB[7]}]_0/[\text{MC4}^{2+}]_0 = 0$; (2) $[\text{CB[7]}]_0/[\text{MC4}^{2+}]_0 = 1.9$; $l = 1 \text{ cm}$; $T = 25.0(1)^\circ\text{C}$. The absorption spectra are not corrected from dilution effects.

The electronic spectra depicted in Figure 19B suggested the formation of a predominant [2]pseudorotaxane $\text{MC4}^{2+} \subset \text{CB}[7]$ ($\log K_{\text{MC4}^{2+} \subset \text{CB}[7]} = 4.68(5)$) (two isosbestic points at 238 and 293.5 nm). The job plot presented in Figure 19B further confirmed the formation of a major 1:1 stoichiometric complex with MC4^{2+} and $\text{CB}[7]$.

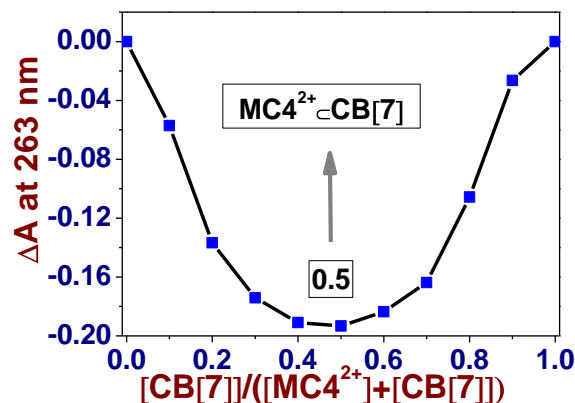


Figure 20. Job plot (ΔA at 263 nm) upon mixing MC4^{2+} with $\text{CB}[7]$ at pH 7. ($[\text{MC4}^{2+}]_0 + [\text{CB}[7]]_0 = 7.0 \times 10^{-5} \text{ M}$; Solvent :water pH 7.0 (0.1 M $\text{Na}_2\text{H}_2\text{PO}_4/\text{NaH}_2\text{PO}_4$); $l = 1 \text{ cm}$; $T = 25.0(1)^\circ\text{C}$).

4.2.3c. Recognition of C23^{4+} by $\text{CB}[7]$

The calix[4]arene-*bis*-viologen C23^{4+} possesses 2 viologen units that can be each encircled by a $\text{CB}[7]$ macrocycle ultimately leading to a [3]pseudorotaxane $\text{C23}^{4+} \subset (\text{CB}[7])_2$. Figure 21A describes the spectral absorption variation that have been measured during the absorption spectrophotometric titration of C23^{4+} by $\text{CB}[7]$. Only an apparent association constant^{30,31} ($\log K^*_{\text{C23}^{4+} \subset (\text{CB}[7])_2} = 4.5(1)$) was deduced from the processing of the absorption data. The job plot presented in Figure 22 further confirmed the predominant formation of the $\text{C23}^{4+} \subset (\text{CB}[7])_2$ species (isosbestic point at 297 nm).

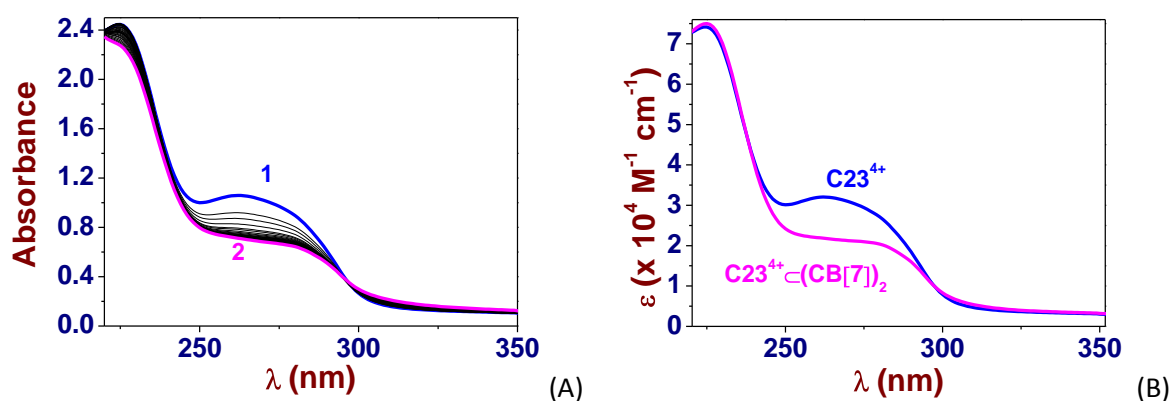


Figure 21. A) UV-Vis. absorption titration of C23^{4+} by $\text{CB}[7]$. B) Electronic spectra of C23^{4+} and its inclusion complex with $\text{CB}[7]$ ($\text{C23}^{4+} \subset (\text{CB}[7])_2$). Solvent: water pH 7.0 (0.1 M $\text{Na}_2\text{H}_2\text{PO}_4/\text{NaH}_2\text{PO}_4$). $[\text{C23}^{4+}]_0 = 3.3 \times 10^{-5} \text{ M}$; (1) $[\text{CB}[7]]_0/[\text{C23}^{4+}]_0 = 0$; (2) $[\text{CB}[7]]_0/[\text{C23}^{4+}]_0 = 42.2$; $l = 1 \text{ cm}$; $T = 25.0(1)^\circ\text{C}$. The absorption spectra are not corrected from dilution effects.

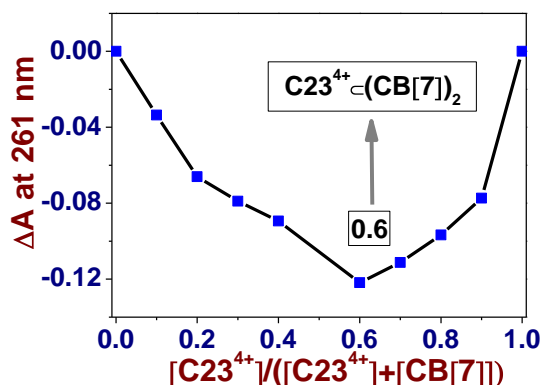


Figure 22. Job plot (ΔA at 261 nm) upon mixing $C23^{4+}$ with $CB[7]$ at pH 7. ($[C23^{2+}]_0 + [CB[7]]_0 = 6.9 \times 10^{-5}$ M; Solvent :water pH 7.0 (0.1 M $Na_2H_2PO_4/NaH_2PO_4$); $l = 1$ cm; $T = 25.0(1)^\circ C$).

4.2.3d. Recognition of $C24^{4+}$ by $CB[7]$

The homologous system $C24^{4+}$ similarly behaves as $C23^{4+}$ in the presence of $CB[7]$. A predominant [3]pseudorotaxane $C24^{4+} \subset (CB[7])_2$ has been evidenced (isosbestic point at 293 nm) by our spectrophotometric measurements (Figure 23). Similarly to $C23^{4+}$, an apparent stability constant was accordingly evaluated ($\log K^*_{C234+(CB[7])2} = 4.44(8)$).

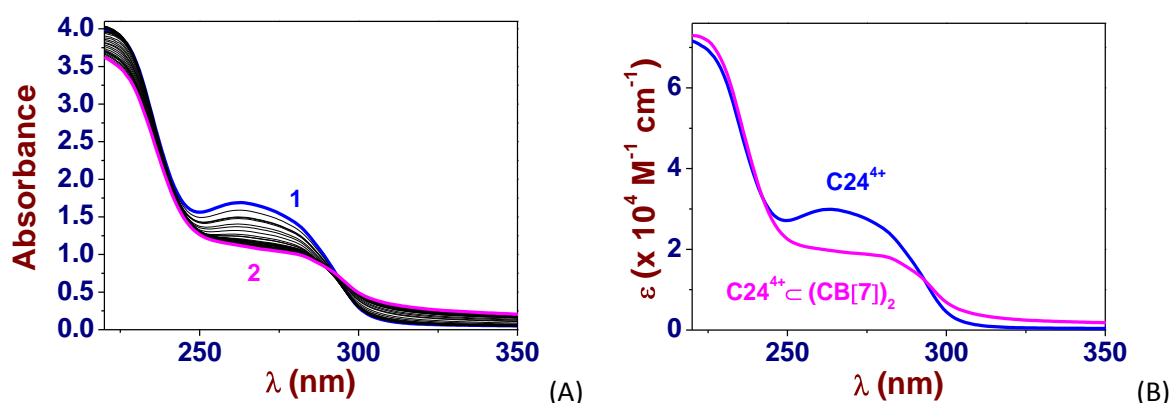


Figure 23. A) UV-Vis. absorption titration of $C24^{4+}$ by $CB[7]$. B) Electronic spectra of $C24^{4+}$ and its inclusion complex with $CB[7]$ ($C24^{4+} \subset (CB[7])_2$). Solvent: water pH 7.0 (0.1 M $Na_2H_2PO_4/NaH_2PO_4$). $[C24^{4+}]_0 = 5.6 \times 10^{-5}$ M; (1) $[CB[7]]_0/[C24^{4+}]_0 = 0$; (2) $[CB[7]]_0/[C24^{4+}]_0 = 24.5$; $l = 1$ cm; $T = 25.0(1)^\circ C$. The absorption spectra are not corrected from dilution effects.

4.2.4. Stoichiometry of the [n]Pseudorotaxane with $MC3^{2+}$, $MC4^{2+}$, $C23^{4+}$ and $C24^{4+}$ Probed by ESI-MS

Electrospray ionization mass spectra (ESI-MS) of the host-guest complexes formed with $MC3^{2+}$, $MC4^{2+}$, $C23^{4+}$ or $C24^{4+}$ with $CB[7]$ (and $CB[8]$) were carried out with an ion-trap instrument (Bruker Esquire 3000plus, Bruker Daltonic, Bremen, Germany) equipped with an Agilent Technologies 6120 quadrupole equipped with an electrospray (ESI) interface. The sample solutions were continuously introduced into the spectrometer source with a syringe pump (Kd Scientific) with a flow rate of $800 \mu L h^{-1}$. For electrospray ionization, the drying gas was heated at $250^\circ C$ and its flow was set at $6 L min^{-1}$. The capillary exit voltage was fixed at

5 kV and the skimmer voltage was varied from 50 to 300 V in order to optimize the signal responses. Scanning was performed from $m/z = 100$ to 1500. The stoichiometries of the pseudorotaxanes were investigated by electrospray mass spectrometry (ESI-MS) in the positive mode in aqueous solutions. The ionization of the viologen derivatives and complexes (mainly observed as mono-, doubly or triply positively charged species) takes place by reduction, deprotonation and/or by addition of sodium cations. Fragmentations such as demethylation or dealkylation of the substituents were also observed.

Figure 24B first depicts the ESI-MS spectrum obtained for a 55 μM solution of MC3^{2+} (Figure 24A) combined to 5 equivalents of $\text{CB}[7]$. Similarly, Figure 24D shows the results of a ESI-MS experiment conducted with a 55 μM solution of MC3^{2+} and 1 equivalent of $\text{CB}[8]$. A [2]pseudorotaxane species $\text{MC3}^{2+}\text{CB}[n]$ ($n = 7,8$) has been clearly identified and its presence matches with the observations made by absorption spectrophotometry (*vide supra*). Interestingly, the measurements done at a higher concentration of MC3^{2+} and with a $[\text{CB}[7]]_0/[\text{MC3}^{2+}]_0 = 10$ evidenced the formation of a second host-guest complex, namely the [3]pseudorotaxane $\text{MC3}^{2+}(\text{CB}[7])_2$ which likely results from the presence of a hydrophobic substituent. Even though this species was also confirmed by ^1H NMR experiments (*vide infra*), we were unable to characterize and quantify this species by absorption titrations (*i.e.* the stability of this complex is expected to be low for steric hindrance reasons and the inclusion of a second $\text{CB}[7]$ macrocycle is anticipated to induce weak absorption variations).

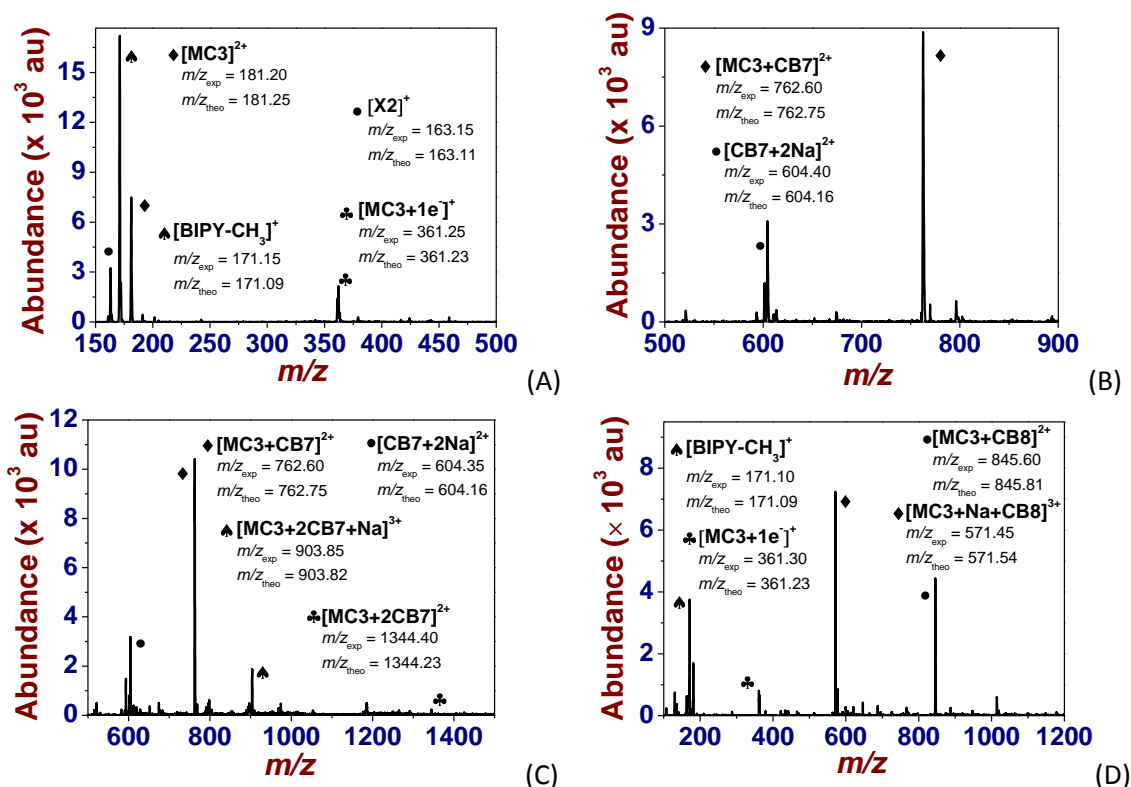


Figure 24. (A) ESI mass spectrum of free MC3^{2+} . $[\text{MC3}^{2+}]_0 = 5.5 \times 10^{-5}$ M. Solvent: H_2O ; positive mode. $V_c = 100$ V. $\bullet = [\text{X2}]^+$, $m/z_{\text{exp}} = 163.15$, $m/z_{\text{theo}} = 163.11$ with $\text{X2} = ^+\text{CH}_2\text{-O-C}_6\text{H}_4\text{-C}(\text{CH}_3)_3$. $\blackspadesuit = [\text{BIPY-CH}_3]^+$, $m/z_{\text{exp}} = 171.15$, $m/z_{\text{theo}} = 171.09$. $\blacklozenge = [\text{MC3}]^{2+}$, $m/z_{\text{exp}} = 181.20$, $m/z_{\text{theo}} = 181.25$. $\blackspade = [\text{MC3}+1\text{e}]^+$, $m/z_{\text{exp}} = 361.25$, $m/z_{\text{theo}} = 361.23$.

(B) ESI mass spectrum of inclusion complexes of MC3^{2+} with $\text{CB}[7]$. $[\text{MC3}^{2+}]_0 = 5.5 \times 10^{-5} \text{ M}$; $[\text{CB}[7]]_0 = 2.75 \times 10^{-4} \text{ M}$. Solvent: H_2O ; positive mode. $V_c = 280 \text{ V}$. $\bullet = [\text{CB}[7]+2\text{Na}]^{2+}$, $m/z_{\text{exp}} = 604.40$, $m/z_{\text{theo}} = 604.16$. $\blacklozenge = [\text{MC3}+\text{CB}[7]]^{2+}$, $m/z_{\text{exp}} = 762.60$, $m/z_{\text{theo}} = 762.75$.

(C) ESI mass spectrum of inclusion complexes of MC3^{2+} with $\text{CB}[7]$. $[\text{MC3}^{2+}]_0 = 10^{-4} \text{ M}$; $[\text{CB}[7]]_0 = 10^{-3} \text{ M}$. Solvent: H_2O ; positive mode. $V_c = 100 \text{ V}$. $\bullet = [\text{CB}[7]+2\text{Na}]^{2+}$, $m/z_{\text{exp}} = 604.35$, $m/z_{\text{theo}} = 604.16$. $\blacklozenge = [\text{MC3}+\text{CB}[7]]^{2+}$, $m/z_{\text{exp}} = 762.60$, $m/z_{\text{theo}} = 762.75$. $\spadesuit = [\text{MC3}+2\text{CB}[7]+\text{Na}]^{3+}$, $m/z_{\text{exp}} = 903.85$, $m/z_{\text{theo}} = 903.82$. $\clubsuit = [\text{MC3}+2\text{CB}[7]]^{2+}$, $m/z_{\text{exp}} = 1344.40$, $m/z_{\text{theo}} = 1344.23$.

(D) ESI mass spectrum of inclusion complexes of MC3^{2+} with $\text{CB}[8]$. $[\text{MC3}^{2+}]_0 = 5.5 \times 10^{-5} \text{ M}$; $[\text{CB}[8]]_0 = 5.5 \times 10^{-5} \text{ M}$. Solvent: H_2O ; positive mode. $V_c = 100 \text{ V}$. $\spadesuit = [\text{BIPY}-\text{CH}_3]^+$, $m/z_{\text{exp}} = 171.10$, $m/z_{\text{theo}} = 171.09$. $\clubsuit = [\text{MC3}+1\text{e}]^+$, $m/z_{\text{exp}} = 361.30$, $m/z_{\text{theo}} = 361.23$. $\blacklozenge = [\text{MC3}+\text{Na}+\text{CB}[8]]^{3+}$, $m/z_{\text{exp}} = 571.45$, $m/z_{\text{theo}} = 571.54$. $\bullet = [\text{MC3}+\text{CB}[8]]^{2+}$, $m/z_{\text{exp}} = 845.60$, $m/z_{\text{theo}} = 845.81$. The ESI-MS spectra were limited to the areas of interest. No peaks were detected in the excluded m/z regions.

The same observations stand for MC4^{2+} with $\text{CB}[7]$ or $\text{CB}[8]$ (Figure 25). A [2]pseudorotaxane $\text{MC3}^{2+} \subset \text{CB}[7]$ has been clearly evidenced. In addition, a $\text{MC3}^{2+} \subset (\text{CB}[7])_2$ has been characterized under high excess of $\text{CB}[7]$ in agreement with the ^1H NMR (*vide infra*) data but was not quantified using absorption spectrophotometry.

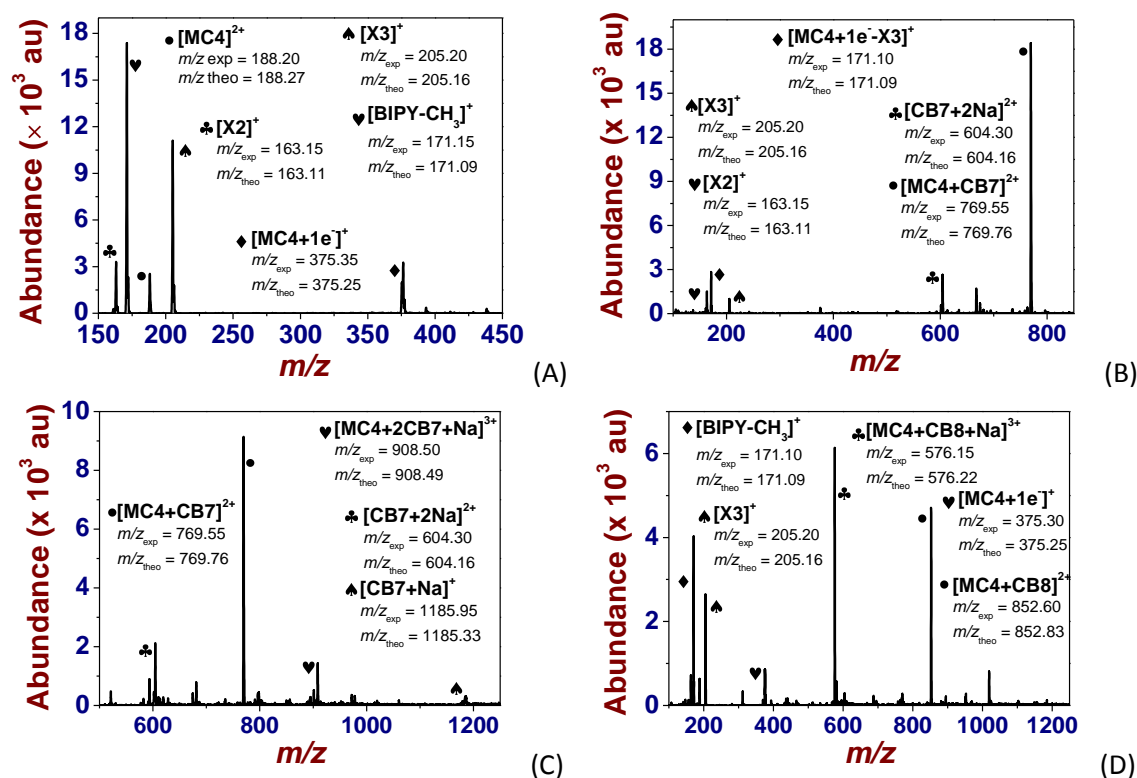


Figure 25. (A) ESI mass spectrum of free MC4^{2+} . $[\text{MC4}^{2+}]_0 = 5.5 \times 10^{-5} \text{ M}$. Solvent: H_2O ; positive mode. $V_c = 100 \text{ V}$. $\clubsuit = [\text{X2}]^+$, $m/z_{\text{exp}} = 163.15$, $m/z_{\text{theo}} = 163.11$ with $\text{X2} = ^+\text{CH}_2\text{-O-C}_6\text{H}_4\text{-C}(\text{CH}_3)_3$. $\heartsuit = [\text{BIPY}-\text{CH}_3]^+$, $m/z_{\text{exp}} = 171.15$, $m/z_{\text{theo}} = 171.09$. $\bullet = [\text{MC4}]^{2+}$, $m/z_{\text{exp}} = 188.20$, $m/z_{\text{theo}} = 188.27$. $\spadesuit = [\text{X3}]^+$, $m/z_{\text{exp}} = 205.20$, $m/z_{\text{theo}} = 205.16$ with $\text{X3} = ^+\text{CH}_2\text{-CH}_2\text{-CH}_2\text{-CH}_2\text{-O-C}_6\text{H}_4\text{-C}(\text{CH}_3)_3$. $\blacklozenge = [\text{MC4}+1\text{e}]^+$, $m/z_{\text{exp}} = 375.35$, $m/z_{\text{theo}} = 375.25$.

(B) ESI mass spectrum of inclusion complexes of MC4^{2+} with $\text{CB}[7]$. $[\text{MC4}^{2+}]_0 = 5.5 \times 10^{-5} \text{ M}$; $[\text{CB}[7]]_0 = 2.75 \times 10^{-4} \text{ M}$. Solvent: H_2O ; positive mode. $V_c = 240 \text{ V}$. $\heartsuit = [\text{X2}]^+$, $m/z_{\text{exp}} = 163.15$, $m/z_{\text{theo}} = 163.11$ with $\text{X2} = ^+\text{CH}_2\text{-O-C}_6\text{H}_4\text{-C}(\text{CH}_3)_3$. $\spadesuit = [\text{X3}]^+$, $m/z_{\text{exp}} = 205.20$, $m/z_{\text{theo}} = 205.16$ with $\text{X3} = ^+\text{CH}_2\text{-CH}_2\text{-CH}_2\text{-}$

$\text{CH}_2\text{-O-C}_6\text{H}_4\text{-C}(\text{CH}_3)_3$. $\clubsuit = [\text{CB}[7]+2\text{Na}]^{2+}$, $m/z_{\text{exp}} = 604.30$, $m/z_{\text{theo}} = 604.16$. $\bullet = [\text{MC4}+\text{CB}[7]]^{2+}$, $m/z_{\text{exp}} = 769.55$, $m/z_{\text{theo}} = 769.76$.

(C) ESI mass spectrum of inclusion complexes of MC4^{2+} with $\text{CB}[7]$. $[\text{MC4}^{2+}]_0 = 10^{-4}$ M; $[\text{CB}[7]]_0 = 10^{-3}$ M. Solvent: H_2O ; positive mode. $V_c = 100$ V. $\clubsuit = [\text{CB}[7]+2\text{Na}]^{2+}$, $m/z_{\text{exp}} = 604.30$, $m/z_{\text{theo}} = 604.16$. $\bullet = [\text{MC4}+\text{CB}[7]]^{2+}$, $m/z_{\text{exp}} = 769.55$, $m/z_{\text{theo}} = 769.76$. $\heartsuit = [\text{MC4}+2\text{CB}[7]+\text{Na}]^{3+}$, $m/z_{\text{exp}} = 908.50$, $m/z_{\text{theo}} = 908.49$. $\spadesuit = [\text{CB}[7]+\text{Na}]^+$, $m/z_{\text{exp}} = 1185.95$, $m/z_{\text{theo}} = 1185.33$.

(D) ESI mass spectrum of inclusion complexes of MC4^{2+} with $\text{CB}[8]$. $[\text{MC4}^{2+}]_0 = 5 \times 10^{-5}$ M; $[\text{CB}[7]]_0 = 5 \times 10^{-5}$ M. Solvent: H_2O ; positive mode. $V_c = 100$ V. $\blacklozenge = [\text{BIPY-CH}_3]^+$, $m/z_{\text{exp}} = 171.15$, $m/z_{\text{theo}} = 171.09$. $\spadesuit = [\text{X3}]^+$, $m/z_{\text{exp}} = 205.20$, $m/z_{\text{theo}} = 205.16$ with $\text{X3} = ^+\text{CH}_2\text{-CH}_2\text{-CH}_2\text{-CH}_2\text{-O-C}_6\text{H}_4\text{-C}(\text{CH}_3)_3$. $\heartsuit = [\text{MC4}+1\text{e}^-]^+$, $m/z_{\text{exp}} = 375.30$, $m/z_{\text{theo}} = 375.25$. $\clubsuit = [\text{MC4}+\text{CB}[8]+\text{Na}]^{3+}$, $m/z_{\text{exp}} = 576.15$, $m/z_{\text{theo}} = 576.22$. $\bullet = [\text{MC4}+\text{CB}[8]]^{2+}$, $m/z_{\text{exp}} = 852.60$, $m/z_{\text{theo}} = 852.83$. The ESI-MS spectra were limited to the areas of interest. No peaks were detected in the excluded m/z regions.

Figure 26 now depicts the ESI-MS spectra that were recorded for aqueous solutions containing $\sim 50 \mu\text{M}$ C23^{4+} mixed with 3 equivalents of $\text{CB}[7]$ (Figure 26B) and 2 equivalents of $\text{CB}[8]$ (Figure 26C), respectively. Similarly, Figure 27 shows the ESI-MS experiments recorded for solutions that contain C24^{4+} ($\sim 50 \mu\text{M}$) mixed with either $\text{CB}[7]$ (3 equivalents, Figure 27B) or $\text{CB}[8]$ (2 equivalents, Figure 27C). As anticipated, a [2]pseudorotaxane $\text{C2x}^{4+} \subset \text{CB}[n]$ and a [3]pseudorotaxane $\text{C2x}^{4+} \subset (\text{CB}[n])_2$ ($x = 3$ or 4 and $n = 7$ or 8) were evidenced regardless the size of the macrocyclic host or the chain length connecting the calix[4]arene platform to the terminal electroactive bipyridinium units.

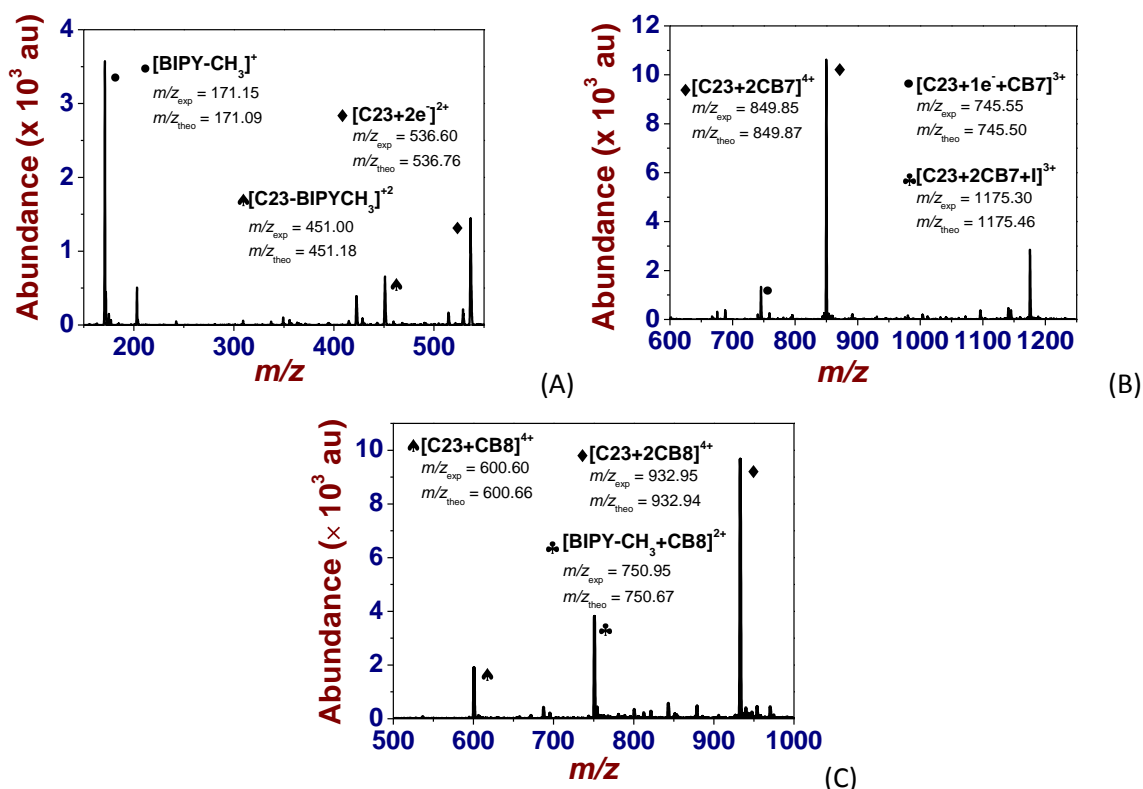


Figure 26. (A) ESI mass spectrum of free C23^{4+} . $[\text{C23}^{4+}]_0 = 4.9 \times 10^{-5}$ M. Solvent: H_2O ; positive mode. $V_c = 150$ V. $\bullet = [\text{BIPY-CH}_3]^+$, $m/z_{\text{exp}} = 171.15$, $m/z_{\text{theo}} = 171.09$. $\heartsuit = [\text{C23}^{4+}\text{-BIPY-CH}_3]^{2+}$, $m/z_{\text{exp}} = 451.00$, $m/z_{\text{theo}} = 451.18$. $\blacklozenge = [\text{C23}^{4+}+2\text{e}^-]^{2+}$, $m/z_{\text{exp}} = 536.60$, $m/z_{\text{theo}} = 536.76$.

(B) ESI mass spectrum of inclusion complexes of C23^{4+} with $\text{CB}[7]$. $[\text{C23}^{4+}]_0 = 4.7 \times 10^{-5} \text{ M}$; $[\text{CB}[7]]_0 = 1.41 \times 10^{-4} \text{ M}$. Solvent: H_2O ; positive mode. $V_c = 300 \text{ V}$. $\bullet = [\text{C23}^{4+} + 1\text{e}^- + \text{CB}[7]]^{3+}$, $m/z_{\text{exp}} = 745.55$, $m/z_{\text{theo}} = 745.50$. $\blacklozenge = [\text{C23}^{4+} + 2\text{CB}[7]]^{4+}$, $m/z_{\text{exp}} = 849.85$, $m/z_{\text{theo}} = 849.87$. $\clubsuit = [\text{C23}^{4+} + 2\text{CB}[7] + \text{I}]^{3+}$, $m/z_{\text{exp}} = 1175.30$, $m/z_{\text{theo}} = 1175.46$.

(C) ESI mass spectrum of inclusion complexes of C23^{4+} with $\text{CB}[8]$. $[\text{C23}^{4+}]_0 = 5 \times 10^{-5} \text{ M}$; $[\text{CB}[8]]_0 = 10^{-4} \text{ M}$. Solvent: H_2O ; positive mode. $V_c = 200 \text{ V}$. $\heartsuit = [\text{C23}^{4+} + \text{CB}[8]]^{4+}$, $m/z_{\text{exp}} = 600.60$, $m/z_{\text{theo}} = 600.66$. $\clubsuit = [\text{BIPY-CH}_3 + \text{CB}[8]]^{2+}$, $m/z_{\text{exp}} = 750.95$, $m/z_{\text{theo}} = 750.67$. $\blacklozenge = [\text{C23}^{4+} + 2\text{CB}[8]]^{4+}$, $m/z_{\text{exp}} = 932.95$, $m/z_{\text{theo}} = 932.94$.

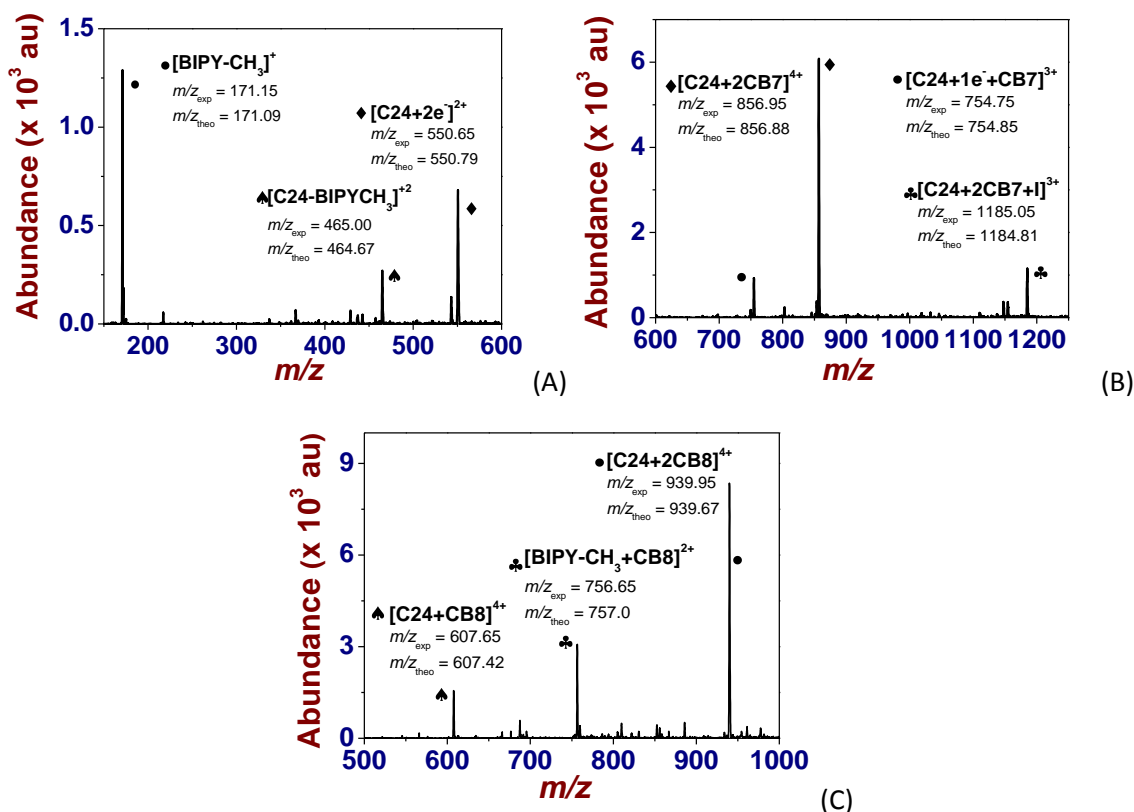


Figure 27. (A) ESI mass spectrum of free C24^{4+} . $[\text{C24}^{4+}]_0 = 4.7 \times 10^{-5} \text{ M}$. Solvent: H_2O ; positive mode. $V_c = 150 \text{ V}$. $\bullet = [\text{BIPY-CH}_3]^+$, $m/z_{\text{exp}} = 171.15$, $m/z_{\text{theo}} = 171.09$. $\heartsuit = [\text{C24}^{4+} - \text{BIPY-CH}_3]^{2+}$, $m/z_{\text{exp}} = 465.00$, $m/z_{\text{theo}} = 464.67$. $\blacklozenge = [\text{C24}^{4+} + 2\text{e}]^{2+}$, $m/z_{\text{exp}} = 550.65$, $m/z_{\text{theo}} = 550.79$.

(B) ESI mass spectrum of inclusion complexes of C24^{4+} with $\text{CB}[7]$. $[\text{C24}^{4+}]_0 = 4.7 \times 10^{-5} \text{ M}$; $[\text{CB}[7]]_0 = 1.41 \times 10^{-4} \text{ M}$. Solvent: H_2O ; positive mode. $V_c = 240 \text{ V}$. $\bullet = [\text{C24}^{4+} + 1\text{e}^- + \text{CB}[7]]^{3+}$, $m/z_{\text{exp}} = 754.75$, $m/z_{\text{theo}} = 754.85$. $\blacklozenge = [\text{C24}^{4+} + 2\text{CB}[7]]^{4+}$, $m/z_{\text{exp}} = 856.95$, $m/z_{\text{theo}} = 856.88$. $\clubsuit = [\text{C24}^{4+} + 2\text{CB}[7] + \text{I}]^{3+}$, $m/z_{\text{exp}} = 1185.05$, $m/z_{\text{theo}} = 1184.81$.

(C) ESI mass spectrum of inclusion complexes of C24^{4+} with $\text{CB}[8]$. $[\text{C24}^{4+}]_0 = 5 \times 10^{-5} \text{ M}$; $[\text{CB}[8]]_0 = 10^{-4} \text{ M}$. Solvent: H_2O ; positive mode. $V_c = 100 \text{ V}$. $\spadesuit = [\text{C24}^{4+} + \text{CB}[8]]^{4+}$, $m/z_{\text{exp}} = 607.65$, $m/z_{\text{theo}} = 607.42$. $\clubsuit = [\text{BIPY-CH}_3 + \text{CB}[8]]^{2+}$, $m/z_{\text{exp}} = 756.65$, $m/z_{\text{theo}} = 757.25$. $\bullet = [\text{C24}^{4+} + 2\text{CB}[8]]^{4+}$, $m/z_{\text{exp}} = 939.95$, $m/z_{\text{theo}} = 939.67$.

4.2.5. $\text{MC3}^{2+}/\text{MC4}^{2+}$ Recognition by $\text{CB}[7]$ Probed by ^1H NMR Spectroscopy

To evaluate the binding mode between the model guests $\text{MC3}^{2+}/\text{MC4}^{2+}$ and $\text{CB}[7]$, titration experiments were carried out in D_2O and monitored using ^1H NMR spectroscopy (Figure 28 for MC3^{2+} and Figure 29 for MC4^{2+}).

4.2.5a. ^1H NMR Titration of MC3^{2+} by $\text{CB}[7]$

Increasing amounts (up to 2 equivalents) of a solution of $\text{CB}[7]$ in D_2O were added to 500 μL of a concentrated solution of MC3^{2+} (3.5×10^{-3} M). Up to 1 equivalent of $\text{CB}[7]$, the ^1H NMR spectra clearly revealed a large upfield shift of the β -protons of the viologen moiety, while the α/α' protons were found to be unaltered by $\text{CB}[7]$ complexation. By contrast with the other systems described so far, a slow exchange with respect to the NMR timescale can be proposed on the basis of the presence of two sets of β/β' resonances (*i.e.* related to free and complexed MC3^{2+}) and important line broadening. In addition, the protons signal arising from the methyl (*i.e.* *a* protons) or propyloxy substituents (*i.e.* *b*, *c* and *d* protons) of the viologen unit were also found to be unchanged. This is a strong indication of the formation of a first inclusion complex between MC4^{2+} and $\text{CB}[7]$, namely the [2]pseudorotaxane $\text{MC3}^{2+} \subset \text{CB}[7]$, for which the macrocyclic guest is likely sitting in the middle of the bipyridinium dication (kinetically inert species). This observation is in excellent agreement with the absorption spectrophotometric studies (Figure 17) and the ES-MS data (Figure 24).

Strikingly, after 1 equivalent and up to the end of the titration (2 equivalents), the *e*, *f* and *g* protons that belong to the *tert*-butyl-phenyl residue experienced marked upfield shifts while those of the α/α' , β/β' and propyloxy chain (*b*, *c* and *d*) remained unaffected. This result strongly suggests that, once the MC4^{2+} thread is encircled by a first $\text{CB}[7]$ macrocycle through its viologen unit, an additional $\text{CB}[7]$ molecule can sterically encapsulate the terminal hydrophobic aromatic unit (*i.e.* *tert*-butyl-phenyl) of the wire ultimately yielding a 2:1 complex ($\text{MC3}^{2+} \subset (\text{CB}[7])_2$) that was previously identified by an ESI-MS approach at a high $[\text{CB}[7]]_0/[\text{MC4}^{2+}]_0$ ratio.

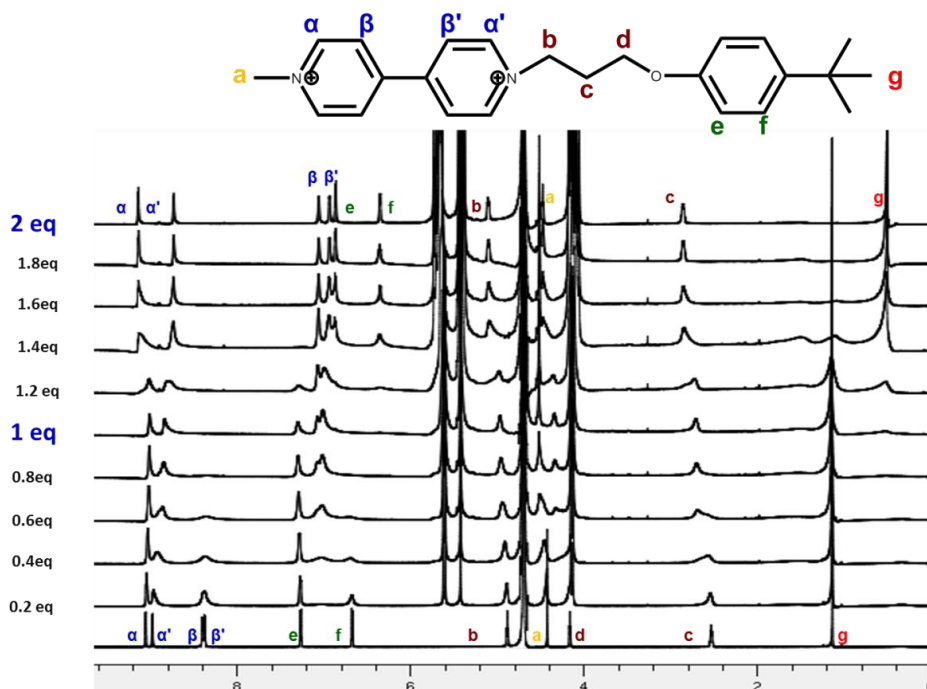


Figure 28. ^1H NMR spectra (600 MHz, D_2O , 298 K) of MC3^{2+} (3.5 mM) in the presence of increasing amounts of $\text{CB}[7]$.

4.2.5b. ^1H NMR Titration of MC3^{2+} by $\text{CB}[7]$

Increasing amounts (up to 2.4 equivalents) of a solution of $\text{CB}[7]$ in D_2O were added to 500 μL of a concentrated solution of MC4^{2+} (8.6×10^{-3} M). The observations made for MC3^{2+} perfectly stand for the titration of MC4^{2+} by $\text{CB}[7]$ (Figure 29) thus suggesting the formation of two complexes, namely a [2]pseudorotaxane $\text{MC3}^{2+}\text{CB}[7]$ (*i.e.* the β/β' signals are the most affected by $\text{CB}[7]$ up to 1 equivalent) and a [3]pseudorotaxane $(\text{MC3}^{2+}\text{CB}[7])_2$ (*i.e.* the e, f and g signals are the most affected by $\text{CB}[7]$ addition from 1 to up to 2.4 equivalents). As previously stated for MC3^{2+} , the formation of these two types of host-guest complexes was already observed by ESI-MS (Figure 25).

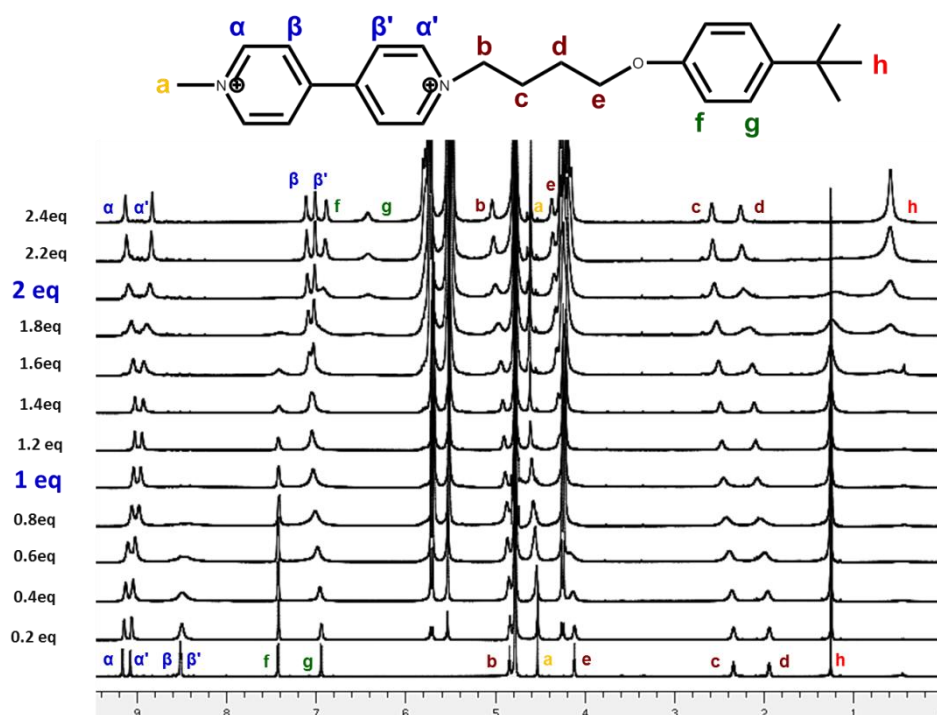


Figure 29. ^1H NMR spectra (600 MHz, D_2O , 298 K) of MC4^{2+} (8.6 mM) in the presence of increasing amounts of $\text{CB}[7]$.

4.2.6. $\text{C23}^{4+}/\text{C24}^{4+}$ Recognition by $\text{CB}[7]$ Probed by ^1H NMR Spectroscopy

In the following section, the ^1H NMR titration experiments of C23^{4+} (Figure 30) and C24^{4+} (Figure 31) by $\text{CB}[7]$ out in D_2O are described.

4.2.6a. ^1H NMR Titration of C23^{4+} by $\text{CB}[7]$

Increasing amounts (up to 2 equivalents) of a solution of $\text{CB}[7]$ in D_2O were added to 500 μL of a concentrated solution of C23^{4+} (7×10^{-4} M). The ^1H NMR spectra only show an upfield shift of the β/β' -protons of the viologen moieties, while the α/α' protons were found to be unaffected by $\text{CB}[7]$ complexation. This feature visibly indicates that both bipyridinium BIPY^{2+} are encircled by a $\text{CB}[7]$ host leading to a [3]pseudorotaxane $\text{C23}^{4+}\text{CB}[7]_2$. By

contrast with MC3^{2+} model system, the other proton signals were found to be unchanged along the ^1H NMR titration thus demonstrating the inability of C23^{4+} to welcome a second $\text{CB}[7]$ host on each of its strands for evident steric reasons. These spectroscopic data are in excellent agreement with the observations made previously (absorption investigation, Figure 21 and ESI-MS, Figure 26).

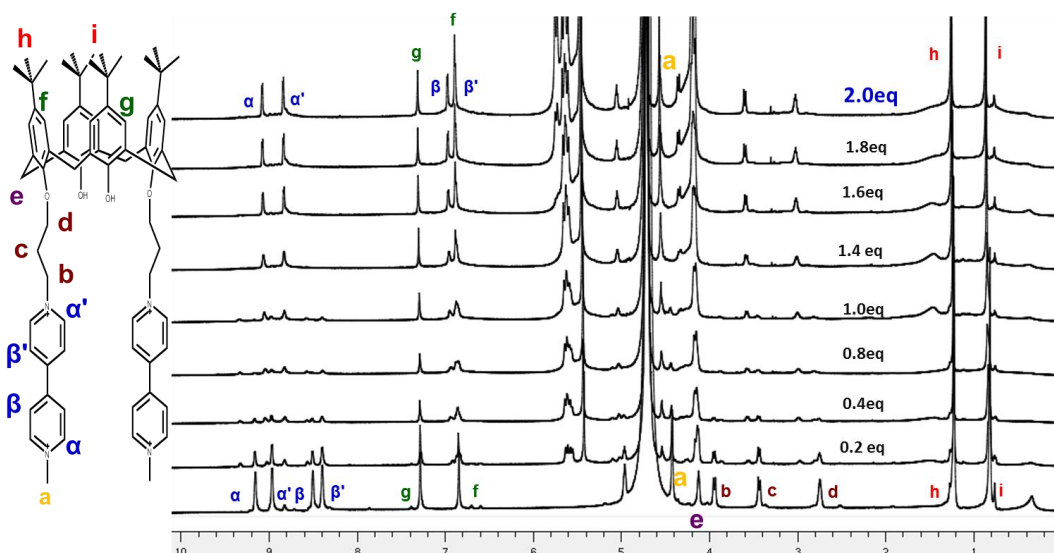


Figure 30. ^1H NMR (600 MHz, D_2O , 298 K) titration of C23 with an excess of $\text{CB}[7]$.

4.2.6b. ^1H NMR Titration of C24^{4+} by $\text{CB}[7]$

The titration of the C24^{2+} could not be achieved with adequate accuracy because of the low solubility of this compound in water. ^1H NMR spectra of a 3×10^{-4} M solution of C24^{2+} in D_2O in the absence and in the presence of $\text{CB}[7]$ were however measured. The comparison of the two ^1H NMR spectra suggested the formation of an inclusion complex (*i.e.* $\text{C23}^{4+} \subset \text{CB}[7]_2$) where each of the viologen moieties is encapsulated within the $\text{CB}[7]$ hydrophobic cavity. As observed with C24^{2+} , only the β/β' protons of the viologen moieties undergo a significant upfield shift in the presence of $\text{CB}[7]$.

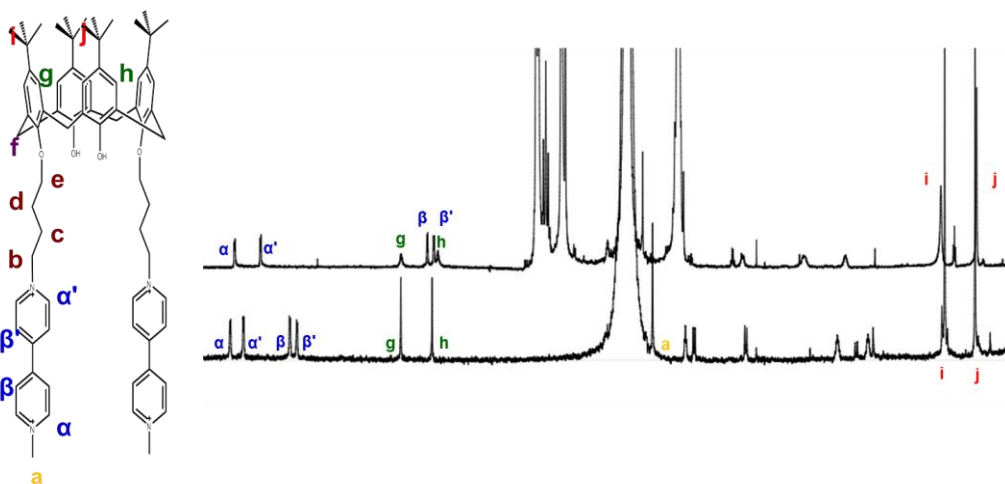


Figure 31. ^1H NMR spectra (600 MHz, D_2O , 298 K) of C24 without and with an excess of $\text{CB}[7]$.

4.2.7. $\text{MC3}^{\bullet+}$ and $\text{MC4}^{\bullet+}$ Pimerization in Aqueous Solution

UV-Vis-NIR absorption spectra (220 nm – 1300 nm) of increasing concentration of $\text{MC3}^{\bullet+}$ or $\text{MC4}^{\bullet+}$ (prepared by addition of sodium dithionite under a controlled atmosphere of argon) in 0.5 ml ($2.0 \times 10^{-4} \text{ M} \leq [\text{MC3}^{\bullet+}]_0 < 4 \times 10^{-4} \text{ M}$; $2.0 \times 10^{-4} \text{ M} \leq [\text{MC4}^{\bullet+}]_0 < 6 \times 10^{-4} \text{ M}$) or 1 ml ($10^{-5} \text{ M} \leq [\text{MC3}^{\bullet+}]_0 < 10^{-4} \text{ M}$; $10^{-5} \text{ M} \leq [\text{MC4}^{\bullet+}]_0 < 10^{-4} \text{ M}$) 0.1 M phosphate solutions (pH 7.0) were recorded in 2 mm or 10 mm optical cell, respectively, at 25°C with a Cary 5000 spectrophotometer.

Figure 32 evidences the formation of a broad and intense absorption in the NIR region ($\lambda > 800 \text{ nm}$) upon increasing the concentration of the $\text{MC3}^{\bullet+}$ monoradical cation in solution, which constitutes a proof of the dimerization process. The data have been processed with the Origin program and allowed us to evaluate the dimerization constant ($\log K_{\text{Dim}}$ value of 3.4(2)).

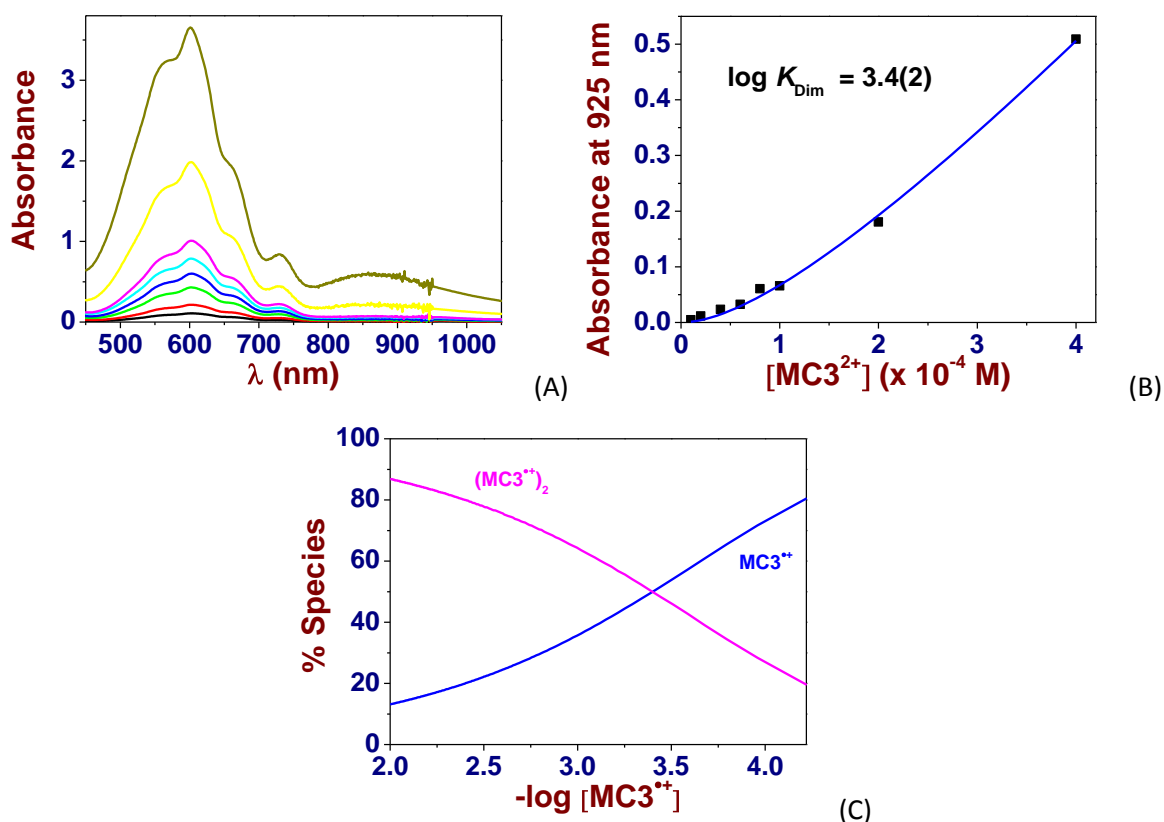


Figure 32. (A) UV-Vis.-NIR absorption titration of $\text{MC3}^{\bullet+}$ in aqueous solution, (B) absorbances at 925 nm as a function of $[\text{MC3}^{\bullet+}]_0$ and (C) distribution diagram of the monomer *versus* dimer as a function of $\text{MC3}^{\bullet+}$ concentration. Solvent: Water pH 7.0 (0.1 M $\text{Na}_2\text{HPO}_4/\text{NaH}_2\text{PO}_4$). For $10^{-5} \text{ M} \leq [\text{MC3}^{\bullet+}]_0 < 10^{-4} \text{ M}$; $l = 1 \text{ cm}$; for $2 \times 10^{-4} \text{ M} \leq [\text{MC3}^{\bullet+}]_0 < 4 \times 10^{-4} \text{ M}$; $l = 2 \text{ mm}$; $T = 25.0(1) \text{ }^\circ\text{C}$. In each of the solutions considered, the $\text{MC3}^{\bullet+}$ species was generated from MC3^{2+} using freshly prepared sodium dithionite solution at *ca.* 10^{-2} M under O_2 free conditions. The absorption spectra are not corrected from dilution effects.

Figure 33 gathers the results obtained for $\text{MC4}^{\bullet+}$ for which a $\log K_{\text{Dim}}$ value of 3.4(2) has been also calculated.

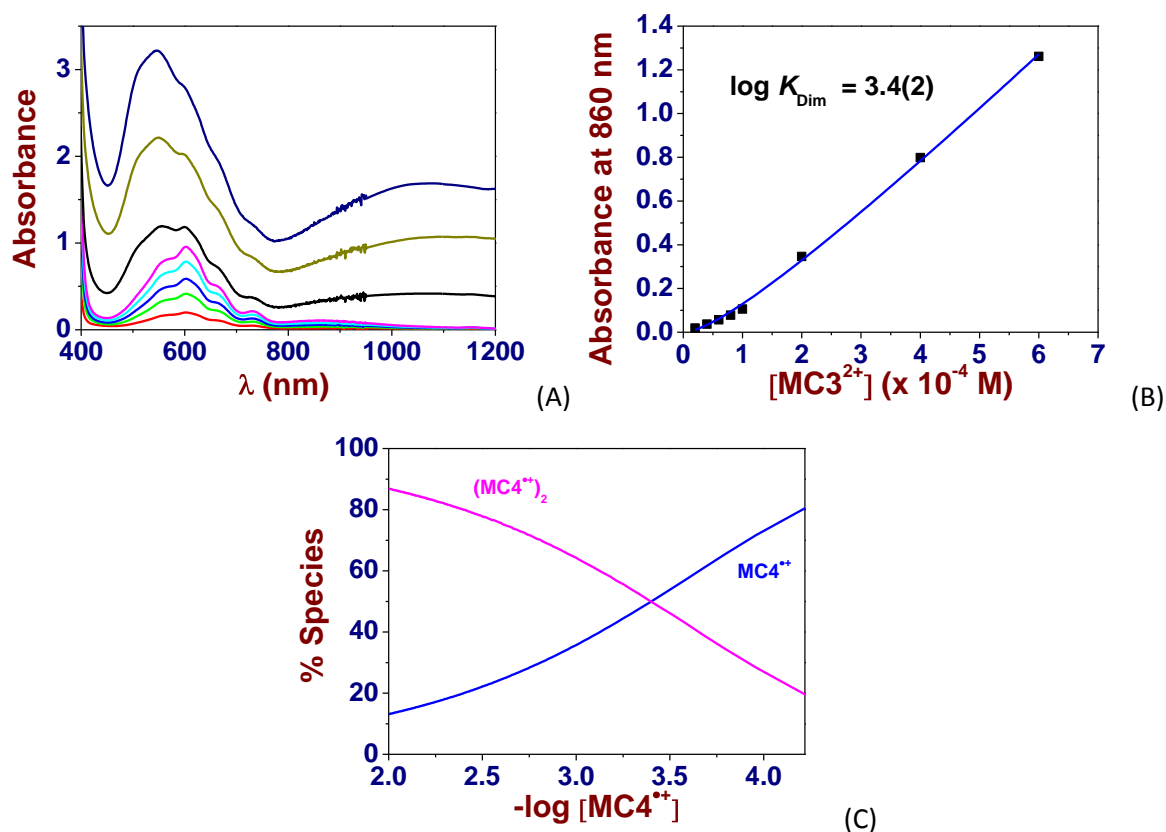


Figure 33. (A) UV-Vis.-NIR absorption titration of $\text{MC4}^{\bullet+}$ in aqueous solution, (B) absorbances at 860 nm as a function of $[\text{MC4}^{\bullet+}]_0$ and (C) distribution diagram of the monomer *versus* dimer as a function of $\text{MC4}^{\bullet+}$ concentration. Solvent: Water pH 7.0 (0.1 M $\text{Na}_2\text{HPO}_4/\text{NaH}_2\text{PO}_4$). For 10^{-5} M $\leq [\text{MC4}^{\bullet+}]_0 < 10^{-4}$ M; $l = 1$ cm; for 2×10^{-4} M $\leq [\text{MC4}^{\bullet+}]_0 < 6 \times 10^{-4}$ M; $l = 2$ mm; $T = 25.0(1)$ °C. In each of the solutions considered, the $\text{MC4}^{\bullet+}$ species was generated from MC4^{2+} using freshly prepared sodium dithionite solution at *ca.* 10^{-2} M under O_2 free conditions. The absorption spectra are not corrected from dilution effects.

4.2.8. Recognition of the Radical Cations by CB[7]

4.2.8a. Recognition of $\text{MC3}^{\bullet+}$ by CB[7]

Figure 34A shows the UV-Vis.-NIR spectra of MC3^{2+} (black line) and of its inclusion complex $\text{MC3}^{2+} \subset \text{CB}[7]$ (red line, *i.e.* we have previously demonstrated that the **CB[7]** host is sitting in the middle of the bipyridinium dication). Chemical reduction of MC3^{2+} led to its monoradical cationic species $\text{MC3}^{\bullet+}$ that is still located within the **CB[7]** cavity (*i.e.* the absorbance measured for the $\text{MC3}^{\bullet+} \subset \text{CB}[7]$ - Figure 34A, green line - is much lower than the one recorded for free $\text{MC3}^{\bullet+}$ under the same experimental conditions, Figure 34B, blue line). Alternatively, Figure 34B shows the UV-Vis.-NIR spectra of MC3^{2+} (black line) and of its monoradical cationic species $\text{MC3}^{\bullet+}$ (blue line). No dimer was observed under these experimental conditions (*i.e.* no NIR absorption, Figure 32). Addition of **CB[7]** up to 4 equivalents induces a significant hypochromic shift of the absorption bands of $\text{MC3}^{\bullet+}$ hence confirming that the monoradical monocation **BIPY** $^{\bullet+}$ unit is encircled by the **CB[7]** host.

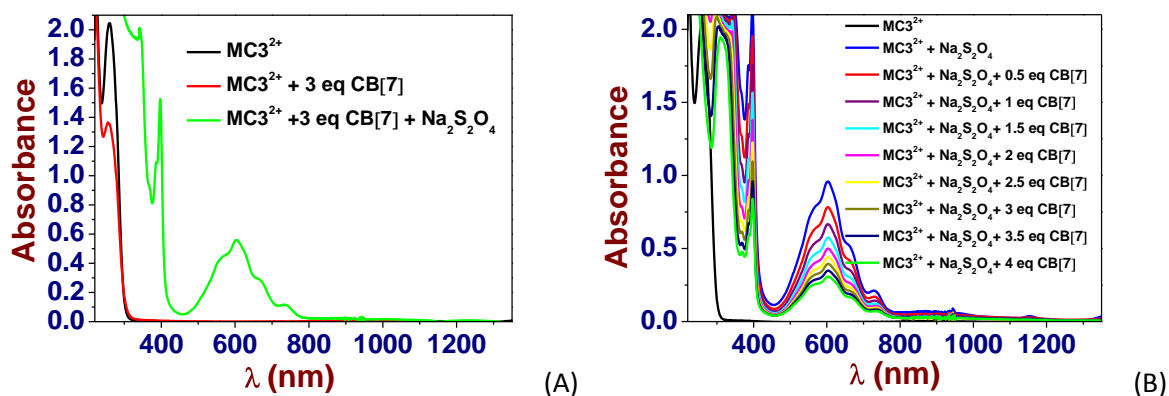


Figure 34. (A) UV-Vis.-NIR spectra of MC3^{2+} ($[\text{MC3}^{2+}]_0 = 10^{-4}$ M, black line) and of its $\text{MC3}^{2+}\text{-CB[7]}$ complex ($[\text{CB[7]}]_0/[\text{MC3}^{2+}]_0 = 3$, red line). Addition of a freshly prepared O_2 -free sodium dithionite (green line) induces formation of absorptions in the Vis. region that are characteristics of the radical species $\text{MC3}^{\bullet+}$. (B) UV-Vis.-NIR spectra of MC3^{2+} ($[\text{MC3}^{2+}]_0 = 10^{-4}$ M, black line) and of its radical species $\text{MC3}^{\bullet+}$ (blue line, addition of freshly prepared and O_2 -free sodium dithionite). Upon addition of CB[7] ($[\text{CB[7]}]_0/[\text{MC3}^{\bullet+}]_0 = 0$, blue line and $[\text{CB[7]}]_0/[\text{MC3}^{\bullet+}]_0 = 4$, green line), the Vis. absorptions experienced a significant hypochromic shift that is indicative of host/guest complexation. Solvent: water buffered at pH 7.0 with 0.1 M $\text{Na}_2\text{H}_2\text{PO}_4/\text{NaH}_2\text{PO}_4$; $l = 1$ cm; $T = 25.0(1)$ °C. In each of the solutions considered, the $\text{MC3}^{\bullet+}$ species was generated from MC3^{2+} using freshly prepared sodium dithionite solution at *ca.* 10^{-2} under O_2 free conditions. The absorption spectra are not corrected from dilution effects.

To determine the association constant of the $\text{MC3}^{\bullet+}\text{-CB[7]}$ inclusion complex, 1 ml of MC3^{2+} (10^{-4} M) were reacted with an excess of sodium dithionite (sodium hydrosulfite or sodium dithionite, $\text{Na}_2\text{S}_2\text{O}_4$, 85%, Sigma Aldrich) in a 10 mm Hellma quartz optical cell in water at pH 7 (0.1 M phosphate buffer).

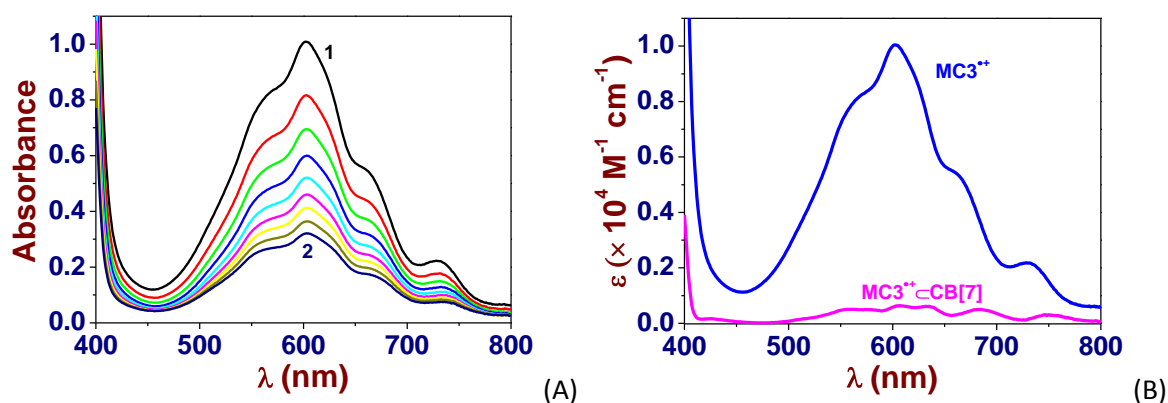


Figure 35. (A) UV-Vis. Absorption batch titration of $\text{MC3}^{\bullet+}$ by CB[7] in water. (B) Electronic spectra of $\text{MC3}^{\bullet+}$ and of its inclusion complex with CB[7] ($\text{MC3}^{\bullet+}\text{-CB[7]}$). Solvent: water pH 7.0 (0.1 M $\text{Na}_2\text{HPO}_4/\text{NaH}_2\text{PO}_4$). $[\text{MC3}^{\bullet+}]_0 = 10^{-4}$ M; (1) $[\text{CB[7]}]_0/[\text{MC3}^{\bullet+}]_0 = 0$; (2) $[\text{CB[7]}]_0/[\text{MC3}^{\bullet+}]_0 = 4.0$; $l = 1$ cm; $T = 25.0(1)$ °C. In each of the solutions considered, the $\text{MC3}^{\bullet+}$ species was generated from MC3^{2+} using freshly prepared sodium dithionite solution at *ca.* 10^{-2} M under O_2 free conditions. The absorption spectra are not corrected from dilution effects.

The solution was constantly flushed with O_2 - free argon to avoid re-oxidation of the $\text{MC3}^{\bullet+}$ radicals. The $[\text{CB[7]}]_0/[\text{MC3}^{\bullet+}]_0$ ratio was varied from 0 to 4. Special care was taken to ensure

that complete equilibration was attained. After each addition, a UV-Vis.-NIR spectrum was recorded from 220 to 1400 nm on a Cary 5000 (Agilent) spectrophotometer maintained at 25.0(2) °C by the flow of a Dual Cell Pelletier Accessory (Cary Varian). Figure 35A depicts the absorption spectrophotometric titration while Figure 35B shows the electronic spectra of $\text{MC3}^{\bullet+}$ and its corresponding inclusion complex $\text{MC3}^{\bullet+}\text{CB}[7]$. The [2]pseudorotaxane $\text{MC3}^{\bullet+}\text{CB}[7]$ is characterized by a stability constant of $\log K_{\text{MC3}^{\bullet+}\text{CB}[7]} = 3.8(4)$.

4.2.8b. Recognition of $\text{MC4}^{\bullet+}$ by $\text{CB}[7]$

Similarly to $\text{MC3}^{\bullet+}$ (Figure 34), Figure 36 shows the effect of $\text{CB}[7]$ on the absorption properties of the $\text{MC4}^{\bullet+}$ that was chemically generated *in situ* in the optical cell with the help of sodium dithionite. As demonstrated for $\text{MC3}^{\bullet+}$, the significant fading of the visible absorption of the $\text{MC4}^{\bullet+}$ radical cation is in agreement with the formation of an inclusion complex $\text{MC4}^{\bullet+}\text{CB}[7]$ for which the binding mode is similar to the $\text{MC4}^{2+}\text{CB}[7]$ pseudorotaxane (*i.e.* $\text{CB}[7]$ is encircling the BIPY^{2+} or $\text{BIPY}^{\bullet+}$ chromophores).

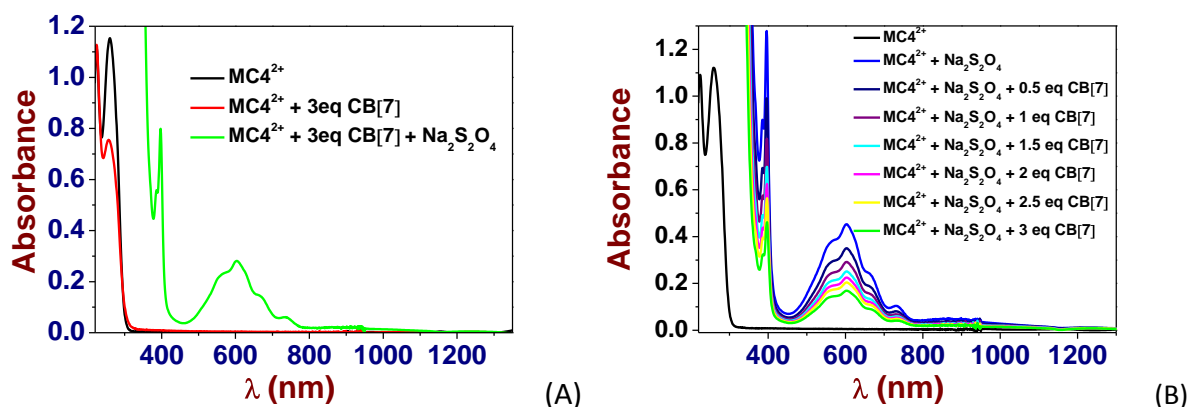


Figure 36. (A) UV-Vis.-NIR spectra of MC4^{2+} ($[\text{MC4}^{2+}]_0 = 2 \times 10^{-5}$ M, black line) and of its $\text{MC4}^{2+}\text{CB}[7]$ complex ($[\text{CB}[7]]_0/[\text{MC4}^{2+}]_0 = 3$, red line). Addition of a freshly prepared O_2 -free sodium dithionite (green line) induces formation of absorptions in the Vis. region that are characteristics of the radical species $\text{MC4}^{\bullet+}$. (B) UV-Vis.-NIR spectra of MC4^{2+} ($[\text{MC4}^{2+}]_0 = 2 \times 10^{-5}$ M, black line) and of its radical species $\text{MC4}^{\bullet+}$ (blue line, addition of freshly prepared and O_2 -free sodium dithionite). Upon addition of $\text{CB}[7]$ ($[\text{CB}[7]]_0/[\text{MC4}^{\bullet+}]_0 = 0$, blue line and $[\text{CB}[7]]_0/[\text{MC4}^{\bullet+}]_0 = 3$, green line), the Vis. absorptions experienced a significant hypochromic shift that is indicative of host/guest complexation. Solvent: water buffered at pH 7.0 with 0.1 M $\text{Na}_2\text{H}_2\text{PO}_4/\text{NaH}_2\text{PO}_4$; $l = 1$ cm; $T = 25.0(1)$ °C. In each of the solutions considered, the $\text{MC4}^{\bullet+}$ species was generated from MC4^{2+} using freshly prepared sodium dithionite solution at *ca.* 10^{-2} under O_2 free conditions. The absorption spectra are not corrected from dilution effects.

Figure 35A shows the absorption spectral variations induced by $\text{CB}[7]$ addition to a solution of $\text{MC4}^{\bullet+}$ and Figure 35B depicts the electronic spectra of $\text{MC4}^{\bullet+}$ and its corresponding inclusion complex $\text{MC4}^{\bullet+}\text{CB}[7]$ that were calculated. The [2]pseudorotaxane $\text{MC4}^{\bullet+}\text{CB}[7]$ is characterized by a stability constant of $\log K_{\text{MC4}^{\bullet+}\text{CB}[7]} = 4.54(5)$.

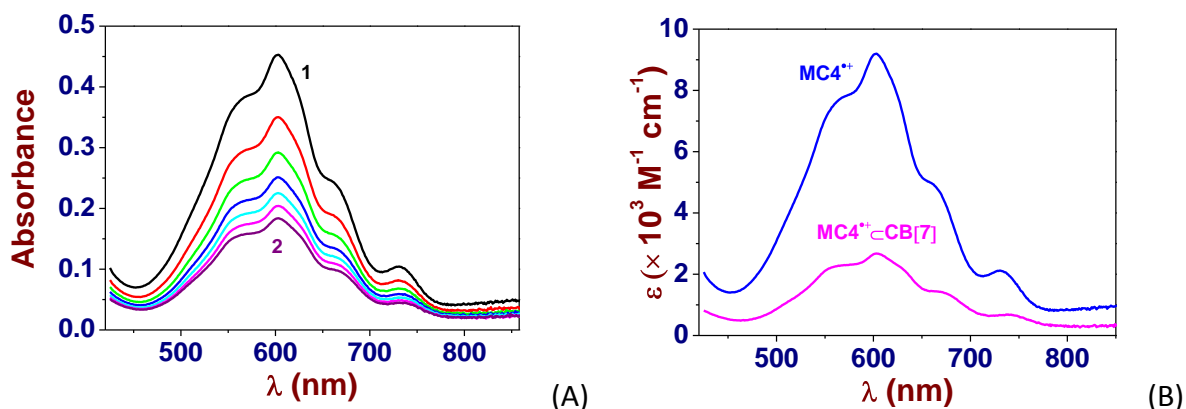


Figure 37. (A) UV-Vis. Absorption batch titration of MC4^{2+} by $\text{CB}[7]$ in water. (B) Electronic spectra of MC4^{2+} and of its inclusion complex with $\text{CB}[7]$ ($\text{MC4}^{2+} \subset \text{CB}[7]$). Solvent: water pH 7.0 (0.1 M $\text{Na}_2\text{HPO}_4/\text{NaH}_2\text{PO}_4$). $[\text{MC4}^{2+}]_0 = 2 \times 10^{-5}$ M; (1) $[\text{CB}[7]]_0/[\text{MC4}^{2+}]_0 = 0$; (2) $[\text{CB}[7]]_0/[\text{MC4}^{2+}]_0 = 3.01$; $l = 1$ cm; $T = 25.0(1)$ °C. In each of the solutions considered, the MC4^{2+} species was generated from MC4^{2+} using freshly prepared sodium dithionite solution at *ca.* 10^{-2} M under O_2 free conditions. The absorption spectra are not corrected from dilution effects.

4.2.8c. Recognition of $\text{C23}^{2(\bullet+)}$ by $\text{CB}[7]$

The recognition properties of $\text{MC3}^{\bullet+}$ and $\text{MC4}^{\bullet+}$ by $\text{CB}[7]$ being well established, we then examined those of $\text{C23}^{2(\bullet+)}$ and $\text{C24}^{2(\bullet+)}$ to assess the influence of the calix[4]arene platform on the dimerization and recognition processes. Figure 38A first shows the UV-Vis-NIR spectra of C23^{4+} (black line) and of its inclusion complex $\text{C23}^{4+} \subset (\text{CB7})_2$ (red line). The reduction of C23^{4+} into its corresponding two electron reduced species (one electron per viologen unit) $\text{C23}^{2(\bullet+)}$ (green line) is characterized by the presence of the broad NIR absorption that is a clear signature of a strong intramolecular dimerization process and therefore of dethreading of the $\text{CB}[7]$ macrocycles. This feature is further confirmed by Figure 38B that confirms that addition of $\text{CB}[7]$ (up to 4.5 equivalents) has no effect on the characteristic absorptions of the $\text{C23}^{2(\bullet+)}$ radical thus demonstrating that intramolecular dimerization overwhelms the inclusion process with $\text{CB}[7]$.

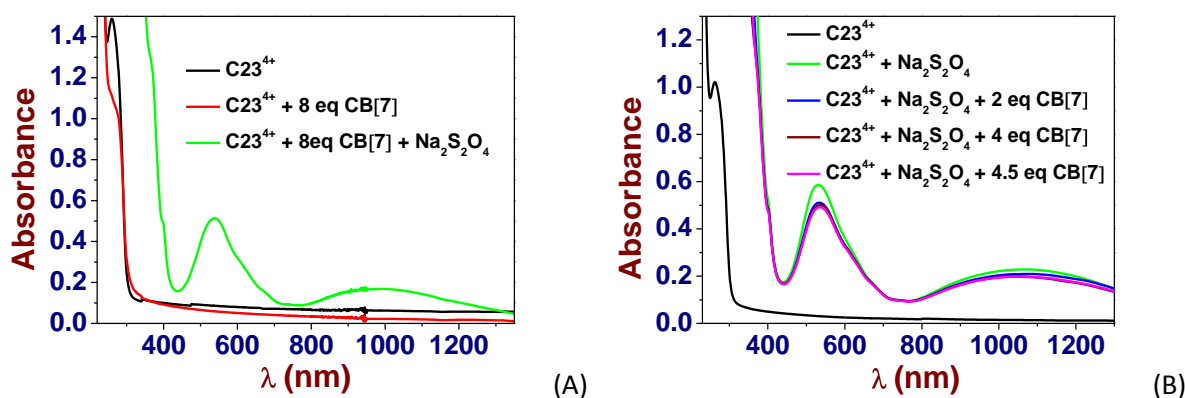


Figure 38. (A) UV-Vis.-NIR spectra of C23^{4+} ($[\text{C23}^{4+}]_0 = 5.0 \times 10^{-5}$ M, black line) and of its $\text{C23}^{4+} \subset (\text{CB7})_2$ complex ($[\text{CB7}]_0/[\text{C23}^{4+}]_0 = 8$, red line). Addition of a freshly prepared O_2 -free sodium dithionite (green line) induces formation of absorptions in the Vis. and NIR regions that are characteristics of the intramolecular radical dimeric species $\text{C23}^{2(\bullet+)}$. (B) UV-Vis.-NIR spectra of C23^{4+}

($[\text{C23}^{4+}]_0 = 5.0 \times 10^{-5} \text{ M}$, black line) and of its radical species $\text{C23}^{2(\bullet+)}$ under its dimeric state (green line, prepared by addition of O_2 -free sodium dithionite). Upon addition of **CB[7]** ($[\text{CB[7]}]_0/[\text{C23}^{4+}]_0 = 0$, green line and $[\text{CB[7]}]_0/[\text{C23}^{4+}]_0 = 4.5$, magenta line), no alteration of the absorption spectrum of $\text{C23}^{2(\bullet+)}$ can be observed thus substantiating the inability of **CB[7]** to revert the intramolecular dimerisation reaction. Solvent: water buffered at pH 7.0 with 0.1 M $\text{Na}_2\text{H}_2\text{PO}_4/\text{NaH}_2\text{PO}_4$; $l = 1 \text{ cm}$; $T = 25.0(1)^\circ \text{ C}$. In each of the solutions considered, the $\text{C23}^{2(\bullet+)}$ species was prepared from C23^{4+} using freshly prepared sodium dithionite solution at *ca.* 10^{-2} under O_2 free conditions. The absorption spectra are not corrected from dilution effects.

4.2.8d. Recognition of $\text{C24}^{2(\bullet+)}$ by **CB[7]**

Similarly to the studies described above with $\text{C23}^{2(\bullet+)}$ and **CB[7]** (Figure 38), the experiments described in Figure 39 also demonstrate that strong intramolecular interactions between the two **BIPY**[•] borne by the calix[4]arene unit of $\text{C24}^{2(\bullet+)}$ overcome the inclusion with the **CB[7]** macrocycles. As a consequence, reduction of the viologen units of the [3]pseudorotaxane $\text{C24}^{4+} \subset (\text{CB7})_2$ led to dethreading of the hosts (Figure 39A). Alternatively, addition of **CB[7]** has no effect on the chemically generated $\text{C24}^{2(\bullet+)}$ (Figure 39B).

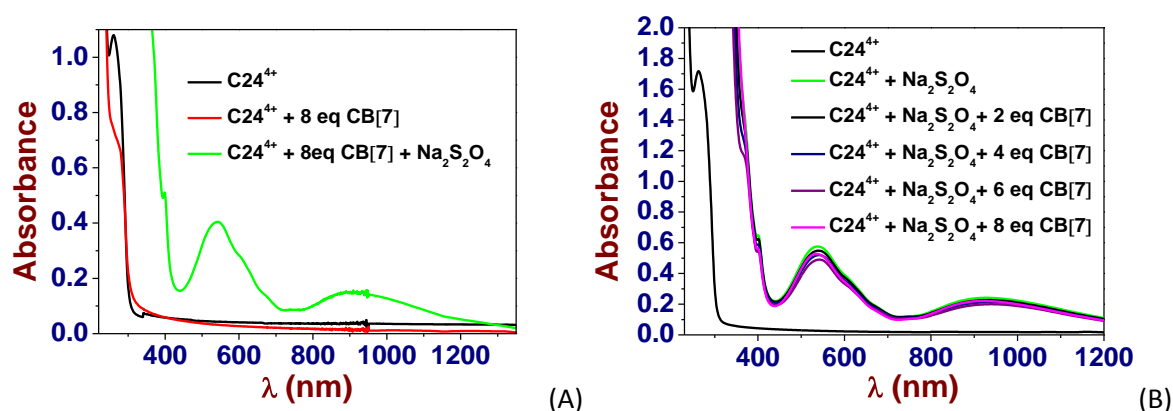


Figure 39. (A) UV-Vis.-NIR spectra of C24^{4+} ($[\text{C24}^{4+}]_0 = 5.0 \times 10^{-5} \text{ M}$, black line) and of its $\text{C24}^{4+} \subset (\text{CB[7]})_2$ complex ($[\text{CB[7]}]_0/[\text{C24}^{4+}]_0 = 8$, red line). Addition of O_2 -free sodium dithionite (green line) induces formation of absorptions in the Vis. and NIR regions that are characteristics of the intramolecular radical dimeric species $\text{C24}^{2(\bullet+)}$. (B) UV-Vis.-NIR spectra of C24^{4+} ($[\text{C24}^{4+}]_0 = 5.0 \times 10^{-5} \text{ M}$, black line) and of its radical species $\text{C24}^{2(\bullet+)}$ under its dimeric state (green line, prepared by addition of O_2 -free sodium dithionite). Upon addition of **CB[7]** ($[\text{CB[7]}]_0/[\text{C24}^{4+}]_0 = 0$, green line and $[\text{CB[7]}]_0/[\text{C24}^{4+}]_0 = 7.9$, magenta line), no alteration of the absorption spectrum of $\text{C24}^{2(\bullet+)}$ can be observed thus substantiating the inability of **CB[7]** to revert the intramolecular dimerisation reaction. Solvent: water buffered at pH 7.0 with 0.1 M $\text{Na}_2\text{H}_2\text{PO}_4/\text{NaH}_2\text{PO}_4$; $l = 1 \text{ cm}$; $T = 25.0(1)^\circ \text{ C}$. In each of the solutions considered, the $\text{C24}^{2(\bullet+)}$ species was prepared from C24^{4+} using freshly prepared sodium dithionite solution at *ca.* 10^{-2} under O_2 free conditions. The absorption spectra are not corrected from dilution effects.

4.2.9. Electrochemical Properties of the Threads and the [n]Pseudorotaxanes

Cyclic Voltammetry (CV) and Square Wave (SW) voltammetry experiments were carried out at room temperature in argon-purged H_2O solutions with a Gamry Multipurpose instrument (Reference 600) interfaced to a PC. The electrochemical experiments were performed using a glassy carbon working electrode (0.071 cm^2 , BASi). The electrode surface

was polished routinely with 0.05 μm alumina-water slurry on a felt surface immediately before use. The counter electrode was a Pt coil and the reference electrode was an Ag/AgCl electrode, unless otherwise noted. The concentration of the supporting electrolyte, tetrabutylammonium chloride (TBACl) was 0.1 M. The experimental errors on the potential values are estimated to ± 10 mV. All measurements were recorded in phosphate buffer solutions (pH 7). The scan rate was set to 200 mV s^{-1} . The cyclic (CV) and square wave (SW) voltammograms of the four viologen derivatives (**MC3²⁺**, **MC4²⁺**, **C23⁴⁺** and **C24⁴⁺**) described below were measured in the absence and in the presence of **CB[7]**. It is noteworthy that the values of $E_{1/2}$ calculated by SWV for each of the redox processes are in excellent agreement with the ones evaluated by CV experiments.

Regardless of the nature of the system considered, the CVs of degassed solutions of the viologen derivatives showed the presence of two reversible redox waves (Figure 40, orange lines) that can be attributed to the successive formation of **BIPY^{•+}** and **BIPY⁰**. The systems remain reversible in the presence of **CB[7]** (Figure 40, blue lines).

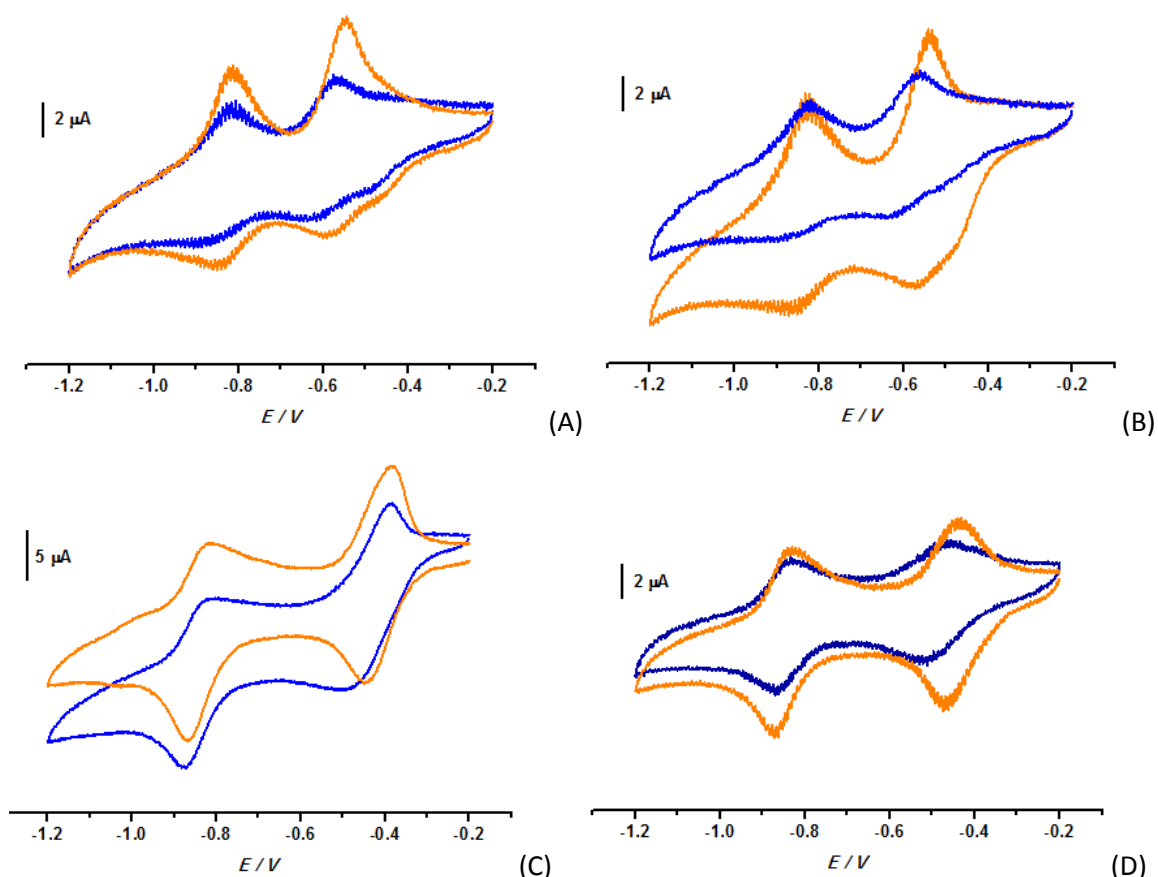


Figure 40. Cyclic voltammograms measured for (A) **MC3²⁺** (5×10^{-5} M), (B) **MC4²⁺** (6.3×10^{-5} M), (C) **C23⁴⁺** (5×10^{-5} M) and (D) **C24⁴⁺** (5×10^{-5} M) in the absence (orange lines) and the presence (blue lines) of **CB[7]** ((A) $[\text{CB[7]}]_0/[\text{MC3}^{2+}]_0 = 3$, (B) $[\text{CB[7]}]_0/[\text{MC4}^{2+}]_0 = 3$, (C) $[\text{CB[7]}]_0/[\text{C23}^{4+}]_0 = 4$ and (D) $[\text{CB[7]}]_0/[\text{C24}^{4+}]_0 = 4$). All voltammograms were recorded in Argon-purged phosphate buffer solutions (pH 7) at 298 K. The scan rate was set at 200 mVs^{-1} . E versus Ag/AgCl.

4.2.10. EPR Spectroscopy

EPR measurements (studies done in close collaboration with the group of Pr Ali Trabolsi, NYUAD, Abu Dhabi, UAE) were carried out with solutions of the calixarene-*bis*-viologens compounds **C23**⁴⁺ and **C24**⁴⁺, along with their model ligands, namely **MC3**²⁺ and **MC4**²⁺, in the absence and in the presence of **CB[7]**. This study was performed to evaluate the nature (dimerized or segregated) of the radical cations³² depending on the composition of the mixture. The radical cations species were produced chemically by addition of an excess of a reducing agent such as sodium dithionite (Na₂S₂O₄). Each of the solution was prepared at a concentration of $\sim 10^{-4}$ M.

4.2.10a. EPR Characterization of the Chemically Generated Radical Cation **MC3**^{•+} and its Inclusion Complex **MC3**^{•+}⊂(**CB7**)₂

10 equivalents of sodium dithionite were added to solutions of **MC3**^{•+} and **MC3**^{•+}⊂(**CB7**)₂ (*i.e.* **MC3**^{•+} mixed to 4 equivalents of **CB[7]**) in order to generate the corresponding radical cation species. The EPR spectra described in Figure 41 are characterized by a hyperfine structure which is characteristic of non-dimerized radical cations. Under the experimental conditions used ($\sim 10^{-4}$ M), these EPR data demonstrate that **MC3**^{•+} predominates (> 80%) under its monomeric form (Figure 32) regardless the presence or the absence of **CB[7]**. The exaltation of the hyperfine peaks is a strong indication of the dissociation of the few amount of dimers (< 20%, Figure 32) upon addition of **CB[7]**. These results are in excellent agreement with the absorption spectrophotometric and electrochemical studies.

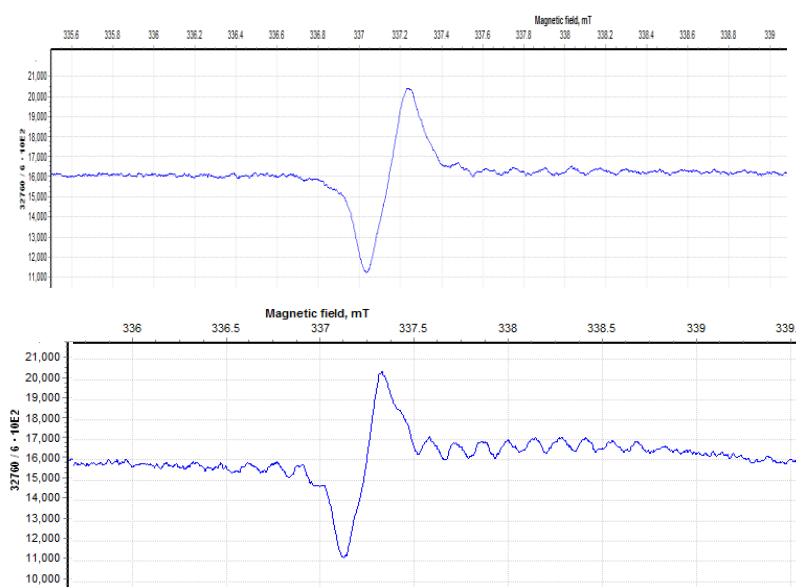


Figure 41. EPR spectra measured for (top) **MC3**^{•+} and (bottom) **MC3**^{•+} and 4 equivalents of **CB[7]**. Solvent: water.

4.2.10b. EPR Characterization of the Chemically Generated Radical Cation $MC4^{\bullet+}$ and its Inclusion Complex $MC4^{\bullet+} \subset (CB7)_2$

Similarly to $MC4^{\bullet+}$, the EPR spectrum measured in the absence of **CB[7]** that is characterized by a hyperfine structure is unchanged by the addition of the **CB[7]** host (Figure 42) thus demonstrating the predominant occurrence of the monomer under the experimental conditions used. The significant exaltation of the hyperfine structure upon addition of **CB[7]** is once again a proof of the dissociation of the few amount of the dimer that exists under these conditions (< 20%, Figure 33).

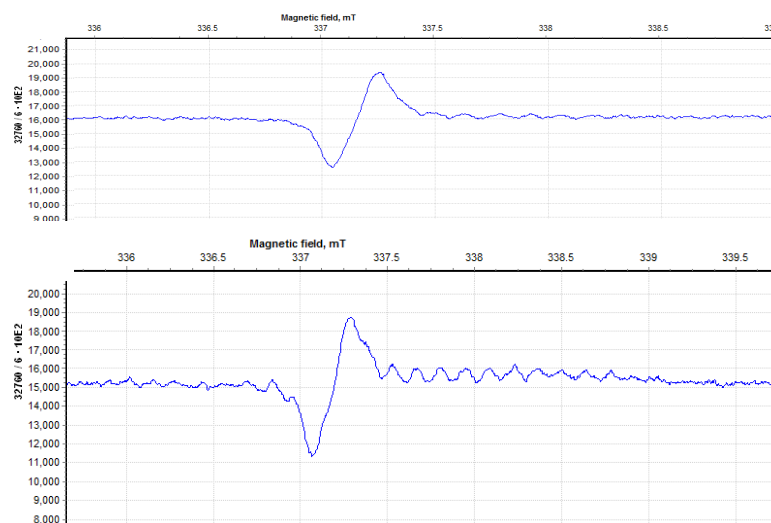
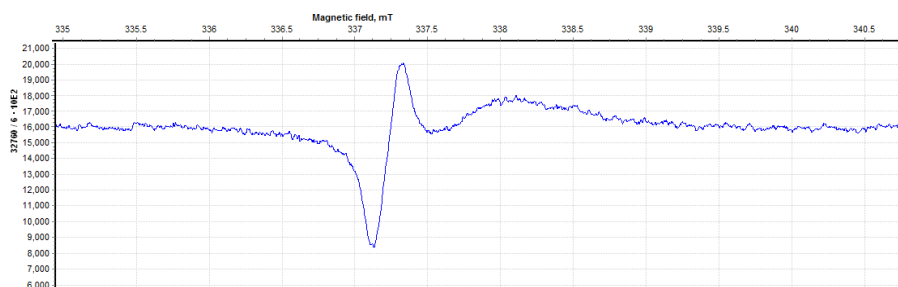


Figure 42. EPR spectra measured for (top) $MC4^{\bullet+}$ and (bottom) $MC4^{\bullet+}$ and 4 equivalents of **CB[7]**. Solvent: water.

4.2.10c. EPR Characterization of the Chemically Generated Radical Cations $C23^{2(\bullet+)}$ and $C24^{2(\bullet+)}$ in the Presence and in the Absence of **CB[7]**

It has been demonstrated upon reduction of the two **BIPY**²⁺ units borne by **C23**⁴⁺ (or **C23**⁴⁺), a spontaneous intramolecular dimerization of the two corresponding **BIPY**^{•+} occurs independently of the concentration (Figure 38). Addition of **CB[7]** does not compete thermodynamically with the strong intramolecular dimerization process. The EPR spectra of **C23**^{2(•+)} (Figure 43) and **C24**^{2(•+)} (Figure 44) measured in the absence and in the presence of **CB[7]** corroborates these observations since in both case, no hyperfine structure can be observed, in good agreement with spin exchange between the unpaired electrons.



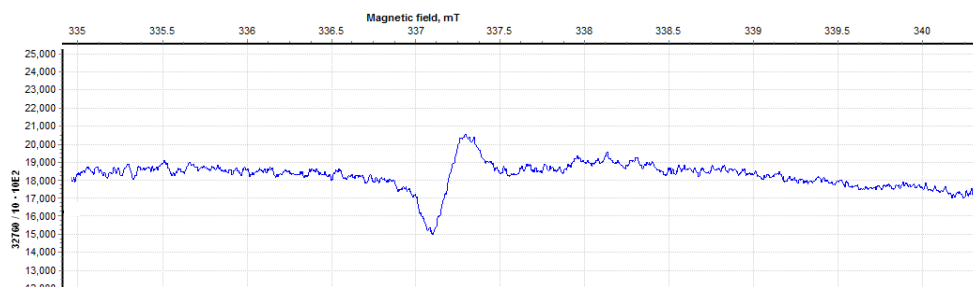


Figure 43. EPR spectra measured for (top) $\text{C23}^{2(\bullet+)}$ and (bottom) $\text{C23}^{2(\bullet+)}$ and 4 equivalents of **CB[7]**. Solvent: water.

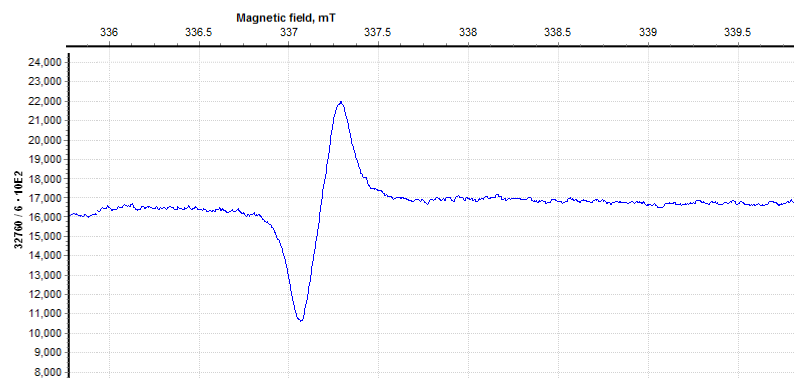
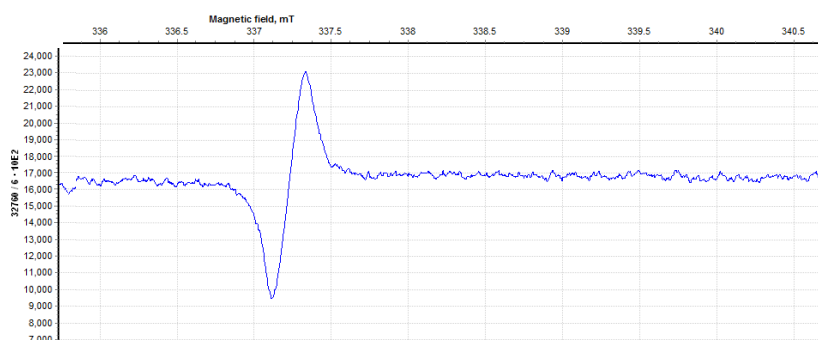


Figure 44. EPR spectra measured for (top) $\text{C24}^{2(\bullet+)}$ and (bottom) $\text{C24}^{2(\bullet+)}$ and 4 equivalents of **CB[7]**. Solvent: water.

In the next section, we will evaluate the ability of the viologen derivatives considered in this work to lead to host-guest complexes with **CB[8]**, a **CB[7]** homologous macrocyclic receptor whose the cavity size is appropriate for the recognition of two different or similar guests (*e.g.* radical cations of viologens)

4.2.11. Recognition of $\text{MC3}^{2+}/\text{MC3}^{\bullet+}$ and $\text{MC4}^{2+}/\text{MC4}^{\bullet+}$ by **CB[8]**

Figure 45A shows the UV-Vis.-NIR spectra of MC3^{2+} (black line) and of its inclusion complex $\text{MC3}^{2+} \subset \text{CB[8]}$ (red line, *i.e.* significant decrease of the BIPY^{2+} π - π^* transitions). Only a 1:1 complex has been characterized by ESI-MS experiments. Addition of a reductant (sodium dithionite) reduces the MC3^{2+} into its monoradical monocationic species $\text{MC3}^{\bullet+}$

(green line) whose the absorption is markedly different from that observed in the presence of **CB[7]** (Figure 34). This UV-Vis.-NIR absorption spectrum is indeed characterized by a broad absorption in the NIR ($\lambda_{\max} = 909$ nm) and an intense and structured absorption in the visible region ($\lambda_{\max} = 557$ nm) that are associated to the dimeric form of **MC3^{•+}** hosted by **CB[8]** (**(MC3^{•+})₂CB[8]**). This confirms that the larger size of **CB[8]** with respect to that of **CB[7]** allows accommodating two monoradical monocations **MC3^{•+}** that are firmly stacked together within the macrocyclic host cavity. Figure 45B further confirmed this result. The monoradical monocationic species **MC3^{•+}** (red line), chemically generated from **MPV²⁺** (red line) is characterized by a series of structured absorptions centred at 602 nm indicative of the monomer occurrence in solution. Incremental additions of **CB[8]** induces a hypsochromic shift of the absorptions lying in the visible region concomitantly to the formation of NIR transitions. This spectral feature is clearly related to the gradual formation of the **(MC3^{•+})₂CB[8]** species in solution. The same host/guest processes can be proposed for the **MC4²⁺/MC4^{•+}** redox couple in presence of **CB[8]** (Figure 46).

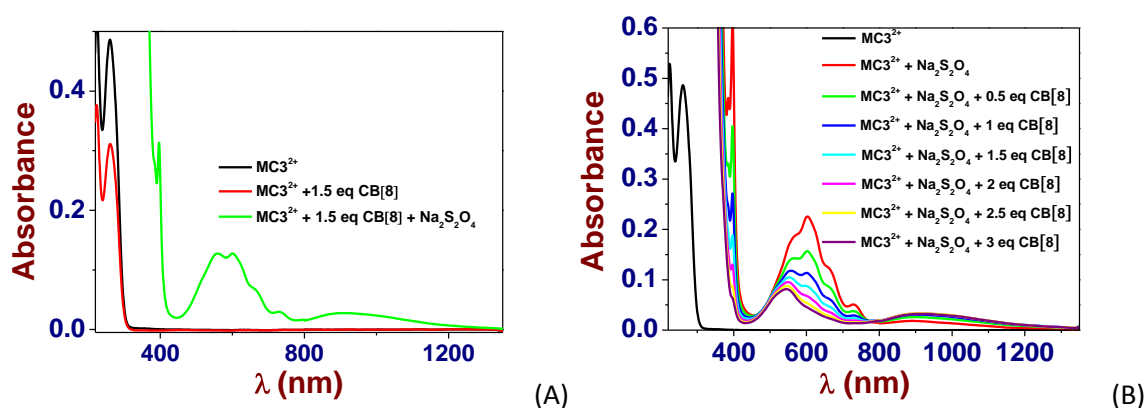


Figure 45. (A) UV-Vis.-NIR spectra of **MC3²⁺** ($[\text{MC3}^{2+}]_0 = 2.0 \times 10^{-5}$ M, black line) and of its **MC3²⁺CB[8]** complex ($[\text{CB[8]}]_0/[\text{MC3}^{2+}]_0 = 1.5$, red line). Addition of O_2 -free sodium dithionite (green line) induces formation of absorptions in the Vis. and NIR regions characteristics of the radical dimeric species **(MC3^{•+})₂** that is favoured by encapsulation with **CB[8]** (*i.e.* **(MC3^{•+})₂CB[8]**, see Figure 34 for comparison propose with **CB[7]**). (B) UV-Vis.-NIR spectra of **MC3²⁺** ($[\text{MC3}^{2+}]_0 = 2.0 \times 10^{-5}$ M, black line) and of its radical species **MC3^{•+}** under its predominant monomeric state (red line, addition of O_2 -free sodium dithionite). Upon addition of **CB[8]** ($[\text{CB[8]}]_0/[\text{MC3}^{•+}]_0 = 0$, green line and $[\text{CB[8]}]_0/[\text{MC3}^{•+}]_0 = 3$, purple line), significant alteration of the Vis. and NIR absorptions of **MC3^{•+}** is observed in line with the dimerization of **MC3^{•+}** triggered by **CB[8]** inclusion. Solvent: water buffered at pH 7.0 with 0.1 M $\text{Na}_2\text{H}_2\text{PO}_4/\text{NaH}_2\text{PO}_4$; $l = 1$ cm; $T = 25.0(1)^\circ\text{C}$. In each of the solutions considered, the **MC3^{•+}** species was generated from **MC3²⁺** using freshly prepared sodium dithionite solution at *ca.* 10^{-2} under O_2 free conditions. The absorption spectra are not corrected from dilution effects.

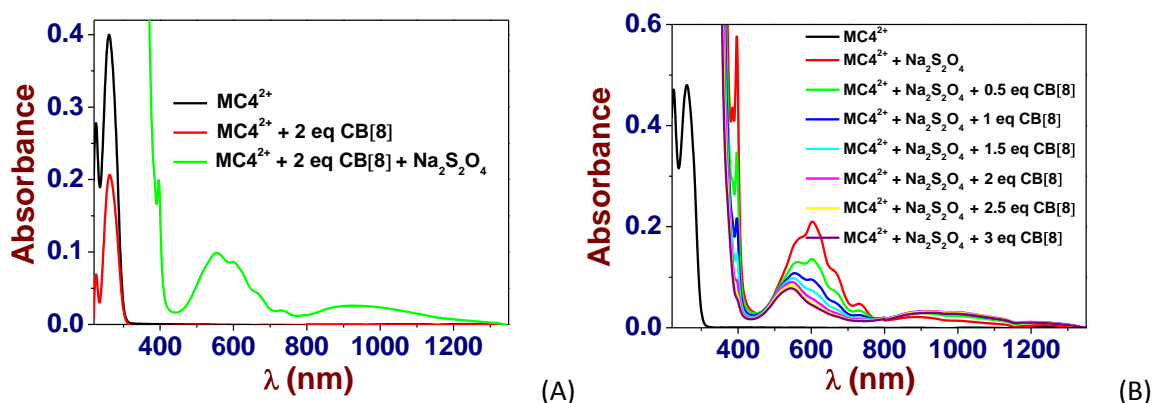


Figure 46. (A) UV-Vis.-NIR spectra of MC4^{2+} ($[\text{MC4}^{2+}]_0 = 2.0 \times 10^{-5}$ M, black line) and of its $\text{MC4}^{2+} \subset \text{CB}[8]$ complex ($[\text{CB}[8]]_0/[\text{MC4}^{2+}]_0 = 1.5$, red line). Addition of sodium dithionite (green line) induces formation of absorptions in the Vis. and NIR regions that are characteristics of the radical dimeric species $(\text{MC4}^{\bullet+})_2$ favoured by encapsulation with $\text{CB}[8]$ (*i.e.* $(\text{MC4}^{\bullet+})_2 \subset \text{CB}[8]$, see Figure 36 for comparison propose with $\text{CB}[7]$). (B) UV-Vis.-NIR spectra of MC4^{2+} ($[\text{MC4}^{2+}]_0 = 2.0 \times 10^{-5}$ M, black line) and of its radical species $\text{MC4}^{\bullet+}$ under its predominant monomeric state (red line, addition of O_2 -free sodium dithionite). Upon addition of $\text{CB}[8]$ ($[\text{CB}[8]]_0/[\text{MC4}^{\bullet+}]_0 = 0$, green line and $[\text{CB}[8]]_0/[\text{MC4}^{\bullet+}]_0 = 3$, purple line), significant alteration of the Vis. and NIR absorptions of $\text{MC4}^{\bullet+}$ is observed in line with the dimerization of $\text{MC4}^{\bullet+}$ guided by $\text{CB}[8]$ inclusion. Solvent: water buffered at pH 7.0 with 0.1 M $\text{Na}_2\text{H}_2\text{PO}_4/\text{NaH}_2\text{PO}_4$; $l = 1$ cm; $T = 25.0(1)^\circ \text{C}$. In each of the solutions considered, the $\text{MC4}^{\bullet+}$ species was generated from MC4^{2+} using freshly prepared sodium dithionite solution at *ca.* 10^{-2} under O_2 free conditions. The absorption spectra are not corrected from dilution effects.

4.2.12. Behaviour of $\text{C23}^{2(\bullet+)}$ and $\text{C24}^{2(\bullet+)}$ Radical Species in the Presence of $\text{CB}[8]$

Figure 47A depicts the UV-Vis.-NIR spectra of C23^{4+} (black line) and its inclusion complex $\text{C23}^{4+} \subset (\text{CB}[8])_2$ (red line, *i.e.* this species has been previously characterized by ESI-MS, Figure 26). Reduction of C23^{4+} led to the formation of the predominant diradical dication species $\text{C23}^{2(\bullet+)}$ for which the two $\text{BIPY}^{\bullet+}$ are firmly stacked together. In the presence of $\text{CB}[7]$, we have already demonstrated that reduction of the BIPY^{2+} units and concomitant intramolecular dimerization of the $\text{BIPY}^{\bullet+}$ radical cation led to the dethreading of the macrocyclic hosts (Figure 38). Alternatively, Figure 47B shows that addition of $\text{CB}[8]$ to a solution of intramolecularly dimerized $\text{C23}^{2(\bullet+)}$ (red line) has no effects on the Vis. and NIR absorptions of the dimeric species. This feature indicates that $\text{CB}[8]$ is not able to accommodate two $\text{BIPY}^{\bullet+}$ radical cations for steric and structural reasons. Figure 48 demonstrates that the increase of the chain length from 3 (C23^{4+}) to 4 carbons (C23^{4+}) (Figure 6) does not influence the recognition by $\text{CB}[8]$.

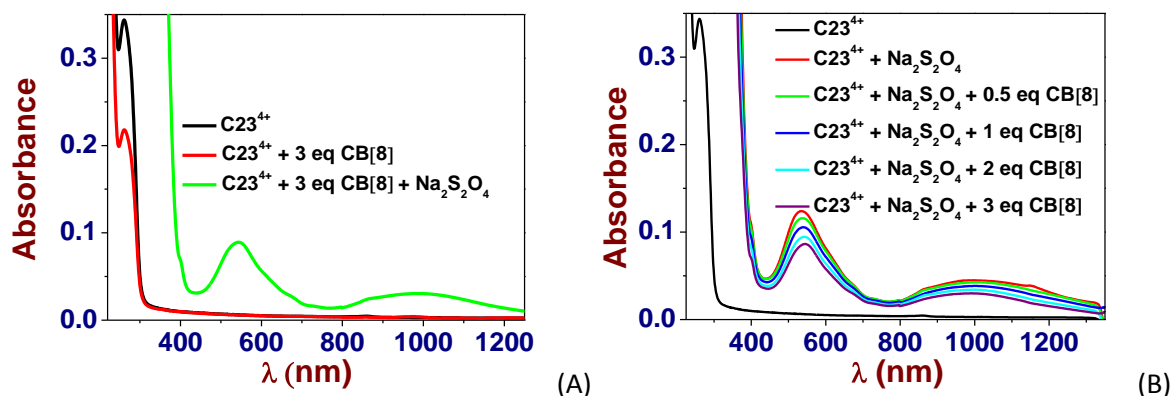


Figure 47. (A) UV-Vis.-NIR spectra of C23^{4+} ($[\text{C23}^{4+}]_0 = 10^{-5}$ M, black line) and of its $\text{C23}^{4+} \subset (\text{CB}[8])_2$ complex ($[\text{CB}[8]]_0/[\text{C23}^{4+}]_0 = 3$, red line). Addition of O_2 -free sodium dithionite (green line) induces formation of absorptions in the Vis. and NIR regions that are characteristics of the stable intramolecular radical dimeric species $\text{C23}^{2(\bullet+)}$, see Figure 38 for comparison propose with $\text{CB}[7]$). (B) UV-Vis.-NIR spectra of C23^{4+} ($[\text{C23}^{4+}]_0 = 10^{-5}$ M, black line) and of its radical species $\text{C23}^{2(\bullet+)}$ under its dimeric state (red line, addition of O_2 -free sodium dithionite). Addition of $\text{CB}[8]$ ($[\text{CB}[8]]_0/[\text{C23}^{2(\bullet+)}]_0 = 0$, red line and $[\text{CB}[8]]_0/[\text{C23}^{2(\bullet+)}]_0 = 3$, purple line) has no effect on the absorption properties of $\text{C23}^{2(\bullet+)}$. Solvent: water buffered at pH 7.0 with 0.1 M $\text{Na}_2\text{H}_2\text{PO}_4/\text{NaH}_2\text{PO}_4$; $l = 1$ cm; $T = 25.0(1)^\circ\text{C}$. In each of the solutions considered, the $\text{C23}^{2(\bullet+)}$ species was generated from C23^{4+} using freshly prepared sodium dithionite solution at *ca.* 10^{-2} under O_2 free conditions. The absorption spectra are not corrected from dilution effects.

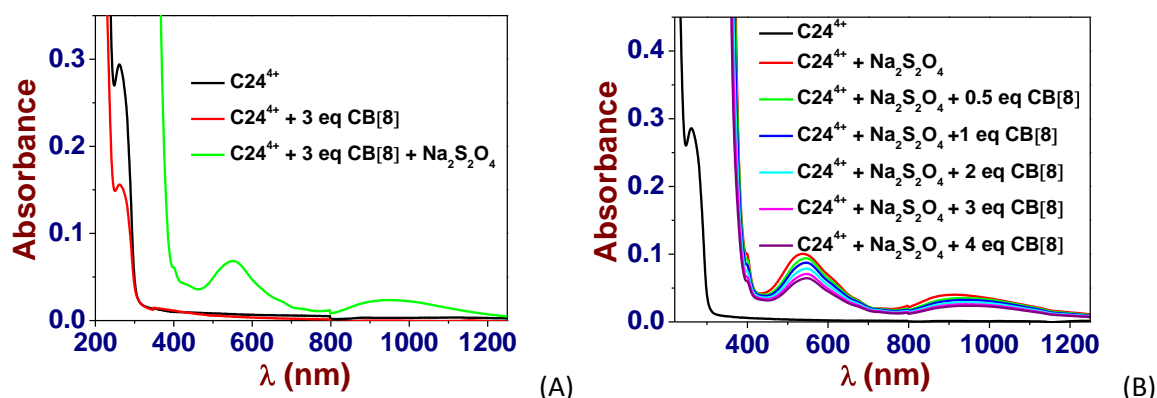


Figure 48. (A) UV-Vis.-NIR spectra of C24^{4+} ($[\text{C24}^{4+}]_0 = 10^{-5}$ M, black line) and of its $\text{C24}^{4+} \subset (\text{CB}[8])_2$ complex ($[\text{CB}[8]]_0/[\text{C24}^{4+}]_0 = 3$, red line). Addition of O_2 -free sodium dithionite (green line) induces formation of absorptions in the Vis. and NIR regions that are characteristics of the stable intramolecular radical dimeric species $\text{C24}^{2(\bullet+)}$, see Figure 39 for comparison propose with $\text{CB}[7]$). (B) UV-Vis.-NIR spectra of C24^{4+} ($[\text{C24}^{4+}]_0 = 10^{-5}$ M, black line) and of its radical species $\text{C24}^{2(\bullet+)}$ under its dimeric state (red line, addition of O_2 -free sodium dithionite). Addition of $\text{CB}[8]$ ($[\text{CB}[8]]_0/[\text{C24}^{2(\bullet+)}]_0 = 0$, red line and $[\text{CB}[8]]_0/[\text{C24}^{2(\bullet+)}]_0 = 4$, purple line) has no effect on the absorption properties of $\text{C24}^{2(\bullet+)}$. Solvent: water buffered at pH 7.0 with 0.1 M $\text{Na}_2\text{H}_2\text{PO}_4/\text{NaH}_2\text{PO}_4$; $l = 1$ cm; $T = 25.0(1)^\circ\text{C}$. In each of the solutions considered, the $\text{C24}^{2(\bullet+)}$ species was generated from C24^{4+} using freshly prepared sodium dithionite solution at *ca.* 10^{-2} under O_2 free conditions. The absorption spectra are not corrected from dilution effects.

4.2.13. Statistical Processing of the Absorption Spectrophotometric Data

The spectrophotometric data were processed using the Specfit program³³⁻³⁶ which adjusts the stability constants and the corresponding extinction coefficients of the species formed at equilibrium. Specfit uses factor analyses to reduce the absorbance matrix and to extract the eigenvalues prior to the multi-wavelength fit of the reduced data set according to the Marquardt algorithm.^{37,38}

4.3. Discussion

4.3.1. Characterization of the Thread/CB[7] [n]pseudorotaxanes

4.3.1a. Recognition of MC3²⁺ and MC4²⁺ by CB[7]

The absorption spectrophotometric binding titration of **MC3²⁺** (Figure 17) and **MC4²⁺** (Figure 19) at *ca.* 5×10^{-5} M with **CB[7]** as well as the Job plot measurements allowed us to evidence 1:1 stoichiometric (**MC3²⁺**⊂**CB[7]** and **MC4²⁺**⊂**CB[7]**) host-guest complexes. Both **MC3²⁺** and **MC4²⁺** are characterized by two main absorptions at ~ 225 nm and 260 nm (Table 2) that can be attributed to the π - π^* transitions of the *tert*-butyl-phenyl and **BIPY²⁺** chromophoric units, respectively. Interestingly, the **CB[7]** complexation mainly induces hypochromic shift of the **BIPY²⁺** transitions while those of the *tert*-butyl-phenyl are unaltered. This would indicate that **CB[7]** resides on the **BIPY²⁺** moiety rather on the apparent more hydrophobic residue such as the alkoxy-*tert*-butyl-phenyl. Steric hindrance due to the *tert*-butyl substitution likely explains this unexpected binding behaviour. The binding constant ($\log K_{\text{MC3}^{2+}\text{⊂CB[7]}} = 4.51(6)$ and $\log K_{\text{MC4}^{2+}\text{⊂CB[7]}} = 4.68(5)$ at 0.1 M phosphate buffer, pH 7.0) that were measured are lower than that calculated for **MV²⁺** as a consequence of statistical effects. Indeed, **MV²⁺** possesses two open faces to welcome a **CB[7]**, while **MC³⁺** and **MC⁴⁺** display only one (*i.e.* the *tert*-butyl-phenyl can be regarded as a bulky stopper). Consequently, the $K_{\text{MC3}^{2+}}/K_{\text{MV}^{2+}}$ (0.16) and $K_{\text{MC4}^{2+}}/K_{\text{MV}^{2+}}$ (0.24) are close to the statistical value (0.25).³⁹ At higher concentrations used for the ¹H NMR (Figure 28 and Figure 29) or high **[CB[7]]/[MC3²⁺]** (or **[CB[7]]/[MC4²⁺]**) ratios employed for the ESI-MS measurements (Figure 24 and Figure 25), another host-guest species has been characterized, namely the [3]pseudorotaxane **MC3²⁺**⊂(**CB[7]**)₂ (or **MC4²⁺**⊂(**CB[7]**)₂). For this latter species, the ¹H NMR titrations have suggested that the second **CB[7]** macrocycle is sitting close to the *tert*-butyl-phenyl unit (Figure 49). Binding of the first **CB[7]** indeed mainly affects the β , β' protons of the **BIPY²⁺** unit, while recognition of the second **CB[7]** macrocycle rather influences the protons of the *tert*-butyl-phenyl residue (Figure 28 and Figure 29). The impossibility to characterize and quantify the second recognition event leading to **MC3²⁺**⊂(**CB[7]**)₂ (or **MC4²⁺**⊂(**CB[7]**)₂) by absorption spectrophotometry likely results from the predictable weak spectral variations (see **BMV²⁺**, **MPV²⁺** and **DPV²⁺** in the previous chapters) and the much lower stability constant (statistical effects, steric interactions).

Table 2. Thermodynamic and spectroscopic parameters of [n]pseudorotaxanes formed with **CB[7]**.

Viologen V	$\log K_{V\text{⊂CB[7]}}$	λ (V) (nm) ϵ^m ($10^4 \text{ M}^{-1} \text{ cm}^{-1}$)	λ (V⊂CB[7]) (nm) ϵ^d ($10^4 \text{ M}^{-1} \text{ cm}^{-1}$)
MV²⁺	5.30(2)	227(2.96) / 257(2.06)	226(3.13) / 281(sh)
MC3²⁺	4.51(6)	224(2.29) / 259(2.17)	223(2.49) / 255(1.51)
MC4²⁺	4.68(5)	224(2.17) / 260(2.29)	224(2.48) / 252(1.40)
C23⁴⁺	4.5(1)	224(7.42) / 262(3.20)	225(7.50) / 275(2.10)
C23⁴⁺	4.44(8)	220(7.16) / 263(2.99)	220(7.29) / 280(1.83)
Solvent: water buffered at pH 7.0 with 0.1 M Na ₂ H ₂ PO ₄ /NaH ₂ PO ₄ ; <i>l</i> = 1 cm; <i>T</i> = 25.0(1)° C.			

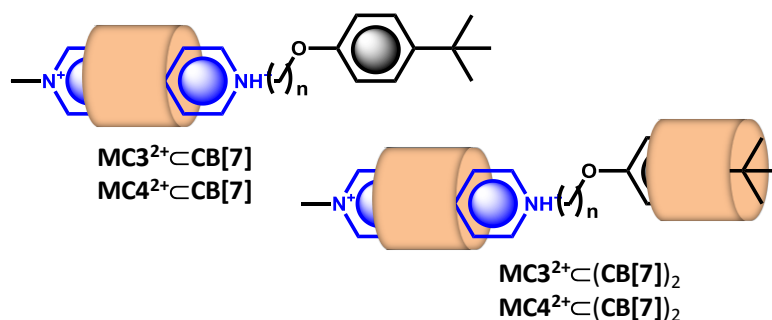


Figure 49. Schematic representation of the [2]pseudorotaxanes $\text{MC3}^{2+}\subset\text{CB}[7]$ and $\text{MC4}^{2+}\subset\text{CB}[7]$ ($\text{CB}[7]$ mainly resides on the bipyridinium group) and of $\text{MC3}^{2+}\subset(\text{CB}[7])_2$ and $\text{MC4}^{2+}\subset(\text{CB}[7])_2$ (the hydrophobic cavity of the second $\text{CB}[7]$ is sitting close to the terminal phenyl group).

To get deeper insight into the recognition properties, diffusion coefficients have been also determined by ^1H NMR-DOSY technique for MC3^{2+} and MC4^{2+} in the absence and in the presence of increasing amounts of $\text{CB}[7]$ (Table 3). First, the comparison of the diffusion coefficients of the free MC3^{2+} and MC4^{2+} revealed similar values which indicates that both model systems share common structural properties (*e.g.* volume) notwithstanding the extended 1 carbon spacer for MC4^{2+} . Secondly, the values of the diffusion coefficients experienced a stepwise decrease as a function of the number of equivalent of $\text{CB}[7]$ demonstrating that the successive formation of host-guest species of increasing volume and weight. Last but not the least, the diffusion coefficients values compare well between MC3^{2+} and MC4^{2+} regardless of the amount of $\text{CB}[7]$ added suggesting that the [2]pseudorotaxanes $\text{MC3}^{2+}\subset\text{CB}[7]/\text{MC4}^{2+}\subset\text{CB}[7]$ and [3]pseudorotaxanes $\text{MC3}^{2+}\subset(\text{CB}[7])_2/\text{MC4}^{2+}\subset(\text{CB}[7])_2$ also display similar structural properties.

Table 3. Diffusion coefficients ($\text{cm}^2 \text{s}^{-1}$) of MC3^{2+} and MC4^{2+} measured by DOSY experiments (600 MHz, D_2O , 298 K) in the absence and the presence of $\text{CB}[7]$.

– $\text{CB}[7]$		+ 1 eq $\text{CB}[7]$		+ 2 eq $\text{CB}[7]$	
MC3^{2+}	MC4^{2+}	MC3^{2+}	MC4^{2+}	MC3^{2+}	MC4^{2+}
6.51×10^{-6}	6.57×10^{-6}	4.89×10^{-6}	4.17×10^{-6}	3.56×10^{-6}	3.29×10^{-6}

4.3.1b. Recognition of C23^{4+} and C24^{4+} by $\text{CB}[7]$

Altogether, absorption binding titrations (Figure 21 and Figure 23), ^1H -NMR data (Figure 30 and Figure 31) and ESI-MS experiments (Figure 26 and Figure 27) demonstrated the predominant formation of [3]pseudorotaxanes $\text{C23}^{4+}\subset(\text{CB}[7])_2$ (or $\text{C24}^{4+}\subset(\text{CB}[7])_2$). Hypochromic and bathochromic shifts of the $\pi\text{--}\pi^*$ transitions centred on the BIPY^{2+} cores were observed in both cases (Table 2) as a consequence of the encapsulation of the terminal BIPY^{2+} chromophores by the hydrophobic macrocyclic cavity. Besides, the $\pi\text{--}\pi^*$ transitions centred on the calix[4]arene core are unaffected by $\text{CB}[7]$ complexation. As shown previously with the MC3^{2+} and MC4^{2+} model systems, the presence of a hydrophobic alkoxy substituent does not alter the recognition properties. As a result, the two $\text{CB}[7]$ macrocycles remain on the middle of the BIPY^{2+} terminal electrophores as evidenced by ^1H NMR spectroscopy (Figure 30 and Figure 31). The apparent (or average) stability constants

($\log K^*_{\text{CB234}+\text{C}(\text{CB}[7])_2} = 4.5(1)$ and $\log K^*_{\text{CB244}+\text{C}(\text{CB}[7])_2} = 4.44(8)$) were found to be close to those evaluated for the corresponding model systems (MC3^{2+} and MC4^{2+} , Table 2). Herein also, a decrease of the stability constant with respect to that of MV^{2+} ($\log K_{\text{MV}^{2+}+\text{C}(\text{CB}[7])} = 5.30(2)$) is observed as a consequence of the presence of the bulky calix[4]arene core (Figure 50).

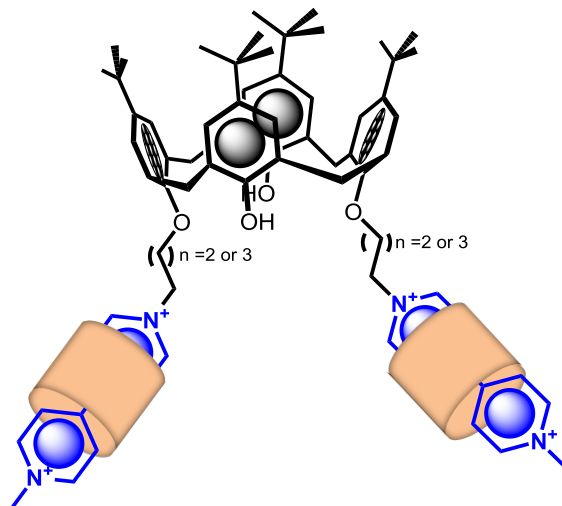


Figure 50. Schematic representation of the [3]pseudorotaxanes $\text{C23}^{4+}\text{C}(\text{CB}[7])_2$ and $\text{C24}^{4+}\text{C}(\text{CB}[7])_2$ ($\text{CB}[7]$ mainly resides on the bipyrindinium groups).

The values of diffusion coefficients have been determined by DOSY measurements for C23^{4+} and C24^{4+} measured by DOSY experiments in the absence and the presence of $\text{CB}[7]$. By contrast with the model ligands, the D value measured for C23^{4+} was found to be much lower than that of C24^{4+} . One would expect that the extended spacer of C24^{4+} increases the global volume of the molecule. This striking result thus might be explained by more flexible arms that minimize electrostatic repulsions between the two BIPY^{2+} units and steric interactions with the bulky calix[4]arene core and thereby by markedly different solvation properties. As a consequence, the diffusion coefficient decreases in the presence of $\text{CB}[7]$ for C24^{4+} , while it increases for C23^{4+} .

Table 4. Diffusion coefficients ($\text{cm}^2 \text{s}^{-1}$) of C23^{4+} and C24^{4+} measured by DOSY experiments (600 MHz, D_2O , 298 K) in the absence and the presence of $\text{CB}[7]$.

– $\text{CB}[7]$		+ 2 eq $\text{CB}[7]$	
C23^{4+}	C24^{4+}	C23^{4+}	C24^{4+}
2.58×10^{-6}	4.30×10^{-6}	3.85×10^{-6}	3.11×10^{-6}

4.3.2. Intermolecular versus Intramolecular Dimerization of the Radical Cations

We have shown that $\text{MC3}^{\bullet+}$ and $\text{MC4}^{\bullet+}$ self-associate (Figure 32 and Figure 33) in aqueous solution with $\log K_{\text{Dim}}$ value of 3.4(2) which is in the same range as the value previously determined the benzyl methyl viologen radical cation $\text{BMV}^{\bullet+}$ ($\log K_{\text{Dim}} = 3.46(5)$) and higher than that reported for the methyl viologen radical cation $\text{MV}^{\bullet+}$ ($\log K_{\text{Dim}} \sim 2.5\text{--}2.9^{40,41}$). The values of K_{Dim} compare well also with those measured for viologens decorated with

hydrophobic alkyl substituents (see previous chapters).⁴² This shows that the increase of hydrophobicity around the **BIPY**^{•+} unit with aryl/alkyl substituents favours the intermolecular pimerization in aqueous solution. Importantly, we herein again demonstrate that the extended spacer for **MC4**^{•+} does not drastically alter its pimerization since similar K_{Dim} values have been calculated for **MC3**^{•+} and **MC4**^{•+}. **MC3**^{•+} and **MC4**^{•+} are characterized by intense and structured absorptions in the visible region (**MC3**^{•+}, $\lambda_{\text{max}} \sim 602$ nm, $\epsilon^{602} = 1.01 \times 10^4 \text{ M}^{-1} \text{ cm}^{-1}$, Figure 32 and **MC4**^{•+}, $\lambda_{\text{max}} \sim 602$ nm, $\epsilon^{602} = 9.56 \times 10^3 \text{ M}^{-1} \text{ cm}^{-1}$, Figure 33), in agreement with the spectroscopic parameters determined for **MV**^{•+} (600-606 nm)^{41,42-44} or **BMV**^{•+} (600 nm, see the previous chapter). Formation of the dimer induces a significant hypsochromic shift of the absorption at ~ 600 nm ($\Delta\lambda \sim 50$ nm) and gives rise to intense radical–radical transitions in the near-IR region ($\lambda_{\text{max}} > 850$ -900 nm).⁴²

The UV-Vis absorption studies depicted in this PhD work demonstrated that no significant π -stacking interaction occurs (pimerization) except if the concentration of the radical cation of the model systems is high enough ($> 10^{-3}$ M, Figure 32 and Figure 33). As shown previously in this work with the hexaviologen derivative **HV**¹²⁺ or by other groups²⁻⁹, subtle preorganization of the **BIPY**²⁺ electrophores around a robust and inert molecular platform can amplify by far the pimerization process and lead to very stable π -dimers in aqueous solution.

Upon chemical generation of the radical cations **C23**^{2(•+)} (Figure 38) and **C24**^{2(•+)} (Figure 39), intense absorptions appeared at ~ 530 nm (Figure 51). Additional and intense absorption centred at 1072 nm for **C23**^{2(•+)} and 925 nm for **C24**^{2(•+)} can be observed and are clearly assigned to the intramolecular charge resonance that is occurring in the dimerized viologen species. This feature indicates that a two-electron reduction led to **C23**^{2(•+)} or **C23**^{2(•+)}, two radical divalent cations, which immediately pimerize intramolecularly to lead to stable radical dimeric species.

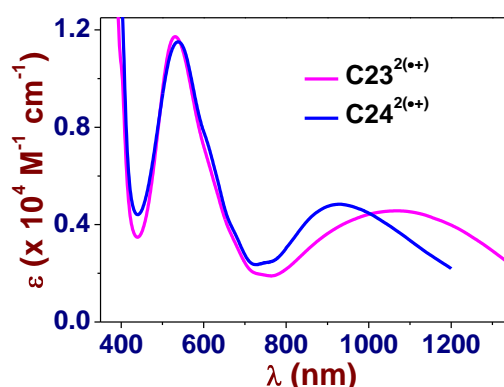


Figure 51. Electronic UV-Vis.-NIR absorption spectra of **C23**^{2(•+)} and **C24**^{2(•+)} in water. Solvent: water buffered at pH 7.0 with 0.1 M Na₂HPO₄/NaH₂PO₄. $T = 25.0(1) \text{ } ^\circ\text{C}$.

The spectroscopic signatures of the π -dimerized complexes (*i.e.* NIR absorption) have been demonstrated to be intimately related to the extent of overlapping between both π -orbitals of the **BIPY**^{•+} radicals.⁹ When a propyloxy chain links the viologens to the

calix[4]arene moiety (**C23**^{2(•+)}, $\lambda_{\max} \sim 960$ nm in CH₃CN⁹ and $\lambda_{\max} \sim 1070$ nm in water), DFT calculations at the BLYP-D3/DZVP levels suggested that only one pyridinium ring per viologen radical is involved in the intramolecular π -dimerization process. This arrangement imposed by geometric constraints that is inherent to the length and structure of the propyl chain is not observed with the ethoxy-derived calix[4]arene-*bis*-viologen (**C22**^{2(•+)}, $\lambda_{\max} \sim 860$ nm in CH₃CN⁹) that affords the fully stacked face to face arrangement. Increasing the length from 3 to 4 carbons (butyloxy derivative, **C24**^{2(•+)}, $\lambda_{\max} \sim 925$ nm in water) seemingly reinstates the face to face dimerized arrangement that was prevented by the use of a shorter propoxy spacer. The nature and size of the linker between the calix[4]arene platform and the terminal radical cations **BIPY**^{•+} as well as the nature of the platform (calix[4]arene displaying a cone conformation) thus appear to be crucial factors that govern the arrangement of the minimized π -dimers. It is noteworthy that the preorganization of the designed systems apparently allows efficient intramolecular dimerization of the two viologens upon reduction in a wide range of solvents (*e.g.* water and CH₃CN⁹).

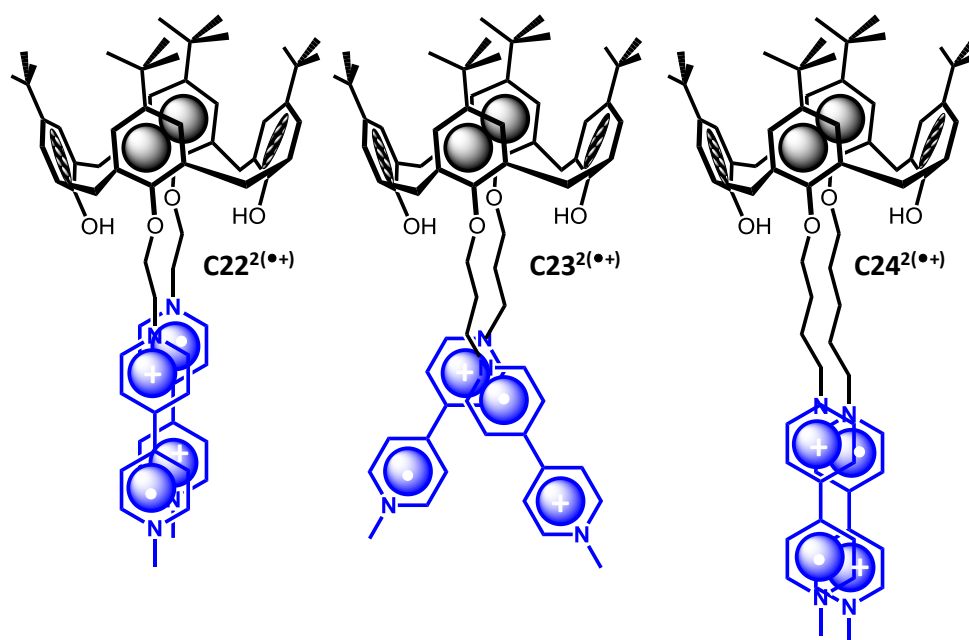


Figure 52. Schematic representation of the putative spatial arrangements of the redox-active **BIPY**^{•+} units within the two electrons reduced calix[4]arene-*bis*-viologens **C22**^{2(•+)}, **C23**^{2(•+)} and **C24**^{2(•+)} that undergo intramolecular pimerization.

4.3.3. Reduction of the [n]Pseudorotaxanes with CB[7]

4.3.3a. Monocationic Monoradicals MC3^{•+} and MC4^{•+}

Cyclic voltammetric (CV, Figure 40) and square-wave voltammetric (SWV, Figure 53) experiments in phosphate-buffered solutions at pH 7 were performed on the model systems **MC3**²⁺ and **MC4**²⁺ in the absence and presence of **CB[7]**. Both systems are characterized by two successive one-electron reversible redox waves: $E_{1/2}^1$ (**MC3**²⁺/**MC3**^{•+}) = -0.56 V and $E_{1/2}^2$ (**MC3**^{•+}/**MC3**⁰) = -0.83 V and $E_{1/2}^1$ (**MC4**²⁺/**MC4**^{•+}) = -0.56 V and $E_{1/2}^2$ (**MC4**^{•+}/**MC4**⁰) = -0.83 V.

Addition of **CB[7]** markedly alters their electrochemical properties. In the presence of three equivalents of **CB[7]** (*i.e.* it is assumed that $\text{MC3}^{2+} \subset (\text{CB}[7])_2$ and $\text{MC4}^{2+} \subset (\text{CB}[7])_2$ predominate), both redox waves shift slightly to a more negative potentials (Table 5) and retain their reversible shapes.

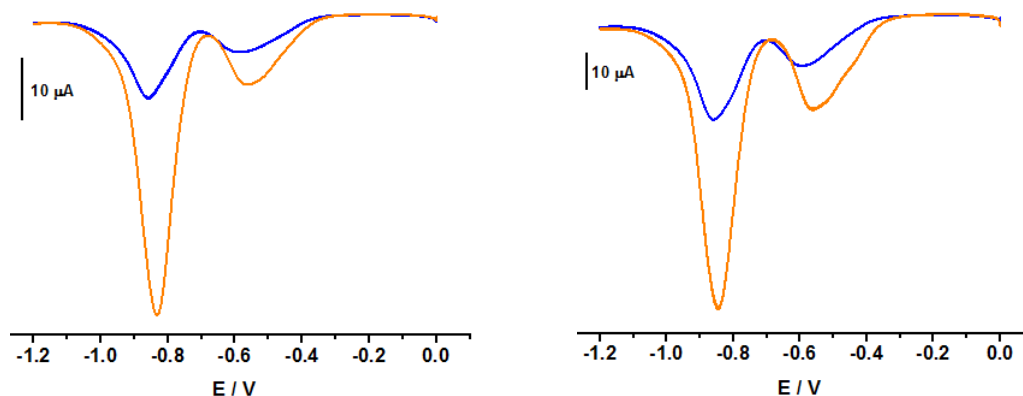


Figure 53. Square Wave voltammograms of MC3^{2+} , $[\text{MC3}^{2+}] = 0.05$ mM (left) and MC4^{2+} , $[\text{MC4}^{2+}] = 0.06$ mM (right) in the absence (orange) and the presence of **CB[7]** (blue, 3 equivalents of **CB[7]**). All voltammograms were recorded in Argon-purged phosphate buffer solutions (pH 7) at 298 K (E versus Ag/AgCl).

Table 5. Values of $E_{1/2}$ (in V) for MC3^{2+} (0.05 mM) and MC4^{2+} (6.3 mM) measured by cyclic voltammetry (CV) and square wave voltammetry (SWV) in the absence and in the presence of 3 equivalents of **CB[7]**.

Composition	$E_{1/2}^1$ (CV)	$E_{1/2}^1$ (SW)	$E_{1/2}^2$ (CV)	$E_{1/2}^2$ (SW)
MC3^{2+}	-0.56 V	-0.56 V	-0.83 V	-0.83 V
$\text{MC3}^{2+} + 3$ eq CB[7]	-0.60 V	-0.59 V	-0.85 V	-0.86 V
Composition	$E_{1/2}^1$ (CV)	$E_{1/2}^1$ (SW)	$E_{1/2}^2$ (CV)	$E_{1/2}^2$ (SW)
MC4^{2+}	-0.56 V	-0.56 V	-0.83 V	-0.84 V
$\text{MC4}^{2+} + 3$ eq CB[7]	-0.58 V	-0.58 V	-0.83 V	-0.86 V

These shifts are therefore the signatures of the relative affinities of **CB[7]** for the different redox states of the model systems. Assuming a $\log K_{\text{MC3}^{2+} \subset \text{CB}[7]} = 4.68$ for $\text{MC3}^{2+} \subset \text{CB}[7]$ that was previously determined using absorption spectrophotometric titrations, $\log K_{\text{MC3}^{\bullet+} \subset \text{CB}[7]} \sim 4-4.2$ and $\log K_{\text{MC3}^{0} \subset \text{CB}[7]} \sim 3.5-3.9$ values can be accordingly calculated.^{45,46} Similarly, using $\log K_{\text{MC4}^{2+} \subset \text{CB}[7]} = 4.5$, $\log K_{\text{MC4}^{\bullet+} \subset \text{CB}[7]} \sim 4.2$ and $\log K_{\text{MC4}^{0} \subset \text{CB}[7]} \sim 3.8$ values are calculated. The calculated values for $\text{MC3}^{2+} \subset \text{CB}[7]$ and $\text{MC3}^{\bullet+} \subset \text{CB}[7]$ using an electrochemical approach are in reasonable good agreement within the reported errors with those derived from direct absorption binding titrations ($\log K_{\text{MC3}^{\bullet+} \subset \text{CB}[7]} = 3.8(4)$ and $\log K_{\text{MC4}^{\bullet+} \subset \text{CB}[7]} = 4.5(5)$). By contrast with BMV^{2+} , MPV^{2+} or DPV^{2+} (*i.e.* a translocation motion of the **CB[7]** occurred on electrochemical reduction of the bipyridinium unit), the **CB[7]** macrocyclic host firmly resides on the BIPY^{2+} electroactive unit whatever its oxidation state.

Assuming that from 0 to -0.7 V, only the first one-electron process is dominating (Figure 40 and Figure 53), one can evaluate by chronocoulometric experiments the diffusion coefficients of MC3^{2+} or MC4^{2+} in the absence and in the presence of **CB[7]** (Table 6). The

differences observed between the values of the diffusion coefficients of $\text{MC3}^{\bullet+}/\text{MC3}^{2+}$ and $\text{MC4}^{\bullet+}/\text{MC4}^{2+}$ are a strong indication of the dimerization of the model systems upon the one-electron reduction reactions. Addition of **CB[7]** has been shown to suppress the pimerization process in favour of the inclusion complexes. As a consequence, the inclusion complexes with **CB[7]** have lower diffusion coefficients than the corresponding free viologens.

Table 6. Diffusion coefficients ($\text{cm}^2 \text{s}^{-1}$) of MC3^{2+} and MC4^{2+} measured by chronocoulometry in the absence and the presence of **CB[7]**.

Species	Diffusion coefficients ($\text{cm}^2 \text{s}^{-1}$)
$\text{MC3}^{\bullet+}$	6.88×10^{-5}
MC3^{2+}	5.4×10^{-5}
$\text{MC3}^{\bullet+} + 2\text{eq CB[7]}$	1.90×10^{-5}
$\text{MC3}^{2+} + 2 \text{ eq CB[7]}$	1.42×10^{-4}
Species	Diffusion coefficients ($\text{cm}^2 \text{s}^{-1}$)
$\text{MC4}^{\bullet+}$	3.12×10^{-5}
MC4^{2+}	8.09×10^{-4}
$\text{MC4}^{\bullet+} + 2 \text{ eq CB[7]}$	6.23×10^{-5}
$\text{MC4}^{2+} + 2\text{eq CB[7]}$	2.16×10^{-4}

UV-Vis.-NIR absorption investigations of MC3^{2+} and MC4^{2+} in water at pH 7.0 in the absence or in the presence of a reducing agent were carried out to evaluate the effect of **CB[7]** addition (Figure 32 to Figure 34). $\text{MC3}^{\bullet+} \subset \text{CB[7]}$ and $\text{MC4}^{\bullet+} \subset \text{CB[7]}$ are both clearly associated to a significant hypochromic shift of the visible absorption signals related to the radical cation, providing a solid evidence for inclusion of the radical cation $\text{BIPY}^{\bullet+}$ within the hydrophobic **CB[7]** cavity which is detrimental to pimerization for thermodynamic reasons.

4.3.3b. Bisradicals $\text{C23}^{2(\bullet+)}$ and $\text{C24}^{2(\bullet+)}$

Cyclic (Figure 40) and square wave (Figure 54) voltammetric studies have been undertaken to evaluate the impact of **CB[7]** addition on the intramolecular pimerization of the $\text{BIPY}^{\bullet+}$ radical cations of the calix[4]arene-bis-viologens C23^{4+} and C24^{4+} . The electrochemical data recorded clearly show two distinct and reversible redox waves. The relative amplitudes and shapes of the peaks for each wave at the anode (oxidation) are similar to those observed at the cathode (reduction). Such a pattern is an indication of the redox reversibility of the system.

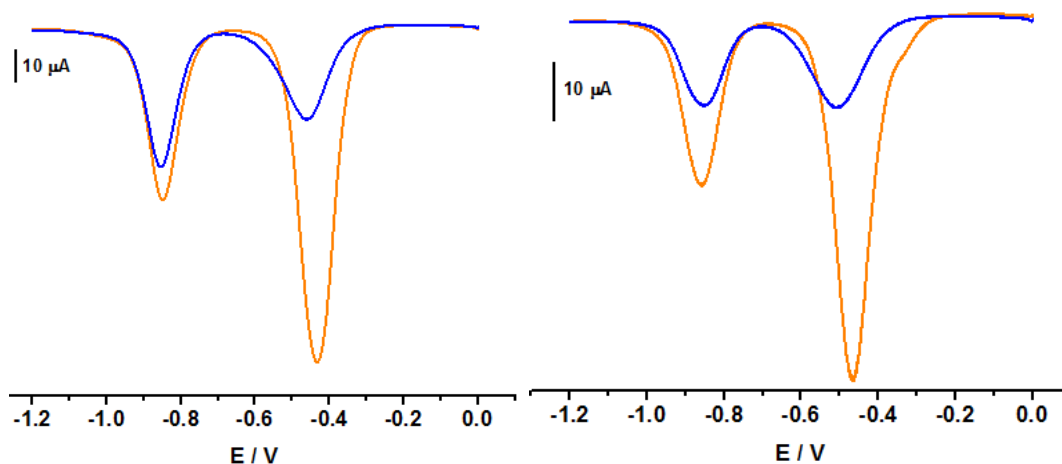


Figure 54. Square Wave voltammograms of C23^{4+} , $[\text{C23}^{4+}] = 0.05$ mM (left) and C24^{4+} , $[\text{C24}^{4+}] = 0.05$ mM (right) in the absence (orange line) and the presence of **CB[7]** (blue line, respectively 3 and 4 equivalents of **CB[7]**). All voltammograms were recorded in Argon-purged phosphate buffer solutions (pH 7) at 298 K (E versus Ag/AgCl).

The SWVs of C23^{4+} and C24^{4+} (Figure 54) display two reversible two-electron processes ($E_{1/2}^1(\text{C23}^{4+}/\text{C23}^{2(\bullet+)}) = -0.43$ V and $E_{1/2}^2(\text{C23}^{2(\bullet+)}/\text{C23}^0) = -0.85$ V and $E_{1/2}^1(\text{C24}^{4+}/\text{C24}^{2(\bullet+)}) = -0.47$ V and $E_{1/2}^2(\text{C24}^{2(\bullet+)}/\text{C24}^0) = -0.85$ V). Interestingly, for the [3]pseudorotaxanes $\text{C23}^{4+}\text{C}(\text{CB}[7])_2$ and $\text{C24}^{4+}\text{C}(\text{CB}[7])_2$, no shift was detected for the second reduction wave (Table 7), which would be expected to correspond to the following reactions: $\text{C23}^{2(\bullet+)}\text{C}(\text{CB}[7])_2 \rightarrow \text{C23}^0\text{C}(\text{CB}[7])_2$ and $\text{C24}^{2(\bullet+)}\text{C}(\text{CB}[7])_2 \rightarrow \text{C24}^0\text{C}(\text{CB}[7])_2$. This indicates that, after the first two-electron reduction process, the threads behave like free $\text{C23}^{2(\bullet+)}$ and $\text{C24}^{2(\bullet+)}$. In other words, the first reduction of $\text{C23}^{4+}\text{C}(\text{CB}[7])_2$ or $\text{C24}^{4+}\text{C}(\text{CB}[7])_2$ induces dethreading of the **CB[7]** macrocycles and is spontaneously followed by intramolecular dimerization of the two terminal **BIPY**^{•+} groups to lead to $\text{C23}^{2(\bullet)}$ and $\text{C24}^{2(\bullet)}$ species under a dimeric arrangement. These results are consistent with the absorption spectrophotometric analyses (Figure 38 and Figure 39) and EPR behaviour (Figure 43 and Figure 44) of the $\text{C23}^{4+}/\text{CB}[7]$ and $\text{C24}^{4+}/\text{CB}[7]$ [3]pseudorotaxanes.

Table 7. Values of $E_{1/2}$ (in V) for C23^{4+} (0.05 mM) and C24^{4+} (0.05 mM) measured by cyclic voltammetry (CV) and square wave voltammetry (SWV) in the absence and in the presence of 3 and 4 equivalents of **CB[7]**, respectively.

Composition	$E_{1/2}^1$ (CV)	$E_{1/2}^1$ (SW)	$E_{1/2}^2$ (CV)	$E_{1/2}^2$ (SW)
C23^{4+}	-0.42 V	-0.43 V	-0.84 V	-0.85 V
$\text{C23}^{4+} + 3$ eq CB[7]	-0.44 V	-0.46 V	-0.84 V	-0.85 V
Composition	$E_{1/2}^1$ (CV)	$E_{1/2}^1$ (SW)	$E_{1/2}^2$ (CV)	$E_{1/2}^2$ (SW)
C24^{4+}	-0.45 V	-0.47 V	-0.85	-0.85
$\text{C24}^{4+} + 4$ eq CB[7]	-0.50	-0.51	-0.85	-0.85

Chronocoulometry was also used to evaluate the diffusion coefficients of the fully oxidized and radical cationic states of the different species in aqueous solution (H_2O , 0.1 M tetrabutylammonium chloride (TBACl) as electrolyte). During the two electrons reduction process ($0\text{V} \rightarrow -0.7\text{V}$) the fully oxidized species predominate and diffuse to the electrode

surface where they are reduced. By measuring the reduction rates, the diffusion constants for **C23⁴⁺** and **C24⁴⁺** species can be calculated in the absence and in the presence of **CB[7]** (Table 8). Alternatively, by setting the voltage to -0.7 V and performing the oxidation process, the rates of oxidation and the diffusion coefficients of the corresponding radical cationic species can be measured as well. In the absence of **CB[7]**, larger diffusion coefficients were observed for **C23⁴⁺** and **C24⁴⁺** than for their corresponding fully reduced forms. This suggests an increase of hydrodynamic size that occurs upon reduction and subsequent pimerization (decrease of the hydrophobic character and markedly different solvation shell). In the presence of **CB[7]**, larger diffusion coefficients were measured for the [3]pseudorotaxanes **C23⁴⁺⊂(CB[7])₂** and **C23⁴⁺⊂(CB[7])₂** than the corresponding reduced species (*i.e.* upon reduction, a dethreading of the **CB[7]** occurs as a consequence of favoured intramolecular pimerization with respect to the recognition process). Here also, one would expect that the [3]pseudorotaxanes **C23⁴⁺⊂(CB[7])₂** and **C23⁴⁺⊂(CB[7])₂** display larger hydrodynamic size by comparison with **C23^{2(•+)}** or **C24^{2(•+)}**. Markedly different solvation of the latter species is suggested to explain these peculiar properties. These calix[4]arene-*bis*-viologen derivatives stand in interesting contrast with the diffusion coefficients values and properties that were measured for **BV⁴⁺** and **HV¹²⁺** (see the previous chapter).

Table 8. Diffusion coefficients ($\text{cm}^2 \text{s}^{-1}$) of **C23⁴⁺** and **C24⁴⁺** measured by chronocoulometry in the absence and the presence of **CB[7]**.

Species	Diffusion coefficients ($\text{cm}^2 \text{s}^{-1}$)
C23^{•+}	1.41×10^{-5}
C23²⁺	7.58×10^{-5}
C23^{•+} + 3 eq CB[7]	2.9×10^{-5}
C23²⁺ + 3 eq CB[7]	3.91×10^{-5}
Species	Diffusion coefficients ($\text{cm}^2 \text{s}^{-1}$)
C24^{•+}	8.13×10^{-6}
C24²⁺	2.01×10^{-4}
C24^{•+} + 4 eq CB[7]	1.6×10^{-6}
C24²⁺ + 4 eq CB[7]	4.21×10^{-4}

4.3.4. Recognition of the Viologen Threads by CB[8]

The characterization of the host-guest complexes formed with **MC3²⁺**, **MC4²⁺**, **C23⁴⁺** or **C24⁴⁺** and **CB[8]** has been investigated by absorption spectrophotometry (Figure 45 to Figure 48) and ESI-MS measurements (Figure 24 to Figure 27). Due to the limited solubility of **CB[8]**, we were not able to perform ^1H NMR titrations of the corresponding viologens. Similarly to the [n]pseudorotaxanes formed with **CB[7]**, we were able to also evidence the formation of [2]pseudorotaxanes with **MC3²⁺** and **MC4²⁺** (namely **MC3²⁺⊂CB[8]** and **MC4²⁺⊂CB[8]**) and [3]pseudorotaxanes with **C23⁴⁺** and **C24⁴⁺** (namely a **C23⁴⁺⊂(CB[8])₂** and **C24⁴⁺⊂(CB[8])₂**).

4.3.5. Reduction of the [n]Pseudorotaxanes with CB[8]

Similarly to the calix[4]arene in the presence of **CB[7]**, chemical reduction of the **BIPY²⁺** electroactive units led to dethreading of the **CB[8]** macrocyclic host despite its larger cavity size (Figure 47 and Figure 48). This suggests strong steric constraints with the calix[4]arene platform and/or poor flexibility of the designed systems even though rather long and apparent flexible spacers have been introduced. This peculiar behaviour can however be rationalized with the model systems **MC3²⁺** and **MC4²⁺** that were clearly demonstrated (Figure 45 and Figure 46) to lead to the expected [3]pseudorotaxanes (**MC3^{•+}**)₂⊂**CB[8]** and (**MC4^{•+}**)₂⊂**CB[8]** thus emphasizing the major role of the anchoring platform rather than the length of the spacers. The occurrence of [3]pseudorotaxanes (**MC3^{•+}**)₂⊂**CB[8]** and (**MC4^{•+}**)₂⊂**CB[8]** in a reducing milieu is in agreement with the published reports⁴⁶⁻⁴⁷⁴⁸ that showed that the stability of methyl viologen dimer (**MV^{•+}**)₂ was significantly increased in the presence of **CB[8]** following the formation of a 2:1 (**MV^{•+}**)₂⊂**CB[8]** supramolecular complex in water.

4.4. Conclusion

In the search of efficient anchoring systems to efficiently preorganize and distribute viologen residues, we have already considered a hexavalent phosphazene which was proven to fulfil most of the targeted requirements (easiness of functionalization, efficient and fast polymerization, and applicability in electrochromic material research, marked recognition properties as function of its redox state). Following this approach, calix[4]arene has then been considered thanks to its numerous conformational and structural properties. Up to four positions can be substituted either on the lower or upper rims (*i.e.* we have considered in this preliminary approach only the disubstituted derivatives). The conformation properties of the calix[4]arene can be easily controlled (*i.e.* only the cone conformation has been evaluated in this first approach).

Two calix[4]arene-*bis*-viologen systems, namely **C23⁴⁺** and **C24⁴⁺** (Figure 6) have been successfully synthesized. The host-guest properties have been extensively studied using a large set of analytical methods and led to the characterization of [3]pseudorotaxanes in combination with either **CB[7]** or **CB[8]**. For each of these host-guest species, the **CB[7]** or **CB[8]** was demonstrated to reside in the middle of the **BIPY²⁺** dications as a result of steric interactions with the anchoring platform. On reduction of the terminal bipyridiniums, these [3]pseudorotaxanes spontaneously dissociate as the result of a strong intramolecular dimerization of the two face-to-face viologen radical cations. The arrangement of the **BIPY^{•+}** radical cations within the dimeric species seemingly relies on the length of the spacer that links the electroactive units to the anchoring moiety. Decomplexation and dimerization do not occur in experiments involving **CB[7]** (or **CB[8]**) and either of the two monomeric viologen guests **MC3²⁺** and **MC4²⁺**, which were used as model systems.

The model compounds provided unexpected and valuable properties. Thanks to the presence of an alkoxy-phenyl substitution, [3]pseudorotaxanes such as **MC3²⁺**⊂(**CB[7]**)₂ and

$\text{MC4}^{2+} \subset (\text{CB}[7])_2$ were characterized. For the $\text{MC3}^{2+} \subset \text{CB}[7]$ and $\text{MC3}^{2+} \subset \text{CB}[7]$ [2]pseudorotaxanes, no translocation of the hydrophobic macrocyclic host between two binding stations, as observed for the previous systems such as BMV^{2+} , MPV^{2+} and DPV^{2+} , were observed indicating that the BIPY^{2+} unit remained the privileged recognition site whatever its redox state. In the presence of the larger **CB[8]** host, similar properties were emphasized with the oxidized form of MC3^{2+} and MC4^{2+} threads. However, [3]pseudorotaxanes ($\text{MC3}^{(\bullet+)} \subset \text{CB}[8]$) and ($\text{MC4}^{(\bullet+)} \subset \text{CB}[8]$) were predominantly formed as a consequence of the larger cavity size of the **CB[8]** host.

This preliminary study provided interesting information for the further development of functional electroactive systems. It is already planned to prepare the *tetrakis* analogues using both a cone or 1,3-alternate arrangement of the anchoring unit.

Bibliographic Section

- 1 (a) Nchimi Nono, K.; Dalvand, P.; Wadhwa, K.; Nuryyeva, S.; Alneyadi, S.; Fahrenbach, A.; Olsen, J.-C.; Asfari, Z.; Platas-Iglesias, C.; Elhabiri, M.; Trabolsi, A. *Chem. Eur. J.* **2014**, *20*, 7334-7344. (b) K. Wadhwa, S. Nuryyeva, A. C. Fahrenbach, M. Elhabiri, C. Platas-Iglesias, A. Trabolsi, *J. Mater. Chem. C* **2013**, *1*, 2302–2307.
- 2 Kannappan, R.; Bucher, C.; Saint-Aman, E.; Moutet, J. C.; Milet, A.; Oltean, M.; Méta y, Pellet-Rostaing, E. S.; Lemaire, M.; Chaix, C. *New J. Chem.* **2010**, *34*, 1373-1386.
- 3 Geuder, W.; Huenig, S.; Suchy, A. *Tetrahedron* **1986**, *42*, 1665-1667.
- 4 Atherton, S. J.; Tsukahara, K.; Wilkins, R. G. *J. Am. Chem. Soc.* **1986**, *108*, 3380-3385.
- 5 Iordache, A.; Retegan, M.; Thomas, F.; Royal, G.; Saint-Aman, E.; Bucher, C. *Chem. Eur. J.* **2012**, *18*, 7648-7653.
- 6 Iordache, A.; Oltean, M.; Milet, A.; Thomas, F.; Saint-Aman, E.; Bucher, C. *J. Am. Chem. Soc.* **2012**, *134*, 2653-2671.
- 7 Mohammad, M. *Electrochim. Acta* 1988, *33*, 417-419.
- 8 J. Iehl, M. Frasconi, H.-P. Jacquot de Rouville, N. Renaud, S. M. Dyar, N. L. Strutt, R. Carmieli, M. R. Wasielewski, M. A. Ratner, J.-F. Nierengarten, J. F. Stoddart *Chem. Sci.* **2013**, *4*, 1462-1469.
- 9 (a) Iordache, A.; Kanappan, R.; Méta y, E.; Duclos, M. C.; Pellet-Rostaing, S.; Lemaire, M.; Milet, A.; Saint-Aman, E.; Bucher, C. *Org. Biomol. Chem.* **2013**, *11*, 4383-4389. (b) Kahlfuss, C.; Méta y, E.; Duclos, M. C.; Lemaire, M.; Oltean, M.; Milet, A.; Saint-Aman, E.; Bucher, C. *R. Chimie* **2014**, *17*, 505–511.
- 10 Gutsche, C. D.; Iqbal, M.; Stewart, D. *J. Org. Chem.* **1986**, *51*, 742-745.
- 11 Gutsche, C. D.; Iqbal, M. *Org. Synth.* **1990**, *68*, 234-237.
- 12 Guo, D.-S.; Liu, Y. *Chem. Soc. Rev.* **2012**, *41*, 5907-5921.
- 13 Gutsche, C. D.; Muthukrishnan, R. *J. Org. Chem.* **1978**, *43*, 4905-4906.
- 14 https://en.wikipedia.org/wiki/Krater#Calyx_krater
- 15 Baeyer, A. *Ber. Dtsch. Chem. Ges.* **1872**, *5*, 25; 280.
- 16 Zinke Synthesis In *Comprehensive Organic Name Reactions and Reagents* **2010**, *70*, 13183-13196.
- 17 Zinke, A.; Ziegler, E. *Ber. Dtsch. Chem. Ges.* **1944**, *77*, 264-272.
- 18 Zinke, A.; Zigeuner, G.; Hössinger, K.; Hoggmann, G. *Monatsh.* **1948**, *77*, 438-439.
19. Conforth, J. W.; D'Arcy Hart P.; Nicholls, G. A.; Rees, R. J. W.; Stock, J. A. *Br. J. Pharmacol.* **1995**, *10*, 73-86.
- 20 Conforth, J. W.; Morgan, E. D.; Potts, K. T.; Rees, R. J. W. *Tetrahedron.* **1973**, *29*, 1659-1667.
- 21 Vocanson, F.; Lamartine, R.; Longery, P.; Gauvrit, J. Y. *New J. Chem.* **1995**, *19*, 825-829.
- 22 Dumazet, I., PhD Thesis Claude Bernard University Lyon 1, **1997**.
- 23 Stewart, D. R.; Gutsche, C. D. *J. Am. Chem. Soc.* **1999**, *121*, 4136-4146.
- 24 Gutsche, C. D.; Dhawan, B.; Levine, J. A.; No, K.H.; Bauer, L. J. *Tetrahedron.* **1983**, *39*, 409-426.
- 25 Groenen, L. C.; Van Loon, J. D.; Verboom, W.; Harkema, S.; Casnati, A.; Ungaro, R.; Pochini, A.; Ugozzoli, F.; Reinhoudt, D. N. *J. Am. Chem. Soc.* **1991**, *113*, 2385-2392.
- 26 Thondorf, I.; Shivanyuk, A.; Bohmer, V. In *Calixarene 2001*, asfari, Z.; Bohmer, V.; Harrowfield, J.; Vicens, J. Eds., Kluwer Academic publisher, Dordrecht, **2001**, *2*, 26.
- 27 Ko, H.-C.; Park, S.-A.; Paik, W.-K.; Lee, H. *Synth. Met.* **2002**, *132*, 15-20.
- 28 Pomecko, R. PhD Thesis University of Strasbourg, **2007**.
- 29 Li, Z.-T.; Ji, G.-Z.; Zhao, C.-X.; Yuan, S.-D.; Ding, H.; Huang, C.; Du, A.-L.; Wei, M. *J. Org. Chem.* **1999**, *64*, 3572-3584.

- 30 Hou, J. L.; Yi, H. P.; Shao, X. B.; Li, C.; Wu, Z. Q.; Jiang, X. K.; Wu, L. Z.; Tung, C. H.; Li, Z. T. *Angew. Chem. Int. Ed.* **2006**, *45*, 796-800.
- 31 Trabolsi, A.; Urbani, M.; Delgado, J. L.; Ajamaa, F.; Elhabiri, M.; Solladié, N.; Nierengarten, J. F.; Albrecht-Gary, A. M. *New J. Chem.* **2008**, *32*, 159-165.
- 32 Alberti, A. In *Organic Photochromic and Thermochromic Compounds*, Crano, J. C.; Guglielmetti, R. J., Eds., Kluwer Academic publisher, **2002**, *4*, 211-240.
- 33 Gampp, H.; Maeder, M.; Meyer, C. J.; Zuberbühler, A. D. *Talanta* **1985**, *32*, 95-101.
- 34 Rossotti, F. J. C.; Rossotti, H. S.; Whewell, R. J. *J. Inorg. Nuc. Chem.* **1971**, *33*, 2051-2065.
- 35 Gampp, H.; Maeder, M.; Meyer, C. J.; Zuberbühler, A. D. *Talanta* **1985**, *32*, 257-264.
- 36 Gampp, H.; Maeder, M.; Meyer, C. J.; Zuberbühler, A. D. *Talanta* **1986**, *33*, 943-951.
- 37 Marquardt, D. W. *J. Soc. Ind. Appl. Math.* **1963**, *11*, 431-441.
- 38 Maeder, M.; Zuberbuehler, A. D. *Anal. Chem.* **1990**, *62*, 2220-2224.
- 39 Perlmutter-Hayman, B. *Acc. Chem. Res.* **1986**, *19*, 90-96.
- 40 Lee, C.; Moon, M. S.; Park, J. W. *J. Electroanal. Chem.* **1996**, *407*, 161-167.
- 41 Stargardt, J. F.; Hawkridge, F. M. *Anal. Chim. Acta* **1983**, *146*, 1-8.
- 42 Kosower, E. M.; Cotter, J. L. *J. Am. Chem. Soc.* **1964**, *86*, 5524-5527.
- 43 Park, J. W.; Choi, N. H.; Kim, J. H. *J. Phys. Chem.*, **1996**, *100*, 769-774.
- 44 Monk, P. M. S.; Hodgkinson, N. M.; Ramzan, S. A. *Dyes Pigm.* **1999**, *43*, 207-217.
- 45 Lee, J. W.; Samal, S.; Selvapalam, N.; Kim, H.-J.; Kim, K. *Acc. Chem. Res.* **2003**, *36*, 621-630.
- 46 Kim, H.-J.; Jeon, W. S.; Ko, Y. H.; Kim, K. *Proc. Natl. Acad. Sci. USA* **2002**, *99*, 5007-5011.
- 47 Ong, W.; Gomez-Kaifer, M.; Kaifer, A. E. *Org. Lett.*, **2002**, *4*, 1791-1794.
- 48 Jeon, W. S.; Kim, H.-J.; Lee, C.; Kim, K. *Chem. Commun.*, **2002**, 1828-9.

**Chapter V: Recognition of
Azo-Aryl-Imidazoles by
Phen-Strapped
Porphyrins**

5.1. Introduction

This last chapter summarizing the main results obtained in the frame of my PhD work was done in close collaboration with the groups of Dr Jean Weiss (synthesis of the phenanthroline strapped porphyrins, Controlled Ligand Architectures in Coordination Chemistry, Institut de Chimie de Strasbourg, UMR 7177 CNRS-UdS, Strasbourg) and Pr. Ali Trabolsi (synthesis of the azo-chromophores, Supramolecular Multifunctional Systems, New York Abu Dhabi University, Abu Dhabi, UAE). It mainly focuses on the physico-chemical characterization of the pentacoordinated complexes of phenanthroline strapped porphyrins with new azo-imidazole substrates (Figure 1). A series of azo-aryl-imidazoles whose bulkiness of the aromatic moiety has been varied have been herein considered. The aim of this study was to use the valuable properties of azo-chromophores (*trans-to-cis* isomerization induced by light) to induce dissociation (“photoejection”) of the pentacoordinated systems. Thermal re-equilibration is thus expected to reinstate the thermodynamically favoured pentacoordinated complexes. This physico-chemical work constituted a preliminary approach to evaluate the strength and kinetic properties of phenanthroline strapped porphyrins toward a homogenous series of azo-aryl-imidazoles. The spectroscopic, thermodynamic and kinetic aspects of the recognition processes leading to the pentacoordinated porphyrinic complexes with these azo-imidazoles substrates have been studied using a set of complementary analytical tools such as absorption/emission spectrophotometries and stopped-flow measurements.

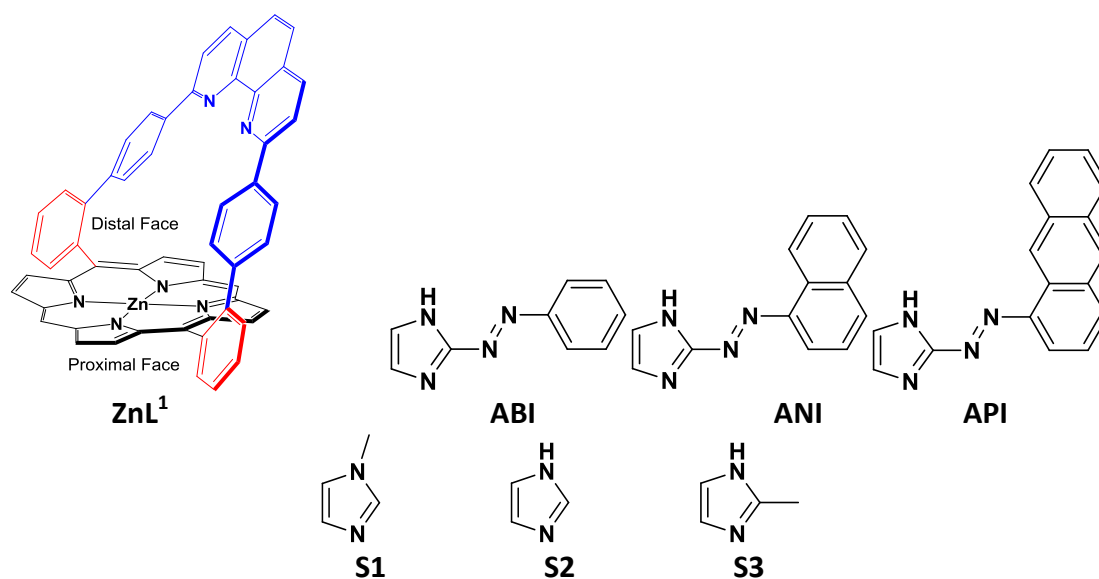


Figure 1. Chemical structures of the strapped Zn(II) porphyrin receptor and the imidazole (**S1-S3**) and azo-aryl-imidazole (**ABI, ANI** and **API**) substrates examined in this work.

Azo-chromophores are well-known photo-responsive systems that undergo *cis/trans* isomerization under UV-Vis light irradiation.¹ The *trans*-isomer of these chromophores is sterically less encumbered than the *cis*-isomer, and the two configurations are characterized by distinct absorption profiles. Moreover, selective excitation in the UV region, where the *trans*-isomer absorbs more intensely, causes displacement of the equilibrium toward the *cis*-

isomer. Irradiation with visible light or application of heat (thermal equilibration) converts *cis* back to *trans*.

The group of Dr Jean Weiss (UMR 7177 CNRS-UdS, Strasbourg) and my hosting have developed and thoroughly studied the selective recognition of imidazoles by phenanthroline superstructured Zn(II) porphyrins^{2,3} that was further used as an efficient assembling tool for the design of self-assembling supramolecular building-blocks.^{4,5} A careful ligand design based on the induced-fit principle indeed led to the selective and strong recognition of imidazoles by various receptors whose bulkiness on the *meso*-positions has been varied. The main outcomes of these studies showed that imidazole recognition results from a strong *N*-imidazolyl-Zn(II) axial coordination⁹ and bifurcated hydrogen bonds between the substrate and the nitrogen atoms of the 1,10-phenanthroline strap of the receptor. Introduction of secondary interactions (π - π stacking, CH- π , hydrophobic interactions) also contributed to strengthen the final assemblies. This self-assembly approach was successfully implemented in photodyads^{5,10} or linear porphyrin arrays.¹¹ The goal of this project is to fruitfully employ these host-guest recognition properties to subtly decorate Zn(II) porphyrinic receptors with azo-chromophores with the aim of developing photoresponsive materials such as Metal-Organic Frameworks (MOFs).

5.2. Experimental Section and Results

5.2.1. Starting Materials and Solvents

Zinc porphyrins (ZnL¹ and ZnTPP) were synthesized according to a previously published procedure.^{2,12} All analyses were carried out with spectroscopic grade 1,2-dichloroethane (Merck, 99.8% or Carlo Erba, 99.8% for spectroscopy), which was further purified by distillation over CaH₂ to remove HCl traces. All solutions were protected from daylight to avoid any photochemical degradation. The imidazole substrates (1-methyl-1*H*-imidazole **S1**, 1*H*-imidazole **S2**, 2-methyl-1*H*-imidazole **S3**) were purchased from commercial sources and used without further purification. The azo-aryl-imidazoles azo-benzene-imidazole (noted **ABI**), azo-naphthyl-imidazole (noted **ANI**) and azo-phenanthryl-imidazole (noted **API**) were synthesized by the group of Pr Ali Trabolsi (Supramolecular Multifunctional Systems, New York Abu Dhabi University, Abu Dhabi, UAE). All stock solutions were prepared using a AG 245 Mettler Toledo analytical balance (precision 0.01mg) and the complete dissolution in dichloroethane was achieved with the help of ultrasonic bath. The concentrations of the reactants were calculated by weighing solid products. The experiments were carried out at 25.0(2) °C maintained with the help of Haake FJ or Lauda E200 thermostats.

5.2.2. UV-Vis. Absorption Spectrophotometric Titrations

The absorption spectrophotometric titration of the receptors ZnL¹ ($\sim 10^{-6}$ M) and ZnTPP ($\sim 10^{-5}$ M) with **S_n** ($n = 1-3$) and **ABI**, **ANI** and **API** were carried out in a Hellma quartz optical cell (1 cm). Microvolumes of a concentrated solution of **Sⁿ** ($n = 1-3$), **ABI**, **ANI** or **API** were added to 2 mL of the porphyrinic receptors with microliter Hamilton syringes (#710 and #750).

Special care was taken to ensure that complete equilibration was attained. Special care was taken to ensure that complete equilibration was attained the corresponding UV-Visible spectra were recorded from (200 nm – 850 nm) on a Cary 5000 (Agilent) spectrophotometer maintained at 25.0(2) °C by the flow of a Dual Cell Pelletier Accessory (Cary Varian).

Figure 2 to Figure 4 first depict the absorption spectrophotometric titrations of ZnTPP with **ABI**, **ANI** and **API**. Those related to the binding titrations of 1-methyl-1*H*-imidazole **S1**, 1*H*-imidazole **S2** and 2-methyl-1*H*-imidazole **S3** have been already described by my hosting group^{4,5} and will not be shown herein. Due to the low stability constants, the absorption study was focussed on the less intense Q bands of the ZnTPP porphyrin which allowed us to increase its analytical concentration and thereby to favour binding in solution for accurate determination. The statistical processing of the absorption data allowed us to calculate the binding constants for **ABI** and **ANI** as well as the electronic spectra of the ZnTPP host and the pentacoordinated complexes. Interestingly, no evidence of complex formation was observed for **API** whose bulkiness (phenanthrene substitution) prevent axial ligation of the Zn(II) metal centre of the porphyrinic receptor. The stability constants are provided in Table 1.

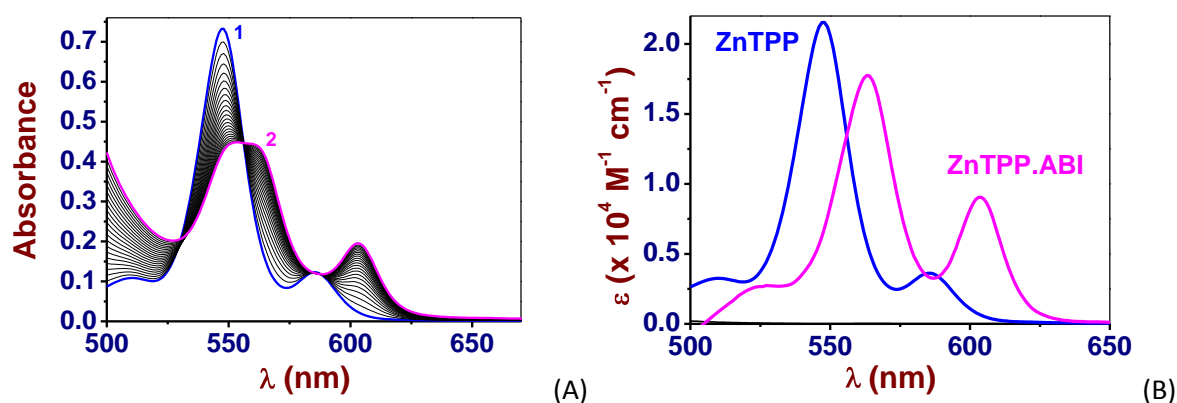


Figure 2. (A) UV-Vis. absorption spectrophotometric titration of ZnTPP by azo-benzene-imidazole (**ABI**). Solvent: 1,2-dichloroethane; $T = 25.0(2) \text{ }^\circ\text{C}$; $l = 1 \text{ cm}$. (1) $[\text{ZnTPP}]_0 = 3.4 \times 10^{-5} \text{ M}$; (2) $[\text{ABI}]_0/[\text{ZnTPP}]_0 = 131$. (B) Electronic spectra of ZnTPP and its pentacoordinated species with **ABI**.

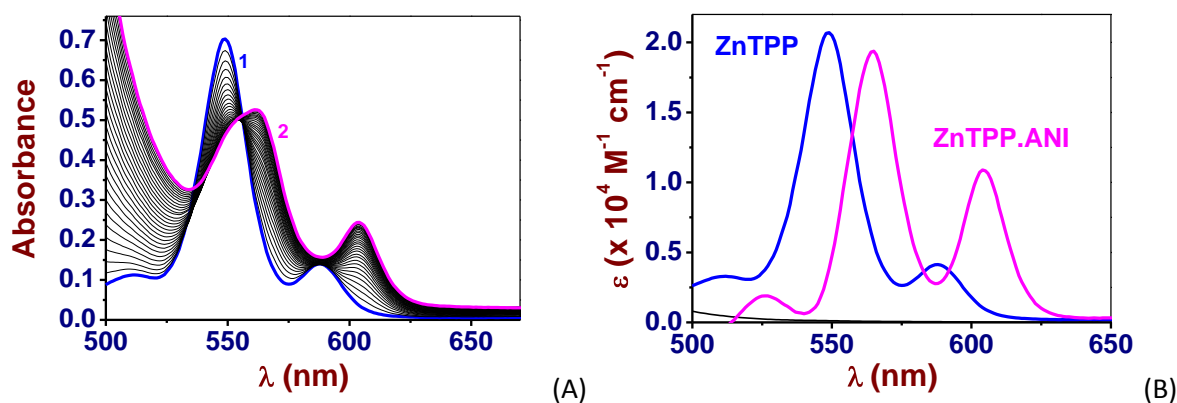


Figure 3. (A) UV-Vis. absorption spectrophotometric titration of ZnTPP by azo-naphthyl-imidazole (**ANI**). Solvent: 1,2-dichloroethane; $T = 25.0(2) \text{ }^\circ\text{C}$; $l = 1 \text{ cm}$. (1) $[\text{ZnTPP}]_0 = 3.4 \times 10^{-5} \text{ M}$; (2) $[\text{ANI}]_0/[\text{ZnTPP}]_0 = 82$. (B) Electronic spectra of ZnTPP and its pentacoordinated species with **ANI**.

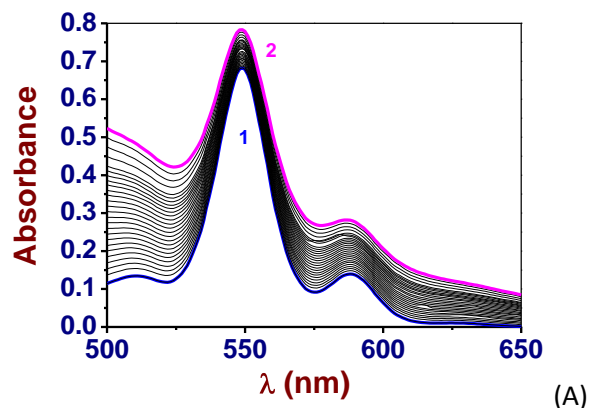


Figure 4. UV-Vis. absorption spectrophotometric titration of ZnTPP by azo-phenanthryl-imidazole (API). Solvent: 1,2-dichloroethane; $T = 25.0(2) \text{ }^\circ\text{C}$; $l = 1 \text{ cm}$. (1) $[\text{ZnTPP}]_0 = 3.4 \times 10^{-5} \text{ M}$; (2) $[\text{API}]_0/[\text{ZnTPP}]_0 = 1015.7$.

Figure 5 to Figure 7 show the absorption spectrophotometric titrations of ZnL^1 with **ABI**, **ANI** and **API**. Those related to the binding titrations of 1-methyl-1*H*-imidazole **S1**, 1*H*-imidazole **S2** and 2-methyl-1*H*-imidazole **S3** will not be described in this report (i.e. see references 4 and 5). Statistical processing of the absorption data allowed calculating the binding constants for **ABI** and **ANI** as well as the electronic spectra of the ZnL^1 host and the pentacoordinated complexes (Table 1). As observed already with ZnTPP, no evidence of complex formation was observed for **API** due to strong steric interactions between the phenanthrene substituent and the tetrapyrrolic/phen units of the ZnL^1 .

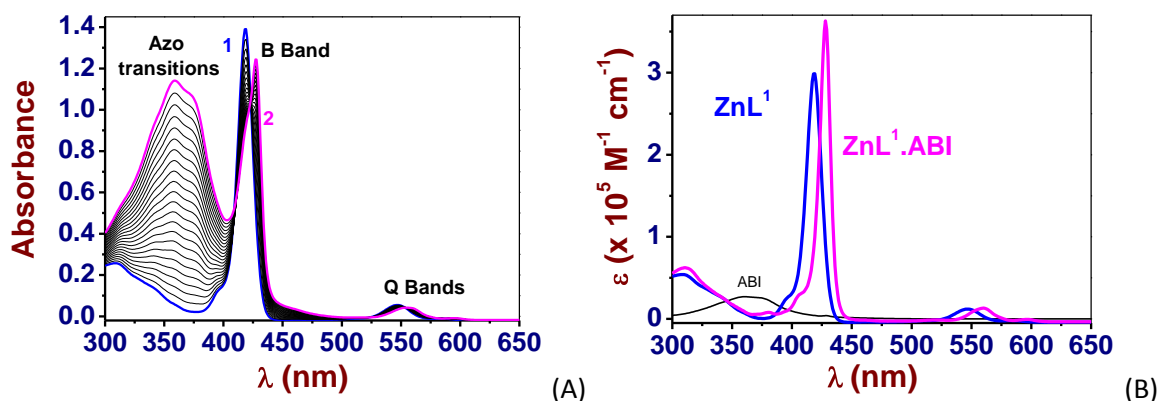


Figure 5. (A) UV-Vis. absorption spectrophotometric titration of ZnL^1 by azo-benzene-imidazole (**ABI**). Solvent: 1,2-dichloroethane; $T = 25.0(2) \text{ }^\circ\text{C}$; $l = 1 \text{ cm}$. (1) $[\text{ZnL}^1]_0 = 4.69 \times 10^{-6} \text{ M}$; (2) $[\text{ABI}]_0/[\text{ZnL}^1]_0 = 35.18$. (B) Electronic spectra of the ZnL^1 receptor and its pentacoordinated species with **ABI**.

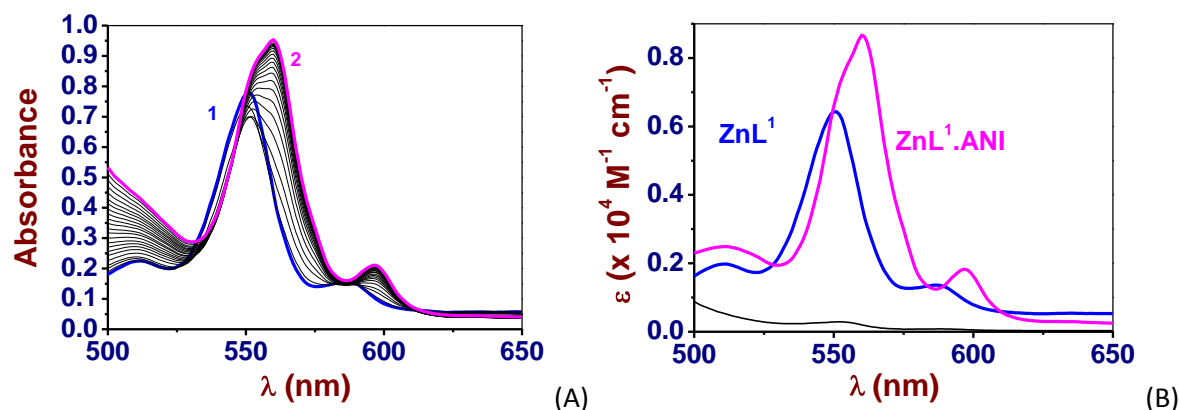


Figure 6. (A) UV-Vis. absorption spectrophotometric titration of ZnL^1 by azo-naphthyl-imidazole (**ANI**). Solvent: 1,2-dichloroethane; $T = 25.0(2)^\circ\text{C}$; $l = 1$ cm. (1) $[\text{ZnL}^1]_0 = 4.80 \times 10^{-6}$ M; (2) $[\text{ANI}]_0/[\text{ZnL}^1]_0 = 3.97$. (B) Electronic spectra of the ZnL^1 receptor and its pentacoordinated species with **ANI**.

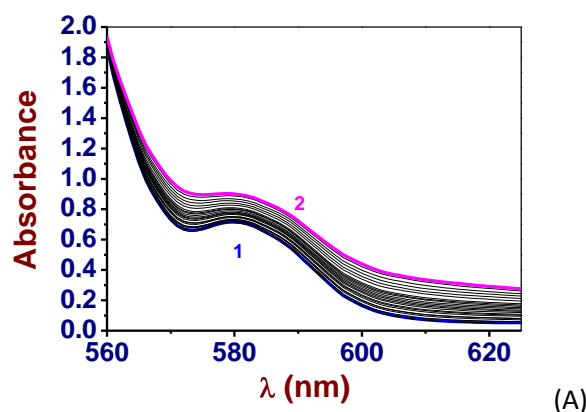


Figure 7. UV-Vis. absorption spectrophotometric titration of ZnL^1 by azo-phenanthryl-imidazole (noted **API**). Solvent: 1,2-dichloroethane; $T = 25.0(2)^\circ\text{C}$; $l = 1$ cm. (1). $[\text{ZnL}^1]_0 = 4.80 \times 10^{-6}$ M; (2) $[\text{API}]_0/[\text{ZnL}^1]_0 = 223.6$.

5.2.3. Luminescence Titrations

Luminescence titrations were carried out on solutions of ZnL^1 or ZnTPP with an absorbance smaller than 0.1 at wavelengths $\geq \lambda_{\text{exc}}$ in order to avoid any errors due to inner filter effect. The titrations of 2 mL of the metalloporphyrins were carried out in a 1 cm Hellma quartz optical cell by addition of known microvolumes of solution of S^n ($n = 1-3$), **ABI**, **ANI** or **API** with microliter Hamilton syringes (#710 and #750). The excitation wavelength corresponds to an isosbestic point (Q bands) between the free receptor and the pentacoordinated complex or to the smallest absorbance amplitudes measured along the absorption spectrophotometric titrations. The Zn(II) porphyrin-centred luminescence spectra were recorded from 550 nm to 800 nm on a Perkin-Elmer LS-50B maintained at 25°C by the flow of a Haake FJ thermostat. The light source was a pulsed xenon flash lamp with a pulse width at half peak height $< 10 \mu\text{s}$ and power equivalent to 20kW.

Figure 8 and Figure 9 illustrate the luminescence spectrophotometric titrations of ZnTPP with ABI and ANI. Those related to the binding titrations of 1-methyl-1*H*-imidazole **S1**, 1*H*-imidazole **S2** and 2-methyl-1*H*-imidazole **S3** can be found in references 4 and 5. The excitation wavelengths were fixed at ~ 550 -560 nm which correspond to isosbestic points evidenced along the absorption spectrophotometric titrations (Figure 2 and Figure 3). Photoexcitation of the Q transitions of the Zn(II) porphyrin ZnTPP resulted in two emission bands in the 550-700 nm spectral window that were attributed to the $S_1 \rightarrow S_0$ (Q(0,0) and Q(0,1)) transitions.¹³⁻¹⁵ Addition of increasing amounts of the two azo-chromophores ABI and ANI resulted in a partial quenching of the ZnTPP-centred emission likely due to electron or energy transfer from the metalloporphyrin to the azo-aryl system. This stands in an interesting contrast with the imidazoles **S2** and **S3** which led to bathochromic shifts of the $S_1 \rightarrow S_0$ transitions as a consequence of the Zn(II) binding^{4,5} thus confirming the major role of the azo-chromophore in the quenching process. The processing of the spectrofluorimetric data allowed determining association constants that were found in good agreement with those derived from absorption binding titrations (Table 1). It is noteworthy that **API** did not lead to significant emission variation as a consequence of its bulkiness (data not shown).

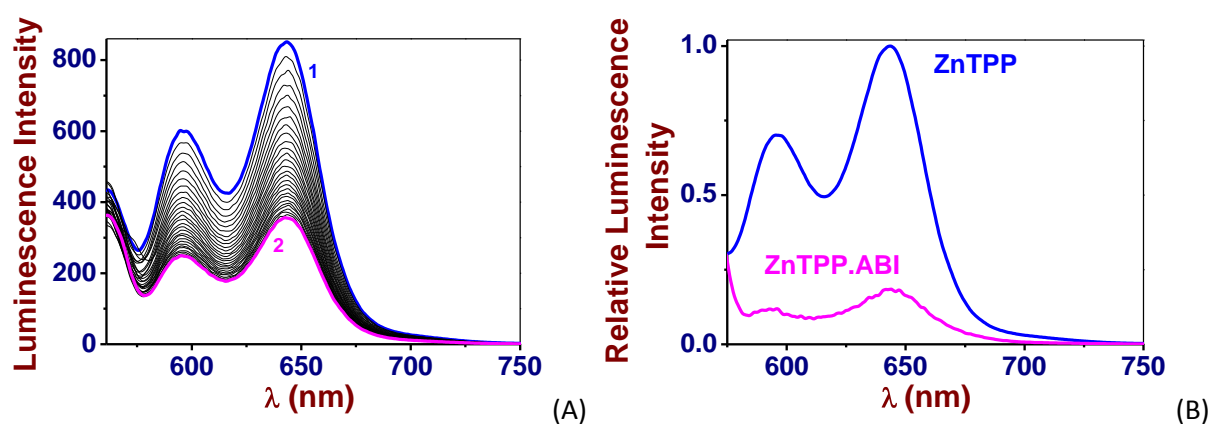


Figure 8. (A) Spectrofluorimetric titration of ZnTPP receptor by azo-benzene-imidazole (**ABI**). $\lambda_{\text{exc}} = 560$ nm; exc. and em. slits 15/20 nm; (1) $[\text{ZnTPP}]_{\text{tot}} = 3.40 \times 10^{-5}$ M; (2) $[\text{ABI}]_0/[\text{ZnTPP}]_{\text{tot}} = 63.5$. (B) Relative reconstituted emission spectra of ZnTPP and its pentacoordinated complex with **ABI**.

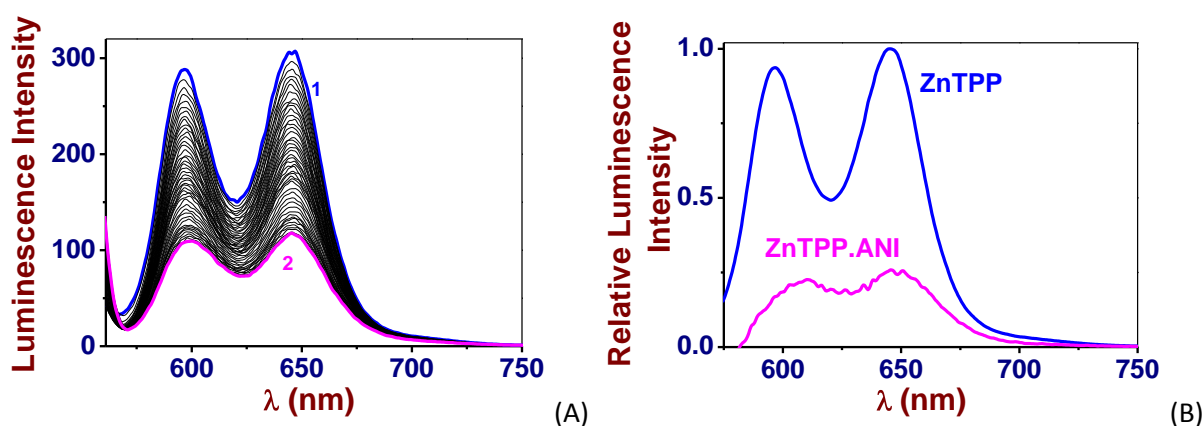


Figure 9. (A) Spectrofluorimetric titration of ZnTPP receptor by azo-naphthyl-imidazole (**ANI**). $\lambda_{\text{exc}} = 555$ nm; exc. and em. slits 10/10 nm; (1) $[\text{ZnTPP}]_{\text{tot}} = 7.10 \times 10^{-6}$ M; (2) $[\text{ANI}]_0/[\text{ZnTPP}]_{\text{tot}} = 93$. (B) Relative reconstituted emission spectra of ZnTPP and its pentacoordinated complex with **ANI**.

Similarly, to **ZnTPP**, the spectrofluorimetric binding titrations of **ZnL¹** by **ABI** and **ANI** revealed a quenching of the **ZnL¹**-centred emission at 600-650 nm ($S_1 \rightarrow S_0$ (Q(0,0) and Q(0,1)) transitions). Those reported by my research group for the substrates **S2** or **S3** which are lacking the azo-chromophores revealed bathochromic shifts of these emission bands. A reasonable good agreement was observed between the thermodynamic data obtained by absorption and emission spectrophotometries.

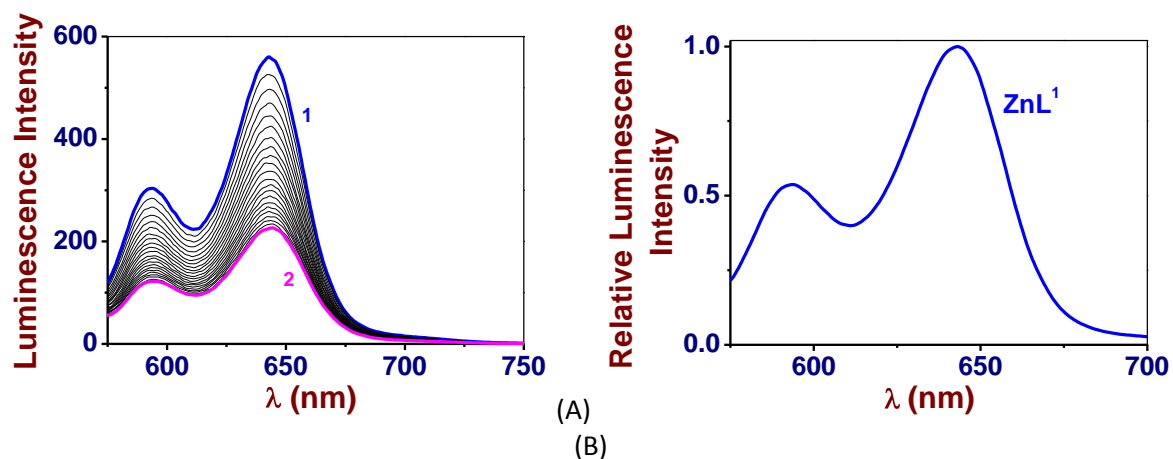


Figure 10. (A) Spectrofluorimetric titration of **ZnL¹** receptor by azo-benzene-imidazole (**ABI**). $\lambda_{exc} = 554$ nm; exc. and em. slits 15/20 nm; (1) $[ZnL^1]_{tot} = 4.7 \times 10^{-6}$ M; (2) $[ABI]_0/[ZnL^1]_0 = 9.66$. (B) Relative reconstituted emission spectra of **ZnL¹** and its pentacoordinated complex with **ABI**.

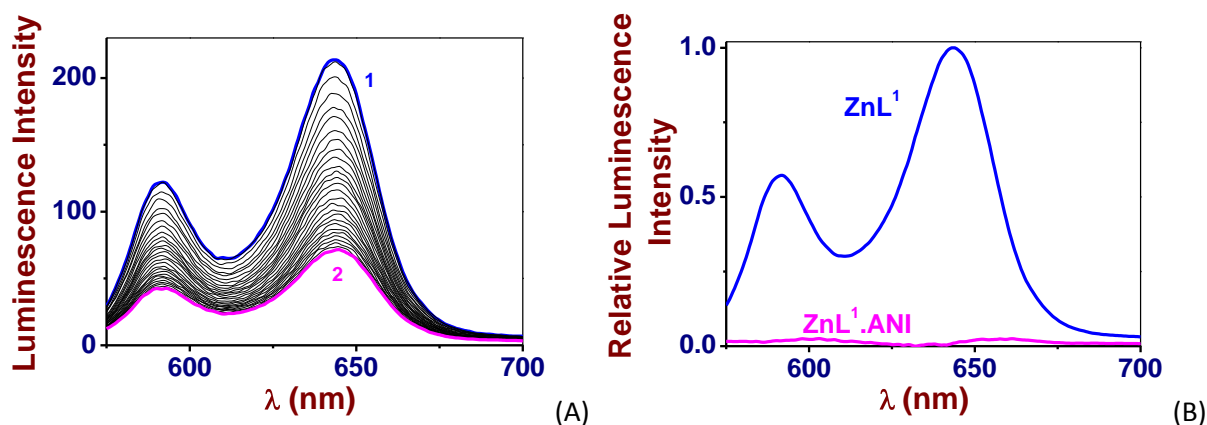


Figure 11. (A) Spectrofluorimetric titration of **ZnL¹** receptor by azo-naphthyl-imidazole (**ANI**). $\lambda_{exc} = 555$ nm; exc. and em. slits 10/10 nm; (1) $[ZnL^1]_{tot} = 1.20 \times 10^{-5}$ M; (2) $[ANI]_0/[ZnL^1]_{tot} = 58.3$. (B) Relative reconstituted emission spectra of **ZnL¹** and its pentacoordinated complex with **ANI**.

5.2.4. Statistical Processing of the Absorption Spectrophotometric Data

The spectrophotometric data were processed using the Specfit program¹⁶⁻¹⁹ which adjusts the stability constants and the corresponding extinction coefficients of the species formed at equilibrium. Specfit uses factor analyses to reduce the absorbance matrix and to extract the eigenvalues prior to the multi-wavelength fit of the reduced data set according to the Marquardt algorithm.^{20,21}

5.2.5. Formation Kinetics and Statistical Analyses

The formation kinetics of the pentacoordinated complex $\text{ZnL}^1\text{-ABI}$ was investigated using an Applied Photophysics SX-18MV stopped-flow spectrophotometer with emission detection. The reactants were thermostated at 25.0(2) °C (Lauda M12 thermostat) and mixed in a 1 cm optical cell. Pseudo-first order conditions with respect to the ABI imidazole were used with imidazole concentrations at least ten times higher than the ZnL^1 receptor concentration. For fluorescence measurements with $\text{ZnL}^1\text{-ABI}$, the excitation monochromator slits were set at 3 nm, and the excitation wavelength corresponds to an isosbestic point ($\lambda_{\text{exc}} = 554$ nm, Q bands) between the free ZnL^1 receptor and the pentacoordinated complex $\text{ZnL}^1\text{-ABI}$. A 550 nm band-pass plastic-glass filter (transparent to light with $\lambda > 550$ nm, Schott KV550) was used for measuring the emitted light. The data sets, averaged out of at least three replicates, were recorded and analyzed with the commercial software Biokine.²² This program fits up to three exponential functions to the experimental curves with the Simplex algorithm²³ after initialization with the Padé-Laplace method.²⁴ Variation of the pseudo-first order rate constants with the analytical concentrations of reagents were processed using commercial programs (Origin 5.0²⁵).

The temperature dependence of the formation kinetic was investigated for $\text{ZnL}^1\text{-ABI}$ complex as well. The experimental protocol described above was herein applied. Kinetic experiments were performed at temperatures ranging from 22.0 to 37.0 (error = ± 0.2 °C). A Lauda cryostat (Ultra Kryomat TK30) was used as the cooling unit whereas a Lauda M12 thermostat was employed as the heating system. The poor solubility of the imidazole at low temperature prevented the decrease of the temperature below 20 °C. Enthalpies and entropies of the reactions were calculated from conventional Eyring plots ($\ln(k/T) = f(1/T)$) using Origin 5.0 program.²⁵

For ZnL^1 and substrates **S2** (1*H*-imidazole) and **S3** (2-methyl-1*H*-imidazole), the kinetic investigations were already reported by my hosting group.^{4,5} For 1-methyl-1*H*-imidazole **S1**, for which a proximal recognition has been characterized (Figure 1), the reaction was too fast to be measured under our experimental conditions, in agreement with data reported, for instance, for ZnTPP and **S2** ($\log k_f = 9.5 \pm 0.5$ at 298 K in chlorobenzene).^{26,27} For **ABI**, the reaction times were slow enough to be recorded with a stopped-flow device and the kinetic measurements were then carried out under pseudo-first order conditions. The presence of the phen strap in ZnL^1 significantly slows down the formation reactions of the corresponding pentacoordinated complexes, thus rendering the formation kinetics accessible to stopped-flow techniques. A single rate-limiting step was observed with no evidence of slowest or fastest steps (Figure 12A). The pseudo-first order rate constants k_{obs} (s^{-1}) vary linearly with the concentration of **ABI** (Figure 12B), and the ordinate at the origin was determined with good accuracy. The bimolecular formation rate constants k_f ($\text{M}^{-1} \text{s}^{-1}$) and the monomolecular dissociation constants k_d (s^{-1}) are given in Table 2 and are compared to those measured for **S2** and **S3**.

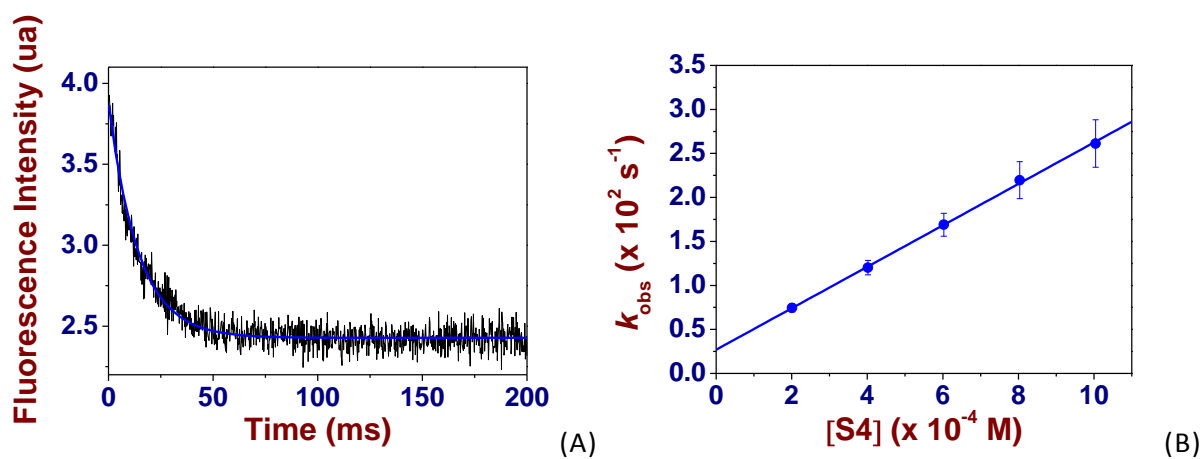


Figure 12. (A) Variation of the luminescence intensity *versus* time for the formation of ZnL^1ABI complex. Solvent: 1,2-dichloroethane; $T = 25.0(2) \text{ }^\circ\text{C}$; $l = 1 \text{ cm}$; $[\text{ZnL}^1] = 1.07 \times 10^{-5} \text{ M}$; $[\text{ABI}]_0/[\text{ZnL}^1]_0 = 10.43$. $\lambda_{\text{exc}} = 554 \text{ nm}$; set of band pass filter ($\lambda > 550 \text{ nm}$). (B) Variation of the pseudo-first order constants k_{obs} (s^{-1}) for the formation of ZnL^1ABI complex *versus* $[\text{ABI}]_{\text{tot}}$. Solvent: 1,2-dichloroethane; $T = 25.0(2) \text{ }^\circ\text{C}$; $[\text{ZnL}^1] = 1.07 \times 10^{-5} \text{ M}$.

5.3. Discussion

5.3.1 Recognition Properties

To evaluate the influence of the phenanthroline strap on the recognition properties of a series of imidazoles (**S1-S3**, **ABI**, **ANI** and **API**), we first considered the reference metalloporphyrin **ZnTPP** that possesses two identical faces. The only interaction that takes place with the imidazoles is indeed the strong *N*-Zn coordination.²⁸ The stability of **ZnTPP-Sⁿ** (**S1-S3**, **ABI**, **ANI** and **API**, Figure 1) were examined in 1,2-dichloroethane at $T = 25$ °C. Absorption and emission titrations were conducted, and the corresponding thermodynamic parameters (Table 1) were calculated by statistical processing of the spectral data.

Table 1. Stability constants of imidazoles **S1-S3**, **ABI**, **ANI** and **API** with ZnL^1 and **ZnTPP** receptors.

	S1	S2	S3	ABI	ANI	API
$\log K_{\text{ZnTPP-S}}$	4.7(2)	4.5(1)	4.9(2)	2.8(2)	3.2(2)	<< 2
$\log K_{\text{ZnL}^1\text{-S}}$	4.3(3)	5.9(1)	7.6(4)	4.4(1)	4.6(1)	<< 2

Solvent: 1,2-dichloroethane; $T = 25.0(2)$ °C. Average stability constants determined from UV-visible absorption and fluorescence spectrophotometric titrations. Uncertainties = 3σ with σ standard deviation.

With respect to **ZnTPP**, the stability constants usually reflect the electronic effects of the substituents on the N_3 -heteroatom, which binds to Zn(II) (Figure 13). The binding constants sequence of imidazoles follow the order of the $\text{p}K_a$ values that are tuned by substituent-induced electronic effects.^{29,30} For the azo-aryl-imidazoles **ABI**, **ANI** and **API**, a marked decrease of the binding constants is observed with respect to the estimated $\text{p}K_a$ values (*i.e.* calculated with ChemAxon $\text{p}K_a$ calculator). This indicates that strong steric interactions take place between the azo-chromophores and the tetrapyrrolic unit. For the phenanthryl substitution (**API**), no Zn(II) binding to **ZnTPP** could be evidenced under our experimental emphasizing this peculiar property.

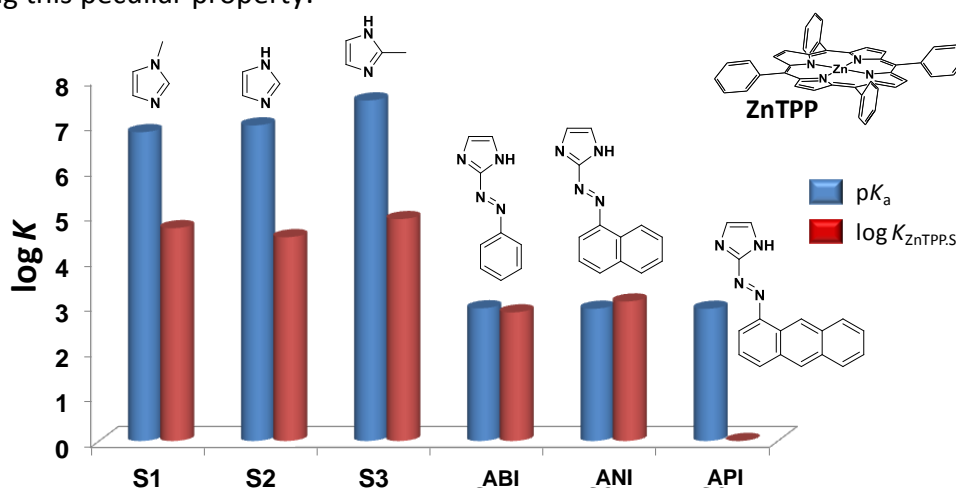


Figure 13. Schematic representation of the $\log K_{\text{ZnTPP,S}}$ values as a function of the $\text{p}K_a$ sequence (simulated with ChemAxon $\text{p}K_a$ calculator) which demonstrate the steric effects induced by the bulkiness of the azo-chromophore substituents.

For ZnL^1 , statistical processing of the spectrophotometric data supported the exclusive formation of 1:1 species corresponding to the axial ligation of an imidazole guest to the metallic centre of the metalloporphyrin.³¹ The corresponding stability constants of the pentacoordinated complexes with ZnL^1 are given in Table 1 and are schematically depicted in Figure 14. These thermodynamic data emphasized that N_1 -unsubstituted substrates are stabilized by 1 to 2 orders of magnitude with respect to ZnTPP . In contrast, 1-methyl-1*H*-imidazole (**S1**) forms a less stable complex with ZnL^1 ($\log K_{\text{ZnL}^1\text{-S1}} = 4.3(3)$) than with unstrapped ZnTPP metalloporphyrin ($\log K_{\text{ZnTPP-S1}} = 4.7(2)$), in agreement with a proximal recognition process.

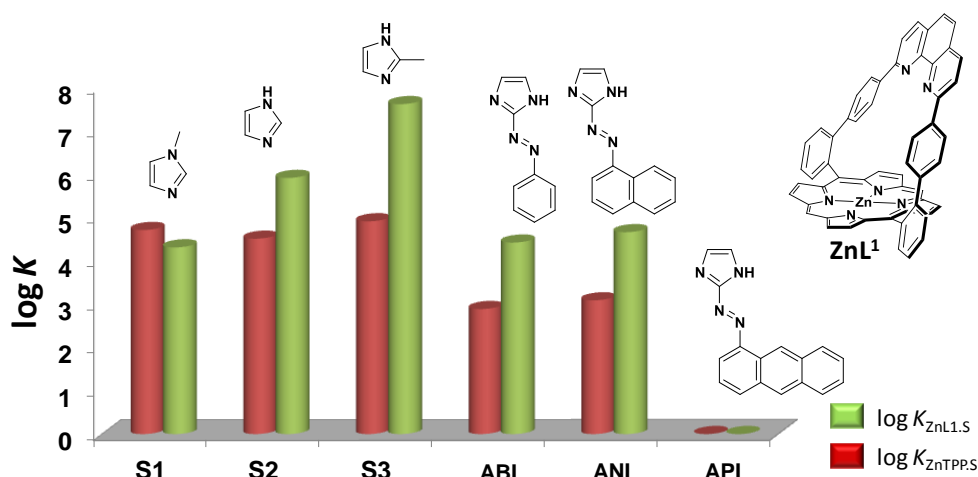


Figure 14. Schematic representation of the $\log K_{\text{ZnTPP.S}}$ and $\log K_{\text{ZnL}^1.S}$ values that shows the effect of hydrogen bonding with the phenanthroline strap on the extra-stabilization of the pentacoordinated complexes notwithstanding the bulkiness of the azo-chromophores.

The stabilization for binding of substrates **S2-S3**, **ABI** and **ANI** within ZnL^1 originates from the presence of the phen strap, which is able to interact with substrates *via* bifurcated hydrogen bonds. Indeed, clear evidence for hydrogen bonding between the imidazole substrates and the two phen nitrogens was previously established by ^1H NMR and 2D ^1H NMR data in solution and X-ray diffraction in the solid state for $\text{ZnL}^1\text{-S2}$ and $\text{ZnL}^1\text{-S3}$.^{2,3b}

For **ABI** and **ANI**, X-ray crystal structures were obtained with ZnL^1 in the frame of this PhD work and are presented in Figure 15. They clearly confirmed the presence of bifurcated hydrogen bonds between the $N_1\text{H}$ hydrogen of the substrate and the two phen-nitrogens. Interestingly, they show that the bulky azo-chromophore is opposed to the tetrapyrrolic aromatic system thus minimizing the steric interactions. The consequence of this arrangement is the steric hindrance that is now induced with the phen strap (*i.e.* almost perpendicular to the tetrapyrrolic system). It was previously demonstrated that the apparently rigid Zn(II) porphyrin ZnL^1 can accommodate on its distal face bulky substrates as a result its ring distortion and large tilt^{2,3b} of its strap above its tetrapyrrolic plane. This allowed the system to minimize steric interactions and maximize the stabilizing ones. In the case of azo-chromophores, the phen strap was

found to be almost perpendicular with respect to the tetrapyrrolic plane (Figure 15) and therefore induces a pronounced distortion of the Zn(II) porphyrin thus explaining the large thermodynamic destabilization of the pentacoordinated species (*i.e.* at least 2 orders of magnitude). For the aza-phenanthryl system **API** for which no binding with ZnL¹ was observed, deleterious steric effects involving the phenanthryl substituent of the substrate and the phenanthroline strap of the receptor as well as important constraints imposed to ZnL¹ prevent complex formation.

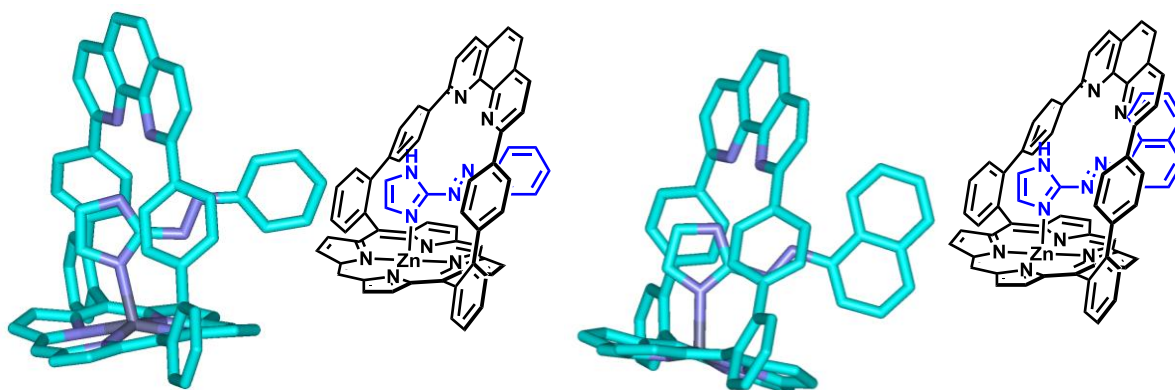


Figure 15. Schematic representation of the X-ray crystal structures of ZnL¹.ABI and ZnL¹.ANI.

5.3.2. Formation Mechanism

Whatever the substrate considered, a single rate limiting step was measured with no evidence of fastest or slowest steps. This suggests that a concerted formation mechanism (*i.e.* the establishments of the secondary stabilizing interactions are concomitant to the limiting Zn(II) coordination by the imidazole substrate) of the pentacoordinated complexes with ZnL¹. The sizeable flexibility of the ZnL¹ porphyrin receptors favors the distal axial coordination of a wide series of substrates without altering the main stabilizing interactions (*N*-Zn coordination and hydrogen bonding). This distal binding, however, induces a significant energetic cost, and leads to severe deformations of the porphyrin receptors. The kinetic data depicted in Table 2 illustrate this tendency and highlight that when binding requires strong distortion of the receptors, because of bulky guests, the resulting assemblies are more labile and are formed more slowly. The k_f values drastically decreases with increasing bulkiness of the substituents in position 2 of the imidazoles (2-phenyl-1*H*-imidazole and **ABI**). Differences of about two to three orders of magnitude are indeed observed between **S3** and 2-phenyl-1*H*-imidazole and between **S3** and **ABI**, respectively. When the 2-position of the imidazole remains unsubstituted, no decrease of the k_f values are observed as exemplified with the bulky 1*H*-benzimidazole.⁵ For **ABI**, introduction of an azo-chromophore in position 2 of the imidazole core has therefore a direct influence on the formation rate of the pentacoordinated complexes with ZnL¹. The k_d values rather result from a subtle balance between secondary stabilizing interactions (CH- π and π - π) and destabilizing steric interactions and structural deformations of the porphyrin host exerted by the bulky substrates. For example, 2-phenyl-1*H*-imidazole⁵ and 2-methyl-1*H*-imidazole (**S3**)

were found to form more inert edifices with ZnL^1 , because of the additional π - π stacking or CH- π interactions that were evidenced from NMR and X-ray data. For **ABI**, the steric interactions of the azo-chromophore with the phen-strap of ZnL^1 increase the lability of the corresponding complexes.

Table 2. Formation and Dissociation rate constants determined by kinetic studies for the formation mechanism of pentacoordinated complexes with ZnL^1 .^a

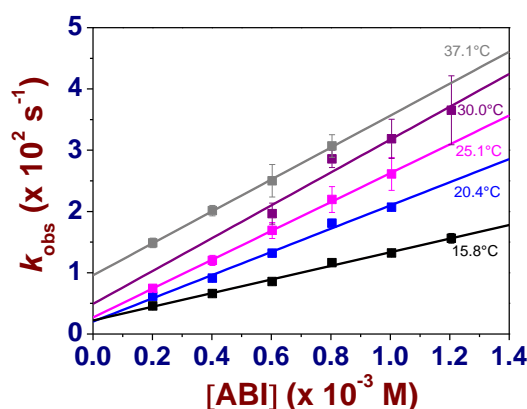
	S2	S3	2-Phenyl-1H-Imidazole ⁵	1H-Benzimidazole ⁵	ABI
$k_f (\text{M}^{-1} \text{s}^{-1})^d$	Too fast	$2.2(9) \times 10^7$	$2.0(7) \times 10^4$	$6.4(8) \times 10^7$	$2.35(4) \times 10^5$
$k_d (\text{s}^{-1})^d$	n.a.	16(8)	1.4(2)	162(51)	27(3)
$\log(k_f/k_d)$	n.a.	6.2	4.2	5.6	9.9
$\log K_{\text{ZnL}^1\text{S}}$	5.9(1)	7.6(4)	3.92(7)	5.8(4)	4.4(1)

^a Solvent: 1,2-dichloroethane; $T = 25.0(2)^\circ\text{C}$. $k_{\text{obs}} = k_f[\text{S}^n]_{\text{tot}} + k_d$. na = not applicable

5.3.3. Activation and Energetic Parameters.

To better understand the self-assembly mechanism, the activation enthalpies and entropies of both the formation and dissociation steps were determined for complexes ZnL^1 -**ABI**. The Eyring plots (k_f and k_d) are given in Figure 16.

ZnL^1 exhibited activation enthalpies for formation and dissociation ($\Delta H_f^\ddagger = +43(10) \text{ kJ mol}^{-1}$ and $\Delta H_d^\ddagger = +71(6) \text{ kJ mol}^{-1}$) that suggest an enthalpically controlled equilibrium ($\Delta\Delta H^\ddagger = -28(2) \text{ kJ mol}^{-1}$). These parameters are completed by comparable $\Delta S_f^\ddagger = -1.2(2) \text{ J mol}^{-1} \text{ K}^{-1}$ and $\Delta S_d^\ddagger = +2.2(2) \text{ J mol}^{-1} \text{ K}^{-1}$. The binding event seemingly proceeds through an associative mechanism with enthalpic contribution. These data are in excellent agreement with those described for ZnL^1 and 2-phenyl-1H-imidazole. Activation enthalpies and entropies for formation and dissociation ($\Delta H_f^\ddagger = 42(2) \text{ kJ mol}^{-1}/\Delta S_f^\ddagger = -26.0(9) \text{ J mol}^{-1} \text{ K}^{-1}$ and $\Delta H_d^\ddagger = 65(4) \text{ kJ mol}^{-1}/\Delta S_d^\ddagger = -28(2) \text{ J mol}^{-1} \text{ K}^{-1}$) also suggested an associative mechanism with enthalpic control.



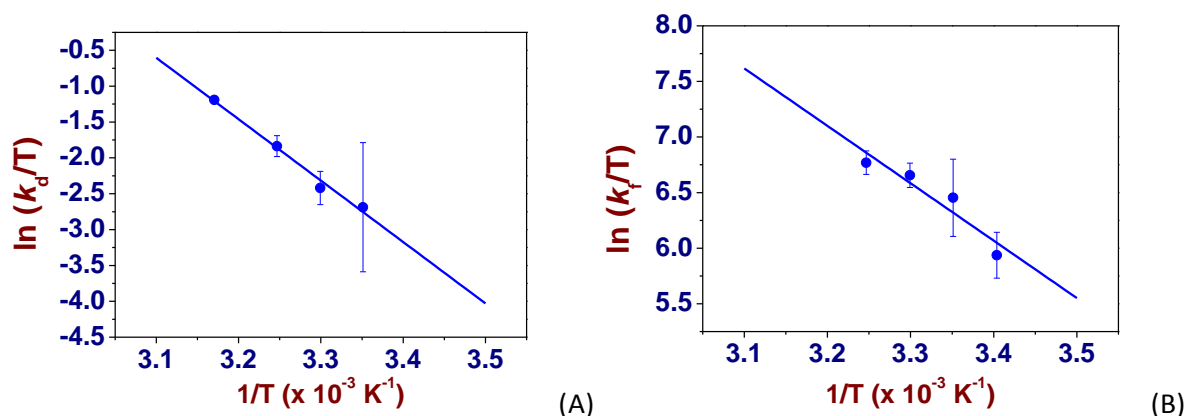


Figure 16. Eyring plots for (A) the formation and (B) the dissociation of $\text{ZnL}^1\text{.ABI}$ complex. Solvent: 1,2-dichloroethane.

These activation parameters have been completed with energetic data (standard entropy and enthalpy) that were calculated for $\text{ZnL}^1\text{.ABI}$ and ZnTPP.ABI (Table 3 and Figure 17) to evaluate the influence of the phen-strap on the global reaction.

Table 3. Binding constants measured for $\text{ZnL}^1\text{.ABI}$ and ZnTPP.ABI at different temperatures. Solvent: 1,2-dichloroethane; $[\text{ZnL}^1] = 4.73 \times 10^{-6} \text{ M}$, $[\text{ZnTPP}] = 6.7 \times 10^{-5} \text{ M}$.

$[\text{ABI}]_{\text{tot}}$	18°C	25°C	30°C	37°C
ZnL^1	4.67(2)	4.41(1)	4.12(6)	3.93(1)
ZnTPP	3.09(0.01)	2.88(0.012)	2.81(0.03)	2.48(0.05)

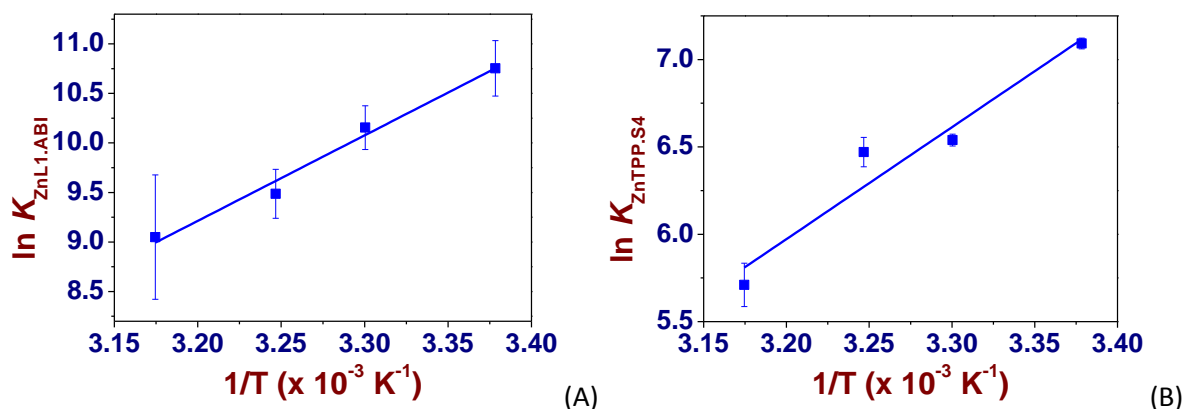


Figure 17. Van't Hoff plots for (A) ZnTPP.ABI and (B) $\text{ZnL}^1\text{.ABI}$. Solvent: 1,2-dichloroethane.

The values of standard enthalpies and entropies that were calculated (Table 4) clearly demonstrate that the reactions are enthalpically driven for either $\text{ZnL}^1\text{.ABI}$ or ZnTPP.ABI in excellent agreement with the activation parameters described above. My hosting group has demonstrated⁵ that the nature of the binding reaction was significantly altered by bulky substituent on the *meso*-positions of the porphyrinic receptor which induced a change of the reaction from enthalpically associative to entropically dissociative. Despite steric interactions with the phen-strap, the presence of bulky azo-chromophores seemingly does not alter the nature of the reaction (no conformational changes of the substrate and no severe distortions of the receptor). The entropies of the binding reactions leading to $\text{ZnL}^1\text{.ABI}$ and ZnTPP.ABI

suggested a minor influence of the strap on conformational properties of the pentacoordinated complexes, while the standard enthalpy measured for $\text{ZnL}^1\text{.ABI}$ is increased by $\sim 20 \text{ kJ mol}^{-1}$ as a consequence of the stabilizing interactions between the phen-strap and the imidazole unit.

Table 4. Standard enthalpies and entropies measured for $\text{ZnTPP}\text{.ABI}$ and $\text{ZnL}^1\text{.ABI}$.

	ΔH^0 ($\text{kJ} \times \text{mol}^{-1}$)	ΔS^0 ($\text{J} \times \text{K}^{-1} \times \text{mol}^{-1}$)	$-T\Delta S^0$ ($\text{kJ} \times \text{mol}^{-1}$)
$\text{ZnL}^1\text{.ABI}$	-72(6)	-150(20)	45(6)
$\text{ZnTPP}\text{.ABI}$	-53(10)	-120(30)	36(9)

5.4. Conclusion

The phen-strapped Zn(II) porphyrin ZnL^1 exhibit a suitable topography tailored to strongly and selectively bind various N_1 -unsubstituted imidazole-type substrates. The distal discrimination of imidazole N -Zn axial binding is favoured by the establishment of bifurcated hydrogen bonds of the N_1H group of the imidazole with the phenanthroline nitrogens of the receptor. This property consequently stabilizes the corresponding pentacoordinated complexes and therefore leads to an efficient multi-point host-guest system. The sizeable flexibility of the ZnL^1 receptor (*i.e.* distortion of the tetrapyrrolic conjugated system and large tilt of the phen-strap) constitutes structural features which minimize the steric interactions along the recognition process.

We clearly demonstrated in this study that imidazole substrates subtly decorated in their position 2 with functional (*trans-to-cis* conformational change upon photo-excitation) and bulky azo-chromophores can still form stable species with ZnL^1 receptor (distal recognition). However, a significant decrease was observed with respect to reference compounds (ZnTPP , 1*H*-imidazole, 1-methyl-1*H*-imidazole or 2-methyl-1*H*-imidazole) as a consequence of steric interactions of the azo-chromophore with the phen-strap and subsequent porphyrin distortions. To a greater extent, the azo-phenanthryl substitution (**API**) was found to prevent complex formation with ZnL^1 .

The mechanism of formation was elucidated using a fast mixing device. The binding reaction proceeded in a concerted single rate limiting step. Important effect was observed on the bimolecular formation rate constant k_f when bulkiness was introduced at the imidazole 2-position (**ABI** and 2-phenyl-1*H*-imidazole). Steric interactions between the azo-chromophore and the phen-strap accounted for the increase of lability of the $\text{ZnL}^1\text{.ABI}$ species with respect to model systems (*e.g.* $\text{ZnL}^1\text{.S3}$). Access to activation and energetic parameters allowed a deeper understanding of the formation mechanism. The formation of $\text{ZnL}^1\text{.ABI}$ was found to an associative mechanism that is enthalpically controlled. An enthalpy energy gain of $\sim 20 \text{ kJ mol}^{-1}$ was measured when comparing $\text{ZnL}^1\text{.ABI}$ to $\text{ZnTPP}\text{.ABI}$ as a consequence of stabilizing interactions occurring between the imidazole substrate and the phen-strap.

To sum up, ZnL^1 and the azo-chromophore substituted to an imidazole vector both display great potential for the preparation of innovative functional systems. It is anticipated that photo-excitation of the azo-chromophore would trigger its conformational change from *trans*- to *cis*- that induces the dissociation of the imidazole guest as a consequence of strong steric interactions. Thermal re-equilibration would invert the reaction and allowed reinstating the thermodynamically favoured pentacoordinated complex (Figure 18). These experiments are under progress and will be reported in due course.

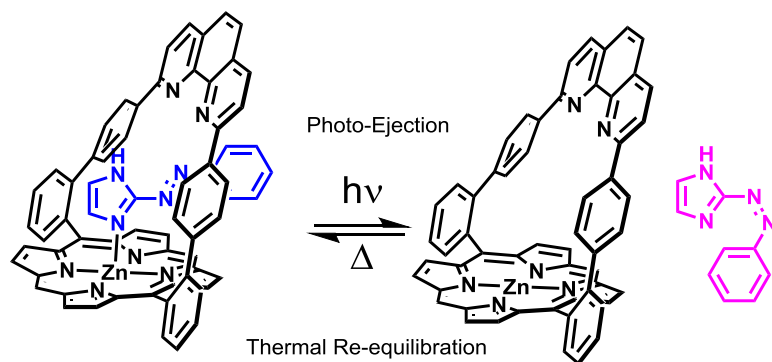


Figure 18. Schematic representation of the principle of photo-ejection of the azo-aryl-imidazole from the pentacoordinated species with ZnL^1 .

Bibliographic Section

- 1 (a) Griffiths, J. *Chem. Soc. Rev.* **1972**, *1*, 481-493. (b) Bandara, H.M.D.; Burdette, S.C. *Chem. Soc. Rev.* **2012**, *41*, 1809-1825.
- 2 Froidevaux, J.; Ochsenbein, P.; Bonin, M.; Schenk, K.; Maltese, P.; Gisselbrecht, J. P.; Weiss, J. *J. Am. Chem. Soc.* **1997**, *119*, 12362-12363.
- 3 (a) Dharam, P.; Wytko, J. A.; Koepf, M.; Weiss, J. *Inorg. Chem.*, **2002**, *41*, 3699-3704. (b) Dharam, P.; Melin, F.; Hirtz, C.; Wytko, J.A.; Ochsenbein, P.; Bonin, M.; Schenk, K.; Maltese, P.; Weiss, J. *Inorg. Chem.* **2003**, *42*, 3779-3787.
- 4 Brandel, J.; Trabolsi, A.; Melin, F.; Elhabiri, M.; Weiss, J.; Albrecht-Gary, A. M. *Inorg. Chem.* **2007**, *46*, 9534-9536.
- 5 Brandel, J.; Trabolsi, A.; Trabolsi, H.; Melin, F.; Koepf, M.; Wytko, J. A.; Elhabiri, M.; Weiss, J.; Albrecht-Gary, A. M. *Inorg. Chem.* **2009**, *48*, 3743-3754.
- 6 Sanders, J. K. M. In *The Porphyrin Handbook*, Kadish, K. M.; Smith, K. M.; Guillard, R., Eds., Academic Press, New York, **2000**, *3*, pp 347-368.
- 7 Imamura, T.; Fukushima, K. *Coord. Chem. Rev.* **2000**, *198*, 133-156.
- 8 (a) Wojaczynski, J.; Latos-Grazynski, L. *Coord. Chem. Rev.* **2000**, *204*, 113-171. (b) Flamigni, L.; Barigelletti, F.; Armaroli, N.; Collin, J. P.; Dixon, I. M.; Sauvage, J. P.; Williams, J. A. G. *Coord. Chem. Rev.* **1999**, *190-192*, 671-682. (c) Tamiaki, H. *Coord. Chem. Rev.* **1996**, *148*, 183-197. (d) Kurreck, H.; Huber, M. *Angew. Chem., Int. Ed. Engl.* **1995**, *34*, 849-866. (e) Gribkova, S. E.; Evstigneeva, R. P.; Luzgina, V. N. *Russ. Chem. Rev.* **1993**, *62*, 963-979. (f) Gust, D.; Moore, T. A. *Topics Curr. Chem.* **1991**, *159*, 103-151.
- 9 (a) Iengo, E.; Zangrando, E.; Alessio, E. *Eur. J. Inorg. Chem.* **2003**, 2371-2384. (b) Wojaczynski, J.; Latos-Grażyński, L. *Coord. Chem. Rev.* **2000**, *204*, 113-171. (c) Heitz, V.; Chambron, J. C.; Sauvage, J. P. In *The Porphyrin Handbook*, Kadish, K. M.; Smith, K. M.; Guillard, R. Eds., Academic Press, New York, **2000**, *6*, 1-42. (d) Haycock, R. A.; Hunter, C. A.; James, D. A.; Michelsen, U.; Sutton, L. R. *Org. Lett.* **2000**, *2*, 2435-2438.
- 10 Leray, I.; Valeur, B.; Paul, D.; Regnier, E.; Koepf, M.; Wytko, J. A.; Boudon, C.; Weiss, J. *Photochem. Photobiol. Sci.* **2005**, *4*, 280-286.
- 11 Koepf, M.; Trabolsi, A.; Elhabiri, M.; Wytko, J. A.; Albrecht-Gary, A. M.; Weiss, J. *Org. Lett.* **2005**, *7*, 1279-1282.
- 12 Wytko, J. A.; Graf, E.; Weiss, J. *J. Org. Chem.* **1992**, *57*, 1015-1018.
- 13 (a) Gouterman, M. In *The Porphyrins*, Dolphin, D., Ed. Academic Press, New York, **1978**, *3*, 1-165. (b) Dorough, G. D.; Miller, J. R.; Huennekens, F. M. *J. Am. Chem. Soc.* **1951**, *73*, 4315-4320. (c) Thomas, D. W.; Martell, A. E. *J. Am. Chem. Soc.* **1956**, *78*, 1338-1343. (d) Edwards, L.; Dolphin, D. H.; Gouterman, M.; Adler, A. D. *J. Mol. Spectrosc.* **1971**, *38*, 16-32. (e) Seybold, P. G.; Gouterman, M. *J. Mol. Spectrosc.* **1969**, *31*, 1-13.
- 14 (a) Humphry-Baker, R.; Kalyanasundaram, K. *J. Photochem.* **1985**, *31*, 105-112. (b) Seely, G. R.; Calvin, M. *J. Chem. Phys.* **1955**, *23*, 1068-1078.
- 15 Nappa, M.; Valentine, J. S. *J. Am. Chem. Soc.* **1978**, *100*, 5075-5080.
- 16 Gampp, H.; Maeder, M.; Meyer, C. J.; Zuberbühler, A. D. *Talanta* **1985**, *32*, 95-101.
- 17 Rossotti, F. J. C.; Rossotti, H. S.; Whewell, R. J. *J. Inorg. Nuc. Chem.* **1971**, *33*, 2051-2065.
- 18 Gampp, H.; Maeder, M.; Meyer, C. J.; Zuberbühler, A. D. *Talanta* **1985**, *32*, 257-264.

- 19 Gampp, H.; Maeder, M.; Meyer, C. J.; Zuberbühler, A. D. *Talanta* **1986**, *33*, 943-951.
- 20 Marquardt, D. W. *J. Soc. Ind. Appl. Math.* **1963**, *11*, 431-441.
- 21 Maeder, M.; Zuberbuehler, A. D. *Anal. Chem.* **1990**, *62*, 2220-2224.
- 22 Bio-Logic Company, Ed. Bio-Logic Company, Echirolles, **1991**.
- 23 Nelder, J. A.; Mead, R. *Comput. J.* **1965**, *7*, 308-313.
- 24 Yeramian, E.; Claverie, P. *Nature* **1987**, *326*, 169-174.
- 25 Microcal Origin, 1997; Microcal Software, Inc.: Northampton, MA.
- 26 Caldin, E.; Field, J. P. *J. Chem. Soc., Faraday Trans. I* **1982**, *78*, 1923-1935.
- 27 Ware, W. R.; Novros, J. S. *J. Phys. Chem.* **1966**, *70*, 3246-3253.
- 28 Satake, A.; Kobuke, Y. *Tetrahedron* **2005**, *61*, 13-41.
- 29 (a) Mc Dermott, G. A.; Walker, F. A. *Inorg. Chim. Acta* **1984**, *91*, 95-102. b) Kadish, K. M.; Shiue, L. R. *Inorg. Chem.* **1982**, *21*, 3623-3630. (c) Kadish, K. M.; Shiue, L. R.; Rhodes, R. K.; Bottomley, L. A. *Inorg. Chem.* **1981**, *20*, 1274-1277. (d) Kadish, K. M.; Rhodes, R. K. *Inorg. Chem.* **1981**, *20*, 2961-2966. (e) Vogel, G. C.; Stahlbusch, J. R. *Inorg. Chem.* **1977**, *16*, 950-953. (f) Valentine, J. S.; Tatsuno, Y.; Nappa, M. *J. Am. Chem. Soc.* **1977**, *99*, 3522-3523. (g) Cole, S. J.; Curthoys, G. C.; Magnusson, E. A.; Phillips, J. N. *Inorg. Chem.* **1972**, *11*, 1024-1028.
- 30 (a) Ogoshi, H.; Mizutani, T.; Hayashi, T.; Kuroda, Y. In *The Porphyrin Handbook*; Kadish, K. M.; Smith, K. M.; Guilard, R., Eds., Academic Press, New York, **2000**; *6*, pp 1-49.
- 31 (a) Miller, J. R.; Dorough, G. D. *J. Am. Chem. Soc.* **1952**, *74*, 3977-3981. (b) Kirskey, C. H.; Hambright, P. *Inorg. Chem.* **1970**, *9*, 958-960.

General Conclusion

The first part of my PhD work that was done under the scientific supervision of Dr Mourad Elhabiri (UMR 7509 CNRS-UdS) and Dr Zouhair Asfari (UMR 7178 CNRS-UdS) has been focused on the synthesis and thorough physico-chemical investigations of host guest complexes using “multimeric” viologen based systems and cucurbituril macrocycles. Particular attention has been paid on the redox properties of these systems which confer them interesting behaviour and high potential for designing new nanometric mechanical or electrochemical tools. This work has been done in close collaboration with the groups of Pr Ali Trabolsi (NYUAD, Abu Dhabi, UAE) and of Pr Carlos Platas-Iglesias (Universidad de Coruña, Spain).

The novel nanomechanical systems that have been developed include among other: a [3]pseudorotaxane, a [4]pseudorotaxane and a [7]pseudorotaxane, each composed of a “multimeric” viologen-based thread molecule and the macrocycles, cucurbit[7]uril (**CB[7]**) and cucurbit[8]uril (**CB[8]**). In aqueous solution, these systems can be electrochemically switched between a complexed state, defined by the pseudorotaxanes themselves, and an uncomplexed state comprising their separate components. The driving force for the disassembly process (*i.e.* "dethreading") is a strong intramolecular or intermolecular dimerization of the viologen radical cations. The recognition and dethreading properties have been analyzed using a set of complementary analytical tools such as UV-visible-NIR absorption spectrophotometry, ^1H NMR, electrochemistry (CV and SWV), ESMS and EPR. These data have been completed by DFT calculations.

In the first section, we have investigated the redox and recognition properties of a hexaviologen dendritic like system (**HV¹²⁺**) that takes advantage of the properties of a phosphazene core. Six terminal **BIPY²⁺** units have been homogeneously distributed along the periphery of this cyclotriphosphazene unit. Model ligands (**BV⁴⁺**, **MV²⁺** and **BMV²⁺**) have also been studied to assess the critical role of the cyclotriphosphazene unit on the recognition of and dimerization processes. The model system **BV⁴⁺** only contains two viologen subunits that are distributed face-to-face along the periphery of the phosphazene core while the benzyl methyl viologen **BMV²⁺** corresponds to a basic electroactive unit.

MV²⁺ and **MV^{•+}** bind to **CB[7]** in a similar fashion, with a viologen unit being encircled inside the hydrophobic cavity of the macrocycle. As a consequence, reduction of the pseudorotaxane **MV²⁺⊂CB[7]** does not induce any conformational changes, although **MV^{•+}⊂CB[7]** is a less stable complex. Substitution of the viologen electrophore with a hydrophobic benzylic unit markedly alters its recognition properties. **BMV²⁺** was found to bind to **CB[7]** with its benzyl substituent inside the hydrophobic cavity of the macrocycle. However, upon one electron reduction, **BMV^{•+}** and **MV^{•+}** are sharing the same binding properties with **CB[7]** with the radical cation moiety being located inside the **CB[7]** cavity. It follows that, when the pseudorotaxane **BMV²⁺⊂CB[7]** is reduced to **BMV^{•+}⊂CB[7]**, the macrocycle translocates from the benzyl unit to the viologen radical cation.

Despite the structural analogy between **BMV²⁺** and the arms of the multimeric threads **BV⁴⁺** and **HV¹²⁺**, these latter bind to **CB[7]** similarly as **MV²⁺** does (*i.e.* a [7]pseudorotaxane

$\text{HV}^{12+} \subset (\text{CB}[7])_6$ and a [3]pseudorotaxane $\text{BV}^{4+} \subset (\text{CB}[7])_2$ have been characterized). This likely originates from the steric effects induced by the cyclophosphazene core, which hamper **CB[7]** to efficiently encircle the benzylic residue of BV^{4+} or HV^{12+} . Upon one electron reduction of each of the bipyridinium units of $\text{BV}^{4+} \subset (\text{CB}[7])_2$ and $\text{HV}^{12+} \subset (\text{CB}[7])_6$, spontaneous dissociation of the **CB[7]** occurs as a result of the thermodynamic favoured intramolecular pimerization of the corresponding radical cations with respect to inclusion to **CB[7]**. $\text{BV}^{2(\bullet+)}$ and $\text{HV}^{6(\bullet+)}$ pimerizes intramolecularly to form one and three pairs of viologen radical cation dimers, respectively (*i.e.* for the hexavalent system the fully pimerized species was referred as $\text{HV}_D^{6(\bullet+)}$). No proof of interactions between **CB[7]** and the hexameric system $\text{HV}_D^{6(\bullet+)}$ was obtained by any of the analytical methods employed so far. This important outcome lend credence to the fact that radical cation dimerization (*i.e.* a relatively weak interaction) can be enhanced intramolecularly and exploited for the design of novel molecular switches (molecular reorganization from six to three directions around a cyclotriphosphazene core) irrespective of the presence of **CB[7]** or not.

Motivated by these findings, we considered in this work other anchoring cores to efficiently preorganize and distribute viologen residues. These molecular anchors have to fulfil a given number of requirements (*e.g.* easiness of functionalization, efficient and fast pimerization, and applicability to electrochromic material research, marked recognition properties as function of its redox state). Calix[4]arene has then selected thanks to its numerous conformational and structural properties. Up to four positions can be substituted either on the lower or the upper rims (*i.e.* we have considered in this work only the face-to-face disubstituted derivatives on the lower rim). The conformation properties of the calix[4]arene can also be controlled.

Two calix[4]arene-*bis*-viologen systems, namely C23^{4+} and C24^{4+} , have been prepared. Two monomeric viologen guests (MC3^{2+} and MC4^{2+}) have been also employed as model systems. [2]pseudorotaxanes, $\text{MC3}^{2+} \subset \text{CB}[7]$ and $\text{MC4}^{2+} \subset \text{CB}[7]$, were characterized. By contrast with BMV^{2+} , the BIPY^{2+} unit was found to be the unique recognition site whatever its redox state. Consequently, no translocation of the macrocyclic host was observed between the two binding stations (*i.e.* BIPY^{2+} and hydrophobic alkoxy-phenyl units). These model compounds provided other unexpected results. As a result of the presence of the alkoxy-phenyl substitution, [3]pseudorotaxanes such as $\text{MC3}^{2+} \subset (\text{CB}[7])_2$ and $\text{MC4}^{2+} \subset (\text{CB}[7])_2$ were also characterized. With the larger **CB[8]** host, similar properties have been emphasized with the oxidized form of MC3^{2+} and MC4^{2+} .

With C23^{4+} and C24^{4+} , we characterized [3]pseudorotaxanes with either **CB[7]** or **CB[8]**. Regardless of the size of the macrocyclic host involved, **CB[7]** and **CB[8]** were shown to reside in the middle of the BIPY^{2+} dications as a result of steric interactions with the calix[4]arene anchor. Similarly to HV^{12+} , these [3]pseudorotaxanes spontaneously dissociate on reduction of the terminal bipyridiniums as the result of a strong intramolecular pimerization of the face-to-face viologen radical cations. Arrangement of the $\text{BIPY}^{\bullet+}$ radical cations within the dimeric species also depends on the nature and length of the spacer that links the electroactive units to the anchoring moiety. Last but not the least, decomplexation

and dimerization do not occur in experiments involving **CB[7]** (or **CB[8]**) and either of the two monomeric viologen guests **MC3²⁺** and **MC4²⁺**.

In another approach, we also demonstrated that using fine tuned intermolecular interactions on multivalent systems, strong dimerization of radical cations can also thermodynamically overwhelm the inclusion to **CB[7]** and induce fast and efficient host-guest dethreading. Reinstating the oxidized bipyridiniums prevent the dimerization process and reversibly led to the initial host-guest species. A circular trimeric system (**TV⁶⁺**) composed of a benzenic core that has been extended on its 1, 3 and 5 positions by methyl-phenyl-viologen (**MPV²⁺**) subunits has been considered. For the sake of comparison, model systems (**MVTP²⁺**, **MPV²⁺** and **DPV²⁺**) have been investigated as well.

In the presence of **CB[7]** or **CB[8]**, **TV⁶⁺** led to the formation of [4]pseudorotaxane **TV⁶⁺⊂[CB[n]]₃** (n = 7, 8). The model ligands stood in interesting contrast. **MVTP²⁺** led to the formation of [2]pseudorotaxane with its **BIPY²⁺** unit being encircled by the macrocyclic host (*i.e.* steric effect of the cucurbituril with the triaryl-phenylene substituent), while **MPV²⁺** (*i.e.* leading to [2]pseudorotaxane) welcomed the macrocyclic host on its phenyl side rather than on its **BIPY²⁺** as a consequence of minimized steric interactions. Last but not the least, **DPV²⁺** which bear two phenyl substituents can form either [2]pseudorotaxane or [3]pseudorotaxane.

The one electron reduction of each of the viologen units of **TV⁶⁺** led to the formation of a trisradical viologen **TV^{3(•••)}** that spontaneously self-associate in solution to afford the dimeric (**TV^{3(•••)}**)₂ species. Unlike viologen derivatives under their monoradical state, pimerization **TV^{3(•••)}** was found to be significantly favoured ($K_{Dim} \gg 10^7 \text{ M}^{-1}$) as a result of the multiple pimerization centres (multivalency effect). The (**TV^{3(•••)}**)₂ dimer thus remains the predominant species even in the sub-micromolar concentrations. Besides, an aggregation process has been observed due to a stacking process between the aromatic dimers that can be reversible prevented by addition of **CB[8]** but not with **CB[7]**. In the presence of **CB[7]**, the one electron reduction of each of the viologen units led to the dethreading of the macrocycles from the (electro)chemically generated **TV^{3(•••)}⊂[CB[7]]₃** species. This process is reversible and oxidation of the viologen monoradical subunits regenerates the initial host-guest species. Similarly to the first strategy (intramolecular pimerization using calix[4]arene or cyclotriphosphazene molecular anchors), the intermolecular pimerization by far competes thermodynamically with the inclusion process. With **CB[8]**, we have shown that two monoradical viologen subunits can be firmly stacked together within the macrocyclic host cavity ultimately leading to (**TV^{3(•••)}**)₂⊂**[CB[8]]₃** species and then preventing oligomerization (and precipitation) of the (**TV^{3(•••)}**)₂ dimers.

In addition to intramolecular pimerization within pre-organized systems, intermolecular interactions can be used as well to enhance the stability of radical dimers in solution thank to a peculiar design (recognition centres judiciously distributed along the periphery of a benzenic central core) and to a multicenter approach.

The last project that was studied in close collaboration with the groups of Dr Jean Weiss (UMR 7177, CNRS-UdS) and Pr Ali Trabolsi (NYUAD, Abu Dhabi, UAE) focused on the physico-chemical characterization of pentacoordinated complexes that are formed when combining new azo-aryl-imidazole substrates and a phenanthroline strapped porphyrin. The phen-strapped Zn(II) porphyrin ZnL^1 exhibit a suitable topography tailored to strongly and selectively bind various N_1 -unsubstituted imidazole-type substrates. The distal discrimination of imidazole N -Zn axial binding is favoured by the establishment of bifurcated hydrogen bonds of the N_1H group of the imidazole with the phenanthroline nitrogens of the receptor. This property stabilizes the corresponding pentacoordinated complexes and therefore leads to an efficient multi-point host-guest system.

A series of new azo-aryl-imidazoles whose bulkiness of the azo-chromophore has been varied has been considered. These substrates display a functional group that might undergo a *trans*-to-*cis* conformational change upon photo-irradiation and ultimately induce a so-called “photo-ejection” of the substrate. We have shown that these apparent bulky imidazole substrates decorated in their position 2 with azo-chromophores can still form stable pentacoordinated species with the ZnL^1 phen-strapped metalloporphyrinic receptor (distal recognition). A significant decrease of stability was, however, observed as a consequence of steric interactions of the azo-chromophore with the phen-strap and subsequent porphyrin distortions. To a greater extent, the azo-phenanthryl substitution (**API**) did not lead to complex formation with ZnL^1 under our experimental conditions.

Binding of these new azo-aryl-imidazoles proceeded according to a concerted mechanism. Bulkiness of the imidazole 2-position (**ABI** azo-benzene-imidazole and 2-phenyl-1*H*-imidazole) was shown to influence both the formation and the inertness of the pentacoordinated complexes with ZnL^1 (*i.e.* strong steric interactions between the azo-chromophore and the phen-strap). Besides, formation of ZnL^1 .**ABI** follows an associative mechanism that is enthalpically controlled. An enthalpy energy gain of ~ 20 kJ mol⁻¹ is observed between ZnL^1 .**ABI** and $ZnTPP$.**ABI** as a consequence of stabilizing interactions (*i.e.* hydrogen bonds) occurring between the imidazole substrate and the phen-strap.

The physico-chemical properties of these pentacoordinated complexes being well established, it is now anticipated that photo-excitation of the azo-chromophore would trigger its conformational change from *trans*- to *cis*- and then impose dissociation of the imidazole guest as a consequence of deleterious steric interactions. Thermal re-equilibration is expected to reverse the reaction and allowed reinstating the thermodynamically favoured pentacoordinated complex.

Multivalent Systems Based on Viologen Units: Redox Behaviour and Recognition Properties by Cucurbit[n]urils

Résumé

Des supramolécules basées sur la reconnaissance de viologènes par des cucurbit[n]urils (CB[n]) ont été étudiées. Les systèmes développés incluent des [3]-, [4]- et [7]pseudorotaxanes, composés de multimères à base de viologène et de CB[7] ou CB[8]. L'étude physicochimique a montré que ces supramolécules sont interconverties électrochimiquement entre un état complexé, défini par les pseudorotaxanes, et un état dissocié comprenant chacun des partenaires. Le désassemblage résulte d'une pimérisation intra/intermoléculaire entre radicaux viologènes.

L'étude physicochimique de complexes pentacoordinés basés sur la reconnaissance d'azo-aryl-imidazoles par une porphyrine à anse phénanthroline a été menée; l'objectif étant d'utiliser les propriétés d'isomérisation photoinduite *trans-cis* d'azo-chromophores pour dissocier ces complexes. Les complexes initiaux sont alors régénérés par relaxation thermique. La stabilité et les propriétés cinétiques des complexes pentacoordinés ont été évaluées.

Mots clés : Bipyridinium, Cucurbit[n]uril, Porphyrine, Azo-chromophore, Multivalence, Reconnaissance, [n]Pseudorotaxanes, Physico-Chimie

Résumé en anglais

Supramolecules based on the recognition of redox-active bipyridiniums by cucurbit[n]uril (CB[n]) have been studied. The investigated systems include a [3]-, a [4]- and a [7]pseudorotaxane, each of them composed of a multimeric viologen-based thread molecule and CB[7] or CB[8]. The physicochemical approach emphasized that these systems can be electrochemically switched between a complexed state, defined by the pseudorotaxanes, and an uncomplexed state comprising their components. The disassembly results from intra/intermolecular pimerization of the viologen radicals.

A physicochemical approach of pentacoordinated complexes of a phen-strapped porphyrin with azo-arylimidazoles has been undertaken with the aim to use the photoinduced *trans-cis* isomerization properties of azo-chromophores to dissociate the complexes. Thermal equilibration reinstates the thermodynamically favoured complexes. The strength and the kinetic properties of these pentacoordinated species have been evaluated.

Keywords: Bipyridinium, Cucurbit[n]uril, Porphyrin, Azo-chromophore, Multivalency, Recognition, [n]Pseudorotaxanes, Physico-chemistry